

Cellular mechanisms affecting Alzheimer's amyloid-beta aggregation in *Saccharomyces cerevisiae*

Author:

Nair, Suresh

Publication Date:

2012

DOI:

<https://doi.org/10.26190/unsworks/15886>

License:

<https://creativecommons.org/licenses/by-nc-nd/3.0/au/>

Link to license to see what you are allowed to do with this resource.

Downloaded from <http://hdl.handle.net/1959.4/52322> in <https://unsworks.unsw.edu.au> on 2024-04-16

**Cellular mechanisms affecting Alzheimer's
amyloid-beta aggregation in *Saccharomyces
cerevisiae***

A thesis presented for the degree of Doctor of Philosophy by

Suresh Nair

School of Biotechnology and Biomolecular Sciences
University of New South Wales

August, 2012

Thesis/Dissertation Sheet

First name: **SURESH**

Other name/s:

Abbreviation for degree as given in the University calendar: **PhD**

School: **Biological Sciences**

Faculty: **SCIENCE**

Title: **Cellular mechanisms affecting Alzheimer's amyloid-beta aggregation in *Saccharomyces cerevisiae***

Amyloid-beta (A β) plaques are a major neuropathological feature of Alzheimer's disease (AD). These plaques are primarily composed of aggregates of A β peptides generated via the amyloidogenic processing of the amyloid precursor protein. The two major isoforms of A β peptide are A β_{40} and A β_{42} , of which the latter is highly prone to aggregation. Increased presence and aggregation of intracellular A β_{42} peptides is an early event in the disease progression of AD. Improved understanding of cellular processes involved in A β_{42} aggregation may have implications for understanding AD progression and development of therapeutic strategies.

Here A β ₄₂ fused to green fluorescent protein (A β ₄₂GFP) was expressed in each mutant of the *Saccharomyces cerevisiae* genome-wide deletion library to identify proteins and cellular processes that affect intracellular A β ₄₂ aggregation by assessing the fluorescence associated with expression of the A β ₄₂GFP fusion protein. This screening identified 110 mutants exhibiting intense A β ₄₂GFP-associated fluorescence. Four major cellular processes were over-represented in the data set, including phospholipid homeostasis and mitochondrial function. Analysis of the *S. cerevisiae* lipidome by quantitative mass spectrometry led to the discovery that disruption of phosphatidylcholine, phosphatidylserine and/or phosphatidylinositol metabolism had a major effect on intracellular A β ₄₂ aggregation and localisation. Distinctive subcellular localisation of A β ₄₂GFP in the phospholipid mutants was observed. Confocal microscopy indicated that A β ₄₂GFP in the phospholipid mutants was juxtaposed to the nucleus of the cell, associated with the endoplasmic reticulum.

A novel outcome of the A β ₄₂GFP fusion protein has been to also identify putative roles for two proteins of previously uncharacterised function. This study further exploited the powerful and flexible platform of applying GFP-derived fluorescence-based assay for the screening of the Library of Pharmacologically Active Compounds (LOPAC) and the SPECTRUM Collection chemical/drug libraries for compounds with amyloidogenic and anti-amyloidogenic properties. These libraries include FDA-approved drugs and identifying such drugs as affecting intracellular A β ₄₂ aggregation may significantly reduce costs and the exhaustive process of introducing new drugs onto the market. These data provide genome-wide evidence of cellular processes and chemical compounds that affect intracellular A β ₄₂GFP aggregation and may have important implications for understanding cellular mechanisms that affect intracellular A β ₄₂ aggregation and ultimately AD progression.

I hereby grant to the University of New South Wales or its agents the right to archive and to make available my thesis or dissertation in whole or in part in the University libraries in all forms of media, now or here after known, subject to the provisions of the Copyright Act 1968. I retain all property rights, such as patent rights. I also retain the right to use in future works (such as articles or books) all or part of this thesis or dissertation.

I also authorise University Microfilms to use the 350 word abstract of my thesis in Dissertation Abstracts International (this is applicable to doctoral theses only).

20 - 12 - 2012

.....
Signature

.....
Witness

.....
Date

The University recognises that there may be exceptional circumstances requiring restrictions on copying or conditions on use. Requests for restriction for a period of up to 2 years must be made in writing. Requests for a longer period of restriction may be considered in exceptional circumstances and require the approval of the Dean of Graduate Research.

FOR OFFICE USE ONLY

Date of completion of requirements for Award:

ORIGINALITY STATEMENT

I hereby declare that this submission is my own work and to the best of my knowledge it contains no materials previously published or written by another person, or substantial proportions of material which have been accepted for the award of any other degree or diploma at UNSW or any other educational institution, except where due acknowledgement is made in the thesis. Any contribution made to the research by others, with whom I have worked at UNSW or elsewhere, is explicitly acknowledged in the thesis.

I also declare that the intellectual content of this thesis is the product of my own work, except to the extent that assistance from others in the project's design and conception or in style, presentation and linguistic expression acknowledged.

Signed

Suresh Nair

Date: 20 – 12 – 2012

COPYRIGHT STATEMENT

I hereby grant the University of New South Wales or its agents the right to archive and to make available my thesis or dissertation in whole or part in the University libraries in all forms of media, now or here after known, subject to the provisions of the Copyright Act 1968. I retain all proprietary rights, such as patent rights. I also retain the right to use in future works (such as articles or books) all or part of this thesis or dissertation.

I also authorise University Microfilms to use the 350 word abstract of my thesis in Dissertation Abstract International (this is applicable to doctoral theses only). I have either used no substantial portions of copyright material in my thesis or I have obtained permission to use copyright material; where permission has not been granted I have applied/will apply for a partial restriction of the digital copy of my thesis or dissertation.

Signed

Suresh Nair

Date: 20 – 12 – 2012

AUTHENTICITY STATEMENT

I certify that the Library deposit digital copy is a direct equivalent of the final officially approved version of my thesis. No emendation of content has occurred and if there are any minor variations in formatting, they are the result of the conversion to digital format.

Signed

Suresh Nair

Date: 20 – 12 – 2012

ABSTRACT

Amyloid-beta ($A\beta$) plaques are a major neuropathological feature of Alzheimer's disease (AD). These plaques are primarily composed of aggregates of $A\beta$ peptides generated via the amyloidogenic processing of the amyloid precursor protein. The two major isoforms of $A\beta$ peptide are $A\beta_{40}$ and $A\beta_{42}$, of which the latter is highly prone to aggregation. Increased presence and aggregation of intracellular $A\beta_{42}$ peptides is an early event in the disease progression of AD. Improved understanding of cellular processes involved in $A\beta_{42}$ aggregation may have implications for understanding AD progression and development of therapeutic strategies.

Here $A\beta_{42}$ fused to green fluorescent protein ($A\beta_{42}$ GFP) was expressed in each mutant of the homozygous diploid *Saccharomyces cerevisiae* genome-wide deletion library (Winzeler et al., 1999) to identify proteins and cellular processes that affect intracellular $A\beta_{42}$ aggregation by assessing the fluorescence associated with expression of the $A\beta_{42}$ GFP fusion protein. This screening identified 110 mutants exhibiting intense $A\beta_{42}$ GFP-associated fluorescence. Four major cellular processes were over-represented in the data set, including phospholipid homeostasis and mitochondrial function. Global analysis of the *S. cerevisiae* lipidome by quantitative shotgun mass spectrometry led to the discovery that disruption of phosphatidylcholine, phosphatidylserine and/or phosphatidylinositol metabolism had a major effect on intracellular $A\beta_{42}$ aggregation and localisation. Distinctive subcellular localisation of $A\beta_{42}$ GFP in the phospholipid mutants was observed. Confocal microscopy indicated that $A\beta_{42}$ GFP in the phospholipid mutants was juxtaposed to the nucleus of the cell, associated with the endoplasmic reticulum.

Another novel outcome of the $A\beta_{42}$ GFP fusion protein has been to identify putative roles for two proteins of previously uncharacterised function. This study further exploited the powerful and flexible platform of applying GFP-derived fluorescence-based assay for the screening of the Library of Pharmacologically Active Compounds (LOPAC) and the SPECTRUM chemical/drug library for compounds with amyloidogenic and anti-amyloidogenic properties. These libraries include FDA-approved drugs and identifying such drugs as affecting intracellular $A\beta_{42}$ aggregation may significantly reduce costs and the exhaustive process of introducing new drugs onto

the market. Compounds identified through this approach may potentially change the way these drugs are currently administered to patients. These data provide the first genome-wide evidence of cellular processes and chemical compounds that affect intracellular A β ₄₂GFP aggregation and may have important implications for understanding cellular mechanisms that affect intracellular A β ₄₂ aggregation and ultimately disease progression of AD.

ACKNOWLEDGEMENTS

I thank Ian, my supervisor, for his guidance and encouragement throughout my candidature. Your passion in science and generosity has allowed me to build a network with fellow researchers through attending conferences and collaborative work. I really appreciate your mentorship. Now that you are an Emeritus, I admit its nice to see you running around the lab with a pipette and lab coat!

I thank Gab, my supervisor, for being an awesome mentor and friend. I cannot thank you enough for being always approachable and positive. I will definitely miss those intense brains storming discussions we've had (and the smell of chilli tuna Hah!). I appreciate the guidance you provided me throughout. Also, thanks to you, I am now hooked onto drawing pathways on A0 paper.

To my review committee members, Marc Wilkins and Robert Yang – thank you for your guidance and advice during these 3 years. I appreciate your important contributions to the development of this study.

To Geoff Kornfeld – thank you for coming to the rescue for all the technical issues and managing the lab so efficiently. Most of all, I really appreciate those science/geeky emails you send that are not directly related to my work. You are my supplier of good distractions and I hope you will still keep sending them! Also, a big thank you for the useful advises you have provided me along the way.

A special thank you to Mat for conjuring up this idea of modelling neurodegeneration in yeasts and having faith in this “Semi-High-Throughput” project. You have been an awesome mentor and friend. Thank you for all the career advice too. To the past and present members of the Dawes Lab - Joyce, Monica, Cristy, Eva, Radhika, May, Chonghan, Shixiong, Duncan and Anita. Thank you all for making this PhD journey a memorable and thoroughly enjoyable one.

I thank Andrej Shevchenko (Max Planck Institute of Cell Biology and Genetics, Germany), Guenter Daum (Institut für Biochemie, Technische Universität Graz,

Austria) and Paul Atkinson (Victoria University of Wellington, New Zealand) for providing me the opportunity to visit your lab to learn techniques that have significantly contributed to this thesis. Thank you to the members of the Shevchenko lab, Daum lab and Atkinson lab for useful discussions and for an absolutely brilliant time during my stay. I can't wait to visit you guys in future!

To my close group of friends here in Sydney – thank you for your constant encouragement and friendship during the last four years. Our friendships have been ones that are special and I hold dearly. Thank you for keeping me sane!

To my dearest parents, grandparents, my sister and brother – your love and continual support for me is immeasurable. Despite being miles away, the regular phone calls and your concern mean so much. I absolutely love you and dedicate this thesis to you.

LIST OF ABBREVIATIONS

A ₆₀₀	absorbance measured at 600nm
A β	amyloid-beta
A β ₄₀	amyloid-beta (40-amino acid peptide)
A β ₄₂	amyloid-beta (42-amino acid peptide)
A β _{EP}	amyloid-beta (42-amino acid EP variant)
A β ₄₀ GFP	amyloid-beta (40-amino acid peptide) fused to enhanced green fluorescent protein
A β ₄₂ GFP	amyloid-beta (42-amino acid peptide) fused to enhanced green fluorescent protein
A β _{EP} GFP	amyloid-beta (42-amino acid EP variant) fused to enhanced green fluorescent protein
AD	Alzheimer's disease
APP	amyloid precursor protein
bp	base pairs
CEN	centromeric
cER	cortical endoplasmic reticulum
d	day(s)
DAG	diacylglycerol
DAPI	4,6-diaminido-2-phenylindole dihydrochloride
DIC	differential interference contrast
DNA	2'deoxyribonucleic acid
<i>E. coli</i>	<i>Escherichia coli</i>
EDTA	ethylenediaminetetraacetic acid
GFP	enhanced green fluorescent protein
ER	endoplasmic reticulum
Erg	ergosterol
EUROSCARF	European <i>Saccharomyces cerevisiae</i> Archive for Functional Analysis
FA	fatty acid
FT MS	Fourier transform ion cyclotron resonance mass spectrometry
GAL1	gene encoding galactokinase
GFP	green fluorescent protein
GL	glycerolipid
GO	Gene Ontology
GP	glycerophospholipid
h	hour(s)
IPC	inositolphosphoceramide
kb	kilo base pairs
kDa	kilo-Daltons
L	litre

LB	luria-bertani broth/media
LCB	long chain base
LCBP	long chain base phosphate
LD	lipid droplet
LOPAC	Library of Pharmacologically Active Compounds
LTQ Orbitrap	hybrid linear ion trap Orbitrap mass spectrometer
lysoPA	lyso-phosphatidic acid
lysoPC	lyso-phosphatidylcholine
lysoPE	lyso-phosphatidylethanolamine
lysoPI	lyso-phosphatidylinositol
lysoPS	lyso-phosphatidylserine
µg	microgram
µl	microliter
mg	milligram
ml	milliliter
mM	millimolar
min	minute(s)
MIPC	mannosyl-inositolphosphoceramide
M(IP) ₂ C	mannosyl-diinositolphosphoceramide
MS/MS	tandem mass spectrometry
mtDNA	mitochondrial DNA
MW	molecular weight
PA	phosphatidic acid
PC	phosphatidylcholine
PCR	polymerase chain reaction
PDME	phosphatidylmethylethanolamine
PE	phosphatidylethanolamine
PEG	polyethylene glycol (MW 3350)
PG	phosphatidylglycerol
PI	phosphatidylinositol
PM	plasma membrane
PMME	phosphatidylmonomethylethanolamine
PS	phosphatidylserine
RNA	ribonucleic acid
<i>S. cerevisiae</i>	<i>Saccharomyces cerevisiae</i>
SE	steryl ester
SGD	<i>Saccharomyces</i> Genome Database
SCM	synthetic complete D-glucose media
SCgal	synthetic complete D-galactose media
SP	sphingolipid
ssDNA	single-stranded deoxyribonucleic acid
TAG	triacylglycerol
TCA	tricarboxylic acid cycle

TLC	thin-layer chromatography
Ura	uracil
YNB	yeast nitrogen base
YPD	media containing yeast extract, peptone and D-glucose
YPG	media containing yeast extract, peptone and D-glucose

Saccharomyces cerevisiae gene names are designated by italicised, capitalised three-letter mnemonic, followed by a number (e.g. *DAK2*). A mutant deleted of a specific gene is in italicised lower case (e.g. *dak2*). The protein product of the gene is designated by Roman type, with the first letter capitalised and suffix “p” (e.g. Dak2p). Open reading frames are designated with three letters, followed by a three digit numerical code and ending in either “c” or “w”. The nomenclature indicates the chromosomal position of the open reading frame (e.g. YIL090W).

LIST OF FIGURES

FIGURE 1-1 AMYLOID-BETA PLAQUES AND NEUROFIBRILLARY TANGLES IN THE AD BRAIN	5
FIGURE 1-2 SCHEMATIC OVERVIEW OF AMYLOID PRECURSOR PROTEIN PROTEOLYTIC CLEAVAGE PATHWAYS.	10
FIGURE 1-3 THREE-DIMENSIONAL STRUCTURE OF AB ₄₂ FIBRIL	13
FIGURE 1-4 THE ‘UPDATED’ AMYLOID CASCADE HYPOTHESIS.....	22
FIGURE 2-1 SCHEMATIC ILLUSTRATION OF AbGFP PLASMID CONSTRUCTS USED IN THIS STUDY.	32
FIGURE 3-1 FLUORESCENT CELL POPULATION IN WILD-TYPE CELLS EXPRESSING AB ₄₂ GFP OR GFP.	54
FIGURE 3-2 FLUORESCENT CELL POPULATION IN WILD-TYPE CELLS EXPRESSING AB ₄₂ GFP, AB ₄₀ GFP, AB _{EP} GFP OR GFP.	56
FIGURE 3-3 WESTERN BLOT ANALYSIS OF SOLUBLE CELL EXTRACTS FROM BY4743 WILD-TYPE CELLS EXPRESSING AB ₄₂ GFP, AB ₄₀ GFP, AB _{EP} GFP AND GFP CONTROL VECTOR	58
FIGURE 3-4 FLUORESCENT CELL POPULATION OF WILD-TYPE CELLS CO-EXPRESSING AB ₄₂ GFP AB ₄₀ GFP OR AB _{EP} GFP.	59
FIGURE 3-5 FLUORESCENT AND LIGHT MICROSCOPIC IMAGES OF REPRESENTATIVE MUTANTS DEPICTING STRONG, WEAK AND WILD-TYPE AB ₄₂ GFP-ASSOCIATED FLUORESCENCE PHENOTYPES.....	61
FIGURE 3-6 GRAPHIC REPRESENTATION OF CELLULAR PROCESSES IDENTIFIED AFFECTING AB ₄₂ GFP-ASSOCIATED FLUORESCENCE IN <i>S. CEREVISIAE</i>	81
FIGURE 3-7 VISUALISATION OF PROTEIN-PROTEIN INTERACTION NETWORK DEPICTING 75 OUT OF 110 PROTEINS IDENTIFIED IN THE GENOME-WIDE SCREEN THAT AFFECT AB ₄₂ GFP AGGREGATION, GENERATED USING GEOMI.....	87
FIGURE 4-1 OVERVIEW OF THE PATHWAYS FOR LIPID METABOLISM AND THEIR SUBCELLULAR LOCALISATION IN <i>S. CEREVISIAE</i>	105
FIGURE 4-2 FLUORESCENT MICROSCOPIC IMAGES OF REPRESENTATIVE MUTANTS EXHIBITING VARIOUS AB ₄₂ GFP LOCALISATION PATTERNS.	107
FIGURE 4-3 FLUORESCENT MICROSCOPIC IMAGES OF REPRESENTATIVE MUTANTS FROM THE PHOSPHOLIPID METABOLISM AND MITOCHONDRIAL FUNCTIONAL GROUPS EXHIBITING VARIOUS AB ₄₂ GFP LOCALISATION PATTERNS	107
FIGURE 4-4 FLUORESCENT MICROSCOPIC IMAGES OF $\Delta OPI3$, $\Delta CHO2$ AND $\Delta ICE2$ STRAINS EXPRESSING AB ₄₂ GFP, AB ₄₀ GFP, AB _{EP} GFP OR GFP.....	108
FIGURE 4-5 WESTERN BLOT ANALYSIS OF SOLUBLE CELL EXTRACTS FROM BY4743 WILD-TYPE AND $\Delta OPI3$ CELLS EXPRESSING AB ₄₂ GFP, AB ₄₀ GFP, AB _{EP} GFP AND GFP CONTROL VECTOR	110
FIGURE 4-6 FLUORESCENT AND CONFOCAL MICROSCOPIC IMAGES OF $\Delta OPI3$, $\Delta CHO2$ AND $\Delta ICE2$ STRAINS EXHIBITING STRONG AB ₄₂ GFP-ASSOCIATED FLUORESCENCE AND DAPI STAINING.	111
FIGURE 4-7 WESTERN BLOT ANALYSIS OF SUBCELLULAR FRACTIONS FROM $\Delta OPI3$ AND BY4743 WILD-TYPE CELLS EXPRESSING AB ₄₂ GFP.....	112
FIGURE 4-8 FLUORESCENT MICROSCOPIC IMAGES OF $\Delta OPI3$ AND $\Delta ICE2$ STRAINS EXPRESSING AB ₄₂ GFP STAINED WITH LIPIDTOX RED.	114
FIGURE 4-9 FLUORESCENT MICROSCOPIC IMAGES OF THE QUADRUPLE MUTANT, $\Delta DGAI \Delta LROI$ $\Delta ARE1 \Delta ARE2$, EXPRESSING AB ₄₂ GFP STAINED WITH DAPI AND LIPIDTOX RED.....	116

FIGURE 4-10 FLUORESCENT MICROSCOPIC IMAGES OF $\Delta CHO2$ AND $\Delta SCS2$ STRAINS EXHIBITING STRONG AB ₄₂ GFP FLUORESCENCE WITH SKL-MDSRED PEROXISOMAL MARKER.	117
FIGURE 4-11 FLUORESCENT MICROSCOPIC IMAGES OF $\Delta OPI3$, $\Delta CHO2$ AND $\Delta ICE2$ STRAINS EXPRESSING AB ₄₂ GFP, AB ₄₀ GFP, AB _{EP} GFP OR GFP GROWN IN MEDIA EITHER LACKING OR SUPPLEMENTED WITH CHOLINE.	120
FIGURE 4-12 FLUORESCENT MICROSCOPIC IMAGES OF WILD-TYPE, $\Delta PSD1$, $\Delta CHO2$, $\Delta OPI3$ AND $\Delta ICE2$ CELLS EXPRESSING A FLUORESCENT BIOSENSOR OF PS AND PA GROWN IN GALACTOSE MEDIA.	124
FIGURE 4-13 FLUORESCENT CELL POPULATION OF WILD-TYPE CELLS EXPRESSING AB ₄₂ GFP, AB ₄₀ GFP OR AB _{EP} GFP AND THE PYES-DEST52 CONTROL PLASMID.	128
FIGURE 4-14 FLUORESCENT MICROSCOPIC IMAGES OF WILD-TYPE CELLS OVER-EXPRESSING <i>CDS1</i> OR <i>DAK2</i> TOGETHER WITH AB ₄₂ GFP, AB ₄₀ GFP OR AB _{EP} GFP.	130
FIGURE 4-15 FLUORESCENT MICROSCOPIC IMAGES OF <i>CDS1</i> -DAMP, <i>PGS1</i> -DAMP AND <i>PIS1</i> -DAMP CELLS EXPRESSING AB ₄₂ GFP GROWN WITH AND WITHOUT <i>CDS1</i> OVER-EXPRESSION.	136
FIGURE 4-16 FLUORESCENT MICROSCOPIC IMAGES OF <i>PGS1</i> AND <i>PIS1</i> OVER-EXPRESSION IN WILD-TYPE AND $\Delta CHO1$ CELLS EXPRESSING AB ₄₂ GFP.	137
FIGURE 4-17 FLUORESCENT MICROSCOPIC IMAGES OF WILD-TYPE CELLS OVER-EXPRESSING <i>URA5</i> OR <i>URA7</i> TOGETHER WITH AB ₄₂ GFP.	141
FIGURE 4-18 FLUORESCENT MICROSCOPIC IMAGES OF WILD-TYPE CELLS OVER-EXPRESSING <i>INM1</i> OR <i>INM2</i> TOGETHER WITH AB ₄₂ GFP.	142
FIGURE 5-1 GENERAL LIPID CATEGORIES OF WILD-TYPE, $\Delta CHO2$, $\Delta OPI3$, $\Delta PSD1$ AND $\Delta ICE2$ CELLS EXPRESSING AB ₄₂ GFP.	160
FIGURE 5-2 GLOBAL LIPIDOMIC PROFILE OF WILD-TYPE, $\Delta OPI3$, $\Delta CHO2$, $\Delta PSD1$ AND $\Delta ICE2$ STRAINS EXPRESSING AB ₄₂ GFP.	161
FIGURE 5-3 GENERAL LIPID CATEGORIES OF WILD-TYPE AND $\Delta ICE2$ CELLS GROWN IN EITHER GLUCOSE (GLU) OR GALACTOSE (GAL) MEDIA.	166
FIGURE 5-4 GLOBAL LIPIDOMIC PROFILE OF WILD-TYPE AND $\Delta ICE2$ CELLS GROWN IN EITHER GLUCOSE (GLU) OR GALACTOSE (GAL) MEDIA.	168
FIGURE 5-5 FLUORESCENT IMAGES OF MUTANTS AFFECTED IN MITOCHONDRIAL FUNCTION EXPRESSING AB ₄₂ GFP.	170
FIGURE 5-6 FLUORESCENCE MICROSCOPIC IMAGES OF RHO ⁰ AND WILD-TYPE GRANDE CELLS EXPRESSING AB ₄₂ GFP.	171
FIGURE 5-7 GENERAL LIPID CATEGORIES IN WILD-TYPE, RHO ⁰ CELLS AND SELECTED TCA CYCLE MUTANTS EXPRESSING AB ₄₂ GFP.	172
FIGURE 5-8 GLOBAL LIPIDOMIC PROFILE OF WILD-TYPE, RHO ⁰ AND SELECTED TCA CYCLE MUTANTS EXPRESSING AB ₄₂ GFP.	174
FIGURE 5-9 GLOBAL LIPIDOMIC PROFILE OF WILD-TYPE, $\Delta OPI3$, $\Delta CHO2$, $\Delta PSD1$, $\Delta ICE2$ AND RHO ⁰ CELLS EXPRESSING AB ₄₂ GFP.	175
FIGURE 5-10 OVERVIEW OF THE PATHWAYS FOR DIHYDROXYACETONE AND GLYCEROL METABOLISM IN <i>S. CEREVISIAE</i>	178
FIGURE 5-11 FLUORESCENT MICROSCOPIC IMAGES OF WILD-TYPE CELLS OVER-EXPRESSING <i>DAK2</i> TOGETHER WITH AB ₄₂ GFP, AB ₄₀ GFP OR AB _{EP} GFP.	181
FIGURE 5-12 DIFFERENTIAL INTERFERENCE CONTRAST (DIC) MICROSCOPIC IMAGES OF WILD-TYPE CELLS OVER-EXPRESSING EITHER <i>DAK1</i> OR <i>DAK2</i>	182

FIGURE 5-13 FLUORESCENT AND CONFOCAL MICROSCOPIC IMAGES OF THE QUADRUPLE MUTANT AND WILD-TYPE CELLS OVER-EXPRESSING <i>DAK2</i> EXHIBITING AB ₄₂ GFP FLUORESCENCE, LIPIDTOX RED AND DAPI STAINING.....	183
FIGURE 5-14 FLUORESCENT AND DIC MICROSCOPIC IMAGES OF WILD-TYPE CELLS OVER- EXPRESSING <i>DAK2</i> STAINED WITH NILE RED	185
FIGURE 5-15 GLOBAL LIPIDOMIC PROFILE OF WILD-TYPE CELLS OVER-EXPRESSING <i>DAK2</i> AND AB ₄₂ GFP	186
FIGURE 5-16 ONE-DIMENSIONAL THIN-LAYER CHROMATOGRAPHIC SEPARATION OF POLAR LIPIDS FROM WILD-TYPE CELLS OVER-EXPRESSING <i>DAK2</i>	187
FIGURE 5-17 FLUORESCENT AND DIC MICROSCOPIC IMAGES OF WILD-TYPE CELLS OVER- EXPRESSING DAK2P-GFP	189
FIGURE 5-18 EFFECT OF DHA SUPPLEMENTATION ON WILD-TYPE CELLS EXPRESSING AB ₄₂ GFP	190
FIGURE 6-1 FLUORESCENT MICROSCOPIC IMAGE ANALYSIS USING EVOTEC TECHNOLOGIES ACAPELLA™ IMAGE ANALYSIS SOFTWARE OF WILD-TYPE CELLS EXPRESSING AB ₄₂ GFP OR AB ₄₀ GFP GROWN IN GALACTOSE (INDUCTION) MEDIUM CONTAINING 0.2 mM DMSO ..	205
FIGURE 6-2 FLUORESCENT MICROSCOPIC IMAGE ANALYSIS USING EVOTEC TECHNOLOGIES ACAPELLA™ IMAGE ANALYSIS SOFTWARE OF WILD-TYPE CELLS EXPRESSING AB ₄₂ GFP GROWN IN MEDIA SUPPLEMENTED WITH 20 mM OF A SPECIFIC DRUG/CHEMICAL COMPOUND FROM THE LOPAC ^{1280®} LIBRARY	213
FIGURE 6-3 FLUORESCENT MICROSCOPIC IMAGE ANALYSIS USING EVOTEC TECHNOLOGIES ACAPELLA™ IMAGE ANALYSIS SOFTWARE OF WILD-TYPE CELLS EXPRESSING AB ₄₂ GFP GROWN IN MEDIA SUPPLEMENTED WITH 20 mM OF A SPECIFIC DRUG/CHEMICAL COMPOUND FROM THE SPECTRUM COLLECTION LIBRARY	214
FIGURE 6-4 FLUORESCENT MICROSCOPIC IMAGE ANALYSIS USING EVOTEC TECHNOLOGIES ACAPELLA™ IMAGE ANALYSIS SOFTWARE OF WILD-TYPE CELLS EXPRESSING AB ₄₀ GFP GROWN IN MEDIA SUPPLEMENTED WITH 20 mM OF A SPECIFIC DRUG/CHEMICAL COMPOUND FROM THE LOPAC ^{1280®} LIBRARY	221
FIGURE 6-5 FLUORESCENT MICROSCOPIC IMAGE ANALYSIS USING EVOTEC TECHNOLOGIES ACAPELLA™ IMAGE ANALYSIS SOFTWARE OF WILD-TYPE CELLS EXPRESSING AB ₄₀ GFP GROWN IN MEDIA SUPPLEMENTED WITH 20 mM OF A SPECIFIC DRUG/CHEMICAL COMPOUND FROM THE SPECTRUM COLLECTION LIBRARY	222
FIGURE 6-6 SCHEMATIC OVERVIEW OF COMPOUNDS IDENTIFIED FROM THE CHEMICAL/DRUG LIBRARIES THAT AFFECTED AB ₄₂ GFP OR AB ₄₀ GFP-ASSOCIATED FLUORESCENCE.....	225

LIST OF TABLES

TABLE 1-1 SUMMARY OF GENES ASSOCIATED WITH INCREASED RISK OF AD.....	3
TABLE 2-1 <i>S. CEREVISIAE</i> AND <i>E. COLI</i> STRAINS USED IN THIS STUDY.....	30
TABLE 2-2 PLASMIDS USED IN THIS STUDY.....	32
TABLE 2-3 PRIMERS USED IN THIS STUDY.....	33
TABLE 2-4 SUPPLEMENTS FOR SYNTHETIC COMPLETE MEDIA.....	36
TABLE 3-1 LIST OF 110 MUTANTS THAT EXHIBITED STRONG AB ₄₂ GFP-ASSOCIATED FLUORESCENCE, THEIR LOCALISATION PATTERNS AND THE BIOLOGICAL FUNCTION OF EACH OF THEIR RESPECTIVE GENE PRODUCTS BASED ON DESCRIPTIONS PROVIDED IN THE <i>SACCHAROMYCES</i> GENOME DATABASE (SGD).....	63
TABLE 3-2 FUNCTIONAL GROUPING OF THE 110 MUTANT IDENTIFIED THROUGH THE GENOME- WIDE SCREEN THAT EXHIBITED STRONG AB ₄₂ GFP-ASSOCIATED FLUORESCENCE, BASED ON MOLECULAR FUNCTION ONTOLOGY (FUNSPEC GO DATABASE).....	77
TABLE 3-3 FUNCTIONAL GROUPING OF THE 110 MUTANT IDENTIFIED THROUGH THE GENOME- WIDE SCREEN THAT EXHIBITED STRONG AB ₄₂ GFP-ASSOCIATED FLUORESCENCE, BASED ON BIOLOGICAL PROCESS ONTOLOGY (FUNSPEC GO DATABASE).	78
TABLE 3-4 FUNCTIONAL GROUPING OF THE 110 MUTANT IDENTIFIED THROUGH THE GENOME- WIDE SCREEN THAT EXHIBITED STRONG AB ₄₂ GFP-ASSOCIATED FLUORESCENCE, BASED ON CELLULAR COMPONENT ONTOLOGY (FUNSPEC GO DATABASE).	79
TABLE 3-5 BROAD FUNCTIONAL GROUPING OF THE 110 MUTANTS IDENTIFIED THROUGH THE GENOME-WIDE SCREEN THAT EXHIBITED STRONG AB ₄₂ GFP-ASSOCIATED FLUORESCENCE, BY MANUAL CATEGORISATION.....	82
TABLE 3-6 PROPORTION OF AB ₄₂ GFP-ASSOCIATED FLUORESCENT CELLS IN REPRESENTATIVE MUTANTS FROM MAJOR OVER-REPRESENTED FUNCTIONAL GROUPS IDENTIFIED BY BIOINFORMATICS ANALYSIS.	84
TABLE 3-7 LIST OF 35 GENES WHICH ENCODE PROTEINS WITH NO KNOWN PROTEIN INTERACTIONS AND WERE NOT MAPPED ON THE PROTEIN-PROTEIN INTERACTION NETWORK	86
TABLE 3-8 HUMAN ORTHOLOGS OF <i>S. CEREVISIAE</i> GENES IDENTIFIED THROUGH THE GENOME- WIDE SCREEN.....	88
TABLE 4-1 PROPORTION OF AB ₄₂ GFP FLUORESCENT CELLS GROWN IN MEDIA LACKING OR SUPPLEMENTED WITH CHOLINE.....	122
TABLE 4-2 LIST OF GENES ENCODING ENZYMES OF THE PHOSPHOLIPID INTERMEDIATES THAT WERE OVER-EXPRESSED IN WILD-TYPE CELLS AND RELEVANT PHOSPHOLIPID MUTANTS	126
TABLE 4-3 PROPORTION OF ABGFP FLUORESCENT CELLS IN STRAINS OVER-EXPRESSING <i>CDS1</i> OR <i>DAK2</i>	131
TABLE 4-4 PROPORTION OF ABGFP FLUORESCENT CELLS GROWN IN MEDIA LACKING OR SUPPLEMENTED WITH CHOLINE.....	133
TABLE 4-5 PHOSPHOLIPID COMPOSITION OF WILD-TYPE AND MUTANTS AFFECTED IN PHOSPHOLIPID METABOLISM.	145
TABLE 5-1 CATEGORISATION OF LIPID SPECIES AND CLASSES INTO GENERAL LIPID CATEGORIES	157
TABLE 5-2 NEGATIVE GENETIC INTERACTION NETWORK OF <i>ICE2</i> AND GENES INVOLVED IN LIPID METABOLISM, BASED ON SIGNIFICANT INTERACTIONS (DRYGIN DATABASE).....	166
TABLE 5-3 LIST OF GENES ENCODING ENZYMES OF THE PHOSPHOLIPID INTERMEDIATES THAT WERE OVER-EXPRESSED IN WILD-TYPE CELLS AND RELEVANT PHOSPHOLIPID MUTANTS	180

TABLE 6-1 SCREENING OF THE LOPAC LIBRARY IDENTIFIED 4 COMPOUNDS WHICH INCREASED LEVELS OF AB ₄₂ GFP FLUORESCENCE IN WILD-TYPE CELLS	207
TABLE 6-2 SCREENING OF THE SPECTRUM COLLECTION LIBRARY IDENTIFIED 21 COMPOUNDS WHICH INCREASED LEVELS OF AB ₄₂ GFP FLUORESCENCE IN WILD-TYPE CELLS	208

TABLE OF CONTENTS

THESIS/ DISSERTATION SHEET

ORIGINALITY STATEMENT

COPYRIGHT STATEMENT

AUTHENTICITY STATEMENT

ABSTRACT	I
ACKNOWLEDGEMENTS.....	III
LIST OF ABBREVIATIONS	V
LIST OF FIGURES	VIII
LIST OF TABLES	XI
TABLE OF CONTENTS	

CHAPTER1: INTRODUCTION

1.1 ALZHEIMER'S DISEASE	1
1.1.1 Prevalence and incidence.....	1
1.1.2 Risk factors and genetics of AD	1
1.1.3 Characteristics and clinical manifestations of AD.....	4
1.1.4 Endoproteolytic processing of APP and generation of amyloid-beta (A β)	7
1.2 PROTEIN MISFOLDING, AGGREGATION AND NEURODEGENERATION.....	11
1.2.1 States of A β oligomerisation and fibril formation, and, their 3-dimensional structures	11
1.2.2 Intracellular A β : physiological roles, localisation and neurotoxicity of soluble oligomers.....	14
1.2.3 The 'updated' amyloid cascade hypothesis – incorporating A β clearance mechanisms	18
1.3 ENHANCED GREEN FLUORESCENT PROTEIN (GFP)-BASED FLUORESCENT REPORTER FOR PROTEIN AGGREGATION	22
1.3.1 Amyloid-beta GFP fusion (A β GFP) in <i>E. coli</i>	23
1.4 MODEL SYSTEMS TO STUDY DISEASE-RELATED PROTEINS IMPLICATED IN NEURODEGENERATION.....	24
1.4.1 Modelling aspects of neurodegeneration and AD in <i>S. cerevisiae</i>	25
1.5 GENERAL AIMS AND SUMMARY OF THIS STUDY	28

CHAPTER 2: MATERIALS AND METHODS

2.1 GENERAL MATERIALS AND REAGENTS	30
2.2 <i>S. CEREVISIAE</i> AND <i>E. COLI</i> STRAINS, PLASMIDS AND PRIMERS	30
2.2.1 <i>S. cerevisiae</i> strains.....	30
2.2.2 <i>E. coli</i> strains	31

2.2.3	Plasmids.....	31
2.2.4	Primers.....	33
2.3	GENERAL METHODS/ LABORATORY PROCEDURES.....	35
2.3.1	Sterilisation and containment of biological waste.....	35
2.4	MEDIA AND GROWTH CONDITIONS.....	35
2.4.1	<i>E. coli</i> growth media and storage conditions.....	35
2.4.2	<i>S. cerevisiae</i> growth media and storage conditions.....	36
2.5	GENERAL MOLECULAR BIOLOGY METHODS.....	37
2.5.1	Polymerase chain reaction.....	37
2.5.2	DNA sequencing.....	37
2.5.3	Small-scale plasmid extraction.....	38
2.5.4	Large-scale plasmid extraction.....	38
2.6	TRANSFORMATION OF <i>S. CEREVISIAE</i> AND <i>E. COLI</i> STRAINS.....	39
2.6.1	Low-throughput transformation of <i>S. cerevisiae</i> strains.....	39
2.6.2	High-throughput transformation of <i>S. cerevisiae</i> genome-wide deletion library in 96-well plate arrays.....	39
2.6.3	Transformation of <i>E. coli</i> strains.....	40
2.7	INDUCTION OF AB ₄₂ GFP EXPRESSION AND SCREENING OF THE <i>S. CEREVISIAE</i> GENOME-WIDE DELETION COLLECTION.....	40
2.8	EPIFLUORESCENCE AND CONFOCAL MICROSCOPY, AND THE VISUALISATION OF ORGANELLES.....	40
2.8.1	Nuclear and mitochondrial DNA staining.....	41
2.8.2	Staining of lipid droplets with LipidTOX Red and Nile Red.....	41
2.8.3	Peroxisome-targeted fluorescent protein (SKL-DsRed).....	42
2.9	SCIENTIFIC DATABASES USED IN THIS STUDY.....	43
2.10	GENERATION OF STRAINS AND PLASMIDS.....	43
2.10.1	Generation and transformation of BY4743 Rho-zero (Rho ⁰) petite cells.....	43
2.10.2	Generation of plasmids.....	44
2.11	PROTEOMIC METHODS.....	45
2.11.1	Protein extraction, SDS-PAGE and western blot analysis.....	45
2.11.2	Protein-protein interaction network analysis.....	45
2.12	LIPIDOMIC METHODS.....	46
2.12.1	Total cellular lipid extraction and lipidomic profiling using mass spectrometry.....	46
2.12.2	Polar lipid extraction and one-dimensional thin-layer chromatography.....	47
2.13	BIOCHEMICAL METHODS.....	48
2.13.1	Assessment of the effects of choline supplementation to mutants exhibiting strong Aβ ₄₂ GFP derived fluorescence.....	48
2.13.2	Assessment of the effects of dihydroxyacetone (DHA) supplementation to wild-type cells expressing Aβ ₄₂ -GFP.....	48
2.13.3	Assessment on the effects of citrate supplementation in BY4743 wild-type cells expressing Aβ ₄₂ GFP.....	48
2.13.4	Subcellular fractionation – Mitochondrial and ER fractions.....	49
2.14	HIGH-CONTENT CHEMICAL AND DRUG LIBRARIES SCREEN.....	50
2.15	STATISTICAL ANALYSES.....	51

CHAPTER 3: GENOME-WIDE DELETION ANALYSIS IDENTIFIES CELLULAR PROCESSES AFFECTING AMYLOID-BETA AGGREGATION IN *S. CEREVISIAE*

3.1	INTRODUCTION AND AIMS	52
3.2	RESULTS – DEVELOPMENT OF THE ABGFP FUSION-ASSOCIATED AGGREGATION/ FLUORESCENCE ASSAY	53
3.2.1	Fluorescence production in wild-type cells expressing enhanced green fluorescent protein fused to A β ₄₂ (A β ₄₂ GFP)	53
3.2.2	Fluorescence production in wild-type <i>S. cerevisiae</i> cells expressing less aggregation- prone forms of A β : A β ₄₀ GFP or A β _{EP} GFP	55
3.2.3	Western blot analysis of wild-type cells expressing A β ₄₂ GFP, A β ₄₀ GFP, A β _{EP} GFP or GFP	57
3.2.4	A β ₄₂ seeds formation of punctate aggregates of A β ₄₀	58
3.2.5	Screening of the <i>Saccharomyces cerevisiae</i> genome-wide deletion library for genetic factors affecting A β ₄₂ GFP fluorescence	60
3.2.6	Pilot-scale screening of the <i>S. cerevisiae</i> deletion library to establish parameters and selection criteria for use in the genome-wide screening	60
3.2.7	Genome-wide screening of deletion mutants that exhibit altered A β ₄₂ GFP-associated fluorescence	62
3.2.8	Identification of over-represented cellular processes affecting A β ₄₂ GFP fluorescence through bioinformatics analysis	76
3.2.9	Quantitative assessment of A β ₄₂ GFP-associated fluorescence in the over-represented functional categories identified by the genome-wide screen	83
3.2.10	Protein-protein interaction network	85
3.2.11	Human orthologs of <i>S. cerevisiae</i> genes identified by the genome-wide screen	88
3.3	DISCUSSION	91
3.3.1	Development and characterisation of A β GFP aggregation assay in <i>S. cerevisiae</i> ...	91
3.3.2	Disruption to phosphatidylcholine biosynthesis/phospholipid metabolism leads to increased A β ₄₂ GFP-associated fluorescence in <i>S. cerevisiae</i> cells	95
3.3.3	Disruption to mitochondrial function leads to increased A β ₄₂ GFP-associated fluorescence in <i>S. cerevisiae</i> cells	98

CHAPTER 4: UNDERSTANDING MECHANISMS OF AMYLOID-BETA AGGREGATION AND LOCALISATION IN *S. CEREVISIAE*

4.1	INTRODUCTION AND AIMS	101
4.2	RESULTS – UNDERSTANDING THE LINK BETWEEN PHOSPHOLIPID METABOLISM AND AB ₄₂ GFP AGGREGATION	105
4.2.1	Investigation of A β ₄₂ GFP localisation in mutants identified by the <i>S. cerevisiae</i> genome-wide screen	105
4.2.2	Localisation of less aggregation-prone A β ₄₀ GFP and A β _{EP} GFP in mutants of the phospholipid metabolism functional group	108
4.2.3	Western blot analysis of mutants affected in phospholipid metabolism expressing A β ₄₂ GFP, A β ₄₀ GFP, A β _{EP} GFP or GFP	109
4.2.4	Perinuclear localisation of fluorescent A β ₄₂ GFP in mutants of the phospholipid metabolism functional group was determined to be interacting with the endoplasmic reticulum (ER) and not lipid droplets (LD)	110

4.2.5	Some, but not all, of the intense fluorescent puncta of A β ₄₂ GFP in mutants affected in phospholipid metabolism co-localise with peroxisomes	117
4.2.6	Effects of choline supplementation on mutants that belong to the phospholipid metabolism functional group.....	118
4.2.7	Investigation of altered localisation of phosphatidic acid (PA) and phosphatidylserine (PS) in mutants that belong to the phospholipid metabolism functional group	123
4.2.8	A ‘reverse-genetics’ approach to identify specific lipid metabolite(s) that influence partitioning of A β ₄₂ GFP in to the ER membrane	125
4.2.9	Over-expression of <i>CDS1</i> , encoding cytidine diphosphate-diacylglycerol synthase, and DAK2, encoding dihydroxyacetone kinase, alter A β ₄₂ GFP-associated fluorescence	128
4.2.10	Choline supplementation alters A β ₄₂ GFP fluorescence in wild-type cells over-expressing <i>CDS1</i> , but not <i>DAK2</i>	132
4.2.11	Investigating the role of essential genes involved in phospholipid metabolism in A β ₄₂ GFP aggregation	134
4.2.12	Effects of intracellular levels of water-soluble lipid precursors on A β ₄₂ GFP aggregation	138
4.2.12.1	Altered levels of <i>S</i> -adenosyl-L-methionine (AdoMet) do not affect A β ₄₂ GFP aggregation	138
4.2.12.2	Over-expression of <i>URA5</i> , encoding orotate phosphoribosyltransferase, and <i>URA7</i> , encoding cytidine-triphosphate (CTP) synthase, give rise to increased A β ₄₂ GFP fluorescence	139
4.2.12.3	Over-expression of inositol monophosphatases Inm1p and Inm2p, but not inositol supplementation, give rise to increased A β ₄₂ GFP fluorescence	141
4.3	DISCUSSION.....	144
4.3.1	Disruption to phospholipid metabolism leads to increased A β ₄₂ GFP-associated fluorescence in <i>S. cerevisiae</i> cells	144
4.3.2	Implications of phosphatidylcholine in human disease	153

CHAPTER 5: GLOBAL YEAST LIPIDOME PROFILING BY QUANTITATIVE SHOTGUN MASS SPECTROMETRY

5.1	INTRODUCTION AND AIMS	155
5.2	RESULTS – GLOBAL LIPIDOME PROFILING OF MUTANTS AFFECTED IN LIPID METABOLISM	158
5.2.1	Global lipidome analysis of mutants exhibiting ER/ER-membrane A β ₄₂ GFP localisation identifies pronounced effect of decreased phospholipids and increased M(IP) ₂ C levels	158
5.2.2	Genetic interaction network supported by a global lipidomic approach provide hints to another possible function of Ice2p	164
5.2.3	Understanding the link between mitochondrial dysfunction and A β ₄₂ GFP aggregation – Investigation of A β ₄₂ GFP localisation in mitochondrial mutants	169
5.2.4	Disruption of mitochondrial DNA does not affect A β ₄₂ GFP expression	170
5.2.5	Global lipidome analysis of TCA cycle mutants exhibiting altered A β ₄₂ GFP fluorescence.....	171
5.2.6	A ‘reverse-genetics’ approach identifies metabolite(s) that may influence increased A β ₄₂ GFP fluorescence in mutants affected in mitochondrial function.....	176

5.2.7	Over-expression of <i>DAK2</i> , but not <i>DAK1</i> , leads to formation of large globular compartment in cells containing fluorescent A β_{42} GFP peptides.....	181
5.2.8	Investigation of A β_{42} GFP localisation in wild-type cells over-expressing <i>DAK2</i> ..	182
5.2.9	Global lipidome analysis of wild-type cells over-expressing <i>DAK2</i> identifies pronounced effect of increased TAG, MIPC and lysoPA levels.....	185
5.2.10	Dak2p localises in the large compartment formed by overexpression of <i>DAK2</i>	188
5.2.11	Dihydroxyacetone supplementation alters A β_{42} GFP fluorescence in wild-type cells	189
5.3	DISCUSSION AND GENERAL SUMMARY	191
5.3.1	Global lipidomic analysis of mutants that exhibit increased A β_{42} GFP fluorescence	191
5.3.2	General summary of the effect of <i>ICE2</i> deletion on A β_{42} GFP	194
5.3.3	General summary of the effect of mitochondrial dysfunction, <i>DAK2</i> over-expression and DHA supplementation on A β_{42} GFP	196

CHAPTER 6: HIGH-CONTENT CHEMICAL AND DRUG SCREENS FOR SMALL MOLECULE MODIFIERS OF AMYLOID-BETA AGGREGATION IN *S. CEREVISIAE*

6.1	INTRODUCTION AND AIMS	202
6.2	RESULTS - DEVELOPMENT OF A YEAST CELL-BASED SYSTEM FOR THE IDENTIFICATION OF COMPOUNDS THAT AFFECT AGGREGATION OF A β_{42} GFP AND A β_{40} GFP IN VIVO BASED ON ABGFP FUSION-ASSOCIATED FLUORESCENCE ASSAY	204
6.2.1	Effect of dimethyl sulfoxide (DMSO) on wild-type (yCG253) <i>S. cerevisiae</i> cells expressing A β_{42} GFP or A β_{40} GFP.....	204
6.2.2	High content screen for small molecule modifiers that affect A β_{42} GFP aggregation in <i>S. cerevisiae</i>	206
6.2.3	High content screen for small molecule modifiers that reduce A β_{40} GFP fluorescence in <i>S. cerevisiae</i>	215
6.3	DISCUSSION.....	223
6.3.1	Tetracycline and it derivatives.....	226
6.3.2	Tetranortriterpenoid compounds and isogedunin	228
6.4	FUTURE DIRECTIONS	228

REFERENCES.....	231
-----------------	-----

APPENDIX A	274
------------------	-----

APPENDIX B	275
------------------	-----

1 INTRODUCTION

1.1 Alzheimer's disease

1.1.1 Prevalence and incidence

Alzheimer's disease (AD), a progressive and irreversible neurodegenerative disorder, is the most common form of dementia in individuals over 65 years of age; and the incidence of AD doubles every five years beyond the age of 65. According to the World Alzheimer Report 2011, it is estimated that 36 million people worldwide are afflicted with dementia, and numbers are expected to double every 20 years to 66 million by 2030, and 115 million by 2050 (Prince et al., 2011). This is of major social and economic concern in both developed and developing countries because living standards and the quality of medical treatment have increased life expectancy and a trend towards aging populations (Cruz and Tsai, 2004). In 2010, the estimated global economic burden of dementia was US\$604 billion. Interestingly, this economic impact is significantly more than the costs of cancer or heart disease (Prince et al., 2011). Onset of AD is characterised by a gradual loss of short-term memory and decision-making capability, which is subsequently associated with a decline in physical function and behavioural changes (Brookmeyer et al., 1998). Therefore, over time, afflicted individuals increase their dependency on others for day to day functioning and survival. Death of AD-affected individuals often occurs due to pneumonia, malnutrition and/or inanition (Walsh et al., 1990). With advances in therapeutic strategies, and possibly preventive interventions, it is predicted that if interventions could delay both disease onset and progression by a single year, there would be approximately 9.2 million fewer cases of disease by 2050 (Brookmeyer et al., 2007).

1.1.2 Risk factors and genetics of AD

The common types of dementia are Alzheimer's disease, vascular dementia, mixed dementia, frontotemporal dementia, and Parkinson's disease. However, Alzheimer's disease accounts for approximately 50-80% of all dementia cases (Abbott, 2011). The two subtypes of AD are based on the age of onset of the disease: early-onset AD (or familial AD) and late-onset AD (or sporadic AD). Familial AD accounts for about 5% of all AD cases with age of onset ranging from 30 to 65 years and shows autosomal dominant inheritance (Bekris et al., 2010). Familial AD has been associated

with mutations in three genes, namely APP (Chartier-Harlin et al., 1991; Goate et al., 1991), PSEN1 (Sherrington et al., 1995) and PSEN2 (Levy-Lahad et al., 1995) (Table 1-1). Late-onset AD is the most common form and it is defined as AD with an age at onset after 65 years of age. This form of AD may also occur in people with a positive family history of AD and studies have estimated the heritability of late-onset AD to be 76% of all ‘sporadic’ AD cases (Blennow et al., 2006; Ferri et al., 2005). An example of this is the epsilon 4 isoform ($\epsilon 4$) allele of apolipoprotein E (*APOE*) gene, which has been consistently identified in individuals with sporadic AD across several genetic studies (Coon et al., 2007; Corder et al., 1993; Roses et al., 1995; Schellenberg, 1995). Apolipoprotein E, and in particular the $\epsilon 2$ allele, has a protective effect against apoptosis (Hayashi et al., 2007). However, this is significantly reduced in the presence of the $\epsilon 4$ allele. Current estimates indicate that presence of the $\epsilon 4$ allele of *APOE* may account for approximately 20% of the genetic risk for late-onset AD (Lambert and Amouyel, 2011), increase the lifetime risk for AD from 20% to 90% and lower the age of onset of AD to 68 years of age as compared to 84 (Corder et al., 1994; Corder et al., 1993). Interestingly, many individuals who carry the $\epsilon 4$ allele of *APOE* live to an old age. This may be indicative of other genetic and/or environmental risk factors affecting late-onset AD that have yet to be identified.

Apart from *APOE*, almost 700 genes have been linked to AD. However, only ~2% of these genetic variants are supported by a strong association based on overall epidemiological credibility (Bertram et al., 2007; Bird, 2008; Chai, 2007; Olgiati et al., 2011). A list of candidate genes is provided in the AlzGene online database, which is a web-based compilation of published association studies on AD (<http://www.alzforum.org/res/com/gen/alzgene/default.asp>) (Bertram et al., 2007). The Alzheimer’ Research Forum (Alzgene) database includes 1,395 studies where 695 genes have been identified with 2973 polymorphisms (updated 18 April 2011). The number of meta-analyses is 320. Analyses of this database suggest that there may be around 10 major late-onset AD susceptibility genes (Table 1-1), many of which were identified and characterised in two of the largest genome-wide association studies (GWAS) performed in AD with a combined sample size of more than 30,000 individuals (including controls) (Harold et al., 2009; Hollingworth et al., 2011b; Lambert et al., 2009). At present, the focus of research is turned towards how these genetic loci identified through the GWAS

studies may be functionally relevant to AD disease progression. Since the identification of these gene loci have been fairly recent, a better understanding is required before the results of gene polymorphisms can be translated into diagnostic implementations or potential targets for therapeutic strategies. Furthermore, sporadic AD appear to be a complex disorder that is likely to involve multiple genetic and environmental factors (Bird, 2008; Kamboh, 2004; Roses, 2006; Serretti et al., 2005). Limitations such as genetic-genetic interactions and genetic-chemical/environment interactions (i.e. lifestyle factors) which are significant aspects in the onset and progression of AD need to be further studied. However, analyses of the Alzgene database and Gene ontology (GO) terms indicate that the late-onset AD susceptibility genes (Table 1-1) may be implicated in cellular processes such as cholesterol metabolism, intracellular transport of amyloid-beta precursor protein, autophagy of damaged organelles and regulation of amyloid-beta (A β) clearance from the brain (discussed in the Section 1.2.3). The role of inflammatory response in AD pathogenesis is also highlighted (Olgiati et al., 2011; van Es and van den Berg, 2009).

Table 1-1 Summary of genes associated with increased risk of AD

Gene name	Chromosome	Inheritance/ Genetic variance	Phenotype relevant to AD	Reference
Amyloid precursor protein (<i>APP</i>)	21q21	Autosomal dominant	Increased A β generation & aggregation	(Goate et al., 1991)
Presenilin 1 (<i>PSEN1</i>)	14q24.2	Autosomal dominant	Increased A β generation	(Sherrington et al., 1995)
Presenilin 2 (<i>PSEN2</i>)	1q42.13	Autosomal dominant	Increased A β generation	(Levy-Lahad et al., 1995)
Apolipoprotein E (<i>APOE</i>)	19q13.32	Autosomal dominant and may also be sporadic	Increased A β aggregation & decreased clearance	(Bekris et al., 2010; Corder et al., 1993; Poirier et al., 1993)
Bridging integrator 1 (<i>BINI</i>)	2q14	Sporadic	Unknown	(Seshadri et al., 2010)
Clusterin (<i>CLU</i>)	8p21-p12	Sporadic	Unknown	(Corneveaux et al., 2010)
ATP-binding cassette, subfamily A, member 7 (<i>ABCA7</i>)	19p13.3	Sporadic	Unknown	(Hollingworth et al., 2011a; Naj et al., 2011)
Complement component (3b/4b) receptor 1 (<i>CR1</i>)	1q32	Sporadic	Unknown	(Corneveaux et al., 2010)

Phosphatidylinositol binding clatherin assembly protein (<i>PICALM</i>)	11q14	Sporadic	Unknown	(Corneveaux et al., 2010)
Membrane-spanning 4-domains, subfamily A, member 6A (<i>MS4A6A</i>)	11q12.1	Sporadic	Unknown	(Hollingworth et al., 2011a; Naj et al., 2011)
Myeloid cell surface antigen CD33 (<i>CD33</i>)	19q13.3	Sporadic	Unknown	(Bettens et al., 2010; Harold et al., 2009)
Membrane-spanning 4-domains, subfamily A, member 4E (<i>MS4A4E</i>)	11q12.2	Sporadic	Unknown	(Hollingworth et al., 2011a; Naj et al., 2011)
CD2-associated protein (<i>CD2AP</i>)	6p12	Sporadic	Unknown	(Hollingworth et al., 2011a; Naj et al., 2011)

Apart from genetic variations, the prevalence and incidence of AD strongly indicate that age is the most prominent risk factor. Incidence of AD cases is ~1% in individuals 60 - 70 years of age, ~5% for those between 70 – 80 years of age, and increases significantly to ~35% for individuals above the age of 85 (Campion et al., 1999; Mayeux, 2003). Age-related changes in the brain include atrophy of the brain, inflammation, oxidative damage by free radicals, and mitochondrial dysfunction which may cause neuronal cell death and ultimately AD (Querfurth and LaFerla, 2010). Although the cellular mechanisms that lead to AD are yet to be established, the disease onset and progression is generally agreed to be accompanied by the presence of A β protein, which is found to accumulate in the brains of AD afflicted individuals (discussed below).

1.1.3 Characteristics and clinical manifestations of AD

In 1907, Alois Alzheimer reported two pathological lesions in the brain of Auguste Deter, a female patient with dementia (Alzheimer et al., 1907). One of the cerebral lesions described by Alzheimer was neurofibrillary tangles (NFTs) that occurred intraneuronally. It was later discovered that these NFTs are composed of aggregated forms of hyperphosphorylated microtubule-binding protein tau (Figure 1-1E) (Goedert and Crowther, 1989; Goedert et al., 1988; Grundke-Iqbal et al., 1986). These NFTs are also identified in asymptomatic individuals and in other neurodegenerative disorders such as progressive supranuclear palsy, corticobasal degeneration, Pick's

disease and frontal temporal dementia (Dickson et al., 1992; Lee et al., 2001b). The biological function of soluble tau is to promote microtubule assembly and its stabilisation. In addition to axonal transport, normal tau is also found to interact with structural proteins and proteins involved in signal transduction indicating that tau may play a crucial role in neuronal architecture (Wang and Liu, 2008). In its pathological state, tau protein forms filamentous structures and is hyperphosphorylated at specific residues (Bramblett et al., 1993; Goedert et al., 1992; Grundke-Iqbal et al., 1986). Even though the mechanism of tau hyperphosphorylation-mediated toxicity is not clearly understood, available data suggest that aggregation prone hyperphosphorylated tau loses its ability to bind to microtubules (Bramblett et al., 1993), sequesters normal microtubule-associated proteins, disrupts microtubule dynamics, blocks intracellular trafficking of the neurons and promotes cell cycle re-entry (Wang and Liu, 2008). Interestingly, *MAPT*, the gene encoding tau, is not genetically linked to AD (Poorkaj et al., 1998). The lack of genetic association to AD together with the identification that tau dysfunction serves to cause neurodegeneration (Hutton et al., 1998) may be indicative of a possible downstream role of tau in AD.

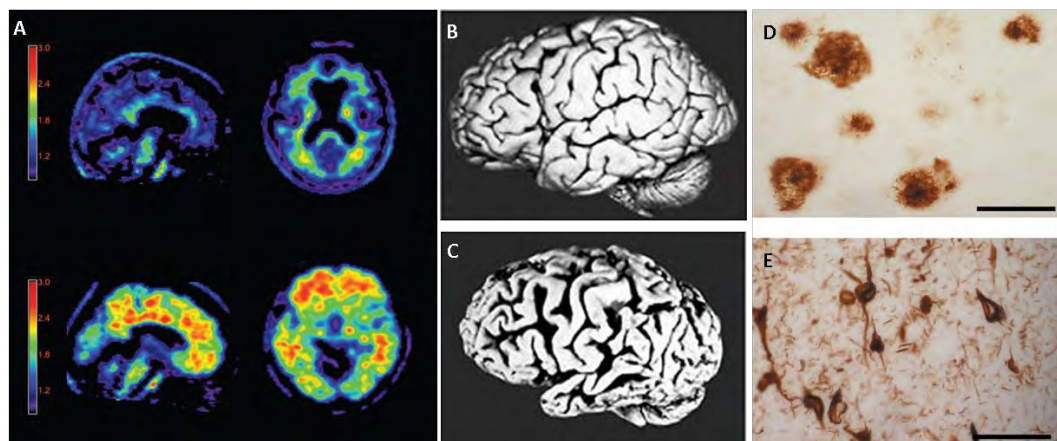


Figure 1-1 Amyloid-beta plaques and neurofibrillary tangles in the AD brain

A) Amyvid (^{18}F florbetapir), a radioactive tracer developed by Eli Lilly, binds to amyloid plaques and allows imaging of amyloid plaque in the brain. The top two images from a cognitively healthy elderly individual indicate absence of $\text{A}\beta$; while, the bottom two images from an AD patient indicates significantly high levels of $\text{A}\beta$ pathology (Sinha, 2011). Compared with the brain of a healthy person (B), the brain of an AD patient (C) demonstrates significant shrinkage of gyri in the temporal lobe (ie. lower part of the brain), frontal lobes (left part of the brain) and in brain regions involved in learning and memory (Mattson, 2004). Representative microphotographs of amyloid plaques in the AD brain visualised by immunostaining with an anti- $\text{A}\beta_{42}$ antibody (D) and of neurofibrillary tangles, visualised by immunostaining with an anti-PHF1 antibody (E) (LaFerla and Oddo, 2005).

The second cerebral lesion described as ‘peculiar substance’ by Alzheimer, is more recently termed amyloid plaques, and occurs as extracellular deposits in specific regions of the brain (Figure 1-1D). It was subsequently established that these compact and extraneuronal amyloid plaques consist of aggregates of a ~4 kDa peptide called amyloid-beta ($A\beta$) (Glennner and Wong, 1984; Masters et al., 1985). Both proteinaceous tau and $A\beta$ aggregates represent the hallmark features of AD, and their presence in the post-mortem observation is necessary for complete diagnosis of AD. Amyloid plaques are typically found in the limbic regions (i.e. hippocampus and amygdala) and in specific cortical regions of the brain. However, according to the Braak Staging of AD, there is a systematic progression of $A\beta$ deposition in the brain where $A\beta$ plaque deposition first commences in the limbic regions and subsequently moves up to other brain regions (Braak and Braak, 1991). Using the Campbell-Switzer silver technique and immunohistochemistry, the first stage of $A\beta$ deposition was observed near the hippocampus and neocortex, and over the next four stages subsequently spread through the allocortical brain regions, diencephalic nuclei, the striatum and finally the cholinergic nuclei of the basal forebrain, which is important in the production of acetylcholine (Braak et al., 2011; MacDonald, 2007; Thal et al., 2002). Together with the presence of proteinaceous aggregates, the AD brain is further characterised by other structural and neuropathological alterations. These include atrophy of the brain, shrinkage of the gyri (Figure 1-1A-C), enlarged ventricles containing cerebrospinal fluid, depletion of specific neurotransmitter systems and extensive degeneration of the hippocampus and neocortex through the loss of neurons and synapses, which subsequently lead to severe cognitive impairment affecting memory, orientation and behavioural changes (Giasson et al., 2003; Hansen et al., 1993; Naslund et al., 2000; Tanzi and Bertram, 2005).

$A\beta$ has been the focus of AD research for almost three decades and is generally accepted as the main causative factor for the onset and progression of AD. The reason for its interest may lie in the initial discovery of *APP*, *PSEN1* and *PSEN2* mutations (Table 1-1) that cause familial AD. All three genes encode proteins that play an important role in the regulation and generation of $A\beta$ (De Strooper et al., 1998; Price et al., 1998) (discussed in Section 1.1.4). Furthermore, mutations in these genes were found to increase the propensity for $A\beta$ to aggregate (Scheuner et al., 1996). The

identification of *APP*, *PSEN1* and *PSEN2* genes further lends support to earlier observations that A β is the major constituent of the amyloid plaque deposits observed in AD brains (Glenner and Wong, 1984). In addition, in late-onset AD, the identification of the ϵ 4 allele of *APOE* gene (Table 1-1) was found to affect the rate of A β aggregation (Bales et al., 1999). These critical studies led to the formulation of the amyloid cascade hypothesis (Hardy and Selkoe, 2002) (discussed in Section 1.2.3) and improved understanding of the role A β played in the onset and progression of AD.

1.1.4 Endoproteolytic processing of APP and generation of amyloid-beta (A β)

The amyloid precursor protein (APP) is a single-transmembrane protein, 695-770 amino acids long, with an *N*-terminal extracellular domain. Of the three major isoforms of APP, the longest isoform (770 amino acids), consists of the Kunitz-type protease inhibitor domain, which is absent in the shortest 695 amino acids long isoform, and the OX-2 antigen domain, absent in both the 695 and 751 amino acids isoforms (Goate et al., 1991). The amyloid-beta (A β) domain is partly embedded in the membrane, with the first 28 amino acids outside the membrane and the remaining 12–14 residues in the transmembrane domain. The cleavage and processing of APP can occur via two pathways (Figure 1-2): the non-amyloidogenic pathway and the amyloidogenic pathway. In the prevalent non-amyloidogenic pathway, APP is cleaved by α -secretase at a position 83 amino acids from the *C*-terminus, producing a large *N*-terminal domain (sAPP α) which is secreted into the extracellular space (Kojro and Fahrenholz, 2005). The resulting 83-amino-acid *C*-terminal fragment (C83) is retained in the membrane and subsequently cleaved by γ -secretase, producing two short fragments termed p3 (Haass and Selkoe, 1993) and the transcriptionally active APP intracellular domain (AICD) (Beckett et al., 2012; Cao and Sudhof, 2001). Importantly, cleavage by the α -secretase occurs within the A β region, thereby abrogating formation of A β (Kojro and Fahrenholz, 2005). In humans, four enzymes with α -secretase activity, ADAM 9, ADAM 10, ADAM 17 and BACE 2, have been identified and all belong to the ADAM (a disintegrin and metalloproteinase) family of enzymes (Allinson et al., 2003; Nowotny et al., 2001).

The amyloidogenic pathway is an alternative cleavage pathway for APP which leads to the generation of A β peptides of various lengths (number of amino acid residues

is indicated by the index). For example, A β ₄₀ and A β ₄₂ are A β peptides of 40 and 42 amino acids in length, respectively. Amyloid beta is generated by sequential endoproteolysis of APP, by classes of enzyme complexes termed β - and γ -secretases. The initial proteolytic cleavage is mediated by the β -secretase at a position located 99 amino acids from the C-terminus of APP. Cleavage of the β -site is performed by β -site APP-cleaving enzyme 1 (BACE1), which is a type I integral membrane protein belonging to the pepsin family of β -secretase (Sinha et al., 1999; Vassar et al., 1999). The γ -secretase is an intramembranous protease complex comprised of presenilin 1 or presenilin 2 (homologous proteins that form the catalytic active site of γ -secretase), nicastrin, anterior pharynx defective 1 homolog A (or 1B) and presenilin enhancer 2 (Edbauer et al., 2003; Francis et al., 2002; Steiner, 2004; Wolfe et al., 1999). This cleavage results in the release of sAPP β leaving the 99-amino-acid C-terminal portion of APP (known as C99) in the membrane. The newly generated N-terminus corresponds to the first amino acid of A β . Subsequent cleavage of this fragment (between residues 38 and 50) by γ -secretase liberates an intact A β peptide (Hartmann et al., 1997; Saito et al., 2011) (Figure 1-2). Due to the varied nature of γ -secretase action, the γ -cleavage of C99 generates A β forms in the range of 38 to 50 amino acids long. The two predominant forms of A β generated are A β ₄₀ (~90%) while about 10% is the A β ₄₂ form, which is more neurotoxic than A β ₄₀ due to its higher hydrophobicity and propensity to aggregate (Jarrett et al., 1993b). Furthermore, mutations associated with early-onset AD identified in *APP*, *PSEN1* and *PSEN2* genes (Table 1-1), were found to increase A β ₄₂ generation and/or the ratio of A β ₄₂/A β ₄₀. Hence these data indicate that A β ₄₂ may be critical for the onset of AD pathogenesis.

However, A β species of various lengths ranging from A β ₃₈ to A β ₅₀ have been found to exist in AD brains and in transgenic mice (Miravalle et al., 2005; Van Vickle et al., 2007). Interestingly, recent studies have shown that A β ₄₃ deposited in amyloid plaques is found more frequently than A β ₄₀ in both early-onset and late-onset AD (Keller et al., 2010; Takami et al., 2009; Welander et al., 2009). It was recently proposed that initially two long A β peptides, A β ₄₈ and A β ₄₉, are produced by γ -secretase and through subsequent stepwise tripeptide release A β ₄₂ and A β ₄₀, are generated respectively (Takami et al., 2009). Therefore, A β ₄₃, which is generated from A β ₄₆ which itself was generated from A β ₄₉, can produce A β ₄₀ by γ -secretase. On the other hand,

A β ₄₂ is generated from A β ₄₈ via A β ₄₅. These data are further supported since only two species of AICD, namely 50-99 and 49-99 amino acids long peptides have been discovered (Sato et al., 2003), indicating that there is significant amount of A β ₄₉ and A β ₄₈ generated. It has also been reported that mutations in the *PSEN1* gene increase the production of longer A β species, such as A β ₄₂, A β ₄₃, A β ₄₅ and longer A β peptides (Welander et al., 2009). The propensity of A β ₄₃ to aggregate is similar to that of A β ₄₂ (Martins et al., 2008; Qi-Takahara et al., 2005). Accumulation of the longer A β peptides, A β ₄₂, A β ₄₃ and A β ₄₅ and/or shortage of the shorter A β peptides, A β ₄₀ and A β ₃₈ may drive neuronal and synaptic dysfunction. However, at present, the possible implications of A β ₄₃ or other varied-length A β species have yet to be fully understood.

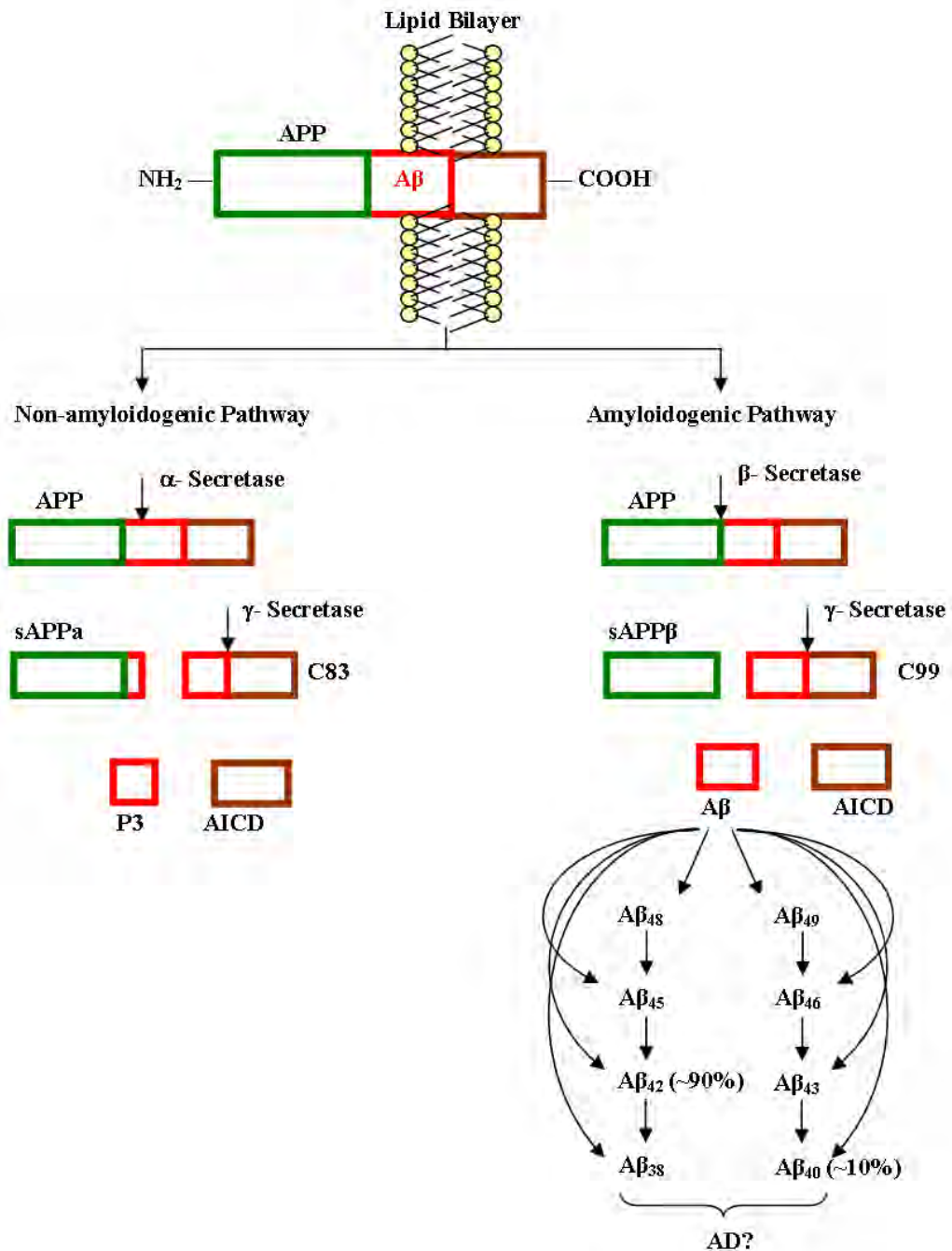


Figure 1-2 Schematic overview of amyloid precursor protein proteolytic cleavage pathways.

A β peptides are derived via proteolysis of the 695–770 amino acid long amyloid precursor protein (APP). APP can undergo proteolytic processing by one of two pathways. Most APP is processed through the non-amyloidogenic pathway, which precludes A β generation. γ -secretase cleaves in the transmembrane domain of APP in a variety of positions leading to the production of A β species of various lengths ranging from A β ₃₈ to A β ₅₀ (indicated by arrows). Generation of A β ₄₂ and A β ₄₀ may also occur via successive tripeptide cleavages at every α -helical turn of A β ₄₈ and A β ₄₉ respectively (Takami et al., 2009). See text for a detailed explanation. Abbreviations: AICD, APP intracellular domain; sAPP β , soluble ectodomain; sAPP α , soluble ectodomain; APP, amyloid precursor protein; C83, carboxy-terminal fragment 83 amino acids in length; C99, carboxy-terminal fragment 83 amino acids in length.

1.2 Protein misfolding, aggregation and neurodegeneration

In neurodegenerative diseases, such as Parkinson's disease, Alzheimer's disease, amyotrophic lateral sclerosis and Huntington's disease, there are characteristic deposits of protein aggregates from abnormal protein folding and interactions in the brain (Dobson, 2003; Dobson and Ellis, 1998; Hammarstrom, 2009; Markossian and Kurganov, 2004; Ross and Poirier, 2004; Selkoe, 2004). In each of these diseases, the distribution and composition of protein aggregates are varied and can be either intracellular (e.g. cytoplasmic or nuclear) and/or extracellular. These protein aggregates are a typical hallmark of neurodegenerative diseases, and while the protein component may vary in each disease, they have similar morphological, structural, and staining characteristics. The accumulated aggregated protein is predominantly composed of the disease protein in a fibrillar aggregated form called amyloid and may potentially contain other proteins as well (Eanes and Glenner, 1968; Sunde and Blake, 1998). While causal factors of protein aggregation are not clearly understood, it has been proposed that genetic mutation(s) causing intracellular accumulation of normal protein, or mutation(s) that leads to production of a disease-linked protein, may play an important role. It has been shown that proteins that generally do not cause aggregation-linked diseases can also form aggregates and cause toxicity (Dobson, 2003; Stefani and Dobson, 2003). Apart from genetic alterations, environmental stress and aging may also trigger protein aggregation (Lindner and Demarez, 2009).

Although protein aggregates are a hallmark of neurodegenerative diseases, there is debate over the possible role of large aggregates in these diseases. While there is clear evidence of protein misfolding and aggregation leading to toxicity, many studies indicate that formation of large aggregates may not be linked directly to toxicity, and possibly represent a cellular protective response (Arrasate et al., 2004; Ross and Poirier, 2005; Saudou et al., 1998; Terry et al., 1991).

1.2.1 States of A β oligomerisation and fibril formation, and, their 3-dimensional structures

A β peptides generated by the amyloidogenic processing of APP are produced as monomers, but they spontaneously self-associate to generate low-molecular weight to high-molecular weight/higher order oligomers. The aggregation state of A β increases in

degree of complexity in the order: monomer < dimer < trimer < tetramer < protofibril < fibril. Therefore, soluble A β peptides have a high propensity to aggregate and the fibrillar complexes are the highest molecular weight assemblies. The term 'oligomer' is imprecise since various species of A β have been identified to exist in constant equilibrium with monomers and higher-order oligomers. Hence the term oligomers used herein refers to dimers to hexamers (i.e. 2 - 6 peptides) of A β . Unlike the A β plaques deposits, which are composed of insoluble A β fibrils, soluble A β oligomers (dimeric, trimeric and tetrameric forms), which are the most neurotoxic species, are found intracellularly and disrupt synaptic function, long term potentiation, learning and memory in AD (Cleary et al., 2005; Gouras et al., 2005; Lesne et al., 2006; Ono et al., 2009; Walsh et al., 2002; Walsh and Selkoe, 2007). Furthermore, the total amount of soluble A β oligomers in the AD brain was found to directly correlate with the degree of cognitive defect in AD individuals (Li et al., 2010; Lue et al., 1999). Studies of mouse models of AD have also corroborated these findings and indicated that increasing levels of A β dodecamers specifically affect cognition and memory (Lesne et al., 2006).

Identification of atomic structures of A β fibrils is extremely challenging and studying the structures of various oligomers and protofibrils is even more challenging. At present, atomic structures of full-length A β fibrils have not been determined since reasonable crystals of full-length A β fibrils for X-ray crystallography have not been obtained (Fandrich et al., 2011). Due to the large size of A β fibrils, conventional solution-state nuclear magnetic resonance (NMR) spectroscopic techniques are not suitable. In the absence of atomic structures of A β fibrils, several structural models have been proposed. The majority of these A β fibril models have a U-shaped peptide fold called a β -arc (Kajava et al., 2010)(Figure 1-3). Interestingly, these U-shaped peptide models have been shown to fit data from cryo-electron microscopic analyses (Sachse et al., 2006; Zhang et al., 2009). Both transmission electron and atomic force microscopy have shown that A β fibrils can have a length of more than 1 μ m, while the lateral width is less than 25 nm (Goldsbury et al., 2000; Luhers et al., 2005; Meinhardt et al., 2009; Sachse et al., 2006; Schmidt et al., 2009). Both the A β ₄₀ and A β ₄₂ superhelical fibrils, which consist of a few protofilaments (Lashuel et al., 2002; Lashuel and Lansbury, 2006; Makin and Serpell, 2005) appear to have a left-handed twist and therefore result in regular crossovers that are visible by transmission electron microscopy (Figure 1-3).

The formation of these fibrils appears to be directional, similar to that of actin filaments or microtubules (Goldsbury et al., 2000; Meinhardt et al., 2009; Sachse et al., 2006; Schmidt et al., 2009). A β fibrils, which form the core of dense A β plaques within the brain parenchyma, are fibrillar polypeptide aggregates with a cross- β structure as demonstrated by X-ray diffraction (Fandrich, 2007; Sunde et al., 1997). The cross- β structure represents intermolecular polypeptide assembly, where the β -sheet plane and the backbone hydrogen bonds that connect the β -strands are oriented parallel to the main fibril axis. Therefore, the β -strands run perpendicular to this direction (Figure 1-3).

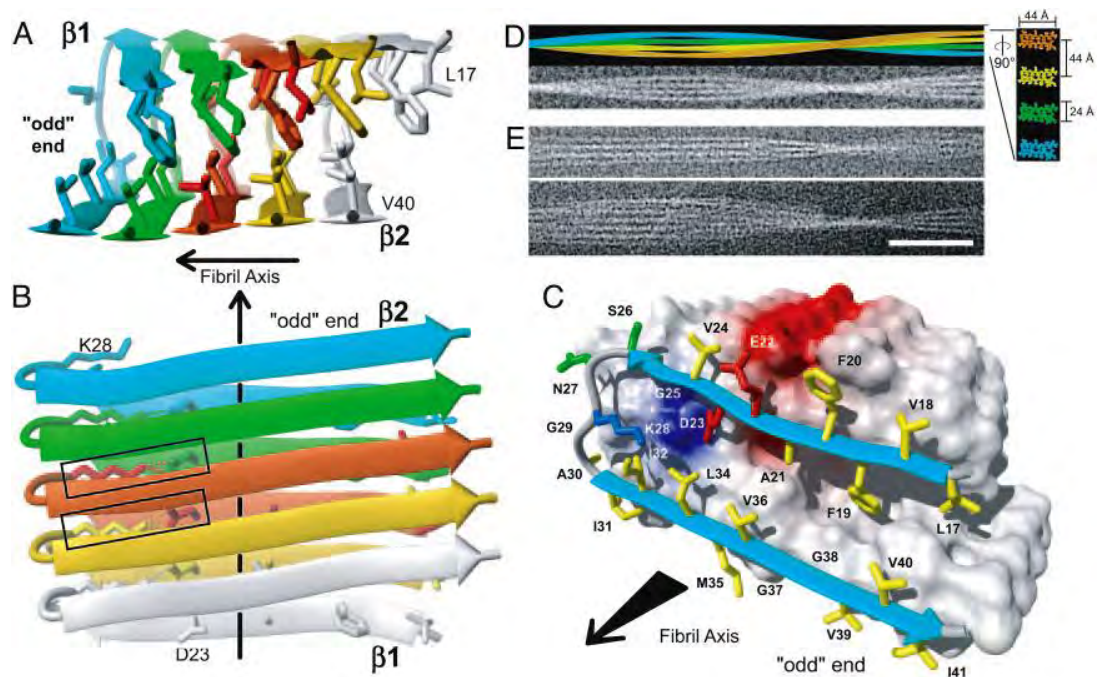


Figure 1-3 Three-dimensional structure of A β_{42} fibril

Individual A β_{42} peptides are coloured. The direction of the fibril axis is indicated by an arrow pointing from even to 'odd' end. A) Using ribbon diagrams, the intermolecular A β -peptide interactions are illustrated. B) Two intermolecular salt bridges formed between D23 and K28 amino acid residues (indicated by black box). C) Ribbon diagram and van der Waals contact surface polarity identifies the hydrophobic, polar, negatively charged, and positively charged amino acid side chains which are illustrated in yellow, green, red, and blue, respectively. The positively and negatively charged surface patches are shown in blue and red, respectively, and all others are shown in white. D and E) Four A β_{42} protofilaments coloured individually with 5 X magnification of the cross section perpendicular to the fibril axis is shown (right). Scale bar, 50 nm. Figure adapted from Luhers et al., 2005.

It is noteworthy that A β fibrils are the end products of a complex fibrillation process involving various A β oligomers, including dimers, trimers, amyloid-derived diffusible ligands, globulomers and protofibrils. However, at present, the isolation and purification of these A β oligomers is a challenge and has not been done (Broersen et al.,

2010). Oligomers and protofibrils, which are the most neurotoxic species found intracellularly, exhibit variable molecular weights and shapes, including spherical oligomers, curvilinear protofibrils and annular pores (Fandrich et al., 2011). Despite these challenges and evidence of random coil-like structure assemblies (Sandberg et al., 2010), data from many studies strongly indicate that A β ₄₀ and A β ₄₂ oligomers also display significant β -sheet content (Ahmed et al., 2010; Cerf et al., 2009; Chimon et al., 2007; Habicht et al., 2007). While A β fibrils are generally localised extracellularly, the formation of these extracellular deposits and their toxicity initiates from intracellular A β oligomeric species (Friedrich et al., 2010; Hu et al., 2009).

1.2.2 Intracellular A β : physiological roles, localisation and neurotoxicity of soluble oligomers

Although the A β peptide was first discovered and reported in many studies as a component of extracellular insoluble A β plaques, Grundke-Iqbal and colleagues (1989) were the first to report the presence of intraneuronal A β in the cerebellum, cerebrum and spinal cord of AD individuals (Grundke-Iqbal et al., 1989). Since then, many post-mortem studies have revealed the presence of intraneuronal A β in AD and Down syndrome individuals (Gyure et al., 2001; Mori et al., 2002; Wegiel et al., 2007). These studies revealed strong correlations between levels of intracellular soluble A β oligomers and synaptic loss (Lue et al., 1999) and cognitive function in AD (McLean et al., 1999). It was further established that the majority of intraneuronal soluble A β in AD is the A β ₄₂ species (D'Andrea et al., 2002; Gouras et al., 2000; Ohyagi et al., 2007; Takahashi et al., 2002) which are localised in multivesicular bodies (MVBs) of neuronal cells displaying synaptic pathology (Takahashi et al., 2002). Furthermore, two independent studies revealed that accumulation of intracellular soluble A β ₄₂ oligomers preceded extracellular plaque formation (Gyure et al., 2001; Wirths et al., 2001) and levels of intraneuronal A β decreased with extracellular plaque build-up (Mori et al., 2002). Taken together, these studies indicate that intracellular soluble A β ₄₂ may play a critical role in the onset and progression of AD compared to the previously thought extracellular insoluble A β deposition. In addition, the increase in intracellular soluble A β ₄₂ may also prove to be an early event in the onset of AD (Gouras et al., 2005; Gouras et al., 2000). The above idea is strongly supported since individuals with mild cognitive impairment were found with

intraneuronal A β in the hippocampus and entorhinal cortex of the brain, where they are likely found in the early stages of AD (Gouras et al., 2000).

Multiple studies have since shown that levels of intraneuronal A β decrease as extracellular A β plaques accumulate (Gyure et al., 2001; Oakley et al., 2006; Oddo et al., 2003; Oddo et al., 2006; Wirths et al., 2001). Two apparent processes have been implicated as causative factors in intracellular A β accumulation. First, since the majority of A β generated intracellularly is secreted from the cell, an impaired secretory pathway where A β generated intracellularly is not secreted would cause a build-up of A β in the cell. Next, extracellular A β can be internalised by neuronal cells through endocytosis to contribute to these intracellular pools. To determine localisation of A β , it is important to understand trafficking and localisation of APP from which A β is released. Studies have showed that APP is localised to cellular plasma membrane (PM) (Kinoshita et al., 2003) and subcellular membranes including the trans-Golgi network (Xu et al., 1995), endocytic network, ER, lysosomal, endosomal (Kinoshita et al., 2003), exosomal (Rajendran et al., 2006) and mitochondrial membranes (Mizuguchi et al., 1992). In the presence of adjacent β - and γ -secretases, A β generation could possibly occur in all the above cellular organelles. Therefore, amyloidogenic processing of APP within subcellular membranes would lead to intracellular A β ; and those within cellular PM and secretory vesicles would be released into the extracellular space (Wertkin et al., 1993). Intraneuronal A β_{42} was also found to localise to outer membranes of MVBs (Langui et al., 2004; Takahashi et al., 2002) and was most often located in the perinuclear region (Langui et al., 2004). Interestingly, intracellular production of A β_{40} and A β_{42} was only found in neuronal cells. In most non-neuronal cells, production of A β predominantly occurred on the plasma membrane (Hartmann et al., 1997). Although the neurotoxicity of various APP mutant forms and their cellular localisation has been well established, detailed cellular functions of APP are not clearly understood. At present, APP has been predicted to have a role in cell adhesion (Kinoshita et al., 2003) and cell movement (Sabo et al., 2001). Data from the loss-of-function phenotypes may also suggest the involvement of APP during development (Zhang et al., 2012).

A β found in senile plaques was initially presumed to be an abnormal protein. Therefore, an important finding was that A β is produced constitutively during normal

cell metabolism (Haass et al., 1992; Wertkin et al., 1993). Soluble A β produced by cells undergoes conformational change to contain high β -sheet content and this increases its aggregation propensity to form soluble oligomers and extracellular fibrils found in plaques. Furthermore, aggregation-prone A β_{42} triggers the misfolding of other A β species (Jarrett et al., 1993b). A β aggregation proceeds by a multistep, nucleation-dependent process (Jarrett and Lansbury, 1993). Formation of nucleation seeds is rate limiting, in the absence of preformed seed fibrils there is a significant lag period for the formation of A β fibrils, followed by a rapid fibril elongation phase once seed fibrils have been generated. The lag time for fibril formation can be dramatically shortened by adding preformed fibril seeds to A β monomer (Jarrett and Lansbury, 1993). The rate of A β fibril formation is controlled by both fibril seed and monomer concentrations (Naiki and Nakakuki, 1996). Initially, only A β deposited in plaques was assumed to be neurotoxic, however, recent data strongly indicate that soluble A β oligomers inhibit hippocampal long-term potentiation and disrupt synaptic plasticity (Walsh and Selkoe, 2004).

Lipid membranes can influence both protein folding and kinetics of protein aggregation. Therefore, alterations to lipid composition in the membranes of subcellular compartment may have an important role in A β aggregation. The formation of A β oligomers can occur during interactions with lipid bilayers, specifically lipid rafts, which are cholesterol- and glycosphingolipid-rich microdomains in plasma membranes (Hicks et al., 2012; Kim et al., 2006; Lai and McLaurin, 2010). Intracellular interactions of soluble A β with clusters of monosialogangliosides in lipid rafts were found to accelerate oligomerisation of A β . This results in the generation of A β bound to GM1 ganglioside, which then acts as a nucleation seed for further A β aggregation (Ikeda et al., 2011; Matsuzaki et al., 2007; Wakabayashi et al., 2005). Interestingly, GM1 ganglioside levels in the lipid rafts of synaptosomes are known to increase with age (Yamamoto et al., 2004). Studies by Wakabayashi et al., (2005) suggest that these ganglioside clusters in lipid rafts serve as a conformational catalyst, generating membrane-bound forms of A β with the ability to act as a seed for aggregation. Interestingly, it was found that A β aggregation is also accelerated in the presence of endosomal, lysosomal and plasma membranes (Waschuk et al., 2001). Taken together, from these data it can be inferred that the plasma membrane and intracellular membranes play a critical role in the

generation of these neurotoxic species of A β . The seeding of toxic intracellular soluble oligomers may be a prelude to pathological events and further seed extracellular plaque formation by exocytosis (Walsh et al., 2002).

There is accumulating evidence that alterations in cholesterol homeostasis in the AD brain may be linked to cerebral A β pathology (Austen et al., 2003). It was recently shown that intracellular A β has a physiological role in maintenance of lipid homeostasis (Grimm et al., 2007), besides its pathological impact. In brain cells, cholesterol was found to increase A β production, and conversely A β production caused a decrease in cholesterol synthesis. The decrease in cholesterol is mediated by the inhibition of 3-hydroxy-3-methylglutaryl-coenzyme A reductase (HMGR) (Grimm et al., 2007). Cholesterol also appears to modulate interaction of A β with neuronal membranes. This may account for the recent finding that statin treatment may afford protection against AD (Grimm et al., 2007). However, the 'AD protection' mediated by statins cannot be simply explained by reduction of cholesterol levels. In addition to their cholesterol-lowering effects (Hartmann, 2001; Wolozin, 2004), statins offer pleiotropic effects such as the reduction in protein isoprenylation (Ostrowski et al., 2007; Reid et al., 2007) and decreasing association of the active form of the γ -secretase complex with membrane rafts (Urano et al., 2005).

Since the first study to implicate the presence of intracellular A β in AD (Grundke-Iqbal et al., 1989), many studies have since reported intraneuronal A β aggregation. Recently, the role of intracellular A β in AD progression has received much more attention (Haass and Selkoe, 2007; LaFerla et al., 2007). Studies using C-terminal-specific antibodies against A β ₄₀ and A β ₄₂ have found that in AD brains most of the intraneuronal A β ends at residue 42 (Gouras et al., 2005) and that the A β ₄₂ localises to the outer membranes of multi-vesicular bodies (MVBs) within neuronal cells (Langui et al., 2004; Takahashi et al., 2002). Interestingly, A β -containing MVBs in mice were most often located in the perinuclear region (Langui et al., 2004). Furthermore, studies using immuno-gold electron microscopy demonstrated that A β ₄₂ can be found in the multivesicular bodies (MVBs) of neuronal cells, where it is implicated in synaptic pathology (Takahashi et al., 2002). These findings have led to the hypothesis that the build-up of intracellular A β may be an early event in the disease progression of AD

(Gouras et al., 2005). Indeed accumulation of intracellular A β precedes extracellular plaque formation in patients with AD (Gyure et al., 2001).

In addition, A β accumulation has been shown to inhibit the proteasome directly (Almeida et al., 2006; Oh et al., 2005) suggesting that intracellular soluble A β is responsible for toxicity. This is the case since A β -induced toxicity was found to increase with impaired function of the proteasome. Gradual accumulation of A β in the mitochondria (Manczak et al., 2006) has also been associated with diminished enzymatic activity of electron transport chain complexes III and IV, and reduced rates of oxygen utilisation (Caspersen et al., 2005).

1.2.3 The ‘updated’ amyloid cascade hypothesis – incorporating A β clearance mechanisms

As indicated in Section 1.1.4, in brain cells, most of the A β peptides produced are A β_{40} , while 10% is the 42 amino acid species (A β_{42}). A β_{42} is more hydrophobic and is more prone to aggregation and fibril formation than A β_{40} (Jarrett et al., 1993b). Interestingly, A β_{42} peptides are the predominant form of A β found in intraneuronal oligomers and the major component of extracellular plaques in AD brains (Younkin, 1998). Data from many studies have shown that deposition of A β in senile plaques play a seminal role in AD pathogenesis. Some of those studies include the identification of multiple autosomal dominant mutations in early-onset AD susceptibility genes *APP*, *PSEN1* and *PSEN2* (Table 1-1). Mutations in these three genes have been found to cause hereditary cerebral hemorrhage with amyloidosis due to excessive A β deposition, reduced flux via the non-amyloidogenic pathway and increased rate of APP endoproteolysis by BACE1 (via the amyloidogenic pathway) (Figure 1-2), increased generation of A β , specifically A β_{42} , and a higher ratio of A β_{42} /A β_{40} (Levy et al., 1990; Nilsberth et al., 2001; Sahlin et al., 2007; Scheuner et al., 1996; Van Broeckhoven et al., 1990). These, as well as other studies have proposed that extracellular A β deposition initiates a pathological cascade that involves the formation of A β plaque deposits, which eventually disrupt neuronal and/or synapse function, resulting in AD. These genetic and histopathological data led to the initiation and development of the amyloid cascade hypothesis by Hardy and Higgins (1992), which posits that deposition of A β protein in the brain parenchyma (Glennner and Wong, 1984; Hardy and Higgins, 1992; Masters et

al., 1985; Selkoe, 1991), is the causative agent of AD pathology and that the neurofibrillary tangles, cell loss, vascular damage, and dementia follow as a direct result of the A β deposition.

However, since the amyloid cascade hypothesis was first proposed in 1992, it has constantly evolved over the last two decades to remain up-to-date with recent developments and to incorporate new data. The amyloid cascade hypothesis received further support with the identification of mutations in the late-onset/sporadic AD ‘susceptibility’ genes (Table 1-1) in the recent genome-wide association studies. Genetic variances identified in two genome-wide association studies point towards cellular processes implicated in A β clearance from the brain (discussed below) (Harold et al., 2009; Hollingworth et al., 2011b; Lambert et al., 2009). Impaired clearance of A β may lead to late-onset AD via the gradual accumulation of A β . A β proteins can be degraded by the peptidases such as the insulin-degrading enzyme, neprilysin, and by endothelin-converting enzyme (Carson and Turner, 2002; Nalivaeva et al., 2012). A β clearance from the brain can also be mediated by low-density lipoprotein receptor related protein across the blood–brain barrier (Tanzi et al., 2004). At present, there is no indication for alterations in these degradative enzymes in AD. However, it is possible that impaired clearance of A β may occur through interactions with ApoE4, decreased cellular catabolism/proteolysis of A β , reduced transport across the blood-brain barrier, or impaired cerebrospinal fluid transport.

Deane and colleagues (2008) showed that in mouse brains, complexes of A β –ApoE2 and A β –ApoE3 were cleared at the blood–brain barrier at a significantly faster rate than A β –ApoE4 complexes (Deane et al., 2008). Interestingly, ApoE is capable of binding to a group of structurally related proteins such as the low-density lipoprotein receptor. Overexpression of this receptor significantly reduced A β aggregation and increased extracellular A β clearance (Kim et al., 2009b). In AD-inflicted brains, the mRNA level of APOE is inversely correlated with the amount of amyloid plaques (Lambert et al., 2005). These data were further supported when it was found that mutations in the promoter region of the APOE gene led to reduced levels of APOE, increased levels of A β plaques and also genetic predisposition to AD (Lambert et al., 2002; Lambert et al., 2004; Lambert et al., 2001; Lambert et al., 2005). Taken together,

these data strongly indicate that APOE isoforms may play an important role in the regulation of extracellular and intracellular A β clearance in the brain (Kim et al., 2009a).

Another apolipoprotein identified by the genome-wide association studies is clusterin (CLU), also known as apolipoprotein J, which is a chaperone involved in cell death and neurodegeneration. Interestingly, it is also one of the most highly expressed apolipoproteins in the central nervous system (Montine et al., 1998; Roheim et al., 1979). Like ApoE, it has been proposed that CLU is involved in the clearance of A β_{42} from the brain via the blood-brain barrier (DeMattos et al., 2004). Gaps remain in our knowledge of the cellular functions of BIN1 and PICALM but both proteins are known to be involved in clathrin-mediated endocytosis, an important step in the intracellular trafficking of neurotransmitters in neuronal cells. Due to their known endocytic functions, both genes were proposed to be involved in APP metabolism (Leprince et al., 1997; Tebar et al., 1999) leading to altered levels of intracellular A β . Therefore, mutations in the PICALM gene may lead to synaptic dysfunction, possibly through altered synaptic vesicle cycling. PICALM is ubiquitously expressed in all tissue types with prominent expression in neurons, where it is randomly distributed at both pre- and postsynaptic structures (Harold et al., 2009), and in the endothelium of blood vessel walls (Baig et al., 2010). Therefore, it has been suggested to be localised in endothelial cells along the blood-brain barrier and may be involved in A β clearance.

Mawuenyega and colleagues (2010) were the first to report a method to measure the generation and clearance of A β in AD individuals. While the average production rate of both A β_{42} and A β_{40} did not differ between the cognitively healthy control group and the AD group, it was found that the average clearance rate of both A β_{42} and A β_{40} was significantly slower in AD individuals compared to the controls (Mawuenyega et al., 2010). It was further established that the 30% impairment in clearance mechanisms of A β_{42} and A β_{40} may be critical in the onset and progression of AD (DeMattos et al., 2004; Mawuenyega et al., 2010).

The amyloid cascade hypothesis has also faced, and still faces, major criticisms. It was recently reported that all A β -centred therapeutic approaches failed and this report was further supported by two independent studies that showed poor correlation between

extracellular insoluble amyloid fibrils/plaque counts and the degree of cognitive impairment/clinical manifestations of AD (Dickson, 1997; Dickson et al., 1995; Greenberg et al., 2003; Morgan et al., 2009; Robinson et al., 2003; Selkoe, 2011; Terry et al., 1991). Interestingly, healthy older individuals, without any AD clinical symptoms, were also found to have significant amount of A β plaque deposits in the limbic and cortical regions of the brain; while in AD individuals, the severity of AD-associated dementia does not correlate with plaque levels and density (Dickson, 1997; Lue et al., 1999). Therefore, at present, it is unclear whether the extracellular insoluble A β aggregates are protective, inert or pathogenic. On the other hand, there are strong correlations between levels of soluble A β oligomers (not A β plaques) and cognitive function/clinical manifestations of AD. Therefore the ‘updated’ amyloid cascade hypothesis posits that AD is caused by an imbalance between A β production and its clearance, which may lead to increased amounts of soluble monomeric, oligomeric, and insoluble fibrillar forms of A β in the central nervous system. The increased level of A β subsequently initiates a cascade of events causing toxicity and neuronal cell death, ultimately leading to AD (Figure 1-4).

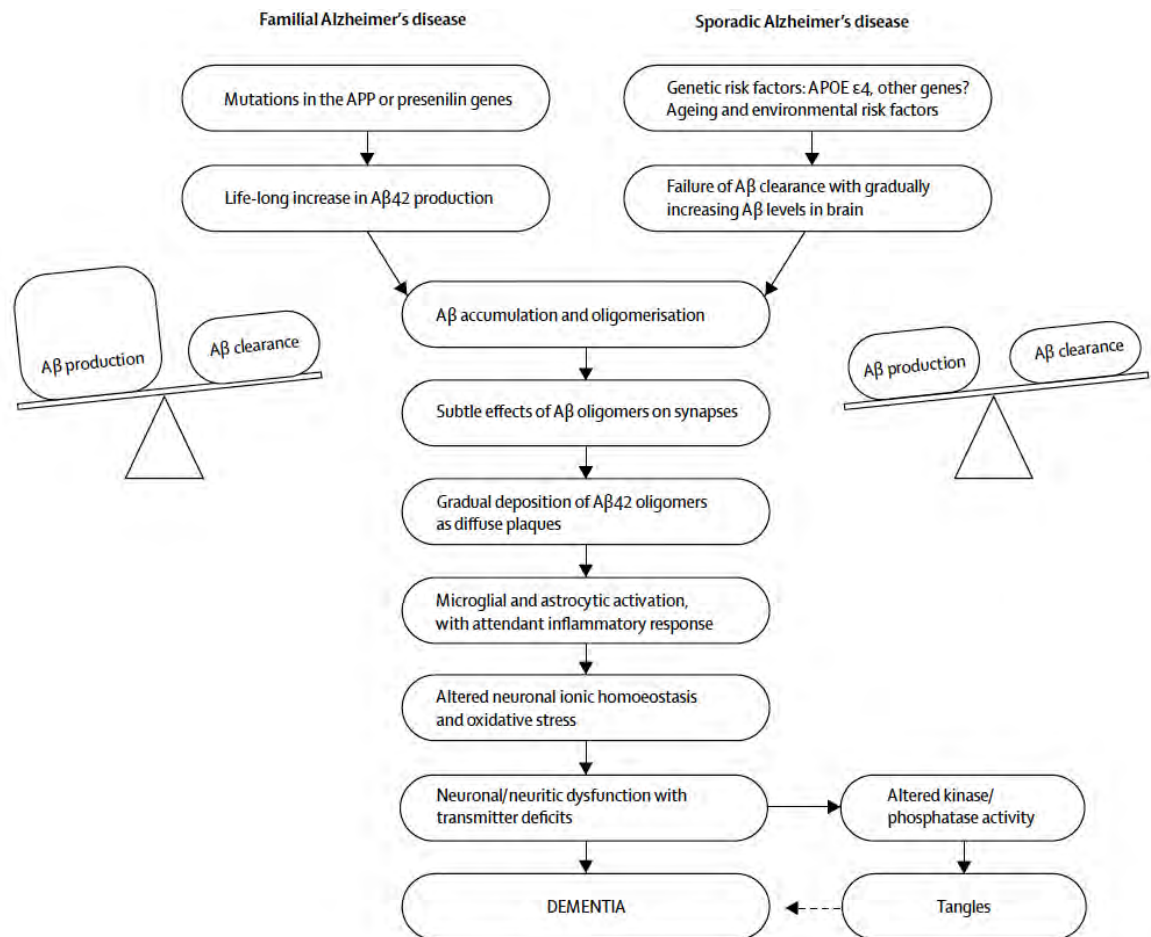


Figure 1-4 The 'updated' amyloid cascade hypothesis

The central events leading to familial AD (early-onset AD) and sporadic AD (or late-onset AD) proposed by the amyloid cascade hypothesis as defined by Hardy and Selkoe (1992) incorporating data from the recent GWAS studies. According to the updated hypothesis, the imbalance between A β production and clearance may be critical in the onset and progression of AD; with increased A β production observed in familial AD and decreased A β clearance in sporadic AD. Instead of A β plaques and fibrils, A β oligomers may inhibit hippocampal long-term potentiation and impair neuronal and synaptic function that lead to cognitive symptoms. While tau pathology may contribute to neurodegeneration, it is likely to play a downstream role in AD. Figure adapted from Blennow et al., 2006.

1.3 Enhanced green fluorescent protein (GFP)-based fluorescent reporter for protein aggregation

The modified enhanced green fluorescent protein (GFP) from the jellyfish *Aequorea victoria* is an important reporter molecule for monitoring gene expression and protein localisation *in vivo* (Kain et al., 1995). Recently, GFP folding has been exploited to study kinetics of protein aggregation in *E. coli* (Waldo et al., 1999). In an aggregation reporter assay developed by Waldo *et al.*, (1999), the exhibition of

fluorescence from the GFP fluorophore is related to the productive folding of the upstream fusion protein and avoidance of inclusion body formation. Therefore, in the event that the fused protein aggregates prior to fluorophore formation, GFP-associated fluorescence would not be observed. Observation of GFP-associated fluorescence would indicate the solubility of correctly folded protein. The expression of GFP can subsequently be qualitatively analysed using fluorescence microscopy and fluorescence-activated cell sorting (FACS).

1.3.1 Amyloid-beta GFP fusion (A β GFP) in *E. coli*

As introduced in Section 1.2.2, the rapid aggregation of the A β ₄₂ peptides is thought to be the main causative role for AD and its disease progression. In applying the GFP-based aggregation assay to study aspects of A β ₄₂ aggregation, consecutive studies by Wurth et al., (2002), and, Kim and Hecht (2005) developed an aggregation assay that used A β fused to GFP (A β GFP). In *E. coli*, it was found that cells expressing A β ₄₂GFP do not exhibit fluorescence, whereas cells expressing A β ₄₀GFP, or unfused GFP exhibited high levels of fluorescence (Kim and Hecht, 2005; Wurth et al., 2002). The lack of fluorescence was attributed to the aggregation of the A β ₄₂-moiety of the fusion protein, prior to the formation of the fluorophore. The influence of the additional two amino acid residues (isoleucine and alanine) in the C-terminal of A β ₄₂ was found to increase the aggregation propensity of this peptide compared to A β ₄₀ (Kim and Hecht, 2006). These data were further confirmed using biophysical analysis, including electron microscopy (Kim and Hecht, 2008).

In an analysis of mutations in the A β ₄₂ peptide that would reduce its propensity to aggregate in *E. coli*, it was found that the C-terminal 41st and 42nd amino acid residues played a significant role in increasing the propensity of the A β ₄₂ peptide to aggregate relative to A β ₄₀. A substitution of the C-terminus isoleucine (41st amino acid) and alanine (42nd amino acid) to glutamic acid and proline respectively resulted in the construction of a highly non-aggregating variant of A β ₄₂ (Kim and Hecht, 2005; Kim and Hecht, 2006). The variant form of A β ₄₂ was termed A β _{EP} and the fluorescence intensity exhibited by A β _{EP} was significantly greater than A β ₄₀ or A β ₄₂ in *E. coli* cells. This supported that A β GFP-derived fluorescence is a reliable indicator of the correct

folding of GFP and highlighted the efficacy of using A β -GFP fusion to gain further insight into mechanisms affecting A β aggregation.

1.4 Model systems to study disease-related proteins implicated in neurodegeneration

The factors affecting A β protein misfolding and aggregation remain elusive. While it may be true that reduced protein quality control and other altered cellular processes associated with aging may contribute to protein misfolding and aggregation ultimately leading to AD (Gaczynska et al., 2001; Lindner and Demarez, 2009), there is a lack of understanding as to why individuals develop various protein-misfolding diseases with aging. It is worth noting that there are individuals who do not develop protein-misfolding diseases or neurodegeneration as they age. Therefore, cellular factors or disease-modifying factors may play a role in the pathogenesis. Identification of genetic/cellular factors that affect A β aggregation would improve our understanding of the underlying molecular basis of protein-misfolding diseases and may have implications for the development of therapeutic strategies.

Genome-wide association studies and epidemiological studies have provided limited mechanistic insight into the cellular processes that determine disease susceptibility or age-at-onset of disease (Carrasquillo et al., 2009; Harold et al., 2009; Hollingworth et al., 2011b; Lambert et al., 2009). Model organisms, such as *Saccharomyces cerevisiae*, *Caenorhabditis elegans* and *Drosophila melanogaster* heterologously expressing neurodegenerative disease-related proteins, together with genome-wide screens, have been exploited to model many aspects of neurodegeneration, including aggregation and toxicity of disease-related proteins and to gain further mechanistic insight about cellular factors affecting protein-misfolding diseases (Fernandez-Funez et al, 2000; Flower et al., 2005; Ghosh and Feany, 2004; Giorgini et al., 2005; Hamamichi et al, 2008; Kazemi-Esfarjani and Benzer, 2000; Komano et al., 1998; Kraemer et al, 2006; Kuwahara et al, 2008; Morley et al, 2002; Outeiro and Lindquist, 2003; Treusch et al., 2011; Van Ham et al, 2008; Wang et al, 2009a; Willingham et al., 2003; Zhang et al., 1994; Zhang et al., 1997). These model organisms share a minimum of 30% homology with human genes and show evolutionary

conservation of many cellular pathways. Interestingly, several regulatory pathways that play a major role in the development of human embryo, regulation of programmed cell death, neuronal function and cellular pathways regulating aging were first elucidated in these organisms (van Ham et al., 2009). Therefore, evolutionarily conserved cellular processes that play important roles in protein misfolding may provide a focal point for future mechanistic studies in neurodegeneration.

A key feature of most neurodegenerative diseases is the late age of onset of the disease. With age being an important factor, an advantage of using model organisms is that they have significantly shorter lifespans compared to humans while exhibiting similar pathobiological hallmarks of aging (Herndon et al., 2002). In the majority of sporadic cases, the late age of onset would impede long term studies in humans directed at identifying early events in the disease progression. Furthermore, there would be serious ethical and practical limitations on the use of human individuals in scientific research. As noted by Khurana and Lindquist (2010), the identification and characterization of the upstream role for A β in AD has been a concerted effort by work within model organisms and human brain tissue. Therefore, it is clear that various complementary approaches will be required for the development of therapeutic strategies for neurodegenerative diseases (Khurana and Lindquist, 2010).

1.4.1 Modelling aspects of neurodegeneration and AD in *S. cerevisiae*

The budding yeast *S. cerevisiae* has served as an important model organism for understanding many aspects of eukaryotic molecular biology. It is the first eukaryote to have its 12,157,105 bp genome (encoding 6607 ORFs; updated as of 2nd August 2012) sequenced (Cherry et al., 2012). While at least 30% of *S. cerevisiae* genes have a corresponding mammalian ortholog, an additional 30% show at least one conserved domain with human genes (Botstein et al., 1997; Winderickx et al., 2008). Approximately 30% of human disease-associated genes also have close yeast orthologs (Bassett et al., 1996; Foury, 1997; Perocchi et al., 2008; Steinmetz et al., 2002). Use of *S. cerevisiae* as a model organism has provided insight into cellular processes such as cell cycle progression, vesicular trafficking, protein synthesis and degradation, and cellular mechanisms involved in aging and cell death. This demonstrates the evolutionarily conserved cellular processes shared between *S. cerevisiae* and human cells.

Recently *S. cerevisiae* has also been used for the study of proteins implicated in neurodegenerative disorders to study aspects related to AD (Bharadwaj et al., 2009; Caine et al., 2007; Caine et al., 2011; Dubey et al., 2009; Komano et al., 1998; Treusch et al., 2011; Zhang et al., 1994; Zhang et al., 1997), frontal temporal lobar degeneration (Braun et al., 2011; Johnson et al., 2008), Parkinson's Disease (Flower et al., 2005; Outeiro and Lindquist, 2003; Zhang et al., 1994) and Huntington's Disease (Giorgini et al., 2005; Willingham et al., 2003). In the majority of these studies, *S. cerevisiae* was used to understand cellular processes involved in the various neurodegenerative diseases caused by misfolded proteins. Disease-related proteins involved in neurodegeneration were heterologously expressed in yeast cells since *S. cerevisiae* lack functional counterparts; thereby constructing so-called 'humanised-yeasts' to study aspects of AD, frontal temporal lobar degeneration, Parkinson's and Huntington's diseases. Genome-wide screens based on the effects on growth have been performed for the identification of genes that suppress or enhance toxicity to *S. cerevisiae* cells expressing A β , α -synuclein or huntingtin proteins (Cooper et al, 2006; Giorgini et al, 2005; Treusch et al., 2011; Willingham et al, 2003). Categorisation of these identified genes on the basis of cellular processes indicated that modifiers of A β toxicity are overrepresented in endocytosis, including the yeast homolog of phosphatidylinositol binding clathrin assembly protein (PICALM); while α -synuclein toxicity mainly play a role in vesicle-mediated transport and lipid metabolism. Modifiers of huntingtin toxicity were found to be overrepresented in stress response pathways, protein folding and degradation. These data strongly indicate that the neurodegenerative disease-related proteins cause toxicity in *S. cerevisiae* through different mechanisms.

While the *S. cerevisiae* genome does not encode β - or γ -secretases, Yap3p and Mkc7p have shown to exhibit α -secretase activity (Edbauer et al., 2003; Luthi et al., 2003; Middendorp et al., 2004; Zhang et al., 1994; Zhang et al., 1997). Intracellular A β may play a causative role in the early progression of AD; therefore, detailed understanding of A β aggregation into soluble oligomers or insoluble aggregates is essential. Yeast cells expressing unfused A β ₄₂ were reported not to produce detectable levels of this protein via western blot analysis (Caine et al., 2007; von der Haar et al., 2007). Whether this phenomenon is due to the toxicity of A β or rapid degradation of A β

remains to be examined. However, A β can be expressed and detected in *S. cerevisiae* cells as a component of N- or C-terminal fusion proteins, and studies with fusion constructs indicated that A β expression slightly lowers growth yield and induces a heat shock response, indicating that expression of A β may exert stress in cells (Caine et al., 2007). Recently, two independent groups developed *S. cerevisiae* models expressing A β -fusions that allowed analysis of A β oligomerisation. By substituting the N-terminal prion forming domain of Sup35p, a transcriptional terminator and prion, with A β ; an oligomerisation assay was developed based on changes in colony colour (Bagriantsev and Liebman, 2006; von der Haar et al., 2007). The aggregation of A β_{42} -Sup35p fusion protein led to loss of function of Sup35p in transcription termination which resulted in the transcriptional read-through of the premature stop codon of the *ade1-14* allele resulting in the expression of Ade1p protein, alleviating the adenine auxotrophy and producing white colonies. Reduced or lack of aggregation of A β_{42} -Sup35p fusion protein led to decreased read-through of the premature stop codon in the mutant *ade1* allele, causing adenine auxotrophy and the accumulation of a red coloured intermediate of the adenine biosynthetic pathway. This led to the growth of pink/red colonies. Therefore, white-coloured colonies indicated that A β -Sup35p had aggregated, while red-coloured colonies indicated a lack of aggregation. Using this approach, it was shown that Hsp104p, a chaperone involved in protein disaggregation, was involved in the formation of A β oligomers by binding directly to A β_{42} -Sup35p. In addition, the prion-curing agent guanidine was found to accelerate oligomerisation of A β_{42} -Sup35p (Bagriantsev and Liebman, 2006). In a separate study, the expression of an A β_{42} -GFP fusion protein allowed visualisation of intracellular A β aggregation and localization in *S. cerevisiae* (Caine et al., 2007). Wild-type cells expressing A β_{42} -GFP exhibited fluorescent cells with large fluorescent puncta in the cytosol, which may correspond to the formation of intracellular oligomers/aggregates. Furthermore, an induction of the heat shock response was noted in these cells. Taken together, these studies may indicate a role for heat shock proteins in response to intracellular accumulation of A β_{42} .

These yeast systems illustrate the value of the *S. cerevisiae* model in understanding cellular processes that are affected or triggered by intracellular A β aggregation. While there may be many important aspects of neurodegenerative diseases that lie beyond the reach of unicellular yeast cells, lacking a brain and a central nervous

system, the evolutionarily conserved cellular processes in *S. cerevisiae* allow it to be used to study fundamental alterations in cellular processes that may be responsible for the onset and progression of neurodegeneration.

1.5 General aims and summary of this study

There are three general aims in this thesis. The first is to understand genetic factors and cellular processes affecting intracellular A β ₄₂ aggregation. To address this aim, the assay for A β ₄₂GFP aggregation reported by Kim and Hecht (2005) was recapitulated in *S. cerevisiae* to facilitate screening of the genome-wide deletion library (Winzeler et al., 1999) for genetic factors and cellular processes affecting intracellular A β ₄₂ aggregation, by assessing the fluorescence associated with expression of the A β ₄₂GFP fusion protein. These data which are presented in Chapter 3, led to identification of 110 mutants exhibiting intense A β ₄₂GFP-associated fluorescence. Four major cellular processes were over-represented in the data set, including phospholipid homeostasis and mitochondrial function. Identification of genetic/cellular factors that affect A β aggregation may lead to the discovery of homologs and conserved pathways in humans, improve our understanding of the underlying molecular basis of intracellular A β ₄₂ aggregation and have implications on the development of therapeutic strategies.

Given the importance of lipid metabolism/homeostasis and mitochondrial TCA cycle function in affecting intracellular A β ₄₂ aggregation in *S. cerevisiae*, the second aim of this study was to better understand underlying cellular mechanisms that contribute to reduced A β ₄₂GFP aggregation. This was carried out using the yeast gene over-expression library (Gelperin et al., 2005) to elucidate specific lipid metabolites that may play a role in reducing the propensity for A β ₄₂GFP to aggregate (Chapter 4). This chapter further explores the distinctive subcellular localisation of A β ₄₂GFP in the phospholipid mutants. Given the recent developments in the analysis of the *S. cerevisiae* lipidome by quantitative shotgun mass spectrometry, this approach was undertaken to identify specific lipid metabolites that may interact with A β ₄₂GFP thus reduce its propensity to aggregate (Chapter 5).

The final aim of this study was to further exploit the powerful and flexible platform of applying the GFP-derived fluorescence-based assay for the screening of chemical/drug libraries for compounds with amyloidogenic and anti-amyloidogenic properties. Both the Library of Pharmacologically Active Compounds (LOPAC¹²⁸⁰®, Sigma-Aldrich), composed of 1280 compounds, and the Spectrum Collection library (MicroSource Discovery Systems, Gaylordsville, CT, USA), containing 1997 compounds, were used in the high-throughput chemical and drug screen for modifiers of A β ₄₂GFP and A β ₄₀GFP aggregation/fluorescence in *S. cerevisiae*. These data are presented in Chapter 6. Identifying such drugs as affecting intracellular A β ₄₂ aggregation may significantly reduce costs and the exhaustive process of introducing new drugs onto the market. Compounds identified through this approach may potentially change the way these drugs are currently administered to patients. These data provide genome-wide evidence of cellular processes and chemical compounds that affect intracellular A β ₄₂GFP aggregation and may have important implications for understanding cellular mechanisms that affect intracellular A β ₄₂ aggregation and ultimately disease progression of AD.

2 MATERIALS AND METHODS

2.1 General Materials and Reagents

General chemicals, reagents and organic solvents used in this study were of analytical grade and were purchased from Invitrogen (Australia), Sigma-Aldrich (Australia) or Ajax Chemicals. MilliQ water was used in all experimental procedures.

2.2 *S. cerevisiae* and *E. coli* strains, plasmids and primers

2.2.1 *S. cerevisiae* strains

The *S. cerevisiae* deletion strains used in this study were derived from the BY4743 wild-type strain (Winzeler et al., 1999) (Open Biosystems). The genotypes of the *S. cerevisiae* strains used in this study are given in Table 2-1. Unless otherwise stated, the term ‘wild-type’ exclusively denotes wild-type *S. cerevisiae* cells of the BY4743 background.

Table 2-1 *S. cerevisiae* and *E. coli* strains used in this study

Strain	Genotype	Source
BY4743 (Wild type)	<i>MATa/MATa; his3Δ1/his3Δ1; leu2Δ0/leu2Δ0; met15Δ0/MET15; LYS2/lys2Δ0; ura3Δ0/ura3Δ0</i>	EUROSCARF
Deletion library	As in BY4743 except homozygous deletion for respective target gene. <i>KanMX4:: target gene</i>	EUROSCARF
BY4743 (rho ⁰)	As in strain BY4743 but rho ⁰	This study
BY4741 (Wild-type)	<i>MATa; his3Δ1; leu2Δ0; met15Δ0; ura3Δ0</i>	EUROSCARF
Quadruple mutant <i>Δdgal1Δlro1Δare1Δare2</i>	<i>MATa; lro1::KanMX4; dgal::KanMX4; are1::KanMX4; are2::KanMX4</i> in BY4741	Karin Athenstaedt (Athenstaedt, 2011)
DAmP collection (heterozygous diploids)	<i>MATa/MATa; his3Δ1/his3Δ1; leu2Δ0/leu2Δ0; met15Δ0/MET15; ura3Δ0/ura3Δ0; CYH2+/cyh2</i>	Open Biosystems
DAmP collection (generated haploids)	<i>MATa; his3Δ1; leu2Δ0; met15Δ0; ura3Δ0</i>	Open Biosystems & this study
yCG253	<i>MATa; can1 Δ::STE2pr-Sp_URA; lyp1Δ::mCherry-Nat; his3Δ1; leu2Δ0; ura3Δ0::NLS-RedStar2-hph; LYS2+</i>	Paul Atkinson (Bircham et al., 2011)

2.2.2 *E. coli* strains

The *E. coli* strain DH5 α TM [F- ϕ 80*lacZ* Δ M15 Δ (*lacZ*YA-*argF*)U169 *recA1* *endA1* *hsdR*17(*r*_k⁻, *m*_k⁺) *phoA* *supE*44 *thi*-1 *gyrA*96 *relA1* λ ⁻] was used for plasmid propagation and the InvitrogenTM Gateway System® reactions. The *E. coli* strains (DH5 α) in the yeast ORF library (YSC3868) were also used for plasmid propagation and the InvitrogenTM Gateway System® reactions.

2.2.3 Plasmids

The plasmids used in this study are listed in Table 2-2. Centromeric plasmids (denoted as CEN) indicate the presence of a centromeric sequence on the plasmid which leads to its maintenance in *S. cerevisiae* cells at a low-copy number (usually as one or two copies). Plasmids that encode a 2 μ origin of replication (denoted as 2 μ ori) are maintained at high-copy number (20-50 copies) in *S. cerevisiae* (Sikorski and Hieter, 1989). The pAG series of plasmids were described in Alberti et al (2007). Yeast ORF collection (BG1805 series of plasmids) was purchased from Open Biosystems. Relevant plasmids were verified by sequencing using the DNA sequencing service provided by the Ramaciotti Centre for Gene Function Analysis, UNSW.

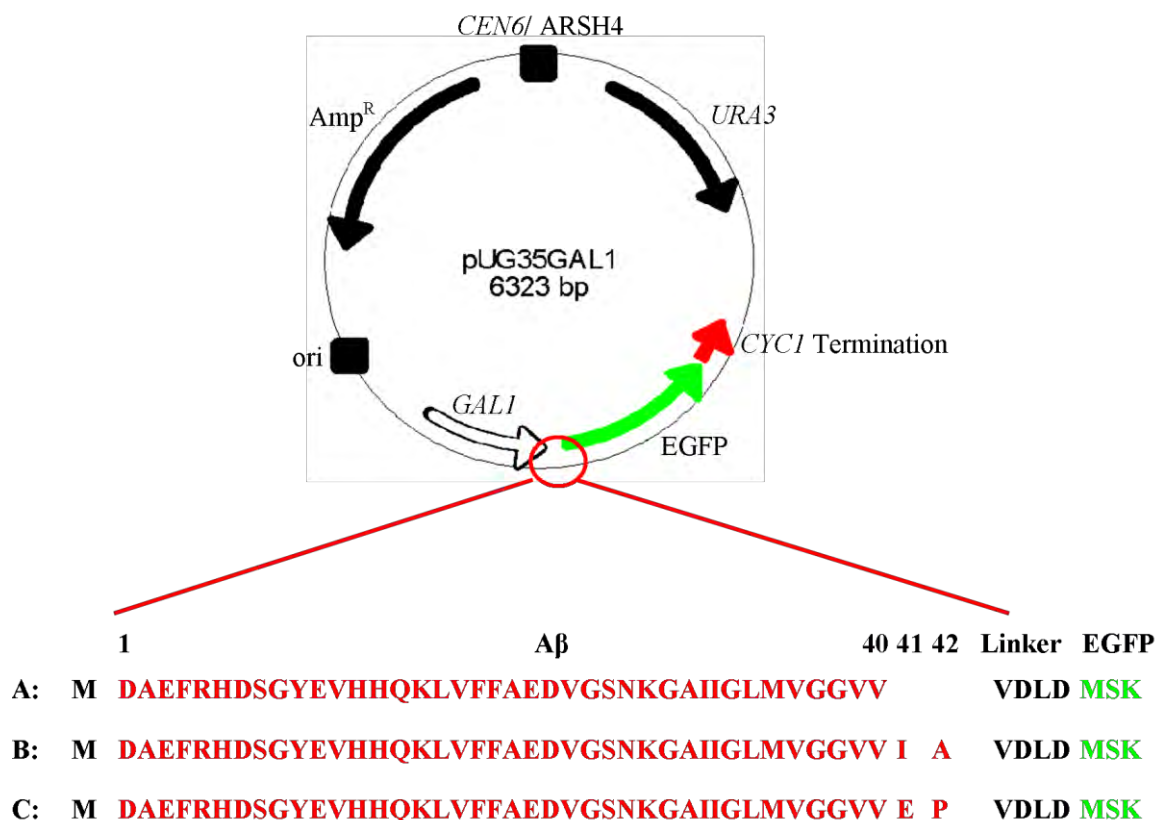


Figure 2-1 Schematic illustration of AβGFP plasmid constructs used in this study.

Using the same plasmid backbone pUG35GAL1 to cater for the expression of C-terminally fused AβGFP fusion proteins A) Aβ₄₀ fused to GFP; B) Aβ₄₂ fused to GFP and C) Aβ_{EP} fused to GFP. Amino acids in red denote the Aβ sequence; fused to the N-terminus of GFP domain via a four amino acid peptide linker, VDLD.

Table 2-2 Plasmids used in this study

Plasmid	Genotype/Description	Source
pUG35GAL1 (Figure 2-1)	Unfused vector for GFP expression under the regulation of <i>GAL1</i> promoter, <i>URA3</i> selection marker; CEN	Mathew Traini
pUG35GAL1-Aβ ₄₀ (Figure 2-1)	As in pUG35GAL1 but encoding human Aβ ₄₀ with a C-terminal fusion to GFP	Mathew Traini
pUG35GAL1-Aβ ₄₂ (Figure 2-1)	As in pUG35GAL1 but encoding human Aβ ₄₂ with a C-terminal fusion to GFP	Mathew Traini
pUG35GAL1-Aβ _{EP} (Figure 2-1)	As in pUG35GAL1 but encoding Aβ ₄₂ variant with a C-terminal fusion to GFP (I41E and A42P substitutions)	Mathew Traini
pJR233-mDsRed	Encodes peroxisome targeting signal 1 (PTS1) tripeptide Ser-Lys-Leu (SKL) fused to the C-terminal of mDsRed. Expression under regulation of the <i>MLS1</i> (constitutive) promoter, <i>LEU2</i> selection marker; 2μ ori	Brocard <i>et al.</i> , (1997)

pDONR221	Vector, KanR	Invitrogen
pAG416GAL-ccdb	Vector, AmpR, CEN, <i>URA3</i>	Addgene
pAG416GAL-A β 42	As in pAG416GAL but encoding human A β ₄₂ with a C-terminal fusion to GFP	This study
pAG416GAL-A β 40	As in pAG416GAL but encoding human A β ₄₀ with a C-terminal fusion to GFP	This study
pAG416GAL-A β EP	As in pAG416GAL but encoding human A β _{EP} with a C-terminal fusion to GFP	This study
pAG416GAL-EGFP	As in pAG416GAL but encoding GFP	This study
pAG415GAL-ccdb	Vector, AmpR, CEN, <i>LEU2</i>	Addgene
pAG415GAL-A β 42	As in pAG415GAL but encoding human A β ₄₂ with a C-terminal fusion to GFP	This study
pAG415GAL-A β 40	As in pAG415GAL but encoding human A β ₄₀ with a C-terminal fusion to GFP	This study
pAG415GAL-A β EP	As in pAG415GAL but encoding human A β _{EP} with a C-terminal fusion to GFP	This study
pAG415GAL-EGFP	As in pAG415GAL but encoding GFP	This study
pAG426GAL-ccdb-EGFP	Vector, AmpR, 2 μ , <i>URA3</i> , GFP	Addgene
pAG426GAL-DAK2-EGFP	As in pAG426GAL but encoding <i>DAK2</i> with a C-terminal fusion to GFP	This study
Yeast ORF collection (BG1805 family)	Yeast ORF/Gene-of-interest expression under the regulation of <i>GALI</i> promoter, <i>URA3</i> selection marker; 2 μ	Open Biosystems
pRS316-STE2pr-SpHIS5	Mata-specific promoter, <i>HIS5</i>	Open Biosystems

2.2.4 Primers

Primers (Table 2-3) were purchased from GeneWorks (Australia) and were used for generating strains or for plasmid construction.

Table 2-3 Primers used in this study

Primer	Sequence	Use(s)
OPI3-KanMXS1	GAGCCATAAACAGCAATTGAAGACAACAA GAATAGCGCAAGTCAAGCGATGATGGGTA AGGAAAAGACTCACG	Deletion of <i>OPI3</i>
OPI3-KanMXS2	GGTAATAGCATAGGCTTCTAACATTATAGA ATATATAGAAATAGAGCACTTATTAGAAAA ACTCATCGAGCATCAAATG	Deletion of <i>OPI3</i>

SLC4S1	ACGCCAAGACAAACCGTGGTGATTTAATTC TGCTGCTGATCGCTTCCAACATGCGTACGC TGCAGGTCGAC	Deletion of <i>SLC4</i>
SLC4S2	ATAAGACAACAAGACTGTGACTTCCACACG CATCTGTCGTTTTTGGCCATCTAATCGATGA ATTCGAGCTCG	Deletion of <i>SLC4</i>
SLC4 – A	CTTTCATGTAAAGCTGTTGAACCTT	Verification of <i>SLC4</i> deletion
SLC4 – D	GGCAGACAATACCAAAGATAAAGAA	Verification of <i>SLC4</i> deletion
AYR1S1	CTTCTATTAATATATACTCAATTCAAATATT GATCAGGATTTCAAAGAGTATGCGTACGCT GCAGGTCGAC	Deletion of <i>AYR1</i>
AYR1S2	GGAATCTTGTATATAAATATAGGTAGCTAT TGACGATGGTGAAACACTAATCGATGAATT CGAGCTCG	Deletion of <i>AYR1</i>
AYR1 – A	GACAGCCTTTTTACTTGAAGAATGA	Verification of <i>AYR1</i> deletion
AYR1 – D	TTGAATATGCTGTTCTCACTTTTGA	Verification of <i>AYR1</i> deletion
SLC1S1	TAGAGAAGTTTAGTGGTTTCCCTCCGTCAG TGAATTCGAGCAAAAAAATAATGCGTACGC TGCAGGTCGAC	Deletion of <i>SLC1</i>
SLC1S2	GATAATTACAGTTTTTGGGTCTATATACTAC TCTAAAAATGTGGTGGTGGCTTAATCGATG AATTCGAGCTCG	Deletion of <i>SLC1</i>
SLC1 – A	TCTTGTTGTGGTTTTTCAGACATTA	Verification of <i>SLC1</i> deletion
SLC1 – D	TTGTTGTTCCCTCGTATTTTTCTTTC	Verification of <i>SLC1</i> deletion
attB1-GFP	GGGGACAAGTTTGTACAAAAAAGCAGGCT TCATGTCTAAAGGTGAAGAATTATTCAC	Construction of pDonr221- GFP
attB1-Abeta- GFP	GGGGACAAGTTTGTACAAAAAAGCAGGCT TCATGGATGCAGAATTCCGAC	Construction of pDonr221- A β GFP
attB2-Abeta- EGFP	GGGGACCACTTTGTACAAGAAAGCTGGGTC CTATTATTTGTACAATTCATCCATAC	Construction of pDonr221- GFP and pDonr221- A β GFP
GPD promoter	CGGTAGGTATTGATTGTAATTCTG	Sequence vectors from Addgene

M13F	GTAAAACGACGGCCAG	Sequence pDONR221 and vectors from Addgene
M13R	CAGGAAACAGCTATGAC	Sequence pDONR221 and vectors from Addgene
BG1805F	GGGGACAAGTTTGTACAAAAAAGCAGGCT	Sequence BG1805- based plasmids
BG1805R	GGGGACCACTTTGTACAAGAAAGCTGGGT	Sequence BG1805- based plasmids

2.3 General methods/ laboratory procedures

2.3.1 Sterilisation and containment of biological waste

Media, labware and heat-stable solutions were sterilised by autoclaving at 121°C (125 kPa) for 15 min with the exception of 70% (w/v) polyethylene glycol (MW 3350; PEG) and 50% (v/v) glycerol which were sterilised at 121°C for 45 min. Heat labile solutions were filter sterilised via passage through 0.22 µm Millex™ sterile filters (Millipore, NSW). DNases were inactivated by autoclaving. All biological materials were autoclaved at 121°C for 20 min prior to disposal.

2.4 Media and growth conditions

2.4.1 *E. coli* growth media and storage conditions

For the purposes of plasmid propagation, the *E. coli* strain (Section 2.2.2) was cultured in 50 ml Luria-Bertani (LB) media (1% tryptone, 0.5% yeast extract, 1% NaCl), supplemented with relevant antibiotics, and incubated at 37°C with shaking (500 rpm) for 12 h. Antibiotics were stored as 1000X concentrated stocks at -20°C and used at the following final working concentrations: 100 µg/ml ampicillin; 50 µg/ml kanamycin sulphate; 50 µg/ml chloramphenicol. For short term storage (<2 weeks), *E. coli* strains were maintained on LB media solidified with 2% (w/v) agar, at 4°C. For long term storage, cells were stored in 50% (v/v) aqueous glycerol at -80°C.

2.4.2 *S. cerevisiae* growth media and storage conditions

The wild-type and mutant strains of *S. cerevisiae* used in this study were predominantly of the BY4743 strain background (Table 2-1). Homozygous diploid deletion mutants of all non-essential genes from the *Saccharomyces* Gene Deletion Project (Winzeler et al., 1999) were obtained from the European *Saccharomyces cerevisiae* Archive for Functional Analysis (EUROSCARF) (Table 2-1) and maintained in YPD media (2% w/v) D-glucose, 2% (w/v) bactopectone, 1% yeast extract). All strains transformed with a plasmid were maintained in synthetic complete D-glucose media (SCM) containing 2% (w/v) glucose, 0.5% ammonium sulfate, 0.17% yeast nitrogen base and appropriate synthetic media supplements (listed in Table 2-4), but lacking the necessary supplement to facilitate maintenance of plasmid. For example synthetic complete medium lacking leucine is denoted as SCM-LEU. 2% (w/v) D-galactose was used as carbon source in the SCM (SCgal) instead of glucose when galactose induction of a gene-of-interest was required. SCgal medium lacking uracil is denoted as SCM-URA. Unless otherwise stated, yeast strains were grown at 30°C, with shaking (600 rpm) using a 96-well plate volume:medium volume of 2:1. For the western blot and quantitative shotgun mass spectrometric lipidome analyses, yeast strains were grown at 30°C, with shaking (500 rpm) using a vessel flask volume:medium volume of 5:1.

Table 2-4 Supplements for synthetic complete media

Supplement	Final conc. (mg L ⁻¹)	Supplement	Final conc. (mg L ⁻¹)
Adenine	18	Leucine	260
Alanine	76	Lysine	76
Arginine	76	Methionine	76
Asparagine	76	p-aminobenzoic acid potassium salt	8
Aspartic acid	76	Phenylalanine	76
Cysteine	76	Proline	76
Glutamic acid	76	Serine	76
Glutamine	76	Threonine	76
Glycine	76	Tryptophan	76
Histidine	211	Tyrosine	76
Myo-inositol	76	Uracil	22
Isoleucine	76	Valine	76

For short-term storage (<2 weeks), *S. cerevisiae* strains were maintained in appropriate solidified media (YPD or SCM), with the addition of agarose 2% (w/v), at 4°C. For long-term storage, *S. cerevisiae* strains were stored in aqueous 15% (v/v) glycerol at -80°C.

2.5 General molecular biology methods

Methods for agarose-gel electrophoresis, ethanol precipitation and DNA isolation were described in Sambrook et al (1989). Restriction enzymes, ligases and associated buffers were purchased from New England Biolabs (NSW). Isolation of DNA from agarose gels was performed using the Qiagen gel extraction kit according to the manufacturer's instruction. DNA ligations were performed for 3 h at room temperature or overnight at 4°C in a 20 µl reaction volume. Conditions such as the length of time for ligation and the vector to insert DNA quantity and ratio were optimised for each ligation reaction.

2.5.1 Polymerase chain reaction

Proof reading polymerase (iProof, Biorad) was used according to the manufacturer's instructions for polymerase chain reactions (PCRs) to amplify DNA. Annealing temperatures were optimised for each primer pair using a gradient temperature function (50°C to 70°C). For verification of DNA amplification, PCR products were run (80 V) on 1.5 % agarose gels run at 70 V using 1 x TAE (40 mM Tris-HCl pH 8.5, 2 mM EDTA pH 8.0, 0.001% glacial acetic acid) as running buffer. DNA was visualised using ethidium bromide (0.00008% final concentration) added from a 10 mg/ml stock solution.

2.5.2 DNA sequencing

DNA was sequenced using the ABI BigDye Terminator system (Applied Biosystems, NSW) according to manufacturer's instructions. Samples were sequenced and analysed by the Ramaciotti Centre for Gene Function Analysis (UNSW, Australia).

2.5.3 Small-scale plasmid extraction

For plasmid purification, *E. coli* strain DH5 α TM cultures were grown in 50 ml LB media (Section 2.4.1) Plasmid DNA was purified using the QIAGEN Plasmid Midi Kit according to the manufacturer's instruction and maintained in TE buffer at -20°C.

2.5.4 Large-scale plasmid extraction

For the high-throughput transformation of the *S. cerevisiae* genome-wide deletion library, large quantities of plasmid DNA were prepared. *E. coli* cultures harbouring the desired plasmid were grown (Section 2.4.1) in LB media, supplemented with ampicillin, for 8 h. Cells were pelleted via centrifugation (3,000 g; 15 min) at 4°C and the supernatant removed. The cell pellet was resuspended in 2 ml GTE pH 8.0 (50 mM D-glucose, 10 mM EDTA, 25 mM Tris) and incubated at room temperature for 5 min. To lyse cells, 4 ml lysis solution (0.2 M NaOH, 1% SDS) was added and mixed gently by inversion of the tube end-over-end until the solution became viscous and clear. The tube was incubated on ice for 5 min and 3 ml of chilled 3 M potassium acetate solution added, and the mixture gently mixed and placed on ice for a further 5 min. The mixture was transferred into a pre-chilled Sorvall SS-34 centrifuge tube and centrifuged (16,000 g; 30 min; 4°C). The supernatant was transferred into a fresh Sorvall SS-34 centrifuge tube containing 5.4 ml absolute isopropanol. After incubation for 5 min at room temperature, the tubes were centrifuged (16,000 g; 30 min; 4°C) and the resulting supernatant discarded. The pellet was washed and resuspended in 1 ml of 70% (v/v) ethanol. The suspension was transferred into a 1.5 ml microfuge tube, and centrifuged (18,000 g; 2 min). The supernatant was discarded and pellet washed in 1 ml of 70% (v/v) ethanol followed by centrifugation (18,000 g; 2 min). The resulting supernatant was discarded and the pellet dried in a Savant SpeedVac for 15 min at medium drying rate. The resulting plasmid DNA pellet was resuspended in 500 μ l of TE buffer and stored at -80°C.

2.6 Transformation of *S. cerevisiae* and *E. coli* strains

2.6.1 Low-throughput transformation of *S. cerevisiae* strains

The transformation of a limited number of *S. cerevisiae* strains was achieved using the high-efficiency lithium acetate-based transformation protocol previously described by (Gietz and Woods, 2002).

2.6.2 High-throughput transformation of *S. cerevisiae* genome-wide deletion library in 96-well plate arrays

The genome-wide *S. cerevisiae* deletion library stored at -80°C freezer in 96-plate format was thawed at room temperature and replicated into 96-well round-bottom plates (Sarstedt, SA) containing YPD media, using a 96-pin replicating tool. Freshly inoculated 96-well plates were incubated at 30°C with shaking (600 rpm) for 48 h. Following centrifugation (800 g; 5 min), the resulting supernatant was removed and cell pellets resuspended in 10 µl of sterile MilliQ water. For the transformation of a single 96-well plate, a 25 ml transformation mix containing 40% (w/v) PEG 3350, 0.1 M lithium acetate, 1 mM EDTA, 10 mM Tris-HCl (pH 7.5), 2 mg single-stranded salmon sperm DNA and 500 µl of the appropriate plasmid DNA dissolved in Tris-EDTA (TE) buffer (e.g. pUG35GAL1-Aβ42; Table 2-2). Yeast strains were resuspended in the transformation mix by gentle pipetting and the 96-well plates were incubated at 30°C with shaking for 24 h. Following the incubation, strains were heat-shocked at 42°C for 30 min. Cells were pelleted after centrifugation (800 g; 5 min), the supernatant was removed and the cell pellet resuspended in SCM-URA (medium lacking uracil to allow auxotrophic selection of transformed cells) and incubated at 30°C with shaking for 48 h. Subsequently, in the second round of selection, 5 µl of each yeast strain was transferred into a fresh 96-well flat-bottom plate (Sarstedt, SA) containing SCM-URA and incubated at 30°C with aeration for 48 h.

For storage purposes, each 96-well plate was centrifuged (800 g; 5 min), supernatant removed and cell pellets resuspended in 15% w/v glycerol and stored at -80°C. Mutants that were not transformed are listed Appendix A.

2.6.3 Transformation of *E. coli* strains

E. coli competent cells were prepared by rubidium chloride treatment as described in Hanahan et al (1991) or purchased from Biolines. Cells were stored at -80°C and thawed on ice when required. Transformations were performed by mixing 50 µl of competent cells with the DNA and incubating on ice for 20 min. Cells were heat-shocked for 45 s at 42°C, incubated on ice for 2 min and then incubated in LB medium for 1 h at 37°C and plated onto the appropriate LB antibiotic selection medium (Hanahan et al., 1991).

2.7 Induction of Aβ₄₂GFP expression and screening of the *S. cerevisiae* genome-wide deletion collection

S. cerevisiae strains transformed with the pUG35GAL1-Aβ₄₂ plasmid in 96-plate format, were thawed from the -80°C freezer and replicated in a fresh plate containing SCM-URA. Plates were incubated at 30°C with aeration for 24 h. 5 µl of each yeast strain was transferred into a fresh 96-well flat-bottom plate containing SCgal-URA, induction medium for the expression of Aβ₄₂GFP (galactose medium lacking uracil to maintain transformed plasmids). For the initial growth in galactose medium, yeast strains were incubated at 30°C with shaking for 48 – 72 h. In preparation for screening mutants via microscopic analysis, yeast strains were replicated into a fresh 96-well flat-bottom plate, containing SCgal-URA and incubated at 30°C with shaking for 12 to 18 h. Through fluorescence microscopy (Section 2.8), yeast strains were screened individually for exhibition of Aβ₄₂GFP-associated fluorescence. Upon completion of the genome-wide analysis, an array of 110 mutants exhibiting strong Aβ₄₂GFP-associated fluorescence was prepared on a fresh 96-well flat-bottom plate and stored at -80°C (Section 2.6.2). This screen was performed in conjunction with Mathew Traini, University of New South Wales, Australia.

2.8 Epifluorescence and confocal microscopy, and the visualisation of organelles

Fluorescence and differential interference contrast (DIC) microscopy was performed using a LEICA DM5500B microscope with a 100X/1.3 oil objective lens (Leica Microsystems, Germany). GFP, DAPI and LipidTOX Red-derived fluorescence

was observed using the I3 FLUO-Filtercube (LEICA; 450-490 nm bandpass excitation filter), C/Y FLUO-Filtercube (LEICA; 360/40 nm bandpass excitation filter) and the TX2 FLUO-Filtercube (LEICA; 560/40 nm bandpass excitation filter) respectively. Images were electronically captured and processed using the Leica Application Suite. Image overlays were performed using NIH ImageJ v1.38 software and saved as TIFF files. False colouring, multiple image overlays and image editing was achieved using the National Institutes of Health (NIH) ImageJ v1.38 software (<http://rsb.info.nih.gov/ij>).

Confocal fluorescence microscopy was performed using an Olympus FV-1000 confocal microscope under 100X objective. GFP, DAPI and LipidTOX Red images were visualised using 488 nm, 405 nm and 633 nm excitation lasers respectively. 3D-Confocal data analysis and image processing were performed using the Imaris 7.2 software package (Bitplane™).

2.8.1 Nuclear and mitochondrial DNA staining

For the visualisation of nuclear and mitochondrial DNA, 4',6'-diamidino-2-phenylindole (DAPI) staining was used in conjunction with fluorescence microscopy. An aliquot of 100 µl from a culture of *S. cerevisiae*, growing at exponential phase, was centrifuged (8000 g; 5 min) and supernatant was discarded. The cell pellet was resuspended in 100 µl of water and DAPI was added to a final concentration of 3 µg/ml. The cell suspension in the DAPI staining solution was incubated in the dark, at room temperature, for 15 min. Cells were examined directly under the fluorescence microscope using the C/Y FLUO-Filtercube (excitation: 360/40 nm), suitable for visualisation of DAPI fluorescence.

2.8.2 Staining of lipid droplets with LipidTOX Red and Nile Red

For the visualisation of lipid droplets, LipidTOX Red staining (Invitrogen) (Nioi et al., 2007) was used in conjunction with fluorescence microscopy. An aliquot of 100 µl from a culture of *S. cerevisiae*, growing at exponential phase, was centrifuged (8000 g; 5 min) and supernatant was discarded. The cell pellet was resuspended in 100 µl of water and LipidTOX Red was added to the cell suspension by diluting the manufacturer-supplied 1000 X stock to a final 1 X working concentration. The cell suspension in the

LipidTOX Red staining solution was incubated in the dark, at room temperature, for 15 min. Cells were examined directly under the fluorescence microscope using the TX2 FLUO-Filtercube (excitation: 560/40 nm), suitable for visualisation of LipidTOX Red fluorescence. LipidTOX Red staining used in the detection of lipid droplets in *S. cerevisiae*, displays an emission spectrum that does not overlap with that of GFP (Invitrogen).

Nile Red (9-diethylamino-5H-benzo[α]phenoxazine-5-one) is another fluorescent lipophilic stain characterised by a shift of emission from red to yellow according to the degree of hydrophobicity of lipids (Fowler and Greenspan, 1985; Greenspan and Fowler, 1985; Greenspan et al., 1985). Therefore, unlike LipidTOX Red, Nile Red stain is able to detect both polar and non-polar/neutral lipids. Polar lipids such as phospholipids appear red while neutral lipids that are present in LDs, stain yellow-gold. Due to the significant emission spectral overlap of GFP and Nile Red fluorescence (Listenberger and Brown, 2007), Nile Red stain was only used in cells not expressing and GFP fusion proteins. As in LipidTOX Red staining, *S. cerevisiae* cells were washed in water and Nile Red was added to the cell suspension by diluting the manufacturer-supplied stock to a final 2 $\mu\text{g/ml}$ working concentration. The cell suspension in the Nile Red staining solution was incubated in the dark, at room temperature, for 15 min. Nile red-stained cells were washed once with water before visualisation. Cells were examined directly under the fluorescence microscope using the TX2 FLUO-Filtercube (excitation: 560/40 nm), suitable for visualisation of Nile Red fluorescence.

2.8.3 Peroxisome-targeted fluorescent protein (SKL-DsRed)

Peroxisome localisation was identified based on a peroxisome-targeted fluorescent protein (SKL-DsRed) (Brocard et al., 1997) (Table 2-3). Plasmids encoding SKL-DsRed (pJR233) were isolated from a culture of *E. coli* strain DH5 α as described in Section 2.4.1 and transformed into the sub-array plate containing all 110 mutants exhibiting strong A β ₄₂GFP-derived fluorescence (Section 2.7). Peroxisomes were visualised in the cells examined directly by fluorescence microscopy using the TX2 FLUO-Filtercube (excitation: 560/40 nm).

2.9 Scientific databases used in this study

The *Saccharomyces* Genome Database (SGD) and the accompanying Gene ontology (GO) annotation tool, GO Term Finder, genetic and physical interactions tools (<http://www.yeastgenome.org>) were used in the analysis of genes that when deleted, led to exhibition of A β ₄₂GFP-associated fluorescence. The Yeast GFP Fusion Localisation Database (<http://yeastgfp.ucsf.edu>) was used in the analysis of protein localisation in *S. cerevisiae* (Huh et al., 2003). Both the Munich Information centre for Protein Sequence (MIPS) Functional Catalogue Database (FunCatDB) (<http://mips.gsf.de/projects/funcat>) (Ruepp et al., 2004) and the FunSpec GO databases (GO-consortium, 2001; Robinson et al., 2002) were used for the analysis of gene function. For the quantitative analysis of determining over-representation of functional groups, FunSpec (Gene Ontology, 2001; Robinson et al., 2002; Ruepp et al., 2004) was used. Homologene (NCBI) is a program that makes use of amino acid sequence searching for the automated detection of homologues among annotated genes of several completely sequenced eukaryotic genomes (Wheeler et al., 2008). This program was used in the identification of human orthologues of *S. cerevisiae* genes. Negative genetic interaction networks were generated and analysed using a web-based database of quantitative genetic interaction networks called Data Repository of Yeast Genetic Function (DRYGIN) (<http://drygin.ccbr.utoronto.ca>) (Baryshnikova et al., 2010; Koh et al., 2010). The Yeast Resource Center Public Data Repository database (www.yeastrc.org/pdr) (Malmstrom et al., 2007; Reynolds et al., 2008; Riffle et al., 2005) was used in the identification of known signal sequences or transmembrane regions encoded by proteins.

2.10 Generation of strains and plasmids

2.10.1 Generation and transformation of BY4743 Rho-zero (Rho⁰) petite cells

The wild-type (BY4743) strain was rendered respiratory incompetent (Rho⁰) by loss of mtDNA according to the method reported by Fox et al., (1991). Briefly, wild type cells were grown in YPD media at 30°C for 24 h shaking at 600 rpm. Cells were inoculated into SCM containing 25 µg/ml ethidium bromide and incubated at 30°C for 72 h with shaking (600 rpm). After the initial ethidium bromide treatment, 50 µl of culture was re-inoculated into fresh SCM containing ethidium bromide and incubated for 72 h at 30°C. After the second round of ethidium bromide treatment, cells were

spread onto YPD agar media to produce single colonies. Following incubation at 30°C for 48 h, single colonies were picked/patched onto YPD and YPG (3% (v/v) glycerol, 2% (w/v) bacteriological peptone and 1% yeast extract) agar media and growth was assessed after 72 h of incubation. Cells that grew on YPD but not on YPG media were tested for complete loss of mitochondrial DNA content using DAPI staining (Section 2.8.1) (Fox et al., 1991). At least five independent rho⁰ cells generated were examined for each experiment.

2.10.2 Generation of plasmids

Aβ-GFP fusion constructs for the over-expression screen were generated using the Invitrogen Gateway system according to the manufacturer's instructions. Briefly, the primer pair attB1-Abeta-GFP and attB2-Abeta-GFP was used to generate the three Aβ-GFP fusion PCR fragments from pUG35GAL1-Aβ42, pUG35GAL1-Aβ40 and pUG35GAL1-AβEP respectively. These PCR fragments were used for the BP reaction of the Gateway system (Invitrogen, San Diego, CA, USA) with the destination vector pDONR221. The resulting plasmids, pDonr221-Aβ42-GFP/pDonr221-Aβ40-GFP/pDonr221-AβEP-GFP, were used for the LR reaction using the destination vector pAG415GAL-ccdB and pAG416GAL-ccdB (Alberti et al., 2007). This generated the following plasmids: pAG415GAL-Aβ42-GFP/ pAG415GAL-Aβ40-GFP/ pAG415GAL-AβEP-GFP/ pAG416GAL-Aβ42-GFP/ pAG416GAL-Aβ40-GFP/ pAG416GAL-AβEP-GFP. Using the method described above, control plasmids pAG415GAL-GFP/ pAG416GAL-GFP were generated using the primer pair attB1-GFP and attB2-Abeta-GFP. Plasmids were maintained and amplified in *E. coli* DH5α cells.

High-copy galactose-inducible plasmids (BG1805 family) containing *S. cerevisiae* open reading frames in the yeast ORF library (Gelperin et al., 2005) were purchased from OpenBiosystems. To generate the pAG426GAL-DAK2-EGFP fusion construct, the 2-step recombination reactions, BP and LR, was utilised to first shuttle *DAK2* into pDONR221 and subsequently into pAG426GAL1-ccdB-EGFP (Alberti et al., 2007). All plasmids were verified by sequencing using the DNA sequencing service provided by the Ramaciotti Centre for Gene Function Analysis, UNSW.

2.11 Proteomic methods

2.11.1 Protein extraction, SDS-PAGE and western blot analysis

Yeast cultures (50 ml) were grown to OD₆₀₀ of 1.5 in induction medium (SD-galactose) lacking uracil at 30°C. Cells were harvested, washed with water and lysed using a mini-bead beater (Biospec Scientific) (1 min high speed, 4°C) with acid-washed glass beads in ice-cold lysis buffer (0.1 mM Tris-HCl pH 8.0, 20% v/v glycerol) supplemented with protease inhibitors (CompleteTM, Roche). Samples were centrifuged (17500 g; 10 min; 4°C) and the protein concentration in the supernatant determined by Bradford protein assay (Pierce) or BioRad microtitre plate assay based on the methods of Bradford (1976) and Wright et al (1996). Total cellular proteins (15 µg per well) in sample loading buffer (Tris-HCl pH 6.8, 40% v/v glycerol, 5% v/v β-mercaptoethanol) were boiled for 10 min and separated by SDS-PAGE on Bis-Tris 4-12% NuPAGE gradient gels with MES running buffer (Invitrogen). Proteins were electroblotted onto nitrocellulose membranes for western blotting, and probed with rabbit anti-GFP (Invitrogen), mouse anti-Aβ (6E10; Covance), rabbit anti-Wbp1p, rabbit anti-Por1p (kind gifts from Prof. Guenter Daum, Institut für Biochemie, Technische Universität Graz), rabbit anti-Pgk1p (Santa Cruz Biotechnology) antibodies for 1 h at a 1:1000 dilution. Immunodetection was performed using appropriate horseradish peroxidase-conjugated secondary antibodies (Jackson Immunolaboratories) at a 1:5000 dilution and Amersham ECL advanced chemiluminescence detection kit (GE Healthcare). Analysis and quantitation of western blot images was performed using NIH ImageJ v1.38 software.

2.11.2 Protein-protein interaction network analysis

To determine protein interactions, protein-protein interaction networks were generated and analysed using the GEOMI visual analytic platform (GEOMetry for Maximum Insight) together with two metadata sets (Bertin et al., 2007; Yu et al., 2008). This work was completed in collaboration with the Systems Biology Initiative at University of New South Wales. Only direct interactions of proteins were mapped where a maximum distance of two interactions from the protein-of-interest was assessed.

2.12 Lipidomic methods

2.12.1 Total cellular lipid extraction and lipidomic profiling using mass spectrometry

Total lipid compositions of samples were determined by quantitative shotgun lipidomic analysis as previously described (Ejsing et al., 2009; Surma et al., 2011). Briefly, cells expressing the A β ₄₂GFP fusion were grown to exponential phase (OD₆₀₀ 1.5) in galactose induction medium, washed and resuspended in 150 mM ammonium bicarbonate. Cells were lysed using 200 μ l of Zirconia beads in the TissueLyser II (Qiagen) (20 min; 4°C) and a volume equivalent to 0.2 OD₆₀₀ units was diluted with ammonium bicarbonate up to 200 ml. Samples were spiked with 30 μ L of internal lipid standard mixture providing a total of 24 pmol diacylglycerol (DAG) 17:0-17:0, 22 pmol PA 17:0-14:1, 41 pmol PE 17:0-14:1, 41 pmol PS 17:0-14:1, 42 pmol PC 17:0-14:1, 40 pmol PI 17:0-14:1, 14 pmol CL 15:0-15:0-15:0-16:1, 22 pmol ceramide 18:0;3/18:0;0, 37 pmol IPC 18:0;2/26:0;0, 36 pmol MIPC 18:0;2/26:0;0, 31 pmol M(IP)₂C 18:0;2/26:0;0 and 57 pmol cholesterol-D7. Two-step lipid extraction described in Klose et al., 2012 was carried out on samples and lipid extracts were dissolved in 100 μ l chloroform/methanol (1:2, v/v). Quantitative mass spectrometric analysis was carried out using an LTQ Orbitrap XL (Thermo Fisher Scientific) equipped with a robotic nanoflow ion source TriVersa NanoMate (Advion Biosciences, Inc.). Glycerophospholipids (phosphatidic acid, PA; phosphatidylcholine, PC; phosphatidylethanolamine, PE; phosphatidylinositol, PI; phosphatidylserine, PS; cardiolipin, CL) and complex sphingolipids (inositolphosphorylceramide, IPC; mannosyl-inositol phosphorylceramide, MIPC; mannosyl-di-(inositolphosphoryl) ceramide, M(IP)₂C) species were analysed by negative ion mode Fourier transform ion cyclotron resonance mass spectrometry (FT MS), while diacylglycerol (DAG) and ceramide species (Cer) were analysed by positive ion mode FT MS. Ergosterol and cholesterol-D7 were derivatised using sulfation and analysed by negative ion mode FT MS (Sandhoff et al., 1999). This quantitative shotgun lipidomic analysis was performed in conjunction with Christian Klose and Andrej Shevchenko, Max Planck Institute – Cell Biology and Genetics, Dresden, Germany.

Lipid species identification and quantitative analysis were performed using LIPIDX software (Herzog et al., 2011). Lipid species were annotated according to their

molecular composition. Glycerophospholipid and diacylglycerol species are annotated as: <lipid class><sum of carbon atoms in the two FAs>:<sum of double bonds in the two FAs> (e.g. PC 36:1). Sphingolipid species are annotated as: <lipid class><sum of carbon atoms in the long chain base (LCB) and fatty acid (FA) moiety>:<sum of double bonds in the LCB and the FA moiety>;<sum of hydroxyl groups in the LCB and the FA moiety> (e.g. MIPC 46:1;2).

2.12.2 Polar lipid extraction and one-dimensional thin-layer chromatography

Total polar lipid extracts were prepared from cells expressing A β ₄₂GFP grown to exponential phase (OD₆₀₀ 1.5) in galactose induction medium based on Folch et al., (1957). Briefly, cells were harvested, washed in distilled water and resuspended in 4 ml breakage buffer (5 mM MES, 1 mM KCl, 0.5 mM EDTA, 0.6 M sorbitol, pH 6.0). Two volumes of acid-washed glass beads were added and cells were lysed using a mini-bead beater for an 1 h at 4 °C. Upon determination of protein concentration (Lowry et al., 1951), 2 mg of protein from the total cell lysates were used for lipid extraction. Appropriate amount of total cell lysate was added to 3 ml of CHCl₃:MeOH (2:1; v/v) and polar lipids were extracted to the organic phase while vortexing at room temperature for 1 h. Contaminating proteins were removed by consecutive washing with 0.2 volumes 0.034 % MgCl₂, 1 ml 2 N KCl/MeOH (4:1; v/v) and 1 ml of an artificial upper phase (CHCl₃:MeOH:H₂O; 3:48:47; per vol.). Upon centrifugation, the aqueous phase was removed by aspiration and lipids dried down under gaseous N₂ (Folch et al., 1957).

Polar lipids were separated by one-dimensional thin-layer chromatography (TLC) on silica gel 60 plates (Merck, Germany) using chloroform/methanol/acetic acid/water (80:10:10:2.5; v/v) as developing solvent (Letts and Dawes, 1983). Individual lipid spots were visualised by staining with iodine vapour in a saturated chamber for 10 min.

2.13 Biochemical methods

2.13.1 Assessment of the effects of choline supplementation to mutants exhibiting strong A β ₄₂GFP derived fluorescence

Selected *S. cerevisiae* strains were grown in SCM-URA in a 96-well flat bottom plate at 30° C with shaking for 48 h. Cells were replicated into 2 fresh 96-well plates; one containing SCgal-URA and the other SCgal-URA supplemented with 1 mM choline. These plates were incubated at 30°C with shaking for 24 h and replicated into a fresh 96-well plate containing the appropriate media prior to screening via microscopic analysis, outlined in Sections 2.7 and 2.8. To identify mutants that were reproducibly able to exhibit a reversal of the A β ₄₂GFP fluorescence, when grown in the presence 1 mM choline, A β ₄₂GFP-associated fluorescence was analysed by counting fluorescent cells in three replicates in a single experiment.

2.13.2 Assessment of the effects of dihydroxyacetone (DHA) supplementation to wild-type cells expressing A β ₄₂-GFP

Wild-type cells were grown in SCM-URA in a 96-well flat bottom plate at 30° C with shaking for 48 h. Cells were replicated into 2 fresh 96-well plates; one containing SCgal-URA and the other SCgal-URA supplemented with 50 μ M DHA. These plates were incubated at 30°C with shaking for 24 h and replicated into a fresh 96-well plate containing the appropriate media prior to screening via microscopic analysis, outlined in Sections 2.7 and 2.8. To identify whether wild-type cells were able to exhibit fluorescence due to an accumulation of dihydroxyacetone or dihydroxyacetone phosphate, when grown in the presence 50 μ M DHA, A β ₄₂GFP-associated fluorescence was analysed by flow cytometry in three replicates in a single experiment. 10,000 cells were counted for each sample.

2.13.3 Assessment on the effects of citrate supplementation in BY4743 wild-type cells expressing A β ₄₂GFP

Wild-type cells (BY4743) expressing A β ₄₂GFP were grown in SCM-URA in a 96-well flat bottom plate at 30°C for 48 h with shaking. Cells were replicated in to fresh plate of SCgal-URA containing no citric acid, 20 mM, 40 mM, 60 mM, 80 mM and 100 mM citric acid and incubated at 30°C with shaking for 48 h. Following incubation, cells

were induced in SCgal-URA supplemented with various concentrations of citric acid and screened for A β ₄₂GFP-derived fluorescence as described in Section 2.7 and 2.8. To identify whether wild-type cells were able to exhibit fluorescence due to an accumulation of citrate, A β ₄₂GFP-associated fluorescence was analysed by counting fluorescent cells in three replicates in a single experiment.

2.13.4 Subcellular fractionation – Mitochondrial and ER fractions

Subcellular fractions of *S. cerevisiae* cells were prepared as previously described (Serrano, 1988; Leber et al., 1994; Zinser and Daum, 1995; Rosenberger et al., 2009) and the purity of the ER and mitochondrial fractions verified by western blot analysis using antibodies against Wbp1p and Por1p respectively. Briefly, cells expressing A β ₄₂GFP were grown to exponential phase (OD₆₀₀ 1.5) in galactose (induction) medium, harvested, washed in distilled water and converted to spheroplasts (Daum et al., 1982). Preparation of spheroplasts was performed using 2 mg zymolyase 20T per gram of cell wet weight and incubating for 1.5 h at 30 °C shaking (600 rpm). Spheroplasts were homogenised on ice using a Dounce homogeniser with a tight fitting pestle and centrifuged to remove unbroken cells and nuclei. For preparation of crude mitochondrial fraction, cell lysates were centrifuged at 30,000 g (30 min; 4°C). In order to enhance the yield and purity of mitochondria, the resulting pellet was thrice resuspended in breakage buffer, re-homogenised and centrifuged as described above. For preparation of crude ER microsomal fraction, the remaining supernatant was centrifuged at 45,000 g (45 min; 4°C). In order to enhance the yield and purity of ER, the resulting pellet was resuspended in breakage buffer, re-homogenised and centrifuged as described above. To determine the purity of the subcellular fractions, proteins from these fractions were precipitated with 50% trichloroacetic acid for an hour on ice, protein concentration was determined (Lowry et al., 1951) and western blot analysis was subsequently performed as described in Section 2.11.1. This subcellular fractionation was performed in conjunction with Vid Vojko Flis and Guenter Daum, Institut für Biochemie, Technische Universität Graz, Austria.

2.14 High-content chemical and drug libraries screen

Both the Library of Pharmacologically Active Compounds (LOPAC¹²⁸⁰®, Sigma-Aldrich), composed of 1280 compounds, and the Spectrum Collection library (MicroSource Discovery Systems, Gaylordsville, CT, USA), containing 1997 compounds, were used in the high-throughput chemical and drug screen for modifiers of A β ₄₂GFP and A β ₄₀GFP aggregation/fluorescence in *S. cerevisiae*. The chemical/drug compounds from the LOPAC and SPECTRUM libraries were diluted in dimethyl sulfoxide (DMSO) to a final concentration of 1 mM and stored at -80°C in 96-well plates. The automated use of the CyBi[®]-Well 96- and 384-Channel Simultaneous Pipettor (CyBio, Germany) and the accompanying CyBio[®] Composer software enabled the precise aliquot of 2 μ l of the chemical/drug compounds from both libraries, in duplicates, into CellCarrier[™] 384-well clear bottomed microplates (PerkinElmer Inc., Waltham, MA, USA) containing SCgal-URA (induction) media to a final concentration of 20 μ M. Plates containing chemical/drug compounds in induction media were prepared two days (maximum) prior to the screening and stored at 4°C.

Wild-type yCG253 cells expressing either A β ₄₂GFP or A β ₄₀GFP co-expressed both a nuclear marker, nuclear localisation signal (NLS) tagged to fluorescent marker RedStar2 (NLS-RedStar2) and a cytosolic marker, mCherry expressed in the cytosol, under the regulation of the constitutive *TEF2* promoter (Table 2-1). Cells were grown to exponential phase (OD₆₀₀ 1.5) in galactose (induction) medium, diluted to an OD₆₀₀ 0.1 and used to inoculate 384-well plates containing 20 μ M chemical/drug compounds in SCgal-URA. The first two columns and last two columns of each 384-well plate were designated as controls where wild-type cells expressing either A β ₄₂GFP or A β ₄₀GFP were grown in SCgal-URA and DMSO. Freshly-inoculated 384-well plates were incubated at 30°C for 4 h (without shaking) and analysed using the Opera[®] High Content Screening System (PerkinElmer, USA) as previously described (Bircham et al., 2011). Two separate images were taken for each sample using the high-throughput microlens-enhanced Nipkow spinning disc confocal microscope on the 60X water immersion lens NA 1.2. GFP, and, RedStar2 and mCherry-associated fluorescence were excited using 488 nm and 561 nm lasers respectively, with emission fluorescence captured through 520/35 and 600/40 dual filter cameras at a focal distance of 4 μ m with 400 ms exposure.

High-throughput image analysis was carried out using Evotec Technologies AcapellaTM image analysis software v2.0 suite of scripts accompanying the Opera high-throughput confocal microscope. Live cells were identified using the NLS-RedStar2 nuclear marker and the mCherry cytosolic marker. During the image analysis, autofluorescence from dead cells, crystallising drugs and other artefacts were omitted by restricting fluorescence intensity, size and roundness of cells. In addition to the automated image analysis described above, manual inspection of the images removed any false-positives. This high-content chemical and drug libraries screen was performed in conjunction with Peter Bircham and Paul Atkinson, Victoria University of Wellington, NZ.

2.15 Statistical analyses

Statistical analysis was performed using the unpaired Student's *t*-test, using Prism 5 for Windows version 5.02 (GraphPad Software, Inc., La Jolla, CA, USA). Data are presented as mean \pm standard deviation. Significant differences are indicated by a *p* – value for data in the text and figures.

For the analysis of the genome-wide screen data, significant terms were determined using the Gene Ontology (GO) and Munich Information Centre for Protein Sequences (MIPS) databases via FunSpec (Robinson et al, 2002), with the *p* – value threshold set at 0.01. FunSpec calculated *p*-values using a hypergeometric distribution, and the *p* – value represent the probability that the intersection of a given list with any given functional category occurs by chance. The *p* – values were Bonferroni corrected which accounts for spurious significance due to multiple testing over the categories of a database.

3 CHAPTER 3: GENOME-WIDE DELETION ANALYSIS IDENTIFIES CELLULAR PROCESSES AFFECTING AMYLOID-BETA AGGREGATION IN *S. CEREVISIAE*

3.1 Introduction and Aims

GFP folding has been exploited to study the kinetics of protein aggregation in *E. coli* (Waldo et al., 1999). In an aggregation reporter assay developed by Waldo et al., (1999), the fluorescence from a GFP fluorophore is related to the productive folding of the upstream fusion protein and avoidance of inclusion body formation. If the GFP-fused protein aggregates prior to fluorophore folding, GFP-associated fluorescence is not observed. In applying the GFP-based aggregation assay to study aspects of A β ₄₂ aggregation, consecutive studies by Wurth et al., (2002), and, Kim and Hecht (2005) (A β GFP) developed an aggregation assay in *E. coli* cells that used A β fused to GFP (A β GFP). It was found that cells expressing A β ₄₂GFP do not exhibit fluorescence, whereas cells expressing the less-aggregation prone A β ₄₀GFP or GFP exhibited high levels of fluorescence (Kim and Hecht, 2005; Wurth et al., 2002). The lack of fluorescence was attributed to the aggregation of the A β ₄₂-moiety of the fusion protein, prior to the formation of the fluorophore. This was further confirmed via biophysical analysis (Kim and Hecht, 2008).

The budding yeast *Saccharomyces cerevisiae* has served as an important eukaryote model organism for understanding many aspects of eukaryotic molecular biology. Interestingly, *S. cerevisiae* has also been exploited for the study of proteins implicated in neurodegenerative disorders including Alzheimer's disease (Komano et al., 1998; Treusch et al., 2011; Zhang et al., 1994; Zhang et al., 1997). In this chapter, a GFP-derived fluorescence-based assay for intracellular A β ₄₂ aggregation was developed and characterised in *S. cerevisiae*. The assay for A β ₄₂GFP aggregation previously reported by Kim and Hecht (2005) in *E. coli* was recapitulated in *S. cerevisiae*. This facilitated screening of the genome-wide deletion library for genes and cellular processes affecting intracellular A β ₄₂ aggregation by assessing the fluorescence associated with A β ₄₂GFP expression. The work described in this chapter further examines these cellular mechanisms. In order to further understand these cellular

processes involved in A β aggregation, A β_{40} GFP fluorescence and intracellular localisation of was also examined.

3.2 Results - Development of the A β GFP fusion-associated aggregation/fluorescence assay

3.2.1 Fluorescence production in wild-type cells expressing enhanced green fluorescent protein fused to A β_{42} (A β_{42} GFP)

Wild-type (BY4743) *S. cerevisiae* cells were transformed with plasmids encoding enhanced green fluorescent protein (GFP) or GFP fused to the C-terminus of A β_{42} (Section 2.1.3). Expression of the plasmid-encoded GFP or the A β_{42} GFP fusion was under the regulation of a *GALI* promoter, which induced expression of GFP or A β_{42} GFP when cells were grown in galactose medium (SCgal-URA). Wild-type cells exhibiting GFP and A β_{42} GFP-associated fluorescence were visualised via microscopic analysis at 10, 20 and 30 h after induction in SCgal-URA. Wild-type cells expressing the A β_{42} GFP fusion peptide yielded very weak A β_{42} GFP-associated fluorescence that was restricted to $5\% \pm 2.0\%$ of the cell population (Figure 3-1A). A β_{42} GFP-associated fluorescence was absent at 30 h post induction, with no fluorescent cells were observed.

In contrast to wild-type cells expressing A β_{42} GFP, wild-type cells expressing GFP (i.e. unfused) yielded a significantly higher ($p < 0.00001$) proportion of fluorescent cells which exhibited cytosolic-diffuse fluorescence in $85\% \pm 5\%$ of the cell population (Figure 3-1B). In wild-type cells GFP-associated fluorescence was maintained at 10, 20 and 30 h post induction in galactose medium. Quantification of fluorescence intensity using the FLUOstar OptimaTM fluorescent plate reader (BMG Labtech, Germany) at 20 h post induction indicated that the average relative intensity of A β_{42} GFP-associated fluorescence in wild-type cells was significantly lower ($p < 0.00001$) than those exhibiting only GFP fluorescence (Figure 3-1).

Acknowledgement: The development of A β constructs, transformation and screening of the genome-wide yeast deletion library was performed in conjunction with Mathew Traini, a previous Doctoral candidate in the laboratory of Prof. Ian Dawes.

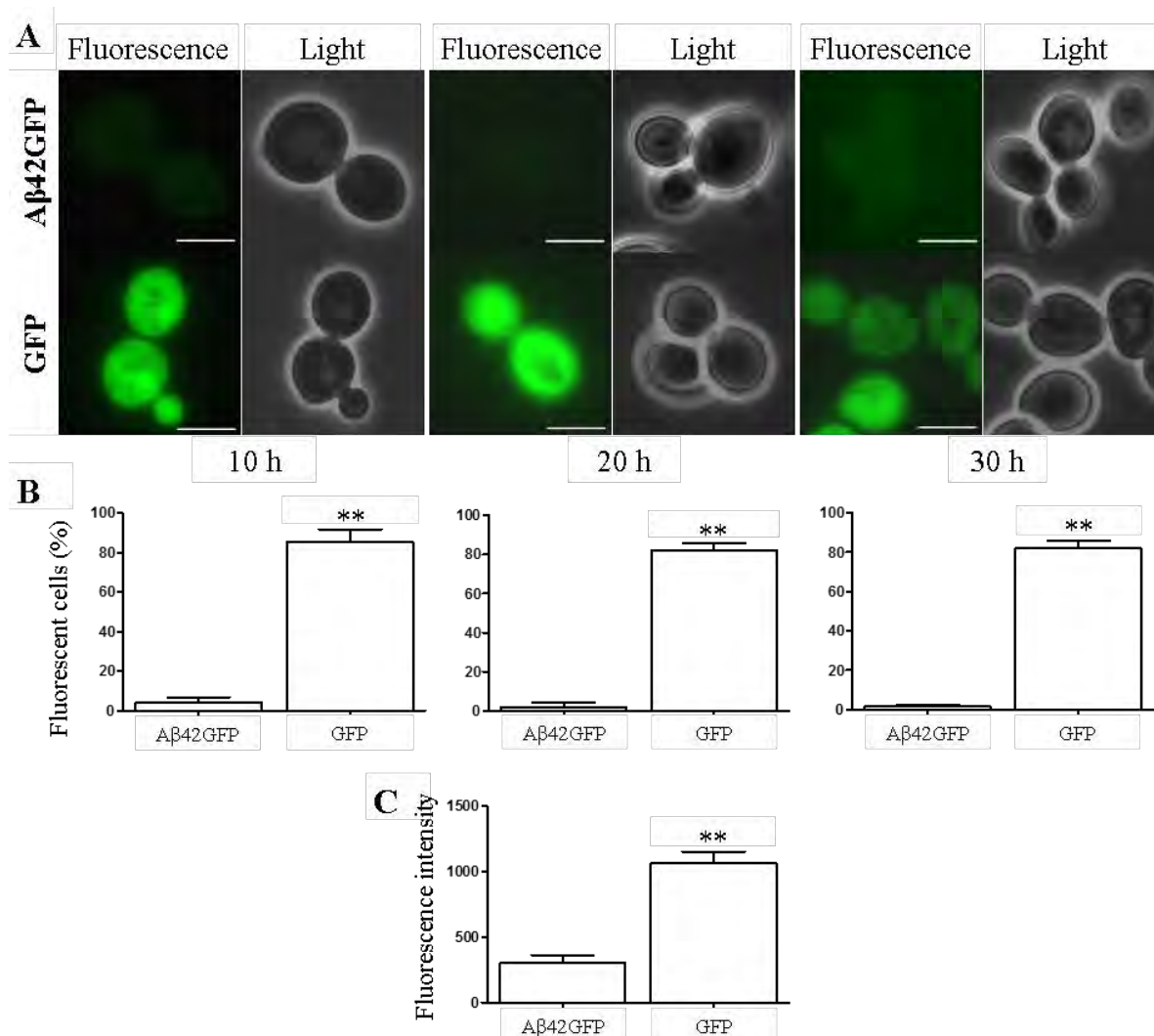


Figure 3-1 Fluorescent cell population in wild-type cells expressing Aβ₄₂GFP or GFP.

A) Fluorescent and light microscopic images (100 X magnification) of wild-type cells expressing GFP or Aβ₄₂GFP at 10, 20 and 30 h post induction in galactose medium (SCgal-URA). B) Quantification of the proportion of fluorescent cells in wild-type cells expressing GFP or Aβ₄₂GFP at 10, 20, and 30 h post induction in galactose medium. C) Quantification of average fluorescence intensity of fluorescing wild-type cells expressing GFP or Aβ₄₂GFP at 20 h post induction. The data shown are the means of triplicate measurements ± standard deviation from two independent experiments. Asterisks (**) denote a significant difference ($p < 0.0001$) in the abundance of fluorescent cells between wild-type cells expressing GFP versus Aβ₄₂GFP. Scale bars indicate 5 μm.

Lack of Aβ₄₂GFP fluorescence by wild-type cells was hypothesised to be due to aggregation of the Aβ₄₂-moiety of the fusion peptide prior to, and/or interfering with, correct folding of the GFP fluorophore. This hypothesis was based on the observation that full length Aβ₄₂GFP was detected at reasonable abundance by western blot analysis of total cellular protein extracts when its expression was induced in wild-type cells (Figure 3-3). These data also indicated that Aβ₄₂GFP fusion protein was expressed intact in wild-type cells and that separate Aβ or GFP proteins were not detected in cells

expressing A β ₄₂GFP fusion peptides. Therefore, the absence of A β ₄₂GFP-associated fluorescence in wild-type cells was likely to be due to aggregation of the A β ₄₂-moiety of the fusion protein. To examine this proposal further, two less aggregation-prone variants of A β (Kim and Hecht, 2005), fused to GFP, specifically A β ₄₀GFP or A β _{EP}GFP, were introduced into wild-type cells. The reduced propensity for aggregation of the A β ₄₀ and A β _{EP} variants of A β is described in more detail in Sections 1.3.1 and 3.3.

3.2.2 Fluorescence production in wild-type *S. cerevisiae* cells expressing less aggregation-prone forms of A β : A β ₄₀GFP or A β _{EP}GFP

Wild-type cells expressing A β ₄₀GFP or A β _{EP}GFP were analysed for A β GFP-associated fluorescence via microscopic analysis 12 h post induction in galactose medium. Expression of A β ₄₀GFP yielded predominantly cytosolic-diffuse fluorescence (Figure 3-2A) in 50% \pm 5% of the cell population, with ~20% of these fluorescent cells exhibiting one or more fluorescent puncta. The proportion of fluorescent cells observed with A β ₄₀GFP was significantly higher ($p < 0.001$) than those expressing A β ₄₂GFP; but, lower ($p = 0.0024$) relative to number of wild-type cells expressing GFP, under identical conditions. The relative intensity of A β ₄₀GFP-associated fluorescence also appeared significantly lower ($p < 0.0001$) compared to wild-type cells expressing GFP alone (Figure 3-2B), but significantly higher ($p = 0.00019$) than those expressing A β ₄₂GFP. Since A β ₄₀ is less prone to aggregation than A β ₄₂, these data indicated that if the A β -moiety of the fusion peptide did not aggregate, prior to the correct folding of the GFP fluorophore, A β GFP-associated fluorescence was observed.

This hypothesis was further supported by experiments performed using wild-type cells expressing A β _{EP}GFP, which exhibited strong cytosolic-diffuse A β _{EP}GFP-associated fluorescence in 60% \pm 8% of the cell population (Figure 3-2A). Approximately 5% of cells expressing A β _{EP}GFP also contained A β _{EP}GFP-associated fluorescent puncta. The proportion of wild-type cells exhibiting A β _{EP}GFP-associated fluorescence was significantly higher than cells expressing A β ₄₂GFP ($p < 0.00001$) or A β ₄₀GFP ($p = 0.15$) (Figure 3-2B); but significantly lower ($p = 0.015$) than those expressing unfused GFP. The average relative fluorescence intensity produced with A β _{EP}GFP also appeared significantly higher than those observed with A β ₄₂GFP ($p <$

0.00001) or A β ₄₀GFP ($p = 0.001$) but comparable to those expressing unfused GFP (Figure 3-2B).

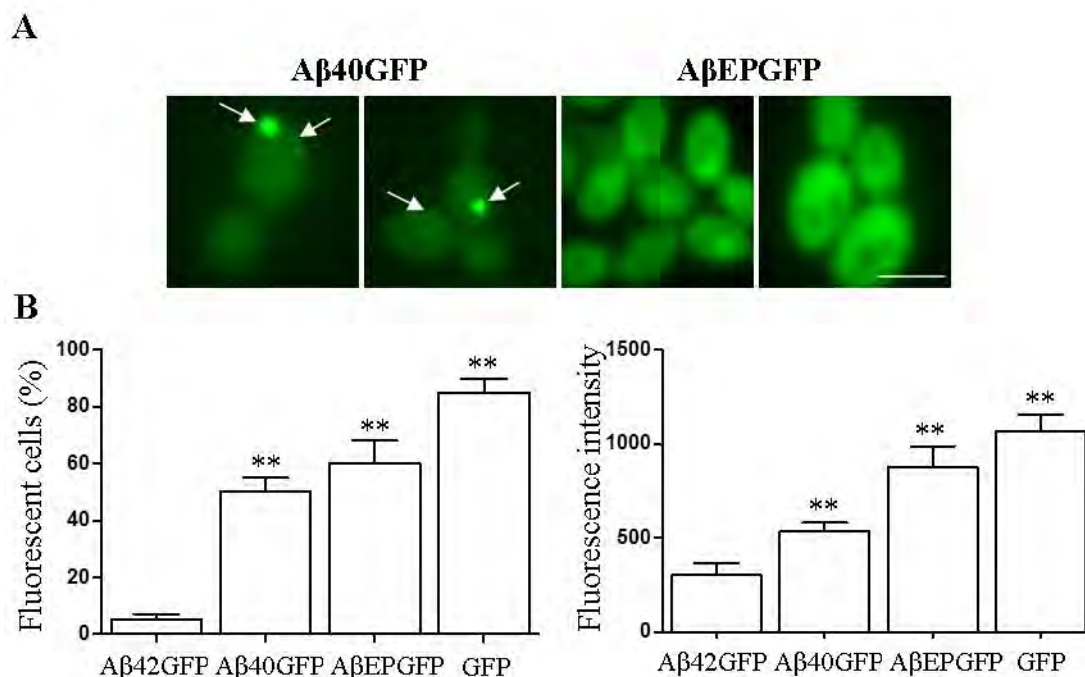


Figure 3-2 Fluorescent cell population in wild-type cells expressing A β ₄₂GFP, A β ₄₀GFP, A β _{EP}GFP or GFP.

A) Wild-type cells expressing A β ₄₀GFP (two left panels) or A β _{EP}GFP (two right panels) were induced in galactose medium (SCgal-URA) and A β GFP-associated fluorescence analysed at 12 h. Wild-type cells expressing A β ₄₀GFP, exhibited moderate cytosolic-diffuse fluorescence with multiple fluorescent puncta (indicated by the arrows). Wild-type cells expressing A β _{EP}GFP (right panels) exhibited strong cytosolic-diffuse fluorescence. Scale bars indicate 5 μ m. B) Quantification of the proportion of fluorescent cells (left panel) and the corresponding fluorescence intensities of fluorescing wild-type cells expressing A β ₄₂GFP, A β ₄₀GFP, A β _{EP}GFP or GFP. The data shown are the means of triplicate measurements \pm standard deviation from a single experiment. Asterisks (**) denote a significant difference ($p < 0.001$) in the abundance of fluorescent cells and higher fluorescence intensities between wild-type cells expressing GFP, A β ₄₀GFP or A β _{EP}GFP versus A β ₄₂GFP.

Both the percentage of fluorescent cells and their relative degree of fluorescence intensity were in the order GFP > A β _{EP}GFP > A β ₄₀GFP > A β ₄₂GFP (Figures 3-1B and 3-2B). This trend in fluorescence inversely correlates with the propensities of A β ₄₂, A β ₄₀, A β _{EP} variants and GFP to undergo aggregation (Kim and Hecht, 2005; Kim and Hecht, 2008). These results are consistent with the hypothesis that aggregation of the A β ₄₂-moiety of the fusion protein affects fluorescence production by interfering with the folding state of the GFP fluorophore. Since A β ₄₀GFP in wild-type cells yielded a higher abundance of intense A β ₄₀GFP-associated fluorescence relative to A β ₄₂GFP, these data also highlight that in terms of aggregation propensity, A β peptides appear to behave in

an analogous manner in *S. cerevisiae*, as in humans (A β ₄₂ and A β ₄₀) (Gouras et al., 2005; Gouras et al., 2000) and in *E. coli* (A β ₄₂, A β ₄₀ and A β _{EP}) (Kim and Hecht, 2005; Kim and Hecht, 2008; Wurth et al., 2002). These observations support the validity of using *S. cerevisiae* to investigate factors affecting intracellular A β ₄₂ aggregation; i.e., through the analysis of fluorescence production by A β GFP fusions.

3.2.3 Western blot analysis of wild-type cells expressing A β ₄₂GFP, A β ₄₀GFP, A β _{EP}GFP or GFP

This inverse correlation between fluorescence intensity and the amyloidogenicity of the A β moiety supported the validity of using A β ₄₂GFP and a fluorescence-based approach in *S. cerevisiae* cells to identify cellular factors that may influence intracellular A β ₄₂ aggregation. However, it was important to investigate if the increased A β ₄₀GFP and A β _{EP}GFP fluorescence was due to increased levels of non-aggregated and soluble A β GFP fusion proteins. In order to assess if increased fluorescence was due to an increase in soluble A β GFP, wild-type BY4743 cells expressing A β ₄₂GFP, A β ₄₀GFP, A β _{EP}GFP fusion proteins or unfused GFP were grown to exponential phase (OD₆₀₀ 1.5) in galactose (induction) medium.

The expected molecular mass of A β GFP fusion protein is approximately 32 kDa. Cells expressing any of the forms of A β GFP fusion exhibited a characteristic band of ~30 kDa expected from the molecular mass of the fusion proteins (Figure 3-3). The relative intensity of this ~30kDa band in soluble cell fractions of wild-type cells expressing A β ₄₂GFP, A β ₄₀GFP or A β _{EP}GFP fusion proteins indicated that the higher fluorescence associated with the expression of a less aggregation-prone moiety of A β fused to GFP (i.e. A β ₄₀GFP and A β _{EP}GFP) was not due to increased expression or accumulation of soluble A β GFP fusion protein. Furthermore, the western blot analysis further validated that the aggregation-prone A β ₄₂GFP was still present in wild-type cells but lacked fluorescence due to aggregation associated with the A β ₄₂ moiety.

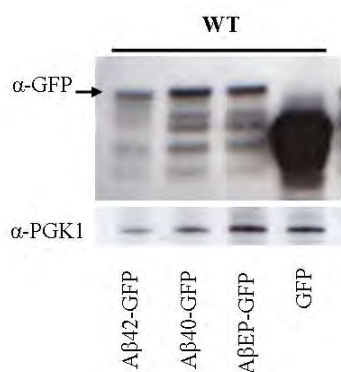


Figure 3-3 Western blot analysis of soluble cell extracts from BY4743 wild-type cells expressing A β ₄₂GFP, A β ₄₀GFP, A β _{EP}GFP and GFP control vector

Load-controlled soluble cell extracts were prepared from wild-type cells expressing A β ₄₂GFP, A β ₄₀GFP, A β _{EP}GFP fusion proteins or unfused GFP were grown to exponential phase (OD₆₀₀ 1.5) in galactose (induction) medium. Analysis by western blot analysis was carried out using anti-GFP antibody. PGK1p was used as a loading control.

3.2.4 A β ₄₂ seeds formation of punctate aggregates of A β ₄₀

A β toxicity has been shown to correlate with the presence of fibrils or β -sheet structures (Howlett et al., 1995; Seilheimer et al., 1997; Simmons et al., 1994). However, gaps remain in understanding mechanisms by which A β aggregation mediates neuronal death. A β aggregation proceeds by a multistep, nucleation-dependent process (Jarrett and Lansbury, 1993). Formation of nucleation seeds is rate limiting. In the absence of preformed seed fibrils there is a significant lag period for the formation of A β fibrils, followed by a rapid fibril elongation phase once seed fibrils have been generated. The lag time for fibril formation can be dramatically shortened by adding preformed fibril seeds to A β monomer (Jarrett and Lansbury, 1993) and the rate of A β fibril formation is controlled by both fibril seed and monomer concentrations (Naiki and Nakakuki, 1996). To examine if the more aggregation prone A β ₄₂GFP affected fluorescence produced by the less aggregation prone A β ₄₀GFP form, parallel expression in wild-type cells of GFP tagged A β ₄₂ and A β ₄₀, A β ₄₂ and A β _{EP}, and, A β ₄₀ and A β _{EP} were undertaken.

The co-expression analysis made use of the various A β GFP fusions constructs in the pUG35GAL1 vector (under the *URA3* selectable marker) and the pAG415GAL1 vector (under the *LEU2* selectable marker) to allow co-expression of various A β GFP fusions in cells. As controls, wild-type BY4743 cells were co-transformed with of A β GFP fusions in the pUG35GAL1 plasmid together with pAG415GAL1 (an empty

LEU2 vector). Co-expression of the A β GFP fusion proteins in each strain was induced by growth in galactose medium and A β GFP-associated fluorescence was analysed 15 h post-induction.

Co-induction of A β_{42} GFP and A β_{40} GFP gave rise to more fluorescent cells (~22%) than those expressing A β_{42} GFP alone (5%) but significantly fewer than cells expressing A β_{40} GFP alone (~40%; Figure 3-4). Cells expressing both A β_{42} GFP and A β_{40} GFP exhibited trace cytosolic fluorescence with intense large puncta and in some cells there were elongated structures (Figure 3-4). Co-induction of A β_{42} GFP and A β_{EP} GFP in wild-type cells also gave rise to more fluorescent cells (~28%; exhibiting cytosolic fluorescence with small intense puncta) compared to those expressing A β_{42} GFP alone but significantly fewer than cells expressing A β_{EP} GFP alone (~70%). Co-induction of A β_{40} GFP and A β_{EP} GFP in wild-type cells gave rise to intense cytosolic fluorescent cells (~60%) comparable to wild-type cells expressing A β_{EP} alone and 30% of the fluorescent cells contained small puncta (Figure 3-4). The increased presence of puncta and lower levels of cytosolic fluorescence in wild-type cells co-expressing either A β_{42} GFP and A β_{40} GFP or A β_{42} GFP and A β_{EP} GFP, indicate that the more aggregation prone A β_{42} GFP can act as a seed for aggregation. Preformed A β_{42} GFP aggregates formed in the cytosol may therefore accelerate nucleation and act as seeds for further formation of intracellular aggregates and fibrils.

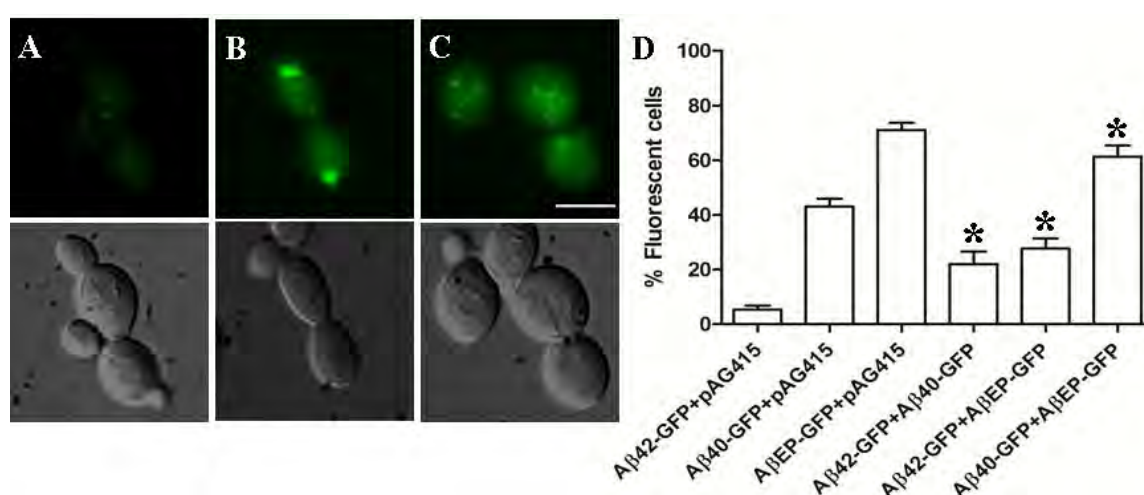


Figure 3-4 Fluorescent cell population of wild-type cells co-expressing A β_{42} GFP A β_{40} GFP or A β_{EP} GFP.

Fluorescent microscopic images of wild-type cells co-expressing (A) A β_{42} GFP and A β_{40} GFP (B) A β_{42} GFP and A β_{EP} GFP (C) A β_{40} GFP and A β_{EP} GFP. Wild-type cells expressing the above constructs were induced in SCgal-URA medium and fluorescence analysed at OD₆₀₀ 1.5. Bar, 5

μm. (D) Proportion of fluorescent wild-type cells expressing GFP, Aβ₄₂GFP, Aβ₄₀GFP or Aβ_{EP}GFP. 900 cells were counted per sample and data shown is an average of three independent experiments. Asterisks (*) denote $p < 0.01$.

3.2.5 Screening of the *Saccharomyces cerevisiae* genome-wide deletion library for genetic factors affecting Aβ₄₂GFP fluorescence

The *S. cerevisiae* genome-wide deletion library utilised in this study consisted of ~4600 diploid strains, otherwise isogenic except that one of each of 4600 non-essential genes was deleted in a given strain (Winzeler et al., 1999). In order to introduce the pUG35GAL1-Aβ₄₂ plasmid, which encodes the Aβ₄₂GFP fusion, into the strains of the *S. cerevisiae* genome-wide library, an established standard lithium acetate *S. cerevisiae* transformation method developed by Gietz and Woods (2002) was modified and implemented for the high-throughput transformation of strains (Section 2.6.2). Transformation of each of the ~4600 strains with the pUG35GAL1-Aβ₄₂ plasmid was attempted. Approximately 95% of the genome-wide deletion mutants were transformed; those not successfully transformed are listed in Appendix A. All transformed strains were maintained in synthetic complete glucose media lacking uracil (SCM-URA) in 96-well plates.

3.2.6 Pilot-scale screening of the *S. cerevisiae* deletion library to establish parameters and selection criteria for use in the genome-wide screening

For screening of the *S. cerevisiae* genome-wide deletion library, expression of Aβ₄₂GFP was induced by growth of cells, transformed with pUG35GAL1-Aβ₄₂, in galactose medium (SCgal-URA) prior to microscopic analysis. Some transformed strains that grew in glucose-supplemented medium, did not grow in galactose-supplemented medium (SCgal-URA) and therefore were not screened. Prior to commencing the high-throughput analysis, it was important to define the selection criteria that would be used for classifying strains during the genome-wide screen. A pilot scale screen of ~600 strains was undertaken to establish suitable parameters and selection criteria to determine the optimal conditions for screening Aβ₄₂GFP-associated fluorescence production on a genome-wide scale. Mutant strains transformed with pUG35GAL1-Aβ₄₂ plasmid were grown in galactose media (SCgal-URA) and fluorescence examined between 12 and 18 h via microscopic analysis. The 12 to 18 h time interval was selected since wild-type cells expressing GFP alone (Figure 3-1) and

the less aggregation-prone A β_{40} GFP or A β_{EP} GFP, exhibited a relatively constant degree of fluorescence between 12 to 18 h post induction. This pilot scale screen also enabled the preliminary investigation of the effect of a subset of the genome-wide deletion library on A β_{42} GFP fluorescence.

In broad terms, three distinct phenotypes were observed with respect to A β_{42} GFP-associated fluorescence. First, most mutants exhibited trace levels of fluorescence in a limited number of cells, which was qualitatively comparable to wild-type cells expressing A β_{42} GFP. These mutants were classified as exhibiting a wild-type (or trace) fluorescence phenotype (hereinafter as wild-type levels/phenotype). Secondly, mutants that exhibited faint or weak A β_{42} GFP-associated fluorescence in a small proportion of the cell population (between 5-10%) were classified as exhibiting a weak/moderate fluorescence phenotype. Finally, mutants that produced intense A β_{42} GFP-associated fluorescence in 10% or more of the cell population were classified as exhibiting a strong fluorescence phenotype. Figure 3-5 displays representative images of mutants scored as exhibiting strong, weak or wild-type fluorescence phenotypes associated with A β_{42} GFP expression. The parameters and selection criteria established during the pilot scale screen were implemented for the screening of the *S. cerevisiae* genome-wide deletion library (Section 3.2.7).

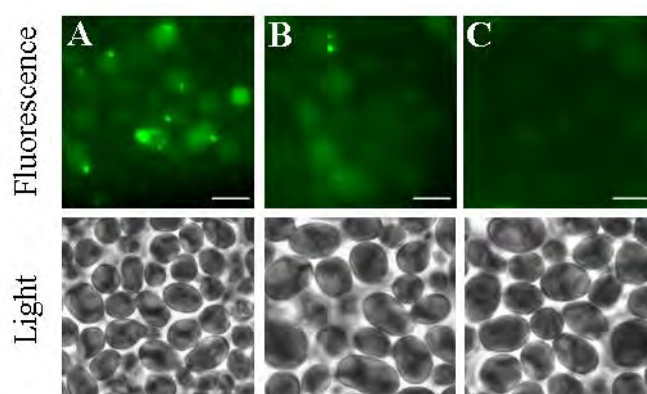


Figure 3-5 Fluorescent and light microscopic images of representative mutants depicting strong, weak and wild-type A β_{42} GFP-associated fluorescence phenotypes.

Strains expressing A β_{42} GFP were induced in galactose medium (SCgal-URA) and A β_{42} GFP-associated fluorescence analysed between 12 to 18 h post induction. The A β_{42} GFP-associated fluorescence exhibited were classified as A) strong fluorescence, as observed in the $\Delta scs2$ strain; B) weak fluorescence, as observed in the $\Delta gln3$ strain; and C) trace or wild-type levels of fluorescence, as observed in the $\Delta elal$ strain. Scale bars indicate 5 μ m.

3.2.7 Genome-wide screening of deletion mutants that exhibit altered A β ₄₂GFP-associated fluorescence

To identify genetic factors that may affect A β ₄₂ aggregation, a genome-wide screen of the *S. cerevisiae* deletion library was performed to identify mutants exhibiting increased A β ₄₂GFP-associated fluorescence relative to wild-type cells (BY4743). Transformation of pUG35GAL1-A β ₄₂ plasmid, encoding the A β ₄₂GFP fusion peptide, was successfully achieved for ~4300 mutant strains of the genome-wide deletion library (Section 2.6.2). The expression of the A β ₄₂GFP fusion protein in strains was induced by the growth in galactose medium (SCgal-URA) and A β ₄₂GFP-associated fluorescence was analysed between 12 to 18 h post induction. Analysis of ~4300 strains identified 344 mutants that appeared to exhibit altered A β ₄₂GFP-associated fluorescence relative to wild-type cells. These 344 mutants were subsequently rescreened for confirmation of altered fluorescence and in mutants exhibiting strong A β ₄₂GFP-associated fluorescence, the proportion of fluorescent cells was quantified. According to the parameters established following the pilot scale screen (Section 3.2.6), 110 of the 344 mutants were classified as exhibiting strong A β ₄₂GFP-associated fluorescence in 15-40% of cells, while the remaining 234 mutants were identified as exhibiting weaker fluorescence in 5-10% of cells. Efforts were focussed on the 110 mutants exhibiting strong A β ₄₂GFP-associated fluorescence and members of this set were considered for further characterisation and experiment (Table 3-1). The list of 234 mutants exhibiting weak fluorescence, as well as details of the biological function of each of their respective gene products is provided in Appendix B.

Table 3-1 List of 110 mutants that exhibited strong A β ₄₂GFP-associated fluorescence, their localisation patterns and the biological function of each of their respective gene products based on descriptions provided in the *Saccharomyces* Genome Database (SGD)

Gene name/ ORF	Gene Functional Description	A β ₄₂ GFP fusion localisation pattern	Respiratory incompetence
Chromatin remodelling/Histone exchange			
<i>SWR1</i>	Component of the Swr1p complex; required for the incorporation of Htz1p into chromatin	Multiple punctates	No
<i>VPS72</i>	Protein of unknown function, component of the Swr1p complex that incorporates Htz1p into chromatin; required for vacuolar protein sorting	Cytosolic with single large punctate	No
<i>SWC5</i>	Protein of unknown function, component of the Swr1p complex that incorporates Htz1p into chromatin	Single small punctate	No
<i>VPS71</i>	Protein of unknown function, component of the Swr1p complex that incorporates Htz1p into chromatin; required for vacuolar protein sorting	Multiple small punctates	No
<i>HTA2</i>	One of histone H2A subtypes; core histone required for chromatin assembly and chromosome function; DNA damage-dependent phosphorylation by Mec1p facilitates DNA repair; acetylated by Nat4p	Single small punctate	No
<i>HIR1</i>	Transcriptional co-repressor involved in cell cycle-regulated transcription of histone H2A, H2B, H3 and H4 genes; contributes to nucleosome formation, heterochromatic gene silencing, and formation of kinetochores	Single small punctate	No
<i>CHD1</i>	Nucleosome remodelling factor that functions in regulation of transcription elongation; contains a chromo domain, a helicase domain and a DNA-binding domain; component of both the SAGA and SILK complexes	Cytosolic	No

YDL041W	Protein of unknown function; overlaps the verified gene <i>SIR2</i> /YDL042C; sporulation defective	Multiple small puncta	No
Mitotic cell cycle			
<i>SWI4</i>	DNA binding component of the SBF complex (Swi4p-Swi6p), a transcriptional activator that in concert with MBF (Mbp1-Swi6p) regulates late G1-specific transcription of targets including cyclins and genes required for DNA synthesis and repair	Cytosolic with single small punctate	No
<i>DCC1</i>	Subunit of a complex with Ctf8p and Ctf18p that shares some components with Replication Factor C, required for sister chromatid cohesion and telomere length maintenance	Single small punctate	Yes
<i>POG1</i>	Putative transcriptional activator that promotes recovery from pheromone induced arrest; inhibits both alpha-factor induced G1 arrest and repression of <i>CLN1</i> and <i>CLN2</i> via SCB/MCB promoter elements; potential Cdc28p substrate; SBF regulated	Single small punctate	No
<i>CTS1</i>	Endochitinase, required for cell separation after mitosis; transcriptional activation during late G and early M cell cycle phases is mediated by transcription factor Ace2p	Cytosolic	No
Gene expression/regulation			
<i>HFII</i>	Adaptor protein required for structural integrity of the SAGA complex, a histone acetyltransferase-coactivator complex that is involved in global regulation of gene expression through acetylation and transcription functions	Cytosolic	Yes
<i>ELC1</i>	Elongin C, forms heterodimer with Ela1p that participates in transcription elongation; expression dramatically upregulated during sporulation; widely conserved among eukaryotes	Single small punctate	No
<i>SYC1</i>	Subunit of the APT subcomplex of cleavage and polyadenylation factor, may have a role in 3' end formation of both polyadenylated	Single small punctate	No

	and non-polyadenylated RNAs		
<i>NCL1</i>	<i>S</i> -adenosyl-L-methionine-dependent tRNA: m5C-methyltransferase, methylates cytosine to m5C at several positions in tRNAs and intron-containing pre-tRNAs; similar to Nop2p and human nucleolar protein p120	Single small punctate	No
<i>MOT2</i>	Component of the Ccr4p-Notp transcription regulatory complex, which represses transcription by inhibiting functional TBP-DNA interactions; aids in transcription elongation; interacts with C-terminal region of Not1p	Single small punctate	Yes
<i>SSN2</i>	Protein required for stable association of Srb10p-Srb11p kinase with RNA polymerase holoenzyme; subunit of the RNA polymerase II mediator complex; essential for transcriptional regulation	Cytosolic with single large punctate	No
<i>MED1</i>	Subunit of the RNA polymerase II mediator complex; associates with core polymerase subunits to form the RNA polymerase II holoenzyme; essential for transcriptional regulation	Cytosolic with 1/2 small punctates	No
<i>SSN3</i>	Cyclin-dependent protein kinase, component of RNA polymerase II holoenzyme; involved in phosphorylation of the RNA polymerase II C-terminal domain; involved in glucose repression	Multiple small punctates	Yes
<i>SRB8</i>	Subunit of the RNA polymerase II mediator complex; associates with core polymerase subunits to form the RNA polymerase II holoenzyme; essential for transcriptional regulation; involved in glucose repression	1/2 small punctates	Yes
<i>CTK1</i>	Catalytic subunit of C-terminal domain kinase I, which phosphorylates the C-terminal repeated domain of the RNA polymerase II large subunit (Rpo21p) to affect both transcription and pre-mRNA 3' end processing	1/2 small punctates	No

<i>TIF4631</i>	Translation initiation factor eIF4G, subunit of the mRNA cap-binding protein complex (eIF4F) that also contains eIF4E (Cdc33p); associates with the poly(A)-binding protein Pab1p, also interacts with eIF4A (Tif1p)	Multiple small punctates	Yes
<i>LSM7</i>	Lsm protein; part of heteroheptameric complexes (Lsm2p-7p and either Lsm1p or 8p); cytoplasmic Lsm1p complex involved in mRNA decay; nuclear Lsm8p complex part of U6 snRNP	Multiple small punctates	Yes
<i>GDT1</i>	Protein of unknown function; expression is reduced in a <i>gcr1</i> null mutant; GFP-fusion protein localises to the vacuole; expression pattern and physical interactions suggest a possible role in ribosome biogenesis	Single small punctate	Yes
<i>SNT309</i>	Component of NineTeen complex (NTC) containing Prp19p involved in mRNA splicing, interacts physically and genetically with Prp19p	Cytosolic with 1/2 small punctates	Yes
<i>DEG1</i>	Non-essential tRNA:pseudouridine synthase, introduces pseudouridines at position 38 or 39 in tRNA, important for maintenance of translation efficiency and normal cell growth, localises to both the nucleus and cytoplasm	Single large punctate	No
<i>GAT1</i>	Transcriptional activator of genes involved in nitrogen catabolite repression, member of the GATA family of DNA binding proteins; activity and localisation regulated by nitrogen limitation and Ure2p	Single small punctate	No
Methionine metabolism			
<i>MET8</i>	Bifunctional dehydrogenase and ferrochelataase, involved in the biosynthesis of siroheme; also involved in the expression of PAPS reductase and sulfite reductase	Single small punctate	No
<i>MXR1</i>	Peptide methionine sulfoxide reductase, reverses the oxidation of methionine residues; involved in oxidative damage repair, providing resistance to oxidative stress and regulation of lifespan	Single small punctate	No

<i>MET16</i>	3'-phosphoadenylylsulfate reductase, reduces 3'-phosphoadenylyl sulfate to adenosine-3',5'-bisphosphate and free sulfite using reduced thioredoxin as cosubstrate, involved in sulfate assimilation and methionine metabolism	Single small punctate	No
Purine metabolism			
<i>ADE12</i>	Adenylosuccinate synthase, catalyses the first committed step in the 'de novo' biosynthesis of adenosine	Single small punctate	No
<i>ADK1</i>	Adenylate kinase, required for purine metabolism; localised to the cytoplasm and the mitochondria	Single small punctate	No
Spindle pole body			
<i>BIM1</i>	Microtubule-binding protein that together with Kar9p makes up the cortical microtubule capture site and delays the exit from mitosis when the spindle is oriented abnormally	Single small punctate	No
<i>BFA1</i>	Component of the GTPase-activating Bfa1p-Bub2p complex involved in multiple cell cycle checkpoint pathways that control exit from mitosis	Single small punctate	No
Phospholipid metabolism			
<i>ICE2</i>	Integral ER membrane protein with type-III transmembrane domains; mutations cause defects in cortical ER morphology in both the mother and daughter cells	Membrane-associated	No
<i>SCS2</i>	Integral ER membrane protein that regulates phospholipid metabolism via an interaction with FFAT motif of Opi1p; involved in telomeric silencing, disruption causes inositol auxotrophy above 34°C, VAP homolog	Single large punctate	No
YER119C-A	Protein of unknown function; deletion mutation blocks replication of Brome mosaic virus in <i>S. cerevisiae</i> , but this is most likely due	Single small punctate	No

	to effects on the overlapping gene <i>SCS2</i>		
<i>CHO2</i>	Phosphatidylethanolamine methyltransferase catalyses the first step in the conversion of phosphatidylethanolamine to phosphatidylcholine (PC) during the methylation pathway of PC biosynthesis	Cytosolic with 1/2 small punctates	No
<i>OPI3</i>	Phospholipid methyltransferase (methylene-fatty-acyl-phospholipid synthase), catalyses the last two steps in phosphatidylcholine biosynthesis	Membrane-associated	No
<i>PSD1</i>	Phosphatidylserine decarboxylase of the mitochondrial inner membrane, converts phosphatidylserine to phosphatidylethanolamine	Membrane-associated	Yes
<i>INO2</i>	Component of the heteromeric Ino2p/Ino4p basic helix-loop-helix transcription activator that binds inositol/choline-responsive elements, required for derepression of phospholipid biosynthetic genes in response to inositol depletion	Membrane-associated	No
<i>INO4</i>	Transcription factor required for derepression of inositol-choline-regulated genes involved in phospholipid synthesis; forms a complex, with Ino2p, that binds the inositol-choline-responsive element through a basic helix-loop-helix domain	Punctate	No
<i>UME6</i>	Key transcriptional regulator of early meiotic genes, binds URS1 upstream regulatory sequence, couples metabolic responses to nutritional cues with initiation and progression of meiosis, forms complex with Ime1p, and with Sin3p-Rpd3p	Single small punctate	No
<i>IPK1</i>	Inositol 1,3,4,5,6-pentakisphosphate 2-kinase, nuclear protein required for synthesis of 1,2,3,4,5,6-hexakisphosphate (phytate), which is integral to cell function	Cytosolic with single large punctate	No
<i>DET1</i>	Acid phosphatase involved in the non-vesicular transport of sterols in both directions between the endoplasmic reticulum and	Cytosolic	No

	plasma membrane; deletion confers sensitivity to nickel		
<i>PDX3</i>	Pyridoxine (pyridoxamine) phosphate oxidase, has homologs in <i>E. coli</i> and <i>Myxococcus xanthus</i> ; transcription is under the general control of nitrogen metabolism	Cytosolic with punctate and nuclear	Yes
Mitochondrial functions			
<i>MRPL7</i>	Mitochondrial ribosomal protein of the large subunit	Cytosolic punctates	Yes
<i>HAP3</i>	Subunit of the heme-activated, glucose-repressed Hap2p/3p/4p/5p CCAAT-binding complex, a transcriptional activator and global regulator of respiratory gene expression; contains sequences contributing to both complex assembly and DNA binding	Single small punctate	Yes
<i>PET112</i>	Protein required for mitochondrial translation; mutation is functionally complemented by a <i>B. subtilis</i> ortholog	Single small punctate	Yes
<i>RSM18</i>	Mitochondrial ribosomal protein of the small subunit, has similarity to <i>E. coli</i> S18 ribosomal protein	Single small punctate	Yes
<i>CYM1</i>	Lysine-specific metalloprotease of the mitochondrial intermembrane space, degrades proteins and presequence peptides cleaved from imported proteins; required for normal mitochondrial morphology	Single small punctate	No
<i>MIC14</i>	Mitochondrial intermembrane space cysteine motif protein of 14 kDa	Cytosolic	No
<i>RIM1</i>	Single-stranded DNA-binding protein essential for mitochondrial genome (mtDNA) maintenance and involved in mtDNA replication	Cytosolic	Yes
<i>KGD1</i>	Component of the mitochondrial alpha-ketoglutarate dehydrogenase complex, which catalyses a key step in the TCA cycle, the oxidative decarboxylation of alpha-ketoglutarate to form succinyl-CoA	Cytosolic	Yes

<i>KGD2</i>	Dihydrolipoyl transsuccinylase, a component of the mitochondrial alpha-ketoglutarate dehydrogenase complex, which catalyses a step in the TCA cycle, the oxidative decarboxylation of alpha-ketoglutarate to succinyl-CoA	Cytosolic	Yes
<i>LPD1</i>	Dihydrolipoamide dehydrogenase, the lipoamide dehydrogenase component (E3) of the pyruvate dehydrogenase and 2-oxoglutarate dehydrogenase multi-enzyme complexes	Cytosolic	Yes
<i>LSC1</i>	Alpha subunit of succinyl-CoA ligase, which is a mitochondrial enzyme of the TCA cycle that catalyses the nucleotide-dependent conversion of succinyl-CoA to succinate	Cytosolic	Yes
<i>LSC2</i>	Beta subunit of succinyl-CoA ligase, which is a mitochondrial enzyme of the TCA cycle that catalyses the nucleotide-dependent conversion of succinyl-CoA to succinate	Cytosolic	No
<i>ATP11</i>	Molecular chaperone, required for the assembly of alpha and beta subunits into the F ₁ sector of mitochondrial F ₁ F ₀ ATP synthase	Cytosolic with 1/2 punctates	Yes
<i>MRPL35</i>	Mitochondrial ribosomal protein of the large subunit	Cytosolic	Yes
<i>PET117</i>	Protein required for assembly of cytochrome c oxidase	Cytosolic	Yes
<i>HAP2</i>	Subunit of the heme-activated, glucose-repressed Hap2p/3p/4p/5p CCAAT-binding complex, a transcriptional activator and global regulator of respiratory gene expression; contains sequences sufficient for both complex assembly and DNA binding	Cytosolic	Yes
<i>RSM7</i>	Mitochondrial ribosomal protein of the small subunit, has similarity to <i>E. coli</i> S7 ribosomal protein	Cytosolic	Yes
<i>COX16</i>	Mitochondrial inner membrane protein, required for assembly of cytochrome c oxidase	Cytosolic	Yes
<i>COX20</i>	Mitochondrial inner membrane protein, required for proteolytic processing of Cox2p and its assembly into cytochrome c oxidase	Cytosolic	Yes
<i>ACO1</i>	Aconitase, required for the TCA cycle and also independently required for mtDNA maintenance; component of the	Cytosolic with 1/2 small punctates	Yes

mitochondrial nucleoid; mutation leads to glutamate auxotrophy

<i>ACO2</i>	Putative mitochondrial aconitase isozyme; similarity to Aco1p, an aconitase required for the TCA cycle; expression induced during growth on glucose, by amino acid starvation via Gcn4p, and repressed on ethanol	Cytosolic	No
<i>CIT1</i>	Citrate synthase, catalyses the condensation of acetyl coenzyme A and oxaloacetate to form citrate; the rate-limiting enzyme of the TCA cycle	Cytosolic with 1/2 small punctates	Yes
<i>CIT3</i>	Dual specificity mitochondrial citrate and methylcitrate synthase; catalyses the condensation of acetyl-CoA and oxaloacetate to form citrate and that of propionyl-CoA and oxaloacetate to form 2-methylcitrate	Cytosolic with 1/2 small punctates	No
<i>FUM1</i>	Fumarase, converts fumaric acid to L-malic acid in the TCA cycle; cytosolic and mitochondrial localization determined by the N-terminal mitochondrial targeting sequence and protein conformation	Cytosolic with punctates	Yes
<i>IDP1</i>	Mitochondrial NADP-specific isocitrate dehydrogenase, catalyses the oxidation of isocitrate to α -ketoglutarate; not required for mitochondrial respiration and may function to divert α -ketoglutarate to biosynthetic processes	Cytosolic with punctates	No
<i>IDH1</i>	Subunit of mitochondrial NAD ⁺ -dependent isocitrate dehydrogenase, which catalyses the oxidation of isocitrate to α -ketoglutarate in the TCA cycle	Cytosolic with punctates	Yes
<i>IDH2</i>	Subunit of mitochondrial NAD ⁺ -dependent isocitrate dehydrogenase, which catalyses the oxidation of isocitrate to α -ketoglutarate in the TCA cycle	Cytosolic with punctates	Yes
<i>MDH1</i>	Mitochondrial malate dehydrogenase, catalyses interconversion of malate and oxaloacetate in the TCA cycle	Cytosolic	No

<i>PYC1</i>	Pyruvate carboxylase isoform, cytoplasmic enzyme that converts pyruvate to oxaloacetate; highly similar to isoform Pyc2p but differentially regulated	Cytosolic with punctates	No
<i>PYC2</i>	Pyruvate carboxylase isoform, cytoplasmic enzyme that converts pyruvate to oxaloacetate; highly similar to isoform Pyc1p but differentially regulated	Cytosolic	No
<i>CBP3</i>	Mitochondrial protein required for assembly of ubiquinol cytochrome-c reductase complex (cytochrome bc1 complex); interacts with Cbp4p and function is partially redundant with that of Cbp4p	Cytosolic with punctates	Yes
<i>AIM4</i>	Protein proposed to be associated with the nuclear pore complex; null mutant displays decreased frequency of mtDNA loss and a severe growth defect in minimal glycerol media	Single small punctate	Yes
<i>YDR230W</i>	Protein of unknown function; partially overlaps the verified gene <i>COX20</i> ; exhibits growth defect on a non-fermentable (respiratory) carbon source	Cytosolic	Yes
<i>SDH1</i>	Flavoprotein subunit of succinate dehydrogenase (Sdh1p, Sdh2p, Sdh3p, Sdh4p), which couples the oxidation of succinate to the transfer of electrons to ubiquinone as part of the TCA cycle and the mitochondrial respiratory chain	Cytosolic	No
<i>SDH2</i>	Iron-sulfur protein subunit of succinate dehydrogenase (Sdh1p, Sdh2p, Sdh3p, Sdh4p), which couples the oxidation of succinate to the transfer of electrons to ubiquinone as part of the TCA cycle and the mitochondrial respiratory chain	Cytosolic	Yes
<i>SDH4</i>	Membrane anchor subunit of succinate dehydrogenase (Sdh1p, Sdh2p, Sdh3p, Sdh4p), which couples the oxidation of succinate to the transfer of electrons to ubiquinone	Cytosolic with punctates	Yes
<i>TUF1</i>	Mitochondrial translation elongation factor Tu; comprises both GTPase and guanine nucleotide exchange factor activities, while these activities are found in separate proteins in <i>S. pombe</i> and	Single small punctate	Yes

humans			
<i>RRG8</i>	Putative protein of unknown function, required for mitochondrial genome maintenance; null mutation results in a decrease in plasma membrane electron transport	Large punctate and nuclear-diffused	Yes
<i>STF2</i>	Protein involved in regulation of the mitochondrial F ₁ F ₀ -ATP synthase; Stf1p and Stf2p act as stabilising factors that enhance inhibitory action of the Inh1p protein	Cytosolic with single large punctate	No
Ubiquitin/Proteasome			
<i>UBR1</i>	Ubiquitin-protein ligase (E3) that interacts with Rad6p/Ubc2p to ubiquitinate substrates of the N-end rule pathway; binds to the Rpn2p, Rpt1p, and Rpt6p proteins of the 19S particle of the 26S proteasome	Cytosol with large punctate	No
<i>SAN1</i>	Ubiquitin-protein ligase, involved in the proteasome-dependent degradation of aberrant nuclear proteins; <i>san1</i> mutations suppress <i>sir4</i> , <i>spt16</i> , and <i>cdc68</i> mutations, suggesting a role in chromatin silencing	Cytosolic	No
<i>SHPI</i>	Ubiquitin regulatory X domain-containing protein that regulates Glc7p phosphatase activity and interacts with Cdc48p; interacts with ubiquitylated proteins and is required for degradation of a ubiquitylated model substrate	Cytosolic with puncta	Yes
MAP kinase activity			
<i>SLG1</i>	Sensor-transducer of the stress-activated Pkc1p-Mpk1p kinase pathway involved in maintenance of cell wall integrity; involved in the organization of actin cytoskeleton	Single small punctate	No
<i>SOK1</i>	Protein overexpression suppresses the growth defect of mutants lacking protein kinase A activity; involved in cAMP-mediated signaling; localised to the nucleus; similar to the mouse testis-	Multiple small punctates	No

specific protein PBS13

<i>PBS2</i>	MAP kinase kinase that plays a pivotal role in the osmosensing signal-transduction pathway, activated under severe osmotic stress	Single small punctate	No
Bud site selection			
<i>BUD31</i>	Protein involved in bud-site selection; diploid mutants display a random budding pattern instead of the wild-type bipolar pattern	Cytosolic with punctates	Yes
<i>BUD23</i>	Protein involved in bud-site selection; diploid mutants display a random budding pattern instead of the wild-type bipolar pattern	Cytosolic with punctate	Yes
Others / Unknown			
<i>APJ1</i>	Putative chaperone of the HSP40 (DNAJ) family; overexpression interferes with propagation of [Psi ⁺] prion	Single small punctate	No
<i>RAD61</i>	Protein of unknown function; mutation confers radiation sensitivity	Cytosolic punctate	No
<i>PHM6</i>	Protein of unknown function, expression is regulated by phosphate levels	Cytosolic punctates	No
<i>GTT3</i>	Protein of unknown function with a possible role in glutathione metabolism, as suggested by computational analysis of large-scale protein-protein interaction data; GFP-fusion protein localises to the nuclear periphery	Single small punctate	No
<i>YIM2</i>	Dubious open reading frame, unlikely to encode a protein; not conserved in closely related <i>Saccharomyces</i> species; 5% of ORF overlaps the verified gene <i>IMP1</i>	Cytosolic	No
<i>RIB1</i>	GTP cyclohydrolase II; catalyses the first step of the riboflavin biosynthesis pathway	Multiple punctates	Yes

<i>EMI2</i>	Non-essential protein of unknown function required for transcriptional induction of the early meiotic-specific transcription factor IME1p, also required for sporulation	Cytosolic with small punctates	No
<i>SNX41</i>	Sorting nexin, involved in the retrieval of late-Golgi SNAREs from the post-Golgi endosome to the trans-Golgi network; forms a complex with Snx4p and Atg20p	Cytosolic with 1/2 small punctates	No
<i>RKM4</i>	Ribosomal lysine methyltransferase specific for monomethylation of Rpl42ap and Rpl42bp (lysine 55); nuclear SET-domain containing protein	Single small punctate	No
<i>ASM4</i>	Nuclear pore complex subunit, part of a subcomplex also containing Nup53p, Nup170p, and Pse1p	Cytosolic with large punctate	No
<i>ICY2</i>	Protein of unknown function; mobilised into polysomes upon a shift from a fermentable to nonfermentable carbon source; potential Cdc28p substrate	Single small punctate	No
<i>PAU11</i>	Putative protein of unknown function; mRNA expression appears to be regulated by <i>SUT1</i> and <i>UPC2</i>	Cytosolic	No
YEL008W	Protein of unknown function; predicted to be involved in metabolism	Single small punctate	No
YDR015C	Protein of unknown function; overlaps the verified gene <i>HED1</i> /YDR014W-A	Cytosolic	No
YOR364W	Protein of unknown function	Single small Punctate	No
YDL242W	Protein of unknown function	Cytosolic	No

3.2.8 Identification of over-represented cellular processes affecting A β ₄₂GFP fluorescence through bioinformatics analysis

The 110 genes (Table 3-1) identified through the genome-wide screen were analysed using the Munich Information centre for Protein Sequence (MIPS) Functional Catalogue Database (FunCatDB) (<http://mips.gsf.de/projects/funcat>) (Ruepp et al., 2004) and the FunSpec GO databases (GO-consortium, 2001; Robinson et al., 2002) with the aim of determining cellular processes affecting A β ₄₂GFP fluorescence and whether these processes or functional groups were over-represented in the data set, relative to their presence in the data set by chance alone. In this analysis, both MIPS FunCatDB and FunSpec GO databases use parameters for calculating probability values based on the premise that every gene in the *S. cerevisiae* genome (6607 genes; updated as of 2nd August 2012) was included in the study. Since ~4600 of the possible 6607 genes were screened in this study, it should be noted that the probability values generated by the above databases would tend to underestimate the presence of over-represented groups; that is, probability values generated were likely to be lower (more significant) in reality. By virtue of this, there is a possibility that additional over-represented groups may be present amongst the 110 genes but were not identified as statistically significant using the above bioinformatics tools.

The FunSpec GO database was used to identify over-representations in process ontology, function ontology and component ontology. Analysis using the process ontology annotation (Tables 3-2, 3-3 and 3-4), to identify broad biological/ cellular processes, indicated that tricarboxylic acid (TCA) cycle (GO: 0008654; $p < 1 \times 10^{-14}$), histone exchange (GO: 0043486; $p = 2.12 \times 10^{-5}$), phospholipid biosynthetic process (GO: 0008654; $p = 0.0005$), ER inheritance (GO: 0048309; $p = 0.005$), methylation (GO: 0032259; $p = 0.008$), chromatin modification (GO: 0016568; $p = 0.001$) and remodelling (GO: 0006338; $p = 0.009$) were significantly over-represented among the 110 mutants identified by the genome-wide screen. Analysis using the function ontology annotation, to identify the individual roles of gene products, indicated that transcription regulator activity, specifically RNA polymerase II transcription cofactor activity (GO: 0001104; $p = 0.005$) and RNA polymerase II core promoter proximal region sequence-specific DNA-binding transcription factor activity involved in positive regulation of transcription (GO: 0001077; $p = 0.001$) was a significantly enriched functional category.

Finally, analysis using the component ontology annotation, to identify cellular components encompassed in subcellular structures, locations, and macromolecular complexes, indicated that components of CCAAT-binding transcription factor complex (GO: 0016602; $p = 0.07$) and Swr1 complex (GO: 0000812; $p = 0.001$) were over-represented in the 110 mutants identified by the screen. A complete list of the biological process, molecular function and cellular component ontologies generated from FunSpec GO database are provided in Tables 3-2, 3-3 and 3-4.

Table 3-2 Functional grouping of the 110 mutants identified through the genome-wide screen that exhibited strong A β ₄₂GFP-associated fluorescence, based on molecular function ontology (FunSpec GO database).

k: number of genes from the input cluster in given category. f: total number of genes in the category.

Category	<i>p</i> -value	Genes in Category	k	f
isocitrate hydro-lyase (cis-aconitate-forming) activity [GO:0052633]	0.00027	<i>ACO2 ACO1</i>	2	2
citrate hydro-lyase (cis-aconitate-forming) activity [GO:0052632]	0.00027	<i>ACO2 ACO1</i>	2	2
oxidoreductase activity, acting on the CH-OH group of donors, NAD or NADP as acceptor [GO:0016616]	0.001214	<i>IDP1 MDH1 IDH1 IDH2</i>	4	29
oxoglutarate dehydrogenase (succinyl-transferring) activity [GO:0004591]	0.001585	<i>LPD1 KGD1</i>	2	4
RNA polymerase II core promoter proximal region sequence-specific DNA binding transcription factor activity involved in positive regulation of transcription [GO:0001077]	0.001989	<i>HAP3 INO2 HAP2 INO4</i>	4	33
succinate dehydrogenase (ubiquinone) activity [GO:0008177]	0.003498	<i>SDH4 SDH1 SDH2</i>	3	19
isocitrate dehydrogenase (NAD ⁺) activity [GO:0004449]	0.003879	<i>IDH1 IDH2</i>	2	6
RNA polymerase II transcription cofactor activity [GO:0001104]	0.005363	<i>SRB8 SSN2 MED1</i>	3	22
transferase activity, transferring acyl groups, acyl groups converted into alkyl on transfer [GO:0046912]	0.005372	<i>CIT1 CIT3</i>	2	7

aconitate hydratase activity [GO:0003994]	0.005372	<i>ACO2 ACO1</i>	2	7
metal ion binding [GO:0046872]	0.006088	<i>RIB1 PYC2 IDP1 SAN1 SDH4 UME6 CYM1 MOT2 GAT1 PYC1 UBR1 ACO2 SDH2 ACO1 VPS71 IDH1 APJ1 ADE12 IDH2 SSN3</i>	20	670
NAD binding [GO:0051287]	0.006094	<i>IDP1 IDH1 IDH2</i>	3	23
transcription regulator activity [GO:0030528]	0.006223	<i>HIR1 INO2 UME6 INO4</i>	4	45
4 iron, 4 sulfur cluster binding [GO:0051539]	0.006881	<i>ACO2 SDH2 ACO1</i>	3	24
pyruvate carboxylase activity [GO:0004736]	0.007085	<i>PYC2 PYC1</i>	2	8
succinate-CoA ligase (ADP- forming) activity [GO:0004775]	0.009012	<i>LSC2 LSC1</i>	2	9
biotin carboxylase activity [GO:0004075]	0.009012	<i>PYC2 PYC1</i>	2	9
magnesium ion binding [GO:0000287]	0.009681	<i>IDP1 IDH1 ADE12 IDH2</i>	4	51

Table 3-3 Functional grouping of the 110 mutants identified through the genome-wide screen that exhibited strong A β ₄₂GFP-associated fluorescence, based on biological process ontology (FunSpec GO database).

Category	<i>p</i> -value	Genes in Category	k	f
tricarboxylic acid cycle [GO:0006099]	<1e-14	<i>IDP1 KGD2 SDH4 LSC2 KGD1 ACO2 MDH1 SDH1 SDH2 ACO1 IDH1 CIT1 IDH2 LSC1 FUM1 CIT3</i>	16	61
2-oxoglutarate metabolic process [GO:0006103]	4.38E-06	<i>KGD2 LPD1 KGD1</i>	3	3
glutamate biosynthetic process [GO:0006537]	1.08E-05	<i>IDP1 ACO1 IDH1 CIT1 IDH2</i>	5	19
histone exchange [GO:0043486]	2.12E-05	<i>SWC5 SWR1 VPS72 VPS71</i>	4	11
mitochondrial electron transport, succinate to ubiquinone [GO:0006121]	4.27E-05	<i>SDH4 SDH1 SDH2</i>	3	5
isocitrate metabolic process [GO:0006102]	0.000342	<i>IDP1 IDH1 IDH2</i>	3	9
phospholipid biosynthetic process [GO:0008654]	0.0005115	<i>INO2 SCS2 CHO2 OPI3 PSD1 INO4</i>	6	62
citrate metabolic process [GO:0006101]	0.0008014	<i>ACO1 CIT1</i>	2	3
nuclear-transcribed mRNA catabolic process, non-stop decay [GO:0070481]	0.0009202	<i>IPK1 SSN2 SSN3 MED1</i>	4	27
transcription, DNA- dependent [GO:0006351]	0.0009433	<i>HIR1 HAP3 SWC5 SRB8 INO2 UME6 SWR1 SSN2 VPS72 MOT2 SWI4 CHD1 GAT1 HAP2 POG1 CTK1 INO4 SSN3 HF11 MED1</i>	20	572

chromatin modification [GO:0016568]	0.001441	<i>HIR1 SWC5 UME6 SWR1 VPS72 CHD1 VPS71 HFI1</i>	8	132
succinyl-CoA metabolic process [GO:0006104]	0.001585	<i>LSC2 LSC1</i>	2	4
cellular respiration [GO:0045333]	0.001723	<i>SDH4 SDH1 SDH2</i>	3	15
regulation of cellular respiration [GO:0043457]	0.002614	<i>HAP3 HAP2</i>	2	5
positive regulation of transcription from RNA polymerase II promoter by galactose [GO:0000435]	0.002614	<i>SSN2 SSN3</i>	2	5
metabolic process [GO:0008152]	0.002908	<i>MET8 PYC2 BUD23 DET1 KGD2 PYC1 LSC2 KGD1 ACO2 MDH1 CTS1 ACO1 IDH1 IDH2 LSC1 MET16</i>	16	453
phosphatidylcholine biosynthetic process [GO:0006656]	0.002981	<i>CHO2 OPI3 PSD1</i>	3	18
cellular carbohydrate metabolic process [GO:0044262]	0.003498	<i>MDH1 CIT1 CIT3</i>	3	19
carbon catabolite activation of transcription from RNA polymerase II promoter [GO:0000436]	0.003879	<i>HAP3 HAP2</i>	2	6
mitochondrial genome maintenance [GO:0000002]	0.004855	<i>RIM1 KGD2 ACO1 RRG8</i>	4	42
NADPH regeneration [GO:0006740]	0.005372	<i>PYC2 PYC1</i>	2	7
endoplasmic reticulum inheritance [GO:0048309]	0.005372	<i>SCS2 ICE2</i>	2	7
propionate metabolic process [GO:0019541]	0.005372	<i>ACO1 CIT3</i>	2	7
mitochondrial translation [GO:0032543]	0.007228	<i>PET112 MRPL7 MRPL35 RSM18 RSM7 TUF1</i>	6	104
methylation [GO:0032259]	0.008612	<i>NCL1 BUD23 RKM4 CHO2 OPI3</i>	5	77
chromatin remodeling [GO:0006338]	0.009084	<i>SWC5 SWR1 VPS72 CHD1 VPS71</i>	5	78

k: number of genes from the input cluster in given category. f: total number of genes in the category.

Table 3-4 Functional grouping of the 110 mutants identified through the genome-wide screen that exhibited strong A β ₄₂GFP-associated fluorescence, based on cellular component ontology (FunSpec GO database).

Category	<i>p</i> -value	Genes in Category	k	f
mitochondrial nucleoid [GO:0042645]	4.20E-08	<i>RIM1 IDP1 KGD2 LPD1 KGD1 ACO1 IDH1 LSC1</i>	8	33
mitochondrial oxoglutarate dehydrogenase complex [GO:0009353]	4.38E-06	<i>KGD2 LPD1 KGD1</i>	3	3

mitochondrial respiratory chain complex II [GO:0005749]	4.27E-05	<i>SDH4 SDH1 SDH2</i>	3	5
mitochondrial isocitrate dehydrogenase complex (NAD ⁺) [GO:0005962]	0.00027	<i>IDH1 IDH2</i>	2	2
mitochondrial matrix [GO:0005759]	0.0002715	<i>LPD1 KGD1 MDH1 ACO1 IDH1 ATP11 CIT1 IDH2 TUF1 FUM1</i>	10	159
Swr1 complex [GO:0000812]	0.001568	<i>SWC5 SWR1 VPS72 VPS71</i>	4	31
CCAAT-binding factor complex [GO:0016602]	0.007085	<i>HAP3 HAP2</i>	2	8

k: number of genes from the input cluster in given category. f: total number of genes in the category.

Analysis using the MIPS FunCatDB also yielded a very similar set of functional categories as the FunSpec GO database but also identified phospholipid metabolism (01.06.02.01; $p = 0.001$), regulation of lipid, fatty acid and isoprenoid metabolism (01.06.10; $p = 0.008$), sulphate assimilation (01.02.03.01; $p = 0.007$) and transcriptional control (11.02.03.04; $p = 0.0005$) to be over-represented in the data set of 110 genes. Functional categories that are over-represented in this group of 110 genes indicate the cellular processes affecting A β ₄₂GFP fluorescence, and by extension intracellular A β ₄₂ aggregation.

In addition to these bioinformatics tools, the 110 gene products were also considered following consultation of available scientific literature on the established or putative cellular roles of each of the respective gene products. From these analyses, it was possible to categorise the 110 genes into broad biological functional groups/cellular processes that affected A β ₄₂GFP-associated fluorescence including: chromatin remodelling complexes/ histone exchange, gene expression, methionine metabolism, phospholipid metabolism, and mitochondrial functions (Table 3-1). A graphical representation of the proportion of mutants in each functional group is illustrated in Figure 3-6. Mutants belonging to each of the groups in Figure 3-6 are given in Table 3-1 where a comprehensive description of the function of each of the 110 encoded gene products and the observed A β ₄₂GFP localisation phenotype is provided.

The use of more than one database increased the possibility of identifying all over-represented functional groups amongst the 110 mutants. Despite this advantage, all

database searches are limited to the gene ontology descriptions used to classify genes, which are often simplifications and generalisations derived from available scientific literature. It was therefore of benefit to also ensure that the 110 genes were considered with respect to the available scientific literature. This required manual categorisation of mutants following analysis of the available literature, relative to each gene. In addition to the functional groups described above, the manual categorisation indicated that among the 110 mutants sulphite reductase activity appeared to affect A β ₄₂GFP-associated fluorescence. This was the case since deletion of *MXR1*, encoding methionine sulphite reductase, *MET16*, encoding PAPS reductase, and *MET8*, encoding a protein required specifically for sulphite reductase activity all affected A β ₄₂GFP-associated fluorescence, while the deletion of the other genes required for sulphur assimilation and synthesis of methionine/cysteine did not (Thomas and Surdin-Kerjan, 1997).

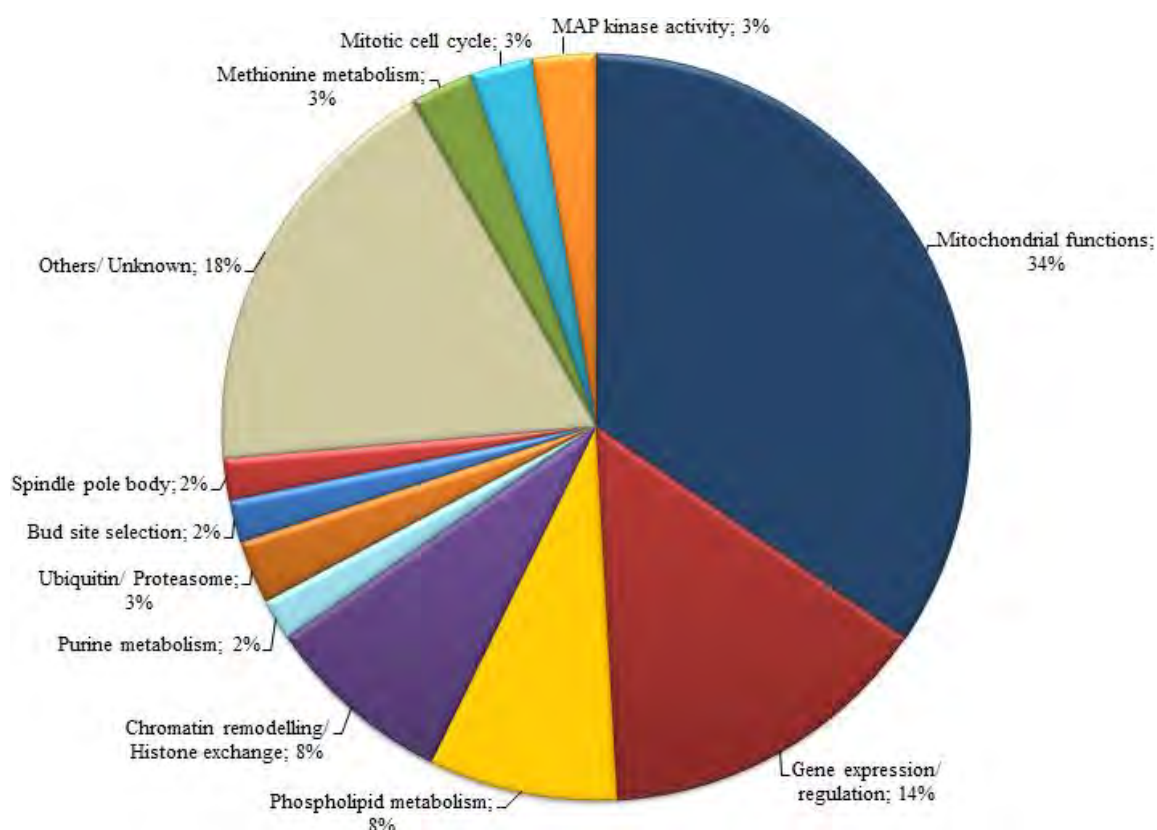


Figure 3-6 Graphic representation of cellular processes identified affecting A β ₄₂GFP-associated fluorescence in *S. cerevisiae*.

Percentages reflect the number of mutants identified in a particular cellular process relative to the total number of mutants identified by the genome-wide screen.

Table 3-5 Broad functional grouping of the 110 mutants identified through the genome-wide screen that exhibited strong A β ₄₂GFP-associated fluorescence, by manual categorisation

Functional group	Deleted gene	Common Aβ₄₂GFP localisation
Bud site selection	<i>BUD23, BUD31</i>	Cytosolic and punctate(s)
Chromatin remodelling/ Histone exchange	<i>CHD1, HIR1, HTA2, IPK1, SWR1, SWC5, VPS71, VPS72, YDL041W</i>	Punctate(s)
Mitotic cell cycle	<i>CTS1, POG1, SWI4</i>	Cytosolic and punctate(s)
MAP kinase activity	<i>PBS2, SLG1, SOK1</i>	Punctate(s)
Methionine metabolism	<i>MET8, MET16, MXR1</i>	Single small punctate
Mitochondrial functions	<i>CIT1, CIT3, ACO1, ACO2, IDH1, IDH2, IDP1, KGD1, KGD2, LPD1, LSC1, LSC2, SDH1, SDH2, SDH4, FUM1, MDH1, PYC1, PYC2, AIM4, ATP11, CBP3, COX16, COX20, CYM1, HAP2, HAP3, MIC14, MRPL7, MRPL35, PET112, PET117, RIM1, RSM7, RSM18, STF2, TUF1, YDR230W</i>	Cytosolic and punctate(s)
Phospholipid metabolism	<i>CHO2, ICE2, INO2, INO4, OPI3, PSD1, SCS2, UME6, YER119C-A</i>	Membrane /Organelle associated and punctate(s)
Purine metabolism	<i>ADE12, ADK1</i>	Single small punctate
Spindle pole body	<i>BFA1, BIM1</i>	Single small punctate
Gene expression/ regulation	<i>CTK1, DEG1, ELC1, GAT1, GDT1, HF11, LSM7, MED1, MOT2, NCL1, SNT309, SRB8, SSN2, SSN3, SYC1, TIF4631</i>	Punctate(s)
Ubiquitin/ Proteasome	<i>SAN1, SHP1, UBR1</i>	Cytosolic and punctate(s)
Others / Unknown	<i>APJ1, ASM4, DCC1, EMI2, GTT3, ICY2, PAU11, PDX3, PHM6, RAD61, RIB1, SET7, SNX41, YIM2, YDL242W, YDR015C, YEL008W, YOR364W, YPR116W, YDR051C</i>	Cytosolic and punctate(s)

As indicated above, bioinformatics analysis identified PC biosynthesis as an over-represented function in the data set of 110 genes. In addition to this, manual categorisation indicated that it was the disruption of genes required for conversion of phosphatidylserine (PS) to phosphatidylcholine (PC), and not other steps in the phospholipid biosynthetic pathway that affected A β ₄₂GFP-associated fluorescence. Refer to Figure 4-1 (page 97) for the PL metabolic pathway. These findings indicate the value of using bioinformatics tools in conjunction with detailed consultation of the broader scientific literature, for identification of the relevant cellular processes that affect A β ₄₂GFP-associated fluorescence.

3.2.9 Quantitative assessment of A β ₄₂GFP-associated fluorescence in the over-represented functional categories identified by the genome-wide screen

The bioinformatic analyses above identified over-represented cellular processes that affect A β ₄₂GFP-associated fluorescence. In order to determine whether some over-represented functional categories had a greater effect on A β ₄₂GFP-associated fluorescence than others, a representative group of mutants from each functional category were selected for further quantitative analysis. For each of the selected mutants, exhibition of A β ₄₂GFP-associated fluorescence was quantified 12 h post induction in galactose medium. In each case, 300 cells were counted in triplicate and the mean and standard deviation for each are given in Table 3-6.

Table 3-6 Proportion of A β ₄₂GFP-associated fluorescent cells in representative mutants from major over-represented functional groups identified by bioinformatics analysis.

Strains expressing A β ₄₂GFP were induced in galactose medium (SCgal-URA) and A β ₄₂GFP-associated fluorescence analysed at 12 h post induction. The data shown are the mean of triplicate measurements \pm standard deviation from a single experiment. All deletion mutants below exhibited a significant increase in the proportion of cells exhibiting A β ₄₂GFP fluorescence compared to those in wild-type cells ($p < 0.0001$).

Strain expressing A β ₄₂ GFP	% Fluorescent cells \pm std. dev.	Strain expressing A β ₄₂ GFP	% Fluorescent cells \pm std. dev.
Phospholipid metabolism			
<i>Δino2</i>	17 \pm 2	<i>Δopi3</i>	23 \pm 2
<i>Δino4</i>	14 \pm 2	<i>Δscs2</i>	26 \pm 2
<i>Δpsd1</i>	18 \pm 2	<i>Δice2</i>	28 \pm 2
<i>Δcho2</i>	18 \pm 2	<i>Δume6</i>	22 \pm 3
Mitochondrial function			
<i>Δcox16</i>	43 \pm 9	<i>Δlpd1</i>	19 \pm 2
<i>Δcox20</i>	25 \pm 7	<i>Δlsc1</i>	20 \pm 1
<i>Δcit1</i>	19 \pm 3	<i>Δlsc2</i>	20 \pm 2
<i>Δcit3</i>	17 \pm 3	<i>Δsdh1</i>	27 \pm 2
<i>Δaco1</i>	38 \pm 7	<i>Δsdh2</i>	22 \pm 1
<i>Δaco2</i>	31 \pm 3	<i>Δsdh4</i>	19 \pm 8
<i>Δidh1</i>	23 \pm 6	<i>Δfum1</i>	42 \pm 5
<i>Δidh2</i>	23 \pm 2	<i>Δmdh1</i>	22 \pm 4
<i>Δkgd1</i>	21 \pm 7	<i>Δpyc1</i>	17 \pm 2
<i>Δkgd2</i>	24 \pm 4	<i>Δpyc2</i>	17 \pm 2
Chromatin remodeling/ Histone exchange*			
<i>Δswr1</i>	23 \pm 3	<i>Δvps71</i>	18 \pm 2
<i>Δvps72</i>	18 \pm 3	<i>Δhta2</i>	15 \pm 2
<i>Δswc5</i>	21 \pm 5	<i>Δhir1</i>	18 \pm 5

*500 cells were counted in triplicates for mutants in this functional group.

The data in Table 3-6 indicate that the average proportion of fluorescent cells that belong to the phospholipid metabolism and the chromatin silencing/ histone functional groups was approximately 21%; whereas the average percentage of fluorescent cells belonging to mitochondrial functional group was approximately 25%. This significant difference ($p = 0.008$) in the proportion of fluorescent cells between functional categories may indicate the relative impact of a given function with respect to A β ₄₂GFP-associated fluorescence. Since all of the mutants that were selected exhibited a significantly higher proportion of fluorescent cells relative to wild-type cells, these data also indicated that most, if not all, mutants categorised as exhibiting strong fluorescence phenotype (Table 3-1), were likely to be significantly different to wild-type cells.

3.2.10 Protein-protein interaction network

To determine if any of the 110 mutants identified in the genome-wide deletion screen were physically associated to each other, protein-protein interaction analyses were undertaken. This work was completed in collaboration with the Systems Biology Initiative at University of New South Wales. To generate and analyse the protein-protein interaction networks, a visual analytic platform called GEOMI (GEOMetry for Maximum Insight) was utilised together with two metadata sets (Bertin et al., 2007; Yu et al., 2008). Protein interaction networks were generated to map *S. cerevisiae* proteins that interact with proteins identified in the genome-wide screen. Out of the 110 proteins identified in the genome-wide deletion screen, 35 have no known protein interactions (Table 3-7). To increase the confidence of a physiologically relevant protein-protein interaction, only direct interactions of the remaining 75 proteins were mapped (Figure 3-7), where a maximum distance of two interactions from the protein-of-interest was assessed.

From the protein-protein interaction analyses, a total of 398 proteins were identified to physically interact with the 75 proteins that were mapped forming a total of 1290 interactions. In an attempt to identify functional interaction or cross-talk between cellular processes identified in the genome-wide deletion screen, data from the protein interaction network were analysed for shared protein interacting partners between cellular processes. Detailed analysis of the protein-protein interaction network indicated that Hap2, Hap3 (subunits of the heme-activated Hap2p/3p/4p/5p CCAAT-binding complex, which regulates respiratory gene expression) and Cox20p (belonging to the mitochondrial functional group), Opi3p (belonging to lipid metabolism functional group) and Met8p (belonging to the methionine metabolism functional group) were found to share a common protein interacting partner in Cmd1p. Calmodulin (Cmd1p), is an essential calcium-binding protein in *S. cerevisiae* and therefore not analysed in the genome-wide screen performed in the above section. It regulates a wide range of cellular processes, both calcium-dependent and independent, including response to stress conditions, mating, budding, and remodelling of the actin cytoskeleton (Cyert, 2001; Eitzen et al., 2002). Identification of this physical interaction between Cmd1p-Hap2p/ Hap3p/Cox20p, Cmd1p-Opi3p and Cmd1p-Met8p is made further interesting by recent data indicating that calcium-dependent phospholipases are an important factor in

the onset and progression of neurodegenerative mechanisms in AD brains (Farooqui et al., 2006; Gentile et al., 2012). Several studies have also demonstrated that A β peptides form channels in cell membranes, causing calcium influx into the cell and subsequently stimulating several cellular processes leading to mitochondrial dysfunction, inflammation and cell death (Ballard et al., 2011; Querfurth and LaFerla, 2010). These data suggest the possibility of an underlying calcium-dependent mechanism which affects A β ₄₂GFP aggregation between mutants of the mitochondrial, lipid metabolism and methionine metabolism functional groups.

Table 3-7 List of 35 genes which encode proteins with no known protein interactions and were not mapped on the protein-protein interaction network

<i>NCL1</i>	<i>MIC14</i>	<i>PET117</i>	<i>ICE2</i>	<i>TUF1</i>
<i>RIB1</i>	<i>SDH4</i>	<i>CHO2</i>	<i>COX16</i>	<i>FUM1</i>
<i>PDX3</i>	<i>RKM4</i>	<i>DEG1</i>	<i>ACO2</i>	<i>CIT3</i>
<i>GDT1</i>	<i>PHM6</i>	<i>GAT1</i>	<i>CTS1</i>	<i>RRG8</i>
<i>PYC2</i>	<i>IPK1</i>	<i>PYC1</i>	<i>ACO1</i>	<i>IDP1</i>
<i>RIM1</i>	<i>MRPL35</i>	<i>PAU11</i>	<i>YIM2</i>	<i>GTT3</i>
<i>BUD23</i>	<i>CYM1</i>	<i>STF2</i>	<i>APJ1</i>	<i>YER119C-A</i>

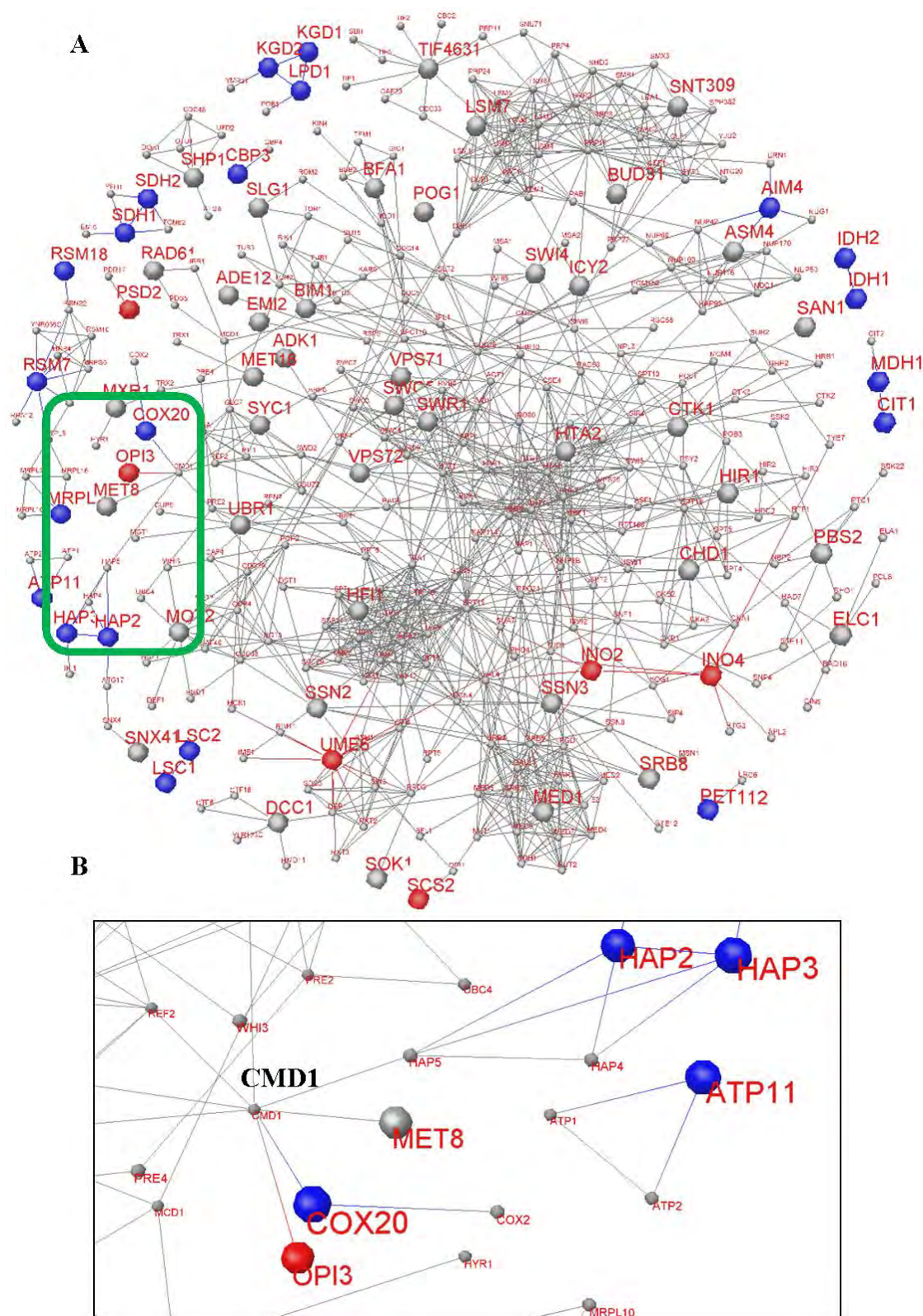


Figure 3-7 Visualisation of protein-protein interaction network depicting 75 out of 110 proteins identified in the genome-wide screen that affect A β ₄₂GFP aggregation, generated using GEOMI

A) 398 proteins (small nodes) were identified to physically interact with the 75 proteins that were identified in the genome-wide screen (large nodes), forming a total of 1290 interactions. Blue and red nodes indicate genes belonging to the mitochondrial function and phospholipid

metabolism functional groups, respectively. Three different functional groups were found to share a common interacting partner in Cmd1p (highlighted within a green box). B) A close-up view of the same protein interaction network within the green box redrawn using the force-directed layout.

Additional insight into common mechanisms through which various biological processes affect A β ₄₂GFP aggregation has been gained through this bioinformatics approach. However, this analysis should be attempted again in future when more protein interaction partners, especially of the remaining 35 proteins, have been identified as this may reveal further insight into common underlying mechanisms between other cellular processes that affect A β ₄₂GFP aggregation in *S. cerevisiae*. Since, cellular processes are usually delivered through biological pathways, rather than individual proteins, in the following chapters, this study attempts to provide possible mechanistic insights into how these cellular processes may affect A β ₄₂GFP aggregation.

3.2.11 Human orthologs of *S. cerevisiae* genes identified by the genome-wide screen

Since many genes of *S. cerevisiae* have human orthologues, identification of these genetic factors may help to identify cellular processes in humans that may play a role in A β ₄₂ aggregation. To identify human orthologues of *S. cerevisiae* genes, an analysis using the NCBI database resource tool, HomoloGene, was performed and the results are presented in Table 3-8.

Table 3-8 Human orthologs of *S. cerevisiae* genes identified through the genome-wide screen.

S. cerevisiae genes have been sorted according to the biological functional groups described in Table 3-5.

<i>S. cerevisiae</i> Gene Name	Human orthologue (Gene name)
Mitochondrial functions	
<i>ACO1</i>	ACO2; aconitase 2, mitochondrial
<i>ATP11</i>	ATPAF1; ATP synthase mitochondrial F1 complex assembly factor 1
<i>CBP3</i>	UQCC; ubiquinol-cytochrome c reductase complex chaperone
<i>CYM1</i>	PITRM1; pitrilysin metalloproteinase 1
<i>SDH1</i>	SDHA; succinate dehydrogenase complex, subunit A, flavoprotein (Fp)
<i>SDH2</i>	SDHB; succinate dehydrogenase complex, subunit B, iron sulfur (Ip)
<i>SDH4</i>	SDHD; succinate dehydrogenase complex, subunit D, integral membrane protein

<i>IDP1</i>	IDH1; isocitrate dehydrogenase 1 (NADP ⁺), soluble
<i>IDH1</i>	IDH3B; isocitrate dehydrogenase 3 (NAD ⁺) beta
<i>IDH2</i>	IDH3A; isocitrate dehydrogenase 3 (NAD ⁺) alpha
<i>LPD1</i>	DLD; dihydrolipoamide dehydrogenase
<i>KGD1</i>	OGDH; oxoglutarate (alpha-ketoglutarate) dehydrogenase (lipoamide)
<i>KGD2</i>	DLST; dihydrolipoamide S-succinyltransferase
<i>LSC1</i>	SUCLG1; succinate-CoA ligase, alpha subunit
<i>MDH1</i>	MDH2; malate dehydrogenase 2, NAD (mitochondrial)
<i>PYC1</i>	PC; pyruvate carboxylase
<i>PYC2</i>	PC; pyruvate carboxylase
<i>MRPL35</i>	MRPL35; mitochondrial ribosomal protein L35
<i>PET112</i>	PET112L; PET112-like (yeast)
<i>FUM1</i>	FH; fumarate hydratase
<i>HAP2</i>	NFYA; nuclear transcription factor Y, beta
<i>HAP3</i>	NFYB; nuclear transcription factor Y, beta
<i>TUF1</i>	TUFM; Tu translation elongation factor, mitochondrial
Phospholipid metabolism	
<i>OPI3</i>	PEMT; phosphatidylethanolamine N-methyltransferase
<i>SCS2</i>	VAPA; VAMP (vesicle-associated membrane protein)
<i>IPK1</i>	IPPK; inositol 1,3,4,5,6-pentakisphosphate 2-kinase
<i>PDX3</i>	PNPO; pyridoxamine 5'-phosphate oxidase
<i>PSD1</i>	PISD; phosphatidylserine decarboxylase
Purine metabolism	
<i>ADE12</i>	ADSSL1; adenylosuccinate synthase like 1
<i>ADK1</i>	AK2; adenylate kinase 2
Bud site selection	
<i>BUD23</i>	WBSCR22; Williams Beuren syndrome chromosome region 22
<i>BUD31</i>	BUD31; BUD31 homolog
Chromatin remodelling/ Histone exchange	
<i>CHD1</i>	CHD2; chromodomain helicase DNA binding protein 1
<i>HIR1</i>	HIRA; HIR histone cell cycle regulation defective homolog A
<i>HTA2</i>	H2AFX; H2A histone family, member X
<i>SWC5</i>	CFDP1; craniofacial development protein 1

Gene expression/regulation	
<i>CTK1</i>	CDC2L5; cell division cycle 2-like 5
<i>DEG1</i>	PUS3; pseudouridylate synthase 3
<i>GDT1</i>	TMEM165; transmembrane protein 165
<i>MED1</i>	MED1; mediator complex subunit 1
<i>NCL1</i>	NSUN2; NOL1/NOP2/Sun domain family, member 2
<i>SRB8</i>	MED12L; mediator complex subunit 12-like
<i>SSN2</i>	MED13L; mediator complex subunit 13-like
<i>SSN3</i>	CDK8; cyclin-dependent kinase 8
<i>TIF4631</i>	EIF4G1; eukaryotic translation initiation factor 4 gamma, 1
<i>LSM7</i>	LSM7; LSM7 homolog, U6 small nuclear RNA associated
Ubiquitin/ Proteasome	
<i>SHP1</i>	NSFL1C; NSFL1 (p97) cofactor (p47)
<i>UBR1</i>	UBR1; ubiquitin protein ligase E3 component n-recognin 1
Methionine homeostasis	
<i>MXR1</i>	MSRA; methionine sulfoxide reductase A
Mitotic cycle	
<i>DCC1</i>	DSCC1; defective in sister chromatid cohesion 1 homolog
Spindle pole body	
<i>BIM1</i>	MAPRE1; microtubule-associated protein, RP/EB family, member 1
MAP kinase activity	
<i>PBS2</i>	MAP2K4; mitogen-activated protein kinase kinase 4

Of the 110 *S. cerevisiae* genes in Table 3-1, 52 were found to have human orthologues. To identify if these human genes have implications in Alzheimer's disease individuals, the 52 human genes should now be screened in AD patients. It is hypothesised that mutations in some of these human genes may affect the onset of AD or may render a degree of protection against AD, by affecting A β ₄₂ aggregation.

3.3 Discussion

3.3.1 Development and characterisation of A β GFP aggregation assay in *S. cerevisiae*

A major histopathological feature of Alzheimer's disease (AD) is the occurrence of insoluble extracellular plaques, composed of aggregates of amyloid- β (A β) peptides, in specific cognitive domains of the brain (Glenner and Wong, 1984; Masters et al., 1985). These A β -plaques were found to be enriched with the A β peptides, specifically A β ₄₀ (40 amino acids) and A β ₄₂ (42 amino acids) peptides in the ratio 10:1 (Jarrett et al., 1993a). The A β ₄₂ peptide is more hydrophobic and prone to aggregation and fibril formation than the A β ₄₀ (Jarrett et al., 1993b). According to the amyloid cascade hypothesis by Hardy and Higgins (1992), "deposition of A β protein, the main component of the plaques (Glenner and Wong, 1984; Hardy and Higgins, 1992; Masters et al., 1985; Selkoe, 1991), is the causative agent of AD pathology and that the neurofibrillary tangles, cell loss, vascular damage, and dementia follow as a direct result of the A β deposition". Despite extracellular plaques being implicated as the causative agent of AD, intraneuronal A β aggregation has also been long reported (Grundke-Iqbal et al., 1989). However, only recently presence of intraneuronal A β ₄₂ aggregation has been implicated as an early event in neuronal dysfunction and in the disease progression of AD (Gouras et al., 2005; Kienlen-Campard et al., 2002; Lesne et al., 2006; Lesne and Kotilinek, 2005; Younkin, 1995; Younkin, 1998).

A β ₄₂ is the predominant form of A β found intraneuronally (Younkin, 1995) and is more neurotoxic than A β ₄₀ (Kienlen-Campard et al., 2002). A β has been found to exist in many assembly states such as monomers, oligomers, protofibrils and fibrils, and it is these assembly states, particularly the oligomeric and protofibrillar forms, that are considered the most neurotoxic (Haass and Selkoe, 2007; Selkoe, 2002; Selkoe, 2008; Walsh et al., 2002). Formation of fibrils or oligomers is nucleation-dependent and A β ₄₂ has been strongly implicated in this role (Jarrett et al., 1993b). Strategies that target A β ₄₂ oligomerisation or aggregation states have been proposed to be possible therapeutic strategies to treat/prevent AD (Gouras et al., 2005). Improved understanding of genetic factors and biological processes that affect intracellular A β ₄₂ aggregation is therefore vital.

S. cerevisiae has served as a useful model to study aspects neurodegeneration; specifically in Huntington's disease (Giorgini et al., 2005; Giorgini et al., 2008; Willingham et al., 2003), Parkinson's disease (Cooper et al., 2006; Flower et al., 2005; Outeiro and Lindquist, 2003; Zhang et al., 1994), frontotemporal lobar degeneration (Johnson et al., 2008; Tardiff et al., 2012) and Alzheimer's disease (Bharadwaj et al., 2010; Caine et al., 2011; Komano et al., 1998; Macreadie et al., 2008; Treusch et al., 2011; Zhang et al., 1994; Zhang et al., 1997). In this study, a GFP-derived fluorescence-based assay for intracellular A β ₄₂ aggregation was developed and characterised in *S. cerevisiae*. The primary aim for this was to identify proteins and cellular processes that affect A β ₄₂GFP aggregation through screening of the *S. cerevisiae* genome-wide deletion library.

Principally, the assay for A β ₄₂ aggregation used in this study is based on the system developed by Kim and Hecht (2005, 2008), who exploited the fusion of enhanced green fluorescent protein (GFP) to the C-terminus of A β ₄₂ (A β ₄₂GFP) to show that a direct correlation exists between fluorescence exhibited and A β ₄₂ aggregation in *E. coli*. In the studies by Kim and Hecht (2005; 2008), it was identified that aggregation of the A β ₄₂-moiety of the A β GFP fusion proteins precludes correct folding of the GFP fluorophore, thus not exhibiting A β ₄₂GFP-associated fluorescence. Detailed biophysical analysis demonstrated that the lack of fluorescence can indeed be attributed to aggregation of the A β ₄₂-moiety (Kim and Hecht, 2008). As such, when A β ₄₂GFP aggregation is reduced, A β ₄₂GFP-associated fluorescence is restored (Kim and Hecht, 2005; Waldo et al., 1999). It was revealed that the last two amino acid residues on the C-terminus of A β ₄₂, isoleucine (residue 41) and alanine (residue 42), strongly influenced the amyloidogenicity of the A β ₄₂ peptide relative to A β ₄₀ peptide (Kim and Hecht, 2005; Wurth et al., 2002). It was also found that substitution of the isoleucine and alanine residues with glutamic acid and proline residues respectively, to generate a variant form of A β ₄₂, termed A β _{EP}, led to dramatically increased fluorescence due to reduced aggregation propensity.

Expression of A β ₄₂GFP in wild-type *S. cerevisiae* cells led to trace levels of A β ₄₂GFP-associated fluorescence in ~5% of the cell population; in contrast to wild-type *S. cerevisiae* cells expressing GFP alone, where ~85% of the cell population exhibited

GFP-derived fluorescence. The lack of A β ₄₂GFP-associated fluorescence in wild-type *S. cerevisiae* cells was hypothesised to be due to aggregation of the fusion protein prior to the correct formation of the GFP fluorophore. This was supported by a number of observations. Western blot analysis of wild-type *S. cerevisiae* cells expressing A β ₄₂GFP fusion protein indicated that the fusion protein was expressed intact and not cleaved/degraded. Expression of the less aggregation-prone A β ₄₀GFP or A β _{EP}GFP led to higher levels of fluorescence in the wild-type *S. cerevisiae* cells. A β _{EP}GFP-associated fluorescence was predominantly intense cytosolic-diffuse observed in ~60% of the cell population; whereas the intensity of A β ₄₀GFP-associated fluorescence was lower relative to A β _{EP}GFP in 50% of the cell population, and this was often accompanied by the presence of one or more intense fluorescent puncta.

Fluorescent puncta were not observed in wild-type *S. cerevisiae* cells expressing GFP alone. The reduced cytosolic-diffuse fluorescence and presence of puncta with A β ₄₀GFP are likely to reflect aggregation of A β ₄₀GFP after correct folding of the GFP fluorophore had occurred. The binding and interaction of one A β peptide to another A β peptide is thought to be facilitated through interaction of one or more of four regions of the A β peptide. These amino acid regions of A β ₄₂ are 15–21, 24–32, 35–37, and 40–42 (Hilbich et al., 1992; Morimoto et al., 2004; Williams et al., 2004). Three of four regions identified to play a role in A β -A β interaction are present in the A β ₄₀ peptide, which accounts for the potential of A β ₄₀ peptide to undergo aggregation. The importance of the 41st and 42nd amino acid residues of A β ₄₂ peptide in influencing aggregation in *S. cerevisiae* is demonstrated by the increased overall fluorescence and size of the fluorescent puncta observed with A β ₄₀GFP relative to A β ₄₂GFP (Kim and Hecht, 2005; Morimoto et al., 2004).

Despite A β ₄₂ and A β ₄₀ sharing ~95% sequence identity, both peptides have been shown to behave characteristically differently *in vivo* (Gouras et al., 2000) and *in vitro* (Jarrett et al., 1993b). Studies by Jarrett *et al* (1993) showed that concentrated solutions of A β ₄₀ did not show signs of aggregation following days of incubation, whereas comparable concentrations of A β ₄₂ aggregated almost immediately (within minutes/hours). These data supported the notion that the aggregation kinetics of A β ₄₂GFP and A β ₄₀GFP were characteristically different and that fluorescent puncta

observed in wild-type *S. cerevisiae* cells expressing A β ₄₀GFP were therefore likely to be aggregates that formed subsequent to folding of the GFP-domain. The difference in overall fluorescence observed with A β ₄₂GFP versus A β ₄₀GFP was also likely to reflect differences in the aggregation kinetics of these A β GFP fusions.

A β aggregation proceeds by a multistep, nucleation-dependent process (Jarrett and Lansbury, 1993). Formation of nucleation seeds is rate limiting, in the absence of preformed seed fibrils there is a significant lag period for the formation of A β fibrils, followed by a rapid fibril elongation phase once seed fibrils have been generated. The lag time for fibril formation can be dramatically shortened by adding preformed fibril seeds to A β monomer (Jarrett and Lansbury, 1993). The rate of A β fibril formation is controlled by both fibril seed and monomer concentrations (Naiki and Nakakuki, 1996). In mammalian cells, it has been proposed that aggregation of A β ₄₂ may act as a nucleation seed for more rapid aggregation of A β ₄₀, the latter being the major component of extracellular plaques found in AD brains (Jarrett et al., 1993b). Data from the seeding experiment demonstrate that A β ₄₂GFP and A β ₄₀GFP fusion proteins appeared to behave in the same way in *S. cerevisiae* cells. Co-induction of A β ₄₂GFP and A β ₄₀GFP gave rise to more fluorescent cells (~22%) than those expressing A β ₄₂GFP alone (5%) but significantly fewer than cells expressing A β ₄₀GFP alone (~40%). Cells expressing both A β ₄₂GFP and A β ₄₀GFP exhibited trace cytosolic fluorescence with intense large puncta and in some cells there were elongated structures. These data lend further support to the use of *S. cerevisiae* as a model system to examine the role of A β ₄₂ in the aggregation of A β ₄₀.

Approximately 50% of wild-type cells expressing A β ₄₀GFP displayed intense cytosolic-diffuse fluorescence but did not exhibit fluorescent puncta. This indicated that a threshold level of A β ₄₀GFP may need to be reached prior to onset of aggregation and generation of fluorescent puncta. Interestingly, in addition to the intense cytosolic-diffuse A β _{EP}GFP-associated fluorescence, ~5% of the fluorescent cells exhibited intense fluorescent puncta. The presence of A β _{EP}GFP-associated fluorescent puncta indicated that A β _{EP} is still capable of aggregation to some extent in *S. cerevisiae*. This finding differs from those of Kim and Hecht (2005) who found that substitution of the 41st and 42nd amino acids of A β ₄₂ with glutamic acid and proline completely prevented

aggregation in *E. coli* cells (Kim and Hecht, 2005), since these two amino acids were found to disrupt β -sheet formation (Creighton, 1992). The differences observed with A β _{EP}GFP in *E. coli* and *S. cerevisiae* may be due to formation of inclusion bodies in the latter. Inclusion bodies appear as small membrane-bound bodies that contain over-expressed protein and their formation does not necessarily reflect aggregation. A more detailed analysis of A β _{EP}GFP in *S. cerevisiae* using biophysical analysis as performed by Kim and Hecht (2008) would be required to determine whether the A β _{EP}GFP puncta observed in *S. cerevisiae* are indeed inclusion bodies.

The identification of factors affecting A β ₄₂ oligomerisation/aggregation are important for the understanding of AD disease progression (Gouras et al., 2005). A primary aim of this study was to identify genes of the *S. cerevisiae* genome that affected intracellular A β ₄₂GFP aggregation. To address this aim, the single gene deletion collection was used to screen for genes that altered the levels of A β ₄₂GFP fluorescence compared to those observed in wild-type cells. Screening of the *S. cerevisiae* genome-wide deletion library identified 110 mutants that exhibited strong A β ₄₂GFP-associated fluorescence and 236 mutants that exhibited weak fluorescence. Analysis of the 110 mutants (that exhibited strong A β ₄₂GFP-associated fluorescence) indicated that four groups were over-represented in the data set with respect to biological function. These over-represented functional groups were: mitochondrial function; transcription/translational regulation; chromatin remodelling/gene silencing/histone exchange; and, phospholipid metabolism and indicated that these cellular processes may play a role in intracellular A β ₄₂ aggregation. Since the mutants belonging to the phospholipid metabolism functional group and mitochondrial functional group were studied in detail, the remainder of this thesis focuses primarily on these mutants.

3.3.2 Disruption to phosphatidylcholine biosynthesis/phospholipid metabolism leads to increased A β ₄₂GFP-associated fluorescence in *S. cerevisiae* cells

Phospholipid (PL) metabolism was over-represented in the data set from the genome-wide screen. Genes in this functional group included *INO2*, *INO4*, *UME6*, *SCS2*, *PSD1*, *CHO2* and *OPI3*. A detailed description of each gene function is given in Table 3-1. Six of these mutants (Δ *ino2*, Δ *ino4*, Δ *psd1*, Δ *cho2*, Δ *opi3* and Δ *ice2*)

exhibited the characteristic arc-shaped organelle/membrane-associated A β ₄₂GFP localisation.

Ino2p and Ino4p form a basic heteromeric helix–loop–helix dimer that functions as a transcriptional regulator, specifically for induction of genes involved in phospholipid biosynthesis in response to choline depletion, including *INO1* and *OPI3*, (Bailis et al., 1987; Hirsch and Henry, 1986). The Ino2p-Ino4p transcriptional regulator is also involved in the regulation of phospholipid methylation in the membranes (Loewy and Henry, 1984). Loewy and Henry (1984) reported that the Δ *ino2* and Δ *ino4* mutants have a reduced capacity to produce phosphatidylcholine (PC) via methylation of phosphatidylethanolamine (PE) and that both Ino2p and Ino4p are specifically involved in the regulation of PC biosynthesis. Δ *ino2* and Δ *ino4* mutants exhibited ~25% decrease in PC and a ~50% and 400% increase in PE and phosphatidyl-*N*-dimethylethanolamine (PDME) respectively in cellular membranes compared to the wild-type strain (Loewy and Henry, 1984).

In a genome-wide microarray analysis, 28 genes were found to be strongly regulated by the Ino2p and Ino4p transcriptional complex, including *OPI3*, *PSD1*, *CDS1*, *INO1*, *CHO1*, *ITR1*, *CKII*, *SAH1* and *HNMI* (Jesch et al., 2005). These target genes are involved in phospholipid biosynthesis and unfolded protein response pathways. The latter is a response used by cells to counter endoplasmic reticulum (ER) stress (Travers et al., 2000). Psd1p, Cho2p and Opi3p, which encode phosphatidylserine decarboxylase, phosphatidyl-*N*-methylethanolamine *N*-methyltransferase or phosphatidylethanolamine-*N*-methyltransferase (PEMT) respectively, are involved in the *de novo* synthesis of PC. Deletion of *PSD1*, *CHO2* or *OPI3* genes affected A β ₄₂GFP fluorescence. Psd1p converts phosphatidylserine (PS) to PE, Cho2p subsequently catalyses the methylation of PE to phosphatidyl-monomethylethanolamine (PMME), while Opi3p, catalyses conversion of PMME to PDME and PC via two sequential steps. *S*-adenosyl-L-methionine (SAM) acts as the methyl-group donor in the reactions catalysed by Cho2p and Opi3p, to form *S*-adenosyl-L-homocysteine (SAH) (Kodaki and Yamashita, 1987; McGraw and Henry, 1989; Summers et al., 1988). Refer to Figure 4-1 (page 97) for an overview of the PC biosynthetic and PL metabolic pathways.

The membranes of both $\Delta cho2$ and $\Delta opi3$ strains were found to be depleted of PC. However, significant differences in phospholipid composition were observed between the $\Delta cho2$ and $\Delta opi3$ strains. The $\Delta cho2$ strain showed a ~70% decrease in PC relative to wild-type cells (Summers et al., 1988) compared to the $\Delta opi3$ strain, where membranes were almost devoid of PC (McGraw and Henry, 1989). The $\Delta opi3$ mutant showed a ~50% decrease in PE but an over-accumulation of PMME (McGraw and Henry, 1989), while $\Delta cho2$ mutants exhibited a 2-fold increase in PE (Summers et al., 1988). Based on the reported phospholipid content of the $\Delta cho2$ and $\Delta opi3$ mutants, it is likely that A β_{42} GFP-associated fluorescence is affected by PC depletion, or, PE/PMME over-accumulation or a combination of both.

The $\Delta cho2$ strain exhibited strong A β_{42} GFP-associated cytosolic and punctate fluorescence, as opposed to the $\Delta opi3$ strain, which exhibited weaker cytosolic fluorescence but intense fluorescent puncta arranged in an arc-shape. Differences in the phospholipid composition of $\Delta cho2$ and $\Delta opi3$ mutants may have led to the different localisation patterns of A β_{42} GFP. Alternatively, since Opi3p was found to efficiently suppress the phospholipid methylation defect in cells with the $\Delta cho2$ mutation by masking the methyltransferase function (Preitschopf et al., 1993), the slight increase in PC in $\Delta cho2$ relative to $\Delta opi3$ mutants may have led to a less profound effect on A β_{42} GFP localisation. It is interesting to note that the mutants exhibiting the characteristic arc-shaped A β_{42} GFP localisation, $\Delta ino2$, $\Delta ino4$ and $\Delta opi3$ strains were all found to have significantly increased levels of PE or PMME respectively.

To understand the link between phosphatidylcholine (PC) biosynthesis/phospholipid (PL) metabolism and A β_{42} GFP aggregation, a ‘reverse-genetics’ approach was used to screen for genes that when over-expressed altered A β_{42} GFP aggregation in *S. cerevisiae*. These data are presented in Chapter 4, which elucidates the important role of phospholipid homeostasis in intracellular membranes of cells.

3.3.3 Disruption to mitochondrial function leads to increased A β ₄₂GFP-associated fluorescence in *S. cerevisiae* cells

The mitochondria functional group represents the largest functional category of mutants over-represented in the data set from the genome-wide screen. Detailed descriptions of each gene belonging to this functional group and its cellular functions are given in Table 3-1. It is also interesting to note that many mutants identified in this screen have disrupted mitochondrial functions indicated by their respiratory incompetence. Increased A β ₄₂GFP fluorescence was detected in mutants affected in assembly of ETC complexes (complex III ($\Delta cbp3$), complex IV ($\Delta cox16$, $\Delta cox20$ and $\Delta pet117$) and ATP synthase ($\Delta atp11$ and $\Delta stf2$), mitochondrial genome maintenance, or the TCA cycle ($\Delta cit1$, $\Delta cit3$, $\Delta aco1$, $\Delta aco2$, $\Delta idh1$, $\Delta idh2$, $\Delta idp1$, $\Delta kgd1$, $\Delta kgd2$, $\Delta lpd1$, $\Delta lsc1$, $\Delta lsc2$, $\Delta sdh1$, $\Delta sdh2$, $\Delta sdh4$, $\Delta fum1$, $\Delta mdh1$, $\Delta pyc1$, $\Delta pyc2$). The very significant over-representation of mutants involved in mitochondrial functions raises the possibility of an interaction between A β ₄₂GFP and mitochondria. Cellular sub-fractionation indicated that A β ₄₂GFP fusion proteins were detected in the mitochondrial fraction in wild-type cells, but mitochondrial co-localisation was not observed using fluorescence microscopy in wild-type or mutant strains affected in mitochondrial function. Therefore, one possible explanation may be that non-fluorescent A β ₄₂GFP aggregates present in cells are co-fractionating with the mitochondria.

During growth in exponential phase on fermentable carbon sources, *S. cerevisiae* is less dependent on mitochondrial ETC function. Since the genome-wide screen for A β ₄₂GFP fluorescence was performed using galactose media, reduced energy metabolism due to mitochondrial respiratory defects is less likely to be the cause of altered A β ₄₂GFP fluorescence. One possibility is that a metabolite in, or derived from, the TCA cycle may affect A β ₄₂GFP aggregation. TCA cycle intermediates, oxaloacetate, α -ketoglutarate, citrate and succinyl-CoA are precursors for several anabolic processes, such as biosynthesis of porphyrins (for heme production), amino acids, purines, pyrimidines, fatty acids, sterols, and neurotransmitters (in neuronal cells). Apart from porphyrins, all other metabolites provide the TCA cycle with the intermediates when turned over by the metabolic activity of the cell. Porphyrins and heme may be possible candidate metabolites to be analysed since its metabolism has been previously found to

be altered in AD (Atamna, 2006; Atamna and Boyle, 2006; Atamna and Frey, 2004; Atamna and Frey, 2007; Chuang et al., 2012).

Heme is tightly linked to the TCA cycle and to several metabolic processes in the cell. Porphyrin, whose cellular functions are not yet properly understood, is an important precursor for heme biosynthesis. The biosynthesis of one mole of heme requires 8 moles of succinyl-CoA and glycine (Woods, 1976; Ponka, 1999) from the TCA cycle and mitochondrial pool of amino acids, respectively. ETC complex IV contains heme-*a* at a stoichiometry of two molecules per ETC complex IV (Mogi et al., 1994) and it is the only protein complex in the cell to contain heme-*a*. Interestingly, it was found that heme and other related porphyrins inhibit *in vitro* aggregation of A β even at very low A β /heme ratios. It was further demonstrated that heme protected neuronal cells against A β -induced toxicity (Howlett et al., 1997). It has been hypothesised that since A β peptide contains three histidines, it can potentially bind heme and subsequently prevent aggregation either by changing conformation of the A β peptide, its hydrophobicity, or by masking sites that binds free iron or copper, which may trigger A β aggregation (Atamna, 2004). However, the effect of endogenous heme on A β aggregation and consequences of metabolic changes on the TCA cycle (such as levels of succinyl-CoA) and heme is not clearly understood.

While glycolysis and oxidative phosphorylation decrease in the aging brain and in AD patients (Blass, 2001; Valla et al., 2001), heme degradation has been found to increase with age and in neurodegeneration (Bitar and Shapiro, 1987; Schipper, 2000; Smith et al., 2000). Bilirubin, a by-product of heme degradation, is found to be increased in the CSF in AD patients (Kimpura et al., 2000). Furthermore, levels of a heme/heme-metabolite which inhibits the muscarinic acetylcholine receptor, isolated from AD brains, was found to be threefold higher in AD brains than in controls (Fawcett et al., 2002). These data strongly suggest a possible link between mitochondrial function, heme and A β aggregation. Although heme is important for metabolic homeostasis, mitochondrial integrity, and regulation of specific transcription factors, the role of endogenous heme in cell metabolism is poorly understood, especially in neurodegeneration. Hence, the consequences of altered levels of heme *in vivo*, especially on the brain are unknown.

The TCA cycle is an amphibolic biochemical pathway, where intermediates of this pathway are involved in both anabolic and catabolic processes either by supplying or receiving the carbon skeleton of several metabolites (Owen et al., 2002). It is tempting to speculate that disruption of the TCA cycle would affect acetyl-CoA metabolism and affect processes including lipid homeostasis. However, a more detailed analysis of the mechanism(s) mediating the changes in A β ₄₂GFP fluorescence in the mitochondrial mutants is required, and a metabolomics approach to identify changes in mitochondrial metabolites may be informative. To understand the link between mitochondrial/respiratory function and A β ₄₂GFP aggregation, biochemical and reverse genetics approaches were used to screen for genes that when over-expressed altered A β ₄₂GFP aggregation in *S. cerevisiae*. These data are presented in Chapter 5, which elucidate the important role of mitochondrial function in A β ₄₂GFP aggregation.

4 CHAPTER 4: UNDERSTANDING MECHANISMS OF AMYLOID-BETA AGGREGATION AND LOCALISATION IN *S. CEREVISIAE*

4.1 Introduction and Aims

Since the genome-wide screen identified phospholipid metabolism as an important biological process affecting A β aggregation, relevant information concerning phosphatidylcholine biosynthesis and phospholipid metabolism in *S. cerevisiae* is provided below.

Phospholipids play important roles in intracellular signalling, membrane structure and identity, membrane trafficking pathways as well as anchoring of membrane proteins (Carman and Henry, 1999; Fujita and Jigami, 2008; Henry et al., 2012; Pittet and Conzelmann, 2007; Roth et al., 2006; Vicinanza et al., 2008). As such, phospholipid biosynthesis is tightly regulated in cells depending on factors such as availability of exogenous supplies of phospholipid precursors/intermediates, membrane trafficking and growth stage. This facilitates biogenesis and maintenance of membranes (Carman and Henry, 1999). Phosphatidylcholine (PC), phosphatidylethanolamine (PE), phosphatidylglycerol (PG), phosphatidylinositol (PI), phosphatidylserine (PS) and cardiolipin (CL) constitute a class of lipids termed glycerophospholipids, which comprise 70-80% of total cellular lipids. These glycerophospholipids as well as neutral glycerolipids diacylglycerol (DAG) and triacylglycerol (TAG) are derived from the precursor lipid phosphatidic acid (PA). On average, intracellular membranes of eukaryotes have a phospholipid composition of 50% PC, 10–25% PE and 1–10% PS (Voelker, 2005).

The *S. cerevisiae* biosynthetic pathways for the synthesis of glycerophospholipids and glycerolipids, the localisation of the enzymes and transporters involved in their metabolism are illustrated in Figure 4-1. *S. cerevisiae* synthesises PC via reactions performed in the endoplasmic reticulum, Golgi and mitochondria (van Meer et al., 2008). Phosphatidylserine decarboxylases Psd1p and Psd2p, which are localised in the mitochondria and Golgi/vacuoles respectively, catalyse the decarboxylation of PS to PE (Clancey et al., 1993; Trotter et al., 1993; Trotter et al., 1995; Trotter and Voelker, 1995). Mitochondria-localised Psd1p contributes almost 90%

of total PS decarboxylase activity in cells. Cho2p subsequently catalyses methylation of PE to phosphatidyl-monomethylethanolamine (PMME), while Opi3p, catalyses conversion of PMME to phosphatidyl-dimethylethanolamine PDME and PC via two sequential steps. *S*-adenosyl-L-methionine (SAM) acts as the methyl-group donor in the reactions catalysed by Cho2p and Opi3p, to form *S*-adenosyl-L-homocysteine (SAH) (Kodaki and Yamashita, 1987; McGraw and Henry, 1989; Summers et al., 1988). Phosphatidylcholine can also be synthesised from uptake of exogenous choline via the Kennedy salvage pathway (Kennedy and Weiss, 1956).

Synthesis of PI, an inositol-containing phospholipid, is regulated in response to inositol levels. Through the activity of Pis1p, cytidine-diphosphate-diacylglycerol (CDP-DAG) donates its phosphatidyl moiety to inositol to form PI (Figure 4-1) (Fischl and Carman, 1983; Paulus and Kennedy, 1960). Supplementation of inositol in the growth media increases PI levels in cells due to increased activity of PI synthase and reduced levels of PS, PE and PC due to inhibition of PS synthase, Cho1p activity (Kelley et al. 1988; Loewen et al. 2004). PI subsequently serves as a precursor for the synthesis of sphingolipids, polyphosphoinositides and glycolipid anchors for a few plasma membrane proteins (Dickson and Lester, 2002; Liu et al., 2005; Strahl and Thorner, 2007).

In view of the link between lipid homeostasis and AD (Jones et al., 2010), this chapter examines the phospholipid mutants which gave rise to increased A β ₄₂GFP fluorescence and exhibited a distinctive subcellular localisation. In addition to identifying this subcellular localisation using confocal microscopy, the GFP-derived fluorescence-based assay for intracellular A β ₄₂ aggregation (described in Chapter 1) was further exploited using gene over-expression analysis. This approach was undertaken to investigate if the increased A β ₄₂GFP fluorescence and partitioning of A β ₄₂GFP into the ER in the relevant phospholipid mutants were caused by an accumulation of a specific phospholipid intermediate upstream of the PC biosynthetic pathway. This ‘reverse-genetics’ approach provided further insight into the link between altered phospholipid homeostasis and A β ₄₂GFP fluorescence. In order to understand the cellular mechanisms involved in A β aggregation in these phospholipid mutants, the work described in this chapter further examines the effects of intracellular levels of important lipid

precursors/co-factors involved in the *de novo* phospholipid biosynthetic pathway on A β ₄₂GFP aggregation.

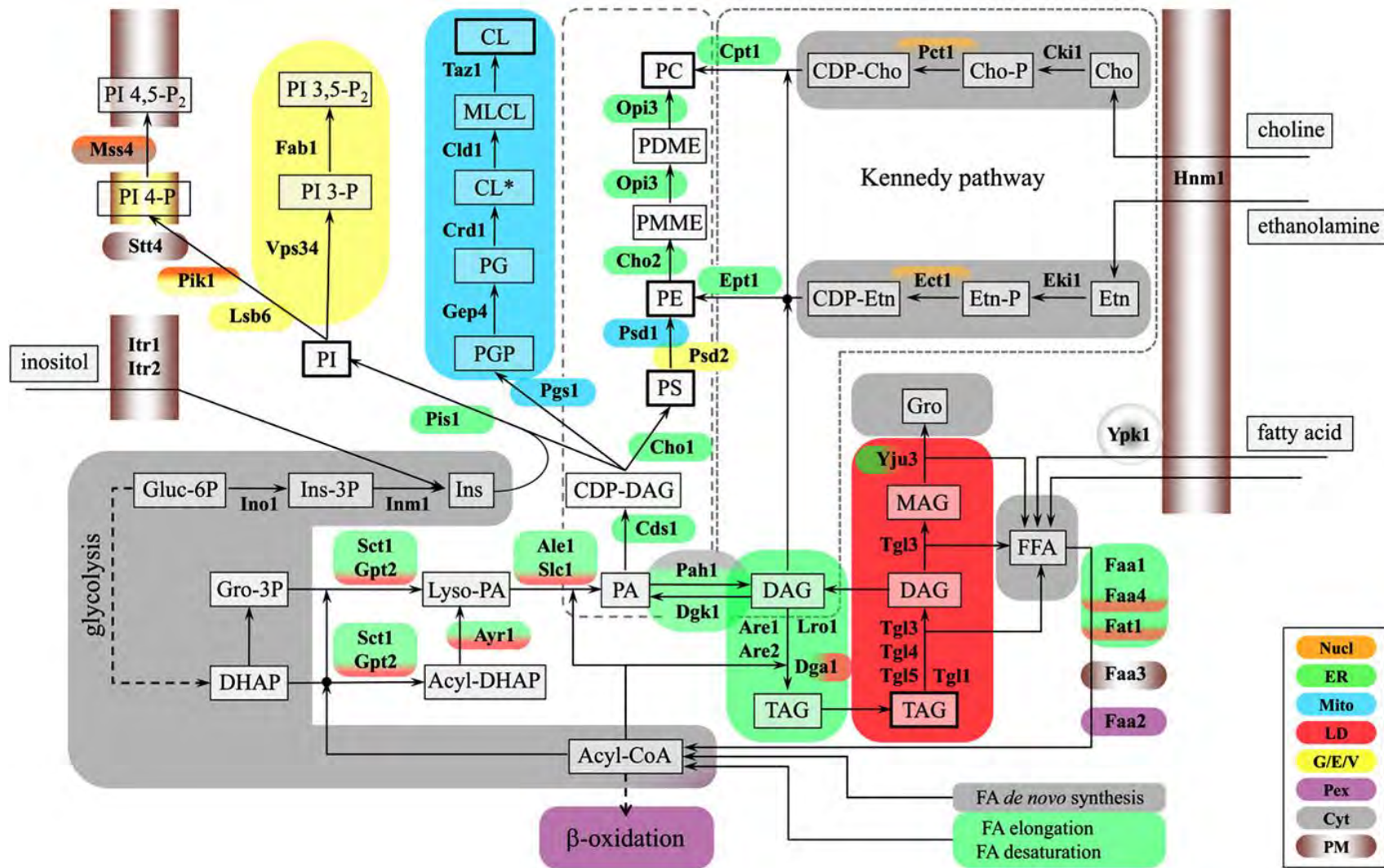


Figure 4-1 Overview of the pathways for lipid metabolism and their subcellular localisation in *S. cerevisiae*

The pathways shown for the synthesis of major glycerophospholipids and the relevant steps discussed in the text. PA serves as the immediate precursor of CDP-DAG, glycerophospholipids and glycerolipids diacylglycerol (DAG) and triacylglycerol (TAG). As illustrated, synthesis of PC from PA is performed in the endoplasmic reticulum, Golgi and mitochondria (van Meer et al., 2008). PS is decarboxylated to form PE via Psd1p and Psd2p, followed by Cho2p which catalyses the first methylation step to convert PE to PMME. Opi3p catalyses two sequential methylation steps to convert PMME to PDME and PC. *S. cerevisiae* cells are able to take up exogenous choline or ethanolamine to synthesise PC via the Kennedy salvage pathway (as indicated). Abbreviations used: TAG, triacylglycerols; PI, phosphatidylinositol; PA, phosphatidic acid; CDP-DAG, CDP-diacylglycerol; DAG, diacylglycerol; MAG, monoacylglycerol; Gro, glycerol; DHAP, dihydroxyacetone phosphate; PS, phosphatidylserine; PE, phosphatidylethanolamine; PG, phosphatidylglycerol; PGP phosphatidylglycerol phosphate; CL* precursor cardiolipin; MLCL, monolyso-cardiolipin; CL, mature cardiolipin; PMME, phosphatidylmonomethylethanolamine; PDME, phosphatidyl-dimethylethanolamine; PC, phosphatidylcholine; FFA, free fatty acids; Cho, choline, Etn, ethanolamine, Ins, inositol; Cho-P, choline phosphate; CDP-Cho, CDP-choline; Etn-P, ethanolamine phosphate; CDP-Etn, CDP-ethanolamine; PI 3-P, phosphatidylinositol 3-phosphate; PI 4-P, phosphatidylinositol 4-phosphate; PI 4,5-P₂, phosphatidylinositol 4,5-bisphosphate; PI 3,5-P₂, phosphatidylinositol 3,5-bisphosphate. Nucl, nucleus; ER, endoplasmic reticulum; Mito, mitochondria; LD, lipid droplets; G/E/V, Golgi, endosomes, vacuole; Pex, peroxisomes; Cyt, cytoplasm; PM, plasma membrane. Figure modified from Henry et al., 2012.

4.2 Results – Understanding the link between phospholipid metabolism and A β ₄₂GFP aggregation

4.2.1 Investigation of A β ₄₂GFP localisation in mutants identified by the *S. cerevisiae* genome-wide screen

In this study, five apparently distinct A β ₄₂GFP localisation patterns were observed among the 110 mutants listed in Table 3-1. These distinct localisation patterns were single punctate (29%), multiple puncta (9%), cytosolic-diffuse (22%), distinct arc-shaped membrane/ organelle associated localisation (5%) and a combination of punctate and cytosolic-diffuse fluorescence (35%). The percentage values provided reflect the number of mutants that exhibit A β ₄₂GFP-associated fluorescence in a specific localisation, with respect to the 110 mutants identified by the screen. A graphical representation of these data and an example of each localisation pattern is given in Figure 4-2.

A structured A β ₄₂GFP fluorescence localisation was likely to be indicative of a distinct cellular localisation; possibly organelle and/ or membrane-associated. Of the A β ₄₂GFP localisation patterns identified, the arc-shaped fluorescence localisation in

mutants affected in phosphatidylcholine biosynthesis/phospholipid homeostasis and the combination of cytosolic-diffused and/or small puncta fluorescence observed in mutants affected in mitochondrial function were distinctive and these mutants were selected for further investigation. Deletion of six genes expressing A β ₄₂GFP exhibited a structured arc-shaped A β ₄₂GFP fluorescence. Of these six genes, three encode consecutive steps in the conversion of phosphatidylserine to phosphatidylcholine (phosphatidylserine decarboxylase, *PSDI*; and phosphatidylethanolamine methyltransferases, *CHO2* and *OPI3*) (Figure 4-1); two encode a heterodimeric transcriptional regulator of phospholipid and inositol biosynthesis (*INO2* and *INO4*) (Ambroziak and Henry, 1994); and lastly *ICE2*, which encodes an integral ER membrane protein involved in cortical ER inheritance (Estrada de Martin et al., 2005). The localisation of A β ₄₂GFP in these six mutant strains as well as mutants affected in mitochondrial function, illustrated in Figure 4-3, and their corresponding genes are discussed in further detail in this chapter and in Chapter 5.

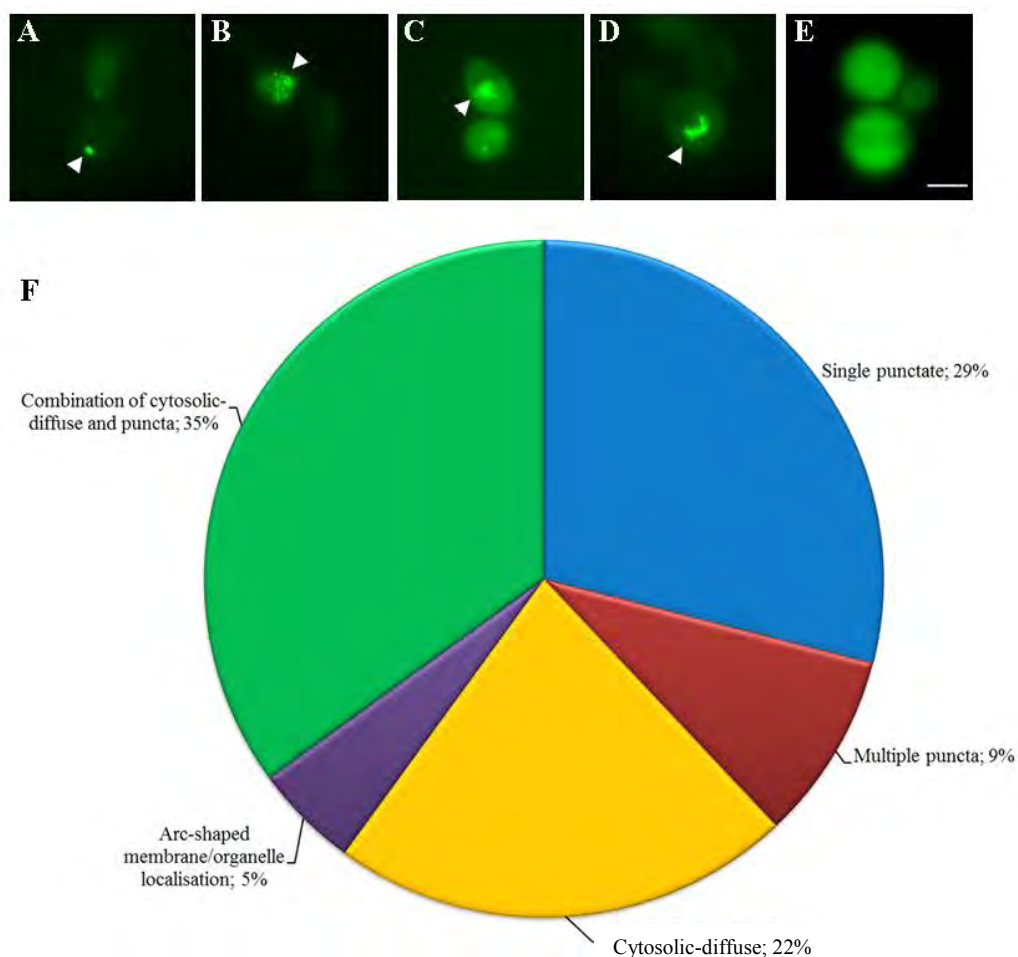


Figure 4-2 Fluorescent microscopic images of representative mutants exhibiting various A β_{42} GFP localisation patterns.

Strains expressing A β_{42} GFP were induced in galactose medium (SCgal-URA) and A β_{42} GFP-associated fluorescence analysed between 12 to 18 h post induction. The A β_{42} GFP-associated localisation patterns were classified as A) fluorescent punctate, $\Delta scs2$; B) multiple fluorescent puncta, $\Delta acol$; C) combination of puncta and cytosolic fluorescence, $\Delta pdx3$; D) arc-shaped organelle/ membrane-associated fluorescence, $\Delta psd1$; and E) cytosolic-diffuse fluorescence, $\Delta kgd2$. Arrows indicate the specific type of localisation in each of the mutants. Scale bars indicate 5 μ m. B) Graphic representation of the various types of A β_{42} GFP localisation described above.

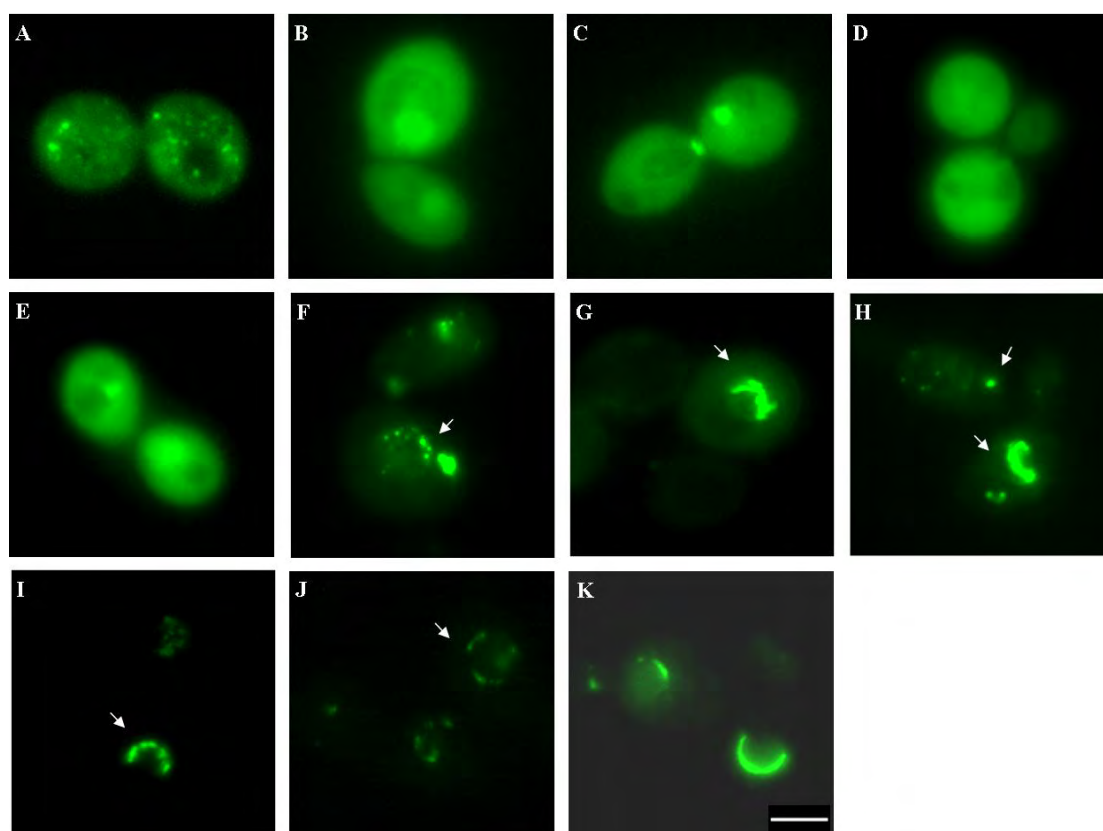


Figure 4-3 Fluorescent microscopic images of representative mutants from the phospholipid metabolism and mitochondrial functional groups exhibiting various A β_{42} GFP localisation patterns

TCA cycle and phospholipid mutants expressing A β_{42} GFP induced in galactose medium and A β_{42} GFP-associated fluorescence analysed at 12 h post induction. TCA cycle mutants (A) $\Delta acol$, (B) $\Delta fum1$, (C) $\Delta idp1$, (D) $\Delta kgd2$ and (E) $\Delta sdh4$ were observed to predominantly exhibit cytosolic-diffuse A β_{42} GFP-associated fluorescence, with some mutants exhibiting fluorescent puncta. Phospholipid mutants (F) $\Delta opi3$, (G) $\Delta psd1$, (H) $\Delta cho2$, (I) $\Delta ino2$, (J) $\Delta ino4$ and (K) $\Delta ice2$ were observed to exhibit a distinct arc-shaped organelle/ membrane-associated fluorescence. Scale bar indicate 5 μ m.

4.2.2 Localisation of less aggregation-prone A β ₄₀GFP and A β _{EP}GFP in mutants of the phospholipid metabolism functional group

To examine whether the distinct localisation of A β ₄₂GFP in Δ *opi3*, Δ *cho2* and Δ *ice2* mutants was dependant on the aggregation propensity of the A β ₄₂-moiety of the fusion protein, the localisations of A β ₄₀GFP and A β _{EP}GFP were analysed. In the Δ *opi3*, Δ *cho2* and Δ *ice2* mutants expressing the less aggregation-prone fusion proteins, A β ₄₀GFP and A β _{EP}GFP was localised in an arc-shaped structure, analogous to the manner in which A β ₄₂GFP localised in these strains (Figure 4-4).

The rationale for this approach is that in wild-type cells A β _{EP}GFP does not appear to aggregate and exhibits a cytosolic-diffuse localisation pattern (Figure 3-2). Comparable localisations of A β ₄₂GFP, A β ₄₀GFP or A β _{EP}GFP in the Δ *opi3*, Δ *cho2* and Δ *ice2* strains indicated that the distinct localisation of A β ₄₂GFP in these strains does not depend on the aggregation propensity of the A β -moiety of the fusion protein i.e. the fluorescent structures observed for A β ₄₂GFP in Δ *opi3*, Δ *cho2* and Δ *ice2* strains are unlikely to be aggregates.

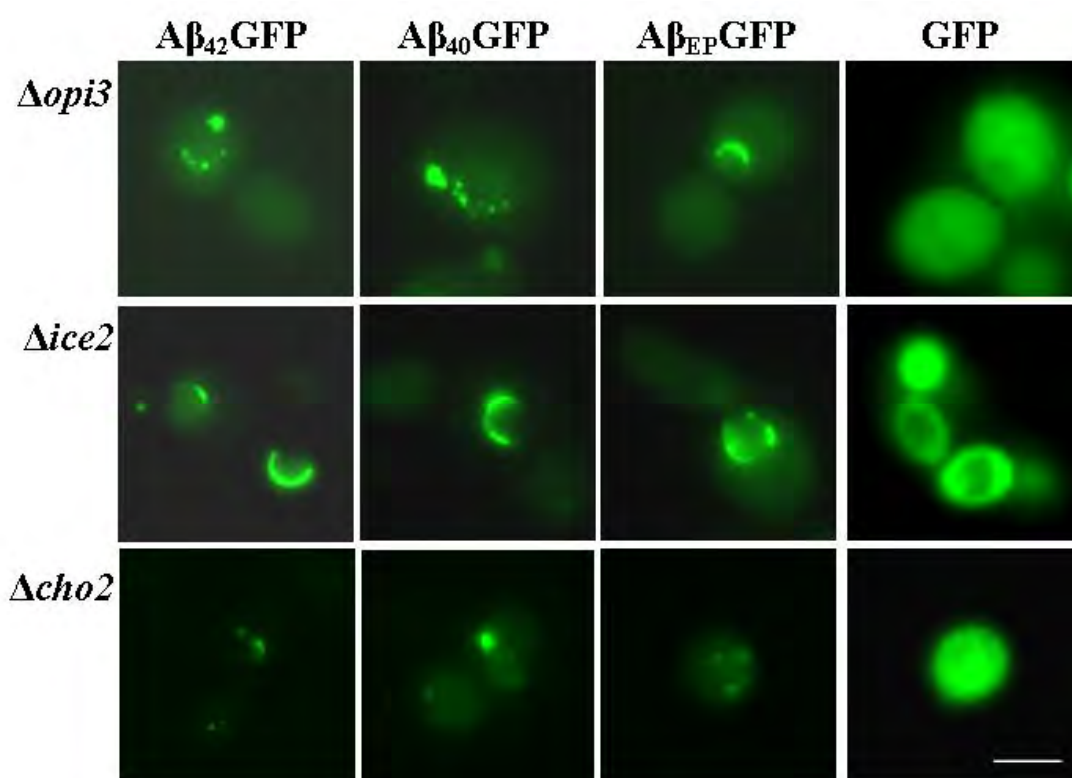


Figure 4-4 Fluorescent microscopic images of Δ *opi3*, Δ *cho2* and Δ *ice2* strains expressing A β ₄₂GFP, A β ₄₀GFP, A β _{EP}GFP or GFP.

Δ *opi3*, Δ *cho2* and Δ *ice2* strains expressing various forms of A β fusion proteins were induced in galactose medium (SCgal-URA) and A β ₄₂GFP-associated fluorescence analysed at 12 h post

induction. The distinct arc-shaped localisation is observed in $\Delta opi3$, $\Delta cho2$ and $\Delta ice2$ strains expressing $A\beta_{42}GFP$, $A\beta_{40}GFP$ and $A\beta_{EP}GFP$. Scale bar indicate 5 μm .

4.2.3 Western blot analysis of mutants affected in phospholipid metabolism expressing $A\beta_{42}GFP$, $A\beta_{40}GFP$, $A\beta_{EP}GFP$ or GFP

The inverse correlation between fluorescence intensity and the amyloidogenicity of the $A\beta$ moiety supported the validity of using $A\beta_{42}GFP$ and a fluorescence-based approach in *S. cerevisiae* cells to identify cellular factors that may influence intracellular $A\beta_{42}$ aggregation. In view of the link between lipid homeostasis and AD (Jones et al., 2010), it was important to investigate in the phospholipid mutants if the increased $A\beta_{42}GFP$ fluorescence was due to increased levels of non-aggregated and soluble $A\beta_{42}GFP$. In order to examine this, wild-type BY4743 and $\Delta opi3$ cells expressing $A\beta_{42}GFP$, $A\beta_{40}GFP$, $A\beta_{EP}GFP$ fusion proteins or GFP were grown to exponential phase (OD₆₀₀ 1.5) in galactose (induction) medium. Soluble proteins were harvested from cell extracts and protein concentration determined by Bradford protein assay. Load-controlled soluble proteins were analysed by western blot analysis using anti-GFP antibody.

Wild-type BY4743 and $\Delta opi3$ cells expressing any of the forms of $A\beta GFP$ fusion exhibited a band of ~30 kDa expected from the molecular mass of the fusion proteins (Figure 4-5). The relative intensity of this band in $\Delta opi3$ cells expressing $A\beta_{42}GFP$ was similar in wild-type cells expressing the same construct, and hence similar expression levels of $A\beta_{42}GFP$ peptide were present in both the $\Delta opi3$ and wild-type cells. Similar intensity of the $A\beta_{40}GFP$ and $A\beta_{EP}GFP$ bands was also observed in both wild-type and $\Delta opi3$ cells (Figure 4-5). These data indicated that the increase in fluorescence in $\Delta opi3$ cells is not due to increased expression of $A\beta_{42}GFP$ protein, but the possible presence of soluble fluorescent $A\beta_{42}GFP$ peptides in deletion mutant strains exhibiting increased level of $A\beta_{42}GFP$ -associated fluorescence.

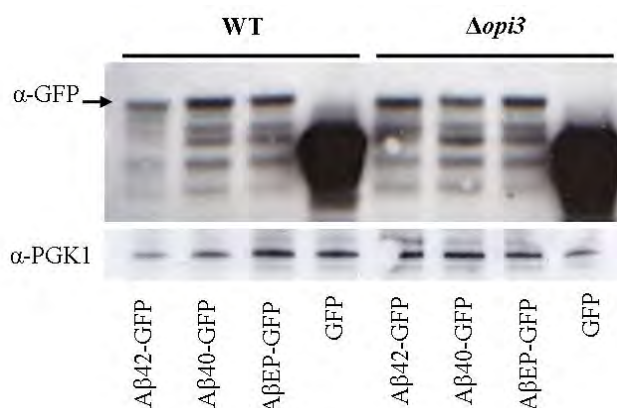


Figure 4-5 Western blot analysis of soluble cell extracts from BY4743 wild-type and $\Delta opi3$ cells expressing A β ₄₂GFP, A β ₄₀GFP, A β _{EP}GFP and GFP control vector

Load-controlled soluble cell extracts were prepared from wild-type cells expressing A β ₄₂GFP, A β ₄₀GFP, A β _{EP}GFP fusion proteins or GFP were grown to exponential phase (OD₆₀₀ 1.5) in galactose (induction) medium. Analysis by western blot analysis was carried out using anti-GFP antibody. PGK1p was used as a loading control.

4.2.4 Perinuclear localisation of fluorescent A β ₄₂GFP in mutants of the phospholipid metabolism functional group was determined to be interacting with the endoplasmic reticulum (ER) and not lipid droplets (LD).

In order to determine the cellular localisation of A β ₄₂GFP in the $\Delta ice2$ mutant, and, $\Delta opi3$ and other mutants of the phosphatidylcholine biosynthetic pathway, A β ₄₂GFP was induced for 12 h and cells were stained with 4',6'-diamidino-2-phenylindole (DAPI). Staining with DAPI showed that in $\Delta ice2$ and $\Delta opi3$ strains, the arc-shaped A β ₄₂GFP localisation was juxtaposed to the nucleus (i.e. perinuclear) in these mutants. Evidence of the perinuclear localisation is indicated by the merged images in Figure 4-6 using both fluorescence microscopy and confocal microscopy.

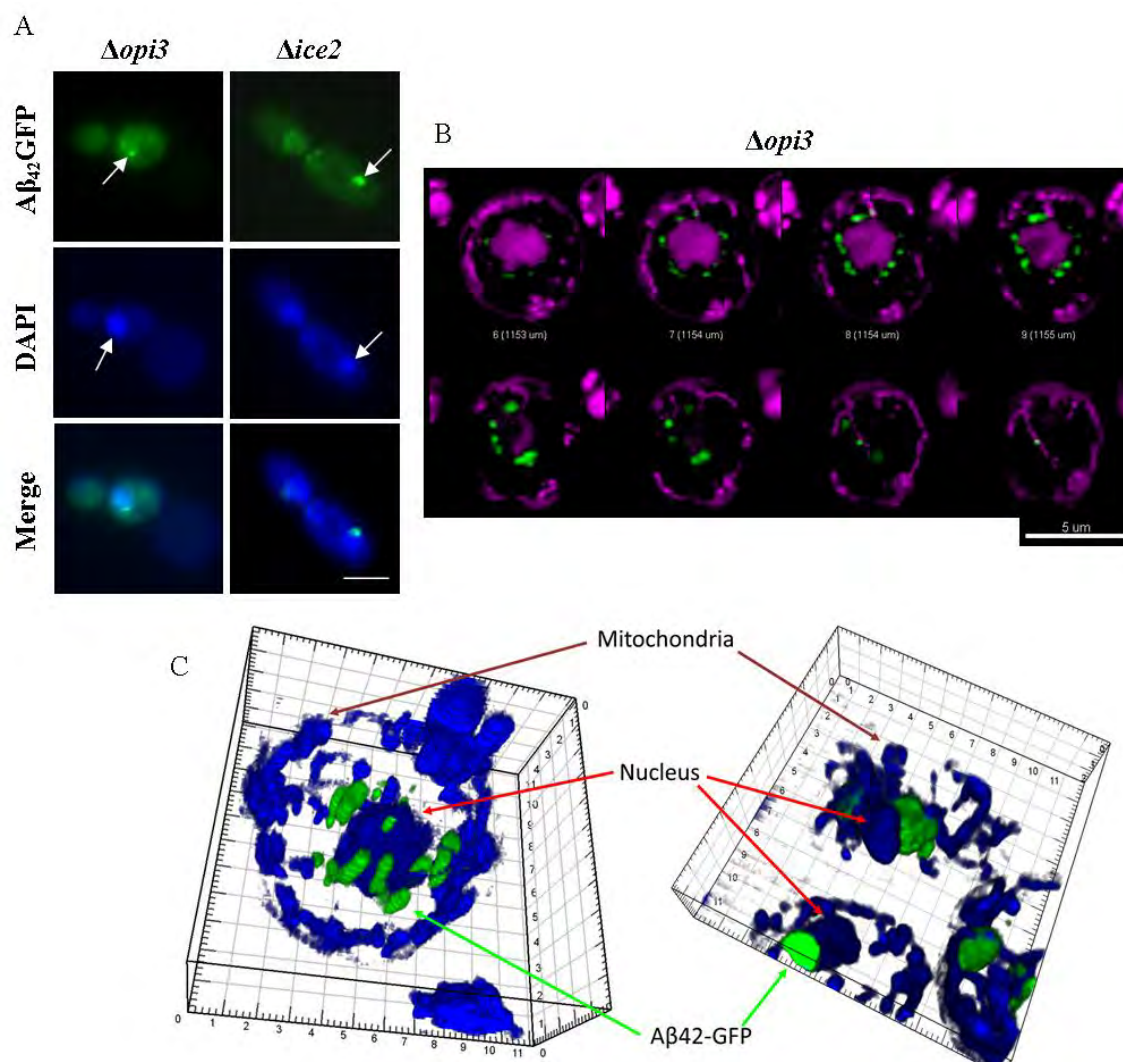


Figure 4-6 Fluorescent and confocal microscopic images of Δopi3 , Δcho2 and Δice2 strains exhibiting strong $\text{A}\beta_{42}\text{GFP}$ -associated fluorescence and DAPI staining.

Strains expressing $\text{A}\beta_{42}\text{GFP}$ were induced in galactose medium (SCgal-URA). Cells were stained with DAPI and the localisation of nuclear and mitochondrial DNA, and $\text{A}\beta_{42}\text{GFP}$ -associated fluorescence were analysed at 12 h post induction. A) $\text{A}\beta_{42}\text{GFP}$ localisation in Δopi3 and Δice2 strains is observed in the top series of panels (arrows indicate $\text{A}\beta_{42}\text{GFP}$ localisation). DAPI staining of mitochondrial and nuclear DNA is observed in the middle series of panels (arrows indicate the nucleus of each cell). Merged images of $\text{A}\beta_{42}\text{GFP}$ and DAPI staining (bottom series of panels) indicate the close proximity of $\text{A}\beta_{42}\text{GFP}$ to the periphery of the nucleus. B) Series of confocal microscopic images, taken at 1 μm intervals (as indicated), of Δopi3 cell exhibiting the distinct arc-shaped localisation, demonstrates that $\text{A}\beta_{42}\text{GFP}$ is juxtaposed to the nucleus. C) 3D construction of the confocal microscopic images from (B) of the Δopi3 cell (left panel) and Δcho2 cell (right panel) exhibiting intense $\text{A}\beta_{42}\text{GFP}$ fluorescence with perinuclear localisation. Scale bars indicate 5 μm .

The perinuclear localisation of fluorescent $\text{A}\beta_{42}\text{GFP}$ in mutants affected in phospholipid metabolism appeared to resemble that of the endoplasmic reticulum (ER). In order to determine the precise localisation of $\text{A}\beta_{42}\text{GFP}$ in the mutants affected in

phospholipid metabolism and assess if the perinuclear localisation of A β ₄₂GFP was interacting and/or adsorbed in to the ER, subcellular fractionation was carried out on wild-type BY4743 and Δ *opi3* cells expressing A β ₄₂GFP (Figure 4-7). Expression of A β ₄₂GFP in both strains was induced in galactose media (SCgal-URA) and grown to exponential phase (OD₆₀₀ 1.5). Pelleted cells were spheroplasted and subcellular fractions collected based on sucrose density gradients. Soluble proteins were harvested from subcellular fractions and load-controlled soluble proteins were analysed by western blot analysis using anti-Por1p antibody (to detect the presence of mitochondrial proteins), anti-Wbp1p antibody (to detect the presence of ER proteins) and anti-GFP antibody (to detect the presence of A β ₄₂GFP) (Figure 4-7).

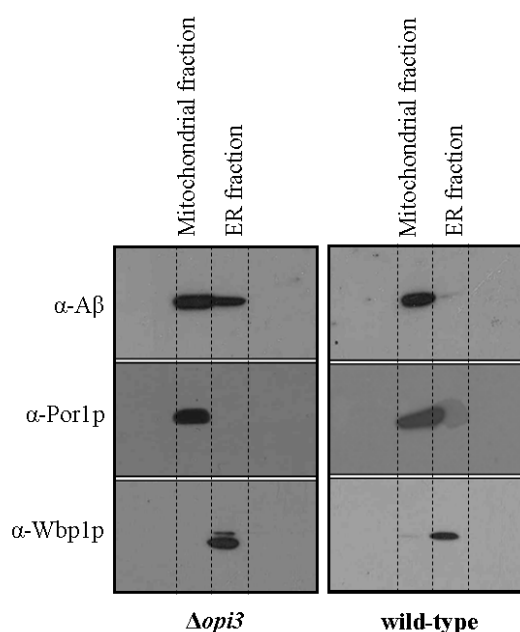


Figure 4-7 Western blot analysis of subcellular fractions from Δ *opi3* and BY4743 wild-type cells expressing A β ₄₂GFP.

Load-controlled soluble proteins were prepared from subcellular fractions (mitochondria and ER) of Δ *opi3* and wild-type cells expressing A β ₄₂GFP. Strains were grown to exponential phase (OD₆₀₀ 1.5) in galactose (induction) medium. Analysis by western blot was carried out using anti-GFP (top panel), anti-Por1p (middle panel) and anti-Wbp1p antibodies (bottom panel). Based on the purity of the subcellular fractions and the lack of cross-contamination between the mitochondrial and ER fractions, presence of A β ₄₂GFP is clearly indicated in the ER fraction of Δ *opi3* cells.

Qualitative assessment using western blot analysis of the mitochondrial and ER fractions indicated that both subcellular fractions were of high purity and lacked cross-contamination between the two organelles during subcellular fractionation. As

previously shown (Figure 4-5), an expected band of molecular mass ~30kDa of A β ₄₂GFP was observed when probed with the anti-GFP antibody. In wild-type cells, A β ₄₂GFP was observed predominantly in the mitochondrial fraction with a very trace amount observed in the ER fraction (Figure 4-7). In contrast, Δ *opi3* cells, which exhibited perinuclear localisation of fluorescent A β ₄₂GFP, had A β ₄₂GFP in both mitochondrial and ER fractions. As indicated by Figure 4-7, a significant increase of A β ₄₂GFP was observed in the ER fraction compared to wild-type cells. These data correlate with the confocal microscopy images indicating that the perinuclear, intensely fluorescent A β ₄₂GFP in the deletion mutants is localised to the ER/ER membrane. The A β ₄₂GFP in the mitochondrial fraction may be due to aggregated non-fluorescent A β ₄₂GFP in these organelles since A β ₄₂GFP-associated fluorescence was not observed in the mitochondria in whole cells via microscopic analysis. This proposition can be tested by carrying out subcellular fractionation of wild-type cells expressing the non-aggregating A β _{EP}GFP fusion protein.

Detailed analysis of Δ *cho2* cells indicated that in addition to the ER/ER-membrane A β ₄₂GFP localisation, these cells also exhibited A β ₄₂GFP-associated fluorescent puncta in an aberrant localisation of punctate bodies not associated to the nucleus or mitochondria. These A β ₄₂GFP-associated fluorescent puncta were also observed in Δ *scs2* cells (Figure 4-2A). The ER/ER-membrane A β ₄₂GFP localisation in these mutants affected in phospholipid metabolism resembled that of lipid droplets (LDs). LDs are composed of a highly hydrophobic core formed by neutral lipids, triacylglycerols (TAG) and sterol esters (SE), surrounded by a phospholipid monolayer containing a well-defined set of proteins (Athenstaedt et al., 1999; Leber et al., 1994). It has recently been shown that SE form several ordered shells below the surface of the phospholipid monolayer and TAG is randomly packed in the core of the LD (Czabany et al., 2008). Both these neutral lipids are highly hydrophobic and are not typically found within the membrane lipid bilayer. The biogenesis of LDs is still a matter of discussion, however, a widely favoured model proposes that accumulation of large amounts of non-polar lipids between the two membrane bilayer leaflets of the ER results in budding of nascent LDs (Athenstaedt and Daum, 2006; Czabany et al., 2007; Rajakumari et al., 2008; Walther and Farese, 2009). It is important to note that while many alternative

mechanisms for LD biogenesis have been proposed (Robenek et al., 2006), all of them agree that LDs originate from the ER.

To further determine the exact localisation of A β ₄₂GFP in the mutants affected in phospholipid metabolism, $\Delta ice2$ and $\Delta opi3$ strains expressing A β ₄₂GFP were stained with LipidTOX Red, which stains the neutral lipid core of LDs. The $\Delta ice2$ and $\Delta opi3$ strains were induced in galactose media (SCgal-URA) for 12 h for A β ₄₂GFP expression and cells were stained with LipidTOX Red to visualise the LDs via fluorescence microscopy. Fluorescent microscopic analysis indicated that in the $\Delta ice2$ and $\Delta opi3$ mutants, A β ₄₂GFP was localised in close association/proximity to, but not co-localised with, lipid droplets (Figure 4-8).

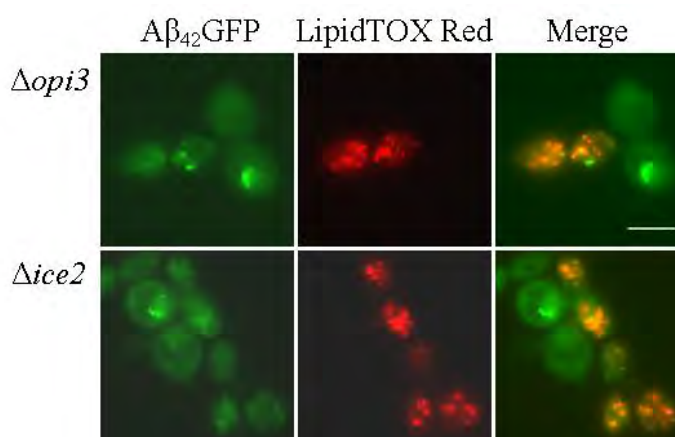


Figure 4-8 Fluorescent microscopic images of $\Delta opi3$ and $\Delta ice2$ strains expressing A β ₄₂GFP stained with LipidTOX Red.

Strains expressing A β ₄₂GFP were induced in galactose medium (SCgal-URA) for 12 h and stained with LipidTOX Red. A β ₄₂GFP localisation in $\Delta opi3$ and $\Delta ice2$ strains is shown in the left panel. LipidTOX Red staining which stains lipid droplets is shown in the middle panel. Merged images of A β ₄₂GFP and LipidTOX Red staining (right panel) indicate that the localisation of A β ₄₂GFP in the $\Delta opi3$ and $\Delta ice2$ mutants was in close association with but not co-localised to lipid droplets. Scale bars indicate 5 μ m.

Given the close association between fluorescent A β ₄₂GFP to lipid droplets in mutants affected in phospholipid metabolism, it was important to understand if the presence and localisation of lipid droplets in the cells played a role in the ER/ER-membrane localisation in these mutants. Approximately forty proteins have been identified on the LD phospholipid monolayer (Athenstaedt et al., 1999; Grillitsch et al., 2011). These include enzymes mainly involved in lipid metabolism, including phosphatidic acid biosynthesis (Athenstaedt and Daum, 1999), fatty acid activation

(Johnson et al., 1994; Watkins et al., 1998), sterol biosynthesis (Watkins et al., 1998), TAG biosynthesis and degradation (Athenstaedt and Daum, 2003; Athenstaedt and Daum, 2005; Sorger et al., 2004) and SE hydrolysis (Jandrositz et al., 2005; Koffel and Schneiter, 2006; Mullner et al., 2005). It is interesting to note that in *S. cerevisiae*, hydrophobic regions of the C-terminus were found to have an influence on the correct targeting of LD proteins to the phospholipid monolayer (Mullner et al., 2004). While the mechanisms by which proteins are targeted to and associated with the LD phospholipid monolayer is still a matter of debate, neutral lipids of LDs have been shown to be involved in protein stabilisation, as demonstrated for squalene epoxidase, Erg1p (Sorger et al., 2004). Interestingly, the last two hydrophobic amino acid residues on the C-terminus of A β ₄₂, isoleucine (41st amino acid) and alanine (42nd amino acid), also strongly influence the amyloidogenicity of the A β ₄₂ peptide (Kim and Hecht, 2005; Wurth et al., 2002).

TAG is synthesised by two TAG synthases Dgalp and Lro1p while SE is synthesised by SE synthases Are1p and Are2p (Dahlqvist et al., 2000; Oelkers et al., 2000; Sandager et al., 2002; Yang et al., 1996; Yu et al., 1996). Therefore a quadruple mutant, $\Delta dgal \Delta lro1 \Delta are1 \Delta are2$, which is devoid of all four acyltransferases is unable to synthesise TAG and SE, and, do not form LDs in cells (Sandager et al., 2002). To determine if the presence and localisation of LDs in cells played a role in the ER/ER-membrane localisation in mutants affected in phospholipid metabolism, the quadruple mutant $\Delta dgal \Delta lro1 \Delta are1 \Delta are2$ (a kind gift from Prof. Guenter Daum, Institut für Biochemie, Technische Universität Graz) was transformed with the pUG35GAL1-A β ₄₂ plasmid. Expression of the A β ₄₂GFP fusion protein in the quadruple mutant was induced by growth in galactose medium and A β ₄₂GFP-associated fluorescence was analysed 15 h post-induction via microscopic analysis.

Prior to the analysis of A β ₄₂GFP-associated fluorescence, wild-type BY4743 cells and the quadruple mutant ($\Delta dgal \Delta lro1 \Delta are1 \Delta are2$) expressing A β ₄₂GFP were stained with LipidTOX Red, to determine the presence of LDs in these cells. As indicated by Figure 4-9A, wild-type cells exhibited intense fluorescent puncta of LDs stained with LipidTOX Red, which were completely absent in the quadruple mutant. A β ₄₂GFP-associated fluorescence levels exhibited in the quadruple mutant expressing

A β_{42} GFP yielded multiple intense fluorescent puncta in ~13% of the cell population, with a majority of these fluorescent puncta localised in close proximity to the nucleus of the cell (Figure 4-9B). Detailed analysis of the quadruple mutant expressing A β_{42} GFP indicated that the ‘discontinuous’ localisation of intensely fluorescent puncta of A β_{42} GFP around the nucleus of the cell differed to that observed in the six deletion mutants belonging to the phospholipid metabolism functional group ($\Delta psd1$, $\Delta cho2$, $\Delta opi3$, $\Delta ino2$, $\Delta ino4$ and $\Delta ice2$ strains) (Figure 4-9B). Interestingly, the quadruple mutant was found to exhibit inositol auxotrophy at elevated growth temperature, indicative of altered *INO1* expression and/or defective PI biosynthesis (Gaspar et al., 2011) and demonstrating the role LDs play in phospholipid homeostasis/metabolism. Taken together, these data lend further support that A β_{42} GFP aggregation is strongly influenced by altered phospholipid homeostasis in *S. cerevisiae* cells.

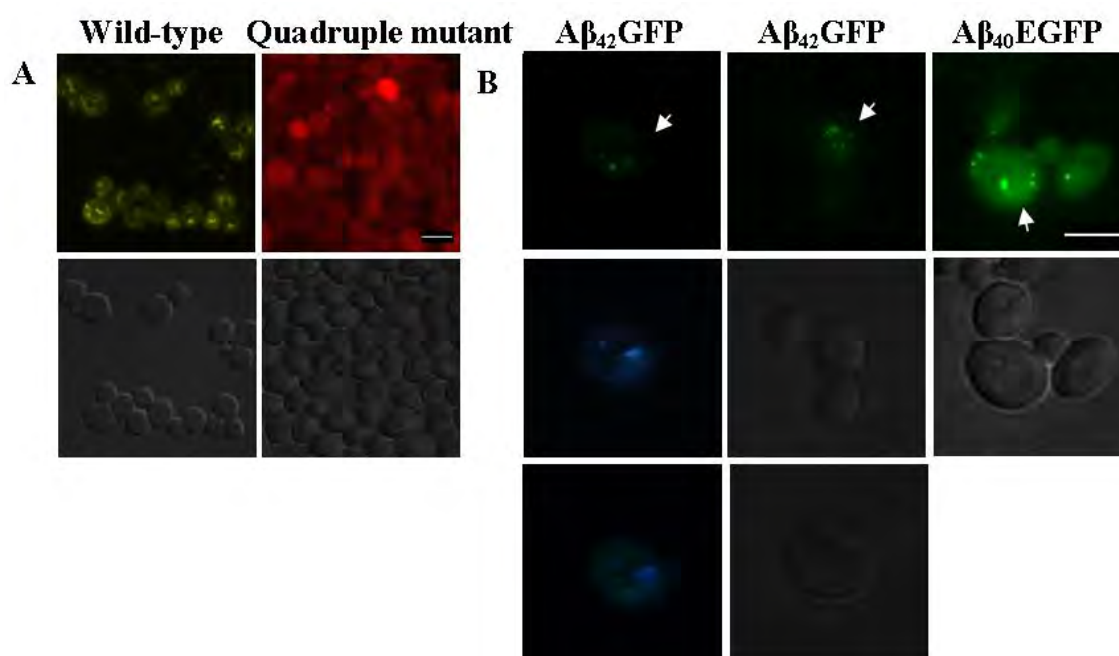


Figure 4-9 Fluorescent microscopic images of the quadruple mutant, $\Delta dgal1 \Delta lro1 \Delta are1 \Delta are2$, expressing A β_{42} GFP stained with DAPI and LipidTOX Red.

Wild-type cells and the quadruple mutant deleted of four acyltransferase genes, ($\Delta dgal1 \Delta lro1 \Delta are1 \Delta are2$), expressing A β_{42} GFP were induced in galactose medium (SCgal-URA) for 15 h and stained with LipidTOX Red or DAPI. A) Wild-type cells exhibit intense fluorescent puncta around the nucleus of the cell while the quadruple mutant completely lacks LDs. B) A β_{42} GFP localisation in the quadruple mutant expressing A β_{42} GFP and A β_{40} GFP is shown in the top panel. DAPI staining which stains nuclear and mitochondrial DNA is shown in the middle panel. Merged images of A β_{42} GFP and DAPI staining (bottom row) indicate that the localisation of A β_{42} GFP in the quadruple mutant was perinuclear. Scale bars indicate 5 μ m.

4.2.5 Some, but not all, of the intense fluorescent puncta of A β ₄₂GFP in mutants affected in phospholipid metabolism co-localise with peroxisomes

Peroxisomes and lipid droplets have been shown to be closely associated with the ER in *S. cerevisiae* (Bascom et al., 2003; Binns et al., 2006). This raised the possibility that the A β ₄₂GFP localisation in the phospholipid mutants may be peroxisomal. The peroxisome targeting signal 1 (PTS1) tripeptide Ser-Lys-Leu (SKL) fused to mDsRed, leads to localisation of the fusion protein to peroxisomes. To examine whether A β ₄₂GFP was co-localised to peroxisomes in the $\Delta ice2$ and $\Delta opi3$ mutants, localisation of SKL-mDsRed and A β ₄₂GFP was examined. Since the intensity of A β ₄₂GFP-associated fluorescence in the phospholipid metabolism mutants (i.e. $\Delta cho2$ and $\Delta scs2$ mutants) was shown to be significantly influenced by choline (Table 4-1) these mutants were also included in analyses with SKL-mDsRed. Expression of the A β ₄₂GFP fusion protein and SKL-mDsRed in each strain was induced by growth in galactose medium and A β ₄₂GFP-associated fluorescence was analysed 15 h post-induction.

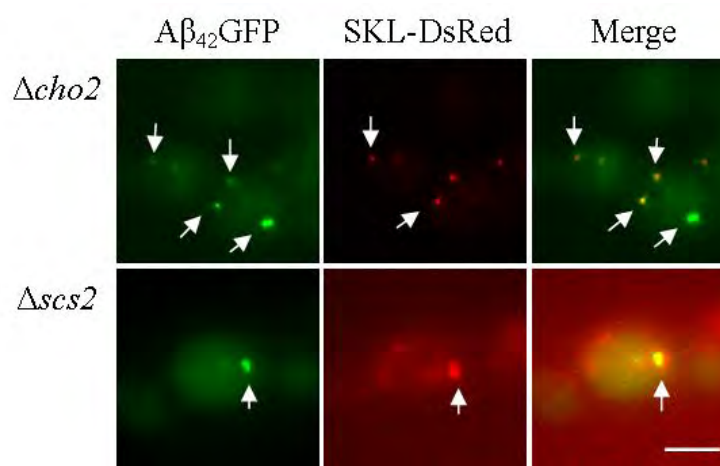


Figure 4-10 Fluorescent microscopic images of $\Delta cho2$ and $\Delta scs2$ strains exhibiting strong A β ₄₂GFP fluorescence with SKL-mDsRed peroxisomal marker.

Strains expressing A β ₄₂GFP were induced in galactose medium (SCgal-URA) and A β ₄₂GFP-associated fluorescence analysed at 12 h post induction. A β ₄₂GFP localisation in the $\Delta cho2$ and $\Delta scs2$ strains is presented in the left panels. SKL-mDsRed peroxisomal marker, which allows for visualisation of peroxisomes, is observed in the middle column. Merged images of A β ₄₂GFP and SKL-mDsRed marker indicate co-localisation (right column). The data indicate that some of the A β ₄₂GFP are in close association with peroxisomes, whereas others are observed to be distal from peroxisomes. Scale bars indicate 5 μ m.

Attempts to visualise SKL-mDsRed in the $\Delta ice2$ and $\Delta opi3$ strains were not successful, due to a very weak fluorescent signal produced by SKL-mDsRed in these strains. Although at present, it is unclear why this occurred; one possible explanation may be that these experiments were conducted at mid-exponential phase where *S. cerevisiae* cells are not as enriched in peroxisomes as compared to cells growing in the late exponential/early stationary phase (Connerth et al., 2010; Thieringer et al., 1991). However, in Figure 4-10, it is observed that some of the intense fluorescent A β_{42} GFP puncta was found to co-localise with SKL-mDsRed in the $\Delta cho2$ and $\Delta scs2$ mutants, indicating that some A β_{42} GFP was localised to peroxisomes in these strains.

4.2.6 Effects of choline supplementation on mutants that belong to the phospholipid metabolism functional group

One of the major functional groups identified through the genome-wide screen approach was the phospholipid metabolism functional group which included the $\Delta psd1$, $\Delta cho2$ and $\Delta opi3$ mutants. Psd1p converts phosphatidylserine (PS) to phosphatidylethanolamine (PE) while Cho2p and Opi3p catalyse the methylation of PE, phosphatidyl-*N*-methylethanolamine (PMME), and phosphatidyl-*N*-dimethylethanolamine (PDME) respectively. Sequential action of Cho2p and Opi3p yields PC. Other mutants that were classified into the phospholipid metabolism functional category were $\Delta scs2$, $\Delta ume6$, $\Delta ino2$ and $\Delta ino4$, which lack genes known to play a role in regulating phospholipid metabolism. Phosphatidylcholine depletion in the $\Delta cho2$ and $\Delta opi3$ mutants can be reversed by the growth of these strains in media supplemented with choline. In *S. cerevisiae*, exogenous choline can be assimilated to produce PC, via the Kennedy salvage pathway (Kennedy and Weiss, 1956). This alternative pathway of PC biosynthesis depends on the availability of precursor molecules such as monomethylethanolamine (MMEA), dimethylethanolamine (DMEA) or choline (McGraw and Henry, 1989; Summers et al., 1988). Since these precursor molecules were not present in the galactose (induction) medium used in the genome-wide deletion screen, it is likely that the membranes of $\Delta psd1$, $\Delta cho2$ and $\Delta opi3$ mutants were PC depleted. It was therefore predicted that the fluorescence of the various forms of A β GFP fusions in *OPI3* mutants would be reversed by choline addition.

In order to investigate this $\Delta opi3$ and $\Delta cho2$ strains expressing $A\beta_{42}$ GFP, $A\beta_{40}$ GFP, $A\beta_{EP}$ GFP, or unfused GFP were grown in medium lacking or supplemented with 1 mM choline. Since the $\Delta ice2$ mutant exhibited an arc-shaped $A\beta_{42}$ GFP localisation, the $\Delta ice2$ mutant was also included in this analysis. Expression of the $A\beta_{42}$ GFP fusion protein in each strain was induced by growth in galactose medium and $A\beta_{42}$ GFP-associated fluorescence was analysed 12 h post-induction. The ER/ER-membrane localisation in the $\Delta opi3$ and $\Delta cho2$ strains was reversed for all three forms of $A\beta$ fusion proteins ($A\beta_{42}$ GFP, $A\beta_{40}$ GFP and $A\beta_{EP}$ GFP) upon choline addition, but not in $\Delta ice2$ strain (Figure 4-11). Interestingly in the $\Delta ice2$ strain, while choline supplementation did not affect the abundance of cells exhibiting fluorescence with $A\beta_{42}$ GFP or $A\beta_{40}$ GFP, a distinct change/reversal of the arc-shaped localisation by $A\beta_{EP}$ GFP, was observed with choline addition. That is, $A\beta_{EP}$ GFP-associated fluorescence in the $\Delta ice2$ strain was predominantly cytosolic (Figure 4-11) under choline supplementation conditions, as observed in the case of wild-type cells expressing $A\beta_{EP}$ GFP (Figure 3-2). Choline supplementation to all three mutants expressing GFP alone had no effect on the intensity or localisation of GFP fluorescence.

These data indicate that appearance of the ER/ER-membrane localisation of $A\beta_{42}$ GFP fluorescence in the phospholipid mutants is dependent on the capacity of the cells to synthesise PC and/or maintain phospholipid homeostasis. However, in the $\Delta ice2$ mutant, these data may suggest otherwise. The underlying mechanism of $A\beta_{42}$ GFP localisation in $\Delta ice2$ cells may be independent of the PC composition of intracellular membranes. Furthermore, a critical evaluation of $A\beta_{42}$ GFP localisation exhibited in $\Delta opi3$ and $\Delta ice2$ strains revealed subtle differences between the ER/ER-membrane localisation observed in both these mutants. It was observed that while $\Delta opi3$ cells exhibited $A\beta_{42}$ GFP-associated fluorescence in multiple puncta aligned contiguously in a structured arc-shape around the nucleus, $\Delta ice2$ cells appeared to exhibit $A\beta_{42}$ GFP-associated fluorescence in a continuous ‘uninterrupted’ arc around the nucleus of the cell (Figure 4-11).

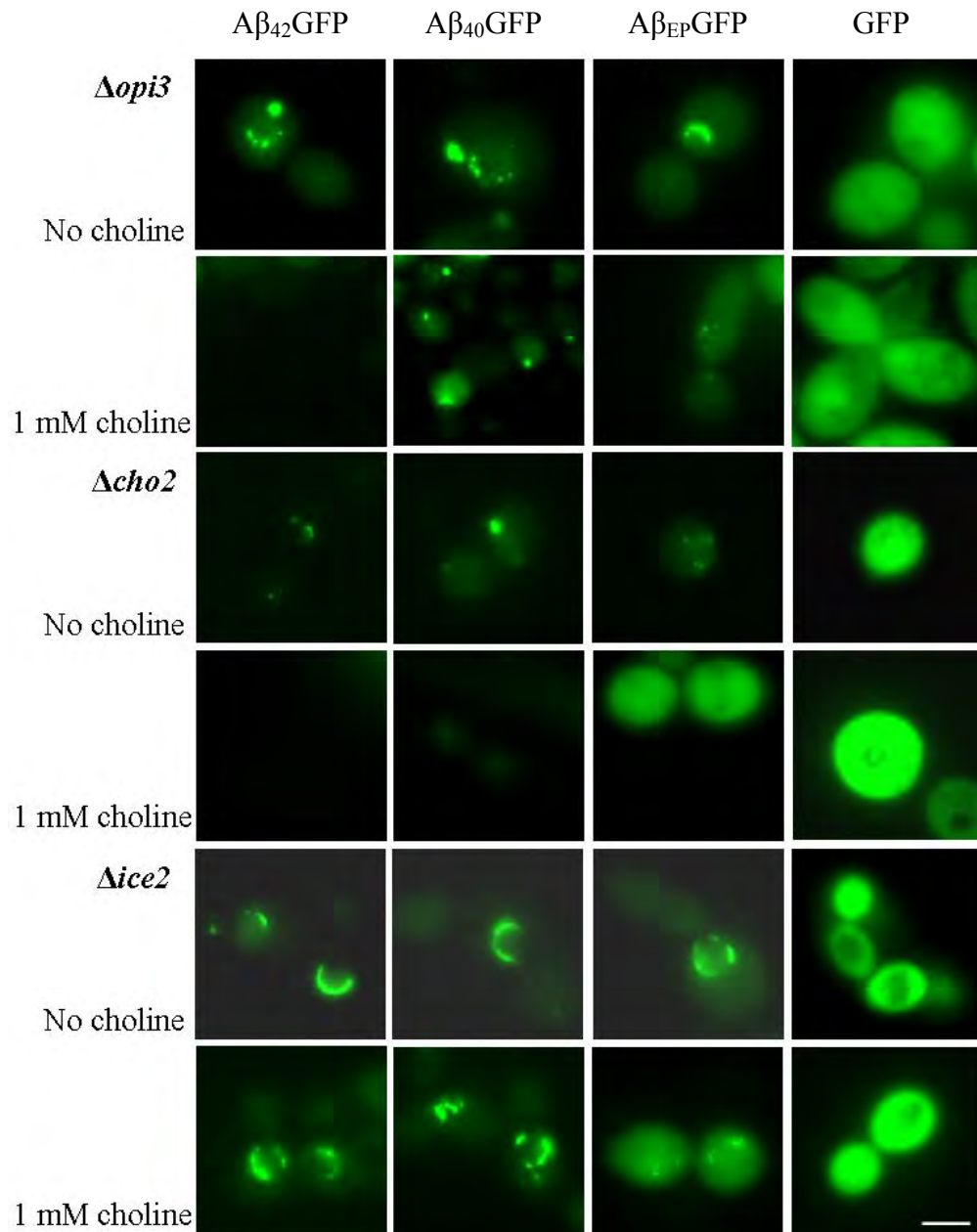


Figure 4-11 Fluorescent microscopic images of $\Delta opi3$, $\Delta cho2$ and $\Delta ice2$ strains expressing $A\beta_{42}$ GFP, $A\beta_{40}$ GFP, $A\beta_{EP}$ GFP or GFP grown in media either lacking or supplemented with choline.

Strains expressing various forms of $A\beta$ fusion proteins (as indicated) were induced in galactose medium (SCgal-URA) either lacking or supplemented with 1 mM choline chloride. $A\beta$ GFP-associated fluorescence was analysed at 12 h post induction. $\Delta opi3$ and $\Delta cho2$ strains, but not the $\Delta ice2$ strain, expressing $A\beta_{42}$ GFP, $A\beta_{40}$ GFP or $A\beta_{EP}$ GFP, indicated that the ER/ER-membrane localisation in both these strains were reversed for all three forms of $A\beta$ fusion proteins upon choline supplementation. Scale bars indicate 5 μ m.

These data indicated that although $\Delta opi3$ and $\Delta cho2$ cells exhibited an arc-shaped A β_{42} GFP localisation, the localisation of A β_{EP} GFP was also reversed by choline supplementation. In order to investigate the effect of choline on the abundance of A β_{42} GFP-associated fluorescence in the $\Delta opi3$ and $\Delta ice2$ strains more quantitatively these strains were grown in media either lacking or supplemented with choline and the percentage of fluorescent cells measured. It was also of interest to determine whether A β_{42} GFP-associated fluorescence in other mutants that were classified into the phospholipid metabolism functional category (Table 3-1) or mutants belonging to the other over-represented groups were also affected by choline addition. This may indicate that $\Delta ice2$ and possibly other mutants, listed in Table 3-1, affected A β_{42} GFP-associated fluorescence due to an effect independent of PC levels in the cells. In each case, 300 cells were counted in triplicate and the mean and standard deviation for each are given in Table 4-1.

A β_{42} GFP-associated fluorescence was analysed following growth of strains in media either lacking or supplemented with 1 mM choline chloride 12 h post induction. The data generated through this analysis are presented in Table 4-1. Choline supplementation did not affect A β_{42} GFP, A β_{40} GFP, A β_{EP} GFP or GFP-associated fluorescence in wild-type cells. The results from the choline supplementation experiment demonstrated that the $\Delta cho2$, $\Delta opi3$ and $\Delta ume6$ strains expressing A β_{42} GFP exhibited a significant decrease in the proportion of fluorescent cells, when the p -value threshold was set at 0.005. However, an increase of the p -value threshold to 0.05 indicated that $\Delta psd1$, $\Delta ino2$, $\Delta ino4$, $\Delta ice2$, $\Delta scs2$, $\Delta swc5$, $\Delta apj1$ and $\Delta san1$ mutants exhibited a significant decrease in the proportion of cells exhibiting A β_{42} GFP-associated fluorescence upon choline addition.

Table 4-1 Proportion of A β ₄₂GFP fluorescent cells grown in media lacking or supplemented with choline

Strains expressing A β ₄₂GFP were induced in galactose medium (SCgal-URA) either lacking or supplemented with choline and A β ₄₂GFP-associated fluorescence analysed at 12 h post induction. 300 cells were counted and the data shown are the mean of triplicate measurements \pm standard deviation. *p* - values denote the significance in the difference of the proportion of cells exhibiting A β ₄₂GFP-associated fluorescence, grown in media either lacking or supplemented with choline.

Strains expressing A β ₄₂ GFP	Percentage of fluorescent cells expressing A β ₄₂ GFP		<i>p</i> - value
	No choline addition	1 mM choline addition	
Wild-type – A β ₄₂ GFP	5 \pm 2	5 \pm 2	1.0
Wild-type – A β ₄₀ GFP	50 \pm 5	50 \pm 3	1.0
Wild-type – A β _{EP} GFP	60 \pm 8	60 \pm 5	1.0
Wild-type – GFP	85 \pm 5	80 \pm 5	0.29
Phospholipid metabolism			
$\Delta cho2$	18 \pm 2	6 \pm 3	0.0045
$\Delta opi3$	23 \pm 2	6 \pm 3	0.0012
$\Delta psd1$	16 \pm 2	9 \pm 2	0.0128
$\Delta ino2$	17 \pm 2	9 \pm 3	0.0184
$\Delta ino4$	14 \pm 2	9 \pm 2	0.0376
$\Delta ume6$	22 \pm 3	10 \pm 2	0.0045
$\Delta scs2$	26 \pm 2	20 \pm 3	0.0449
$\Delta ice2$	28 \pm 2	21 \pm 2	0.0128
Mitochondrial function			
$\Delta fum1$	42 \pm 5	36 \pm 2	0.1258
$\Delta acol$	38 \pm 7	38 \pm 2	1.0
$\Delta mdh1$	22 \pm 4	20 \pm 3	0.5265
$\Delta pyc1$	17 \pm 2	15 \pm 2	0.2879
$\Delta pyc2$	17 \pm 2	17 \pm 2	1.0
$\Delta sdh1$	27 \pm 2	22 \pm 1	0.0179
$\Delta sdh4$	19 \pm 8	16 \pm 2	0.5628
$\Delta lsc1$	20 \pm 1	20 \pm 1	1.0
$\Delta lsc2$	20 \pm 2	20 \pm 1	1.0
$\Delta kgd1$	21 \pm 7	20 \pm 2	0.8236
$\Delta kgd2$	24 \pm 4	22 \pm 1	0.1963
$\Delta idh1$	23 \pm 6	21 \pm 3	0.6328
$\Delta idh2$	23 \pm 2	22 \pm 2	0.5734
$\Delta cit1$	19 \pm 3	20 \pm 1	0.613
Chromatin remodelling/ Silencing/ Histone exchange			
$\Delta swr1$	23 \pm 3.1	21 \pm 2.8	0.401
$\Delta vps72$	18 \pm 3.5	20 \pm 4.3	0.403
$\Delta swc5$	21 \pm 4.6	15 \pm 2.3	0.045
$\Delta hta2$	15 \pm 2	20 \pm 4	0.168
Heat shock protein			
$\Delta apj1$	18 \pm 4.9	11 \pm 1.8	0.018
Ubiquitin/ Proteosome			
$\Delta san1$	45 \pm 4.6	36 \pm 3.4	0.016

4.2.7 Investigation of altered localisation of phosphatidic acid (PA) and phosphatidylserine (PS) in mutants that belong to the phospholipid metabolism functional group

In *S. cerevisiae*, exogenous choline can be assimilated to produce phosphatidylcholine, via the Kennedy salvage pathway (Kennedy and Weiss, 1956) and the PC depletion in the $\Delta cho2$ and $\Delta opi3$ mutants can be reversed by the growth of these strains in media supplemented with choline. However, it is interesting to note that while choline supplementation leads to repletion of PC levels, it also reverses the PE and PMME over-accumulation phenotype of these mutants respectively. Hence, data from the choline supplementation study may be indicative that the ER/ER-membrane localisation of A β_{42} GFP fluorescence in mutants affected in phosphatidylcholine biosynthesis/phospholipid metabolism may be due to a possible depletion or over-accumulation of one or more lipid metabolites in the yeast lipidome. Within the cell, each membrane compartment has a unique lipid composition and may be enriched in specific lipid types (Schneider et al., 1999). Since the sequential action of Psd1p, Cho2p and Opi3p yields PE and PC (Figure 4-1) and growth of $\Delta cho2$ and $\Delta opi3$ strains expressing A β_{42} GFP in choline supplemented media led to significant reduction in ER-localised A β_{42} GFP fluorescence, it was hypothesised that altered accumulation and localisation of phospholipid intermediates upstream of PC, such as PS and PA, may have led to the ER-localised A β_{42} GFP fluorescence in these mutants. Interestingly, $\Delta cho2$ cells exhibit a four-fold increase in PA (Daum et al., 1999) while $\Delta opi3$ cells show a two-fold increase in PS, PI and PE (Kodaki and Yamashita, 1987).

In order to investigate the subcellular distribution of PA, the four deletion mutants which exhibited the ER-localised A β_{42} GFP fluorescence ($\Delta psd1$, $\Delta cho2$, $\Delta opi3$ and $\Delta ice2$) together with wild-type cells were transformed with pRS426-G20, encoding GFP-Spo20p⁵¹⁻⁹¹ under the regulation of a *TEF2* promoter (Nakanishi et al., 2004), to allow *in vivo* visualisation of PA localisation via direct GFP fluorescence. Diploid *S. cerevisiae* cells undergo meiosis and differentiate into haploid spores in response to starvation conditions. Prospore membranes form during this process of sporulation by coalescing post-Golgi secretory vesicles from the plasma membrane (PM), to encapsulate each of the daughter nuclei (Moens, 1971; Moens and Rapport, 1971; Neiman, 1998). Spo20p, which is a member of the soluble *N*-ethylmaleimide sensitive

factor attachment protein receptor (SNARE) subfamily, mediates the fusion of these vesicles with the prospore membrane, where it plays an important step in spore formation. Expression of GFP-Spo20p⁵¹⁻⁹¹ was induced by growth of cells, in galactose medium (SCgal-URA) prior to microscopic analysis. Analysis of these strains expressing the fluorescent biosensor of PA indicated that in all strains except $\Delta cho2$ cells, PA is localised predominantly to the PM (Figure 4-12). Approximately 35% of the cells also exhibited PA localisation in the prospore membranes, where it has been previously reported (Nakanishi et al., 2004). Interestingly, $\Delta cho2$ cells exhibited a perinuclear GFP-Spo20p⁵¹⁻⁹¹ localisation, analogous to the ER/ER-membrane localisation of A β ₄₂GFP fluorescence in the six deletion mutants affected in phospholipid metabolism. When $\Delta cho2$ cells were subsequently analysed following growth in media supplemented with 1 mM choline chloride, the apparent accumulation and localisation of PA in the ER of $\Delta cho2$ cells was reversed to those observed in the case of wild-type cells expressing GFP-Spo20p⁵¹⁻⁹¹ (Figure 4-12). While intracellular accumulation of lipid metabolite(s) has been previously reported in the mutants affected in lipid metabolism, these data indicate that the lipid metabolites may be localised in specific subcellular compartments of the cell.

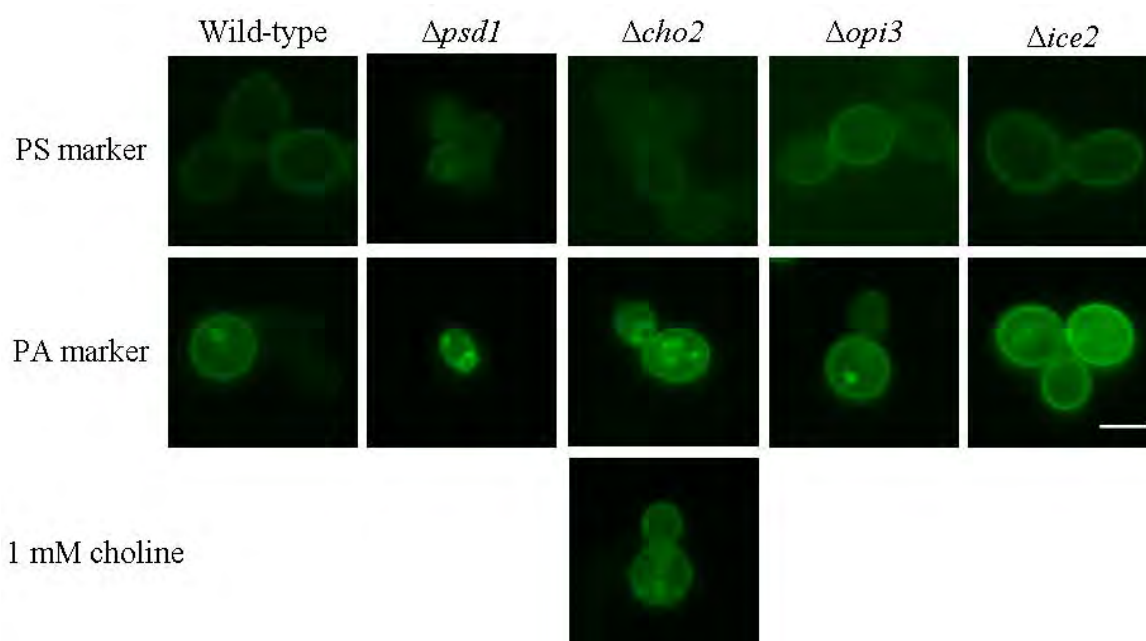


Figure 4-12 Fluorescent microscopic images of wild-type, $\Delta psd1$, $\Delta cho2$, $\Delta opi3$ and $\Delta ice2$ cells expressing a fluorescent biosensor of PS and PA grown in galactose media.

Strains expressing either GFP-Spo20p⁵¹⁻⁹¹ for the detection of PA, or GFP-Lact-C2 for the detection of PS, (as indicated) were induced in galactose medium and analysed at 15 h post

induction. PS is localised predominantly to the PM (top panel) in all mutants including $\Delta psd1$ cells which exhibited trace levels of GFP-Lact-C2 associated fluorescence. All strains, except $\Delta cho2$, also indicated that PA is localised predominantly to the PM with ~35% of the cell population exhibiting PA localisation in prospore membranes (middle panel). In addition to the PM localisation, $\Delta cho2$ cells also exhibited perinuclear PA localisation which was reversed to a wild-type phenotype upon choline supplementation in the media (bottom panel). Scale bars indicate 5 μ m.

Similarly, to investigate the subcellular distribution of PS, the four deletion mutants that exhibited the ER-localised A β_{42} GFP fluorescence (described above) together with wild-type cells were transformed with p416-GFP-Lact-C2, encoding GFP fused to the C2 domain of lactadherin under the regulation of a *GPD* promoter (Yeung et al., 2008), to allow *in vivo* visualisation of PS localisation via direct GFP fluorescence. Lactadherin is a glycoprotein found in milk which binds to PS in a calcium-independent manner. Within the lactadherin protein, the major PS-binding motif is associated with its C2 domain (Andersen et al., 2000; Shi et al., 2004). Expression of GFP-Lact-C2 was induced by growth of cells, in galactose medium (SCgal-URA) prior to microscopic analysis. The analysis of strains expressing the fluorescent biosensor of PS indicated that in all four deletion strains, PS is localised predominantly to the PM (Figure 4-12).

These data indicated that it was unlikely that accumulation of PA and/or PS in the ER-membranes of the six deletion mutants led to partitioning of A β_{42} GFP into the ER in those strains. However, the accumulation of PA in the ER of $\Delta cho2$ cells indicated the possibility of other lipid metabolite(s) influencing the partitioning of A β_{42} GFP into the ER/ER-membrane in mutants affected in phospholipid metabolism.

4.2.8 A ‘reverse-genetics’ approach to identify specific lipid metabolite(s) that influence partitioning of A β_{42} GFP in to the ER membrane

Gene over-expression analysis was undertaken to investigate if the increased A β_{42} GFP fluorescence and partitioning of A β_{42} GFP into the ER in the phospholipid mutants were caused by an accumulation of a specific phospholipid intermediate upstream of the PC biosynthetic pathway. This ‘reverse-genetics’ approach was undertaken to provide further insight into the link between altered phospholipid homeostasis and A β_{42} GFP fluorescence. In wild-type cells, over-expression of a gene in a cellular pathway is likely to increase flux through that particular pathway. In an attempt to force accumulation of a specific phospholipid metabolite, the upstream

gene(s) leading to its synthesis was over-expressed and the gene(s) leading to the utilisation of the ‘target’ phospholipid metabolite was deleted. The genes encoding enzymes of the phospholipid precursors and intermediates that were over-expressed included those involving 1-acyl-dihydroxyacetone phosphate, lyso-phosphatidic acid, phosphatidic acid, 1,2-diacylglycerol (DAG), triacylglycerol (TAG), cytidine-diphosphate-diacylglycerol (CDP-DAG), phosphatidylserine (PS), phosphatidylethanolamine (PE), phosphatidyl-mono-methylethanolamine (PMME), phosphatidyl-dimethylethanolamine (PDME), phosphatidylcholine (PC), glycerophosphocholine and lysophosphocholine (refer to Figure 4-1 for an overview of the PC biosynthetic and PL metabolic pathways). A list of all target lipid metabolites analysed, the strains and plasmids used in this ‘reverse-genetics’ approach are summarised in Table 4-2.

Table 4-2 List of genes encoding enzymes of the phospholipid intermediates that were over-expressed in wild-type cells and relevant phospholipid mutants

Accumulation of metabolite-of-interest	Gene over-expressed	Strains		
Diacylglycerol (DAG)	<i>DPPI1</i>	Wild-type	$\Delta cho2$	$\Delta lro1$
	<i>PAH1</i>	$\Delta opi3$	$\Delta psd1$	$\Delta dga1$
	<i>PLC1</i>	$\Delta ice2$	$\Delta psd2$	
1-acyl-Dihydroxyacetone-Phosphate (1-acyl-DHAP) and lyso-phosphatidic-acid (lysoPA)		Wild-type	$\Delta cho2$	$\Delta ayr1$
	<i>GAT1</i>	$\Delta opi3$	$\Delta psd1$	$\Delta slc1$
	<i>GAT2</i>	$\Delta ice2$	$\Delta psd2$	$\Delta slc4$
Cystidine-Diphosphate-DAG (CDP-DAG)		$\Delta fum1$		
	<i>CDS1</i>	Wild-type	$\Delta cho2$	$\Delta psd2$
		$\Delta opi3$	$\Delta psd1$	$\Delta cho1$
Dihydroxyacetone phosphate (DHAP)		$\Delta ice2$		
	<i>DAK1</i>	Wild-type	$\Delta psd1$	$\Delta gpt2$
	<i>DAK2</i>	$\Delta opi3$	$\Delta psd2$	$\Delta sct1$
Phosphatidic acid (PA)		$\Delta ice2$	$\Delta gpd1$	$\Delta fum1$
	<i>SLC1</i>	Wild-type	$\Delta cho2$	$\Delta fum1$
	<i>SPO14</i>	$\Delta opi3$	$\Delta psd1$	$\Delta lpp1$
Phosphatidylserine (PS)		$\Delta ice2$	$\Delta psd2$	$\Delta dpp1$
	<i>CHO1</i>	Wild-type	$\Delta opi3$	$\Delta psd1$
		$\Delta ice2$	$\Delta cho2$	$\Delta psd2$
Phosphatidylethanolamine (PE)	<i>PSD1</i>	Wild-type	$\Delta opi3$	$\Delta psd1$
	<i>PSD2</i>	$\Delta ice2$	$\Delta cho2$	$\Delta psd2$
Phosphatidylcholine (PC) and phosphatidyl-dimethyl-ethanolamine (PDME)		Wild-type	$\Delta psd1$	$\Delta spo14$
	<i>OPI3</i>	$\Delta ice2$	$\Delta psd2$	$\Delta nte1$
		$\Delta cho2$	$\Delta plb1$	

The over-expression screen made use of pAG415GAL1-A β 42-GFP (under the *LEU2* selectable marker) to allow co-expression of the genes in the yeast ORF library

(under the *URA3* selectable marker) (Gelperin et al., 2005). Plasmids containing the 2 μ origin of replication are maintained at high-copy number (20-50 copies) and are useful in over-expression studies in *S. cerevisiae* (Sikorski and Hieter, 1989). High-copy galactose-inducible plasmids (BG1805 family) containing 5854 *S. cerevisiae* open reading frames (ORFs) in the yeast ORF library (Gelperin et al., 2005) (OpenBiosystemsTM) were utilised in this study. Wild-type BY4743 cells and the appropriate deletion mutants were co-transformed with pAG415GAL-A β ₄₂-GFP construct and BG1805 plasmids carrying lipid gene ORFs as indicated in Table 4-2. As controls, both wild-type BY4743 cells and deletion mutants were co-transformed with pAG415GAL-A β ₄₂-GFP and pYES-DEST52 (an empty *URA3* vector) (Invitrogen, San Diego, CA, USA). In this ‘reverse-genetics’ approach, successful transformants over-expressing a particular lipid ORF were examined to identify those exhibiting increased A β ₄₂GFP fluorescence and/or altered fluorescence localisation compared to wild-type cells.

Expression of the A β ₄₂GFP fusion protein and the lipid gene ORF in each strain was induced by growing cells in galactose medium and A β ₄₂GFP-associated fluorescence was analysed 15 h post-induction. Fluorescence levels exhibited in wild-type cells co-expressing pAG415GAL-A β ₄₂-GFP, pAG415GAL-A β ₄₀-GFP, pAG415GAL-A β _{EP}-GFP, or, pAG415GAL-GFP and the control pYES-DEST52 plasmid yielded similar levels of fluorescence to those observed in wild-type cells expressing pUG35GAL1-A β ₄₂, pUG35GAL1-A β ₄₀, pUG35GAL1-A β _{EP}, or, pUG35GAL1, respectively (Figure 4-13); as described in Section 3.3.2. Wild-type cells expressing A β ₄₂GFP yielded very weak A β ₄₂GFP fluorescence that was restricted to 8% \pm 3% of the cell population whereas expression of A β ₄₀GFP yielded predominantly cytosolic-diffuse fluorescence (Figure 4-13) in 65% \pm 4% of the cell population, with ~20% of these fluorescent cells exhibiting one or more fluorescent puncta. The proportion of fluorescent cells observed in wild-type cells expressing A β _{EP}GFP was significantly higher than those expressing A β ₄₂GFP ($p < 0.0001$) or A β ₄₀GFP ($p = 0.05$), where intense cytosolic-diffuse fluorescence in 75% \pm 5% of the cell population was observed, under identical conditions (Figure 4-13).

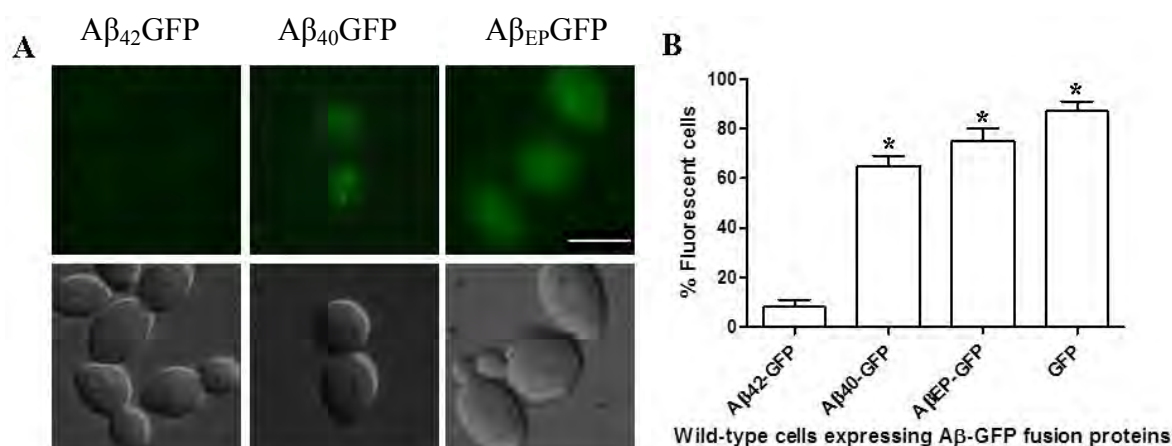


Figure 4-13 Fluorescent cell population of wild-type cells expressing Aβ₄₂GFP, Aβ₄₀GFP or Aβ_{EP}GFP and the pYES-DEST52 control plasmid.

A) Fluorescent microscopic images of wild-type cells expressing Aβ₄₂GFP, Aβ₄₀GFP or Aβ_{EP}GFP (as indicated) together with the pYES-DEST52 control plasmid. Wild-type cells expressing the above constructs were induced in galactose medium and fluorescence was analysed 15 h post-induction. Bar, 5 μm. (B) Proportion of fluorescent wild-type cells expressing Aβ₄₂GFP, Aβ₄₀GFP or Aβ_{EP}GFP. 300 cells were counted per sample and data shown is an average of three independent experiments. Asterisks (*) denote $p < 0.001$.

4.2.9 Over-expression of *CDS1*, encoding cytidine diphosphate-diacylglycerol synthase, and *DAK2*, encoding dihydroxyacetone kinase, alter Aβ₄₂GFP-associated fluorescence

Aβ₄₂GFP-associated fluorescence was analysed following growth of strains in galactose induction media 15 h post induction. Analysis of ~170 strains in the over-expression screen identified two genes that when over-expressed appeared to exhibit altered Aβ₄₂GFP fluorescence relative to wild-type cells. Strains over-expressing *CDS1* or *DAK2* were subsequently rescreened for confirmation of altered levels of fluorescence and the proportion of fluorescent cells was quantified (Figure 4-14; Table 4-3). *CDS1* encodes cytidine diphosphate-diacylglycerol (CDP-DAG) synthase, which is responsible for CDP-DAG-dependent synthesis of phospholipids from phosphatidic acid (PA) (Figure 4-1) (Homann et al., 1985). Wild-type cells over-expressing *CDS1* and Aβ₄₂GFP gave rise to more fluorescent cells (~27%) than those observed in wild-type control cells. *CDS1* over-expression in wild-type cells also expressing Aβ₄₂GFP exhibited ER/ER-membrane localisation of intensely fluorescent puncta analogous to that observed in the six deletion mutants belonging to the phospholipid metabolism functional group (*Δpsd1*, *Δcho2*, *Δopi3*, *Δino2*, *Δino4* and *Δice2* strains) (Figure 4-14A). *CDS1* over-expression in these six deletion strains, identified from the genome-wide

deletion screen, appeared to exacerbate the phenotype since the proportion of cells with ER/ER-membrane localised intensely fluorescent puncta of A β ₄₂GFP was significantly increased in these six deletion mutants compared to their relevant control strains. In each case, 500 cells were counted in triplicate and the mean and standard deviation for each are presented in Table 4-3. *CDS1* over-expression in wild-type cells expressing either A β ₄₀GFP or A β _{EP}GFP gave rise to 42% \pm 5% and 64% \pm 3% of the cell population, respectively. These two strains exhibited slightly more cytosolic-diffuse fluorescence compared to wild-type cells over-expressing *CDS1* with A β ₄₂GFP (Figure 4-14A). These data further support that A β ₄₂GFP aggregation is strongly influenced by altered phospholipid homeostasis in *S. cerevisiae* cells. This effect of *CDS1* over-expression on A β ₄₂GFP aggregation in cells is further investigated in the following section.

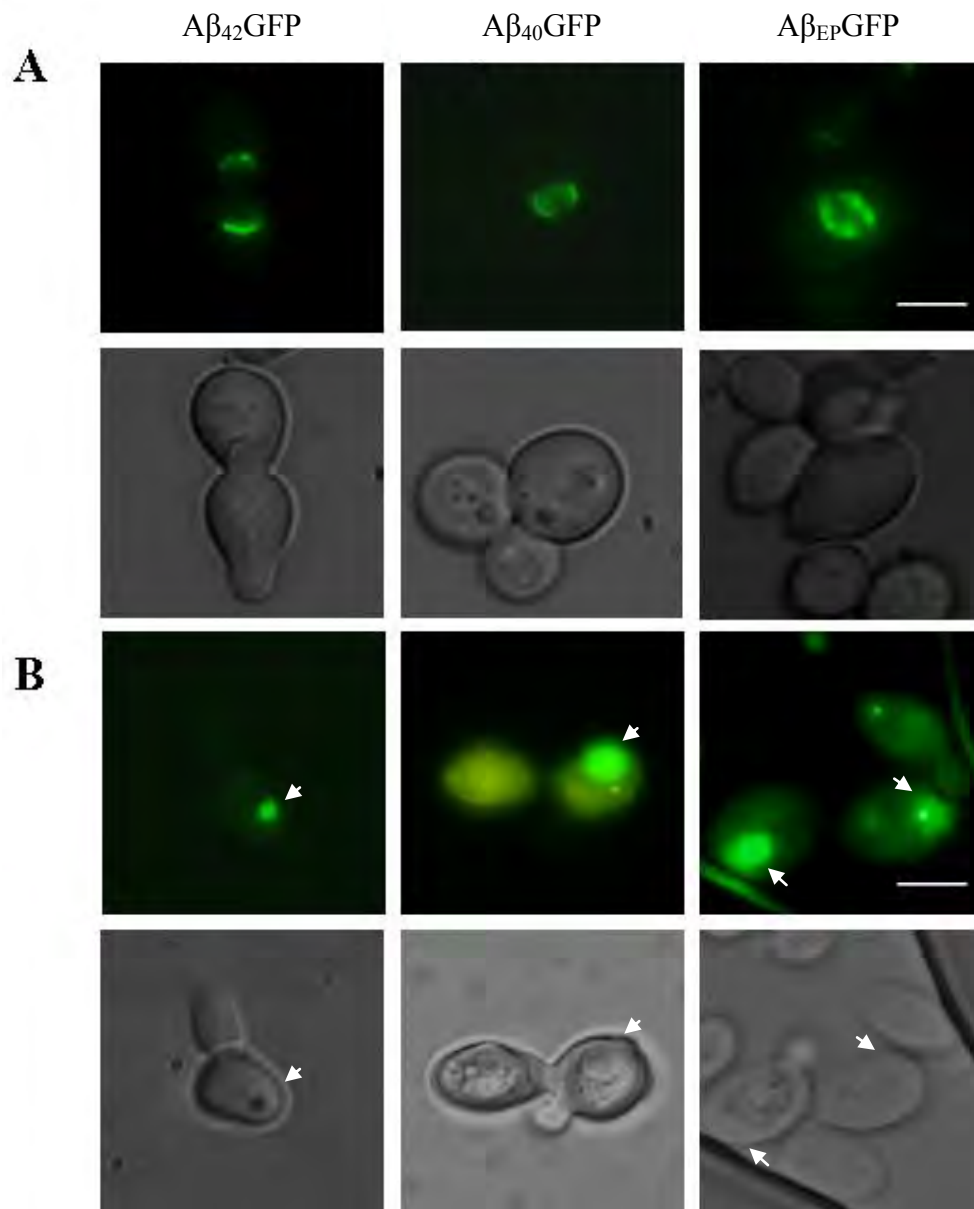


Figure 4-14 Fluorescent microscopic images of wild-type cells over-expressing *CDS1* or *DAK2* together with A β ₄₂GFP, A β ₄₀GFP or A β _{EP}GFP

Wild-type cells over-expressing A) *CDS1* or B) *DAK2* together with various forms of A β fusion proteins (as indicated) were induced in galactose medium (SCgal-URA). A β GFP-associated fluorescence was analysed at 15 h post induction. A) *CDS1* over-expression in wild-type cells yielded ER/ER-membrane localisation of A β ₄₂GFP, A β ₄₀GFP and A β _{EP}GFP. B) *DAK2* over-expression in wild-type cells exhibited a structured localisation of fluorescent A β GFP fusion proteins in a large globular compartment in the cell (as indicated by arrowheads). Scale bars indicate 5 μ m.

Table 4-3 Proportion of A β GFP fluorescent cells in strains over-expressing *CDS1* or *DAK2*

Strains over-expressing either *CDS1* or *DAK2* were induced for A β_{42} GFP expression in galactose medium (SCgal-URA) and A β_{42} GFP-associated fluorescence analysed at 15 h post induction. 500 cells were counted and the data shown are the mean of triplicate measurements \pm standard deviation. *p* - values denote the significance in the difference of the proportion of cells exhibiting A β_{42} GFP-associated fluorescence either in the absence or presence of *CDS1* or *DAK2* over-expression.

Strains expressing A β_{42} GFP	Percentage of fluorescent cells				
	Controls	<i>CDS1</i> over-expression	<i>p</i> - value	<i>DAK2</i> over-expression	<i>p</i> -value
Wild-type – A β_{42} GFP	8 \pm 3	26 \pm 2	0.001	35 \pm 2	0.0002
Wild-type – A β_{40} GFP	65 \pm 4	42 \pm 5	0.0034	52 \pm 5	0.0245
Wild-type – A β_{EP} GFP	75 \pm 5	64 \pm 3	0.0309	60 \pm 5	0.0213
Phospholipid metabolism					
$\Delta cho2$	15 \pm 3	24 \pm 3	0.0213	20 \pm 2	0.0742
$\Delta opi3$	17 \pm 2	24 \pm 2	0.0128	21 \pm 2	0.0705
$\Delta ice2$	23 \pm 2	27 \pm 2	0.0705	23 \pm 2	1.00

DAK2 encodes dihydroxyacetone kinase, which is responsible for detoxification of dihydroxyacetone (Molin et al., 2003; Norbeck and Blomberg, 1997). Wild-type cells over-expressing *DAK2* also gave rise to more fluorescent cells (~35%) than those in wild-type control cells. Interestingly, however, *DAK2* over-expression in wild-type cells exhibited a structured localisation of fluorescent A β_{42} GFP in a large globular compartment in the cell (Figure 4-14B). Based on the intensity of A β_{42} GFP fluorescence, it appeared that fluorescent A β_{42} GFP peptides accumulated inside this large globular compartment, which was found to be visible under differential interference contrast (DIC) microscopic images. *DAK2* over-expression in wild-type cells expressing either A β_{40} GFP or A β_{EP} GFP gave rise to 52% \pm 5% and 60% \pm 5% of the cell population, respectively. Interestingly, expressing the less-aggregation prone A β_{40} GFP or A β_{EP} GFP in these strains, yielded almost no cytosolic-diffuse fluorescence. This is unlike what was observed in wild-type cells where predominantly cytosolic-diffuse fluorescence was seen in cells expressing either A β_{40} GFP or A β_{EP} GFP. Almost all fluorescent A β_{40} GFP or A β_{EP} GFP fusion proteins were contained within the large globular compartment in cells over-expressing *DAK2* (Figure 4-14B). *DAK2* over-expression in mutants affected in phospholipid metabolism gave rise to similar levels of fluorescent cells compared to their relevant control strains; however the ER/ER-membrane localisation of A β_{42} GFP appeared to be less prominent in these lipid mutants. In each case, 500 cells were counted in triplicate and the mean and standard deviation for each are given in Table 4-4.

The relationship between *DAK2* over-expression and A β ₄₂GFP aggregation in cells is further investigated in Chapter 5.

4.2.10 Choline supplementation alters A β ₄₂GFP fluorescence in wild-type cells over- expressing *CDS1*, but not *DAK2*.

In *S. cerevisiae*, exogenous choline can be assimilated to produce PC, via the Kennedy salvage pathway (Kennedy and Weiss, 1956). The PC depletion in $\Delta cho2$ and $\Delta opi3$ strains can be reversed by the growth of these strains in media supplemented with choline. In Section 4.2.6, it was shown that the increased fluorescence of the various forms of A β GFP fusion proteins in $\Delta opi3$ and $\Delta cho2$ cells was reversed by choline supplementation in the growth medium. Cds1p is responsible for CDP-DAG-dependent synthesis of phospholipids from phosphatidic acid (PA) (Figure 4-1) (Homann et al., 1985). Shen and colleagues (1996) previously reported that galactose-induced *CDS1* over-expression in wild-type cells led to a ten-fold increase of Cds1p activity relative to the wild-type control strain. While an increase in CDP-diacylglycerol synthase activity led to significantly higher levels of PA, PI, PE, DMPE and cardiolipin (CL) compared to wild-type cells, a significant decrease in PS and PC was also reported (Shen et al., 1996).

In order to investigate if PC depletion influenced the increased proportion of fluorescent cells and partitioning of fluorescent A β ₄₂GFP in to the ER/ER-membrane of wild-type cells over-expressing *CDS1*, these cells expressing A β ₄₂GFP were grown in medium lacking or supplemented with choline. Since wild-type cells over-expressing *DAK2* exhibited increased fluorescence and accumulation of fluorescent A β ₄₂GFP in a large globular compartment in the cell, this strain was also included in the choline supplementation analysis. A β ₄₂GFP-associated fluorescence was analysed following growth of strains in media either lacking or supplemented with 1 mM choline chloride 15 h post induction. In each case, 300 cells were counted in triplicate and the data generated through this analysis are presented in Table 4-4.

Over-expression of *CDS1* in wild-type, $\Delta opi3$ and $\Delta cho2$ cells expressing A β ₄₂GFP indicated that the ER/ER-membrane localisation in these strains was significantly reduced upon choline supplementation (Table 4-4). It is worth noting that in Section 4.2.6, the ER/ER-membrane localisation of fluorescent A β ₄₂GFP in $\Delta opi3$

and $\Delta cho2$ cells were successfully reversed to wild-type levels upon choline addition. However, with the over-expression of *CDS1* in these strains, levels of $A\beta_{42}$ GFP-associated fluorescence were not completely reversed to those of the wild-type, $\Delta opi3$ and $\Delta cho2$ control cells. Since Cds1p activity is associated with both the ER and mitochondria (Shen et al., 1996), this may indicate that lipid metabolites, other than PC, may be involved in the partitioning of $A\beta_{42}$ GFP in to the ER/ER-membrane of mutants affected in lipid metabolism. Data from the choline supplementation experiments support this hypothesis since PC repletion via choline addition to the media did not reverse the ER/ER-membrane localisation of $A\beta_{42}$ GFP to the extent observed in the wild-type controls. The possible effects of *CDS1* over-expression in cells is further investigated in the following section.

In wild-type cells over-expressing *DAK2*, choline supplementation did not affect the proportion of cells exhibiting $A\beta_{42}$ GFP-associated fluorescence (Table 4-4). These data may suggest a phospholipid-independent mechanism affecting $A\beta_{42}$ GFP aggregation by partitioning into a distinct cellular compartment in the cell. The effect of *DAK2* over-expression in cells is further investigated in Chapter 5.

Table 4-4 Proportion of $A\beta$ GFP fluorescent cells grown in media lacking or supplemented with choline

Strains over-expressing either *CDS1* or *DAK2* were induced for $A\beta_{42}$ GFP expression in galactose medium (SCgal-URA) either lacking or supplemented with choline and $A\beta_{42}$ GFP-associated fluorescence analysed at 15 h post induction. 300 cells were counted and the data shown are the mean of triplicate measurements \pm standard deviation from a single experiment. *p* - values denote the significance in the difference of the proportion of cells exhibiting $A\beta_{42}$ GFP-associated fluorescence, grown in media either lacking or supplemented with choline.

Strains expressing $A\beta_{42}$ GFP and <i>CDS1</i> or <i>DAK2</i>	Percentage of fluorescent cells		<i>p</i> - value
	No choline addition	1 mM choline addition	
Wild-type – $A\beta_{42}$ GFP	8 \pm 3	6 \pm 2	0.3911
Wild-type – $A\beta_{40}$ GFP	65 \pm 4	61 \pm 4	0.2879
Wild-type – $A\beta_{EP}$ GFP	75 \pm 5	69 \pm 6	0.2541
Phospholipid metabolism			
Wild-type – <i>CDS1</i>	26 \pm 2	17 \pm 2	0.0053
$\Delta cho2$ – <i>CDS1</i>	24 \pm 3	15 \pm 3	0.0213
$\Delta opi3$ – <i>CDS1</i>	24 \pm 2	14 \pm 2	0.0036
$\Delta ice2$ – <i>CDS1</i>	27 \pm 2	21 \pm 2	0.0213
Wild-type – <i>DAK2</i>	35 \pm 2	33 \pm 3	0.3911
$\Delta cho2$ – <i>DAK2</i>	20 \pm 2	18 \pm 3	0.3911
$\Delta opi3$ – <i>DAK2</i>	21 \pm 2	18 \pm 2	0.1401
$\Delta ice2$ – <i>DAK2</i>	23 \pm 2	22 \pm 4	0.7183

4.2.11 Investigating the role of essential genes involved in phospholipid metabolism in A β ₄₂GFP aggregation

Over-expression of *CDS1* in wild-type cells and the single-gene deletion mutants, *Δcho2*, *Δopi3* and *Δice2* strains, not only gave rise to increased levels of fluorescence but these mutants also exhibited the ER/ER-membrane-localised A β ₄₂GFP fluorescence. It was hypothesised that A β ₄₂GFP may be interacting with specific lipid metabolite(s) in these mutants with altered phospholipid homeostasis giving rise to the characteristic localisation. As illustrated in the *S. cerevisiae* phospholipid biosynthetic pathway (Figure 4-1), Cds1p catalyses the generation of CDP-DAG from PA using CTP as a co-factor and plays an essential role in the biosynthesis of all major phospholipids. CDP-DAG is subsequently partitioned between PC, PI or CL biosynthesis. Therefore, the over-expression of *CDS1* may have caused increased flux into these three separate pathways leading to altered phospholipid composition in intracellular membranes. Interestingly, Shen and colleagues (1996) previously reported that galactose-induced *CDS1* over-expression in wild-type cells led to significantly higher levels of PA, PI, PE, DMPE and CL; and significantly reduced levels of PS and PC compared to wild-type cells (Shen et al., 1996). These data indicated that cells over-expressing *CDS1* favoured an increased flux into the PI and CL biosynthetic pathways compared to the PS/PC biosynthetic pathway. In a subsequent study, this regulation of phospholipid biosynthesis, particularly of Cho1p (PS synthase), Pis1p, (PI synthase) and Ino1p (inositol 1-phosphate synthase) activities by intracellular levels of Cds1p activity, was further reported (Shen and Dowhan, 1997).

To investigate if the increased fluorescence in phospholipid mutants was caused by an increased flux into one of these three branched pathways (ie. biosynthesis of PC, PI or CL; Figure 4-1), a targeted screen approach using *CDS1* over-expression in selected single gene-deletion mutants (*Δplc1*, *Δcrd1* and *Δcho1*) was undertaken. As controls, wild-type BY4743, *Δplc1*, *Δcrd1* and *Δcho1* cells were co-transformed with pAG415GAL-A β ₄₂-GFP and pYES-DEST52 (an empty *URA3* vector) (Invitrogen, San Diego, CA, USA). Expression of the A β ₄₂GFP fusion protein in each strain was induced by growth in galactose medium and A β ₄₂GFP-associated fluorescence was analysed 15 h post-induction. In addition to the use of non-essential gene deletion mutants, essential genes for viability of *S. cerevisiae* were also analysed.

In the *S. cerevisiae* genome, 1033 genes (~18% of ORFs) have been identified to be essential for viability (Nash et al., 2007). Since *CDS1* (which encodes phosphatidate cytidylyltransferase to produce CDP-DAG from PA), *PIS1* (which encodes phosphatidylinositol synthase to produce PI from CDP-DAG) and *PGS1* (which encodes phosphatidylglycerolphosphate synthase to produce CL from CDP-DAG), are essential genes for viability, selected strains from the Decrease Abundance mRNA Perturbation (DAmP) yeast library were used. The DAmP yeast library of hypomorphic alleles (alleles with reduced gene function) for 970 heterozygous diploid DAmP essential genes was purchased from OpenBiosystems™ and sporulated into 842 *MATa* haploid strains. In the haploid strains, the insertion of a kanamycin resistance cassette between the stop codon and the 3' untranslated region of an ORF leads to destabilisation in the resulting mRNA transcript and a 2-10 fold reduction in mRNA levels present in the cell relative to the heterozygous diploid (Breslow et al., 2008). Haploid DAmP strains of *CDS1* (*cds1*-DAmP), *PGS1* (*pgs1*-DAmP) and *PIS1* (*pis1*-DAmP) were transformed with pAG415GAL-A β ₄₂-GFP and successful transformants were examined to identify those exhibiting increased A β ₄₂GFP fluorescence and/or altered fluorescence localisation compared to wild-type cells. Expression of the A β ₄₂GFP fusion protein in each of these three strains was induced by growth in galactose medium and A β ₄₂GFP-associated fluorescence was analysed 20 h post-induction, as they were generally slow-growers.

Control strains, Δ *plc1*, Δ *crd1* and Δ *cho1* cells, yielded trace levels of A β ₄₂GFP fluorescence similar to those observed in wild-type cells. Fluorescence levels in Δ *plc1*, Δ *crd1* and Δ *cho1* cells over-expressing *CDS1* exhibited an increased proportion of fluorescent cells (~14%, ~14% and ~16% of the cell population, respectively) compared to their appropriate control strains and similar to those observed in wild-type cells over-expressing *CDS1* where intensely fluorescent puncta of A β ₄₂GFP appeared continuous and in an ordered-manner in the ER/ER-membrane localisation. Analysis of *cds1*-DAmP, *pgs1*-DAmP and *pis1*-DAmP cells expressing A β ₄₂GFP indicated that in all three strains, intensely fluorescent puncta of A β ₄₂GFP were localised in a 'discontinuous' arrangement around the nucleus of the cell (Figure 4-15); unlike those observed in wild-type cells over-expressing *CDS1* or in the six deletion mutants belonging to the phospholipid metabolism functional group (Δ *psd1*, Δ *cho2*, Δ *opi3*, Δ *ino2*, Δ *ino4* and Δ *ice2* strains). *CDS1* over-expression in the *cds1*-DAmP, *pgs1*-DAmP

and *pis1*-DAmP cells was able to restore the ‘continuous’ arrangement of fluorescent A β ₄₂GFP puncta in the ER/ER-membrane localisation in these cells (Figure 4-15).

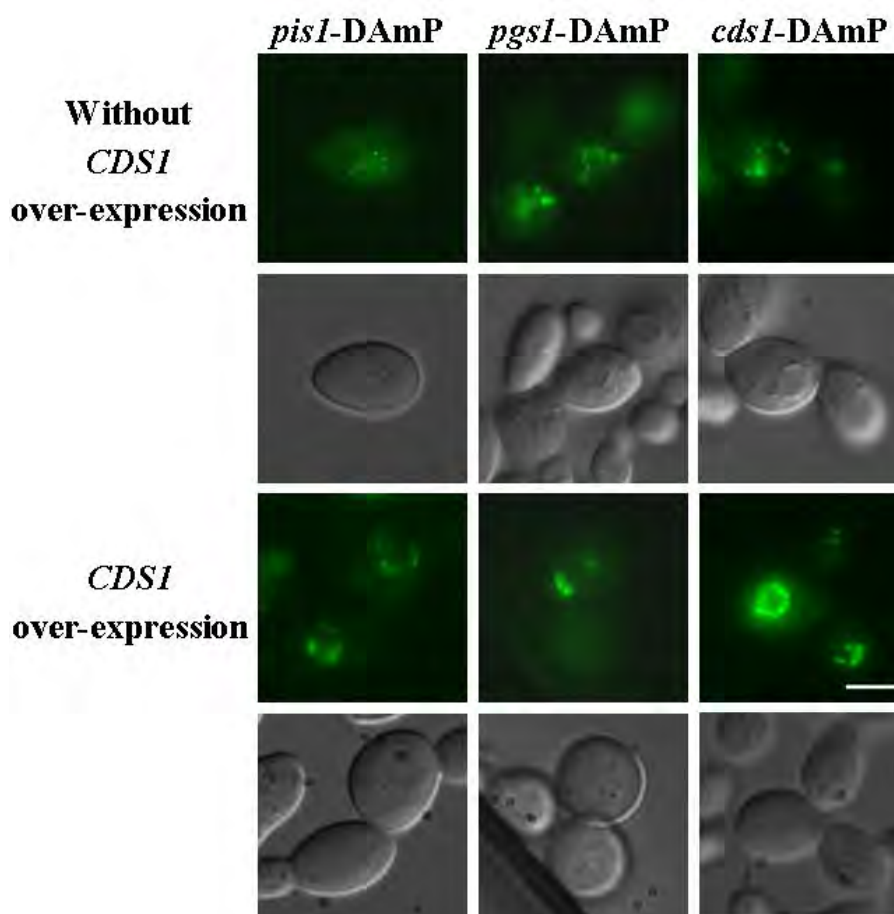


Figure 4-15 Fluorescent microscopic images of *cds1*-DAmP, *pgs1*-DAmP and *pis1*-DAmP cells expressing A β ₄₂GFP grown with and without *CDS1* over-expression.

cds1-DAmP, *pgs1*-DAmP and *pis1*-DAmP cells expressing A β ₄₂GFP grown with or without *CDS1* over-expression (as indicated) were induced in galactose medium (SCgal-URA) and A β GFP-associated fluorescence was analysed at 20 h post induction. All three strains without *CDS1* over-expression yielded intense A β ₄₂GFP fluorescent puncta localised in a ‘discontinuous’ arrangement around the nucleus of the cell while the same strains over-expressing *CDS1* led to the characteristic ER/ER-membrane localisation of A β ₄₂GFP. Scale bars indicate 5 μ m.

To determine if the partitioning of A β ₄₂GFP in to the ER/ER-membrane of the phospholipid mutants was caused by an increased flux into the CL or PI biosynthetic pathways, *PGS1* and *PIS1* over-expression in wild-type and Δ *cho1* cells was undertaken. Over-expression of *PIS1* in wild-type and Δ *cho1* cells expressing A β ₄₂GFP indicated that in both strains intense A β ₄₂GFP fluorescent puncta were localised in a ‘discontinuous’ arrangement around the nucleus of the cell (Figure 4-16). Interestingly, over-expression of *PGS1* in wild-type and Δ *cho1* cells expressing A β ₄₂GFP yielded

multiple A β_{42} GFP fluorescent puncta of various sizes in a randomly distributed manner in both these strains (Figure 4-16). Taken together with results from the $\Delta dgal1 \Delta lro1 \Delta are1 \Delta are2$ quadruple mutant analysis (Section 4.2.4), *pgs1*-DAmP and the *pis1*-DAmP cells (above), these data clearly indicate that reduced flux into PI biosynthesis, and by extension reduced levels of PI may contribute to the ER/ER-membrane localisation of A β_{42} GFP in mutants affected in phospholipid metabolism. To validate these data from a genetic approach, quantitative lipidomics using shotgun mass spectrometry was undertaken in mutants that gave rise to A β_{42} GFP in the ER/ER-membrane localisation. These data are presented in Chapter 5.

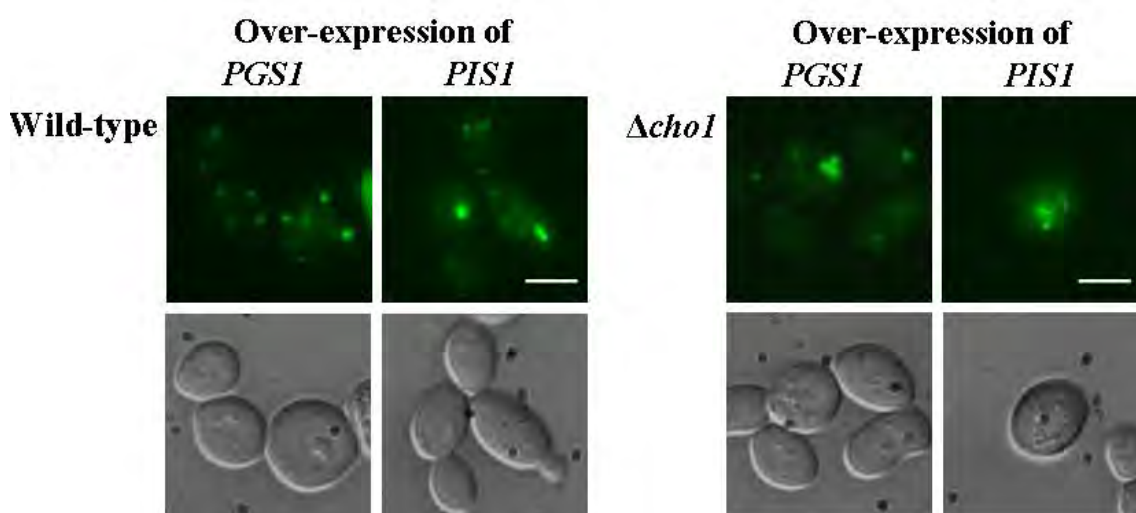


Figure 4-16 Fluorescent microscopic images of *PGS1* and *PIS1* over-expression in wild-type and $\Delta cho1$ cells expressing A β_{42} GFP.

All four strains over-expressing either *PIS1* or *PGS1* (as indicated) were induced in galactose medium (SCgal-URA) and A β GFP-associated fluorescence was analysed at 15 h post induction. *PIS1* over-expression in both wild-type and $\Delta cho1$ cells indicated A β_{42} GFP fluorescent puncta was localised in a ‘discontinuous’ arrangement around the nucleus of the cell. However, *PGS1* over-expression in both wild-type and $\Delta cho1$ cells yielded multiple A β_{42} GFP fluorescent puncta of various sizes in a randomly distributed manner. Scale bars indicate 5 μ m.

4.2.12 Effects of intracellular levels of water-soluble lipid precursors on A β ₄₂GFP aggregation

4.2.12.1 Altered levels of S-adenosyl-L-methionine (AdoMet) do not affect A β ₄₂GFP aggregation

The data provided thus far strongly suggest that A β ₄₂GFP aggregation is influenced by altered phospholipid homeostasis in *S. cerevisiae* cells. Important co-factors involved in the *de novo* phospholipid biosynthetic pathway (Figure 4-1) include cytidine-triphosphate (CTP), myo-inositol, serine and S-adenosyl-L-methionine (AdoMet). The genome-wide deletion mutant analysis identified that the deletion of *CHO2*- and *OPI3*-encoded phospholipid methyltransferases resulted in an increased proportion of A β ₄₂GFP fluorescent cells. Cho2p and Opi3p catalyse the AdoMet-dependent methylation of phosphatidylethanolamine (PE), phosphatidyl-N-methylethanolamine (PMME), and phosphatidyl-N-dimethylethanolamine (PDME) respectively, to sequentially yield PC. S-adenosyl-L-homocysteine (AdoHcy), which is produced as a result of the above methylation reactions, is a competitive inhibitor of Cho2p and Opi3p (Gaynor and Carman 1990). To determine if altered levels of the rate-limiting AdoMet affect A β ₄₂GFP aggregation, analysis of genes involved in the S-adenosyl-L-methionine biosynthetic cycle was undertaken. Wild-type BY4743 cells were co-transformed with pAG415GAL-A β ₄₂-GFP construct and BG1805 plasmids carrying one of the genes: *SAM1*, *SAM2*, *SAH1* and *MET6*. As controls, wild-type, $\Delta sam1$, $\Delta sam2$ and $\Delta met6$ cells were co-transformed with pAG415GAL-A β ₄₂-GFP and pYES-DEST52 (an empty *URA3* vector) (Invitrogen, San Diego, CA, USA). Successful transformants over-expressing a particular ORF were examined to identify those exhibiting increased A β ₄₂GFP fluorescence and/or altered fluorescence localisation. $\Delta sam1$, $\Delta sam2$ and $\Delta met6$ strains, also included in this analysis, were transformed with pUG35GAL1-A β ₄₂. Expression of the A β ₄₂GFP fusion protein and gene ORF in each strain was induced by growth in galactose medium and A β ₄₂GFP-associated fluorescence was analysed 15 h post-induction.

Fluorescence levels exhibited in $\Delta sam1$, $\Delta sam2$ and $\Delta met6$ strains expressing pUG35GAL1-A β ₄₂ yielded weak A β ₄₂GFP fluorescence that was restricted to ~6% of the cell population, similar to that observed in wild-type cells (data not shown). Wild-type cells over-expressing *SAM1*, *SAM2*, *SAH1* or *MET6* also gave rise to similar trace

levels of A β ₄₂GFP fluorescence as the wild-type control cells. These data indicate that while intracellular levels of AdoMet and AdoHcy may be altered in mutants affected in phospholipid metabolism, these water-soluble lipid precursor molecules are unlikely to influence the A β ₄₂GFP aggregation and partitioning in to the ER/ER-membrane directly.

4.2.12.2 Over-expression of *URA5*, encoding orotate phosphoribosyltransferase, and *URA7*, encoding cytidine-triphosphate (CTP) synthase, give rise to increased A β ₄₂GFP fluorescence

Over-expression of *CDS1*-encoded phosphatidate cytidylyltransferase, identified through the ‘reverse-genetics’ approach (Section 4.2.8), also led to an increased proportion of A β ₄₂GFP fluorescent cells. The nucleotide cytidine-triphosphate (CTP), derived from uridine-triphosphate (UTP), is required by Cds1p for the catalytic conversion of PA to CDP-DAG (Chang and Carman, 2008; Ozier-Kalogeropoulos et al., 1991). To determine if altered levels of intracellular CTP affect A β ₄₂GFP aggregation, analysis of genes involved in the *de novo* biosynthesis of pyrimidine ribonucleotides was undertaken. Wild-type BY4743 cells were co-transformed with pAG415GAL-A β ₄₂-GFP construct and BG1805 plasmids carrying one of the genes: *URA1*, *URA4*, *URA5*, *URA6*, and *URA7*. As controls, both wild-type BY4743 cells were co-transformed with pAG415GAL-A β ₄₂-GFP and pYES-DEST52 (an empty *URA3* vector) (Invitrogen, San Diego, CA, USA). Δ *ura2*, Δ *ura4*, Δ *ura1*, Δ *ura5*, Δ *ura10*, Δ *ura7* and Δ *ura8* strains, also included in this analysis, were transformed with pUG35GAL1-A β ₄₂. Expression of the A β ₄₂GFP fusion protein and gene ORF in each strain was induced by growth in galactose medium and A β ₄₂GFP-associated fluorescence was analysed 15 h post-induction.

Single gene deletion mutants of the pyrimidine ribonucleotides biosynthetic pathway (Δ *ura2*, Δ *ura4*, Δ *ura1*, Δ *ura5*, Δ *ura10*, Δ *ura7* and Δ *ura8* cells) and wild-type BY4743 cells over-expressing *URA1*, *URA4*, and *URA6* and A β ₄₂GFP gave rise to similar trace levels of fluorescence (~8% of the cell population) as those observed in wild-type cells. However, wild-type cells over-expressing *URA5*, encoding orotate phosphoribosyltransferase, or *URA7*, encoding CTP synthase, gave rise to a significant increase in the proportion of A β ₄₂GFP fluorescent cells; ~14% and ~12% of the cell population respectively (Figure 4-17). Interestingly, in wild-type cells over-expressing

URA5, A β ₄₂GFP exhibited the ordered localisation of intensely fluorescent puncta of A β ₄₂GFP in a perinuclear arrangement analogous to that observed in the six deletion mutants affected in phospholipid metabolism and in wild-type cells over-expressing *CDS1* (Figure 4-17A). In *S. cerevisiae*, *URA5* and *URA10* encode orotate phosphoribosyltransferase and both share greater than 75% amino acid similarity (de Montigny et al., 1989; de Montigny et al., 1990). Interestingly, over-expression of *URA10* in wild-type cells did not give rise to increased fluorescence compared to *URA5* over-expression in these cells. One possible explanation for this may be that Ura5p contributes around 80% of the OPRase activity found in *S. cerevisiae* (de Montigny et al., 1989; de Montigny et al., 1990). Transcription regulation of *URA5* and *URA10* also appears to differ under various conditions. While the expression of *URA5* is not regulated by any known molecule, *URA10* was found to be down regulated by both inositol and choline in an Opi1p-dependent manner (Santiago and Mamoun, 2003), and upregulated by the presence of lithium (Bro et al., 2003) or by zinc depletion in a Zap1p-dependent manner (Lyons et al., 2000).

Wild-type cells over-expressing *URA7* were observed to exhibit large intense A β ₄₂GFP fluorescent puncta in the cell (Figure 4-17B). Cells over-expressing *URA7* are forced to accumulate CTP intracellularly (Chang and Carman, 2008) and this increased level of CTP has been shown to alter synthesis of membrane phospholipids especially in the pathway leading to PC biosynthesis. Elevated levels of CTP have been found to decrease levels of PS due to direct inhibition of Cho1p (McDonough et al., 1995) and increase levels of PC, PE, and PA (Ostrander et al., 1998) due to activation of the Kennedy salvage pathway. Increased levels of PC and PE are attributed to the activation of choline-phosphate cytidylyltransferase Pct1p and ethanolamine-phosphate cytidylyltransferase Ect1p respectively, due to increased availability of CTP (Kent and Carman, 1999; McDonough et al., 1995; Ostrander et al., 1998); while increased levels of PA may have resulted from the activation of DAG kinase Dgk1p (Han et al., 2008) and inhibition of PA phosphatase Pah1p (Wu and Carman, 1994). Without available literature on the direct relationship between intracellular levels of CTP and A β peptides, these data may further indicate that disruption to phospholipid homeostasis affects A β ₄₂GFP aggregation in cells.

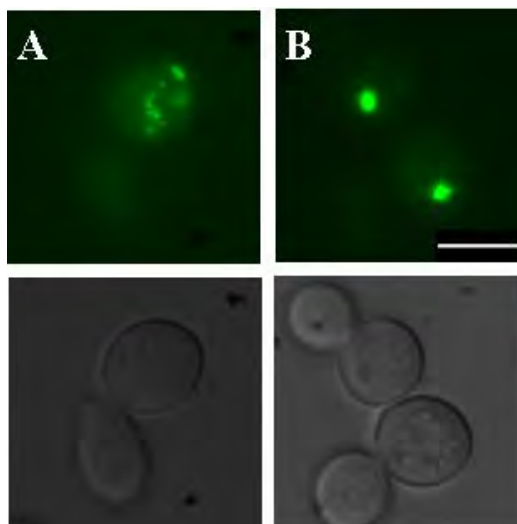


Figure 4-17 Fluorescent microscopic images of wild-type cells over-expressing *URA5* or *URA7* together with A β ₄₂GFP

Wild-type cells over-expressing A) *URA5* or B) *URA7* together with A β ₄₂GFP were induced in galactose medium (SCgal-URA) and A β GFP-associated fluorescence was analysed at 15 h post induction. A) *URA5* over-expression in wild-type cells yielded ER/ER-membrane localisation of A β ₄₂GFP while; B) *DAK2* over-expression in wild-type cells exhibited a large fluorescent A β ₄₂GFP puncta in the cell. Scale bars indicate 5 μ m.

4.2.12.3 Over-expression of inositol monophosphatases Inm1p and Inm2p, but not inositol supplementation, give rise to increased A β ₄₂GFP fluorescence

In Section 4.2.11, it was identified that *pis1*-DAmP cells expressing A β ₄₂GFP exhibited intensely fluorescent puncta of A β ₄₂GFP around the nucleus of the cell. Pis1p requires myo-inositol to yield phosphatidylinositol (PI), which is subsequently utilised in the synthesis of other lipids such as polyphosphoinositides (Strahl and Thorner, 2007) and sphingolipids (Cowart and Obeid, 2007; Dickson, 2010). To investigate if altered levels of intracellular inositol affect A β ₄₂GFP aggregation, analysis of genes involved in the biosynthesis of myo-inositol and inositol phosphate was undertaken. Wild-type BY4743 cells were co-transformed with pAG415GAL-A β ₄₂-GFP construct and BG1805 plasmids carrying one of the genes: *INO1*, *INM1*, *INM2*, *PLC1*, *ARG82*, *KCS1* and *IPK1*. As controls, both wild-type BY4743 cells were co-transformed with pAG415GAL-A β ₄₂-GFP and pYES-DEST52 (an empty *URA3* vector) (Invitrogen, San Diego, CA, USA). Δ *ino1*, Δ *inm1*, Δ *inm2*, Δ *arg82*, Δ *kcs1* and Δ *ipk1* strains, also included in this analysis, were transformed with pUG35GAL1-A β ₄₂. Expression of the A β ₄₂GFP fusion protein and gene ORF in each strain was induced by growth in

galactose medium and A β ₄₂GFP-associated fluorescence was analysed 15 h post-induction.

Single gene deletion mutants of the myo-inositol and inositol phosphate biosynthetic pathways ($\Delta ino1$, $\Delta inm1$, $\Delta inm2$, $\Delta arg82$ and $\Delta kcs1$ cells) and the wild-type BY4743 cells over-expressing *INO1*, *PLC1*, *ARG82*, *KCS1* or *IPK1* and A β ₄₂GFP gave rise to similar trace levels of fluorescence (~10% of the cell population) to that observed in wild-type cells. However, $\Delta ipk1$ cells, and, wild-type cells over-expressing *INM1* and *INM2*, encoding inositol monophosphatases, gave rise to increased A β ₄₂GFP fluorescent cells (~18% of the cell population in both strains) compared to wild-type control cells. $\Delta ipk1$ cells exhibited cytosolic fluorescence with intense fluorescent A β ₄₂GFP arranged in tubular structures around the nucleus and the periphery of the cell (Figure 4-18C), while wild-type cells over-expressing *INM1* or *INM2*, exhibited intense cytosolic diffused A β ₄₂GFP fluorescence (Figure 4-18A and B). It is interesting to note that TCA cycle mutants belonging to the mitochondria functional group were the only group of cells identified thus far in this study to exhibit a similar intensity of cytosolic fluorescence.

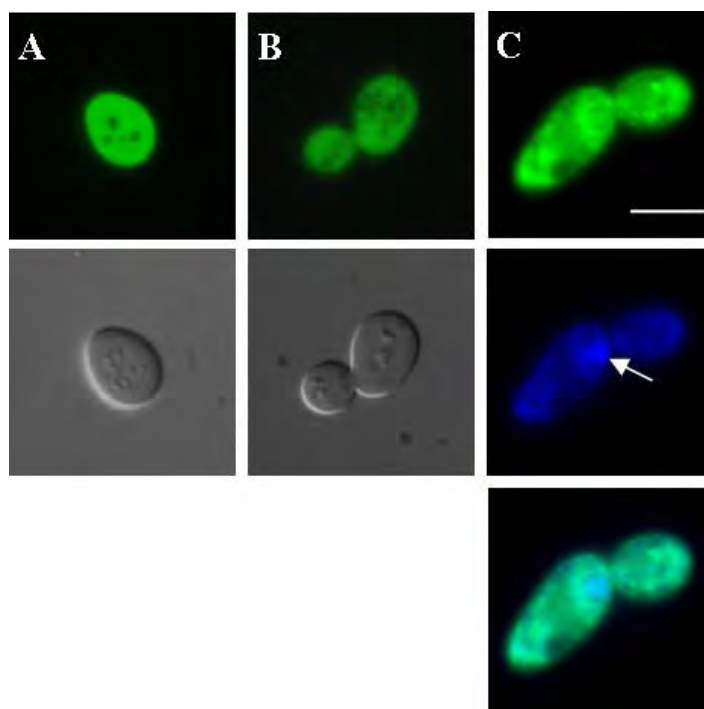


Figure 4-18 Fluorescent microscopic images of wild-type cells over-expressing *INM1* or *INM2* together with A β ₄₂GFP

Wild-type cells over-expressing A) *INM1* or B) *INM2* together with A β ₄₂GFP were induced in galactose medium (SCgal-URA) and A β GFP-associated fluorescence was analysed at 15 h post induction. Both *INM1* and *INM2* over-expression in wild-type cells yielded intense cytosolic

A β_{42} GFP fluorescence. C) A β_{42} GFP localisation in $\Delta ipk1$ cells is observed in the top panel. DAPI staining of mitochondrial and nuclear DNA is observed in the middle (arrow indicates the nucleus). Merged images of A β_{42} GFP and DAPI staining (bottom panel) indicate the close proximity of A β_{42} GFP to the nuclear and cellular periphery. Scale bars indicate 5 μ m.

Biosynthesis of inositol is evolutionarily conserved throughout the biological kingdom (Majumder et al., 2003). Inositol is an essential polyol in eukaryotes as its phospholipid derivative PI is an essential component of phospholipid membranes. Out of the eight naturally-occurring isomers of inositol, myo-inositol is the most common stereoisomer found physiologically. It was previously reported that overexpression of inositol monophosphatase Inm1p, which converts myo-inositol monophosphate to myo-inositol, led to an increased presence of intracellular inositol (Murray and Greenberg, 2000). Since over-expression of inositol monophosphatases Inm1p and Inm2p in wild-type cells gave rise to a significant increase in the proportion of fluorescent cells exhibiting intense cytosolic diffused A β_{42} GFP fluorescence, it was proposed that increased levels of intracellular inositol may have contributed to the increased fluorescence observed in these strains. To examine this, wild-type cells expressing A β_{42} GFP were grown in medium lacking or supplemented with inositol. The concentration of inositol at 75 μ M was selected since studies have previously shown that *S. cerevisiae* cells grown in media supplemented with inositol at this concentration was sufficient to affect phospholipid metabolism (Kelley et al., 1988; Loewen et al., 2004). Expression of the A β_{42} GFP fusion protein in wild-type cells was induced by growth in galactose medium lacking or supplemented with 75 μ M inositol and A β_{42} GFP-associated fluorescence was analysed 15 h post-induction.

Wild-type cells grown in medium lacking or supplemented with inositol exhibited similar trace levels (~5% of the cell population) of A β_{42} GFP fluorescence. A possible explanation for the lack of fluorescence upon inositol supplementation may be that exogenously supplied inositol led to increased PI synthesis instead of inositol accumulation in the cells. It has been previously described that presence of exogenous inositol stimulates Pis1p in wild-type cells which subsequently leads to increased PI levels and reduced levels of CDP-DAG, PA and PS (Kelley et al., 1988; Loewen et al., 2004). Therefore, to be able to force an intracellular accumulation of inositol in cells, a higher concentration of exogenous inositol may be attempted. The human brain has the highest concentration of inositol in the body; ~5 mM myo-inositol and 0.5 mM scyllo-

inositol (Michaelis et al., 1993). Interestingly, using ^1H magnetic resonance spectroscopy, it was demonstrated that AD brains contain high levels of myo-inositol (Moats et al., 1994; Parnetti et al., 1997; Shetty et al., 1996). Post-mortem studies have also shown a 15% increase in myo-inositol compared to controls (Stokes and Hawthorne, 1987) and a significant increase of more than 50% increase in myo-inositol levels in adults with Down syndrome (Huang et al., 1999). At present, however, it is not clearly known if increased levels of myo-inositol are present just before the onset of AD.

4.3 Discussion

4.3.1 Disruption to phospholipid metabolism leads to increased $\text{A}\beta_{42}\text{GFP}$ -associated fluorescence in *S. cerevisiae* cells

Of the main cellular functions affecting $\text{A}\beta_{42}\text{GFP}$ aggregation and localisation, phospholipid metabolism was chosen for more extensive analysis since most of the genes directly involved in phospholipid synthesis were over-represented in the screens, and there is evidence of perturbed phospholipid metabolism in AD (Frisardi et al., 2011; Grimm et al., 2011; Hung et al., 2008). Genes in the phospholipid metabolism functional group include *INO2*, *INO4*, *UME6*, *SCS2*, *PSD1*, *CHO2*, and *OPI3* all of which directly or indirectly regulate levels of PC in cells. Furthermore, $\text{A}\beta_{42}$ was identified in perinuclear localised multi-vesicular bodies (MVBs) of neuronal cells, (Langui et al., 2004; Takahashi et al., 2002). The Δino2 , Δino4 , Δpsd1 , Δcho2 , Δopi3 and Δice2 mutants also exhibited the characteristic ER/ER-membrane associated $\text{A}\beta_{42}\text{GFP}$ localisation. Through these genetic approaches alone, it was not possible to identify any specific phospholipid that affected $\text{A}\beta_{42}\text{GFP}$ fluorescence/ localisation, however data presented in this chapter clearly indicate that perturbation of phospholipid homeostasis, specifically the ER membranes, may affect $\text{A}\beta_{42}\text{GFP}$ aggregation. This may subsequently allow partitioning of $\text{A}\beta_{42}\text{GFP}$ into the ER/ER membranes in the six mutants affected in phospholipid metabolism leading to the different localisation patterns of $\text{A}\beta_{42}\text{GFP}$.

In *S. cerevisiae* cells, PC can be synthesised from exogenous choline via the Kennedy salvage pathway and choline supplementation leads to repletion of PC in the Δcho2 and Δopi3 mutants to wild-type levels (Kennedy and Weiss, 1956; McGraw and

Henry, 1989) (Table 4-5). Choline supplementation of the growth medium led to a reduced extent of the A β ₄₂GFP-associated fluorescence in $\Delta psd1$, $\Delta cho2$ and $\Delta opi3$ cells. While choline supplementation leads to repletion of PC levels in $\Delta cho2$ and $\Delta opi3$ cells it also reverses the PE and PMME over-accumulation phenotype of these mutants, respectively (McGraw and Henry, 1989) (Table 4-5). Therefore, based on these data alone it is not possible to postulate whether it is the PC depletion and/or the over-accumulation of PE/PMME in $\Delta cho2$ and $\Delta opi3$ cells that led to increased A β ₄₂GFP-associated fluorescence. However, evaluation of the phenotype of the $\Delta psd1$ and $\Delta scs2$ mutants may resolve this issue (discussed below).

Table 4-5 Phospholipid composition of wild-type and mutants affected in phospholipid metabolism.

The values represent percentage of phospholipid from total cellular lipids. ND refers to not detectable and NM denotes not measured.

Strain	Media	PI	PS	PE	PMME	PDME	PC	Ref.
Wild-type	No choline	28.3	5.9	13.3	trace	trace	43.2	1
	1 mM choline	NM	14.7	16.3	trace	0.5	57.3	2
Wild-type	No choline	28	5.5	12.1	0.9	1.8	39.7	3
$\Delta opi3$	No choline	35.0	3.0	5.60	44.0	2.00	ND	1
	1 mM choline	24.7	5.1	12.2	8.90	1.80	39.4	1
$\Delta cho2$	No choline	25	5.0	39	NM	NM	15	4
	1 mM choline	18	6.0	21	NM	NM	39	4
$\Delta cho2-1$	No choline	33.8	6.3	44.0	ND	ND	4.2	5
$\Delta ino2-2$	No choline	36.5	4.6	28.3	1.3	9.5	11.9	3
$\Delta ino4-38$	No choline	36.3	4.1	23.8	2.0	7.8	11.1	3

Ref, Reference; 1: McGraw and Henry (1989); 2: Waechter and Lester (1973); 3: Loewy and Henry (1984); 4: Mayerhofer (unpublished); 5: Summers *et al.*, (1988)

The $\Delta psd1$ mutant exhibited the characteristic ER/ER membrane-associated A β ₄₂GFP localisation. Phosphatidylserine decarboxylases Psd1p and Psd2p, which are localised in the mitochondria and Golgi/vacuoles respectively, catalyse the decarboxylation of PS to PE (Trotter *et al.*, 1993; Trotter *et al.*, 1995; Trotter and Voelker, 1995). Mitochondria-localised Psd1p contributes almost 90% of total PS decarboxylase activity in cells. As expected, $\Delta psd1$ cells grown in glucose media were found to exhibit a significant decrease in PE and increase in PI; while PC and PS levels were similar compared to wild-type cells (Storey *et al.*, 2001). Assuming the lipid

composition in membranes are similar when cells are grown in galactose, this may suggest that PC depletion or PE accumulation may not be the underlying cause of altered A β ₄₂GFP-associated fluorescence in Δ *opi3* and Δ *cho2* cells.

Dihydrosphingosine phosphate lyase Dpl1 regulates intracellular levels of sphingolipid long-chain base phosphates (LCBPs) and catabolises dihydrosphingosine-1-phosphate to produce phosphoethanolamine (Gottlieb et al., 1999; Saba et al., 1997). This by-product serves as an intermediate in the Kennedy salvage pathway. To determine if reduced levels of PE influenced the partitioning of A β ₄₂GFP in to the ER/ER membranes, a double deletion mutant (Δ *psd1* Δ *psd2* or Δ *psd1* Δ *dpl1*) needs to be generated to confirm that the A β ₄₂GFP-associated fluorescence was due to the reduced levels of PE. A triple mutant Δ *psd1* Δ *psd2* Δ *dpl1* may not be as useful since PE is completely depleted in this strain and it requires ethanolamine supplementation for growth (Storey et al., 2001). Furthermore, it is very unlikely that PE levels were depleted in the mutants identified in the screens that exhibit the ER/ER membrane A β ₄₂GFP localisation.

Apart from PC synthesis, PE also plays a role in protein modification and has unique physical properties. Unlike PS and PC, which are bilayer lipids, PE is a hexagonal phase lipid (non-bilayer forming lipid) (Birner et al., 2001; de Kruijff, 1997; Ellens et al., 1986; van der Does et al., 2000). Therefore, PE levels within membranes can influence its structure and fluidity implicating its role in membrane cytokinesis and in transmembrane protein folding and translocation (Bogdanov and Dowhan, 1999; Bogdanov et al., 1999; Emoto and Umeda, 2000; Mikhaleva et al., 2001; Schatz and Dobberstein, 1996; Umeda and Emoto, 1999). It has been demonstrated that PE can also directly modify proteins to allow association with membranes. Atg8p, a component of autophagosomes and cytoplasm-to-vacuole targeted vesicles, undergoes a reversible conjugation to PE through a covalent bond formed between the C-terminus glycine and the amine group of PE (Hanada et al., 2007; Kirisako et al., 2000; Komatsu et al., 2001). Direct lipidation by PE is essential to the function of Atg8p (Lang et al., 1998), where Atg8p-PE is anchored to membranes and plays an important role in phagophore expansion and import into the vacuole for protein degradation (Nakatogawa et al., 2007; Xie et al., 2008). While the Δ *atg8* mutant was not identified in the genome-wide

deletion screen (Chapter 3), the $\Delta atg15$ mutant was identified as exhibiting weak A β_{42} GFP-associated fluorescence by the genome-wide screen. *ATG15* encodes for a glycosylated transmembrane lipase required for the degradation of the autophagic vesicles in the vacuole (Teter et al., 2001; Yorimitsu and Klionsky, 2005). In the absence of available literature indicating the role of PE on all proteins involved in autophagy, the exact underlying cause of altered A β_{42} GFP-associated fluorescence in the $\Delta atg15$ mutant can only be speculated. Since Atg15p is a transmembrane protein, it is possible that an altered level of A β_{42} GFP-associated fluorescence was yielded in this mutant due to the availability of phospholipids, such as PE, to interact with A β_{42} GFP.

While it is still unknown whether A β_{42} GFP or A β_{42} interacts with PE *in vivo*, this hypothesis appears to be supported by *in vitro* studies that show that synthetic A β_{40} and A β_{42} peptides are adsorbed onto synthetic phospholipid membranes (Ege and Lee, 2004; Ege et al., 2005; Kanfer et al., 1999; Terzi et al., 1997), and adsorbed onto lipid monolayers enriched with either dipalmitoyl-phosphatidylethanolamine or dimyristoyl-phosphatidylethanolamine (Maltseva and Brezesinski, 2004; Maltseva et al., 2005). In addition to the higher rate of adsorption/insertion of A β onto/into membranes enriched with PE-derivatives compared to other phospholipids, it has also been shown that A β_{40} peptides cannot penetrate into zwitterionic lipid monolayers, consisting of dimyristoyl-phosphatidylcholine (Maltseva and Brezesinski, 2004; Terzi et al., 1997). Instead, A β electrostatically interacted with these outer layer polar headgroups without penetrating them (Terzi et al., 1997). The data from the above studies support the hypothesis that A β peptides have an increased adsorption rate onto lipid membranes enriched with derivatives of PE and this may account for the altered A β_{42} GFP-associated fluorescence observed in the mutants affected in phospholipid metabolism.

The $\Delta scs2$ mutant exhibited strong A β_{42} GFP-associated fluorescent puncta. Scs2p is a type-II integral ER transmembrane protein that interacts with a complex of proteins (Gavin et al., 2002) and acts as a positive regulator for inositol metabolism by interacting with Opi1p (Greenberg et al., 1982; Kagiwada et al., 1998; Loewen et al., 2003). Opi1p is a leucine zipper protein that binds DNA to repress *INO1* expression (Greenberg et al., 1982), for the production of inositol. In the absence of inositol, Scs2p interacts with Opi1p to tether this complex in the ER and produce inositol. However, in

strains lacking the *SCS2* gene, *Opilp* is translocated to the nucleus where it represses *INO1* expression (Loewen et al., 2003).

Kagiwada and Zen (2003) found that $\Delta scs2$ cells accumulate 10% more PC than wild-type cells (Kagiwada and Zen, 2003), whereas the intracellular phosphatidylinositol (PI) level was similar. This indicates that PC depletion alone may not be the underlying cause of altered $A\beta_{42}$ GFP-associated fluorescence in $\Delta opi3$ and $\Delta cho2$ cells. Although choline supplementation reduced $A\beta_{42}$ GFP-associated fluorescence in $\Delta psd1$ and $\Delta scs2$ cells, addition of exogenous choline may also have affected levels of other phospholipids such as PMME, PE, PS and PI in both these strains in a similar manner as in the $\Delta opi3$ and $\Delta cho2$ strains with choline supplementation (Table 4-1). However, in the absence of lipidomic analysis indicating the effects of *SCS2* deletion on intermediates of the phospholipid biosynthetic pathway, the exact underlying cause of altered $A\beta_{42}$ GFP-associated fluorescence in the phospholipid mutants can only be speculated. Despite this, it is very likely that it stems from altered levels of one or more intermediates of the phospholipid biosynthetic pathway, including PA, PS, PE, PC and PI. This possibility is further supported by data using the fluorescent biosensor of PA where $\Delta cho2$ cells exhibited accumulation of PA in a perinuclear/ER localisation.

Interestingly, addition of choline to the growth medium of the $\Delta ino2$ and $\Delta ino4$ mutants did not reduce the levels of $A\beta_{42}$ GFP-associated fluorescence. This may be explained by the fact that one of the target genes strongly regulated by the Ino2p and Ino4p transcriptional complex is the *CKII* gene (Jesch et al., 2005). *CKII* encodes choline kinase, which converts exogenous choline to cytidine diphosphate choline (CDP-choline), as the first enzymatic step in the Kennedy salvage pathway (Hosaka et al., 1990). As such, the lack of response of $\Delta ino2$ and $\Delta ino4$ mutants to choline supplementation, in terms of $A\beta_{42}$ GFP-associated fluorescence, may be attributed to the altered functioning of the Kennedy salvage pathway. To study this aspect further, a double deletion mutant ($\Delta opi3\Delta cki1$ or $\Delta cho2\Delta cki1$) needs to be generated to confirm that the lack of reversal of the $A\beta_{42}$ GFP-associated fluorescence was due to the affected expression of *CKII*.

The Δ ume6 mutant exhibited strong A β ₄₂GFP-associated fluorescence in the form of fluorescent puncta. Ume6p, which functions in a protein complex comprised of Sin3p and Rpd3p, positively regulates *INO2* and *CHO1* genes, where Cho1p is the PS synthase. The production of PS is important since it is the main phospholipid intermediate for the production of PC (Elkhaimi et al., 2000). Since A β ₄₂GFP-associated fluorescence in the Δ ume6 mutant was decreased by choline supplementation, this further indicated that the altered A β ₄₂GFP phenotype in these cells was probably due to altered phospholipid homeostasis.

In this study, it was observed that expression of the non-aggregating form of A β , A β _{EP}GFP, led to a similar localisation pattern as was observed with A β ₄₂GFP. This indicated that the arc-shaped localisation observed in Δ opi3 was not necessarily dependent on the aggregation propensity of the A β peptide and was likely to be due to another characteristic common to A β ₄₂ and A β _{EP}. Since A β ₄₂ is derived from the trans-membrane region of APP, insertion of A β ₄₂ into phospholipid membranes may be attributed to the amphipathic nature of the C-terminus of A β peptides (Ege and Lee, 2004). Altered membrane phospholipid composition, such as that occurring in the PC mutants including Δ cho2 and Δ opi3 may facilitate insertion of A β ₄₂ into distinct membranes of *S. cerevisiae* cells. Insertion of A β ₄₂GFP produced in the cytosol of *S. cerevisiae* (i.e. in this study) would require its translocation/partitioning from the aqueous phase of the cytosol to a membranous environment. This possibility is supported by the observation that in *in vitro* studies soluble A β ₄₀ is capable of re-inserting back into synthetic membranes (Ege and Lee, 2004).

The data above support the idea that altered phospholipid homeostasis, which may include depletion of PC, facilitated in the partitioning of A β ₄₂GFP from the cytosol to a distinct cellular location in the mutants affected in phospholipid metabolism. This redistribution affected the ability of the A β ₄₂-moiety to interfere with the correct folding of the GFP domain of the fusion protein. An important finding was that in Δ cho2 and Δ scs2 mutants some of the intense A β ₄₂GFP fluorescent puncta is likely to be the peroxisome or peroxisomal membrane. A β ₄₂GFP localisation was found to be perinuclear and in very close association with lipid droplets in both Δ cho2 and Δ opi3 cells. In this study, it was found that altered phospholipid metabolism led to A β ₄₂GFP

localisation into the peroxisomes. In *S. cerevisiae*, lipid droplets have been shown to form a very close association with peroxisomes (Binns et al., 2006). The membrane of the peroxisomes often forms extensions into lipid droplets (LDs) and it is thought that the close association of peroxisomes and LDs facilitates lipid metabolic processes. The localisation of A β ₄₂GFP in the Δ *opi3* mutant may therefore have been to peroxisomes. This may be supported by the inability to visualise peroxisomes in the Δ *opi3* cells using SKL-mDsRed, as this mutant was found to produce large LDs around 50 times the volume of those observed in wild-type cells (Fei et al., 2008; Fei et al., 2011).

Peroxisomes are subcellular organelles found in most animal cells that perform diverse metabolic functions, including lipid metabolism, fatty acid β -oxidation (Binns et al., 2006) and detoxification of reactive oxygen species (ROS) (Lazarow, 2003). The peroxisomal membrane is formed from specific regions of the endoplasmic reticulum (ER). Peroxisomes are bound by a single phospholipid monolayer, in which the major phospholipids are PC and PE (Fagarasanu et al., 2007; Purdue and Lazarow, 2001; Schneider et al., 1999). Δ *cho2* and Δ *scs2* mutants exhibited co-localisation of A β ₄₂GFP to peroxisomes. The altered phospholipid composition of PC mutants may facilitate A β insertion into membranes. Since it has been shown that A β peptides can adsorb onto membranes enriched with PE or its derivatives (Ege and Lee, 2004), it is hypothesised that depletion of PC or over-accumulation of PE/PMME in the peroxisomal phospholipid monolayer in Δ *cho2*, Δ *scs2* and probably other PC mutants, may facilitate insertion/adsorption of A β ₄₂GFP either into/onto its membrane monolayer or into the organelle. Fagarasanu *et al.*, (2007) proposed that the peroxisomal membrane lipid composition is important for peroxisome maintenance and growth (Fagarasanu et al., 2007). As such, modification of phospholipid composition of the peroxisomal phospholipid monolayer may also cause alteration in the morphology or function of the peroxisomes, thus leading to distinct localisation of A β ₄₂GFP in Δ *opi3* cells (into the lumen of peroxisomes).

Interestingly, two peroxisome mutants, Δ *pex31* and Δ *pex32*, were identified as exhibiting weak cytosolic-diffuse A β ₄₂GFP-associated fluorescence by the genome-wide screen. *PEX31* and *PEX32* encode for peroxisomal integral membrane proteins that are involved in negative regulation of peroxisome size and number, but are

dispensable for peroxisome biogenesis (Vizeacoumar et al., 2006). Since the function of Pex31p is partially redundant with Pex32p, this may account for the weak effect of their deletion on A β ₄₂GFP-associated fluorescence. Studies of a double deletion mutant of $\Delta pex31\Delta pex32$ would help to examine this possibility. Despite this, the data indicated that altered peroxisome phospholipid content and/or changes in peroxisome proliferation state affect A β ₄₂GFP localisation and aggregation in *S. cerevisiae*. The data obtained in *S. cerevisiae* appear to be supported by the observations reported in the AD literature.

Studies of hippocampal neurons indicated that addition of drugs that promoted peroxisome proliferation afforded protection against A β ₄₂ cytotoxicity since there is mounting evidence of over-accumulation of ROS in AD pathology (Lovell et al., 1995). This suggests that A β -toxicity may be mediated through an oxidative mechanism (Butterfield et al., 1999). It was proposed that the protective effect of peroxisome proliferation was mediated through decreased accumulation of reactive oxygen species (ROS). It has been shown that loss of peroxisomes makes neurons more vulnerable to oxidative stress (Stamer et al., 2002); whereas increased peroxisome proliferation, induced by drugs that promote peroxisome proliferation, ameliorated AD progression in animal models (Landreth, 2006). Neuroprotective properties of peroxisomes were also described when these organelles were induced to proliferate in rat hippocampal neurons (Santos et al., 2005). At present, however, it is unclear whether altered ROS metabolism plays a role in the altered localisation of A β ₄₂GFP in the phospholipid biosynthetic pathway and peroxisome proliferation mutants in *S. cerevisiae*.

The PPARs are a family of receptors consisting of PPAR α , β/δ and γ whose predominant actions are in regulation of lipid metabolism (Berger and Moller, 2002). Activation of PPAR α specifically, which increases catalase activity and the number of peroxisomes, was shown to reduce toxicity associated with A β ₄₂. Activation of PPAR α led to reduced intraneuronal ROS production, prevented the cytoplasmic calcium influx and protected cells from β -catenin degradation; thus, preventing toxicity caused by A β (Santos et al., 2005). It has also been shown that high expression levels of PPAR α strongly reduce the level of secreted and intracellular A β (Camacho et al., 2004). These results indicate that activation of PPAR α prevented A β -toxicity via a mechanism that

involved increased peroxisome proliferation. The modulation of PPAR α activity is currently being investigated as a possible strategy to treat AD (Santos et al., 2005).

The localisation of A β_{42} GFP fluorescent puncta in the ER/ER membrane of $\Delta opi3$ cells may indicate that peroxisome morphology distribution is altered upon PC depletion. This hypothesis is based on the proposal that A β_{42} GFP localised to peroxisomes in $\Delta opi3$ in an analogous manner to that observed in $\Delta cho2$ cells. While the role of PC in peroxisome morphology/function has not been studied in detail, it has been shown that PC plays a role in determining morphology of lipid droplets. Studies carried out in *Drosophila melanogaster* demonstrated that phospholipid biosynthesis is an important determinant of size and number of LDs. PC was particularly important for regulating size, abundance, membrane fusion and curvature of membranes of LDs (Guo et al., 2008). PC depletion also affected fusion of the LD membranes. RNA interference (RNAi) was used to knockdown *Cct1*, which encodes an isoform of phosphatidylcholine cytidyltransferase that catalyses PC synthesis in *Drosophila* (Kent, 2005). Knockdown of *Cct1* led to ~60% decrease in PC levels and significant increase in PE concentration on the LD monolayer, which led to a profound effect on LD size, number and morphology (Guo et al., 2008; Weber et al., 2003).

Lipid droplets (LDs) are bounded by a phospholipid monolayer (Martin and Parton, 2006) and are derived from the endoplasmic reticulum (ER). The monolayer of LDs is primarily composed of PC and lysophosphatidylcholine (Tauchi-Sato et al., 2002). At present it is unclear whether disruption of PC biosynthesis affects the morphology and function of peroxisomes in a similar manner to LDs. It is worth noting that both LDs and peroxisomes are derived from the ER and are bounded by a phospholipid monolayer, where the primary phospholipid is PC. If A β_{42} GFP localises to peroxisomes in $\Delta opi3$ cells, as it does in $\Delta cho2$ and $\Delta scs2$ cells, then the arrangement of fluorescent puncta in $\Delta opi3$ may indicate that peroxisome morphology was altered in the $\Delta opi3$ cells, relative to wild-type cells. In wild-type *S. cerevisiae* cells peroxisomes are randomly distributed throughout the cell (Binns et al., 2006). Altered distribution of peroxisomes in $\Delta opi3$ strain may stem from the direct effect of PC depletion or PE/PMME over-accumulation on peroxisome morphology and distribution. Alternatively, given the close association of peroxisomes with LDs, if altered

phospholipid metabolism affects LD morphology in a similar manner to *Drosophila melanogaster* (Guo et al., 2008) then altered peroxisome distribution in $\Delta opi3$ cells may be an indirect consequence of altered phospholipid metabolism on LD morphology and distribution.

Altered peroxisome function in $\Delta opi3$ cells may account for the problems encountered with trying to visualise SKL-mDsRed in these cells. Targeting of SKL-mDsRed to the peroxisome would have required recognition by a complex of peroxisomal membrane proteins that import proteins into the peroxisome (Agne et al., 2003; Rayapuram and Subramani, 2006). A detailed study of the effect of altered phospholipid metabolism on LD and peroxisome morphology in $\Delta opi3$ cells and other mutants of the PC pathway would help shed light on these issues.

4.3.2 Implications of phosphatidylcholine in human disease

The level of PC has been shown to be reduced in the membranes of cortical domains of Alzheimer's disease (AD) patient brains (Nitsch et al., 1992). PC levels were also found to be reduced in erythrocytes from AD patients (Selley, 2007). In humans, PC biosynthesis occurs solely in hepatic cells and in a similar manner to the pathway in *S. cerevisiae* cells, whereby PE is sequentially methylated to produce PC (Vance et al., 1997). In humans, as in *S. cerevisiae*, *S*-Adenosylmethionine (SAM) serves as the donor for the methyltransferase reaction which liberates *S*-adenosylhomocysteine (SAH) as an end product (Chiang, 1998) (Figure 1-2). SAH binds to methyltransferases with higher affinity than SAM and acts as an inhibitor of cellular methylation. SAH can be hydrolysed by *S*-adenosylhomocysteine hydrolase (SAH hydrolase) to form homocysteine and adenosine (Hu et al., 1999). Homocysteine is an inhibitor of SAH hydrolase and increased concentrations of homocysteine in cells have been shown to lead to increased accumulation of intracellular SAH and thus increased inhibition of methyltransferases (Yi et al., 2000). It has been demonstrated that hyperhomocysteinemia, a disease state associated with increased concentrations of circulating homocysteine, is a strong risk factor for AD (Clarke et al., 1998; McCaddon et al., 1998; Seshadri et al., 2002). Hyperhomocysteinemia is also associated with other diseases including arteriosclerosis (Selhub et al., 1995), hypercholesterolemia (Nygard et al., 1995), hypertension (Sutton-Tyrrell et al., 1997), type 2 diabetes (Drzewoski et al.,

2000) and stroke (Bostom et al., 1999). These diseases have also shown to be risk factors for AD (Selley, 2007). Although the exact mechanism involved is unclear, it is known that SAH inhibits phosphatidylethanolamine *N*-methyltransferase (PEMT) in hepatic cells and reduces conversion of PE to PC (Vance et al., 1997; Watkins et al., 2003). Interestingly, PEMT is the human orthologue of Opi3p in *S. cerevisiae*. Another important role of PEMT is the delivery of essential fatty acids from the liver to plasma and peripheral tissues (Watkins et al., 2003). This role of PEMT may also account for the association between hyperhomocysteinemia and AD.

APP metabolism is central to AD progression, and increased production of A β has been shown to be a key factor in promoting AD progression (Hardy and Higgins, 1992). As such, it is possible that PC deficiency and/or PE accumulation (e.g. in individuals with hyperhomocysteinemia) may also cause membrane stress and abnormal membrane curvature leading to higher rate of cleavage of APP by β -secretases, in the amyloidogenic pathway. While the magnitude of phosphatidylcholine depletion in *S. cerevisiae* is unlikely to be mirrored in humans in general, decreased levels of PC and increased levels of PE and circulating homocysteine are closely associated to AD. Therefore, these data strongly indicate that maintaining a physiological balance of phospholipids in human cells is necessary to prevent the formation of soluble/oligomeric A β that has been shown to inhibit synaptic plasticity and lead to disease progression of AD.

5 CHAPTER 5: GLOBAL YEAST LIPIDOME PROFILING BY QUANTITATIVE SHOTGUN MASS SPECTROMETRY

5.1 Introduction and Aims

Metabolomics is developing as an important functional genomics tool. The combination of both genetics and metabolomics is an emerging approach for biological research. Within the metabolomics field, lipidomics is a distinct subgroup. Lipidomics defined as the “systems-level analysis of lipids and their interacting moieties”, aims to quantitatively describe all lipids and their functions at the cellular level. While lipids may appear to be structurally simple, they have the potential to generate thousands of structurally diverse molecular species (Wenk, 2005); thus, presenting a formidable challenge. Recent technological advances, which include enhanced sensitivity and resolution of mass spectrometry, development of electrospray ionization and matrix assisted laser desorption ionization and computational bioinformatics approaches for data-processing and statistical-analysis allow high-throughput concurrent analysis of complex lipid mixtures (Ejsing et al., 2009; Guan and Wenk, 2006; Han and Gross, 2003). For example, the LIPID Metabolites And Pathways Strategy project (The LIPID MAPS Lipidomics Gateway; <http://www.lipidmaps.org>) aims to qualitatively and quantitatively measure using a systems biology approach and mass spectrometry, all lipid species in mammalian cells and quantify changes in lipid species in response to various conditions (Fahy et al., 2009; Fahy et al., 2007). Complete elucidation of the mammalian lipidome will lead to a thorough understanding of lipid metabolism and its role in diseases such as AD, diabetes, stroke, cancer and other lipid-based diseases. This may allow the development of more effective therapeutic strategies.

Recently, lipidomic analyses of many model organisms have provided detailed insights into the role of various lipids in cellular processes (Gaspar et al., 2007; Odorizzi et al., 2000; York et al., 2001). Since the use of *S. cerevisiae* for lipidomic analysis offers many advantages including its readily accessible molecular genetics, ease of cultivation and short generation time, the use of this model organism has proved to be very valuable. Importantly, it is worth noting that while the lipid composition of *S. cerevisiae* is much simpler compared to higher eukaryotes and multicellular organisms, the fundamental architecture of metabolic and signalling pathways involving lipid

metabolism in *S. cerevisiae* is similar to that in mammalian cells. Some of the significant differences between yeast and mammalian lipidomes include the synthesis of ergosterol in yeast cells as compared to cholesterol in mammalian cells as the major sterol (Zinser et al., 1993); yeast sphingolipids contain inositol instead of choline found in mammalian sphingomyelin. In addition, yeast cells synthesise phytosphingosine and phytoceramide (Gaspar et al., 2007; Perry and Ridgway, 2005). Since the genome of *S. cerevisiae* encodes a single fatty acid desaturase (Ole1p) which introduces a double bond in the $\Delta 9$ position on fatty acids (e.g. palmitoleic acid (16:1 cis-9) and oleic acid (18:1 cis-9) (Stukey et al., 1990), yeast cells do not synthesise polyunsaturated fatty acids, but can incorporate those obtained exogenously. Finally, while yeast cells synthesise PS through the catalytic activity of Cho1p using CDP-DAG and free serine, mammalian cells synthesise PS via an exchange reaction with PE (Kiyono et al., 1987; Letts et al., 1983; Vance, 2003).

As described above, recent advances in mass spectrometry-based shotgun lipidomics has allowed a comprehensive and quantitative analysis of *S. cerevisiae* lipidome in a single experiment (Ejsing et al., 2009; Guan et al., 2009; Klose et al., 2012). Major lipid classes include phosphatidic acid (PA), phosphatidylcholine (PC), phosphatidylethanolamine (PE), phosphatidylinositol (PI), phosphatidylserine (PS), diacylglycerol (DAG), their respective lyso-species, phosphatidylglycerol (PG) and cardiolipin (CL), triacylglycerols (TAG), diacylglycerol (DAG) and ergosterol (Erg). The fatty acid composition of these lipid classes is predominantly restricted to palmitic acid (C16:0), palmitoleic acid (C16:1) and oleic acid (C18:1), with negligible levels of shorter fatty acids. The sphingolipid (SP) category is comprised of inositolphosphorylceramide (IPC), mannosyl-inositol phosphorylceramide (MIPC) and mannosyl-di-(inositolphosphoryl) ceramide (M(IP)₂C) (Table 5-1).

Table 5-1 Categorisation of lipid species and classes into general lipid categories

Lipid species were annotated according to their molecular composition. Glycerophospholipid (GP) and glycerolipids (GL) species are annotated as: <sum of carbon atoms in the fatty acids (FA) >:<sum of double bonds in the FA> (e.g. PC 34:1). Sphingolipid (SP) species are annotated as: <sum of carbon atoms in the long chain base (LCB) and FA moiety>:<sum of double bonds in the LCB and FA moiety>:<sum of hydroxyl groups in the LCB and FA moiety> (e.g. MIPC 44:0:3).

GL	DAG	24:0	24:1	26:0	26:1	28:0	28:1	30:0	30:1	30:2
		32:1	32:2	34:1	34:2	36:1	36:2	38:0	38:1	
	TAG	42:0	42:1	42:2	42:3	44:0	44:1	44:2	44:3	46:0
		46:1	46:2	46:3	48:1	48:2	48:3	50:1	50:2	50:3
		52:0	52:1	52:2	52:3	54:0	54:1	54:2	54:3	56:1
		56:2	56:3	58:1	58:2	58:3	60:1	60:2	60:3	62:1
		62:2								
GP	CL	60:3	62:2	62:3	64:3	64:4	66:2	66:4	68:2	68:4
		70:4	72:2	72:4						
	PA	24:0	26:0	26:1	28:0	28:1	30:1	30:2	32:1	32:2
		34:1	34:2	36:1	36:2					
	PC	24:0	24:1	26:0	26:1	28:0	28:1	28:2	30:0	30:1
		30:2	32:1	32:2	34:1	34:2	36:1	36:2	38:2	
	PE	26:0	26:1	28:0	28:1	29:0	30:1	30:2	32:1	32:2
		34:1	34:2	36:1	36:2	38:2				
	PG	32:1	32:2	34:1	34:2					
	PI	24:0	25:0	26:0	26:1	28:0	28:1	28:2	30:0	30:1
		30:2	32:0	32:1	32:2	34:0	34:1	34:2	36:0	36:1
		36:2	38:1	38:2	40:1	42:1	44:1			
	PS	24:1	26:0	26:1	28:0	28:1	30:1	32:1	32:2	34:1
		34:2	36:0	36:1	36:2					
	lysoPA	12:0	14:0	14:1	16:0	16:1	17:0	18:0	18:1	20:0
		20:1								
	lysoPC	12:0	14:0	14:1	16:0	16:1	18:0	18:1		
	lysoPE	14:0	14:1	16:0	16:1	17:0	18:0	18:1	20:1	
	lysoPI	10:0	12:0	14:0	14:1	16:0	16:1	17:0	18:0	18:1
		20:0								
	lysoPS	14:0	14:1	16:0	16:1	17:0	18:1			
SP	Cer	34:0:2	34:0:3	34:0:4	36:0:2	36:0:4	38:0:2	38:0:3	38:0:5	42:0:2
		42:0:3	44:0:2	44:0:3	44:0:4	44:0:5	46:0:3	46:0:4	46:0:5	
	IPC	36:0:3	38:0:2	42:0:2	42:0:3	42:0:4	42:0:5	44:0:3	44:0:4	44:0:5
		46:0:2	46:0:3	46:0:4	46:0:5					
	LCB	18:0:2	18:0:3							
	LCBP	18:0:3	20:0:3							
ST	Erg									

Abbreviations used: Sphingolipids (SP) include Cer, ceramides; IPC, inositolphosphorylceramide; MIPC, mannosyl-inositol phosphorylceramide; M(IP)2C, mannosyl-di-(inositolphosphoryl) ceramide. Glycerophospholipids (GP) include PA, phosphatidic acid; PC, phosphatidylcholine; PE, phosphatidylethanolamine; PI,

phosphatidylinositol; PS, phosphatidylserine; CL, cardiolipin; the respective lysospecies lysoPA, lysoPC, lysoPE, lysoPI and lysoPS. Glycerolipids (GL) include DAG, diacylglycerol; TAG, triacylglycerol. Sterols (ST) include Erg, ergosterol.

Due to the natural ability of the eukaryotic lipidome to undergo changes in response to various growth conditions (Klose et al., 2012), the work described in this chapter aimed to understand the lipidomic factors involved in the increased A β ₄₂GFP fluorescence and partitioning of A β ₄₂GFP into the ER in the phospholipid mutants. This chapter describes a quantitative shotgun mass spectrometric approach undertaken to investigate if the increased A β ₄₂GFP fluorescence and partitioning of A β ₄₂GFP into the ER in the phospholipid mutants were caused by an accumulation or depletion of a specific lipid metabolite in the glycerophospholipid (GP), glycerolipid (GL), sterol (ST) and/or sphingolipid (SP) biosynthetic pathways. The term shotgun lipidomics is derived on the basis that polar and non-polar lipid extracts are directly injected into the MS for analysis without prior liquid chromatographic separation. This approach was also used to determine if the predominantly cytosolic-diffuse A β ₄₂GFP fluorescence in TCA cycle mutants and the structured localisation of fluorescent A β ₄₂GFP in a large globular compartment in wild-type cells over-expressing *DAK2* might result from altered lipid composition. The mass spectra acquisition of lipid profiles from these samples allowed quantification of a total of ~240 individual lipid species belonging to 21 lipid classes, which in turn belong to four major lipid categories: GP, GL, SP and ST. This categorisation of lipid species and classes into general lipid categories is outlined in Table 5-1.

5.2 Results – Global lipidome profiling of mutants affected in lipid metabolism

5.2.1 Global lipidome analysis of mutants exhibiting ER/ER-membrane A β ₄₂GFP localisation identifies pronounced effect of decreased phospholipids and increased M(IP)₂C levels

Since phospholipid metabolism appears to affect A β ₄₂GFP aggregation, it is important to determine which aspect(s) of phospholipid metabolism are involved. Major rearrangements of membrane lipid compositions and changes in the global lipidomic profile may be caused by altered growth conditions or mutations. Recently, it was demonstrated that minor changes in growth conditions, temperature, growth phase of cells and the utilisation of various carbon sources in the media have a profound

influence on the global lipidomic profile of *S. cerevisiae* cells (Klose et al., 2012; Natter et al., 2005). Therefore, these changes may affect lipid composition-dependent phenotypes. A quantitative shotgun mass spectrometric approach was therefore undertaken to investigate if the increased A β ₄₂GFP fluorescence and partitioning of A β ₄₂GFP into the ER in the phospholipid mutants were caused by an accumulation or depletion of a specific lipid metabolite in the glycerophospholipid (GP), glycerolipid (GL), sterol (ST) and/or sphingolipid (SP) biosynthetic pathways.

Expression of the A β ₄₂GFP fusion protein in wild-type BY4743 cells and the relevant mutants affected in phospholipid metabolism ($\Delta psd1$, $\Delta cho2$, $\Delta opi3$ and $\Delta ice2$) was induced by growing cells in galactose medium to exponential phase (OD₆₀₀ 1.5). Analyses of the global lipid composition from whole cell lipid extracts were determined using quantitative shotgun mass spectrometry based on the methods previously described by Ejlsing et al., (2009), Surma et al., (2011) and Klose et al., (2012) (Section 2.12.1). Cells were harvested from the exponential phase culture, washed in MilliQ water and frozen at -80°C for lipid extraction. In order to determine the influence of lipid composition on A β ₄₂GFP aggregation, it was important to ensure other factors such as manual handling of the cells during lipid extraction and data acquisition by mass spectrometry were not a source of variations of the yeast lipidome. As such, for each sample, the data presented are the mean of triplicate measurements from a single experiment.

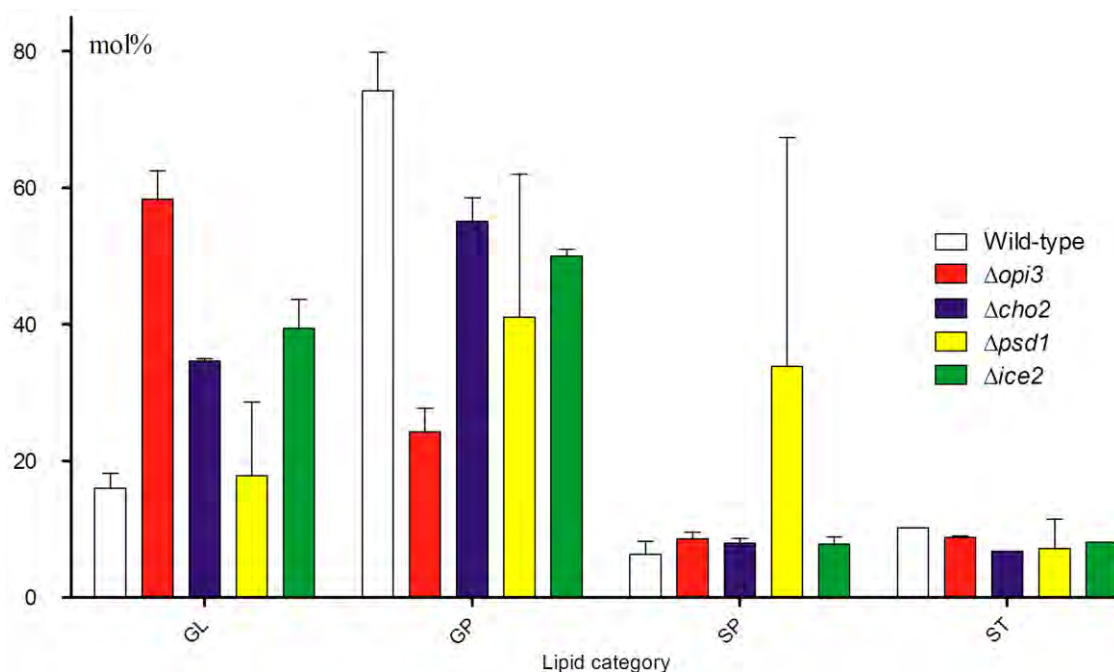


Figure 5-1 General lipid categories of wild-type, Δcho2 , Δopi3 , Δpsd1 and Δice2 cells expressing $\text{A}\beta_{42}\text{GFP}$

Quantitative representation of four major lipid categories in wild-type, Δcho2 , Δopi3 , Δpsd1 and Δice2 cells (as indicated). Each lipid category shows the sum of all the lipid classes belonging to that particular category. Data presented are the mean of triplicate measurements from three independent experiments. Error bars indicate standard deviation of these three MS acquisitions.

Analysis of the general lipid categories indicated that overall sterol levels were similar in all five strains (wild-type, Δcho2 , Δopi3 , Δpsd1 and Δice2) (Figure 5-2). However, total glycerophospholipid levels were significantly lower in all strains displaying the ER/ER-membrane $\text{A}\beta_{42}\text{GFP}$ localisation compared to wild-type cells ($p < 0.05$). Interestingly, Δcho2 , Δopi3 and Δice2 cells, which exhibited the most significant decrease in total glycerophospholipid levels also showed the most significant increase in total glycerolipid levels ($p < 0.0001$). This corroborates previous reports that TAG accumulates in Δcho2 and Δopi3 cells. Total sphingolipid levels were also similar in the four strains, except Δpsd1 (due to larger error bar), displaying the ER/ER-membrane $\text{A}\beta_{42}\text{GFP}$ localisation compared to wild-type cells. To gain further insight into the global lipidome in these mutants affected in phospholipid metabolism, the lipid classes belonging to the glycerolipid, glycerophospholipid and sphingolipid categories were analysed (Figure 5-2).

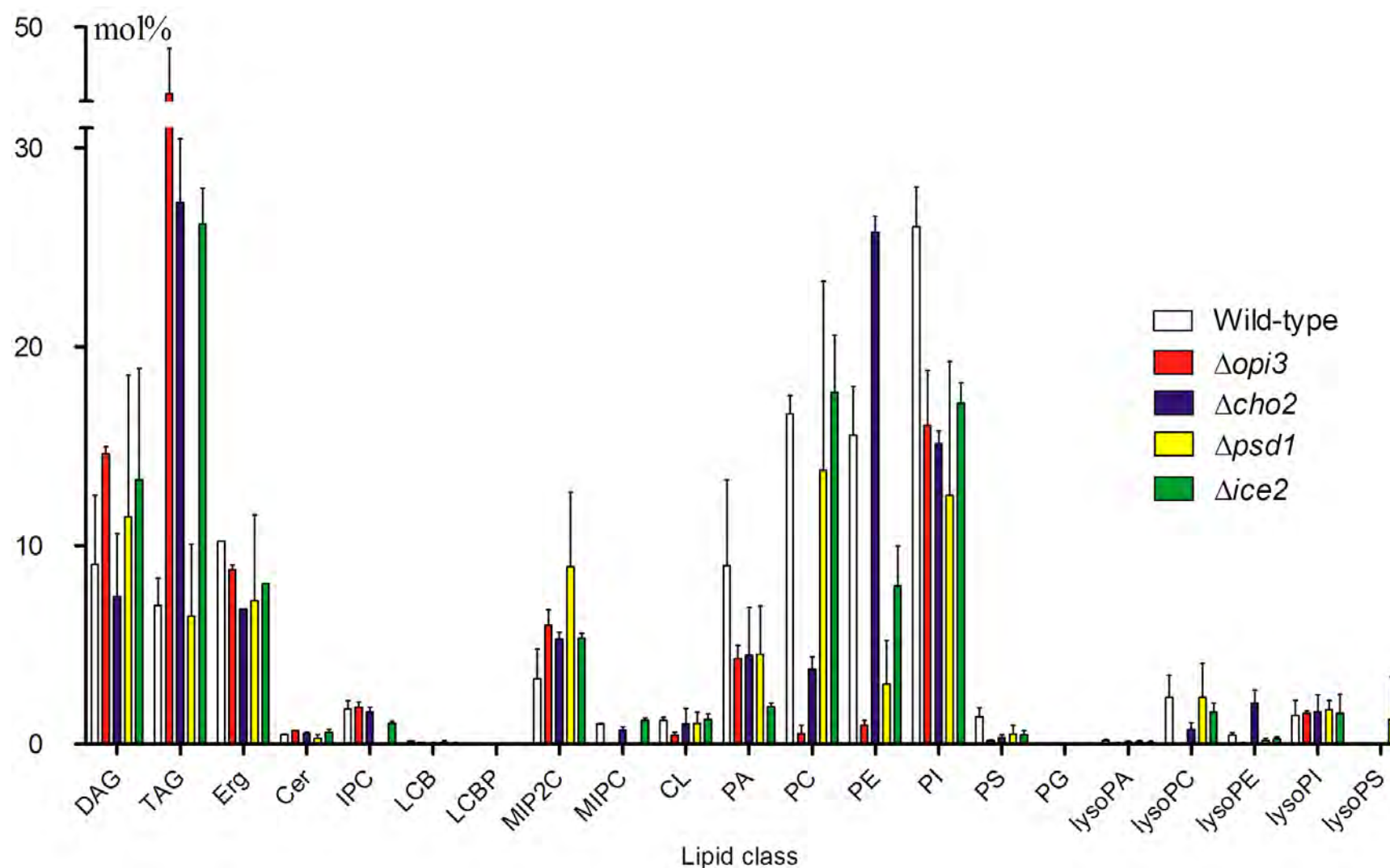


Figure 5-2 Global lipidomic profile of wild-type, Δopi3 , Δcho2 , Δpsd1 and Δice2 strains expressing $\text{A}\beta_{42}\text{GFP}$

Quantitative global lipid class composition in wild-type, Δcho2 , Δopi3 , Δpsd1 and Δice2 cells (as indicated). Data presented are the mean of triplicate measurements from three independent experiments. Error bars indicate standard deviation of these three MS acquisitions.

The quantification of the lipid classes in these five strains led to three important observations (discussed below). First, the expected major lipid changes based on the gene deletion in the cells were observed. Secondly, in the strains exhibiting the ER/ER-membrane A β_{42} GFP localisation there was a pronounced decrease in PA, PI, PS, PE (except in $\Delta cho2$ cells) and PC (except in $\Delta ice2$ cells) levels compared to wild-type cells. Finally, increased levels of M(IP) $_2$ C were observed in these mutants compared to wild-type cells.

This study provides the first lipidomic analysis of *S. cerevisiae* cells grown in galactose media (Figure 5-2). As previously reported for $\Delta opi3$ and $\Delta cho2$ cells grown in glucose media (Summers et al., 1988; McGraw and Henry, 1989), both strains grown expressing A β_{42} GFP in galactose media showed significantly reduced levels of PC ($p < 0.0001$) and increased levels of TAG ($p < 0.0006$) compared to wild-type cells. Interestingly, while PE was found to accumulate in $\Delta cho2$ cells (~26 mol%), its level was almost depleted in $\Delta opi3$ cells (~1 mol%), even lower than that of $\Delta psd1$ cells (~3 mol%). This is in contrast to previous studies where increased accumulation of PE in $\Delta opi3$ cells was observed when they were grown in glucose media (Summers et al., 1988; McGraw and Henry, 1989). The above data appear to also conflict with previous findings by Kodaki and Yamashita (1987) who demonstrated that $\Delta opi3$ cells grown in glucose medium exhibit ~2-fold increase in PE. A general trend of significantly low levels of PS compared to wild-type cells was observed in $\Delta opi3$, $\Delta cho2$ and $\Delta ice2$ strains ($p < 0.03$) and to a lesser extent in $\Delta psd1$ cells. Interestingly, these data differ from the previously reported 3% increase in PS levels in $\Delta psd1$ cells compared to wild-type cells grown in YPD media (Nebauer et al., 2007). These differences in PE and PS levels may be possibly due to difference in the strain backgrounds, growth of cells in galactose media and/or the expression of A β_{42} GFP. While the effect of A β_{42} GFP expression on the lipidome of cells was not analysed in this study, the possible contribution of strain background, utilisation of various carbon sources and the growth phase of cells in influencing the lipidome is further supported by the demonstration that lipidomes of cells grown in glucose media cluster separately using principal component analysis compared to the lipidomes of raffinose- and glycerol-grown cells (Klose et al., 2012).

A significant reduction in PA, PI, PS, PE (except in $\Delta cho2$ cells) and PC (except in $\Delta ice2$ cells) was observed in all mutant strains exhibiting an increased level of A β_{42} GFP-associated fluorescence (Figure 5-2). PA accounted for ~9 mol% in wild-type cells but was generally reduced to only ~4 mol% in $\Delta psd1$, $\Delta cho2$ and $\Delta opi3$ strains and significantly reduced to ~2% in the $\Delta ice2$ strain ($p < 0.008$). PC was present at ~17 mol% in wild-type cells but was significantly reduced only in both $\Delta cho2$ (~4 mol%; $p < 0.0001$) and $\Delta opi3$ (~0.5 mol%; $p < 0.0001$) mutants but comparable to both $\Delta psd1$ and $\Delta ice2$ strains. PI (~26 mol% in wild-type cells) was significantly reduced in all four strains $\Delta psd1$ (~12 mol%; $p < 0.02$), $\Delta cho2$ (~15 mol%; $p < 0.0009$), $\Delta opi3$ (~16 mol%; $p < 0.007$) and $\Delta ice2$ (~17 mol%; $p < 0.002$) mutants respectively. PE accounted for ~15 mol% in wild-type cells but was significantly reduced in $\Delta psd1$ (~3 mol%; $p < 0.002$), $\Delta opi3$ (~1 mol%; $p < 0.0005$) and $\Delta ice2$ (~8 mol%; $p < 0.01$) mutants however, significantly increased in $\Delta cho2$ (~26 mol%; $p < 0.002$) strain. Finally, PS was present at ~1.4 mol% in wild-type cells but was significantly reduced in all four strains $\Delta psd1$ (~0.5 mol%; $p < 0.07$), $\Delta cho2$ (~0.3 mol%; $p < 0.01$), $\Delta opi3$ (~0.1 mol%; $p < 0.009$) and $\Delta ice2$ (~0.5 mol%; $p < 0.03$) mutants respectively. Since the synthesis of PA, PC, PI and PS occur in the ER (Carman and Han, 2011; Daum et al., 1998), a depletion of these lipid species may influence A β_{42} GFP interaction with, and/or partitioning in to the ER membrane reducing A β_{42} aggregation sufficiently for the GFP moiety to fold correctly.

While overall phospholipid levels, including PA, PC, PE, PI, and PS, were reduced in mutants exhibiting the ER/ER-membrane A β_{42} GFP localisation there was a pronounced effect of increased M(IP) $_2$ C levels in these strains compared to wild-type cells. M(IP) $_2$ C (~3 mol% in wild-type cells) was significantly increased in all four strains $\Delta psd1$ (~9 mol%; $p < 0.06$), $\Delta cho2$ (~5 mol%; $p < 0.01$), $\Delta opi3$ (~6 mol%; $p < 0.01$) and $\Delta ice2$ (~5 mol%; $p < 0.01$) mutants respectively (Figure 5-2). Interestingly, increased M(IP) $_2$ C levels showed a noticeable trend: a significant reduction in PI in all mutants exhibiting the ER/ER-membrane A β_{42} GFP localisation led to increased levels of M(IP) $_2$ C in those strains.

5.2.2 Genetic interaction network supported by a global lipidomic approach provide hints to another possible function of Ice2p

The gene *ICE2* encodes an integral ER membrane protein with type III transmembrane domains. In *S. cerevisiae* cells, two types of ER are present; namely perinuclear ER and the cortical ER (Preuss et al., 1991; Rose et al., 1989). While the perinuclear ER is a polygonal network of membranous tubular structures (Palade, 1956) connected to the outer nuclear envelope, the cortical ER forms a membranous tubular network along the periphery of the cells, juxtaposed to the plasma membrane (Prinz et al., 2000). Ice2p, which is localised to both the cortical and perinuclear ER, plays an important role in cortical ER inheritance (Estrada de Martin et al., 2005; Huh et al., 2003). In this study, $\Delta ice2$ cells expressing A β_{42} GFP exhibited a strong level of A β_{42} GFP-associated fluorescence in a perinuclear ER/ER-membrane localisation, similar to the localisation observed for A β_{42} GFP in the mutants affected in phospholipid metabolism.

In *S. cerevisiae*, the deletion of a single gene may not always present a phenotype or a lethal phenotype. Since a vast majority of predicted ORFs/genes (>80%) are not essential for viability of *S. cerevisiae* cells, the phenotypes exhibited through genetic manipulation are usually buffered by the genome (Costanzo et al., 2010; Tong et al., 2001). Therefore to assist in determining gene function, systematic construction of double mutants, termed synthetic genetic array (SGA) analysis was developed by Tong and colleagues (2001), in which a query mutation or gene deletion was crossed to an array of ~4700 deletion mutants (Tong et al., 2001; Tong et al., 2004). The resulting double-mutants that are inviable identify functional interactions between genes and these interactions are known as negative genetic interactions or synthetic lethality. Synthetic sick interactions refer to a lower fitness of the double-mutant compared to the expected combined effect of the single mutant growth phenotypes; while positive genetic interactions usually refer to greater fitness of the double mutant than expected. These genetic interactions occur between pairs of genes that operate in functionally related pathways, and provide deeper understanding of underlying biological/cellular processes (Costanzo et al., 2010; Tong et al., 2001; Tong et al., 2004). To understand the function of *ICE2*, the negative genetic interaction network of *ICE2* was generated and analysed using a web-based database of quantitative genetic interaction networks called

Data Repository of Yeast Genetic Function (DRYGIN) (<http://drygin.ccbr.utoronto.ca>) (Baryshnikova et al., 2010; Koh et al., 2010). The latest version of DRYGIN contains more than 5.4 million measurements of genetic interactions involving approximately 4500 genes. Based on default parameters set by the DRYGIN database showed that both reproducible and functionally informative interactions are determined at $p < 0.05$ which indicate the genetic interaction score confidence. Therefore only these genetic interactions were considered for further analysis.

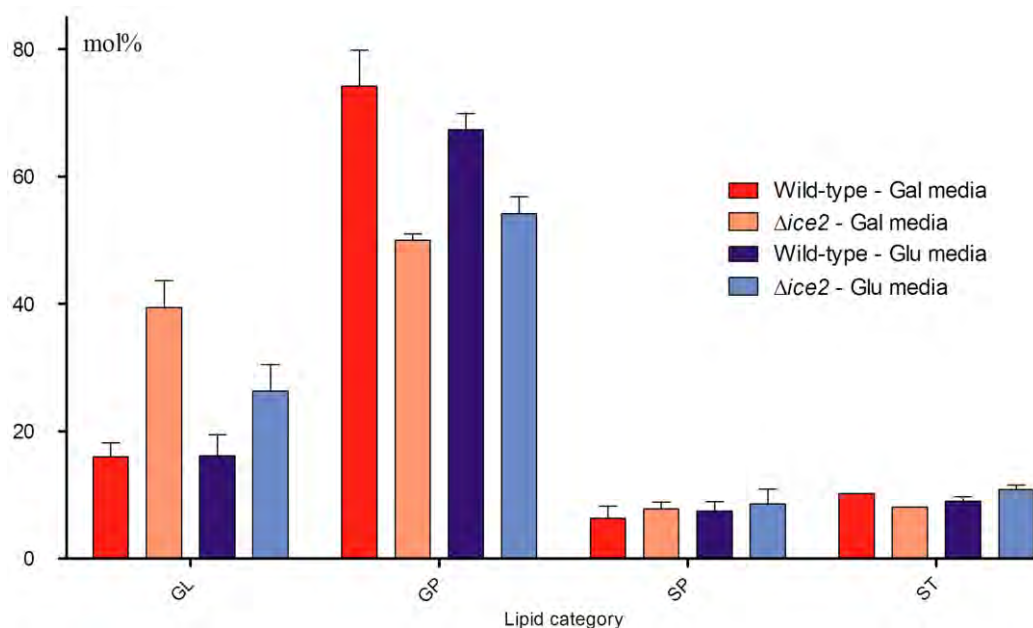
Analysis of the negative genetic interaction network of *ICE2* identified genes involved in cellular processes, such as stabilisation of actin cables and filaments, which direct polarised cell growth, inheritance and distribution of organelles, homolog segregation during meiosis I and nuclear migration and spindle partitioning during mitotic anaphase B. Interestingly, while Ice2p has not been previously associated with a function in lipid/phospholipid metabolism, detailed analysis of negative interaction network data highlight the strong association to genes involved in lipid metabolism and displayed significant genetic interactions with *ICE2* (Table 5-2). These include genes involved in phospholipid metabolism *INO2*, *INO4*, *PSD1*, *PSD2*, *CHO2*, *OPI3*, and *SCS2*; glycerolipid metabolism *PAH1* and *DGK1*; sphingolipid metabolism *SCS7* and *ORM2*; and sterol metabolism *ERG6*. Taken together with results from the global lipidomic analysis of strains exhibiting the ER/ER-membrane A β ₄₂GFP localisation (Figure 5-2) these data strongly suggest that Ice2p may play a role in lipid metabolism in *S. cerevisiae* cells.

To determine if the lipid composition in $\Delta ice2$ cells was altered in any of the 21 lipid classes, global lipidome analysis using a quantitative shotgun mass spectrometric approach was undertaken. Wild-type BY4743 and $\Delta ice2$ cells not containing or expressing any of the A β GFP fusion proteins were grown in synthetic complete glucose media to exponential phase (OD₆₀₀ 1.5). Cells were harvested from the exponential phase culture, washed in MilliQ water and frozen at -80°C for lipid extraction. Since mass spectrometric data was acquired for both wild-type and $\Delta ice2$ cells expressing A β ₄₂GFP in galactose media, these data were also included in this analysis.

Table 5-2 Negative genetic interaction network of *ICE2* and genes involved in lipid metabolism, based on significant interactions (DRYGIN database)

The p – values indicate the genetic interaction score confidence.

Common names		p - value
Query gene	Array gene	
<i>ICE2</i>	<i>DGK1</i>	2.111E-82
<i>DGK1</i>	<i>ICE2</i>	2.111E-82
<i>SCS2</i>	<i>ICE2</i>	8.237E-94
<i>ICE2</i>	<i>SCS2</i>	8.237E-94
<i>INO2</i>	<i>ICE2</i>	8.266E-58
<i>ICE2</i>	<i>INO2</i>	8.266E-58
<i>SCS3</i>	<i>ICE2</i>	3.847E-75
<i>ICE2</i>	<i>SCS3</i>	3.847E-75
<i>PSD2</i>	<i>ICE2</i>	1.635E-20
<i>ICE2</i>	<i>PSD2</i>	1.635E-20
<i>ORM2</i>	<i>ICE2</i>	0.00001117
<i>INO4</i>	<i>ICE2</i>	3.601E-07
<i>CHO2</i>	<i>ICE2</i>	0.000215
<i>ICE2</i>	<i>CHO2</i>	0.000215
<i>ICE2</i>	<i>OPI3</i>	3.41E-11
<i>OPI3</i>	<i>ICE2</i>	3.41E-11
<i>PSD1</i>	<i>ICE2</i>	0.0004931
<i>ERG6</i>	<i>ICE2</i>	0.0000555
<i>PAH1</i>	<i>ICE2</i>	0.01134
<i>ICE2</i>	<i>SCS7</i>	0.02285
<i>SCS7</i>	<i>ICE2</i>	0.02285

**Figure 5-3 General lipid categories of wild-type and $\Delta ice2$ cells grown in either glucose (Glu) or galactose (Gal) media**

Quantitative representation of four major lipid categories in wild-type and $\Delta ice2$ cells grown in either glucose (Glu) or galactose (Gal) media (as indicated). Each lipid category shows the sum

of all the lipid classes belonging to that particular category. Data presented are the mean of triplicate measurements from three independent experiments. Error bars indicate standard deviation of these three MS acquisitions.

This study provides the first global lipidomic analysis of $\Delta ice2$ cells. Analysis of the general lipid categories indicated that overall sterol and sphingolipid levels were more or less comparable in wild-type and $\Delta ice2$ cells grown in glucose or galactose media (Figure 5-3). However, total glycerophospholipid levels were significantly lower in $\Delta ice2$ cells grown in both media compared to wild-type cells ($p < 0.003$). Similar to the earlier observations made in galactose media, $\Delta ice2$ cells also showed a significant increase in total glycerolipid levels ($p < 0.02$) when grown in glucose. To gain further insight into the global lipidome in $\Delta ice2$ cells, the lipid classes belonging to the four major lipid categories were analysed (Figure 5-4). The quantification and analysis of the lipid classes in wild-type and $\Delta ice2$ cells grown in either glucose or galactose led to two major observations. First, $\Delta ice2$ cells showed a pronounced effect of decreased PA ($p < 0.04$) and PE ($p < 0.01$) levels in both glucose and galactose media compared to wild-type cells. Interestingly, significant decreases in PI ($p < 0.002$) and PS ($p < 0.03$) levels were also observed in $\Delta ice2$ cells grown in galactose media but not those grown in glucose media. Finally, general trend of increased DAG and TAG levels were observed in $\Delta ice2$ cells grown in both glucose and galactose media, compared to wild-type cells. Comparison of the lipidomes between $\Delta ice2$, $\Delta cho2$ and $\Delta opi3$ cells indicated that, apart from the PC depletion phenotype, $\Delta ice2$ cells show similar a trend in lipid classes as those observed in the phospholipid mutants.

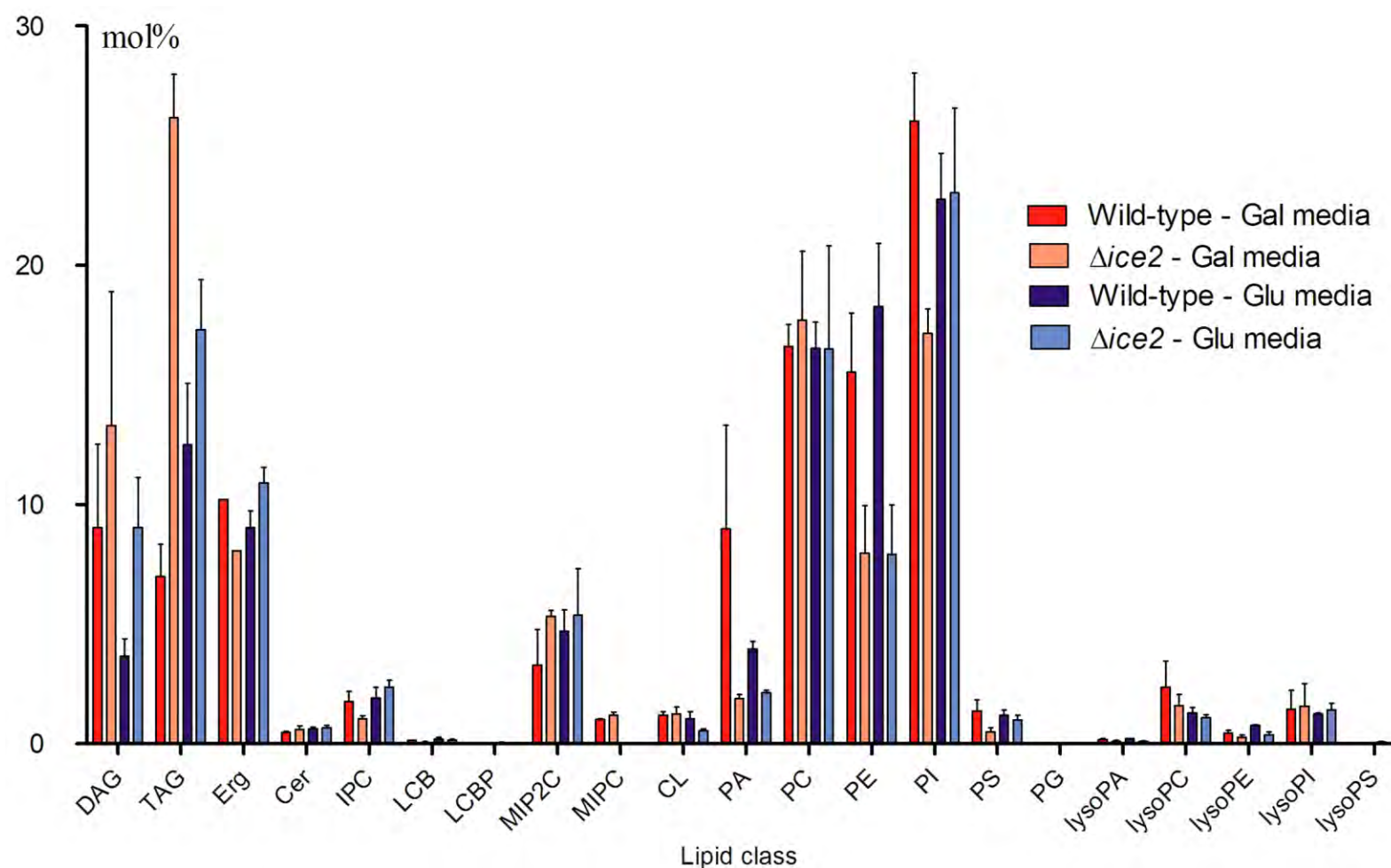


Figure 5-4 Global lipidomic profile of wild-type and $\Delta ice2$ cells grown in either glucose (Glu) or galactose (Gal) media.

Quantitative global lipid class composition in wild-type and $\Delta ice2$ cells grown in either glucose (Glu) or galactose (Gal) media (as indicated). Data presented are the mean of triplicate measurements from three independent experiments. Error bars indicate standard deviation of these three MS acquisitions.

5.2.3 Understanding the link between mitochondrial dysfunction and A β ₄₂GFP aggregation – Investigation of A β ₄₂GFP localisation in mitochondrial mutants

Of the 110 mutants identified in the genome-wide screen, 39.1% (43 mutants from 110) were annotated in the *Saccharomyces* Genome Database as exhibiting disrupted mitochondrial respiratory function. The significant over-representation of mutants involved in processes such as the TCA cycle, oxidative phosphorylation, mitochondrial protein translation and protein import indicates that normal mitochondrial function is closely linked to the folding and aggregation of the A β ₄₂GFP fusion protein in yeast. Further analysis of process ontology also identified acetyl-CoA catabolism and enzymes of the tricarboxylic acid (TCA) cycle, including isocitrate dehydrogenase (Idp1p), alpha-ketoglutarate dehydrogenase (Kgd2p), succinate dehydrogenase (Sdh4p), aconitase (Aco1p) and fumarase (Fum1p) to be significantly over-represented ($p = 7.71 \times 10^{-22}$). Fluorescent A β ₄₂GFP in TCA cycle mutants was localised as cytosolic-diffuse or cytosolic-diffuse with single to multiple small puncta (Figure 5-5), which did not appear to occur in a distinct structure in the cell. Since the mitochondrial mutants that affected A β ₄₂GFP-associated fluorescence were mainly defective in the TCA cycle, disruption of respiratory energy production may account for the altered A β ₄₂GFP-associated fluorescence phenotype observed in these mitochondrial respiration-deficient strains.

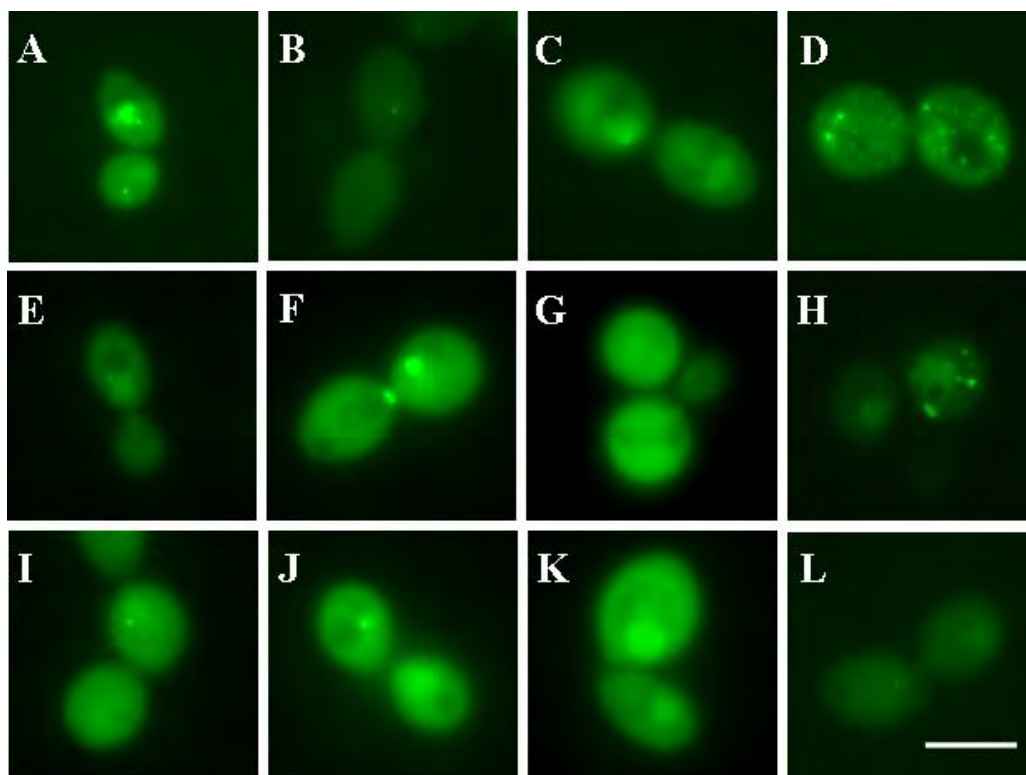


Figure 5-5 Fluorescent images of mutants affected in mitochondrial function expressing A β_{42} GFP.

Mitochondrial mutants expressing A β_{42} GFP were induced in galactose medium (SCgal-URA) and A β_{42} GFP-associated fluorescence analysed at 12 h post induction. TCA cycle mutants A) $\Delta rim1$, B) $\Delta pye2$, C) $\Delta cit3$, D) $\Delta aco1$, E) $\Delta idh2$, F) $\Delta idp1$, G) $\Delta kgd2$, H) $\Delta lsc1$, I) $\Delta sdh2$, J) $\Delta sdh4$, K) $\Delta fum1$ and L) $\Delta mdh1$ and were observed to predominantly exhibit cytosolic-diffuse A β_{42} GFP-associated fluorescence, with some mutants exhibiting fluorescent puncta. Scale bars indicate 5 μ m.

5.2.4 Disruption of mitochondrial DNA does not affect A β_{42} GFP expression

The mitochondrial genome (mtDNA) of *S. cerevisiae* encodes eight proteins that are all essential for oxidative phosphorylation (Tzagoloff and Dieckmann, 1990) and deletion of mtDNA leads to respiratory incompetence due to disruption of the mitochondrial electron transport chain and oxidative phosphorylation of ATP functions. *S. cerevisiae* is a facultative aerobe, and respiratory-incompetent cells can grow on carbon sources such as glucose or galactose. To examine whether the disruption of respiratory function *per se* affected A β_{42} GFP fluorescence, rho-zero (ρ^0) cells lacking mtDNA derived from wild-type BY4743 *S. cerevisiae* were generated and grown in galactose (induction) media and the effect on A β_{42} GFP analysed. The absence of mtDNA was confirmed by DAPI staining (data not shown). Respiratory incompetent ρ^0 cells yielded only a similar trace level of A β_{42} GFP fluorescence ($\sim 5\%$), comparable to wild-type grande (ρ^+) cells, indicating loss of respiratory function *per se* does not

affect $A\beta_{42}$ GFP-associated fluorescence. Therefore, the increased $A\beta_{42}$ GFP fluorescence in the TCA cycle mutants was not due to a general loss of respiration energy production but possibly via another mechanism.

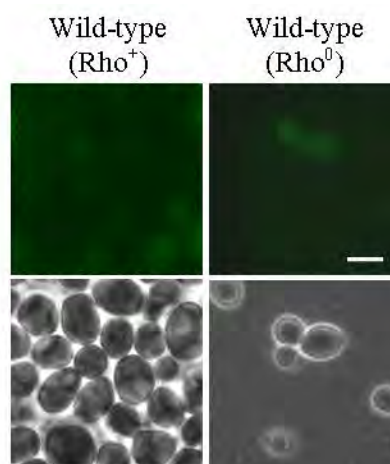


Figure 5-6 Fluorescence microscopic images of Rho^0 and wild-type grande cells expressing $A\beta_{42}$ GFP.

Respiratory incompetent (rho^0) and wild-type grande (rho^+) cells expressing $A\beta_{42}$ GFP were induced in galactose medium (SCgal-URA) and $A\beta_{42}$ GFP-associated fluorescence analysed at 12 h post induction. Rho^0 cells yielded similar trace level of $A\beta_{42}$ GFP fluorescence ($\sim 5\%$), comparable to wild-type cells. Scale bars indicate 5 μm .

5.2.5 Global lipidome analysis of TCA cycle mutants exhibiting altered $A\beta_{42}$ GFP fluorescence

Since affecting the TCA cycle also affected $A\beta_{42}$ GFP-associated fluorescence, accumulation of a specific metabolite of the TCA cycle or upstream of it may be involved since the mutants deleted for aconitase and citrate synthase were affected in $A\beta_{42}$ GFP aggregation. Disruption of the TCA cycle may affect acetyl-CoA metabolism and possibly affect processes including lipid metabolism and/or homeostasis. To determine if the predominantly cytosolic-diffuse $A\beta_{42}$ GFP fluorescence in TCA cycle mutants might result from altered lipid composition, a quantitative shotgun mass spectrometric approach was undertaken to provide insight into the global lipidomic profile of the relevant mutants affected in the TCA cycle. Since wild-type and the respiratory-deficient rho^0 cells did not affect $A\beta_{42}$ GFP aggregation, these strains were also included in this analysis to allow their lipidomes to be compared to that of the TCA cycle mutants.

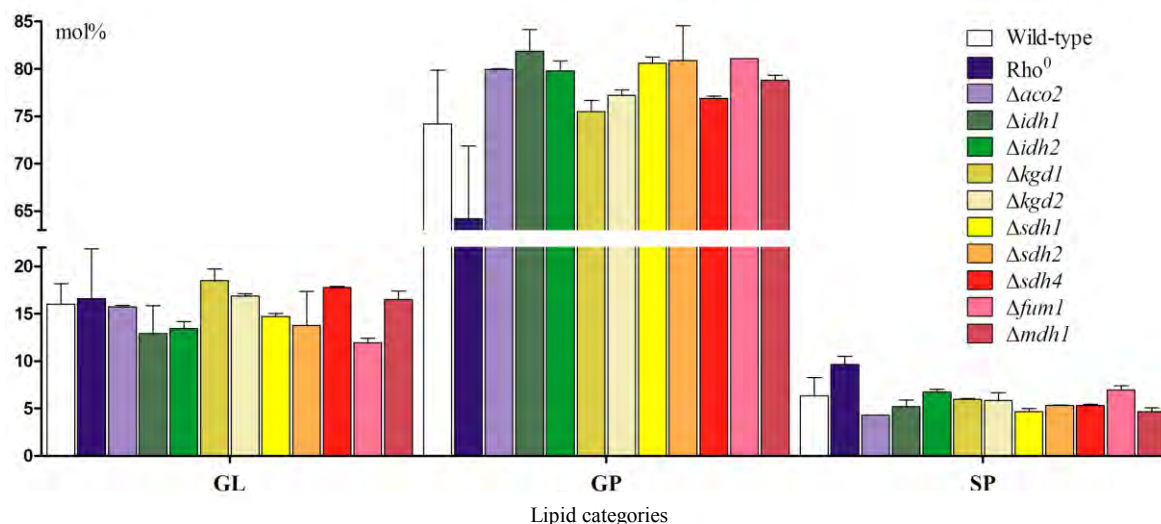


Figure 5-7 General lipid categories in wild-type, rho⁰ cells and selected TCA cycle mutants expressing Aβ₄₂GFP

Quantitative representation of the four major lipid categories in wild-type, rho⁰, Δaco2, Δidh1, Δidh2, Δkgd1, Δkgd2, Δsdh1, Δsdh2, Δsdh4, Δfum1 and Δmdh1 cells (as indicated). Each lipid category shows the sum of all the lipid classes belonging to that particular category. Data presented are the mean of triplicate measurements from three independent experiments. Error bars indicate standard deviation of these three MS acquisitions.

This study provides the first global lipidomic analysis of TCA cycle mutants. Analysis of the general lipid categories, except sterols, indicated that overall glycerolipid levels were more or less comparable in wild-type cells, rho⁰ cells and in all ten TCA cycle mutants (Δaco2, Δidh1, Δidh2, Δkgd1, Δkgd2, Δsdh1, Δsdh2, Δsdh4, Δfum1 and Δmdh1) (Figure 5-7). However, variations within the TCA cycle mutants were observed; while Δidh2 and Δfum1 mutants exhibited the lowest levels of overall glycerolipid content, Δkgd1, Δsdh4 and Δmdh1 showed the highest. While no general trends were observed in the glycerophospholipid and sphingolipid categories; within the TCA cycle mutants, strains that exhibited lower levels of total GL, were found to have higher levels of GP and vice-versa, including Δidh2, Δfum1, Δkgd1, Δsdh4 and Δmdh1 strains. Rho⁰ cells show slightly lower total GP levels and higher total SP levels compared to wild-type cells. Overall SP levels were also comparable in wild-type cells and in all ten TCA cycle mutants.

Unlike the trends of reduced levels of GPs, including PA, PI, PS, PE and PC, and increased levels of TAG and M(IP)₂C observed in mutants affected in phospholipid metabolism, TCA cycle mutants did not exhibit a general trend across any of the 20 lipid categories. Instead, varying levels of lipid classes were observed within the

selected TCA cycle mutants (Figure 5-8). For example, reduced levels of DAG and TAG were found in $\Delta idh2$ and $\Delta fum1$ mutants while, increased levels of DAG were observed in $\Delta kgd1$, $\Delta sdh4$ and $\Delta mdh4$ mutants. Analysis of the sphingolipids indicated that while M(IP)₂C levels in $\Delta idh2$, $\Delta kgd1$, $\Delta kgd2$, and $\Delta fum1$ mutants were comparable to wild-type cells, all other TCA cycle mutants showed a ~2-fold reduction. Analysis of phospholipids indicated that all TCA cycle mutants except $\Delta kgd1$ have significantly increased levels of PE while $\Delta sdh2$ mutant also showed significantly high PC levels compared to wild-type cells. Analysis of the lipidome of ρ^0 cells indicated that TAG ($p = 0.001$) and IPC ($p = 0.004$) levels were significantly increased while CL ($p = 0.005$), PA ($p = 0.03$), PE ($p = 0.003$), PI ($p = 0.04$), and their corresponding lyso-species were significantly reduced in these strains compared to wild-type cells (Figure 5-8).

Since the lipidome of ρ^0 cells is significantly altered, an analysis comparing the lipidomes between ρ^0 cells, which do not give rise to increased A β_{42} GFP-associated fluorescence, and the relevant phospholipid mutants that exhibit the ER/ER-membrane A β_{42} GFP localisation was undertaken. Interestingly, ρ^0 cells exhibited a similar TAG accumulation phenotype, as well as trends involving reduced PA, PE and PI levels to a similar extent to that observed in the phospholipid mutants (Figure 5-9). However, the decrease of PC and PS levels in the phospholipid mutants was not observed in ρ^0 cells. Taken together, it can be surmised that the additional decrease of PC and PS levels in the phospholipid mutants may have given rise to the ER/ER-membrane A β_{42} GFP localisation. These data indicate that alterations to specific phospholipids may affect A β_{42} GFP localisation and aggregation in *S. cerevisiae*.

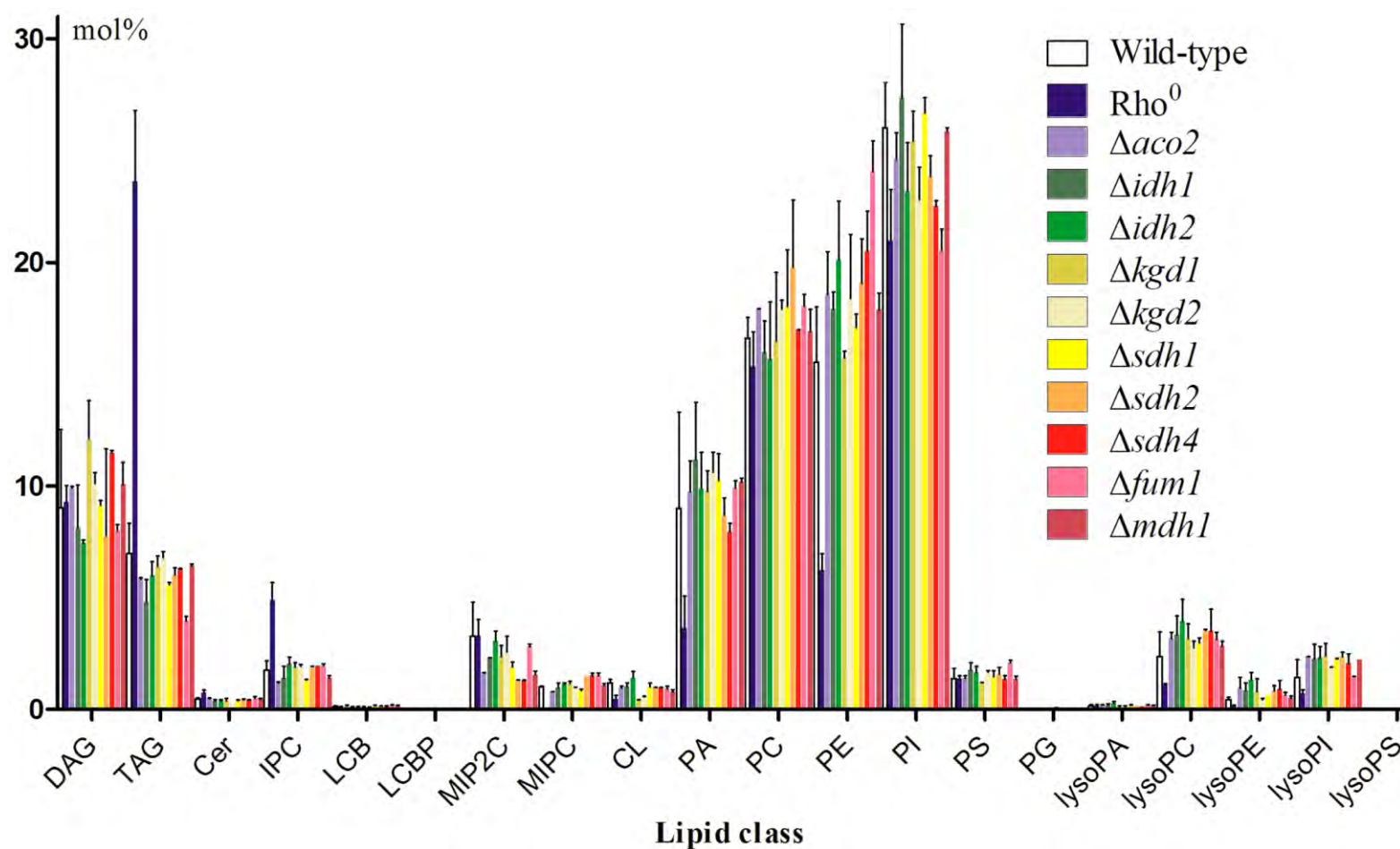


Figure 5-8 Global lipidomic profile of wild-type, ρ^0 and selected TCA cycle mutants expressing $A\beta_4$ GFP

Quantitative global lipid class composition in wild-type, ρ^0 , $\Delta aco2$, $\Delta idh1$, $\Delta idh2$, $\Delta kgd1$, $\Delta kgd2$, $\Delta sdh1$, $\Delta sdh2$, $\Delta sdh4$, $\Delta fum1$ and $\Delta mdh1$ cells (as indicated). Data presented are the mean of triplicate measurements from three independent experiments. Error bars indicate standard deviation of these three MS acquisitions.

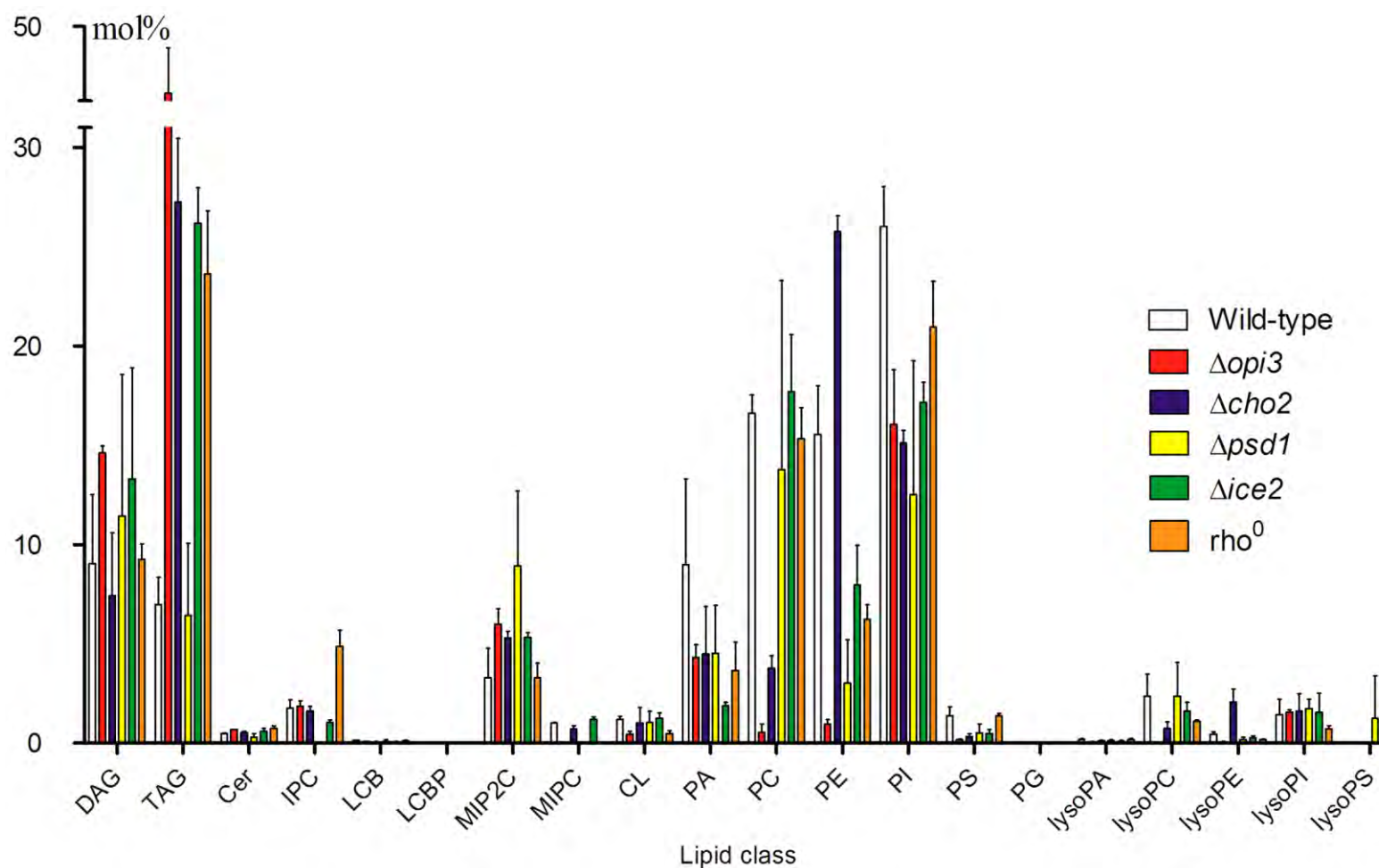


Figure 5-9 Global lipidomic profile of wild-type, Δopi3 , Δcho2 , Δpsd1 , Δice2 and rho^0 cells expressing $\text{A}\beta_{42}\text{GFP}$

Quantitative global lipid class composition in wild-type, Δopi3 , Δcho2 , Δpsd1 , Δice2 and rho^0 cells (as indicated). Data presented are the mean of triplicate measurements from three independent experiments. Error bars indicate standard deviation of these three MS acquisitions.

While TCA cycle mutants gave rise to increased A β ₄₂GFP-associated fluorescence predominantly as cytosolic-diffuse or cytosolic-diffuse with single to multiple small puncta, respiratory incompetent rho⁰ cells yielded similar trace level of A β ₄₂GFP fluorescence (~5%), comparable to wild-type grande (rho⁺) cells indicating loss of respiratory function *per se* does not affect A β ₄₂GFP-associated fluorescence. Interestingly, through detailed comparisons between the lipidomes of wild-type, rho⁰ cells and TCA cycle mutants further indicated altered lipid metabolism and/or homeostasis did not A β ₄₂GFP-associated fluorescence. Although at present, it is unclear how loss of nuclear-encoded mitochondrial proteins affect A β ₄₂GFP-associated fluorescence; one possible explanation may be that a metabolite in, or derived from, the TCA cycle may affect A β ₄₂GFP aggregation. TCA cycle intermediates, oxaloacetate, α -ketoglutarate, citrate and succinyl-CoA are precursors for several anabolic processes, such as biosynthesis of porphyrins (for heme production), amino acids, purines, pyrimidines, fatty acids, sterols, and neurotransmitters (in neuronal cells). Apart from porphyrins, all other metabolites provide the TCA cycle with the intermediates when turned over by the metabolic activity of the cell. Porphyrins and heme may be possible candidate metabolites to be analysed since its metabolism has been previously found to be altered in AD (Atamna, 2006; Atamna and Boyle, 2006; Atamna and Frey, 2004; Atamna and Frey, 2007; Chuang et al., 2012). It is tempting to speculate that disruption of the TCA cycle would affect porphyrins and heme metabolism and alter intracellular levels of these metabolites. However, a more detailed analysis of the mechanism(s) mediating the changes in A β ₄₂GFP fluorescence in the TCA mutants is required, and a metabolomics approach to identify changes in mitochondrial metabolites may be informative. A good starting point can be the intermediate metabolites accumulating in and upstream of the TCA cycle.

5.2.6 A ‘reverse-genetics’ approach identifies metabolite(s) that may influence increased A β ₄₂GFP fluorescence in mutants affected in mitochondrial function

Reduction of NAD⁺ to NADH occurs in dissimilatory as well as in assimilatory reactions in *S. cerevisiae*. Only catalytic amounts of these pyridine nucleotides are present and intracellular concentrations of NAD⁺/NADH of 1 mM have been reported (de Koning and van Dam, 1992; Richard et al., 1993). As such, the reduction of NAD⁺

has to be matched by a continuous reoxidation of NADH. To allow this balance, multiple redox couples exist in cells. While NADH serves as a source of electrons and is required in reductive cellular reactions, NAD^+ serves as a sink for electrons and is required in oxidative cellular reactions (Bakker et al., 2001; Schafer and Buettner, 2001). One of the major mechanisms that allows for the reoxidation of NADH is the production of glycerol via glycerol-3-phosphate dehydrogenase which detoxifies dihydroxyacetone phosphate by utilising NADH (Compagno et al., 1996; Larsson et al., 1998). The glycerol-3-phosphate shuttle is an indirect mechanism to oxidise cytosolic NADH and transfer the electrons to the respiratory chain (Bakker et al., 2001). There are two major processes of glycerol formation; i) reduction of dihydroxyacetone phosphate to glycerol-3-phosphate via NADH-dependent glycerol-3-phosphate dehydrogenase Gpd1p and Gpd2p. This is followed by hydrolysis of the phosphate group to produce glycerol Gpp1p and Gpp2p. ii) Direct conversion of dihydroxyacetone to glycerol via Ypr1p and Gcy1p (Figure 5-10) (Albertyn et al., 1994b; Ansell et al., 1997; Eriksson et al., 1995; Norbeck et al., 1996; Wang et al., 1994). Upon disruption to mitochondrial electron transport, *S. cerevisiae* cells use glycerol production to serve as a redox sink by utilising glycerol-3-phosphate dehydrogenases Gpd1p and Gpd2p to maintain intracellular concentrations and availability of NAD^+ (Bakker et al., 2001). However, unlike the TCA cycle mutants, rho^0 cells and mutants affected in mitochondrial electron transport chain function, do not affect $\text{A}\beta_{42}\text{GFP}$ fluorescence. Three reactions in the TCA cycle utilise NAD^+ as a cofactor; they are, oxidation of isocitrate to α -ketoglutarate by Idh1p and Idh2p, and the subsequent oxidative decarboxylation of α -ketoglutarate to succinyl-CoA by Kgd1p, Kgd2p and Lpd1p, and finally the conversion of malate to oxaloacetate by Mdh1p. Therefore upon disruption to the TCA cycle, cells may have increased levels of NAD^+ and thereby reduced flux into glycerol production.

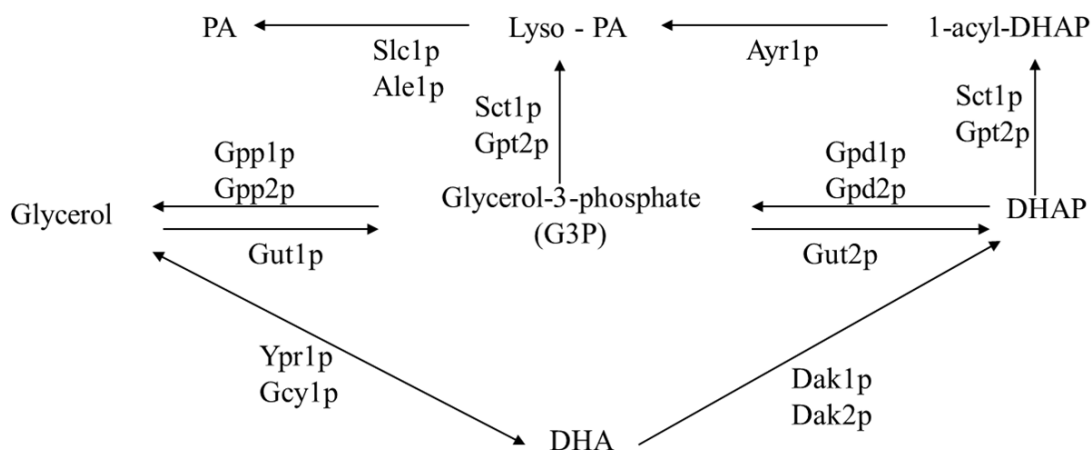


Figure 5-10 Overview of the pathways for dihydroxyacetone and glycerol metabolism in *S. cerevisiae*

The pathways shown for the synthesis of glycerol, DHA, PA and the relevant steps discussed in the text. As illustrated, two major processes of glycerol formation; i) reduction of dihydroxyacetone phosphate to glycerol-3-phosphate via NADH-dependent glycerol-3-phosphate dehydrogenase Gpd1p and Gpd2p. This is followed by hydrolysis of the phosphate group to produce glycerol Gpp1p and Gpp2p. ii) Direct conversion of dihydroxyacetone to glycerol via Ypr1p and Gcylp. Abbreviations used: DHA, dihydroxyacetone; DHAP, dihydroxyacetone phosphate; 1-acyl-DHAP, 1-acyl-dihydroxyacetone phosphate; G3P, glycerol-3-phosphate; lyso-PA, lyso-phosphatidic acid; PA, phosphatidic acid.

In the previous chapter (Section 4.2.8), a ‘reverse-genetics’ approach using gene over-expression analysis was undertaken to investigate if the increased A β ₄₂GFP fluorescence in the phospholipid mutants were caused by an accumulation of a specific phospholipid intermediate. Through this over-expression screen, two genes were identified that when over-expressed appeared to exhibit altered A β ₄₂GFP fluorescence relative to wild-type cells. Strains over-expressing *CDS1* (discussed in Section 4.2.9) or *DAK2* were subsequently rescreened for confirmation of altered levels fluorescence and the proportion of fluorescent cells. *DAK2* encodes dihydroxyacetone kinase, which is responsible for detoxification of dihydroxyacetone (Figure 5-10) (Molin et al., 2003; Norbeck and Blomberg, 1997). Wild-type cells over-expressing *DAK2* gave rise to more fluorescent cells (~35%) than those in wild-type control cells. To determine if the increased A β ₄₂GFP fluorescence in the TCA cycle mutants were caused by an accumulation of a specific intermediate metabolite in the glycerol biosynthetic pathway (eg. glycerol or dihydroxyacetone), gene over-expression analysis was undertaken. This ‘reverse-genetics’ approach was undertaken to provide insight into the link between altered levels of glycerol and/or dihydroxyacetone, and, A β ₄₂GFP fluorescence.

In wild-type cells, over-expression of a gene in a cellular pathway is likely to increase flux through that particular pathway. In an attempt to force accumulation of a specific metabolite, the upstream gene(s) leading to its synthesis was over-expressed and the gene(s) leading to the utilisation of the ‘target’ metabolite was deleted. The genes encoding enzymes of the glycerol precursors and intermediates that were over-expressed included those involving dihydroxyacetone, dihydroxyacetone phosphate, glycerol-3-phosphate and glycerol. A list of all target metabolites analysed, the strains and plasmids used in this ‘reverse-genetics’ approach are summarised in Table 5-3. The over-expression screen made use of pAG415GAL1-A β 42-GFP (under the *LEU2* selectable marker) to allow co-expression of the genes in the yeast ORF library (under the *URA3* selectable marker) (Gelperin et al., 2005). Plasmids containing the 2 μ origin of replication are maintained at high-copy number (20-50 copies) and are useful in over-expression studies in *S. cerevisiae* (Sikorski and Hieter, 1989). High-copy galactose-inducible plasmids (BG1805 family) containing 5854 *S. cerevisiae* open reading frames (ORFs) in the yeast ORF library (Gelperin et al., 2005) (OpenBiosystemsTM) were utilised in this study. Wild-type BY4743 cells and the appropriate deletion mutants were co-transformed with pAG415GAL-A β 42-GFP construct and BG1805 plasmids carrying lipid gene ORFs as indicated in Table 5-3. As controls, both wild-type BY4743 cells and deletion mutants were co-transformed with pAG415GAL-A β 42-GFP and pYES-DEST52 (an empty *URA3* vector) (Invitrogen, San Diego, CA, USA). In this ‘reverse-genetics’ approach, successful transformants over-expressing a particular gene were examined to identify those exhibiting increased A β ₄₂GFP fluorescence and/or altered fluorescence localisation compared to wild-type cells. Expression of the A β ₄₂GFP fusion protein and the gene ORF in each strain was induced by growing cells in galactose medium and A β ₄₂GFP-associated fluorescence was analysed 15 h post-induction.

Table 5-3 List of genes encoding enzymes of the phospholipid intermediates that were over-expressed in wild-type cells and relevant phospholipid mutants

Attempted accumulation of metabolite-of-interest	ORF over-expressed	Strains		
Dihydroxyacetone phosphate (DHAP)	<i>DAK1</i>	Wild-type	<i>Δpsd1</i>	<i>Δgpt2</i>
	<i>DAK2</i>	<i>Δopi3</i>	<i>Δpsd2</i>	<i>Δsct1</i>
	<i>GUT2</i>	<i>Δice2</i>	<i>Δgpd1</i>	<i>Δfum1</i>
		<i>Δcho2</i>	<i>Δgpd2</i>	<i>Δayr1</i>
Dihydroxyacetone (DHA) and dihydroxyacetone phosphate (DHAP)	<i>YPR1</i>	Wild-type	<i>Δpsd1</i>	<i>Δdak2</i>
		<i>Δopi3</i>	<i>Δpsd2</i>	<i>Δgut1</i>
		<i>Δice2</i>	<i>Δfum1</i>	<i>Δgut2</i>
		<i>Δcho2</i>	<i>Δdak1</i>	<i>Δgcy1</i>
Glycerol-3-phosphate (G3P)		Wild-type	<i>Δpsd1</i>	<i>Δdak2</i>
	<i>GPD1</i>	<i>Δopi3</i>	<i>Δpsd2</i>	<i>Δgut1</i>
	<i>GPD2</i>	<i>Δice2</i>	<i>Δfum1</i>	<i>Δgut2</i>
	<i>GUT1</i>	<i>Δcho2</i>	<i>Δdak1</i>	<i>Δgcy1</i>
		<i>Δgpt2</i>	<i>Δsct1</i>	<i>Δfum1</i>
Glycerol		Wild-type	<i>Δpsd1</i>	<i>Δdak2</i>
	<i>GPP1</i>	<i>Δopi3</i>	<i>Δpsd2</i>	<i>Δgut1</i>
	<i>GPP2</i>	<i>Δice2</i>	<i>Δfum1</i>	<i>Δgut2</i>
		<i>Δcho2</i>	<i>Δdak1</i>	<i>Δgcy1</i>
		<i>Δgpt2</i>	<i>Δsct1</i>	<i>Δfum1</i>

Analysis of ~120 strains in the over-expression screen confirmed that only over-expression of *DAK2* in all strains led to an increased proportion of fluorescent cells (~35%) compared to wild-type control cells. As discussed in Section 4.2.8, *DAK2* over-expression in wild-type cells exhibited a structured localisation of fluorescent Aβ₄₂GFP in a large globular compartment in the cell (Figure 5-11). Based on the intensity of Aβ₄₂GFP fluorescence, it appeared that fluorescent Aβ₄₂GFP peptides accumulated inside this large globular compartment which was visible using DIC microscopy (Figure 5-11). *DAK2* over-expression in wild-type cells expressing either Aβ₄₀GFP or Aβ_{EP}GFP gave rise to 52% ± 5% and 60% ± 5% of the cell population, respectively. Interestingly, expressing in these strains the less-aggregation prone Aβ₄₀GFP or Aβ_{EP}GFP yielded almost no cytosolic-diffuse fluorescence. This is unlike wild-type cells where predominantly cytosolic-diffuse fluorescence was seen in cells expressing either Aβ₄₀GFP or Aβ_{EP}GFP. Almost all fluorescent Aβ₄₀GFP or Aβ_{EP}GFP fusion proteins were contained within the large globular compartment in cells over-expressing *DAK2* (Figure 5-11). In addition, choline supplementation did not affect the proportion of *DAK2* over-expressing cells exhibiting Aβ₄₂GFP-associated fluorescence.

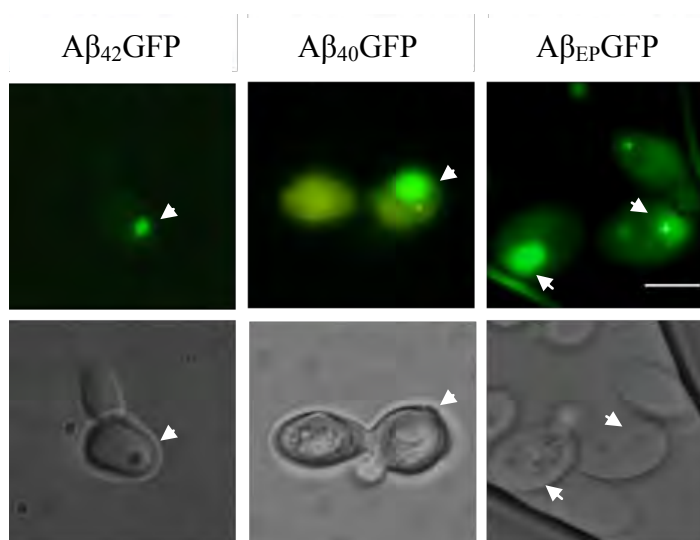


Figure 5-11 Fluorescent microscopic images of wild-type cells over-expressing *DAK2* together with A β ₄₂GFP, A β ₄₀GFP or A β _{EP}GFP

Wild-type cells over-expressing *DAK2* together with various forms of A β fusion proteins (as indicated) were induced in galactose medium (SCgal-URA). A β GFP-associated fluorescence was analysed at 15 h post induction. *DAK2* over-expression in wild-type cells exhibited a structured localisation of fluorescent A β GFP fusion proteins in a large globular compartment in the cell (as indicated by arrowheads). Scale bars indicate 5 μ m.

5.2.7 Over-expression of *DAK2*, but not *DAK1*, leads to formation of large globular compartment in cells containing fluorescent A β ₄₂GFP peptides.

There are two dihydroxyacetone kinases in *S. cerevisiae*, Dak1p and Dak2p, and they share 46% amino acid identity (Molin et al., 2003; Norbeck and Blomberg, 1997). Interestingly, the over-expression of *DAK2* but not *DAK1* led to the formation of a large globular compartment containing fluorescent A β ₄₂GFP peptides. To determine if the formation of this large cellular compartment was dependent on the expression and accumulation of A β ₄₂GFP, wild-type cells were transformed with either *DAK1* or *DAK2* over-expression plasmid alone, induced by growing cells in galactose medium and analysed 15 h post-induction. Analysis using DIC microscopic imaging indicated that wild-type cells over-expressing *DAK2* exhibited a large globular compartment/organelle (Figure 5-12). These large structures were not found in wild-type cell over-expressing *DAK1* (Figure 5-12). Taken together these data indicate that the formation of this cellular compartment was independent of the presence and expression of A β GFP fusion proteins and the A β ₄₂GFP peptides and the less-aggregation prone A β ₄₀GFP or A β _{EP}GFP peptides may have partitioned into this large compartment/organelle of the cell.

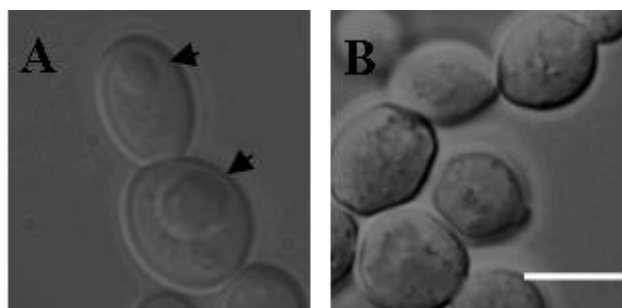


Figure 5-12 Differential interference contrast (DIC) microscopic images of wild-type cells over-expressing either *DAK1* or *DAK2*

Wild-type cells over-expressing either *DAK1* or *DAK2* (as indicated) were induced in galactose medium (SCgal-URA). Strains were analysed at 15 h post induction. *DAK2* over-expression in wild-type cells exhibited a structured large globular compartment/organelle in the cells (as indicated by arrowheads). Scale bars indicate 5 μ m.

5.2.8 Investigation of A β ₄₂GFP localisation in wild-type cells over-expressing *DAK2*

In Section 4.2.4, data from confocal microscopic analysis indicated that A β ₄₂GFP was unlikely to interact with LDs. This was further supported by the ER/ER-membrane localisation of A β ₄₂GFP in the quadruple mutant $\Delta dga1 \Delta lro1 \Delta are1 \Delta are2$, which do not form LDs. Recently it was described that certain *S. cerevisiae* mutants were able to produce ‘super-sized’ LDs that are up to 50 times the volume than those found in wild-type cells (Fei et al., 2008; Fei et al., 2011). In order to determine if this large globular compartment found in wild-type cells over-expressing *DAK2* was a ‘super-sized’ lipid droplet, wild-type BY4743 and the quadruple mutant $\Delta dga1 \Delta lro1 \Delta are1 \Delta are2$ were transformed with the pAG415GAL1-A β ₄₂-GFP and *DAK2* over-expression plasmids. Over-expression of *DAK2* and A β ₄₂GFP in both strains was induced by growth in galactose medium and analysed 15 h post-induction via microscopic analysis. Cells were stained with LipidTOX Red and 4’,6’-diamidino-2-phenylindole (DAPI) to allow co-visualisation of lipid droplets, nuclear and mitochondrial DNA respectively. Data from confocal microscopic analysis indicated that in wild-type cells, the large globular compartment containing fluorescent A β ₄₂GFP peptides did not co-localise to LipidTOX Red or the DAPI stains (Figure 5-13A). The quadruple mutant lacking LDs also exhibited a similar phenotype in that fluorescent A β ₄₂GFP peptides were found localised in the large globular compartment in cells (Figure 5-13B). These data indicate that the large globular compartment/organelle

formed by the over-expression of *DAK2* is not a traditional LD, a ‘super-sized’ LD or the nucleus of the cell. Based on the cellular function of Dak2p, the over-expression of a dihydroxyacetone kinase in cells may lead to an increased DHAP in cells, which is an integral part of the glycerophospholipid backbone. Therefore, it was proposed that in manner analogous to neutral lipid and sterol accumulation in LDs, strains over-expressing *DAK2* may accumulate polar lipids/phospholipids in these large cellular compartments.

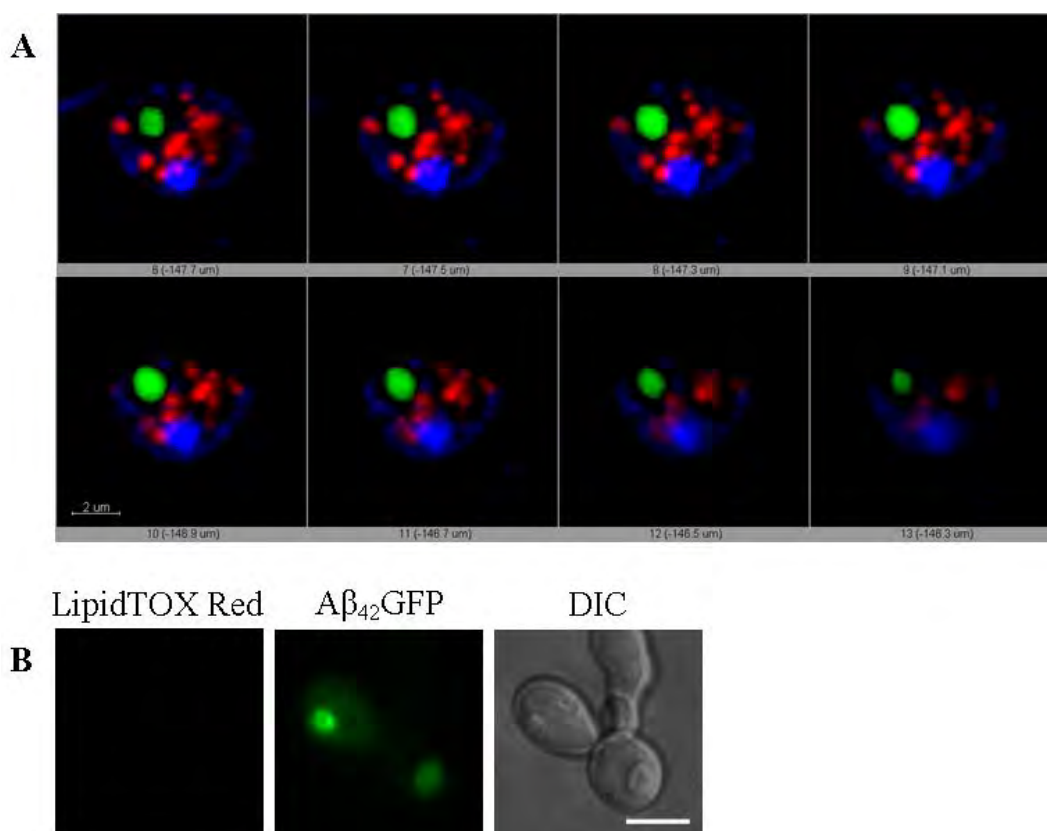


Figure 5-13 Fluorescent and confocal microscopic images of the quadruple mutant and wild-type cells over-expressing *DAK2* exhibiting $A\beta_{42}$ GFP fluorescence, LipidTOX Red and DAPI staining.

Wild-type cells and the quadruple mutant $\Delta dgal \Delta lro1 \Delta are1 \Delta are2$ over-expressing *DAK2* and $A\beta_{42}$ GFP were induced in galactose medium (SCgal-URA). Cells were stained with DAPI and LipidTOX Red; and localisation of LDs, nuclear DNA, and $A\beta_{42}$ GFP fluorescence were analysed at 15 h post induction. A) Series of confocal microscopic images, taken at 1 μ m intervals (as indicated) of a wild-type cell exhibiting distinct $A\beta_{42}$ GFP localisation in a large globular compartment/organelle (in green), demonstrates that this compartment/organelle is not a LD (in red) or the nucleus (in blue). B) Lack of fluorescence signal using LipidTOX Red indicates the lack of LDs in the quadruple mutant (left panel), while $A\beta_{42}$ GFP localises in the large globular compartment/organelle in these cells (middle panel). Bar, 5 μ m.

Nile Red (9-diethylamino-5H-benzo[α]phenoxazine-5-one) is a fluorescent lipophilic stain which is characterised by a shift of emission from red to yellow according to the degree of hydrophobicity of lipids (Fowler and Greenspan, 1985; Greenspan and Fowler, 1985; Greenspan et al., 1985). Therefore, unlike LipidTOX Red used previously, Nile Red stain is able to detect both polar and non-polar/neutral lipids. Polar lipids such as phospholipids appear red while neutral lipids that are present in LDs, appear to be yellow. Interestingly, quantitative ratiometric data of Nile Red red and yellow emissions is able to differentiate lipids based on their polarity/hydrophobic strength (Diaz et al., 2008). It is important to note that this red/yellow emission ratio is unable to evaluate the exact composition of lipid mixtures, but it may indicate a general change in lipid composition based on the difference between the hydrophobicity of polar lipids and neutral lipids. Since the data above indicated that the large globular compartment in wild-type cells over-expressing *DAK2* was not a traditional LD, these cells were stained with Nile Red to determine if there was an accumulation of polar lipid species in these cells. Due to the significant spectral overlap of GFP and Nile Red fluorescence emission (Listenberger and Brown, 2007), wild-type cells over-expressing *DAK2*, without A β ₄₂GFP, were induced for 15 h and stained with Nile Red. The large globular compartment in wild-type cells over-expressing *DAK2* stained with Nile Red appeared to be red in colour in contrast to the yellow coloured LDs (Figure 5-14). This may indicate an accumulation of polar lipid species or DHAP in the large compartment formed in these cells, subsequently causing A β ₄₂GFP to partition into this compartment within this strain leading to the altered localisation of A β ₄₂GFP.

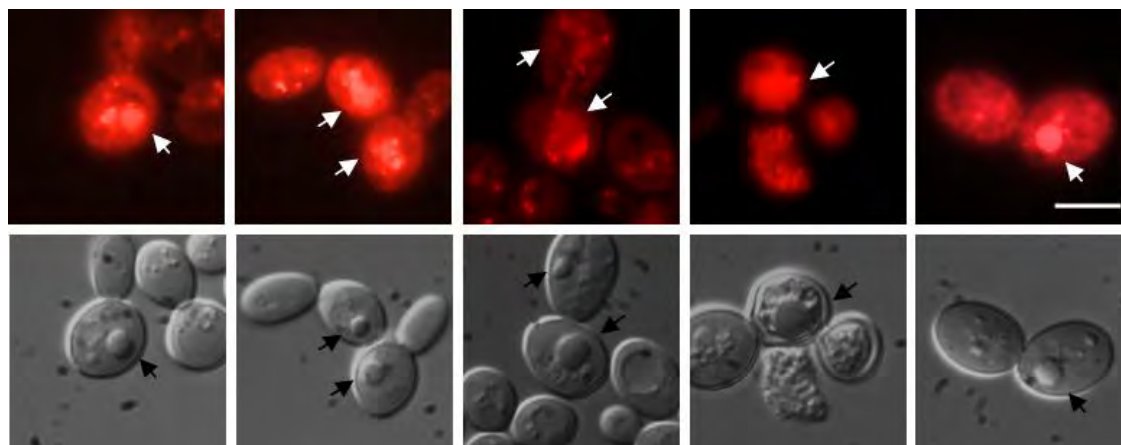


Figure 5-14 Fluorescent and DIC microscopic images of wild-type cells over-expressing *DAK2* stained with Nile Red

Over-expression of *DAK2* in wild-type cells was induced by growth in galactose medium (SCgal-URA). Cells were stained with Nile Red and analysed at 15 h post induction. Wild-type cells over-expressing *DAK2* exhibited the formation of a large globular compartment in cells (black arrows in DIC images) which exhibited red fluorescence with Nile Red stain; unlike the intense yellow fluorescence observed from LDs. Yellow fluorescence is not visible in these images due to false colouring applied. Bar, 5 μ m.

5.2.9 Global lipidome analysis of wild-type cells over-expressing *DAK2* identifies pronounced effect of increased TAG, MIPC and lysoPA levels

To determine if the large globular compartment containing fluorescent A β ₄₂GFP peptides in wild-type cells over-expressing *DAK2* was possibly connected with altered lipid composition, a quantitative shotgun mass spectrometric approach on whole cells was undertaken to provide insight into the global lipidomic profile in this strain. Expression of the A β ₄₂GFP fusion protein in wild-type BY4743 cells and wild-type cells over-expressing *DAK2* was induced by growing cells in galactose medium to exponential phase (OD₆₀₀ 1.5). Cells were harvested from the exponential phase culture, washed in MilliQ water and frozen at -80°C for lipid extraction.

Analysis of the lipid classes, indicated that wild-type cells over-expressing *DAK2* exhibited significantly higher levels of TAG ($p < 0.02$), MIPC ($p < 0.06$) and lysoPA ($p < 0.004$) and lower levels of PE ($p < 0.05$) compared to wild-type cells. Dak2p phosphorylates DHA to DHAP which is subsequently converted to 1-acyl dihydroxyacetone phosphate (1-acyl-DHAP) and lysoPA via sequential action of Gpt2, Sct1p and Ayr1p. Interestingly, of the four lipids classes found elevated in wild-type cells over-expressing *DAK2*, lysoPA is the most polar and exhibited more than 2.5 fold increase compared to lysoPA levels in wild-type cells.

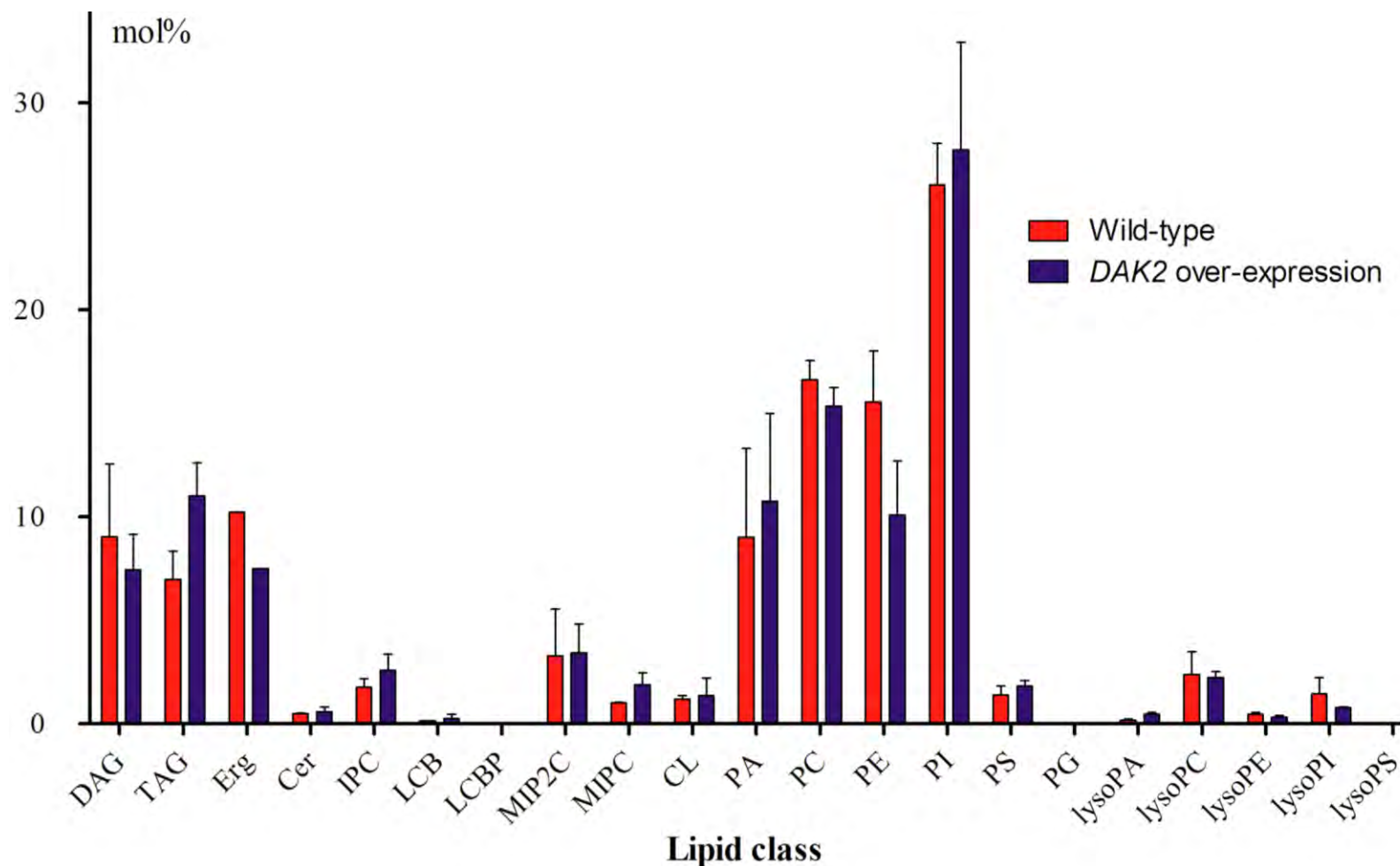


Figure 5-15 Global lipidomic profile of wild-type cells over-expressing *DAK2* and $A\beta_{42}$ GFP

Quantitative global lipid class composition in wild-type and $\Delta ice2$ cells grown in either glucose or galactose media (as indicated). Data presented are the mean of triplicate measurements from three independent experiments. Error bars indicate standard deviation of these three MS acquisitions.

In order to further establish a possible link between altered levels of polar lipids and over-expression of *DAK2*, one-dimensional thin-layer chromatography of the total polar lipid extract was undertaken. Expression of the A β ₄₂GFP fusion protein in wild-type BY4743 cells and wild-type cells over-expressing *DAK2* was induced by growing cells in galactose medium to exponential phase (OD₆₀₀ 1.5). Cells were harvested from the exponential phase culture, washed and polar lipid extracts from total cell lysates were prepared. Chromatograms were developed and analysed as described in Section 2.12.2.

Analysis of the polar lipid separation using TLC indicated that there was a significant increase of a particular lipid species (Figure 5-16). This polar lipid species migrated close to PA, however, at present it is unclear which lipid species accumulated in wild-type cells over-expressing *DAK2*. Identification of this accumulated polar lipid species is currently underway via mass spectrometry, using scrapings of the reddish-yellow band from the TLC plate.

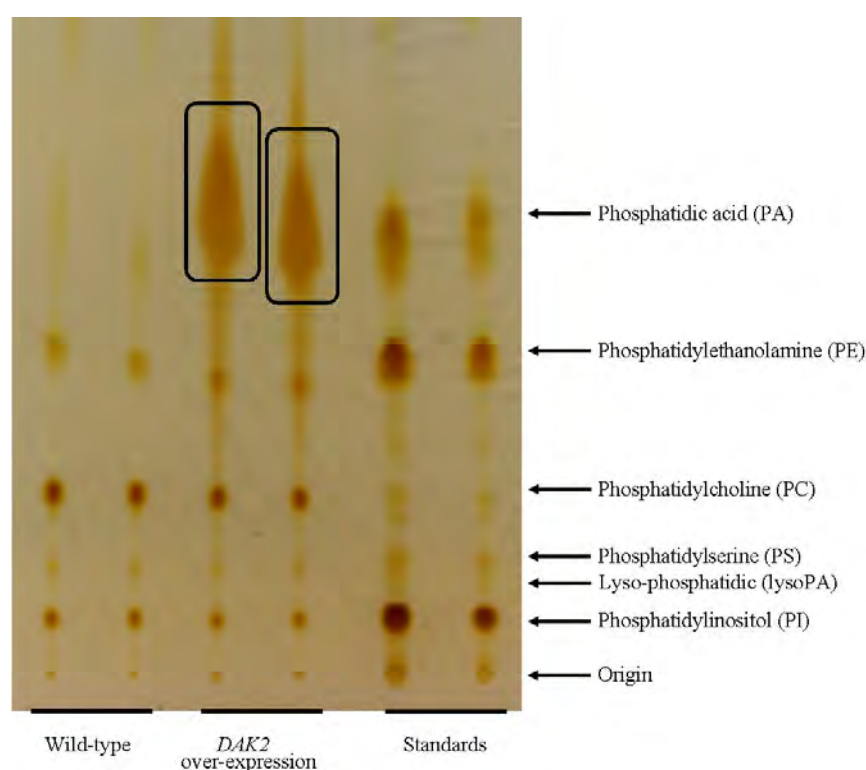


Figure 5-16 One-dimensional thin-layer chromatographic separation of polar lipids from wild-type cells over-expressing *DAK2*

Load-controlled polar lipid extracts were prepared from wild-type cells expressing *DAK2* and wild-type control cells grown to exponential phase (OD₆₀₀ 1.5) in galactose medium. Chromatograms were developed together with phospholipid standards as described in Section

2.12.2, and stained using iodine vapour. The significant increase of a particular lipid species is indicated by a box.

5.2.10 Dak2p localises in the large compartment formed by overexpression of *DAK2*

Though dihydroxyacetone kinases Dak1p and Dak2p are associated with similar cellular functions and share 46% amino acid similarity (Molin et al., 2003; Norbeck and Blomberg, 1997), over-expression of *DAK2* but not *DAK1* in wild-type cells gave rise to increased A β ₄₂GFP fluorescence. Interestingly, the over-expression of *DAK2* led to the formation of a large globular compartment containing fluorescent A β ₄₂GFP peptides. While the Dak1p is found predominantly in the cytosol of *S. cerevisiae* cells, the cellular localisation of Dak2p is not clearly understood (Huh et al., 2003). To determine the exact localisation of Dak2p activity, wild-type cells were transformed with pAG426GAL1-*DAK2*-GFP for the expression of GFP tagged *DAK2*. Expression of the Dak2p-GFP fusion protein in wild-type BY4743 cells was induced by growing cells in galactose medium and fluorescence was analysed 15 h post-induction.

Analysis of the microscopic images indicated that Dak2p was localised in the large globular compartment/organelle formed in wild-type cells over-expressing *DAK2*-GFP (Figure 5-17). Unlike the intensity of A β ₄₂GFP observed in wild-type cells over-expressing *DAK2*, cells expressing Dak2p-GFP appeared more intense as if to indicate that Dak2p-GFP was localised to the surface of this large globular compartment. Taken together with data above, it appears that both Dak2p and fluorescent A β ₄₂GFP peptides were directed to the large compartment found in these cells. To further understand the cellular function and partitioning of Dak2p into the cellular compartment/organelle, a number of key experiments need be conducted in the future. Work is currently underway to determine if the cellular compartment/organelle is derived from the ER. However, a more detailed analysis of the possible proteins and lipids accumulating in the large globular compartments of wild-type cells overexpressing *DAK2* is required. Analysis of subcellular fractions of this compartment/organelle using a lipidomic/metabolomic approach to identify changes in cellular metabolites may be informative.

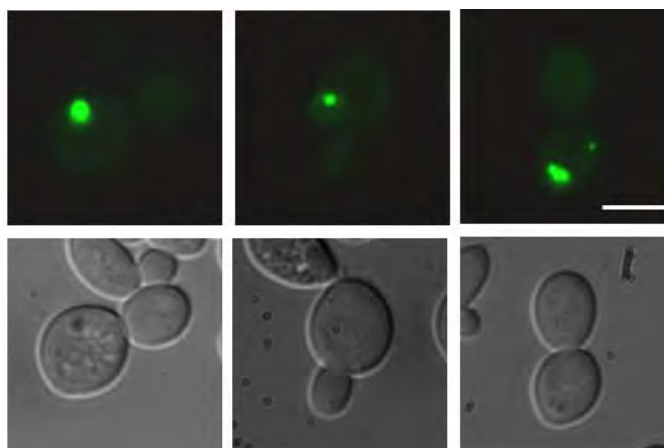


Figure 5-17 Fluorescent and DIC microscopic images of wild-type cells over-expressing Dak2p-GFP

Over-expression of Dak2p-GFP in wild-type cells was induced by growth in galactose medium (SCgal-URA) and analysed at 15 h post induction. The large globular compartment/organelle formed in these cells exhibited co-localisation with Dak2p-GFP associated fluorescence. Bar, 5 μ m.

5.2.11 Dihydroxyacetone supplementation alters A β ₄₂GFP fluorescence in wild-type cells

Dihydroxyacetone (DHA) is toxic to yeast cells and dihydroxyacetone kinases play an important role by detoxifying these molecules to dihydroxyacetone phosphate (DHAP). While the double mutant $\Delta dak1 \Delta dak2$ is highly sensitive to DHA, overexpression of either *DAK1* or *DAK2* allows cells to grow on media using DHA as the only carbon source and also provides the capacity for the $\Delta dak1 \Delta dak2$ double mutant to be highly resistant to DHA. To determine if altered levels of intracellular DHA and/or DHAP influenced the increased proportion of fluorescent cells in the TCA cycle mutants and in wild-type cells over-expressing *DAK2*, wild-type cells expressing A β ₄₂GFP were grown in medium lacking or supplemented with DHA. Since wild-type cells over-expressing *DAK2* exhibited increase fluorescence and accumulation of fluorescent A β ₄₂GFP in a large globular compartment in the cell, this strain was also included in the DHA supplementation analysis. A β ₄₂GFP-associated fluorescence was analysed following growth of strains in media either lacking or supplemented with 50 μ M DHA 15 h post induction. In each case, 10,000 cells were counted in triplicate using flow cytometry. The data was generated were analysed with FlowJo version 7.4 software and presented in Figure 5-18A.

DHA supplementation gave rise to increased A β ₄₂GFP-associated fluorescence (~12%) in wild-type cells. Fluorescent A β ₄₂GFP in wild-type cells was predominantly cytosolic-diffuse or cytosolic-diffuse with single small puncta (Figure 5-18B), which did not appear to occur in a distinct compartment/structure in the cell. However, the large globular compartment formed in cells over-expressing *DAK2* was not observed under DIC microscopy when wild-type cells were supplemented with 50 μ M DHA. No change in the proportion of cells over-expressing *DAK2* exhibiting the A β ₄₂GFP-associated fluorescence was observed with DHA supplementation.

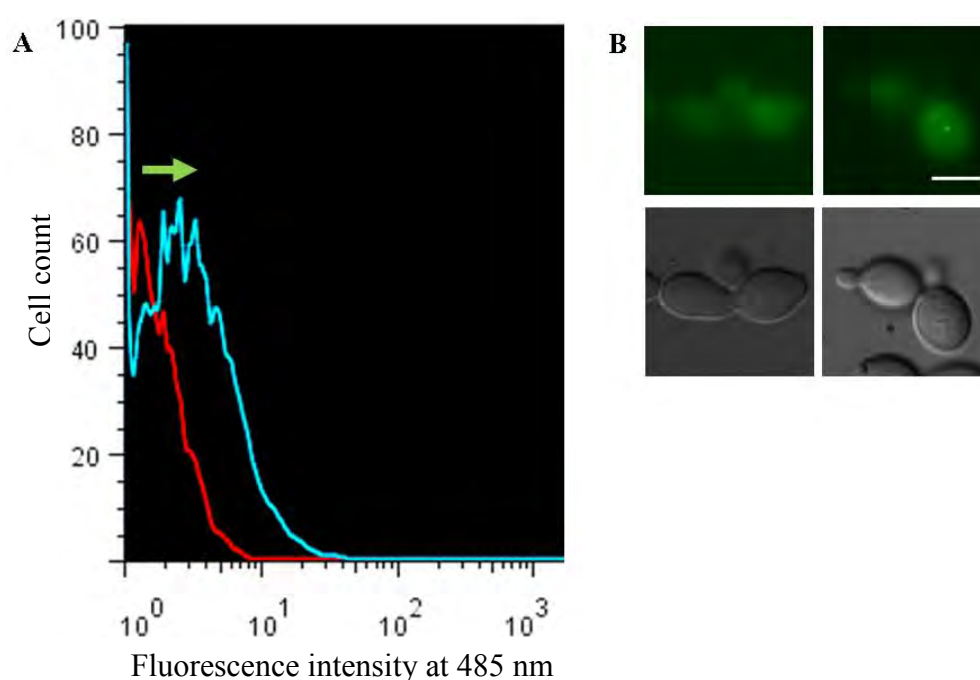


Figure 5-18 Effect of DHA supplementation on wild-type cells expressing A β ₄₂GFP

Wild-type cells expressing A β ₄₂GFP were induced in galactose medium (SCgal-URA) either lacking or supplemented with 50 μ M DHA. A β GFP-associated fluorescence was analysed at 15 h post induction. A) Flow cytometric analysis of 10,000 cells for each sample demonstrates a significant shift (green arrow) indicating an increase in the proportion of fluorescent cells upon DHA supplementation (blue line) compared to control cells (red line). The x-axis indicates GFP-derived fluorescence intensity while the y-axis indicates cell count. B) Fluorescent microscopic images of wild-type cells expressing A β ₄₂GFP upon DHA supplementation. Scale bars indicate 5 μ m.

5.3 Discussion and general summary

5.3.1 Global lipidomic analysis of mutants that exhibit increased A β ₄₂GFP fluorescence

The yeast lipidome is typically characterised by glycerolipids (TAG and DAG) and glycerophospholipid classes found in mammalian cells, but in addition has phytosphingolipids (characterised by the long-chain base and the fatty acyl amide moieties which are hydroxylated) and the presence of ergosterol rather than the cholesterol found in mammalian cells (Gaspar et al., 2007; Perry and Ridgway, 2005; Zinser et al., 1993). Previously, the majority of the knowledge of the yeast lipidome were gathered from analysis of enzymes involved in lipid metabolism via simple thin-layer chromatography, gene sequencing and genetic manipulation (Carman and Henry, 2007). However, it is well understood that genes and transcripts do not accurately predict the levels of active proteins/enzymes or metabolites. Over the last decade, knowledge of physiological levels of lipid metabolites has been found to be more predictive of gene functions and metabolic implications. This study provides a quantitative measure of the changes in lipid metabolites in specific deletion mutants and for cells grown on galactose medium, which may contribute to further understanding of lipid metabolism in *S. cerevisiae*. Interestingly, lipid metabolism is of particular importance for the central nervous system, as it is composed of high concentrations of lipids. The essential role of lipids in cell signalling and physiology is validated by altered lipid metabolism present in many neurodegenerative diseases such as AD and Parkinson's disease (Adibhatla et al., 2006).

Major rearrangements of membrane lipid composition and changes in the global lipidomic profile may be caused by altered growth conditions or mutations. Recently, it was demonstrated that minor changes in growth conditions, temperature, growth phase of cells and the utilisation of various carbon sources in the media have a profound influence on the global lipidomic profile of *S. cerevisiae* cells (Klose et al., 2012; Natter et al., 2005). Therefore, these changes may affect lipid composition-dependent phenotypes. In this study, phospholipid metabolism was chosen for more extensive analysis since most of the genes directly involved in phospholipid synthesis were over-represented in the screens relative to A β ₄₂GFP aggregation and localisation, and there is evidence of perturbed phospholipid metabolism in AD (Frisardi et al., 2011; Grimm et

al., 2011; Hung et al., 2008). Genes in the phospholipid metabolism functional group include *INO2*, *INO4*, *UME6*, *SCS2*, *PSD1*, *CHO2* and *OPI3* all of which, directly or indirectly, regulate levels of PC in cells. Furthermore, A β ₄₂ was identified in perinuclear localised multi-vesicular bodies (MVBs) of neuronal cells, (Langui et al., 2004; Takahashi et al., 2002). The Δ *ino2*, Δ *ino4*, Δ *psd1*, Δ *cho2*, Δ *opi3* and Δ *ice2* mutants also exhibited this characteristic ER/ER-membrane associated A β ₄₂GFP localisation. Through the genetic and lipidomic approaches, it was not possible to identify any specific phospholipid class/species that affected A β ₄₂GFP fluorescence and localisation; however data presented in this chapter clearly indicate that perturbation of phospholipid homeostasis, specifically in the ER membranes, may affect A β ₄₂GFP aggregation. In all of these mutants a decrease in PA, PC, PI and PS was observed and it is clear that perturbation of phospholipid homeostasis may subsequently allow partitioning of A β ₄₂GFP into the ER/ER-membranes in the six mutants affected in phospholipid metabolism leading to the different localisation patterns of A β ₄₂GFP.

While overall phospholipid levels, including PA, PC, PE, PI, and PS, were reduced in mutants exhibiting the ER/ER-membrane A β ₄₂GFP localisation there was also a pronounced effect of increased M(IP)₂C levels in these strains compared to wild-type cells. M(IP)₂C was significantly increased in all four strains Δ *psd1*, Δ *cho2*, Δ *opi3* and Δ *ice2* mutants respectively. Interestingly, increased M(IP)₂C levels showed a noticeable trend: a significant reduction in PI in all mutants exhibiting the ER/ER-membrane A β ₄₂GFP localisation was associated with increased levels of M(IP)₂C in those strains. A possible explanation for this trend may be a shift in lipid metabolism in the relevant phospholipid mutants. By down-regulating *PIS1* or reducing activity of *Pis1p*, for the synthesis of PI, the resulting increased inositol/inositol phosphates in the cells may have been channelled into biosynthesis of phosphoinositol-containing complex sphingolipids: inositol-phosphoceramide (IPC), mannose-inositol-phosphoceramide (MIPC), and mannose-(inositol phosphate)₂-ceramide (M(IP)₂C). Alternatively, since most phospholipids undergo rapid turnover and acyl-chain remodeling yielding complex patterns of lipid species (Schneider et al. 1999; Guan and Wenk 2006; Ejlsing et al. 2009), a high turnover rate of PI may also have led to increased inositol/inositol phosphates levels. In *S. cerevisiae* cells, several PI specific phospholipases and phosphatases are present. *Plb3p*-encoded phospholipase B utilises

PI as a substrate to produce glycerophosphoinositol (Fyrst et al. 1999; Lee et al. 1994; Merkel et al. 1999, 2005), which can be hydrolysed by a phosphodiesterase to produce inositol (Patton-Vogt 2007). Plc1p-encoded phospholipase C is specific for PI 4,5-P₂ and produces DAG and inositol 1,4,5-trisphosphate (Flick and Thorner 1993; Yoko-O et al. 1993). Phosphatases that catalyse the dephosphorylation of the polyphosphoinositides: Ymr1p (Taylor et al. 2000), Fig4p (Gary et al. 2002), and, Inp51p (Stolz et al. 1998b) and Innp54p (Wiradjaja et al. 2001) are specific for PI 3-P, PI 3,5-P₂, and PI 4,5-P₂ respectively. While Inp52p and Inp53, phosphatases with broad specificity utilise any polyphosphoinositide as a substrate (Stolz et al. 1998; Guo et al. 1999), Sac1p mainly utilises PI 3-P, PI 4-P, and PI 3,5-P₂ (Guo et al. 1999). This increase in inositol/inositol phosphates production may have led to increased biosynthesis of phosphoinositol-containing complex sphingolipids, including M(IP)₂C. This hypothesis may be further supported by the increased levels of TAG observed in $\Delta cho2$, $\Delta opi3$ and $\Delta ice2$ strains and DAG in $\Delta opi3$ (Figure 5-2).

While there is a significant increase in M(IP)₂C levels in strains exhibiting the ER/ER-membrane A β ₄₂GFP localisation, it is noteworthy that the Golgi is the primary site for complex sphingolipid synthesis, including M(IP)₂C. In a recent study by Natter and colleagues (2005) in which localisation of enzymes involved in lipid metabolism were studied using GFP fusions, enzymes involved in ceramide and complex sphingolipid synthesis were shown to be predominantly in both the ER membrane and vesicles. Interestingly, while this may be indicative of translocation into COP vesicles and Golgi; it was demonstrated that the relative distribution of enzymes involved in the ceramide and complex sphingolipid biosynthetic pathway between ER and vesicles changes considerably between the various enzymes in this pathway (Natter et al., 2005). In the absence of available literature indicating the localisation of ceramide and complex sphingolipid biosynthetic enzymes in mutants affected in phospholipid metabolism, it is tempting to speculate that the relative distribution of these enzymes may be in favour of the ER compared to the vesicles or Golgi in these phospholipid mutants. This possibility is further supported by data indicating that inositol phosphotransferase Ipt1p, involved in the synthesis of M(IP)₂C, is also localised to the ER. Ceramide biosynthesis is mainly carried out by ER-bound enzymes; however, many of these enzymes show dual localisation to ER and vesicular structures. Examples of such enzymes with dual

localisation include Tsc10p, Csg2p Ydc1p and Scs7p; Ypc1p localises to both the nuclear envelope and vesicles; Sur1p localises to the vacuole lumen and vesicles; while, Csh1p localises to vacuolar membranes and vesicles. Therefore, if there was altered localisation of Ipt1p in the ER of the phospholipid mutants, there is an increased possibility of M(IP)₂C accumulation in the ER-membrane, which may have subsequently led to the ER/ER-membrane A β ₄₂GFP localisation in these mutants. However, proteomic and lipidomic analyses on the subcellular fractions of these mutants using quantitative mass spectrometry would be required to test this hypothesis.

Unlike the trends of reduced levels of GPs, including PA, PI, PS, PE and PC, and increased levels of TAG and M(IP)₂C observed in mutants affected in phospholipid metabolism, TCA cycle mutants did not exhibit a general trend across any of the 20 lipid categories. Instead, varying levels of lipid classes were observed within the selected TCA cycle mutants. Interestingly, the lipidome of rho⁰ cells was significantly altered; rho⁰ cells exhibited a similar TAG accumulation phenotype as observed in the phospholipid mutants, as well as trends involving reduced PA, PE and PI levels. CL, which is found only in the mitochondrial inner membrane and is essential for several aspects of mitochondrial function such as cytochrome oxidase activity (Joshi et al., 2009), was found to be 3-fold lower compared to wild-type cells and corroborates previously reported levels of CL levels in rho⁰ cells (Gaynor et al., 1991). Interestingly, a significant decrease of PC and PS levels in the phospholipid mutants was not observed in rho⁰ cells. Taken together, it can be surmised that the additional decrease of PC and PS levels in the phospholipid mutants may have given rise to the ER/ER-membrane A β ₄₂GFP localisation. Future studies using a ‘double mutant’ of rho⁰ Δ *opi3*, rho⁰ Δ *cho2* and rho⁰ Δ *cho1* mutant would help to examine this possibility. Despite this, these data strongly indicate that alterations to specific phospholipids may affect A β ₄₂GFP localisation and aggregation in *S. cerevisiae*.

5.3.2 General summary of the effect of *ICE2* deletion on A β ₄₂GFP

In *S. cerevisiae* cells, two types of ER are present; namely perinuclear ER and the cortical ER (Preuss et al., 1991; Rose et al., 1989). While the nuclear ER is a polygonal network of membranous tubular structures (Palade, 1956) connected to the outer nuclear envelope, the cortical ER forms a membranous tubular network along the

periphery of the cells, juxtaposed to the plasma membrane (Prinz et al., 2000). Ice2p, is predicted to be a type-III integral ER transmembrane protein that localises to both the cortical and perinuclear endoplasmic reticulum (ER) in *S. cerevisiae* (Huh et al., 2003). While the exact cellular functions of *ICE2* is unclear, $\Delta ice2$ strains were found to exhibit abnormal distribution of the cortical ER tubular network from mother to daughter cells. This led to the proposal that Ice2p is involved in forming and/or maintaining the cortical ER network in *S. cerevisiae* (Estrada de Martin et al., 2005). In this study, $\Delta ice2$ cells expressing A β_{42} GFP exhibited a strong level of A β_{42} GFP-associated fluorescence in a perinuclear ER/ER-membrane localisation, similar to the localisation observed for A β_{42} GFP in the mutants affected in phospholipid metabolism. Although similar to the perinuclear localisation observed for A β_{42} GFP in the $\Delta ino2$, $\Delta ino4$, $\Delta psd1$ and $\Delta opi3$ mutants, subtle differences were observed. In the phospholipid mutants, while a series of fluorescent puncta was organised around the nucleus of the cell, a continuous A β_{42} GFP fluorescent band was observed in the $\Delta ice2$ mutant.

Expression of A β_{40} GFP and A β_{EP} GFP in $\Delta ice2$ cells also produced an arc-shaped fluorescence; and therefore, this indicates that the specific localisation of A β_{42} GFP in the $\Delta ice2$ and mutant was not due to the aggregation propensity of the A β_{42} -moiety of the fusion protein. Although differences were observed in the nature of the fluorescent A β_{42} GFP localisation in the phospholipid mutants and $\Delta ice2$ cells, it is possible that at a fundamental level, a similar underlying mechanism was responsible in both cases. That is, altered lipid composition of subcellular membranes was hypothesised to facilitate A β_{42} GFP localisation to the ER in the phospholipid mutants, a similar mechanism may occur in the $\Delta ice2$ cells. It is worth noting that the abundance of A β_{42} GFP and A β_{40} GFP fluorescence was not affected by exogenous choline addition in $\Delta ice2$ cells. In contrast, A β_{EP} GFP localisation was affected by choline addition. This indicates that the $\Delta ice2$ mutation may be partially suppressed by the addition of exogenous choline. Interestingly, analysis of the negative genetic interaction network of *ICE2*, further highlights a strong association to genes involved in lipid metabolism and displayed significant genetic interactions with *ICE2*. These include genes involved in phospholipid metabolism *INO2*, *INO4*, *PSD1*, *PSD2*, *CHO2*, *OPI3*, and *SCS2*; glycerolipid metabolism *PAH1* and *DGK1*; sphingolipid metabolism *SCS7* and *ORM2*; and sterol metabolism *ERG6*. Using quantitative mass spectrometry, $\Delta ice2$

demonstrated a pronounced effect of decreased PA and PE levels compared to wild-type cells. Significant decrease in PI and PS levels were also observed in $\Delta ice2$ cells grown in galactose media but not those grown in glucose media. Interestingly, a significant increase in the levels of DAG, TAG and M(IP)₂C was observed in $\Delta ice2$ compared to wild-type cells. With the availability of global lipidomes of phospholipid mutants, a comparison of the lipidomic profile of the $\Delta ice2$ mutant indicated that apart from the PC depletion phenotype found in $\Delta opi3$ and $\Delta cho2$ mutants, $\Delta ice2$ cells showed a very similar pattern of lipid classes to those observed in these phospholipid mutants. Taken together with results from the global lipidomic analysis of strains exhibiting the ER/ER-membrane A β ₄₂GFP localisation, these data strongly indicate that Ice2p plays a role in lipid metabolism in *S. cerevisiae* cells.

In this context, the data obtained for A β ₄₂GFP in $\Delta ice2$ may extend our understanding of the role of Ice2p in *S. cerevisiae* cells. While it may be tempting to speculate that Ice2p plays a role in phospholipid metabolism, in addition to the role in cortical ER maintenance and inheritance, further experimental work is required to understand the function of Ice2p. One such experiment might be the direct measure of Ice2p activity *in vivo* and/or *in vitro* using radiolabelled phospholipid precursors such as CDP-DAG, PA, PE, PI and PS. It may also be important to further examine if the lipid composition of subcellular membranes in $\Delta ice2$ cells is altered relative to wild-type cells. If the altered localisation of A β ₄₂GFP localisation in $\Delta ice2$ was due to a change in the phospholipid composition of the ER membrane, then it is tempting to speculate that altered lipid composition may account for the cortical ER inheritance defect observed in the $\Delta ice2$ strain.

5.3.3 General summary of the effect of mitochondrial dysfunction, *DAK2* over-expression and DHA supplementation on A β ₄₂GFP

To allow the reduction of NAD⁺ to be matched by a continuous reoxidation of NADH, multiple mechanisms exist in *S. cerevisiae* cells. While NADH serves as a source of electrons and is required in reductive cellular reactions, NAD⁺ serves as a sink for electrons and is required in oxidative cellular reactions (Bakker et al., 2001; Schafer and Buettner, 2001). One of the major mechanisms that allows for the reoxidation of NADH is the production of glycerol via glycerol-3-phosphate dehydrogenase which

detoxifies dihydroxyacetone phosphate by utilising NADH (Compagno et al., 1996; Larsson et al., 1998). The glycerol-3-phosphate shuttle is an indirect mechanism to oxidise cytosolic NADH and transfer the electrons to the respiratory chain (Bakker et al., 2001). As indicated previously, there are two major processes of glycerol formation; i) reduction of dihydroxyacetone phosphate to glycerol-3-phosphate via NADH-dependent glycerol-3-phosphate dehydrogenase Gpd1p and Gpd2p. This is followed by hydrolysis of the phosphate group to produce glycerol Gpp1p and Gpp2p. ii) Direct conversion of dihydroxyacetone to glycerol via glycerol dehydrogenases Ypr1p and Gcy1p (Albertyn et al., 1994b; Ansell et al., 1997; Eriksson et al., 1995; Norbeck et al., 1996; Norbeck and Blomberg, 1997; Wang et al., 1994).

There are two dihydroxyacetone kinases in *S. cerevisiae*, Dak1p and Dak2p (Molin et al., 2003; Norbeck and Blomberg, 1997). Wild-type cells over-expressing *DAK2* gave rise to increased fluorescent cells than those in wild-type control cells. Interestingly, however, *DAK2* over-expression in wild-type cells exhibited a structured localisation of fluorescent A β ₄₂GFP in a large globular compartment in the cell, which was visible under DIC microscopy. Based on the intensity of A β ₄₂GFP fluorescence, it appeared that fluorescent A β ₄₂GFP peptides accumulated inside this large globular compartment. Interestingly, the over-expression of *DAK2* but not *DAK1* led to the formation of a large globular compartment containing fluorescent A β ₄₂GFP peptides. The formation of this large cellular compartment was independent of the expression and accumulation of A β ₄₂GFP. Interestingly, *DAK2* over-expression in wild-type cells expressing either A β ₄₀GFP or A β _{EP}GFP yielded almost no cytosolic-diffuse fluorescence. This is unlike what was observed in wild-type cells where predominantly cytosolic-diffuse fluorescence was seen in cells expressing either A β ₄₀GFP or A β _{EP}GFP. Almost all fluorescent A β ₄₀GFP or A β _{EP}GFP fusion proteins were contained within the large globular compartment in cells over-expressing *DAK2*. In addition, unlike the reversal of A β ₄₂GFP fluorescence upon choline supplementation in phospholipid mutants, choline supplementation did not affect the proportion of wild-type cells over-expressing *DAK2* exhibiting A β ₄₂GFP, A β ₄₀GFP or A β _{EP}GFP-associated fluorescence.

At present, the exact localisation of the large globular compartment/organelle found in wild-type cells over-expressing *DAK2* is unclear; however, confocal

microscopic analysis indicated that this compartment/organelle was unlikely to be a classical lipid droplet (LD), a ‘super-sized’ LD or the nucleus of the cell. This was further supported by the appearance of this large compartment/organelle in the quadruple mutant $\Delta dgal \Delta lro1 \Delta are1 \Delta are2$, which does not form LDs. Interestingly, analysis of the large compartment/organelle in wild-type cells over-expressing *DAK2* using Nile Red stain, which detects polar and non-polar/neutral lipids, indicated that this compartment/organelle may be a site of accumulation of polar lipid species in these cells. Based on the cellular function of Dak2p, the over-expression of a dihydroxyacetone kinase in cells may lead to an increased DHAP in cells, which is an integral part of the glycerophospholipid backbone. Therefore, it may be possible that in manner analogous to neutral lipid and sterol accumulation in LDs, strains over-expressing *DAK2* may accumulate polar lipids/phospholipids in these large cellular compartments.

Taken together, these data indicate that the formation of this large cellular compartment/organelle, which is independent of the presence and expression of A β GFP fusion proteins, may occur via an accumulation of polar metabolites and/or lipid species such as DHAP or 1-acyl DHAP and subsequently allow A β_{42} GFP and the less-aggregation prone A β_{40} GFP or A β_{EP} GFP peptides to partition into this large compartment/organelle of the cell leading to the altered localisation of A β GFP fusion proteins. Analysis of the global lipidome of wild-type cells over-expressing *DAK2* indicated that significantly higher levels of TAG, MIPC and lysoPA were present in these cells compared to wild-type cells. Dak2p phosphorylates DHA to DHAP which is subsequently converted to 1-acyl dihydroxyacetone phosphate and lysoPA via sequential action of Gpt2, Sct1p and Ayr1p. Due to the unavailability of internal standards for dihydroxyacetone phosphate and 1-acyl dihydroxyacetone phosphate, these lipids were not quantified in this lipidomic approach. However, it is possible that over-expression of *DAK2* may affect lipid metabolism by causing intracellular accumulation of 1-acyl dihydroxyacetone phosphate and lysoPA.

Interestingly, of the four lipids classes found elevated in wild-type cells over-expressing *DAK2*, lysoPA is the most polar and was significantly increased compared to wild-type cells. Due to the unavailability of internal standards for dihydroxyacetone phosphate and 1-acyl-DHAP, these metabolites were not quantified in this lipidomic

approach. It is possible that over-expression of *DAK2* would affect lipid metabolism by causing intracellular accumulation of 1-acyl-DHAP and lysoPA. The compartmentalisation of these polar lipid species may have also led to the red spectral emission observed with Nile Red staining. Separation of total polar lipids from wild-type cells over-expressing *DAK2* using TLC indicated that there was a significant increase of a particular lipid species that migrated close to PA. While at present it is unclear which lipid species accumulated in these cells, identification of this accumulated polar lipid species is currently underway via mass spectrometry, using scrapings of the reddish-yellow band from the TLC plate.

While Dak1p is found predominantly in the cytosol of *S. cerevisiae* cells, the cellular localisation of Dak2p was not previously known (Huh et al., 2003). This study demonstrated that Dak2p is localised in the large compartment/organelle formed in wild-type cells over-expressing *DAK2*-GFP. Based on the intensity of Dak2p-GFP fluorescence, it appeared that Dak2p localised around the periphery of the large globular compartment. This is interesting since redistribution of Dak2p-GFP produced in the cytosol of cells would require translocation/partitioning from the aqueous phase of the cytosol onto the large globular compartment/organelle. Interestingly, no known signal sequences or transmembrane regions were identified on Dak2p using the Yeast Resource Center Public Data Repository database (www.yeastrc.org/pdr) (Malmstrom et al., 2007; Reynolds et al., 2008; Riffle et al., 2005).

To further understand the cellular function of Dak2p and its translocation onto the periphery of the cellular compartment/organelle, a number of key future experiments need be conducted. For example, to determine if the cellular compartment/organelle is derived from the ER, wild-type cells over-expressing *DAK2* can be transformed with an ER protein tagged with a red fluorescent marker such as Erg6p-DsRed. While Erg6p is found mainly on LDs, it is also localised on the ER membrane prior to budding of LDs (Athenstaedt, et al., 1999; Binns, et al., 2006). Use of DsRed fluorescent marker allows for co-localisation studies with A β ₄₂GFP since its emission spectrum does not overlap with that of GFP. Furthermore, detailed analysis of the possible proteins and lipids accumulating in the large globular compartments of wild-type cells overexpressing *DAK2* is required. Analysis of subcellular fractions of this compartment/organelle using

a lipidomic/metabolomic approach to identify changes in metabolites may be informative. Examples of such metabolites/intermediates may be dihydroxyacetone (DHA) or dihydroxyacetone phosphate (DHAP).

Interestingly, upon DHA supplementation a significant increase in the proportion of wild-type cells exhibiting A β ₄₂GFP-associated fluorescence was observed. Fluorescent A β ₄₂GFP in wild-type cells was predominantly cytosolic-diffuse or cytosolic-diffuse with single small puncta, which did not appear to occur in a distinct compartment/structure in the cell. DHA is toxic to yeast cells and dihydroxyacetone kinases play an important role by detoxifying these molecules to DHAP. While the double mutant $\Delta dak1 \Delta dak2$ is highly sensitive to DHA, overexpression of either *DAK1* or *DAK2* allows cells to grow on media using DHA as the only carbon source and also makes the $\Delta dak1 \Delta dak2$ double mutant highly resistant to DHA. The uptake of external DHA appears to be via simple diffusion and not protein-mediated (Molin et al., 2003). The large globular compartment formed by *DAK2* over-expression was not present in wild-type cells supplemented with 50 μ M DHA. A possible explanation may be that Dak1p, which converts DHA into DHAP, localises in the cytosol. In a study by Molin and colleagues (2003), it was found that $\Delta dak1$ cells did not exhibit any detectable dihydroxyacetone kinase activity. $\Delta dak2$ cells exhibited similar levels of dihydroxyacetone kinase activity as wild-type cells. Interestingly, while *DAK1* over-expression in the $\Delta dak1 \Delta dak2$ double mutant led to a ~250 fold increase in dihydroxyacetone kinase specific activity, over-expression of *DAK2* in this mutant did not exhibit any dihydroxyacetone kinase specific activity. While this may indicate that Dak2p does not significantly contribute to the overall dihydroxyacetone kinase activity when grown in glucose media, it was shown in cells grown on 50 mM DHA, as carbon source that over-expression of *DAK2* led to significantly higher enzyme specific activity compared to cells over-expressing *DAK1*. Dak2p exhibited a high affinity for DHA in these conditions. At present, the mechanism for the carbon source variability of dihydroxyacetone kinase or DHA-dependent activity of Dak2p is not clearly understood. It is worthwhile noting that the study by Molin and colleagues (2003), over-expression of *DAK1* and *DAK2* genes was under the regulation of the constitutive triose phosphate isomerase *TPH1* promoter.

Interestingly, apart from DHA detoxification, other roles for dihydroxyacetone kinases in *S. cerevisiae* have been proposed. These include the regulation of intracellular glycerol, involvement in the multienzyme transhydrogenase system (Norbeck and Blomberg, 1997) and playing an important role in cellular ATP homeostasis during sudden shifts in growth potential (Blomberg, 2000). Upon disruption of mitochondrial electron transport, *S. cerevisiae* cells use glycerol production to serve as a redox sink by utilising glycerol-3-phosphate dehydrogenases Gpd1p and Gpd2p to maintain intracellular concentrations and availability of NAD⁺ (Bakker et al., 2001).

Interestingly, glycerol production not only serves as a redox sink, but is important for osmoregulation, protecting cells against osmotic stress (Albertyn et al., 1994a; Blomberg and Adler, 1989; Nevoigt and Stahl, 1997). Small organic molecules called osmolytes protect cells from the potentially damaging effects of osmotic stress caused by altered protein structure and folding. The three main osmolyte classes are polyhydric alcohols and sugars (polyols), amino acids and their derivatives and methyl ammonium compounds (Macchi et al., 2012; Yancey et al., 1982). Osmolytes are widely used to stabilise and facilitate protein folding since they are able to act as “chemical chaperones” (Meng et al., 2001; Welch and Brown, 1996). Polyols such as trehalose, sucrose, mannitol, sorbitol, erythritol, glucose, myo-inositol and glycerol are effective in preventing protein aggregation during refolding of many proteins (Buckle et al., 2005; De Bernardez Clark et al., 1999; Mishra et al., 2005). Glycerol, which is one of the smallest and simplest molecules of the polyols, is most widely used to stabilise proteins (Bolen, 2004; Davis-Searles et al., 2001; Feng and Yan, 2008; Gekko and Timasheff, 1981; Tiwari and Bhat, 2006; Vagenende et al., 2009). Taken together with results from the analysis of mutants affected in mitochondrial functions, it is tempting to speculate that disruption of the TCA cycle would affect DHA and glycerol metabolism and alter intracellular levels of these metabolites. However, a more detailed analysis of the mechanism(s) mediating the changes in A β ₄₂GFP fluorescence in the TCA mutants is required, and a metabolomics approach to identify changes in mitochondrial metabolites may be informative.

6 CHAPTER 6: HIGH-CONTENT CHEMICAL AND DRUG SCREENS FOR SMALL MOLECULE MODIFIERS OF AMYLOID-BETA AGGREGATION IN *S. CEREVISIAE*

6.1 Introduction and Aims

Oligomeric forms of the A β in the brain and cerebrospinal fluid have been proposed to play a crucial role in the onset and progression of Alzheimer's disease (AD) (Hardy and Higgins, 1992; Selkoe, 1991; Younkin, 1995). Oligomers of A β that are detergent-stable have been found to be effective neurotoxins against mice and mammalian cell culture (Dahlgren et al., 2002; Kayed et al., 2003; Lambert et al., 1998; Lesne et al., 2006; Walsh et al., 2002a). Unlike monomeric A β , dimeric forms of A β were shown to induce synaptic dysfunction (Klyubin et al., 2008; Walsh et al., 2002a). Previously, identification of drugs/chemical compounds that prevent A β ₄₂ aggregation that ultimately lead to fibrilisation and large plaques were of interest (De Felice and Ferreira, 2002; Estrada and Soto, 2007; Soto et al., 1998). However, with the increasing data indicating a pathological role of soluble oligomeric forms of A β in the onset and early progression of AD, it has been proposed that inhibition of intracellular A β oligomer formation or promotion of large fibril formation may be a viable therapeutic strategy in the prevention and/or treatment of AD (Klein et al., 2001; Walsh et al., 2002b). At present, the dynamic relationship between intracellular oligomers and extracellular plaques is unclear. However, it has been suggested that large fibrillar aggregates or plaques may be inert and possibly aid in preventing formation of highly toxic oligomers (Chen et al., 2010; Cheng et al., 2007; Glabe, 2005; Harper et al., 1999; Kaye et al., 2003; Necula et al., 2007a). Therefore, an effective therapeutic strategy may be to prevent the formation of oligomeric species by allowing it to form large fibrillar forms.

Most studies aimed at analysing inhibition of A β ₄₂ oligomers have mostly been done *in vitro* using synthetic A β ₄₂ peptides under conditions that allow formation of oligomers instead of fibrils (Chang et al., 2003; Chromy et al., 2003; Hamaguchi et al., 2009; Necula et al., 2007b; Yang et al., 2005). However, oligomers formed by synthetic A β ₄₂ peptides are much less stable than those produced in mouse brains or mammalian cell cultures (Walsh et al., 2005). This stability is indicated by the increased proportion

of dimer, trimer and tetramer oligomers in biologically-derived samples compared to synthetic peptide oligomers. In addition, oligomers formed by synthetic A β ₄₂ peptides are less stable than biologically-derived oligomers to SDS. Therefore, *in vitro* screening assays of A β ₄₂ oligomer formation using synthetic peptides may overestimate the effectiveness of a possible ‘disaggregating’ agent (LeVine, 2007; Walsh et al., 2005). However, it is worthwhile to note that ‘disaggregating’ or disassembling A β ₄₂ fibrils appears to be a rare characteristic of small molecule compounds. Unlike compounds that inhibit A β fibrilisation, these so-called ‘fibril disaggregators’ have been a challenge to identify due to the thermodynamic stability of A β fibrils (O’Nuallain et al., 2006). In addition, attempts to characterise the *in vitro* effects of small molecule compounds on oligomer formation have faced many challenges due to the countless number of possible A β ₄₂ oligomeric species that can form *in vitro* and the difficulty in monitoring oligomer formation (Bitan et al., 2005; Hepler et al., 2006). Interestingly, many of the compounds that were first discovered to have an effect on oligomer formation *in vitro* were later found to be toxic when tested *in vivo* (Liu and Schubert, 2006). Studies in mice have shown that it may not be necessary for complete depletion of oligomeric A β species for therapeutic effectiveness, since low levels of trimers and tetramers do not exert toxicity (Lesne et al., 2006). This may be indicative of the presence of cellular clearance or protein degradation mechanisms to get rid of the residual A β oligomers in the brain.

This chapter aimed at developing a yeast *in vivo* high-throughput assay that allows identification of drug/chemical compounds that reduce aggregation of A β ₄₂ and/or increase aggregation of A β ₄₀, based on the A β GFP fusion-associated fluorescence assay, described in Chapter 1. Using this yeast cell-based platform, both the Library of Pharmacologically Active Compounds (LOPAC^{1280®}; Sigma-Aldrich), composed of 1280 compounds, and the Spectrum Collection library (MicroSource Discovery Systems, Gaylordsville, CT, USA), containing 1997 compounds, were screened. In total, 37 drug/chemical compounds that affected A β ₄₂GFP and A β ₄₀GFP aggregation/fluorescence were identified in a pilot screen. Since this work was carried out towards the end of the thesis research candidature, further work needs to be done in the future to validate these chemical/drug compounds to determine interaction between A β ₄₂GFP/A β ₄₀GFP aggregation and the identified compounds.

6.2 Results - Development of a yeast cell-based system for the identification of compounds that affect aggregation of A β ₄₂GFP and A β ₄₀GFP *in vivo* based on A β GFP fusion-associated fluorescence assay

6.2.1 Effect of dimethyl sulfoxide (DMSO) on wild-type (yCG253) *S. cerevisiae* cells expressing A β ₄₂GFP or A β ₄₀GFP

All 3277 chemical/drug compounds from both the LOPAC^{1280®} (Sigma-Aldrich) and the Spectrum Collection (MicroSource Discovery Systems) libraries were solubilised in dimethyl sulfoxide (DMSO). To determine, as a control, whether incubation of wild-type cells expressing A β ₄₂GFP and A β ₄₀GFP in galactose (induction) medium containing 0.2 mM DMSO would affect A β ₄₂GFP and A β ₄₀GFP-associated fluorescence, wild-type (yCG253) *S. cerevisiae* cells (kind gift from Prof. Paul Atkinson, Victoria University of Wellington) were transformed with plasmids encoding GFP fused to the C-terminus of A β ₄₂ or A β ₄₀ (pUG35GAL1-A β ₄₂ and pUG35GAL1-A β ₄₀). Expression of the plasmid-encoded A β GFP fusions was under the regulation of a *GALI* promoter, which induced expression of A β ₄₂GFP or A β ₄₀GFP in galactose medium (SCgal-URA). Wild-type yCG253 cells expressing either A β ₄₂GFP or A β ₄₀GFP co-expressed both a nuclear marker, with a nuclear localisation signal (NLS) tagged to fluorescent marker RedStar2 (NLS-RedStar2) and a cytosolic marker, mCherry expressed in the cytosol, under the regulation of the constitutive *TEF2* promoter (Section 2.14). Both strains were grown to exponential phase (OD₆₀₀ 1.5) in SCgal-URA media, diluted to an OD₆₀₀ 0.1 and re-inoculated into SCgal-URA media lacking or supplemented with 0.2 mM DMSO. Wild-type cells exhibiting A β GFP-associated fluorescence were analysed 4 h after incubation using the Opera[®] High Content Screening System (PerkinElmer, USA) as previously described (Bircham et al., 2011).

Live cells were identified using the NLS-RedStar2 nuclear marker and the mCherry cytosolic marker. During the image analysis, results due to autofluorescence from dead cells and other artefacts were omitted by restricting fluorescence intensity, size and roundness of cells. Wild-type cells expressing the A β ₄₂GFP in media lacking or supplemented with 0.2 mM DMSO yielded very weak A β ₄₂GFP-associated fluorescence that was restricted to 4% \pm 2.0 % of the cell population (Figure 6-1A). In contrast wild-type cells expressing A β ₄₀GFP in media lacking or supplemented with 0.2 mM DMSO yielded a significantly higher ($p < 0.00001$) proportion of fluorescent cells which

exhibited cytosolic-diffuse fluorescence in $45 \% \pm 8\%$ of the cell population (Figure 6-1B). Quantification of fluorescence intensity using the OPERATM high-throughput confocal microscope (PerkinElmer, USA) indicated that the average relative intensity of A β ₄₂GFP-associated fluorescence in wild-type cells was significantly lower ($p < 0.00001$) than those exhibiting A β ₄₀GFP fluorescence. These data indicate that the 0.2 mM DMSO in the galactose (induction) medium and the incubation conditions for the chemical/drug library screens do not alter the A β ₄₂GFP and A β ₄₀GFP-associated fluorescence exhibited by the wild-type cells. Therefore, this supports the use of this yeast model to be used in the screening of chemical libraries (given below) for compounds with amyloidogenic and anti-amyloidogenic properties that may affect intracellular aggregation of A β ₄₂GFP and A β ₄₀GFP.

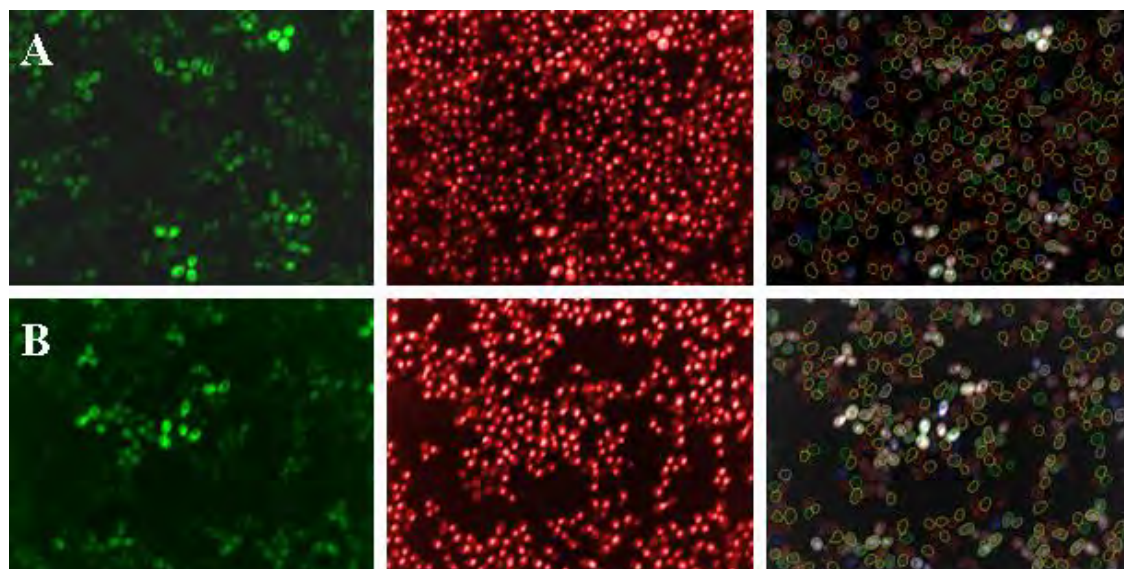


Figure 6-1 Fluorescent microscopic image analysis using Evotec Technologies AcapellaTM image analysis software of wild-type cells expressing A β ₄₂GFP or A β ₄₀GFP grown in galactose (induction) medium containing 0.2 mM DMSO

Wild-type (yCG253) cells expressing (A) A β ₄₂GFP or (B) A β ₄₀GFP were induced in galactose medium supplemented with 0.2 mM DMSO since all the chemical/drug compounds from both LOPAC^{1280®} and the Spectrum Collection libraries were solubilised in DMSO. The presence of DMSO and the incubation conditions for the chemical/drug library screens do not alter the A β ₄₂GFP and A β ₄₀GFP-associated fluorescence exhibited by the wild-type cells. Representative images of A β GFP-associated fluorescence are shown in the left panel. NLS-RedStar2 nuclear and mCherry cytoplasmic RFP fluorescence is shown in the middle panel. Using the RFP fluorescence, whole cells were identified based on whole cell stencils drawn (right panel) for the measurement of fluorescent cell population. 300-500 cells were analysed for each sample.

6.2.2 High content screen for small molecule modifiers that affect A β ₄₂GFP aggregation in *S. cerevisiae*

While cellular processes that affect A β ₄₂ aggregation was investigated in this study, drugs/chemical compounds that may also affect A β ₄₂ aggregation remained to be examined. To identify FDA-approved drugs and other chemical compounds with anti-amyloidogenic properties that may reduce the aggregation propensity of A β ₄₂GFP, a high-throughput screen using the LOPAC^{1280®} (Sigma-Aldrich) and the Spectrum Collection libraries was undertaken. Wild-type cells expressing A β ₄₂GFP were incubated in SCgal-URA (induction) medium lacking or supplemented with 20 μ M chemical/drug compounds and A β GFP-associated fluorescence was analysed at 4 h after incubation using the Opera[®] High Content Screening System (PerkinElmer, USA) as described in Section 2.14.

The high-content screening identified a total of 25 compounds that increased the proportion of cells exhibiting A β ₄₂GFP-associated fluorescence in wild-type cells. HE-NECA, 4-Amino-1,8-naphthalimide, Captopril, GYKI 52466 hydrochloride and Semicarbazide hydrochloride from the LOPAC^{1280®} library (Figure 6-2) and Merbromin, Acriflavinium hydrochloride, Calcein, Isosorbide dinitrate, Aklavine hydrochloride, Hydroxyprogesterone caproate, Hecogenin, Helenine, Tolbutamide, Thiotepa, Isogedunin, Aspartame, Sulfinpyrazone, Glucosaminic acid, Artemisinin, Salicin, Telenzepine hydrochloride, Prednisolone acetate, Carmofur, Euphol and Trazodone hydrochloride from the Spectrum Collection library led to a significant increase in the proportion of fluorescent cells, when the *p*-value threshold was set at 0.001 (Figure 6-3). The data, presented in Table 6-1 and Table 6-2, generated through the analyses of LOPAC and SPECTRUM Collection libraries are the mean of quadruplicate measurements from two biological replicates.

Table 6-1 Screening of the LOPAC library identified 4 compounds which increased levels of A β ₄₂GFP fluorescence in wild-type cells

The *p* – values indicate the significant difference between the proportion of fluorescent cells in control and treated conditions.

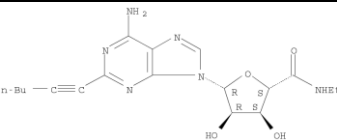
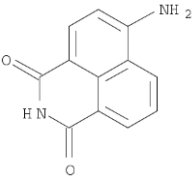
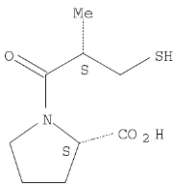
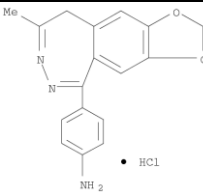
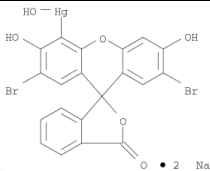
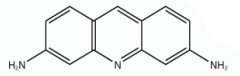
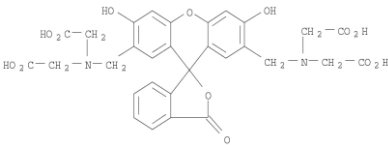
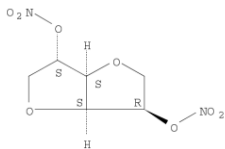
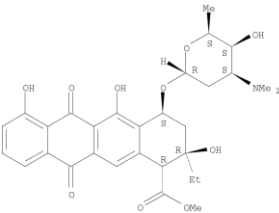
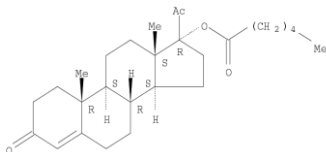
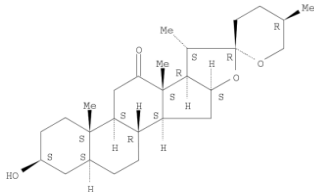
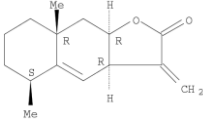
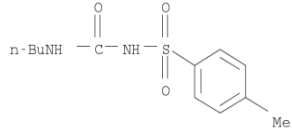
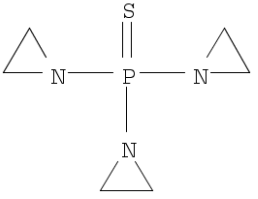
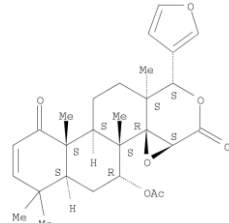
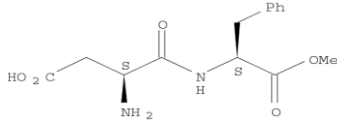
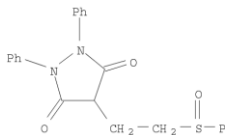
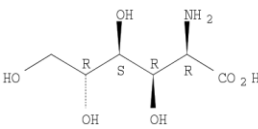
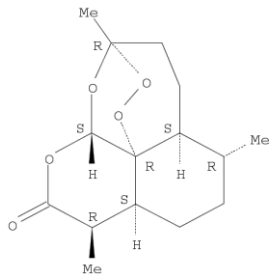
Name of drug	CAS number	Molecular formula	Molecular weight	Structure	Bioactivity	<i>p</i> – value
HE-NECA	141018-30-6	C ₁₈ H ₂₄ N ₆ O ₄	388.42		A2A and A3 adenosine receptor agonist; Hypotensive and antipsychotic agent via A2A receptor.	3.2E-05
4-Amino-1,8-naphthalimide	1742-95-6	C ₁₂ H ₈ N ₂ O ₂	212.20		Sensitises cells to radiation-induced cell damage and enhances the cytotoxicity of 1-methyl-3-nitro-1-nitrosoguanidine.	5.5E-05
Captopril	62571-86-2	C ₉ H ₁₅ NO ₃ S	217.29		Angiotensin converting enzyme inhibitor (similar to enalapril, which lacks one sulfhydryl group and is more potent). Inhibits the formation of angiotensin II, a bioactive peptide that stimulates angiogenesis and increases microvessel density.	7.7E-05
GYKI 52466 hydrochloride	192065-56-8	C ₁₇ H ₁₅ N ₃ O ₂ · HCl	329.78		Selective allosteric AMPA receptor antagonist; anti-convulsant; skeletal muscle relaxant.	0.00011

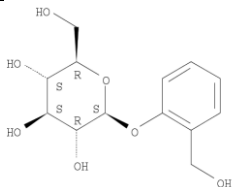
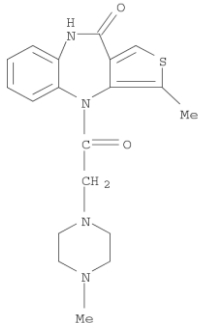
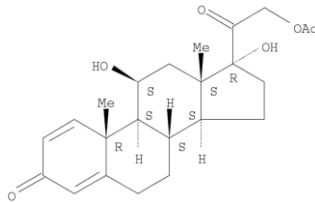
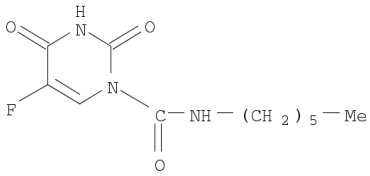
Table 6-2 Screening of the SPECTRUM Collection library identified 21 compounds which increased levels of A β ₄₂GFP fluorescence in wild-type cells

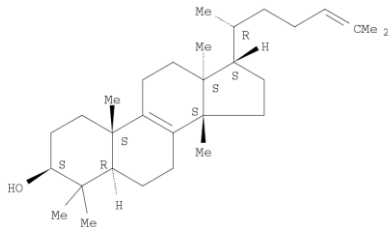
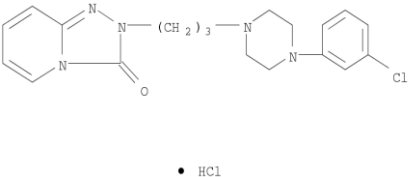
The *p* – values indicate the significant difference between the proportion of fluorescent cells in control and treated conditions.

Name of drug	CAS number	Molecular Formula	Molecular Weight	Structure	Bioactivity	<i>p</i> – value
Merbromin	129-16-8	C ₂₀ H ₈ Br ₂ Hg Na ₂ O ₆	750.66		Antibacterial	1.9E-34
Acridflavinium Hydrochloride	8018-07-3	C ₁₄ H ₁₄ ClN ₃	259.74		Anti-infective, intercalating agent	2.6E-32
Calcein	1461-15-0	C ₃₀ H ₂₆ N ₂ O ₁₃	622.55		Chelating agent (Ca, Mg)	2.6E-32
Isosorbide Dinitrate	87-33-2	C ₆ H ₈ N ₂ O ₈	236.14		Anti-anginal	2.6E-32
Aklavine Hydrochloride	60504-57-6	C ₃₀ H ₃₆ ClNO 10	606.08		Antibacterial, antineoplastic	3.5E-12

Name of drug	CAS number	Molecular Formula	Molecular Weight	Structure	Bioactivity	<i>p</i> – value
Hydroxyprogesterone Caproate	630-56-8	C ₂₇ H ₄₀ O ₄	428.62		Progestogen	6.4E-12
Hecogenin	467-55-0	C ₂₇ H ₄₂ O ₄	430.63		Anti-inflammatory	1.4E-08
Helenine	546-43-0	C ₁₅ H ₂₀ O ₂	232.33		Anthelmintic, antibacterial, antineoplastic	3.8E-06
Tolbutamide	64-77-7	C ₁₂ H ₁₈ N ₂ O ₃ S	270.35		Antidiabetic, sulfonylurea compound that is a hypoglycemic agent	4.3E-06
Thiotepa	52-24-4	C ₆ H ₁₂ N ₃ PS	189.22		Antineoplastic, polyfunctional alkylating agent; DNA alkylating and crosslinking drug to induce chromosome aberrations and nucleotide and base excision repair-type DNA damage.	9.1E-06

Name of drug	CAS number	Molecular Formula	Molecular Weight	Structure	Bioactivity	<i>p</i> – value
Isogedunin	5574-02-07	C ₂₈ H ₃₄ O ₇	482.58			1.7E-05
Aspartame	22839-47-0	C ₁₄ H ₁₈ N ₂ O ₅	294.31		Sweetener	2.3E-05
Sulfinpyrazone	57-96-5	C ₂₃ H ₂₀ N ₂ O ₃ S	404.49		Uricosuric	5.8E-05
Glucosaminic Acid	3646-68-2	C ₆ H ₁₃ NO ₆	195.17			9.9E-05
Artemisinin	63968-64-9	C ₁₅ H ₂₂ O ₅	282.34		Sesquiterpene lactone; highly active anti-malarial (falciparum malaria); anthelmintic (parasitic worm) effective against the blood fluke, schistosomiasis	0.0001

Name of drug	CAS number	Molecular Formula	Molecular Weight	Structure	Bioactivity	<i>p</i> – value
Salicin	138-52-3	C ₁₃ H ₁₈ O ₇	286.28		Analgesic, antipyretic	0.0003
Telenzepine Hydrochloride	80880-90-6	C ₁₉ H ₂₃ ClN ₄ O ₂ S	406.94		Antiulcer, M1 muscarinic antagonist	0.0003
Prednisolone Acetate	52-21-1	C ₂₃ H ₃₀ O ₆	402.49		Glucocorticoid	0.0004
Carmofur	61422-45-5	C ₁₁ H ₁₆ FN ₃ O ₃	257.27		Derivative of fluorouracil, an antimetabolite used as an antineoplastic agent	0.0006

Name of drug	CAS number	Molecular Formula	Molecular Weight	Structure	Bioactivity	<i>p</i> – value
Euphol	514-47-6	C ₃₀ H ₅₀ O	426.73			0.0008
Trazodone Hydrochloride	25332-39-2, 19794-93-5	C ₁₉ H ₂₃ Cl ₂ N ₅ O	408.33		Antidepressant that potentiates the activity of serotonin uptake blockers; 5-HT _{2C} serotonin receptor agonist activity. It is metabolised to the 5-HT ₁ serotonin receptor agonist 1-(3-Chlorophenyl) piperazine.	0.0008

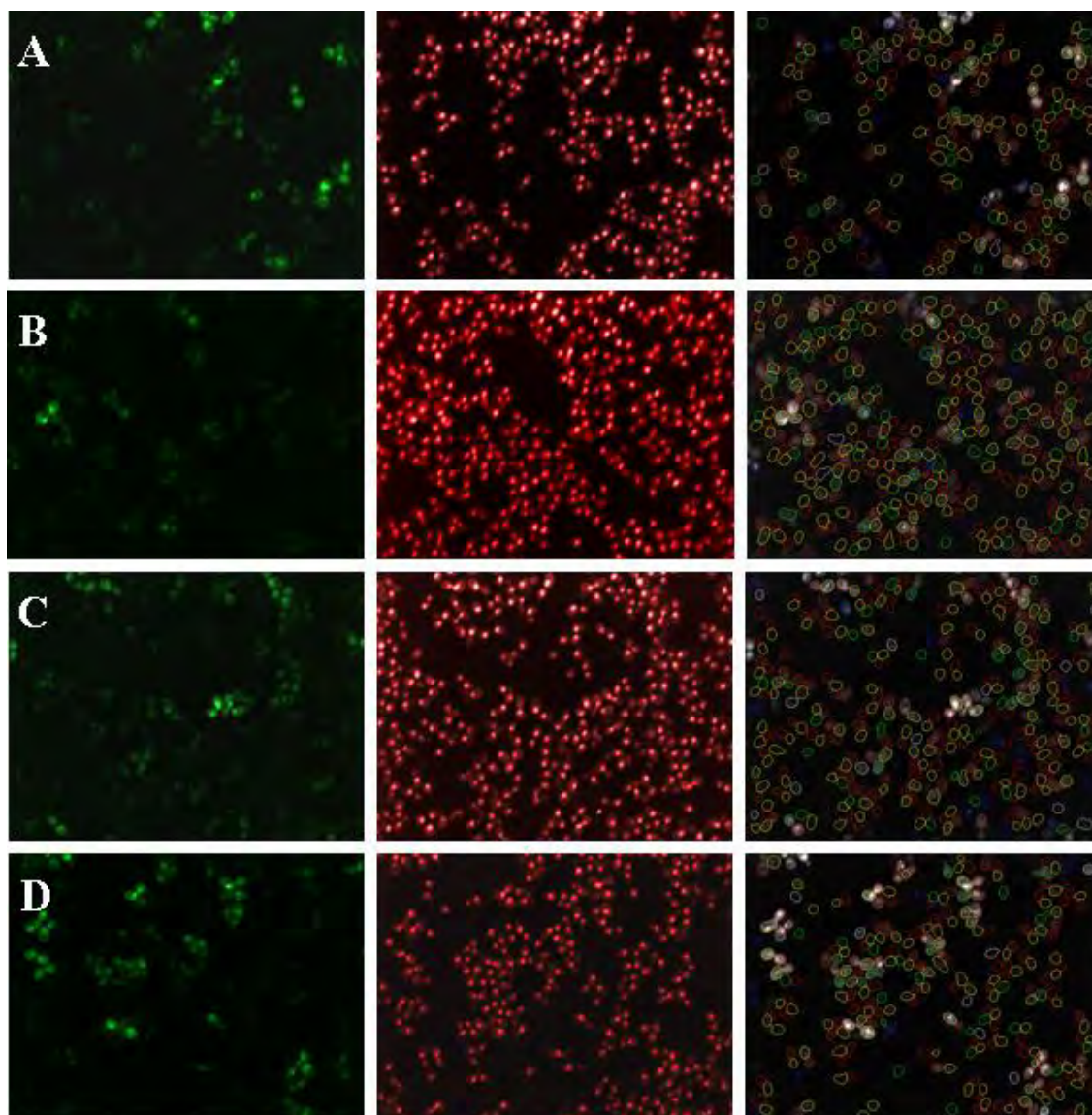


Figure 6-2 Fluorescent microscopic image analysis using Evotec Technologies Acapella™ image analysis software of wild-type cells expressing Aβ₄₂GFP grown in media supplemented with 20 μM of a specific drug/chemical compound from the LOPAC^{1280®} library

Wild-type cells expressing Aβ₄₂GFP were induced in galactose medium supplemented with a specific drug/chemical compound from the LOPAC^{1280®} library that increased the proportion of fluorescent cells compared to control cells: A) HE-NECA, B) 4-Amino-1,8-naphthalimide, C) Captopril and D) GYKI 52466 hydrochloride. Representative images of Aβ₄₂GFP-associated fluorescence are shown in the left panel. NLS-RedStar2 nuclear and mCherry cytoplasmic RFP fluorescence is shown in the middle panel. Using the RFP fluorescence, whole cells were identified based on whole cell stencils drawn (right panel) for the measurement of fluorescent cell population. 300-500 cells were analysed for each sample.

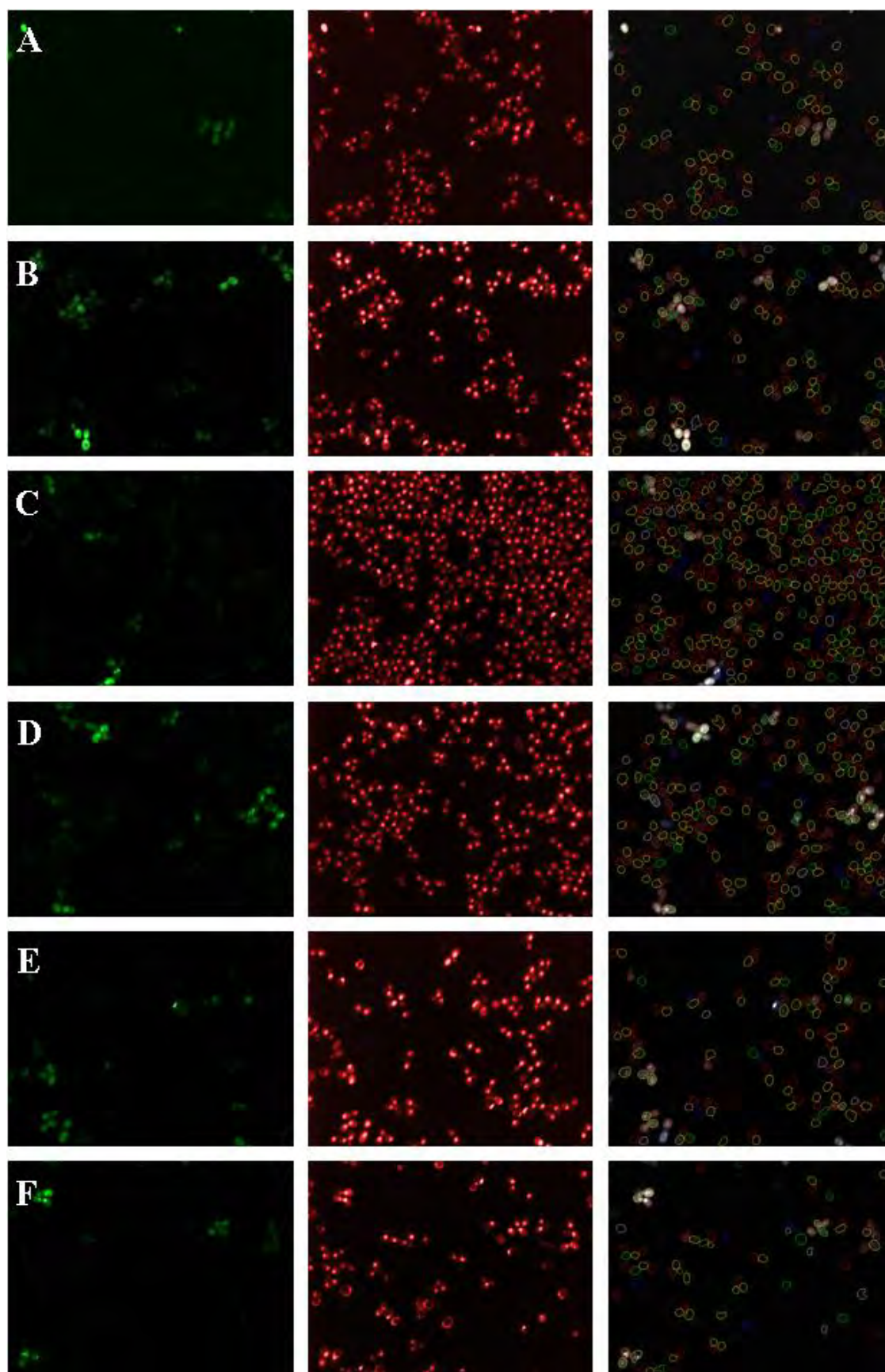


Figure 6-3 Fluorescent microscopic image analysis using Evotec Technologies Acapella™ image analysis software of wild-type cells expressing Aβ₄₂GFP grown in

media supplemented with 20 μ M of a specific drug/chemical compound from the SPECTRUM Collection library.

Wild-type cells expressing A β ₄₂GFP were induced in galactose medium supplemented with specific drug/chemical compound from the SPECTRUM Collection library that increased the proportion of fluorescent cells compared to control cells: A) Isosorbide dinitrate, B) Thiotepe, C) Isogedunin, D) Aspartame, E) Salicin and F) Euphol. Representative images of A β ₄₂GFP-associated fluorescence are shown in the left panel. NLS-RedStar2 nuclear and mCherry cytoplasmic RFP fluorescence is shown in the middle panel. Using the RFP fluorescence, whole cells were identified based on whole cell stencils drawn (right panel) for the measurement of fluorescent cell population. 300-500 cells were analysed for each sample.

6.2.3 High content screen for small molecule modifiers that reduce A β ₄₀GFP fluorescence in *S. cerevisiae*

A β toxicity has been shown to correlate with the presence of β -sheet structures (Howlett et al., 1995; Seilheimer et al., 1997; Simmons et al., 1994). A β aggregation proceeds by a multistep, nucleation-dependent process (Jarrett and Lansbury, 1993). Formation of nucleation seeds is rate limiting, in the absence of preformed seed fibrils there is a significant lag period for the formation of A β fibrils, followed by a rapid fibril elongation phase once seed fibrils have been generated. The lag time for fibril formation can be dramatically shortened by adding preformed fibril seeds to A β monomer (Jarrett and Lansbury, 1993) and the rate of A β fibril formation is controlled by both fibril seed and monomer concentrations (Naiki and Nakakuki, 1996). In Section 3.2.4, it was demonstrated that the co-induction of A β ₄₂GFP and A β ₄₀GFP in wild-type cells gave rise to more fluorescent cells (~22%) than those expressing A β ₄₂GFP alone (5%) but significantly fewer than cells expressing A β ₄₀GFP alone (~40%). Cells expressing both A β ₄₂GFP and A β ₄₀GFP exhibited trace cytosolic fluorescence with intense large puncta and in some cells there were elongated structures. The increased presence of puncta and lower levels of cytosolic fluorescence in wild-type cells co-expressing A β ₄₂GFP and A β ₄₀GFP indicate that the more aggregation prone A β ₄₂GFP can act as a seed for aggregation. While, preformed A β ₄₂GFP aggregates formed in the cytosol may accelerate nucleation and act as seeds for further formation of intracellular aggregates; A β ₄₀GFP, which has a less propensity to aggregate may favour aggregation under certain conditions or in the presence of certain metabolites or compounds.

Therefore, to identify FDA-approved drugs and other chemical compounds with amyloidogenic properties that may increase the aggregation propensity of A β ₄₀GFP, a high-throughput screen using the LOPAC^{1280®} (Sigma-Aldrich) and the Spectrum

Collection libraries was undertaken. Wild-type cells expressing A β ₄₀GFP were incubated in SCgal-URA (induction) media lacking or supplemented with 20 μ M chemical/drug compounds and A β GFP-associated fluorescence was analysed after 4 h incubation using the Opera[®] High Content Screening System (PerkinElmer, USA) as described in Section 2.14.

The high-content screening identified a total of 17 compounds that decreased the proportion of cells exhibiting A β ₄₀GFP-associate fluorescence in wild-type cells. Tulobuterol hydrochloride, cis-Azetidine-2,4-dicarboxylic acid, Doxycycline hydrochloride and SKF 89976A hydrochloride from the LOPAC^{1280®} library (Figure 6-4) and Merbromin, Acriflavinium hydrochloride, Calcein, Isosorbide dinitrate, Tolbutamide, Rosolic acid, Broxyquinoline, Griseofulvin analog A, 18 α -glycyrrhetic acid, Clioquinol, Periplocymarin, Cycloheximide and Haematoporphyrin dihydrochloride from the Spectrum Collection library led a significant decrease in the proportion of fluorescent cells, when the *p*-value threshold was set at 0.001 (Figure 6-5). The data, presented in Table 6-3 and Table 6-4, generated through the analyses of LOPAC and SPECTRUM Collection libraries are the mean of quadruplicate measurements from two biological replicates.

Table 6-3 Screening of the LOPAC library identified 4 compounds which decreased levels of A β ₄₀GFP fluorescence in wild-type cells**The *p* – values indicate the significant difference between the proportion of fluorescent cells in control and treated conditions.**

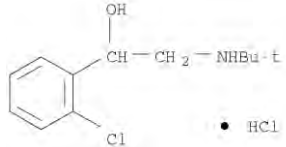
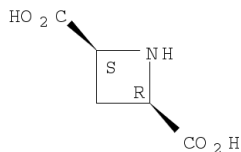
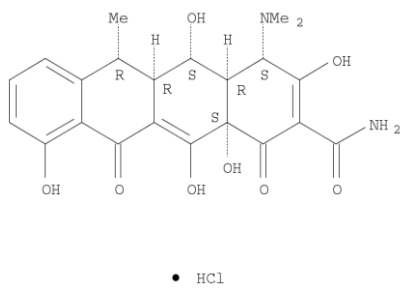
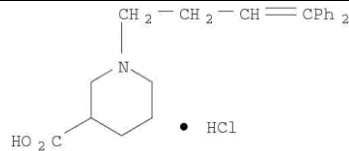
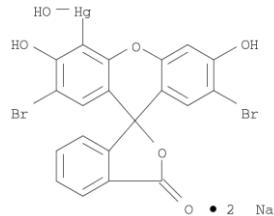
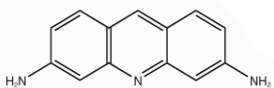
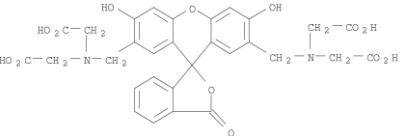
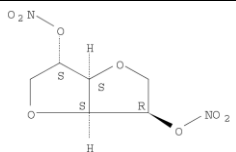
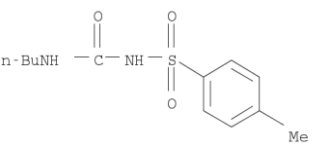
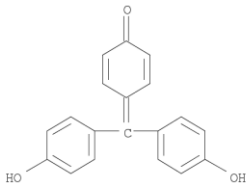
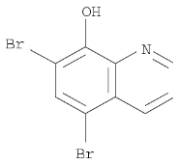
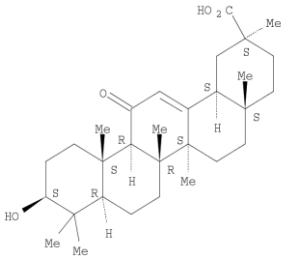
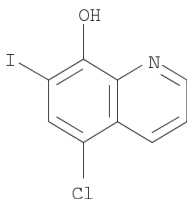
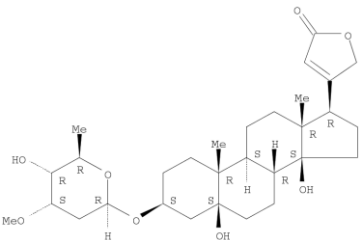
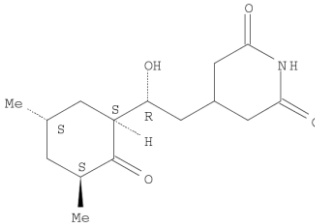
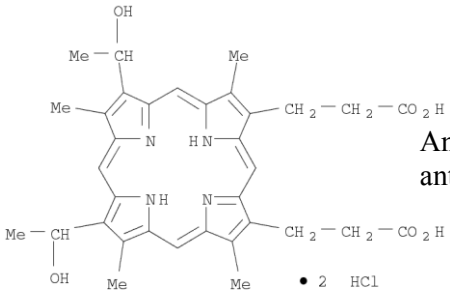
Name of drug	CAS number	Molecular formula	Molecular weight	Structure	Bioactivity	<i>p</i> – value
Tulobuterol hydrochloride	56776-01-3	C ₁₂ H ₁₈ ClNO · HCl	264.19			0.0001
cis-Azetidine-2,4-dicarboxylic acid	121050-04-2	C ₅ H ₇ NO ₄	145.12		NMDA glutamate receptor modulator.	0.0005
Doxycycline hydrochloride	10592-13-9	C ₂₂ H ₂₄ N ₂ O ₈ · HCl · 0.5H ₂ O · 0.5C ₂ H ₆ O	512.94		Derivative of oxytetracycline; broad spectrum antibiotic and bacteriostatic agent; antiprotozoal; used in the treatment of chlamydia, rickettsia, mycoplasma, and some spirochete infections; broad spectrum inhibitor used to inhibit matrix metallo-proteinases such as type 1 collagenase	0.001
SKF 89976A hydrochloride	85375-85-5	C ₂₂ H ₂₅ NO ₂ · HCl	371.9		GABA transporter type 1 (GAT-1) inhibitor that crosses the blood brain barrier.	0.001

Table 6-4 Screening of the SPECTRUM Collection library identified 13 compounds which decreased levels of A β ₄₀GFP fluorescence in wild-type cells

The *p* – values indicate the significant difference between the proportion of fluorescent cells in control and treated conditions.

Name of drug	CAS number	Molecular Formula	Molecular Weight	Structure	Bioactivity	<i>p</i> – value
Merbromin	129-16-8	C ₂₀ H ₈ Br ₂ HgNa ₂ O ₆	750.66		Antibacterial	1.5E-20
Acriflavinium Hydrochloride	8018-07-3	C ₁₄ H ₁₄ ClN ₃	259.74		Antiinfective, intercalating agent	3.0E-20
Calcein	1461-15-0	C ₃₀ H ₂₆ N ₂ O ₁₃	622.55		Chelating agent (Ca, Mg)	3.0E-20
Isosorbide Dinitrate	87-33-2	C ₆ H ₈ N ₂ O ₈	236.14		Antianginal	1.0E-08
Tolbutamide	64-77-7	C ₁₂ H ₁₈ N ₂ O ₃ S	270.35		Antidiabetic	7.2E-07

Name of drug	CAS number	Molecular Formula	Molecular Weight	Structure	Bioactivity	<i>p</i> – value
Rosolic Acid	603-45-2	C ₁₉ H ₁₄ O ₃	290.32		Diagnostic aid	9.3E-06
Broxyquinoline	521-74-4	C ₉ H ₅ Br ₂ NO	302.95		Antiinfectant, disinfectant	0.0003
Griseofulvin Analog A		C ₁₅ H ₁₀ Cl ₂ O ₅	341.15		Antifungal	0.0004
18α-Glycyrrhetic Acid	1449-05-4	C ₃₀ H ₄₆ O ₄	470.70		Anti-inflammatory	0.0005
Clioquinol	130-26-7	C ₉ H ₅ ClINO	305.50		Antiseptic, antiamebic	0.0006

Name of drug	CAS number	Molecular Formula	Molecular Weight	Structure	Bioactivity	<i>p</i> – value
Periplocymarin	32476-67-8	C ₃₀ H ₄₆ O ₈	534.70			0.0007
Cycloheximide	66-81-9	C ₁₅ H ₂₃ NO ₄	281.35		Protein synthesis inhibitor	0.0009
Haemato-porphyrin Dihydro-chloride	17696-69-4	C ₃₄ H ₄₀ Cl ₂ N ₄ O ₆	671.63	 • 2 HCl	Antidepressant, antineoplastic	0.0009

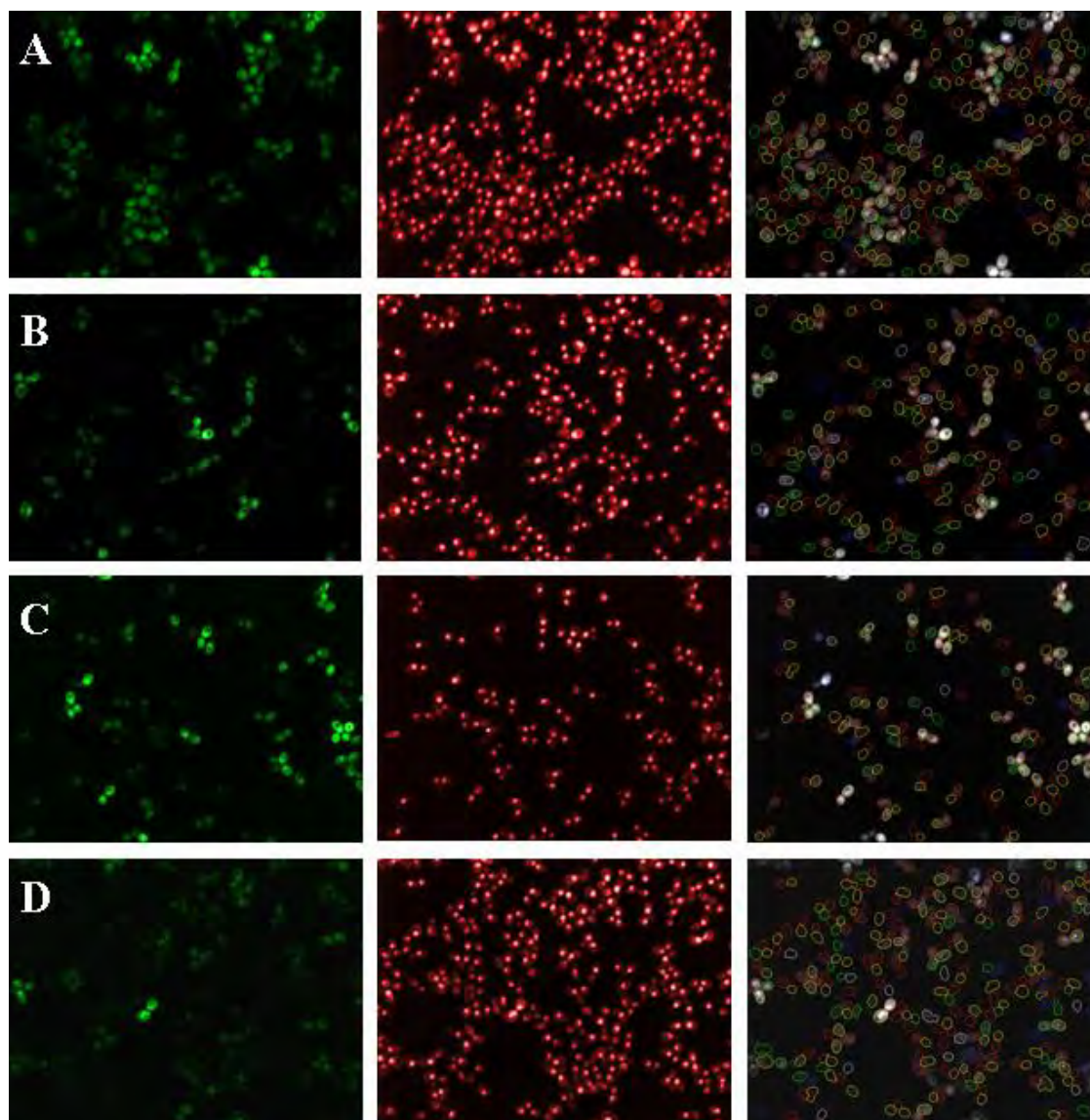


Figure 6-4 Fluorescent microscopic image analysis using Evotec Technologies Acapella™ image analysis software of wild-type cells expressing A β ₄₀GFP grown in media supplemented with 20 μ M of a specific drug/chemical compound from the LOPAC^{1280®} library.

Wild-type cells expressing A β ₄₀GFP were induced in galactose medium supplemented with a specific drug/chemical compound from the LOPAC^{1280®} library that decreased the proportion of fluorescent cells compared to control cells: A) Doxycycline hydrochloride, B) SKF 89976A hydrochloride, C) Tulobuterol hydrochloride and D) cis-Azetidine-2,4-dicarboxylic acid. Representative images of A β ₄₀GFP-associated fluorescence are shown in the left panel. NLS-RedStar2 nuclear and mCherry cytoplasmic RFP fluorescence is shown in the middle panel. Using the RFP fluorescence, whole cells were identified based on whole cell stencils drawn (right panel) for the measurement of fluorescent cell population. 300-500 cells were analysed for each sample.

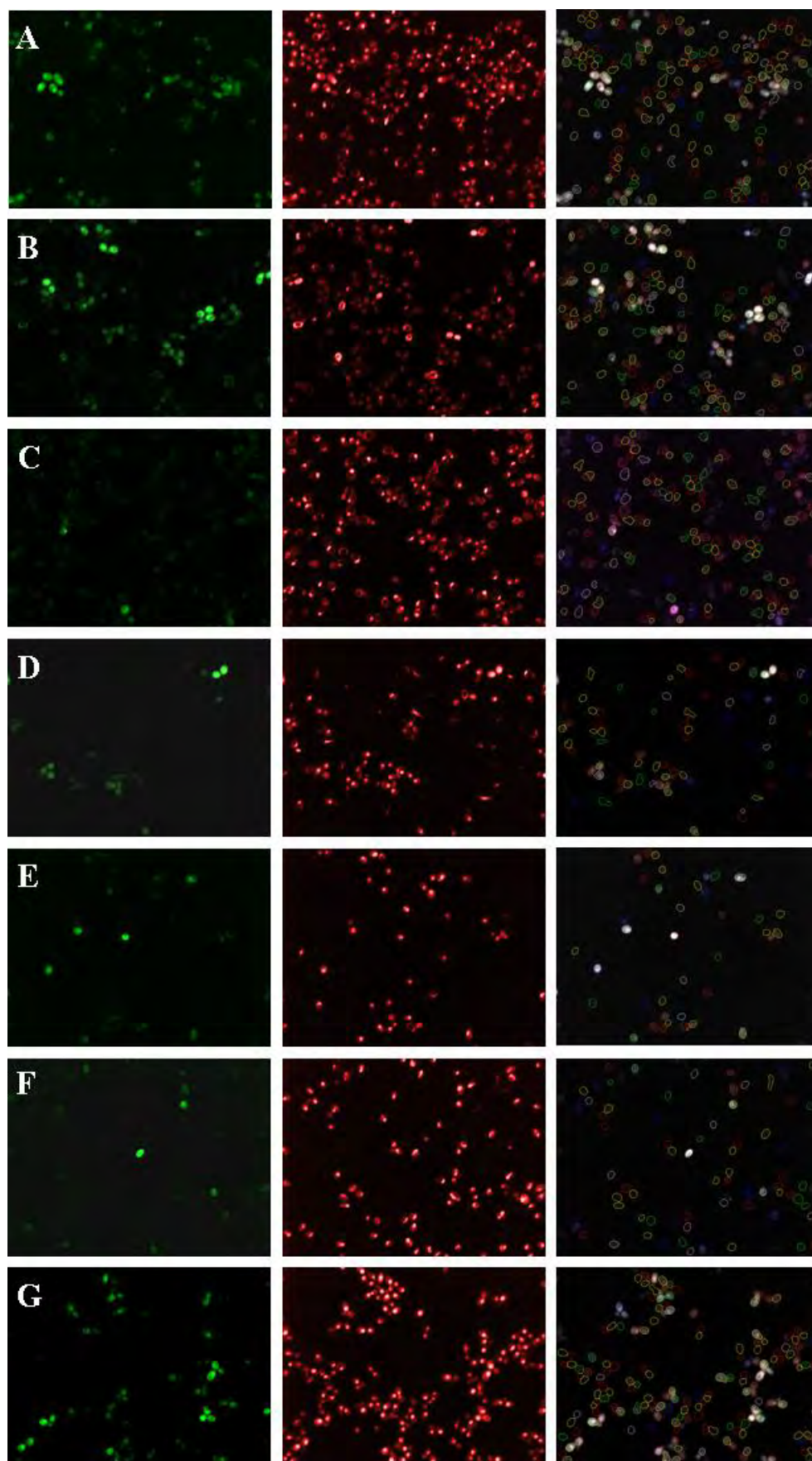


Figure 6-5 Fluorescent microscopic image analysis using Evotec Technologies Acapella™ image analysis software of wild-type cells expressing Aβ₄₀GFP grown in

media supplemented with 20 μ M of a specific drug/chemical compound from the SPECTRUM Collection library.

Wild-type cells expressing A β ₄₀GFP were induced in galactose medium supplemented with a specific drug/chemical compound from the SPECTRUM Collection library that decreased the proportion of fluorescent cells compared to control cells: A) Isosorbide dinitrate, B) Rosolic acid, C) Broxyquinoline, D) 18 α -glycyrrhetic acid, E) Clioquinol, F) Cycloheximide and G) Haematoporphyrin dihydrochloride. Representative images of A β ₄₀GFP-associated fluorescence are shown in the left panel. NLS-RedStar2 nuclear and mCherry cytoplasmic RFP fluorescence is shown in the middle panel. Using the RFP fluorescence, whole cells were identified based on whole cell stencils drawn (right panel) for the measurement of fluorescent cell population. 300-500 cells were analysed for each sample.

6.3 Discussion

The highly conserved cellular processes shared between *S. cerevisiae* and higher eukaryotes, ease of genetic manipulation, amenability to large scale genome-wide functional studies and the relatively lower cost of culturing yeast cells compared to mammalian cells collectively make *S. cerevisiae* an attractive organism for performing high-throughput yeast cell-based screens for drug discovery and development of therapeutic targets. While fibrillar forms of A β are found extracellularly, oligomeric species of A β found intracellularly are more toxic (Lesne et al., 2006; Walsh et al., 2000). Therefore, drugs that reduce the A β load in the interstitial fluid may be less effective than compounds that inhibit A β oligomer formation. This may mean that drugs need to be able to be taken up across the cell membrane for maximum therapeutic effectiveness. This may be another advantage of using the *S. cerevisiae* model.

However, it is also important to appreciate that *S. cerevisiae* cells may present certain disadvantages: i) presence of a cell wall, composed of ~25% helical β (1-3) and β (1-6)-D-glucans and ~25% oligo-mannans, ~20 % protein, ~10% lipids and chitin (Kapteyn et al., 1996; Kollar et al., 1995), may limit permeability to some compounds; ii) presence of highly efficient membrane efflux pumps comprised of ATP-binding cassette (ABC) transporters. Transcriptional regulators Pdr1p and Pdr3p play an important role in cellular detoxification by co- and auto-regulation of these ABC drug efflux pumps and the circuits of pleiotropic drug resistance in *S. cerevisiae*, analogous to the mammalian multiple drug resistance (Balzi and Goffeau, 1995; Decottignies and Goffeau, 1997; Kolaczowski et al., 1998). It has been shown previously that deleting *PDR1* and *PDR3* genes disrupts the efflux pump system, alleviates drug resistance and

instead causes drug hypersensitivity (Egner and Kuchler, 1996). In a recent study, it was shown that strains deleted for *PDR1*, *PDR3*, *PDR5* and other genes associated with pleiotropic drug resistance exhibited remarkably different phenotypes to lovastatin, a statin drug which disrupts sterol biosynthesis in *S. cerevisiae*. Interestingly, deletion of *ERG6*, involved in ergosterol biosynthesis, was found to enhance chemical uptake and counter drug resistance in cells. Ergosterol is important for membrane stability and altered sterol composition in the $\Delta erg6$ mutant was found to enhance chemical uptake (Dunstan et al., 2002; Sharma, 2006; Welihinda et al., 1994). This is verified by the increased sensitivity to cycloheximide in cells (Park et al., 2011). Since data from the previous chapters in this study, including the genome-wide screen, identified lipid homeostasis/metabolism as an important biological process affecting A β aggregation, the $\Delta erg6$ mutant and the $\Delta pdr1 \Delta pdr3$ double mutant were not used in this study. However, it is interesting to note that cycloheximide was identified to affect A β_{40} GFP-associated fluorescence.

In this study a yeast cell-based *in vivo* high-throughput assay that allows identification of drug/chemical compounds that affect A β_{42} and A β_{40} aggregation was developed based on the A β GFP fusion-associated fluorescence assay, described in Chapter 1. Briefly, compounds were identified that increased or decreased the proportion of wild-type cells expressing A β_{42} GFP or A β_{40} GFP-associated fluorescence, respectively. Using this yeast cell-based platform, both the Library of Pharmacologically Active Compounds (LOPAC¹²⁸⁰®; Sigma-Aldrich), composed of 1280 compounds, and the Spectrum Collection library (MicroSource Discovery Systems, Gaylordsville, CT, USA), containing 1997 compounds, were screened. Of the 3277 drug/chemical compounds screened in the pilot screen, 25 compounds were identified that reduced A β_{42} GFP aggregation since increased levels of A β_{42} GFP-associated fluorescence were observed in wild-type cells; while 17 compounds were found to increase A β_{40} GFP aggregation since significantly reduced levels of A β_{40} GFP-associated fluorescence were observed. Interestingly, five compounds, Merbromin, Acriflavinium hydrochloride, Calcein, Isosorbide dinitrate and Tolbutamide were found to exhibit both amyloidogenic and anti-amyloidogenic properties since increased levels of A β_{42} GFP fluorescence as well as reduced levels of A β_{40} GFP fluorescence were observed in wild-type cells (Figure 6-6). At present, it is unclear why this occurred; one

possible explanation may be that these compounds interact differently with both A β ₄₂GFP and A β ₄₀GFP peptides, leading to differences in the aggregation kinetics of these A β GFP fusions. Due to the capacity of these compounds to form soluble A β ₄₂GFP and aggregated forms of A β ₄₀GFP, these data may potentially change the way these five chemical/drug compounds are currently prescribed and/or administered since they may potentially exacerbate AD symptoms and/or disease progression. Work is currently underway, through detailed biochemical analyses, to verify if these compounds do indeed directly affect A β ₄₂GFP or A β ₄₀GFP aggregation *in vivo*. Here, a few compounds were selected from the pilot screen for further discussion.

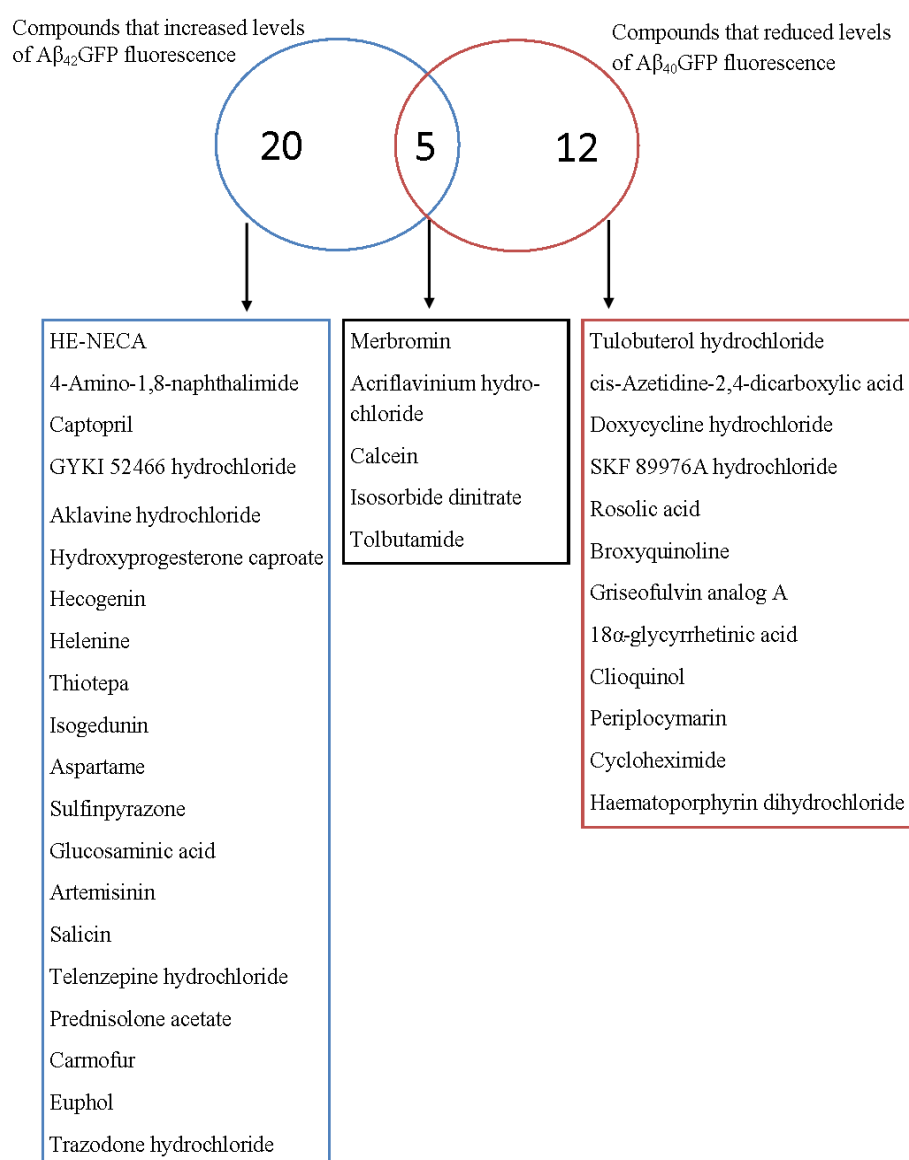


Figure 6-6 Schematic overview of compounds identified from the chemical/drug libraries that affected A β ₄₂GFP or A β ₄₀GFP-associated fluorescence.

6.3.1 Tetracycline and its derivatives

Treatment with doxycycline, a synthetic derivative of oxytetracycline, significantly reduced ($p < 0.001$) the proportion of wild-type cells expressing A β ₄₀GFP-associated fluorescence. Doxycycline appeared to increase the aggregation propensity of A β ₄₀GFP therefore causing a reduction in the portion of wild-type cells expressing A β ₄₀GFP-associated fluorescence. No effects were observed on wild-type cells expressing A β ₄₂GFP when treated with doxycycline. Doxycycline belongs to the class of bacteriostatic tetracycline antibiotics. It is also a broad spectrum inhibitor used to inhibit matrix metallo-proteinases such as type 1 collagenase. The pluripotency of tetracycline drugs is demonstrated by their ability to affect mammalian cellular processes including cell proliferation, migration, apoptosis and matrix remodelling (Bendeck et al., 2002). Interestingly, it was shown that tetracycline and doxycycline exhibited anti-amyloidogenic properties by inhibiting A β aggregation and disaggregating preformed fibrils (Forloni et al., 2001). It was also shown recently that doxycycline inhibits immunoglobulin light chain amyloid fibrilisation in both *in vivo* and *in vitro* studies (Ward et al., 2011). Systemic amyloidosis results from the aggregation of an amyloidogenic immunoglobulin light chain and amyloid fibrils rapidly accumulate in many organs. Ward and colleagues (2011) further demonstrated that doxycycline treatment reduced the number of intact immunoglobulin light chain fibrils which subsequently led to large disordered aggregates forming. However, this anti-amyloidogenic effect of tetracyclines, including doxycycline, does not appear to be limited to only A β and immunoglobulin light chain fibrils. A pathological hallmark of familial amyloidotic polyneuropathy, an autosomal dominant disease, is the extracellular deposition of variant forms of transthyretin protein in fibrillar structures in association with peripheral nerves (Coimbra and Andrade, 1971; Saraiva, 2001). It was shown that treatment of transthyretin fibrils using tetracycline and three other derivatives of tetracycline, including rolitetracycline, minocycline and doxycycline, disrupted fibril formation by disaggregating fibrillar structures. Interestingly, doxycycline demonstrated the highest disaggregation activity.

The molecular mechanism of the anti-amyloidogenic activity of this class of antibiotics is unclear. However, since tetracycline and its derivatives appear to affect amyloid fibrils in general, it may be related to the propensity of these drugs to bind the

fibrillar structures. Since the hydrophobic interactions mediated by the C-terminus of the A β peptide are important for the stability of fibril formation (De Felice et al., 2001; Kim and Hecht, 2005), one possible explanation may be that hydrophobic compounds may be effective in destabilising and disaggregating A β fibrils. Congo red, a charged and hydrophilic molecule, is widely used to stain amyloid oligomers and fibrils since it binds with these aggregated species with high affinity both *in vitro* and *in vivo*. Tetracyclines, which share structural analogies with Congo red, contain an extended hydrophobic core formed by aromatic moieties. Therefore, these antibiotics are lipophilic and readily accessible to the central nervous system (Yrjanheikki et al., 1998). This makes it an important factor to consider in individuals with neurodegenerative diseases caused by amyloidogenesis. Interestingly, minocycline is able to cross the blood–brain barrier and exert a neuroprotective effect in transgenic models of amyotrophic lateral sclerosis and Huntington disease. This neuroprotective effect has been proposed to be caused by inhibition of caspase-1 and 3 (Chen et al., 2000; Zhu et al., 2002). However, characterisation of tetracycline and its derivatives for their anti-amyloidogenic activity and neuroprotection requires further examination.

While doxycycline has a safe toxicological profile, it is unlikely that it would be used as a potential AD drug at higher concentrations because of the pluripotent nature of the drug (described above). Since there is a high degree of similarity between the protein synthesis machinery in prokaryotes and eukaryotic mitochondria, tetracycline drugs and its derivatives inhibit mitochondrial protein synthesis by not allowing binding of the aminoacyl t-RNA to the ribosome; therefore, disrupting mitochondrial protein synthesis (Clark and Chang, 1965; Kroon and Van den Bogert, 1983). However, chemical modifications to its structure can be used to eliminate its bacteriostatic property to generate compounds that affect oligomer formation without inhibiting fibril formation. For example, Col-3 (4-dedimethylaminosancycline), a chemically modified tetracycline that lacks antimicrobial activity but inhibits matrix metalloproteinases and possesses anticollagenase activity, is now the subject of clinical trials in cancer patients (Fife et al., 2000; Gu et al., 2001; Lee et al., 2001a; Rudek et al., 2001a; Rudek et al., 2001b). Chemical modifications to existing tetracycline drugs may be interesting to study since the current therapeutic strategy is to discover molecules that do not affect fibril formation. Since the presence of fibrils might be beneficial or inert, it is proposed

that this specificity might be crucial for clinical success (Chen et al., 2010; Cheng et al., 2007; Necula et al., 2007a; Treusch et al., 2009). Although *in vivo* studies carried out in mammalian cells will be important to determine the efficacy of anti-amyloidogenic property of tetracyclines, these data may potentially change the way tetracycline and doxycycline antibiotics are currently prescribed and/or administered to older patients.

6.3.2 Tetranortriterpenoid compounds and isogedunin

Treatment with isogedunin, a tetranortriterpenoid compound extracted from *Guarea Thompsonii*, significantly increased ($p < 0.001$) the proportion of wild-type cells expressing A β ₄₂GFP-associated fluorescence. Isogedunin appeared to reduce the aggregation propensity of A β ₄₂GFP therefore causing an increasing the portion of wild-type cells expressing A β ₄₂GFP-associated fluorescence. No effects were observed on wild-type cells expressing A β ₄₀GFP when treated with isogedunin. Interestingly, gedunin, also a tetranortriterpenoid compound which shares a similar chemical structure to isogedunin, has been shown to demonstrate anti-parasitic, anti-secretory, antifungal, and neuroprotective activities. Gedunin, which is extracted from *Azadirachta indica* (Indian neem tree) has also been shown to inhibit Hsp90 while gedunin derivatives such as deacetylgedunin, deoxygedunin and deacetoxy-7-oxogedunin have been shown to increase levels of Hsp70p. Currently a patent is held for the use of tetranortriterpenoid compounds for the reduction and/or inhibition of the aggregation of amyloidogenic proteins, such as huntingtin, as well as for increasing proteasome activity for the use in the treatment, diagnosis and/or prevention of trinucleotide repeat disorders (e.g Huntington's disease), amyloid diseases, neurodegenerative disease, protein misfolding diseases or tumors (Patent application number: US 2010/0298280 A1). Interestingly, isogedunin exhibited the strongest inhibitory activity with an EC₅₀ of 2 μ M. In the absence of available data, it is tempting to speculate that altered proteasomal activity and/or heat shock response may have led to the increased proportion of wild-type cells expressing A β ₄₂GFP-associated fluorescence.

6.4 Future directions

In this study, a yeast *in vivo* assay that assesses the aggregation of A β ₄₂ based on the A β ₄₂GFP fusion-associated fluorescence was developed. Using this platform, a

high-throughput assay to screen drug/chemical compounds for an effect on A β ₄₂ and A β ₄₀ aggregation was developed. Here, 37 drug/chemical compounds were identified in a pilot screen that altered A β ₄₂GFP and A β ₄₀GFP aggregation/fluorescence. To resolve the potentially confounding interactions between the drug/chemical compounds that were identified and A β ₄₂GFP aggregation, a few important experiments need to be undertaken in future. Work is currently underway, through detailed biochemical analyses, to verify if these compounds do indeed directly affect A β ₄₂GFP or A β ₄₀GFP aggregation *in vivo* and determine their effectiveness in terms of dose. Biophysical analyses using electron microscopy may be required to identify if these compounds affect A β ₄₂GFP oligomer or fibril formation as this may be crucial for clinical success since the presence of fibrils might be beneficial or inert (Chen et al., 2010; Cheng et al., 2007; Necula et al., 2007a; Treusch et al., 2009).

Yeast cell-based assays for compounds that inhibit A β ₄₂ aggregation are advantageous since compounds that cause toxicity can be eliminated immediately (Bharadwaj et al., 2010; Caine et al., 2007; Kim et al., 2006; Lee et al., 2009; Macreadie et al., 2008). In this study, to eliminate false positives from the dataset, samples were analysed for the appearance of autofluorescence. For example, compounds that formed crystals which led to emission at 485 nm were removed from the data set. However, compounds that may possibly fluoresce without forming crystals were not identified. To resolve this, it is necessary to screen target drugs incubated with wild-type cells not expressing any form of A β GFP fusion constructs. In addition, the effects of target drugs need to be validated based on a dose-dependent assay by serially diluting the drug/chemical compounds in DMSO to varying concentrations.

Recently, small molecule compounds that inhibit formation of toxic A β oligomers and aggregation in general have been well studied (Amijee et al., 2009; Amijee and Scopes, 2009; Scherzer-Attali et al., 2010). Examples of these compounds that are known to inhibit A β ₄₂ oligomerisation and have a therapeutic effect in AD animal models include curcumin, hydroxyaniline (RS-0406), hydroxyaniline derivative (SEN1269; Senexis), scylloinositol (AZD-103), Clioquinol (PBT1; 8-hydroxyquinoline) (also identified in this study to reduce A β ₄₀GFP fluorescence) and PBT2 (a copper/zinc ionophore, 8-hydroxyquinoline) (Yang et al., 2005; Nakagami et al., 2002; O'Hare et al.,

2010; Walsh et al., 2005; McLaurin et al., 2000; McLaurin et al., 2006; Townsend et al., 2006; Hsiao et al., 1996; Adlard et al., 2008; Faux et al., 2010). At present, PBT2 (Prana Biotechnology) and scyllo-inositol (Transition Therapeutics and Elan) are undergoing clinical trials. Since some of these compounds are known to inhibit the formation of A β ₄₂ oligomers, it may be worthwhile to validate these drugs using the *S. cerevisiae* platform described in this study. This may lend further support to the use of yeast high-content screening as an effective strategy in screening for potential inhibitors of A β ₄₂ oligomerisation. These compounds that bind to and inhibit A β ₄₂ oligomerisation may also prevent A β ₄₂-induced toxicity (Alavez et al., 2011; Chen et al., 2010; Scherzer-Attali et al., 2010). In this study, a total of 3277 compounds were analysed. Additional high-content screening with much larger chemical compound libraries including FDA-approved drugs may have the potential to uncover novel and more effective drugs. Identifying such drugs as affecting intracellular A β ₄₂ aggregation may significantly reduce costs and the exhaustive process of introducing new drugs onto the market. The compounds identified through this approach may potentially change the way these drugs are currently administered to patients.

Although amyloidogenic and anti-amyloidogenic properties of compounds that inhibit A β ₄₂ oligomerisation have been investigated in other studies (Chang et al., 2003; Chromy et al., 2003; Hamaguchi et al., 2009; Necula et al., 2007b; Yang et al., 2005), the majority of them were conducted *in vitro* using synthetic A β ₄₂ peptides under conditions that allow formation of oligomers instead of fibrils. The A β GFP fusion-associated fluorescence assay characterised and validated in *S. cerevisiae*, described in this study, allows real-time determination and identification of cellular localisation of A β ₄₂. The study demonstrated it to be a useful tool in the investigation of intracellular factors affecting A β ₄₂ aggregation. The data in this thesis contribute to our current understanding of how cellular mechanisms affect intracellular A β ₄₂ aggregation and begin to address the idea that altered lipid homeostasis and mitochondrial function in cells as well as certain drugs/chemical compounds may have implications for A β ₄₂ aggregation and altered localisation in cells.

7 REFERENCES

- Abbott, A. 2011. Dementia: a problem for our age. *Nature*. 475:S2-4.
- Adibhatla, R.M., J.F. Hatcher, and R.J. Dempsey. 2006. Lipids and lipidomics in brain injury and diseases. *The AAPS journal*. 8:E314-321.
- Adlard, P.A., R.A. Cherny, D.I. Finkelstein, E. Gautier, E. Robb, M. Cortes, I. Volitakis, X. Liu, J.P. Smith, K. Perez, K. Laughton, Q.X. Li, S.A. Charman, J.A. Nicolazzo, S. Wilkins, K. Deleva, T. Lynch, G. Kok, C.W. Ritchie, R.E. Tanzi, R. Cappai, C.L. Masters, K.J. Barnham, and A.I. Bush. 2008. Rapid restoration of cognition in Alzheimer's transgenic mice with 8-hydroxy quinoline analogs is associated with decreased interstitial Abeta. *Neuron*. 59:43-55.
- Agne, B., N.M. Meindl, K. Niederhoff, H. Einwachter, P. Rehling, A. Sickmann, H.E. Meyer, W. Girzalsky, and W.H. Kunau. 2003. Pex8p: an intraperoxisomal organizer of the peroxisomal import machinery. *Molecular cell*. 11:635-646.
- Ahmed, M., J. Davis, D. Aucoin, T. Sato, S. Ahuja, S. Aimoto, J.I. Elliott, W.E. Van Nostrand, and S.O. Smith. 2010. Structural conversion of neurotoxic amyloid-beta(1-42) oligomers to fibrils. *Nat Struct Mol Biol*. 17:561-567.
- Alavez, S., M.C. Vantipalli, D.J. Zucker, I.M. Klang, and G.J. Lithgow. 2011. Amyloid-binding compounds maintain protein homeostasis during ageing and extend lifespan. *Nature*. 472:226-229.
- Alberti, S., A.D. Gitler, and S. Lindquist. 2007. A suite of Gateway cloning vectors for high-throughput genetic analysis in *Saccharomyces cerevisiae*. *Yeast (Chichester, England)*. 24:913-919.
- Albertyn, J., S. Hohmann, and B.A. Prior. 1994a. Characterization of the osmotic-stress response in *Saccharomyces cerevisiae*: osmotic stress and glucose repression regulate glycerol-3-phosphate dehydrogenase independently. *Current genetics*. 25:12-18.
- Albertyn, J., S. Hohmann, J.M. Thevelein, and B.A. Prior. 1994b. GPD1, which encodes glycerol-3-phosphate dehydrogenase, is essential for growth under osmotic stress in *Saccharomyces cerevisiae*, and its expression is regulated by the high-osmolarity glycerol response pathway. *Molecular and cellular biology*. 14:4135-4144.
- Allinson, T.M., E.T. Parkin, A.J. Turner, and N.M. Hooper. 2003. ADAMs family members as amyloid precursor protein alpha-secretases. *J Neurosci Res*. 74:342-352.
- Almeida, C.G., R.H. Takahashi, and G.K. Gouras. 2006. Beta-amyloid accumulation impairs multivesicular body sorting by inhibiting the ubiquitin-proteasome system. *J Neurosci*. 26:4277-4288.
- Alzheimer, A., R.A. Stelzmann, H.N. Schnitzlein, and F.R. Murtagh. 1907. An English translation of Alzheimer's 1907 paper, "Über eine eigenartige Erkrankung der Hirnrinde". *Clinical anatomy (New York, N.Y.)*. 8:429-431.
- Ambroziak, J., and S.A. Henry. 1994. INO2 and INO4 gene products, positive regulators of phospholipid biosynthesis in *Saccharomyces cerevisiae*, form a complex that binds to the INO1 promoter. *The Journal of biological chemistry*. 269:15344-15349.
- Amijee, H., J. Madine, D.A. Middleton, and A.J. Doig. 2009. Inhibitors of protein aggregation and toxicity. *Biochemical Society transactions*. 37:692-696.
- Amijee, H., and D.I. Scopes. 2009. The quest for small molecules as amyloid inhibiting therapies for Alzheimer's disease. *J Alzheimers Dis*. 17:33-47.

- Andersen, M.H., H. Graversen, S.N. Fedosov, T.E. Petersen, and J.T. Rasmussen. 2000. Functional analyses of two cellular binding domains of bovine lactadherin. *Biochemistry*. 39:6200-6206.
- Ansell, R., K. Granath, S. Hohmann, J.M. Thevelein, and L. Adler. 1997. The two isoenzymes for yeast NAD⁺-dependent glycerol 3-phosphate dehydrogenase encoded by GPD1 and GPD2 have distinct roles in osmoadaptation and redox regulation. *The EMBO journal*. 16:2179-2187.
- Arrasate, M., S. Mitra, E.S. Schweitzer, M.R. Segal, and S. Finkbeiner. 2004. Inclusion body formation reduces levels of mutant huntingtin and the risk of neuronal death. *Nature*. 431:805-810.
- Atamna, H. 2004. Heme, iron, and the mitochondrial decay of ageing. *Ageing research reviews*. 3:303-318.
- Atamna, H. 2006. Heme binding to Amyloid-beta peptide: mechanistic role in Alzheimer's disease. *J Alzheimers Dis*. 10:255-266.
- Atamna, H., and K. Boyle. 2006. Amyloid-beta peptide binds with heme to form a peroxidase: relationship to the cytopathologies of Alzheimer's disease. *Proceedings of the National Academy of Sciences of the United States of America*. 103:3381-3386.
- Atamna, H., and W.H. Frey, 2nd. 2004. A role for heme in Alzheimer's disease: heme binds amyloid beta and has altered metabolism. *Proceedings of the National Academy of Sciences of the United States of America*. 101:11153-11158.
- Atamna, H., and W.H. Frey, 2nd. 2007. Mechanisms of mitochondrial dysfunction and energy deficiency in Alzheimer's disease. *Mitochondrion*. 7:297-310.
- Athenstaedt, K. 2011. YALI0E32769g (DGA1) and YALI0E16797g (LRO1) encode major triacylglycerol synthases of the oleaginous yeast *Yarrowia lipolytica*. *Biochimica et biophysica acta*. 1811:587-596.
- Athenstaedt, K., and G. Daum. 1999. Phosphatidic acid, a key intermediate in lipid metabolism. *European journal of biochemistry / FEBS*. 266:1-16.
- Athenstaedt, K., and G. Daum. 2003. YMR313c/TGL3 encodes a novel triacylglycerol lipase located in lipid particles of *Saccharomyces cerevisiae*. *The Journal of biological chemistry*. 278:23317-23323.
- Athenstaedt, K., and G. Daum. 2005. Tgl4p and Tgl5p, two triacylglycerol lipases of the yeast *Saccharomyces cerevisiae* are localized to lipid particles. *The Journal of biological chemistry*. 280:37301-37309.
- Athenstaedt, K., and G. Daum. 2006. The life cycle of neutral lipids: synthesis, storage and degradation. *Cell Mol Life Sci*. 63:1355-1369.
- Athenstaedt, K., D. Zweytick, A. Jandrositz, S.D. Kohlwein, and G. Daum. 1999. Identification and characterization of major lipid particle proteins of the yeast *Saccharomyces cerevisiae*. *Journal of bacteriology*. 181:6441-6448.
- Austen, B.M., C. Sidera, C. Liu, and E. Frears. 2003. The role of intracellular cholesterol on the processing of the beta-amyloid precursor protein. *The journal of nutrition, health & aging*. 7:31-36.
- Bagriantsev, S., and S. Liebman. 2006. Modulation of Abeta42 low-n oligomerization using a novel yeast reporter system. *BMC biology*. 4:32.
- Baig, S., S.A. Joseph, H. Tayler, R. Abraham, M.J. Owen, J. Williams, P.G. Kehoe, and S. Love. 2010. Distribution and expression of picalm in Alzheimer disease. *J Neuropathol Exp Neurol*. 69:1071-1077.

- Bailis, A.M., M.A. Poole, G.M. Carman, and S.A. Henry. 1987. The membrane-associated enzyme phosphatidylserine synthase is regulated at the level of mRNA abundance. *Molecular and cellular biology*. 7:167-176.
- Bakker, B.M., K.M. Overkamp, A.J. van Maris, P. Kotter, M.A. Luttik, J.P. van Dijken, and J.T. Pronk. 2001. Stoichiometry and compartmentation of NADH metabolism in *Saccharomyces cerevisiae*. *FEMS microbiology reviews*. 25:15-37.
- Bales, K.R., T. Verina, D.J. Cummins, Y. Du, R.C. Dodel, J. Saura, C.E. Fishman, C.A. DeLong, P. Piccardo, V. Petegnief, B. Ghetti, and S.M. Paul. 1999. Apolipoprotein E is essential for amyloid deposition in the APP(V717F) transgenic mouse model of Alzheimer's disease. *Proceedings of the National Academy of Sciences of the United States of America*. 96:15233-15238.
- Ballard, C., S. Gauthier, A. Corbett, C. Brayne, D. Aarsland, and E. Jones. 2011. Alzheimer's disease. *Lancet*. 377:1019-1031.
- Balzi, E., and A. Goffeau. 1995. Yeast multidrug resistance: the PDR network. *Journal of bioenergetics and biomembranes*. 27:71-76.
- Baryshnikova, A., M. Costanzo, Y. Kim, H. Ding, J. Koh, K. Toufighi, J.Y. Youn, J. Ou, B.J. San Luis, S. Bandyopadhyay, M. Hibbs, D. Hess, A.C. Gingras, G.D. Bader, O.G. Troyanskaya, G.W. Brown, B. Andrews, C. Boone, and C.L. Myers. 2010. Quantitative analysis of fitness and genetic interactions in yeast on a genome scale. *Nature methods*. 7:1017-1024.
- Bascom, R.A., H. Chan, and R.A. Rachubinski. 2003. Peroxisome biogenesis occurs in an unsynchronized manner in close association with the endoplasmic reticulum in temperature-sensitive *Yarrowia lipolytica* Pex3p mutants. *Molecular biology of the cell*. 14:939-957.
- Bassett, D.E., Jr., M.S. Boguski, and P. Hieter. 1996. Yeast genes and human disease. *Nature*. 379:589-590.
- Beckett, C., N.N. Nalivaeva, N.D. Belyaev, and A.J. Turner. 2012. Nuclear signalling by membrane protein intracellular domains: The AICD enigma. *Cellular signalling*. 24:402-409.
- Bekris, L.M., C.E. Yu, T.D. Bird, and D.W. Tsuang. 2010. Genetics of Alzheimer disease. *Journal of geriatric psychiatry and neurology*. 23:213-227.
- Bendeck, M.P., M. Conte, M. Zhang, N. Nili, B.H. Strauss, and S.M. Farwell. 2002. Doxycycline modulates smooth muscle cell growth, migration, and matrix remodeling after arterial injury. *The American journal of pathology*. 160:1089-1095.
- Berger, J., and D.E. Moller. 2002. The mechanisms of action of PPARs. *Annual review of medicine*. 53:409-435.
- Bertin, N., N. Simonis, D. Dupuy, M.E. Cusick, J.D. Han, H.B. Fraser, F.P. Roth, and M. Vidal. 2007. Confirmation of organized modularity in the yeast interactome. *PLoS biology*. 5:e153.
- Bertram, L., M.B. McQueen, K. Mullin, D. Blacker, and R.E. Tanzi. 2007. Systematic meta-analyses of Alzheimer disease genetic association studies: the AlzGene database. *Nature genetics*. 39:17-23.
- Bettens, K., N. Brouwers, H. Van Miegroet, A. Gil, S. Engelborghs, P.P. De Deyn, R. Vandenberghe, C. Van Broeckhoven, and K. Sleegers. 2010. Follow-up study of susceptibility loci for Alzheimer's disease and onset age identified by genome-wide association. *J Alzheimers Dis*. 19:1169-1175.
- Bharadwaj, P., R. Martins, and I. Macreadie. 2010. Yeast as a model for studying Alzheimer's disease. *FEMS yeast research*. 10:961-969.

- Bharadwaj, P.R., A.K. Dubey, C.L. Masters, R.N. Martins, and I.G. Macreadie. 2009. Abeta aggregation and possible implications in Alzheimer's disease pathogenesis. *Journal of cellular and molecular medicine*. 13:412-421.
- Binns, D., T. Januszewski, Y. Chen, J. Hill, V.S. Markin, Y. Zhao, C. Gilpin, K.D. Chapman, R.G. Anderson, and J.M. Goodman. 2006. An intimate collaboration between peroxisomes and lipid bodies. *The Journal of cell biology*. 173:719-731.
- Bircham, P.W., D.R. Maass, C.A. Roberts, P.Y. Kiew, Y.S. Low, M. Yegambaram, J. Matthews, C.A. Jack, and P.H. Atkinson. 2011. Secretory pathway genes assessed by high-throughput microscopy and synthetic genetic array analysis. *Molecular bioSystems*. 7:2589-2598.
- Bird, T.D. 2008. Genetic aspects of Alzheimer disease. *Genetics in medicine : official journal of the American College of Medical Genetics*. 10:231-239.
- Birner, R., M. Burgermeister, R. Schneiter, and G. Daum. 2001. Roles of phosphatidylethanolamine and of its several biosynthetic pathways in *Saccharomyces cerevisiae*. *Molecular biology of the cell*. 12:997-1007.
- Bitan, G., E.A. Fradinger, S.M. Spring, and D.B. Teplow. 2005. Neurotoxic protein oligomers--what you see is not always what you get. *Amyloid*. 12:88-95.
- Bitar, M.S., and B.H. Shapiro. 1987. Aberration of heme and hemoprotein in aged female rats. *Mechanisms of ageing and development*. 38:189-197.
- Blass, J.P. 2001. Brain metabolism and brain disease: is metabolic deficiency the proximate cause of Alzheimer dementia? *J Neurosci Res*. 66:851-856.
- Blennow, K., M.J. de Leon, and H. Zetterberg. 2006. Alzheimer's disease. *Lancet*. 368:387-403.
- Blomberg, A. 2000. Metabolic surprises in *Saccharomyces cerevisiae* during adaptation to saline conditions: questions, some answers and a model. *FEMS microbiology letters*. 182:1-8.
- Blomberg, A., and L. Adler. 1989. Roles of glycerol and glycerol-3-phosphate dehydrogenase (NAD⁺) in acquired osmotolerance of *Saccharomyces cerevisiae*. *Journal of bacteriology*. 171:1087-1092.
- Bogdanov, M., and W. Dowhan. 1999. Lipid-assisted protein folding. *The Journal of biological chemistry*. 274:36827-36830.
- Bogdanov, M., M. Umeda, and W. Dowhan. 1999. Phospholipid-assisted refolding of an integral membrane protein. Minimum structural features for phosphatidylethanolamine to act as a molecular chaperone. *The Journal of biological chemistry*. 274:12339-12345.
- Bolen, D.W. 2004. Effects of naturally occurring osmolytes on protein stability and solubility: issues important in protein crystallization. *Methods (San Diego, Calif)*. 34:312-322.
- Bostom, A.G., I.H. Rosenberg, H. Silbershatz, P.F. Jacques, J. Selhub, R.B. D'Agostino, P.W. Wilson, and P.A. Wolf. 1999. Nonfasting plasma total homocysteine levels and stroke incidence in elderly persons: the Framingham Study. *Annals of internal medicine*. 131:352-355.
- Botstein, D., S.A. Chervitz, and J.M. Cherry. 1997. Yeast as a model organism. *Science (New York, N.Y)*. 277:1259-1260.
- Braak, H., and E. Braak. 1991. Neuropathological staging of Alzheimer-related changes. *Acta neuropathologica*. 82:239-259.
- Braak, H., D.R. Thal, E. Ghebremedhin, and K. Del Tredici. 2011. Stages of the pathologic process in Alzheimer disease: age categories from 1 to 100 years. *J Neuropathol Exp Neurol*. 70:960-969.

- Bradford MM (1976) A rapid and sensitive method for the quantitation of microgram quantities of protein utilizing the principle of protein-dye binding. *Analytical Biochemistry* 72: 248-254
- Bramblett, G.T., M. Goedert, R. Jakes, S.E. Merrick, J.Q. Trojanowski, and V.M. Lee. 1993. Abnormal tau phosphorylation at Ser396 in Alzheimer's disease recapitulates development and contributes to reduced microtubule binding. *Neuron*. 10:1089-1099.
- Braun, R.J., C. Sommer, D. Carmona-Gutierrez, C.M. Khoury, J. Ring, S. Buttner, and F. Madeo. 2011. Neurotoxic 43-kDa TAR DNA-binding protein (TDP-43) triggers mitochondrion-dependent programmed cell death in yeast. *The Journal of biological chemistry*. 286:19958-19972.
- Breslow, D.K., D.M. Cameron, S.R. Collins, M. Schuldiner, J. Stewart-Ornstein, H.W. Newman, S. Braun, H.D. Madhani, N.J. Krogan, and J.S. Weissman. 2008. A comprehensive strategy enabling high-resolution functional analysis of the yeast genome. *Nature methods*. 5:711-718.
- Bro, C., B. Regenberg, G. Lagniel, J. Labarre, M. Montero-Lomeli, and J. Nielsen. 2003. Transcriptional, proteomic, and metabolic responses to lithium in galactose-grown yeast cells. *The Journal of biological chemistry*. 278:32141-32149.
- Brocard, C., G. Lametschwandtner, R. Koudelka, and A. Hartig. 1997. Pex14p is a member of the protein linkage map of Pex5p. *The EMBO journal*. 16:5491-5500.
- Broersen, K., F. Rousseau, and J. Schymkowitz. 2010. The culprit behind amyloid beta peptide related neurotoxicity in Alzheimer's disease: oligomer size or conformation? *Alzheimer's research & therapy*. 2:12.
- Brookmeyer, R., S. Gray, and C. Kawas. 1998. Projections of Alzheimer's disease in the United States and the public health impact of delaying disease onset. *American journal of public health*. 88:1337-1342.
- Brookmeyer, R., E. Johnson, K. Ziegler-Graham, and H.M. Arrighi. 2007. Forecasting the global burden of Alzheimer's disease. *Alzheimer's & dementia : the journal of the Alzheimer's Association*. 3:186-191.
- Buckle, A.M., G.L. Devlin, R.A. Jodun, K.F. Fulton, N. Faux, J.C. Whisstock, and S.P. Bottomley. 2005. The matrix refolded. *Nature methods*. 2:3.
- Butterfield, D.A., B. Howard, S. Yatin, T. Koppal, J. Drake, K. Hensley, M. Aksenov, M. Aksenova, R. Subramaniam, S. Varadarajan, M.E. Harris-White, N.W. Pedigo, Jr., and J.M. Carney. 1999. Elevated oxidative stress in models of normal brain aging and Alzheimer's disease. *Life sciences*. 65:1883-1892.
- Caine, J., S. Sankovich, H. Antony, L. Waddington, P. Macreadie, J. Varghese, and I. Macreadie. 2007. Alzheimer's Aβ fused to green fluorescent protein induces growth stress and a heat shock response. *FEMS yeast research*. 7:1230-1236.
- Caine, J.M., P.R. Bharadwaj, S.E. Sankovich, G.D. Ciccotosto, V.A. Streltsov, and J. Varghese. 2011. Oligomerization and toxicity of Aβ fusion proteins. *Biochemical and biophysical research communications*. 409:477-482.
- Camacho, I.E., L. Serneels, K. Spittaels, P. Merchiers, D. Dominguez, and B. De Strooper. 2004. Peroxisome-proliferator-activated receptor gamma induces a clearance mechanism for the amyloid-beta peptide. *J Neurosci*. 24:10908-10917.
- Campion, D., C. Dumanchin, D. Hannequin, B. Dubois, S. Belliard, M. Puel, C. Thomas-Anterion, A. Michon, C. Martin, F. Charbonnier, G. Raux, A. Camuzat, C. Penet, V. Mesnage, M. Martinez, F. Clerget-Darpoux, A. Brice, and T. Frebourg. 1999. Early-onset autosomal dominant Alzheimer disease: prevalence, genetic heterogeneity, and mutation spectrum. *American journal of human genetics*. 65:664-670.

- Cao, X., and T.C. Sudhof. 2001. A transcriptionally [correction of transcriptively] active complex of APP with Fe65 and histone acetyltransferase Tip60. *Science (New York, N.Y.)* 293:115-120.
- Carman, G.M., and G.S. Han. 2011. Regulation of phospholipid synthesis in the yeast *Saccharomyces cerevisiae*. *Annual review of biochemistry*. 80:859-883.
- Carman, G.M., and S.A. Henry. 1999. Phospholipid biosynthesis in the yeast *Saccharomyces cerevisiae* and interrelationship with other metabolic processes. *Progress in lipid research*. 38:361-399.
- Carman, G.M., and S.A. Henry. 2007. Phosphatidic acid plays a central role in the transcriptional regulation of glycerophospholipid synthesis in *Saccharomyces cerevisiae*. *The Journal of biological chemistry*. 282:37293-37297.
- Carrasquillo, M.M., F. Zou, V.S. Pankratz, S.L. Wilcox, L. Ma, L.P. Walker, S.G. Younkin, C.S. Younkin, L.H. Younkin, G.D. Bisceglia, N. Ertekin-Taner, J.E. Crook, D.W. Dickson, R.C. Petersen, N.R. Graff-Radford, and S.G. Younkin. 2009. Genetic variation in PCDH11X is associated with susceptibility to late-onset Alzheimer's disease. *Nature genetics*. 41:192-198.
- Carson, J.A., and A.J. Turner. 2002. Beta-amyloid catabolism: roles for neprilysin (NEP) and other metallopeptidases? *Journal of neurochemistry*. 81:1-8.
- Caspersen, C., N. Wang, J. Yao, A. Sosunov, X. Chen, J.W. Lustbader, H.W. Xu, D. Stern, G. McKhann, and S.D. Yan. 2005. Mitochondrial Abeta: a potential focal point for neuronal metabolic dysfunction in Alzheimer's disease. *FASEB J.* 19:2040-2041.
- Cerf, E., R. Sarroukh, S. Tamamizu-Kato, L. Breydo, S. Derclaye, Y.F. Dufrene, V. Narayanaswami, E. Goormaghtigh, J.M. Ruysschaert, and V. Raussens. 2009. Antiparallel beta-sheet: a signature structure of the oligomeric amyloid beta-peptide. *The Biochemical journal*. 421:415-423.
- Chai, C.K. 2007. The genetics of Alzheimer's disease. *American journal of Alzheimer's disease and other dementias*. 22:37-41.
- Chang, L., L. Bakhos, Z. Wang, D.L. Venton, and W.L. Klein. 2003. Femtomole immunodetection of synthetic and endogenous amyloid-beta oligomers and its application to Alzheimer's disease drug candidate screening. *J Mol Neurosci*. 20:305-313.
- Chang, Y.F., and G.M. Carman. 2008. CTP synthetase and its role in phospholipid synthesis in the yeast *Saccharomyces cerevisiae*. *Progress in lipid research*. 47:333-339.
- Chartier-Harlin, M.C., F. Crawford, H. Houlden, A. Warren, D. Hughes, L. Fidani, A. Goate, M. Rossor, P. Roques, J. Hardy, and et al. 1991. Early-onset Alzheimer's disease caused by mutations at codon 717 of the beta-amyloid precursor protein gene. *Nature*. 353:844-846.
- Chen, J., A.H. Armstrong, A.N. Koehler, and M.H. Hecht. 2010. Small molecule microarrays enable the discovery of compounds that bind the Alzheimer's Abeta peptide and reduce its cytotoxicity. *Journal of the American Chemical Society*. 132:17015-17022.
- Chen, M., V.O. Ona, M. Li, R.J. Ferrante, K.B. Fink, S. Zhu, J. Bian, L. Guo, L.A. Farrell, S.M. Hersch, W. Hobbs, J.P. Vonsattel, J.H. Cha, and R.M. Friedlander. 2000. Minocycline inhibits caspase-1 and caspase-3 expression and delays mortality in a transgenic mouse model of Huntington disease. *Nature medicine*. 6:797-801.
- Chen, X., J.F. Wagener, D.H. Morgan, L. Hui, O. Ghribi, and J.D. Geiger. 2010. Endolysosome mechanisms associated with Alzheimer's disease-like pathology in rabbits ingesting cholesterol-enriched diet. *J Alzheimers Dis*. 22:1289-1303.
- Cheng, I.H., K. Searce-Levie, J. Legleiter, J.J. Palop, H. Gerstein, N. Bien-Ly, J. Puolivali, S. Lesne, K.H. Ashe, P.J. Muchowski, and L. Mucke. 2007. Accelerating amyloid-beta fibrillization

- reduces oligomer levels and functional deficits in Alzheimer disease mouse models. *The Journal of biological chemistry*. 282:23818-23828.
- Cherry, J.M., E.L. Hong, C. Amundsen, R. Balakrishnan, G. Binkley, E.T. Chan, K.R. Christie, M.C. Costanzo, S.S. Dwight, S.R. Engel, D.G. Fisk, J.E. Hirschman, B.C. Hitz, K. Karra, C.J. Krieger, S.R. Miyasato, R.S. Nash, J. Park, M.S. Skrzypek, M. Simison, S. Weng, and E.D. Wong. 2012. *Saccharomyces* Genome Database: the genomics resource of budding yeast. *Nucleic acids research*. 40:D700-705.
- Chiang, P.K. 1998. Biological effects of inhibitors of S-adenosylhomocysteine hydrolase. *Pharmacology & therapeutics*. 77:115-134.
- Chimon, S., M.A. Shaibat, C.R. Jones, D.C. Calero, B. Aizezi, and Y. Ishii. 2007. Evidence of fibril-like beta-sheet structures in a neurotoxic amyloid intermediate of Alzheimer's beta-amyloid. *Nat Struct Mol Biol*. 14:1157-1164.
- Chromy, B.A., R.J. Nowak, M.P. Lambert, K.L. Viola, L. Chang, P.T. Velasco, B.W. Jones, S.J. Fernandez, P.N. Lacor, P. Horowitz, C.E. Finch, G.A. Krafft, and W.L. Klein. 2003. Self-assembly of A β (1-42) into globular neurotoxins. *Biochemistry*. 42:12749-12760.
- Chuang, J.Y., C.W. Lee, Y.H. Shih, T. Yang, L. Yu, and Y.M. Kuo. 2012. Interactions between amyloid-beta and hemoglobin: implications for amyloid plaque formation in Alzheimer's disease. *PLoS ONE*. 7:e33120.
- Clancey, C.J., S.C. Chang, and W. Dowhan. 1993. Cloning of a gene (PSD1) encoding phosphatidylserine decarboxylase from *Saccharomyces cerevisiae* by complementation of an *Escherichia coli* mutant. *The Journal of biological chemistry*. 268:24580-24590.
- Clark, J.M., Jr., and A.Y. Chang. 1965. Inhibitors of the transfer of amino acids from aminoacyl soluble ribonucleic acid to proteins. *The Journal of biological chemistry*. 240:4734-4739.
- Clarke, R., A.D. Smith, K.A. Jobst, H. Refsum, L. Sutton, and P.M. Ueland. 1998. Folate, vitamin B12, and serum total homocysteine levels in confirmed Alzheimer disease. *Archives of neurology*. 55:1449-1455.
- Cleary, J.P., D.M. Walsh, J.J. Hofmeister, G.M. Shankar, M.A. Kuskowski, D.J. Selkoe, and K.H. Ashe. 2005. Natural oligomers of the amyloid-beta protein specifically disrupt cognitive function. *Nature neuroscience*. 8:79-84.
- Coimbra, A., and C. Andrade. 1971. Familial amyloid polyneuropathy: an electron microscope study of the peripheral nerve in five cases. II. Nerve fibre changes. *Brain*. 94:207-212.
- Compagno, C., F. Boschi, and B.M. Ranzi. 1996. Glycerol production in a triose phosphate isomerase deficient mutant of *Saccharomyces cerevisiae*. *Biotechnology progress*. 12:591-595.
- Connerth, M., T. Czabany, A. Wagner, G. Zellnig, E. Leitner, E. Steyrer, and G. Daum. 2010. Oleate inhibits steryl ester synthesis and causes liposensitivity in yeast. *The Journal of biological chemistry*. 285:26832-26841.
- Coon, K.D., A.J. Myers, D.W. Craig, J.A. Webster, J.V. Pearson, D.H. Lince, V.L. Zismann, T.G. Beach, D. Leung, L. Bryden, R.F. Halperin, L. Marlowe, M. Kaleem, D.G. Walker, R. Ravid, C.B. Heward, J. Rogers, A. Papassotiropoulos, E.M. Reiman, J. Hardy, and D.A. Stephan. 2007. A high-density whole-genome association study reveals that APOE is the major susceptibility gene for sporadic late-onset Alzheimer's disease. *The Journal of clinical psychiatry*. 68:613-618.
- Cooper, A.A., A.D. Gitler, A. Cashikar, C.M. Haynes, K.J. Hill, B. Bhullar, K. Liu, K. Xu, K.E. Strahearn, F. Liu, S. Cao, K.A. Caldwell, G.A. Caldwell, G. Marsischky, R.D. Kolodner, J. Labaer, J.C. Rochet, N.M. Bonini, and S. Lindquist. 2006. Alpha-synuclein blocks ER-Golgi

- traffic and Rab1 rescues neuron loss in Parkinson's models. *Science (New York, N.Y.)* 313:324-328.
- Corder, E.H., A.M. Saunders, N.J. Risch, W.J. Strittmatter, D.E. Schmechel, P.C. Gaskell, Jr., J.B. Rimmler, P.A. Locke, P.M. Conneally, K.E. Schmader, and et al. 1994. Protective effect of apolipoprotein E type 2 allele for late onset Alzheimer disease. *Nature genetics*. 7:180-184.
- Corder, E.H., A.M. Saunders, W.J. Strittmatter, D.E. Schmechel, P.C. Gaskell, G.W. Small, A.D. Roses, J.L. Haines, and M.A. Pericak-Vance. 1993. Gene dose of apolipoprotein E type 4 allele and the risk of Alzheimer's disease in late onset families. *Science (New York, N.Y.)* 261:921-923.
- Corneveaux, J.J., A.J. Myers, A.N. Allen, J.J. Pruzin, M. Ramirez, A. Engel, M.A. Nalls, K. Chen, W. Lee, K. Chewning, S.E. Villa, H.B. Meechoovet, J.D. Gerber, D. Frost, H.L. Benson, S. O'Reilly, L.B. Chibnik, J.M. Shulman, A.B. Singleton, D.W. Craig, K.R. Van Keuren-Jensen, T. Dunckley, D.A. Bennett, P.L. De Jager, C. Heward, J. Hardy, E.M. Reiman, and M.J. Huentelman. 2010. Association of CR1, CLU and PICALM with Alzheimer's disease in a cohort of clinically characterized and neuropathologically verified individuals. *Human molecular genetics*. 19:3295-3301.
- Costanzo, M., A. Baryshnikova, J. Bellay, Y. Kim, E.D. Spear, C.S. Sevier, H. Ding, J.L. Koh, K. Toufighi, S. Mostafavi, J. Prinz, R.P. St Onge, B. VanderSluis, T. Makhnevych, F.J. Vizeacoumar, S. Alizadeh, S. Bahr, R.L. Brost, Y. Chen, M. Cokol, R. Deshpande, Z. Li, Z.Y. Lin, W. Liang, M. Marback, J. Paw, B.J. San Luis, E. Shuteriqi, A.H. Tong, N. van Dyk, I.M. Wallace, J.A. Whitney, M.T. Weirauch, G. Zhong, H. Zhu, W.A. Houry, M. Brudno, S. Ragibizadeh, B. Papp, C. Pal, F.P. Roth, G. Giaever, C. Nislow, O.G. Troyanskaya, H. Bussey, G.D. Bader, A.C. Gingras, Q.D. Morris, P.M. Kim, C.A. Kaiser, C.L. Myers, B.J. Andrews, and C. Boone. 2010. The genetic landscape of a cell. *Science (New York, N.Y.)* 327:425-431.
- Cowart, L.A., and L.M. Obeid. 2007. Yeast sphingolipids: recent developments in understanding biosynthesis, regulation, and function. *Biochimica et biophysica acta*. 1771:421-431.
- Creighton, T. 1992. Proteins. *Proteins, 2nd Ed.*, . 2nd Ed., pp. 171-200.
- Cruz, J.C., and L.H. Tsai. 2004. Cdk5 deregulation in the pathogenesis of Alzheimer's disease. *Trends in molecular medicine*. 10:452-458.
- Cyert, M.S. 2001. Genetic analysis of calmodulin and its targets in *Saccharomyces cerevisiae*. *Annual review of genetics*. 35:647-672.
- Czabany, T., K. Athenstaedt, and G. Daum. 2007. Synthesis, storage and degradation of neutral lipids in yeast. *Biochimica et biophysica acta*. 1771:299-309.
- Czabany, T., A. Wagner, D. Zweytick, K. Lohner, E. Leitner, E. Ingolic, and G. Daum. 2008. Structural and biochemical properties of lipid particles from the yeast *Saccharomyces cerevisiae*. *The Journal of biological chemistry*. 283:17065-17074.
- D'Andrea, M.R., R.G. Nagele, H.Y. Wang, and D.H. Lee. 2002. Consistent immunohistochemical detection of intracellular beta-amyloid42 in pyramidal neurons of Alzheimer's disease entorhinal cortex. *Neuroscience letters*. 333:163-166.
- Dahlgren, K.N., A.M. Manelli, W.B. Stine, Jr., L.K. Baker, G.A. Krafft, and M.J. LaDu. 2002. Oligomeric and fibrillar species of amyloid-beta peptides differentially affect neuronal viability. *The Journal of biological chemistry*. 277:32046-32053.
- Dahlqvist, A., U. Stahl, M. Lenman, A. Banas, M. Lee, L. Sandager, H. Ronne, and S. Stymne. 2000. Phospholipid:diacylglycerol acyltransferase: an enzyme that catalyzes the acyl-CoA-independent formation of triacylglycerol in yeast and plants. *Proceedings of the National Academy of Sciences of the United States of America*. 97:6487-6492.

- Daum, G., P.C. Bohni, and G. Schatz. 1982. Import of proteins into mitochondria. Cytochrome b2 and cytochrome c peroxidase are located in the intermembrane space of yeast mitochondria. *The Journal of biological chemistry*. 257:13028-13033.
- Daum, G., N.D. Lees, M. Bard, and R. Dickson. 1998. Biochemistry, cell biology and molecular biology of lipids of *Saccharomyces cerevisiae*. *Yeast* (Chichester, England). 14:1471-1510.
- Daum, G., G. Tuller, T. Nemec, C. Hrastnik, G. Balliano, L. Cattell, P. Milla, F. Rocco, A. Conzelmann, C. Vionnet, D.E. Kelly, S. Kelly, E. Schweizer, H.J. Schuller, U. Hojad, E. Greiner, and K. Finger. 1999. Systematic analysis of yeast strains with possible defects in lipid metabolism. *Yeast* (Chichester, England). 15:601-614.
- Davis-Searles, P.R., A.J. Saunders, D.A. Erie, D.J. Winzor, and G.J. Pielak. 2001. Interpreting the effects of small uncharged solutes on protein-folding equilibria. *Annual review of biophysics and biomolecular structure*. 30:271-306.
- De Bernardez Clark, E., E. Schwarz, and R. Rudolph. 1999. Inhibition of aggregation side reactions during in vitro protein folding. *Methods in enzymology*. 309:217-236.
- De Felice, F.G., J.C. Houzel, J. Garcia-Abreu, P.R. Louzada, Jr., R.C. Afonso, M.N. Meirelles, R. Lent, V.M. Neto, and S.T. Ferreira. 2001. Inhibition of Alzheimer's disease beta-amyloid aggregation, neurotoxicity, and in vivo deposition by nitrophenols: implications for Alzheimer's therapy. *FASEB J*. 15:1297-1299.
- De Felice, F.G., and S.T. Ferreira. 2002. Beta-amyloid production, aggregation, and clearance as targets for therapy in Alzheimer's disease. *Cellular and molecular neurobiology*. 22:545-563.
- de Koning, W., and K. van Dam. 1992. A method for the determination of changes of glycolytic metabolites in yeast on a subsecond time scale using extraction at neutral pH. *Analytical biochemistry*. 204:118-123.
- de Kruijff, B. 1997. Lipid polymorphism and biomembrane function. *Current opinion in chemical biology*. 1:564-569.
- de Montigny, J., A. Belarbi, J.C. Hubert, and F. Lacroute. 1989. Structure and expression of the URA5 gene of *Saccharomyces cerevisiae*. *Mol Gen Genet*. 215:455-462.
- de Montigny, J., L. Kern, J.C. Hubert, and F. Lacroute. 1990. Cloning and sequencing of URA10, a second gene encoding orotate phosphoribosyl transferase in *Saccharomyces cerevisiae*. *Current genetics*. 17:105-111.
- De Strooper, B., P. Saftig, K. Craessaerts, H. Vanderstichele, G. Guhde, W. Annaert, K. Von Figura, and F. Van Leuven. 1998. Deficiency of presenilin-1 inhibits the normal cleavage of amyloid precursor protein. *Nature*. 391:387-390.
- Deane, R., A. Sagare, K. Hamm, M. Parisi, S. Lane, M.B. Finn, D.M. Holtzman, and B.V. Zlokovic. 2008. apoE isoform-specific disruption of amyloid beta peptide clearance from mouse brain. *The Journal of clinical investigation*. 118:4002-4013.
- Decottignies, A., and A. Goffeau. 1997. Complete inventory of the yeast ABC proteins. *Nature genetics*. 15:137-145.
- DeMattos, R.B., J.R. Cirrito, M. Parsadanian, P.C. May, M.A. O'Dell, J.W. Taylor, J.A. Harmony, B.J. Aronow, K.R. Bales, S.M. Paul, and D.M. Holtzman. 2004. ApoE and clusterin cooperatively suppress A β levels and deposition: evidence that ApoE regulates extracellular A β metabolism in vivo. *Neuron*. 41:193-202.
- Diaz, G., M. Melis, B. Batetta, F. Angius, and A.M. Falchi. 2008. Hydrophobic characterization of intracellular lipids in situ by Nile Red red/yellow emission ratio. *Micron*. 39:819-824.

- Dickson, D.W. 1997. The pathogenesis of senile plaques. *J Neuropathol Exp Neurol*. 56:321-339.
- Dickson, D.W., H.A. Crystal, C. Bevana, W. Honer, I. Vincent, and P. Davies. 1995. Correlations of synaptic and pathological markers with cognition of the elderly. *Neurobiology of aging*. 16:285-298; discussion 298-304.
- Dickson, D.W., H.A. Crystal, L.A. Mattiace, D.M. Masur, A.D. Blau, P. Davies, S.H. Yen, and M.K. Aronson. 1992. Identification of normal and pathological aging in prospectively studied nondemented elderly humans. *Neurobiology of aging*. 13:179-189.
- Dickson, R.C. 2010. Roles for sphingolipids in *Saccharomyces cerevisiae*. *Advances in experimental medicine and biology*. 688:217-231.
- Dickson, R.C., and R.L. Lester. 2002. Sphingolipid functions in *Saccharomyces cerevisiae*. *Biochimica et biophysica acta*. 1583:13-25.
- Dobson, C.M. 2003. Protein folding and misfolding. *Nature*. 426:884-890.
- Dobson, C.M., and R.J. Ellis. 1998. Protein folding and misfolding inside and outside the cell. *The EMBO journal*. 17:5251-5254.
- Drzewoski, J., L. Czupryniak, G. Chwatko, and E. Bald. 2000. Hyperhomocysteinemia in poorly controlled type 2 diabetes patients. *Diabetes, nutrition & metabolism*. 13:319-324.
- Dubey, A.K., P.R. Bharadwaj, J.N. Varghese, and I.G. Macreadie. 2009. Alzheimer's amyloid-beta rescues yeast from hydroxide toxicity. *J Alzheimers Dis*. 18:31-33.
- Dunstan, H.M., C. Ludlow, S. Goehle, M. Cronk, P. Szankasi, D.R. Evans, J.A. Simon, and J.R. Lamb. 2002. Cell-based assays for identification of novel double-strand break-inducing agents. *Journal of the National Cancer Institute*. 94:88-94.
- Eanes, E.D., and G.G. Glenner. 1968. X-ray diffraction studies on amyloid filaments. *J Histochem Cytochem*. 16:673-677.
- Edbauer, D., E. Winkler, J.T. Regula, B. Pesold, H. Steiner, and C. Haass. 2003. Reconstitution of gamma-secretase activity. *Nature cell biology*. 5:486-488.
- Ege, C., and K.Y. Lee. 2004. Insertion of Alzheimer's A beta 40 peptide into lipid monolayers. *Biophysical journal*. 87:1732-1740.
- Ege, C., J. Majewski, G. Wu, K. Kjaer, and K.Y. Lee. 2005. Templating effect of lipid membranes on Alzheimer's amyloid beta peptide. *Chemphyschem*. 6:226-229.
- Egner, R., and K. Kuchler. 1996. The yeast multidrug transporter Pdr5 of the plasma membrane is ubiquitinated prior to endocytosis and degradation in the vacuole. *FEBS letters*. 378:177-181.
- Eitzen, G., L. Wang, N. Thorngren, and W. Wickner. 2002. Remodeling of organelle-bound actin is required for yeast vacuole fusion. *The Journal of cell biology*. 158:669-679.
- Ejsing, C.S., J.L. Sampaio, V. Surendranath, E. Duchoslav, K. Ekroos, R.W. Klemm, K. Simons, and A. Shevchenko. 2009. Global analysis of the yeast lipidome by quantitative shotgun mass spectrometry. *Proceedings of the National Academy of Sciences of the United States of America*. 106:2136-2141.
- Elkhaimi, M., M.R. Kaadige, D. Kamath, J.C. Jackson, H. Biliran, Jr., and J.M. Lopes. 2000. Combinatorial regulation of phospholipid biosynthetic gene expression by the UME6, SIN3 and RPD3 genes. *Nucleic acids research*. 28:3160-3167.

- Ellens, H., J. Bentz, and F.C. Szoka. 1986. Destabilization of phosphatidylethanolamine liposomes at the hexagonal phase transition temperature. *Biochemistry*. 25:285-294.
- Emoto, K., and M. Umeda. 2000. An essential role for a membrane lipid in cytokinesis. Regulation of contractile ring disassembly by redistribution of phosphatidylethanolamine. *The Journal of cell biology*. 149:1215-1224.
- Eriksson, P., L. Andre, R. Ansell, A. Blomberg, and L. Adler. 1995. Cloning and characterization of GPD2, a second gene encoding sn-glycerol 3-phosphate dehydrogenase (NAD⁺) in *Saccharomyces cerevisiae*, and its comparison with GPD1. *Molecular microbiology*. 17:95-107.
- Estrada de Martin, P., Y. Du, P. Novick, and S. Ferro-Novick. 2005. Ice2p is important for the distribution and structure of the cortical ER network in *Saccharomyces cerevisiae*. *Journal of cell science*. 118:65-77.
- Estrada, L.D., and C. Soto. 2007. Disrupting beta-amyloid aggregation for Alzheimer disease treatment. *Current topics in medicinal chemistry*. 7:115-126.
- Fagarasanu, A., M. Fagarasanu, and R.A. Rachubinski. 2007. Maintaining peroxisome populations: a story of division and inheritance. *Annual review of cell and developmental biology*. 23:321-344.
- Fahy, E., S. Subramaniam, R.C. Murphy, M. Nishijima, C.R. Raetz, T. Shimizu, F. Spener, G. van Meer, M.J. Wakelam, and E.A. Dennis. 2009. Update of the LIPID MAPS comprehensive classification system for lipids. *Journal of lipid research*. 50 Suppl:S9-14.
- Fahy, E., M. Sud, D. Cotter, and S. Subramaniam. 2007. LIPID MAPS online tools for lipid research. *Nucleic acids research*. 35:W606-612.
- Fandrich, M. 2007. On the structural definition of amyloid fibrils and other polypeptide aggregates. *Cell Mol Life Sci*. 64:2066-2078.
- Fandrich, M., M. Schmidt, and N. Grigorieff. 2011. Recent progress in understanding Alzheimer's beta-amyloid structures. *Trends in biochemical sciences*. 36:338-345.
- Farooqui, A.A., W.Y. Ong, and L.A. Horrocks. 2006. Inhibitors of brain phospholipase A2 activity: their neuropharmacological effects and therapeutic importance for the treatment of neurologic disorders. *Pharmacological reviews*. 58:591-620.
- Faux, N.G., C.W. Ritchie, A. Gunn, A. Rembach, A. Tsatsanis, J. Bedo, J. Harrison, L. Lannfelt, K. Blennow, H. Zetterberg, M. Ingelsson, C.L. Masters, R.E. Tanzi, J.L. Cummings, C.M. Herd, and A.I. Bush. 2010. PBT2 rapidly improves cognition in Alzheimer's Disease: additional phase II analyses. *J Alzheimers Dis*. 20:509-516.
- Fawcett, J.R., E.Z. Bordayo, K. Jackson, H. Liu, J. Peterson, A. Svitak, and W.H. Frey, 2nd. 2002. Inactivation of the human brain muscarinic acetylcholine receptor by oxidative damage catalyzed by a low molecular weight endogenous inhibitor from Alzheimer's brain is prevented by pyrophosphate analogs, bioflavonoids and other antioxidants. *Brain research*. 950:10-20.
- Fei, W., G. Shui, B. Gaeta, X. Du, L. Kuerschner, P. Li, A.J. Brown, M.R. Wenk, R.G. Parton, and H. Yang. 2008. Fld1p, a functional homologue of human seipin, regulates the size of lipid droplets in yeast. *The Journal of cell biology*. 180:473-482.
- Fei, W., G. Shui, Y. Zhang, N. Krahmer, C. Ferguson, T.S. Kapterian, R.C. Lin, I.W. Dawes, A.J. Brown, P. Li, X. Huang, R.G. Parton, M.R. Wenk, T.C. Walther, and H. Yang. 2011. A role for phosphatidic acid in the formation of "supersized" lipid droplets. *PLoS genetics*. 7:e1002201.
- Feng, S., and Y.B. Yan. 2008. Effects of glycerol on the compaction and stability of the wild type and mutated rabbit muscle creatine kinase. *Proteins*. 71:844-854.

- Fernandez-Funez, P., M.L. Nino-Rosales, B. de Gouyon, W.C. She, J.M. Luchak, P. Martinez, E. Turiegano, J. Benito, M. Capovilla, P.J. Skinner, A. McCall, I. Canal, H.T. Orr, H.Y. Zoghbi, and J. Botas. 2000. Identification of genes that modify ataxin-1-induced neurodegeneration. *Nature*. 408:101-106.
- Ferri, C.P., M. Prince, C. Brayne, H. Brodaty, L. Fratiglioni, M. Ganguli, K. Hall, K. Hasegawa, H. Hendrie, Y. Huang, A. Jorm, C. Mathers, P.R. Menezes, E. Rimmer, and M. Scazufca. 2005. Global prevalence of dementia: a Delphi consensus study. *Lancet*. 366:2112-2117.
- Fife, R.S., G.W. Sledge, Jr., S. Sissons, and B. Zerler. 2000. Effects of tetracyclines on angiogenesis in vitro. *Cancer letters*. 153:75-78.
- Fischl, A.S., and G.M. Carman. 1983. Phosphatidylinositol biosynthesis in *Saccharomyces cerevisiae*: purification and properties of microsome-associated phosphatidylinositol synthase. *Journal of bacteriology*. 154:304-311.
- Flick, J.S., and J. Thorner. 1993. Genetic and biochemical characterization of a phosphatidylinositol-specific phospholipase C in *Saccharomyces cerevisiae*. *Molecular and cellular biology*. 13:5861-5876.
- Flower, T.R., L.S. Chesnokova, C.A. Froelich, C. Dixon, and S.N. Witt. 2005. Heat shock prevents alpha-synuclein-induced apoptosis in a yeast model of Parkinson's disease. *Journal of molecular biology*. 351:1081-1100.
- Folch, J., M. Lees, and G.H. Sloane Stanley. 1957. A simple method for the isolation and purification of total lipides from animal tissues. *The Journal of biological chemistry*. 226:497-509.
- Forloni, G., L. Colombo, L. Girola, F. Tagliavini, and M. Salmona. 2001. Anti-amyloidogenic activity of tetracyclines: studies in vitro. *FEBS letters*. 487:404-407.
- Foury, F. 1997. Human genetic diseases: a cross-talk between man and yeast. *Gene*. 195:1-10.
- Fowler, S.D., and P. Greenspan. 1985. Application of Nile red, a fluorescent hydrophobic probe, for the detection of neutral lipid deposits in tissue sections: comparison with oil red O. *J Histochem Cytochem*. 33:833-836.
- Fox, T.D., L.S. Folley, J.J. Mulero, T.W. McMullin, P.E. Thorsness, L.O. Hedin, and M.C. Costanzo. 1991. Analysis and manipulation of yeast mitochondrial genes. *Methods in enzymology*. 194:149-165.
- Francis, R., G. McGrath, J. Zhang, D.A. Ruddy, M. Sym, J. Apfeld, M. Nicoll, M. Maxwell, B. Hai, M.C. Ellis, A.L. Parks, W. Xu, J. Li, M. Gurney, R.L. Myers, C.S. Himes, R. Hiebsch, C. Ruble, J.S. Nye, and D. Curtis. 2002. aph-1 and pen-2 are required for Notch pathway signaling, gamma-secretase cleavage of betaAPP, and presenilin protein accumulation. *Developmental cell*. 3:85-97.
- Friedrich, R.P., K. Tepper, R. Ronicke, M. Soom, M. Westermann, K. Reymann, C. Kaether, and M. Fandrich. 2010. Mechanism of amyloid plaque formation suggests an intracellular basis of Abeta pathogenicity. *Proceedings of the National Academy of Sciences of the United States of America*. 107:1942-1947.
- Frisardi, V., F. Panza, D. Seripa, T. Farooqui, and A.A. Farooqui. 2011. Glycerophospholipids and glycerophospholipid-derived lipid mediators: a complex meshwork in Alzheimer's disease pathology. *Progress in lipid research*. 50:313-330.
- Fujita, M., and Y. Jigami. 2008. Lipid remodeling of GPI-anchored proteins and its function. *Biochimica et biophysica acta*. 1780:410-420.

- Fyrst, H., B. Oskouian, F.A. Kuypers, and J.D. Saba. 1999. The PLB2 gene of *Saccharomyces cerevisiae* confers resistance to lysophosphatidylcholine and encodes a phospholipase B/lysophospholipase. *Biochemistry*. 38:5864-5871.
- Gaczynska, M., P.A. Osmulski, and W.F. Ward. 2001. Caretaker or undertaker? The role of the proteasome in aging. *Mechanisms of ageing and development*. 122:235-254.
- Gary, J.D., T.K. Sato, C.J. Stefan, C.J. Bonangelino, L.S. Weisman, and S.D. Emr. 2002. Regulation of Fab1 phosphatidylinositol 3-phosphate 5-kinase pathway by Vac7 protein and Fig4, a polyphosphoinositide phosphatase family member. *Molecular biology of the cell*. 13:1238-1251.
- Gaspar, M.L., M.A. Aregullin, S.A. Jesch, L.R. Nunez, M. Villa-Garcia, and S.A. Henry. 2007. The emergence of yeast lipidomics. *Biochimica et biophysica acta*. 1771:241-254.
- Gaspar, M.L., H.F. Hofbauer, S.D. Kohlwein, and S.A. Henry. 2011. Coordination of storage lipid synthesis and membrane biogenesis: evidence for cross-talk between triacylglycerol metabolism and phosphatidylinositol synthesis. *The Journal of biological chemistry*. 286:1696-1708.
- Gavin, A.C., M. Bosche, R. Krause, P. Grandi, M. Marzioch, A. Bauer, J. Schultz, J.M. Rick, A.M. Michon, C.M. Cruciat, M. Remor, C. Hofert, M. Schelder, M. Brajenovic, H. Ruffner, A. Merino, K. Klein, M. Hudak, D. Dickson, T. Rudi, V. Gnau, A. Bauch, S. Bastuck, B. Huhse, C. Leutwein, M.A. Heurtier, R.R. Copley, A. Edelmann, E. Querfurth, V. Rybin, G. Drewes, M. Raida, T. Bouwmeester, P. Bork, B. Seraphin, B. Kuster, G. Neubauer, and G. Superti-Furga. 2002. Functional organization of the yeast proteome by systematic analysis of protein complexes. *Nature*. 415:141-147.
- Gaynor, P.M., S. Hubbell, A.J. Schmidt, R.A. Lina, S.A. Minskoff, and M.L. Greenberg. 1991. Regulation of phosphatidylglycerolphosphate synthase in *Saccharomyces cerevisiae* by factors affecting mitochondrial development. *Journal of bacteriology*. 173:6124-6131.
- Gekko, K., and S.N. Timasheff. 1981. Mechanism of protein stabilization by glycerol: preferential hydration in glycerol-water mixtures. *Biochemistry*. 20:4667-4676.
- Gelperin, D.M., M.A. White, M.L. Wilkinson, Y. Kon, L.A. Kung, K.J. Wise, N. Lopez-Hoyo, L. Jiang, S. Piccirillo, H. Yu, M. Gerstein, M.E. Dumont, E.M. Phizicky, M. Snyder, and E.J. Grayhack. 2005. Biochemical and genetic analysis of the yeast proteome with a movable ORF collection. *Genes & development*. 19:2816-2826.
- Gene Ontology, C. 2001. Creating the gene ontology resource: design and implementation. *Genome research*. 11:1425-1433.
- Gentile, M.T., M.G. Reccia, P.P. Sorrentino, E. Vitale, G. Sorrentino, A.A. Puca, and L. Colucci-D'Amato. 2012. Role of Cytosolic Calcium-Dependent Phospholipase A2 in Alzheimer's Disease Pathogenesis. *Molecular neurobiology*.
- Ghosh, S., and M.B. Feany. 2004. Comparison of pathways controlling toxicity in the eye and brain in *Drosophila* models of human neurodegenerative diseases. *Human molecular genetics*. 13:2011-2018.
- Giasson, B.I., V.M. Lee, and J.Q. Trojanowski. 2003. Interactions of amyloidogenic proteins. *Neuromolecular medicine*. 4:49-58.
- Gietz, R.D., and R.A. Woods. 2002. Transformation of yeast by lithium acetate/single-stranded carrier DNA/polyethylene glycol method. *Methods in enzymology*. 350:87-96.
- Giorgini, F., P. Guidetti, Q. Nguyen, S.C. Bennett, and P.J. Muchowski. 2005. A genomic screen in yeast implicates kynurenine 3-monooxygenase as a therapeutic target for Huntington disease. *Nature genetics*. 37:526-531.

- Giorgini, F., T. Moller, W. Kwan, D. Zwillig, J.L. Wacker, S. Hong, L.C. Tsai, C.S. Cheah, R. Schwarcz, P. Guidetti, and P.J. Muchowski. 2008. Histone deacetylase inhibition modulates kynurenine pathway activation in yeast, microglia, and mice expressing a mutant huntingtin fragment. *The Journal of biological chemistry*. 283:7390-7400.
- Glabe, C.C. 2005. Amyloid accumulation and pathogenesis of Alzheimer's disease: significance of monomeric, oligomeric and fibrillar A β . *Sub-cellular biochemistry*. 38:167-177.
- Glenner, G.G., and C.W. Wong. 1984. Alzheimer's disease: initial report of the purification and characterization of a novel cerebrovascular amyloid protein. *Biochemical and biophysical research communications*. 120:885-890.
- GO-consortium. 2001. Creating the gene ontology resource: design and implementation. *Genome research*. 11:1425-1433.
- Goate, A., M.C. Chartier-Harlin, M. Mullan, J. Brown, F. Crawford, L. Fidani, L. Giuffra, A. Haynes, N. Irving, L. James, and et al. 1991. Segregation of a missense mutation in the amyloid precursor protein gene with familial Alzheimer's disease. *Nature*. 349:704-706.
- Goedert, M., and R.A. Crowther. 1989. Amyloid plaques, neurofibrillary tangles and their relevance for the study of Alzheimer's disease. *Neurobiology of aging*. 10:405-406; discussion 412-404.
- Goedert, M., M.G. Spillantini, N.J. Cairns, and R.A. Crowther. 1992. Tau proteins of Alzheimer paired helical filaments: abnormal phosphorylation of all six brain isoforms. *Neuron*. 8:159-168.
- Goedert, M., C.M. Wischik, R.A. Crowther, J.E. Walker, and A. Klug. 1988. Cloning and sequencing of the cDNA encoding a core protein of the paired helical filament of Alzheimer disease: identification as the microtubule-associated protein tau. *Proceedings of the National Academy of Sciences of the United States of America*. 85:4051-4055.
- Goldsbury, C.S., S. Wirtz, S.A. Muller, S. Sunderji, P. Wicki, U. Aepli, and P. Frey. 2000. Studies on the in vitro assembly of a β 1-40: implications for the search for a β fibril formation inhibitors. *Journal of structural biology*. 130:217-231.
- Gottlieb, D., W. Heideman, and J.D. Saba. 1999. The DPL1 gene is involved in mediating the response to nutrient deprivation in *Saccharomyces cerevisiae*. *Mol Cell Biol Res Commun*. 1:66-71.
- Gouras, G.K., C.G. Almeida, and R.H. Takahashi. 2005. Intraneuronal A β accumulation and origin of plaques in Alzheimer's disease. *Neurobiology of aging*. 26:1235-1244.
- Gouras, G.K., J. Tsai, J. Naslund, B. Vincent, M. Edgar, F. Checler, J.P. Greenfield, V. Haroutunian, J.D. Buxbaum, H. Xu, P. Greengard, and N.R. Relkin. 2000. Intraneuronal A β 42 accumulation in human brain. *The American journal of pathology*. 156:15-20.
- Greenberg, M.L., B. Reiner, and S.A. Henry. 1982. Regulatory mutations of inositol biosynthesis in yeast: isolation of inositol-excreting mutants. *Genetics*. 100:19-33.
- Greenberg, S.M., B.J. Bacsikai, and B.T. Hyman. 2003. Alzheimer disease's double-edged vaccine. *Nature medicine*. 9:389-390.
- Greenspan, P., and S.D. Fowler. 1985. Spectrofluorometric studies of the lipid probe, Nile red. *Journal of lipid research*. 26:781-789.
- Greenspan, P., E.P. Mayer, and S.D. Fowler. 1985. Nile red: a selective fluorescent stain for intracellular lipid droplets. *The Journal of cell biology*. 100:965-973.
- Grillitsch, K., M. Connerth, H. Kofeler, T.N. Arrey, B. Rietschel, B. Wagner, M. Karas, and G. Daum. 2011. Lipid particles/droplets of the yeast *Saccharomyces cerevisiae* revisited: lipidome meets proteome. *Biochimica et biophysica acta*. 1811:1165-1176.

- Grimm, M.O., H.S. Grimm, and T. Hartmann. 2007. Amyloid beta as a regulator of lipid homeostasis. *Trends in molecular medicine*. 13:337-344.
- Grimm, M.O., S. Grosgen, M. Riemenschneider, H. Tanila, H.S. Grimm, and T. Hartmann. 2011. From brain to food: analysis of phosphatidylcholins, lyso-phosphatidylcholins and phosphatidylcholin-plasmalogens derivatives in Alzheimer's disease human post mortem brains and mice model via mass spectrometry. *Journal of chromatography*. 1218:7713-7722.
- Grundke-Iqbal, I., K. Iqbal, L. George, Y.C. Tung, K.S. Kim, and H.M. Wisniewski. 1989. Amyloid protein and neurofibrillary tangles coexist in the same neuron in Alzheimer disease. *Proceedings of the National Academy of Sciences of the United States of America*. 86:2853-2857.
- Grundke-Iqbal, I., K. Iqbal, Y.C. Tung, M. Quinlan, H.M. Wisniewski, and L.I. Binder. 1986. Abnormal phosphorylation of the microtubule-associated protein tau (tau) in Alzheimer cytoskeletal pathology. *Proceedings of the National Academy of Sciences of the United States of America*. 83:4913-4917.
- Gu, Y., H.M. Lee, E.J. Roemer, L. Musacchia, L.M. Golub, and S.R. Simon. 2001. Inhibition of tumor cell invasiveness by chemically modified tetracyclines. *Current medicinal chemistry*. 8:261-270.
- Guan, X.L., C.M. Souza, H. Pichler, G. Dewhurst, O. Schaad, K. Kajiwara, H. Wakabayashi, T. Ivanova, G.A. Castillon, M. Piccolis, F. Abe, R. Loewith, K. Funato, M.R. Wenk, and H. Riezman. 2009. Functional interactions between sphingolipids and sterols in biological membranes regulating cell physiology. *Molecular biology of the cell*. 20:2083-2095.
- Guan, X.L., and M.R. Wenk. 2006. Mass spectrometry-based profiling of phospholipids and sphingolipids in extracts from *Saccharomyces cerevisiae*. *Yeast (Chichester, England)*. 23:465-477.
- Guo, Y., T.C. Walther, M. Rao, N. Stuurman, G. Goshima, K. Terayama, J.S. Wong, R.D. Vale, P. Walter, and R.V. Farese. 2008. Functional genomic screen reveals genes involved in lipid-droplet formation and utilization. *Nature*. 453:657-661.
- Guo, S., L.E. Stolz, S.M. Lemrow, and J.D. York. 1999. SAC1-like domains of yeast SAC1, INP52, and INP53 and of human synaptojanin encode polyphosphoinositide phosphatases. *The Journal of biological chemistry*. 274:12990-12995.
- Gyure, K.A., R. Durham, W.F. Stewart, J.E. Smialek, and J.C. Troncoso. 2001. Intraneuronal abeta-amyloid precedes development of amyloid plaques in Down syndrome. *Archives of pathology & laboratory medicine*. 125:489-492.
- Haass, C., M.G. Schlossmacher, A.Y. Hung, C. Vigo-Pelfrey, A. Mellon, B.L. Ostaszewski, I. Lieberburg, E.H. Koo, D. Schenk, D.B. Teplow, and et al. 1992. Amyloid beta-peptide is produced by cultured cells during normal metabolism. *Nature*. 359:322-325.
- Haass, C., and D.J. Selkoe. 1993. Cellular processing of beta-amyloid precursor protein and the genesis of amyloid beta-peptide. *Cell*. 75:1039-1042.
- Haass, C., and D.J. Selkoe. 2007. Soluble protein oligomers in neurodegeneration: lessons from the Alzheimer's amyloid beta-peptide. *Nature reviews. Molecular cell biology*. 8:101-112.
- Habicht, G., C. Haupt, R.P. Friedrich, P. Hortschansky, C. Sachse, J. Meinhardt, K. Wieligmann, G.P. Gellermann, M. Brodhun, J. Gotz, K.J. Halbhauer, C. Rocken, U. Horn, and M. Fandrich. 2007. Directed selection of a conformational antibody domain that prevents mature amyloid fibril formation by stabilizing Abeta protofibrils. *Proceedings of the National Academy of Sciences of the United States of America*. 104:19232-19237.

- Hamaguchi, T., K. Ono, A. Murase, and M. Yamada. 2009. Phenolic compounds prevent Alzheimer's pathology through different effects on the amyloid-beta aggregation pathway. *The American journal of pathology*. 175:2557-2565.
- Hamamichi, S., R.N. Rivas, A.L. Knight, S. Cao, K.A. Caldwell, and G.A. Caldwell. 2008. Hypothesis-based RNAi screening identifies neuroprotective genes in a Parkinson's disease model. *Proceedings of the National Academy of Sciences of the United States of America*. 105:728-733.
- Hammarstrom, P. 2009. Protein folding, misfolding and disease. *FEBS letters*. 583:2579-2580.
- Han, G.S., L. O'Hara, S. Siniosoglou, and G.M. Carman. 2008. Characterization of the yeast DGK1-encoded CTP-dependent diacylglycerol kinase. *The Journal of biological chemistry*. 283:20443-20453.
- Han, X., and R.W. Gross. 2003. Global analyses of cellular lipidomes directly from crude extracts of biological samples by ESI mass spectrometry: a bridge to lipidomics. *Journal of lipid research*. 44:1071-1079.
- Hanada, T., N.N. Noda, Y. Satomi, Y. Ichimura, Y. Fujioka, T. Takao, F. Inagaki, and Y. Ohsumi. 2007. The Atg12-Atg5 conjugate has a novel E3-like activity for protein lipidation in autophagy. *The Journal of biological chemistry*. 282:37298-37302.
- Hanahan, D., J. Jessee, and F.R. Bloom. 1991. Plasmid transformation of *Escherichia coli* and other bacteria. *Methods in enzymology*. 204:63-113.
- Hansen, L.A., E. Masliah, D. Galasko, and R.D. Terry. 1993. Plaque-only Alzheimer disease is usually the lewy body variant, and vice versa. *J Neuropathol Exp Neurol*. 52:648-654.
- Hardy, J., and D.J. Selkoe. 2002. The amyloid hypothesis of Alzheimer's disease: progress and problems on the road to therapeutics. *Science (New York, N.Y.)*. 297:353-356.
- Hardy, J.A., and G.A. Higgins. 1992. Alzheimer's disease: the amyloid cascade hypothesis. *Science (New York, N.Y.)*. 256:184-185.
- Harold, D., R. Abraham, P. Hollingworth, R. Sims, A. Gerrish, M.L. Hamshere, J.S. Pahwa, V. Moskvina, K. Dowzell, A. Williams, N. Jones, C. Thomas, A. Stretton, A.R. Morgan, S. Lovestone, J. Powell, P. Proitsi, M.K. Lupton, C. Brayne, D.C. Rubinsztein, M. Gill, B. Lawlor, A. Lynch, K. Morgan, K.S. Brown, P.A. Passmore, D. Craig, B. McGuinness, S. Todd, C. Holmes, D. Mann, A.D. Smith, S. Love, P.G. Kehoe, J. Hardy, S. Mead, N. Fox, M. Rossor, J. Collinge, W. Maier, F. Jessen, B. Schurmann, H. van den Bussche, I. Heuser, J. Kornhuber, J. Wiltfang, M. Dichgans, L. Frolich, H. Hampel, M. Hull, D. Rujescu, A.M. Goate, J.S. Kauwe, C. Cruchaga, P. Nowotny, J.C. Morris, K. Mayo, K. Sleegers, K. Bettens, S. Engelborghs, P.P. De Deyn, C. Van Broeckhoven, G. Livingston, N.J. Bass, H. Gurling, A. McQuillin, R. Gwilliam, P. Deloukas, A. Al-Chalabi, C.E. Shaw, M. Tsolaki, A.B. Singleton, R. Guerreiro, T.W. Muhleisen, M.M. Nothen, S. Moebus, K.H. Jockel, N. Klopp, H.E. Wichmann, M.M. Carrasquillo, V.S. Pankratz, S.G. Younkin, P.A. Holmans, M. O'Donovan, M.J. Owen, and J. Williams. 2009. Genome-wide association study identifies variants at CLU and PICALM associated with Alzheimer's disease. *Nature genetics*. 41:1088-1093.
- Harper, J.D., S.S. Wong, C.M. Lieber, and P.T. Lansbury, Jr. 1999. Assembly of A beta amyloid protofibrils: an in vitro model for a possible early event in Alzheimer's disease. *Biochemistry*. 38:8972-8980.
- Hartmann, T. 2001. Cholesterol, A beta and Alzheimer's disease. *Trends in neurosciences*. 24:S45-48.
- Hartmann, T., S.C. Bieger, B. Bruhl, P.J. Tienari, N. Ida, D. Allsop, G.W. Roberts, C.L. Masters, C.G. Dotti, K. Unsicker, and K. Beyreuther. 1997. Distinct sites of intracellular production for Alzheimer's disease A beta40/42 amyloid peptides. *Nature medicine*. 3:1016-1020.

- Hayashi, H., R.B. Campenot, D.E. Vance, and J.E. Vance. 2007. Apolipoprotein E-containing lipoproteins protect neurons from apoptosis via a signaling pathway involving low-density lipoprotein receptor-related protein-1. *J Neurosci.* 27:1933-1941.
- Henry, S.A., S.D. Kohlwein, and G.M. Carman. 2012. Metabolism and regulation of glycerolipids in the yeast *Saccharomyces cerevisiae*. *Genetics.* 190:317-349.
- Hepler, R.W., K.M. Grimm, D.D. Nahas, R. Breese, E.C. Dodson, P. Acton, P.M. Keller, M. Yeager, H. Wang, P. Shughrue, G. Kinney, and J.G. Joyce. 2006. Solution state characterization of amyloid beta-derived diffusible ligands. *Biochemistry.* 45:15157-15167.
- Herndon, L.A., P.J. Schmeissner, J.M. Dudaronek, P.A. Brown, K.M. Listner, Y. Sakano, M.C. Paupard, D.H. Hall, and M. Driscoll. 2002. Stochastic and genetic factors influence tissue-specific decline in ageing *C. elegans*. *Nature.* 419:808-814.
- Herzog, R., D. Schwudke, K. Schuhmann, J.L. Sampaio, S.R. Bornstein, M. Schroeder, and A. Shevchenko. 2011. A novel informatics concept for high-throughput shotgun lipidomics based on the molecular fragmentation query language. *Genome biology.* 12:R8.
- Hicks, D.A., N.N. Nalivaeva, and A.J. Turner. 2012. Lipid rafts and Alzheimer's disease: protein-lipid interactions and perturbation of signaling. *Frontiers in physiology.* 3:189.
- Hilbich, C., B. Kisters-Woike, J. Reed, C.L. Masters, and K. Beyreuther. 1992. Substitutions of hydrophobic amino acids reduce the amyloidogenicity of Alzheimer's disease beta A4 peptides. *Journal of molecular biology.* 228:460-473.
- Hirsch, J.P., and S.A. Henry. 1986. Expression of the *Saccharomyces cerevisiae* inositol-1-phosphate synthase (INO1) gene is regulated by factors that affect phospholipid synthesis. *Molecular and cellular biology.* 6:3320-3328.
- Hollingworth, P., D. Harold, R. Sims, A. Gerrish, J.C. Lambert, M.M. Carrasquillo, R. Abraham, M.L. Hamshere, J.S. Pahwa, V. Moskvina, K. Dowzell, N. Jones, A. Stretton, C. Thomas, A. Richards, D. Ivanov, C. Widdowson, J. Chapman, S. Lovestone, J. Powell, P. Proitsi, M.K. Lupton, C. Brayne, D.C. Rubinsztein, M. Gill, B. Lawlor, A. Lynch, K.S. Brown, P.A. Passmore, D. Craig, B. McGuinness, S. Todd, C. Holmes, D. Mann, A.D. Smith, H. Beaumont, D. Warden, G. Wilcock, S. Love, P.G. Kehoe, N.M. Hooper, E.R. Vardy, J. Hardy, S. Mead, N.C. Fox, M. Rossor, J. Collinge, W. Maier, F. Jessen, E. Ruther, B. Schurmann, R. Heun, H. Kolsch, H. van den Bussche, I. Heuser, J. Kornhuber, J. Wiltfang, M. Dichgans, L. Frolich, H. Hampel, J. Gallacher, M. Hull, D. Rujescu, I. Giegling, A.M. Goate, J.S. Kauwe, C. Cruchaga, P. Nowotny, J.C. Morris, K. Mayo, K. Sleegers, K. Bettens, S. Engelborghs, P.P. De Deyn, C. Van Broeckhoven, G. Livingston, N.J. Bass, H. Gurling, A. McQuillin, R. Gwilliam, P. Deloukas, A. Al-Chalabi, C.E. Shaw, M. Tsolaki, A.B. Singleton, R. Guerreiro, T.W. Muhleisen, M.M. Nothen, S. Moebus, K.H. Jockel, N. Klopp, H.E. Wichmann, V.S. Pankratz, S.B. Sando, J.O. Aasly, M. Barcikowska, Z.K. Wszolek, D.W. Dickson, N.R. Graff-Radford, R.C. Petersen, et al. 2011a. Common variants at ABCA7, MS4A6A/MS4A4E, EPHA1, CD33 and CD2AP are associated with Alzheimer's disease. *Nature genetics.* 43:429-435.
- Hollingworth, P., D. Harold, R. Sims, A. Gerrish, J.C. Lambert, M.M. Carrasquillo, R. Abraham, M.L. Hamshere, J.S. Pahwa, V. Moskvina, K. Dowzell, N. Jones, A. Stretton, C. Thomas, A. Richards, D. Ivanov, C. Widdowson, J. Chapman, S. Lovestone, J. Powell, P. Proitsi, M.K. Lupton, C. Brayne, D.C. Rubinsztein, M. Gill, B. Lawlor, A. Lynch, K.S. Brown, P.A. Passmore, D. Craig, B. McGuinness, S. Todd, C. Holmes, D. Mann, A.D. Smith, H. Beaumont, D. Warden, G. Wilcock, S. Love, P.G. Kehoe, N.M. Hooper, E.R. Vardy, J. Hardy, S. Mead, N.C. Fox, M. Rossor, J. Collinge, W. Maier, F. Jessen, E. Ruther, B. Schurmann, R. Heun, H. Kolsch, H. van den Bussche, I. Heuser, J. Kornhuber, J. Wiltfang, M. Dichgans, L. Frolich, H. Hampel, J. Gallacher, M. Hull, D. Rujescu, I. Giegling, A.M. Goate, J.S. Kauwe, C. Cruchaga, P. Nowotny, J.C. Morris, K. Mayo, K. Sleegers, K. Bettens, S. Engelborghs, P.P. De Deyn, C. Van Broeckhoven, G. Livingston, N.J. Bass, H. Gurling, A. McQuillin, R. Gwilliam, P. Deloukas, A. Al-Chalabi, C.E. Shaw, M. Tsolaki, A.B. Singleton, R. Guerreiro, T.W. Muhleisen, M.M.

- Nothen, S. Moebus, K.H. Jockel, N. Klopp, H.E. Wichmann, V.S. Pankratz, S.B. Sando, J.O. Aasly, M. Barcikowska, Z.K. Wszolek, D.W. Dickson, N.R. Graff-Radford, R.C. Petersen, et al. 2011b. Common variants at ABCA7, MS4A6A/MS4A4E, EPHA1, CD33 and CD2AP are associated with Alzheimer's disease. *Nature genetics*. 43:429-435.
- Homann, M.J., S.A. Henry, and G.M. Carman. 1985. Regulation of CDP-diacylglycerol synthase activity in *Saccharomyces cerevisiae*. *Journal of bacteriology*. 163:1265-1266.
- Hosaka, K., T. Murakami, T. Kodaki, J. Nikawa, and S. Yamashita. 1990. Repression of choline kinase by inositol and choline in *Saccharomyces cerevisiae*. *Journal of bacteriology*. 172:2005-2012.
- Howlett, D., P. Cutler, S. Heales, and P. Camilleri. 1997. Hemin and related porphyrins inhibit beta-amyloid aggregation. *FEBS letters*. 417:249-251.
- Howlett, D.R., K.H. Jennings, D.C. Lee, M.S. Clark, F. Brown, R. Wetzel, S.J. Wood, P. Camilleri, and G.W. Roberts. 1995. Aggregation state and neurotoxic properties of Alzheimer beta-amyloid peptide. *Neurodegeneration*. 4:23-32.
- Hsiao, K., P. Chapman, S. Nilsen, C. Eckman, Y. Harigaya, S. Younkin, F. Yang, and G. Cole. 1996. Correlative memory deficits, Abeta elevation, and amyloid plaques in transgenic mice. *Science (New York, N.Y.)*. 274:99-102.
- Hu, X., S.L. Crick, G. Bu, C. Frieden, R.V. Pappu, and J.M. Lee. 2009. Amyloid seeds formed by cellular uptake, concentration, and aggregation of the amyloid-beta peptide. *Proceedings of the National Academy of Sciences of the United States of America*. 106:20324-20329.
- Hu, Y., J. Komoto, Y. Huang, T. Gomi, H. Ogawa, Y. Takata, M. Fujioka, and F. Takusagawa. 1999. Crystal structure of S-adenosylhomocysteine hydrolase from rat liver. *Biochemistry*. 38:8323-8333.
- Huang, W., G.E. Alexander, E.M. Daly, H.U. Shetty, J.S. Krasuski, S.I. Rapoport, and M.B. Schapiro. 1999. High brain myo-inositol levels in the predementia phase of Alzheimer's disease in adults with Down's syndrome: a 1H MRS study. *The American journal of psychiatry*. 156:1879-1886.
- Huh, W.K., J.V. Falvo, L.C. Gerke, A.S. Carroll, R.W. Howson, J.S. Weissman, and E.K. O'Shea. 2003. Global analysis of protein localization in budding yeast. *Nature*. 425:686-691.
- Hung, L.W., G.D. Ciccotosto, E. Giannakis, D.J. Tew, K. Perez, C.L. Masters, R. Cappai, J.D. Wade, and K.J. Barnham. 2008. Amyloid-beta peptide (Abeta) neurotoxicity is modulated by the rate of peptide aggregation: Abeta dimers and trimers correlate with neurotoxicity. *J Neurosci*. 28:11950-11958.
- Hutton, M., C.L. Lendon, P. Rizzu, M. Baker, S. Froelich, H. Houlden, S. Pickering-Brown, S. Chakraverty, A. Isaacs, A. Grover, J. Hackett, J. Adamson, S. Lincoln, D. Dickson, P. Davies, R.C. Petersen, M. Stevens, E. de Graaff, E. Wauters, J. van Baren, M. Hillebrand, M. Joosse, J.M. Kwon, P. Nowotny, L.K. Che, J. Norton, J.C. Morris, L.A. Reed, J. Trojanowski, H. Basun, L. Lannfelt, M. Neystat, S. Fahn, F. Dark, T. Tannenberg, P.R. Dodd, N. Hayward, J.B. Kwok, P.R. Schofield, A. Andreadis, J. Snowden, D. Craufurd, D. Neary, F. Owen, B.A. Oostra, J. Hardy, A. Goate, J. van Swieten, D. Mann, T. Lynch, and P. Heutink. 1998. Association of missense and 5'-splice-site mutations in tau with the inherited dementia FTDP-17. *Nature*. 393:702-705.
- Ikeda, K., T. Yamaguchi, S. Fukunaga, M. Hoshino, and K. Matsuzaki. 2011. Mechanism of amyloid beta-protein aggregation mediated by GM1 ganglioside clusters. *Biochemistry*. 50:6433-6440.
- Jandrositz, A., J. Petschnigg, R. Zimmermann, K. Natter, H. Scholze, A. Hermetter, S.D. Kohlwein, and R. Leber. 2005. The lipid droplet enzyme Tgl1p hydrolyzes both sterol esters and triglycerides in the yeast, *Saccharomyces cerevisiae*. *Biochimica et biophysica acta*. 1735:50-58.

- Jarrett, J.T., E.P. Berger, and P.T. Lansbury, Jr. 1993a. The C-terminus of the beta protein is critical in amyloidogenesis. *Annals of the New York Academy of Sciences*. 695:144-148.
- Jarrett, J.T., E.P. Berger, and P.T. Lansbury, Jr. 1993b. The carboxy terminus of the beta amyloid protein is critical for the seeding of amyloid formation: implications for the pathogenesis of Alzheimer's disease. *Biochemistry*. 32:4693-4697.
- Jarrett, J.T., and P.T. Lansbury, Jr. 1993. Seeding "one-dimensional crystallization" of amyloid: a pathogenic mechanism in Alzheimer's disease and scrapie? *Cell*. 73:1055-1058.
- Jesch, S.A., X. Zhao, M.T. Wells, and S.A. Henry. 2005. Genome-wide analysis reveals inositol, not choline, as the major effector of Ino2p-Ino4p and unfolded protein response target gene expression in yeast. *The Journal of biological chemistry*. 280:9106-9118.
- Johnson, B.S., J.M. McCaffery, S. Lindquist, and A.D. Gitler. 2008. A yeast TDP-43 proteinopathy model: Exploring the molecular determinants of TDP-43 aggregation and cellular toxicity. *Proceedings of the National Academy of Sciences of the United States of America*. 105:6439-6444.
- Johnson, D.R., L.J. Knoll, D.E. Levin, and J.I. Gordon. 1994. *Saccharomyces cerevisiae* contains four fatty acid activation (FAA) genes: an assessment of their role in regulating protein N-myristoylation and cellular lipid metabolism. *The Journal of cell biology*. 127:751-762.
- Jones, L., D. Harold, and J. Williams. 2010. Genetic evidence for the involvement of lipid metabolism in Alzheimer's disease. *Biochimica et biophysica acta*. 1801:754-761.
- Joshi, A.S., J. Zhou, V.M. Gohil, S. Chen, and M.L. Greenberg. 2009. Cellular functions of cardiolipin in yeast. *Biochimica et biophysica acta*. 1793:212-218.
- Kagiwada, S., K. Hosaka, M. Murata, J. Nikawa, and A. Takatsuki. 1998. The *Saccharomyces cerevisiae* SCS2 gene product, a homolog of a synaptobrevin-associated protein, is an integral membrane protein of the endoplasmic reticulum and is required for inositol metabolism. *Journal of bacteriology*. 180:1700-1708.
- Kagiwada, S., and R. Zen. 2003. Role of the yeast VAP homolog, Scs2p, in INO1 expression and phospholipid metabolism. *J Biochem*. 133:515-522.
- Kain, S.R., M. Adams, A. Kondepudi, T.T. Yang, W.W. Ward, and P. Kitts. 1995. Green fluorescent protein as a reporter of gene expression and protein localization. *BioTechniques*. 19:650-655.
- Kajava, A.V., U. Baxa, and A.C. Steven. 2010. Beta arcades: recurring motifs in naturally occurring and disease-related amyloid fibrils. *Faseb J*. 24:1311-1319.
- Kamboh, M.I. 2004. Molecular genetics of late-onset Alzheimer's disease. *Annals of human genetics*. 68:381-404.
- Kanfer, J.N., G. Sorrentino, and D.S. Sitar. 1999. Amyloid beta peptide membrane perturbation is the basis for its biological effects. *Neurochem Res*. 24:1621-1630.
- Kapteyn, J.C., R.C. Montijn, E. Vink, J. de la Cruz, A. Llobell, J.E. Douwes, H. Shimoï, P.N. Lipke, and F.M. Klis. 1996. Retention of *Saccharomyces cerevisiae* cell wall proteins through a phosphodiester-linked beta-1,3-/beta-1,6-glucan heteropolymer. *Glycobiology*. 6:337-345.
- Kayed, R., E. Head, J.L. Thompson, T.M. McIntire, S.C. Milton, C.W. Cotman, and C.G. Glabe. 2003. Common structure of soluble amyloid oligomers implies common mechanism of pathogenesis. *Science (New York, N.Y.)*. 300:486-489.
- Kazemi-Esfarjani, P., and S. Benzer. 2000. Genetic suppression of polyglutamine toxicity in *Drosophila*. *Science (New York, N.Y.)*. 287:1837-1840.

- Keller, L., H. Welander, H.H. Chiang, L.O. Tjernberg, I. Nennesmo, A.K. Wallin, and C. Graff. 2010. The PSEN1 I143T mutation in a Swedish family with Alzheimer's disease: clinical report and quantification of A β in different brain regions. *Eur J Hum Genet.* 18:1202-1208.
- Kelley, M.J., A.M. Bailis, S.A. Henry, and G.M. Carman. 1988. Regulation of phospholipid biosynthesis in *Saccharomyces cerevisiae* by inositol. Inositol is an inhibitor of phosphatidylserine synthase activity. *The Journal of biological chemistry.* 263:18078-18085.
- Kennedy, E.P., and S.B. Weiss. 1956. The function of cytidine coenzymes in the biosynthesis of phospholipides. *The Journal of biological chemistry.* 222:193-214.
- Kent, C. 2005. Regulatory enzymes of phosphatidylcholine biosynthesis: a personal perspective. *Biochimica et biophysica acta.* 1733:53-66.
- Kent, C., and G.M. Carman. 1999. Interactions among pathways for phosphatidylcholine metabolism, CTP synthesis and secretion through the Golgi apparatus. *Trends in biochemical sciences.* 24:146-150.
- Khurana, V., and S. Lindquist. 2010. Modelling neurodegeneration in *Saccharomyces cerevisiae*: why cook with baker's yeast? *Nature reviews.* 11:436-449.
- Kienlen-Campard, P., S. Miolet, B. Tasiaux, and J.N. Octave. 2002. Intracellular amyloid-beta 1-42, but not extracellular soluble amyloid-beta peptides, induces neuronal apoptosis. *The Journal of biological chemistry.* 277:15666-15670.
- Kim, J., J.M. Basak, and D.M. Holtzman. 2009a. The role of apolipoprotein E in Alzheimer's disease. *Neuron.* 63:287-303.
- Kim, J., J.M. Castellano, H. Jiang, J.M. Basak, M. Parsadanian, V. Pham, S.M. Mason, S.M. Paul, and D.M. Holtzman. 2009b. Overexpression of low-density lipoprotein receptor in the brain markedly inhibits amyloid deposition and increases extracellular A β clearance. *Neuron.* 64:632-644.
- Kim, S.I., J.S. Yi, and Y.G. Ko. 2006. Amyloid beta oligomerization is induced by brain lipid rafts. *Journal of cellular biochemistry.* 99:878-889.
- Kim, W., and M.H. Hecht. 2005. Sequence determinants of enhanced amyloidogenicity of Alzheimer A β ₄₂ peptide relative to A β ₄₀. *The Journal of biological chemistry.* 280:35069-35076.
- Kim, W., and M.H. Hecht. 2006. Generic hydrophobic residues are sufficient to promote aggregation of the Alzheimer's A β ₄₂ peptide. *Proceedings of the National Academy of Sciences of the United States of America.* 103:15824-15829.
- Kim, W., and M.H. Hecht. 2008. Mutations Enhance the Aggregation Propensity of the Alzheimer's A β Peptide. *Journal of molecular biology.*
- Kimpara, T., A. Takeda, T. Yamaguchi, H. Arai, N. Okita, S. Takase, H. Sasaki, and Y. Itoyama. 2000. Increased bilirubins and their derivatives in cerebrospinal fluid in Alzheimer's disease. *Neurobiology of aging.* 21:551-554.
- Kinoshita, A., H. Fukumoto, T. Shah, C.M. Whelan, M.C. Irizarry, and B.T. Hyman. 2003. Demonstration by FRET of BACE interaction with the amyloid precursor protein at the cell surface and in early endosomes. *Journal of cell science.* 116:3339-3346.
- Kirisako, T., Y. Ichimura, H. Okada, Y. Kabeya, N. Mizushima, T. Yoshimori, M. Ohsumi, T. Takao, T. Noda, and Y. Ohsumi. 2000. The reversible modification regulates the membrane-binding state of Apg8/Aut7 essential for autophagy and the cytoplasm to vacuole targeting pathway. *The Journal of cell biology.* 151:263-276.

- Kiyono, K., K. Miura, Y. Kushima, T. Hikiji, M. Fukushima, I. Shibuya, and A. Ohta. 1987. Primary structure and product characterization of the *Saccharomyces cerevisiae* CHO1 gene that encodes phosphatidylserine synthase. *J Biochem.* 102:1089-1100.
- Klein, W.L., G.A. Krafft, and C.E. Finch. 2001. Targeting small Abeta oligomers: the solution to an Alzheimer's disease conundrum? *Trends in neurosciences.* 24:219-224.
- Klose, C., M.A. Surma, M.J. Gerl, F. Meyenhofer, A. Shevchenko, and K. Simons. 2012. Flexibility of a eukaryotic lipidome--insights from yeast lipidomics. *PLoS ONE.* 7:e35063.
- Klyubin, I., V. Betts, A.T. Welzel, K. Blennow, H. Zetterberg, A. Wallin, C.A. Lemere, W.K. Cullen, Y. Peng, T. Wisniewski, D.J. Selkoe, R. Anwyl, D.M. Walsh, and M.J. Rowan. 2008. Amyloid beta protein dimer-containing human CSF disrupts synaptic plasticity: prevention by systemic passive immunization. *J Neurosci.* 28:4231-4237.
- Kodaki, T., and S. Yamashita. 1987. Yeast phosphatidylethanolamine methylation pathway. Cloning and characterization of two distinct methyltransferase genes. *The Journal of biological chemistry.* 262:15428-15435.
- Koffel, R., and R. Schneider. 2006. Yeh1 constitutes the major steryl ester hydrolase under heme-deficient conditions in *Saccharomyces cerevisiae*. *Eukaryot Cell.* 5:1018-1025.
- Koh, J.L., H. Ding, M. Costanzo, A. Baryshnikova, K. Toufighi, G.D. Bader, C.L. Myers, B.J. Andrews, and C. Boone. 2010. DRYGIN: a database of quantitative genetic interaction networks in yeast. *Nucleic acids research.* 38:D502-507.
- Kojro, E., and F. Fahrenholz. 2005. The non-amyloidogenic pathway: structure and function of alpha-secretases. *Sub-cellular biochemistry.* 38:105-127.
- Kolaczowski, M., A. Kolaczowska, J. Luczynski, S. Witek, and A. Goffeau. 1998. In vivo characterization of the drug resistance profile of the major ABC transporters and other components of the yeast pleiotropic drug resistance network. *Microbial drug resistance.* 4:143-158.
- Kollar, R., E. Petrakova, G. Ashwell, P.W. Robbins, and E. Cabib. 1995. Architecture of the yeast cell wall. The linkage between chitin and beta(1-->3)-glucan. *The Journal of biological chemistry.* 270:1170-1178.
- Komano, H., M. Seeger, S. Gandy, G.T. Wang, G.A. Krafft, and R.S. Fuller. 1998. Involvement of cell surface glycosyl-phosphatidylinositol-linked aspartyl proteases in alpha-secretase-type cleavage and ectodomain solubilization of human Alzheimer beta-amyloid precursor protein in yeast. *The Journal of biological chemistry.* 273:31648-31651.
- Komatsu, M., I. Tanida, T. Ueno, M. Ohsumi, Y. Ohsumi, and E. Kominami. 2001. The C-terminal region of an Apg7p/Cvt2p is required for homodimerization and is essential for its E1 activity and E1-E2 complex formation. *The Journal of biological chemistry.* 276:9846-9854.
- Kraemer, B.C., J.K. Burgess, J.H. Chen, J.H. Thomas, and G.D. Schellenberg. 2006. Molecular pathways that influence human tau-induced pathology in *Caenorhabditis elegans*. *Human molecular genetics.* 15:1483-1496.
- Kroon, A.M., and C. Van den Bogert. 1983. Antibacterial drugs and their interference with the biogenesis of mitochondria in animal and human cells. *Pharmaceutisch weekblad. Scientific edition.* 5:81-87.
- Kuwahara, T., A. Koyama, S. Koyama, S. Yoshina, C.H. Ren, T. Kato, S. Mitani, and T. Iwatsubo. 2008. A systematic RNAi screen reveals involvement of endocytic pathway in neuronal dysfunction in alpha-synuclein transgenic *C. elegans*. *Human molecular genetics.* 17:2997-3009.

- LaFerla, F.M., K.N. Green, and S. Oddo. 2007. Intracellular amyloid-beta in Alzheimer's disease. *Nature reviews*. 8:499-509.
- LaFerla, F.M., and S. Oddo. 2005. Alzheimer's disease: Abeta, tau and synaptic dysfunction. *Trends in molecular medicine*. 11:170-176.
- Lai, A.Y., and J. McLaurin. 2010. Mechanisms of amyloid-Beta Peptide uptake by neurons: the role of lipid rafts and lipid raft-associated proteins. *International journal of Alzheimer's disease*. 2011:548380.
- Lambert, J.C., and P. Amouyel. 2011. Genetics of Alzheimer's disease: new evidences for an old hypothesis? *Current opinion in genetics & development*. 21:295-301.
- Lambert, J.C., L. Araria-Goumidi, L. Myllykangas, C. Ellis, J.C. Wang, M.J. Bullido, J.M. Harris, M.J. Artiga, D. Hernandez, J.M. Kwon, B. Frigard, R.C. Petersen, A.M. Cumming, F. Pasquier, I. Sastre, P.J. Tienari, A. Frank, R. Sulkava, J.C. Morris, D. St Clair, D.M. Mann, F. Wavrant-DeVrieze, M. Ezquerro-Trabalón, P. Amouyel, J. Hardy, M. Haltia, F. Valdivieso, A.M. Goate, J. Perez-Tur, C.L. Lendon, and M.C. Chartier-Harlin. 2002. Contribution of APOE promoter polymorphisms to Alzheimer's disease risk. *Neurology*. 59:59-66.
- Lambert, J.C., N. Coyle, and C. Lendon. 2004. The allelic modulation of apolipoprotein E expression by oestrogen: potential relevance for Alzheimer's disease. *J Med Genet*. 41:104-112.
- Lambert, J.C., S. Heath, G. Even, D. Campion, K. Sleegers, M. Hiltunen, O. Combarros, D. Zelenika, M.J. Bullido, B. Tavernier, L. Letenneur, K. Bettens, C. Berr, F. Pasquier, N. Fievet, P. Barberger-Gateau, S. Engelborghs, P. De Deyn, I. Mateo, A. Franck, S. Helisalmi, E. Porcellini, O. Hanon, M.M. de Pancorbo, C. Lendon, C. Dufouil, C. Jaillard, T. Leveillard, V. Alvarez, P. Bosco, M. Mancuso, F. Panza, B. Nacmias, P. Bossu, P. Piccardi, G. Annoni, D. Seripa, D. Galimberti, D. Hannequin, F. Licastro, H. Soininen, K. Ritchie, H. Blanche, J.F. Dartigues, C. Tzourio, I. Gut, C. Van Broeckhoven, A. Alperovitch, M. Lathrop, and P. Amouyel. 2009. Genome-wide association study identifies variants at CLU and CR1 associated with Alzheimer's disease. *Nature genetics*. 41:1094-1099.
- Lambert, J.C., D. Mann, L. Goumidi, J. Harris, P. Amouyel, T. Iwatsubo, C. Lendon, and M.C. Chartier-Harlin. 2001. Effect of the APOE promoter polymorphisms on cerebral amyloid peptide deposition in Alzheimer's disease. *Lancet*. 357:608-609.
- Lambert, J.C., D. Mann, F. Richard, J. Tian, J. Shi, U. Thaker, S. Merrot, J. Harris, B. Frigard, T. Iwatsubo, C. Lendon, and P. Amouyel. 2005. Is there a relation between APOE expression and brain amyloid load in Alzheimer's disease? *Journal of neurology, neurosurgery, and psychiatry*. 76:928-933.
- Lambert, M.P., A.K. Barlow, B.A. Chromy, C. Edwards, R. Freed, M. Liosatos, T.E. Morgan, I. Rozovsky, B. Trommer, K.L. Viola, P. Wals, C. Zhang, C.E. Finch, G.A. Krafft, and W.L. Klein. 1998. Diffusible, nonfibrillar ligands derived from Abeta1-42 are potent central nervous system neurotoxins. *Proceedings of the National Academy of Sciences of the United States of America*. 95:6448-6453.
- Landreth, G. 2006. PPARgamma agonists as new therapeutic agents for the treatment of Alzheimer's disease. *Experimental neurology*. 199:245-248.
- Lang, T., E. Schaeffeler, D. Bernreuther, M. Bredschneider, D.H. Wolf, and M. Thumm. 1998. Aut2p and Aut7p, two novel microtubule-associated proteins are essential for delivery of autophagic vesicles to the vacuole. *The EMBO journal*. 17:3597-3607.
- Langui, D., N. Girardot, K.H. El Hachimi, B. Allinquant, V. Blanchard, L. Pradier, and C. Duyckaerts. 2004. Subcellular topography of neuronal Abeta peptide in APPxPS1 transgenic mice. *The American journal of pathology*. 165:1465-1477.

- Larsson, C., I.L. Pahlman, R. Ansell, M. Rigoulet, L. Adler, and L. Gustafsson. 1998. The importance of the glycerol 3-phosphate shuttle during aerobic growth of *Saccharomyces cerevisiae*. *Yeast (Chichester, England)*. 14:347-357.
- Lashuel, H.A., D. Hartley, B.M. Petre, T. Walz, and P.T. Lansbury, Jr. 2002. Neurodegenerative disease: amyloid pores from pathogenic mutations. *Nature*. 418:291.
- Lashuel, H.A., and P.T. Lansbury, Jr. 2006. Are amyloid diseases caused by protein aggregates that mimic bacterial pore-forming toxins? *Quarterly reviews of biophysics*. 39:167-201.
- Lazarow, P.B. 2003. Peroxisome biogenesis: advances and conundrums. *Current opinion in cell biology*. 15:489-497.
- Leber, R., E. Zinser, G. Zellnig, F. Paltauf, and G. Daum. 1994. Characterization of lipid particles of the yeast, *Saccharomyces cerevisiae*. *Yeast (Chichester, England)*. 10:1421-1428.
- Lee, H.M., L.M. Golub, J. Cao, O. Teronen, M. Laitinen, T. Salo, S. Zucker, and T. Sorsa. 2001a. CMT-3, a non-antimicrobial tetracycline (TC), inhibits MT1-MMP activity: relevance to cancer. *Current medicinal chemistry*. 8:257-260.
- Lee, K.S., J.L. Patton, M. Fido, L.K. Hines, S.D. Kohlwein, F. Paltauf, S.A. Henry, and D.E. Levin. 1994. The *Saccharomyces cerevisiae* PLB1 gene encodes a protein required for lysophospholipase and phospholipase B activity. *The Journal of biological chemistry*. 269:19725-19730.
- Lee, L.L., H. Ha, Y.T. Chang, and M.P. DeLisa. 2009. Discovery of amyloid-beta aggregation inhibitors using an engineered assay for intracellular protein folding and solubility. *Protein Sci*. 18:277-286.
- Lee, V.M., M. Goedert, and J.Q. Trojanowski. 2001b. Neurodegenerative tauopathies. *Annual review of neuroscience*. 24:1121-1159.
- Leprince, C., F. Romero, D. Cussac, B. Vayssiere, R. Berger, A. Tavitian, and J.H. Camonis. 1997. A new member of the amphiphysin family connecting endocytosis and signal transduction pathways. *The Journal of biological chemistry*. 272:15101-15105.
- Lesne, S., M.T. Koh, L. Kotilinek, R. Kaye, C.G. Glabe, A. Yang, M. Gallagher, and K.H. Ashe. 2006. A specific amyloid-beta protein assembly in the brain impairs memory. *Nature*. 440:352-357.
- Lesne, S., and L. Kotilinek. 2005. Amyloid plaques and amyloid-beta oligomers: an ongoing debate. *J Neurosci*. 25:9319-9320.
- Letts, V.A., and I.W. Dawes. 1983. Temperature-sensitive *Saccharomyces cerevisiae* mutant defective in lipid biosynthesis. *Journal of bacteriology*. 156:212-221.
- Letts, V.A., L.S. Klig, M. Bae-Lee, G.M. Carman, and S.A. Henry. 1983. Isolation of the yeast structural gene for the membrane-associated enzyme phosphatidylserine synthase. *Proceedings of the National Academy of Sciences of the United States of America*. 80:7279-7283.
- LeVine, H., 3rd. 2007. Small molecule inhibitors of Abeta assembly. *Amyloid*. 14:185-197.
- Levy-Lahad, E., W. Wasco, P. Poorkaj, D.M. Romano, J. Oshima, W.H. Pettingell, C.E. Yu, P.D. Jondro, S.D. Schmidt, K. Wang, and et al. 1995. Candidate gene for the chromosome 1 familial Alzheimer's disease locus. *Science (New York, N.Y.)*. 269:973-977.
- Levy, E., M.D. Carman, I.J. Fernandez-Madrid, M.D. Power, I. Lieberburg, S.G. van Duinen, G.T. Bots, W. Luyendijk, and B. Frangione. 1990. Mutation of the Alzheimer's disease amyloid gene in hereditary cerebral hemorrhage, Dutch type. *Science (New York, N.Y.)*. 248:1124-1126.

- Li, S., G.M. Shankar, and D.J. Selkoe. 2010. How do Soluble Oligomers of Amyloid beta-protein Impair Hippocampal Synaptic Plasticity? *Frontiers in cellular neuroscience*. 4:5.
- Lindner, A.B., and A. Demarez. 2009. Protein aggregation as a paradigm of aging. *Biochimica et biophysica acta*. 1790:980-996.
- Listenberger, L.L., and D.A. Brown. 2007. Fluorescent detection of lipid droplets and associated proteins. *Current protocols in cell biology / editorial board, Juan S. Bonifacino ... [et al.* Chapter 24:Unit 24 22.
- Liu, K., X. Zhang, C. Sumanasekera, R.L. Lester, and R.C. Dickson. 2005. Signalling functions for sphingolipid long-chain bases in *Saccharomyces cerevisiae*. *Biochemical Society transactions*. 33:1170-1173.
- Liu, Y., and D. Schubert. 2006. Treating Alzheimer's disease by inactivating bioactive amyloid beta peptide. *Current Alzheimer research*. 3:129-135.
- Loewen, C.J., M.L. Gaspar, S.A. Jesch, C. Delon, N.T. Ktistakis, S.A. Henry, and T.P. Levine. 2004. Phospholipid metabolism regulated by a transcription factor sensing phosphatidic acid. *Science (New York, N.Y.* 304:1644-1647.
- Loewen, C.J., A. Roy, and T.P. Levine. 2003. A conserved ER targeting motif in three families of lipid binding proteins and in Opi1p binds VAP. *The EMBO journal*. 22:2025-2035.
- Loewy, B.S., and S.A. Henry. 1984. The INO2 and INO4 loci of *Saccharomyces cerevisiae* are pleiotropic regulatory genes. *Molecular and cellular biology*. 4:2479-2485.
- Lovell, M.A., W.D. Ehmann, S.M. Butler, and W.R. Markesbery. 1995. Elevated thiobarbituric acid-reactive substances and antioxidant enzyme activity in the brain in Alzheimer's disease. *Neurology*. 45:1594-1601.
- Lowry, O.H., N.J. Rosebrough, A.L. Farr, and R.J. Randall. 1951. Protein measurement with the Folin phenol reagent. *The Journal of biological chemistry*. 193:265-275.
- Lue, L.F., Y.M. Kuo, A.E. Roher, L. Brachova, Y. Shen, L. Sue, T. Beach, J.H. Kurth, R.E. Rydel, and J. Rogers. 1999. Soluble amyloid beta peptide concentration as a predictor of synaptic change in Alzheimer's disease. *The American journal of pathology*. 155:853-862.
- Luhrs, T., C. Ritter, M. Adrian, D. Riek-Loher, B. Bohrmann, H. Dobeli, D. Schubert, and R. Riek. 2005. 3D structure of Alzheimer's amyloid-beta(1-42) fibrils. *Proceedings of the National Academy of Sciences of the United States of America*. 102:17342-17347.
- Luthi, U., C. Schaerer-Brodbeck, S. Tanner, O. Middendorp, K. Edler, and A. Barberis. 2003. Human beta-secretase activity in yeast detected by a novel cellular growth selection system. *Biochimica et biophysica acta*. 1620:167-178.
- Lyons, T.J., A.P. Gasch, L.A. Gaither, D. Botstein, P.O. Brown, and D.J. Eide. 2000. Genome-wide characterization of the Zap1p zinc-responsive regulon in yeast. *Proceedings of the National Academy of Sciences of the United States of America*. 97:7957-7962.
- Macchi, F., M. Eisenkolb, H. Kiefer, and D.E. Otzen. 2012. The effect of osmolytes on protein fibrillation. *International journal of molecular sciences*. 13:3801-3819.
- MacDonald, A.B. 2007. Alzheimer's disease Braak Stage progressions: reexamined and redefined as Borrelia infection transmission through neural circuits. *Medical hypotheses*. 68:1059-1064.
- Macreadie, I., M. Lotfi-Miri, S. Mohotti, D. Shapira, L. Bennett, and J. Varghese. 2008. Validation of folate in a convenient yeast assay suited for identification of inhibitors of Alzheimer's amyloid-beta aggregation. *J Alzheimers Dis*. 15:391-396.

- Majumder, A.L., A. Chatterjee, K. Ghosh Dastidar, and M. Majee. 2003. Diversification and evolution of L-myo-inositol 1-phosphate synthase. *FEBS letters*. 553:3-10.
- Makin, O.S., and L.C. Serpell. 2005. Structures for amyloid fibrils. *The FEBS journal*. 272:5950-5961.
- Malmstrom, L., M. Riffle, C.E. Strauss, D. Chivian, T.N. Davis, R. Bonneau, and D. Baker. 2007. Superfamily assignments for the yeast proteome through integration of structure prediction with the gene ontology. *PLoS biology*. 5:e76.
- Maltseva, E., and G. Brezesinski. 2004. Adsorption of amyloid beta (1-40) peptide to phosphatidylethanolamine monolayers. *Chemphyschem*. 5:1185-1190.
- Maltseva, E., A. Kerth, A. Blume, H. Mohwald, and G. Brezesinski. 2005. Adsorption of amyloid beta (1-40) peptide at phospholipid monolayers. *Chembiochem*. 6:1817-1824.
- Manczak, M., T.S. Anekonda, E. Henson, B.S. Park, J. Quinn, and P.H. Reddy. 2006. Mitochondria are a direct site of A beta accumulation in Alzheimer's disease neurons: implications for free radical generation and oxidative damage in disease progression. *Human molecular genetics*. 15:1437-1449.
- Markossian, K.A., and B.I. Kurganov. 2004. Protein folding, misfolding, and aggregation. Formation of inclusion bodies and aggresomes. *Biochemistry. Biokhimiia*. 69:971-984.
- Martin, S., and R.G. Parton. 2006. Lipid droplets: a unified view of a dynamic organelle. *Nature reviews*. 7:373-378.
- Martins, I.C., I. Kuperstein, H. Wilkinson, E. Maes, M. Vanbrabant, W. Jonckheere, P. Van Gelder, D. Hartmann, R. D'Hooze, B. De Strooper, J. Schymkowitz, and F. Rousseau. 2008. Lipids revert inert A beta amyloid fibrils to neurotoxic protofibrils that affect learning in mice. *The EMBO journal*. 27:224-233.
- Masters, C.L., G. Simms, N.A. Weinman, G. Multhaup, B.L. McDonald, and K. Beyreuther. 1985. Amyloid plaque core protein in Alzheimer disease and Down syndrome. *Proceedings of the National Academy of Sciences of the United States of America*. 82:4245-4249.
- Matsuzaki, K., T. Noguch, M. Wakabayashi, K. Ikeda, T. Okada, Y. Ohashi, M. Hoshino, and H. Naiki. 2007. Inhibitors of amyloid beta-protein aggregation mediated by GM1-containing raft-like membranes. *Biochimica et biophysica acta*. 1768:122-130.
- Mattson, M.P. 2004. Pathways towards and away from Alzheimer's disease. *Nature*. 430:631-639.
- Mawuenyega, K.G., W. Sigurdson, V. Ovod, L. Munsell, T. Kasten, J.C. Morris, K.E. Yarasheski, and R.J. Bateman. 2010. Decreased clearance of CNS beta-amyloid in Alzheimer's disease. *Science (New York, N.Y.)*. 330:1774.
- Mayeux, R. 2003. Epidemiology of neurodegeneration. *Annual review of neuroscience*. 26:81-104.
- McCaddon, A., G. Davies, P. Hudson, S. Tandy, and H. Cattell. 1998. Total serum homocysteine in senile dementia of Alzheimer type. *International journal of geriatric psychiatry*. 13:235-239.
- McDonough, V.M., R.J. Buxeda, M.E. Bruno, O. Ozier-Kalogeropoulos, M.T. Adeline, C.R. McMaster, R.M. Bell, and G.M. Carman. 1995. Regulation of phospholipid biosynthesis in *Saccharomyces cerevisiae* by CTP. *The Journal of biological chemistry*. 270:18774-18780.
- McGraw, P., and S.A. Henry. 1989. Mutations in the *Saccharomyces cerevisiae* opi3 gene: effects on phospholipid methylation, growth and cross-pathway regulation of inositol synthesis. *Genetics*. 122:317-330.

- McLaurin, J., R. Golomb, A. Jurewicz, J.P. Antel, and P.E. Fraser. 2000. Inositol stereoisomers stabilize an oligomeric aggregate of Alzheimer amyloid beta peptide and inhibit abeta -induced toxicity. *The Journal of biological chemistry*. 275:18495-18502.
- McLaurin, J., M.E. Kierstead, M.E. Brown, C.A. Hawkes, M.H. Lambermon, A.L. Phinney, A.A. Darabie, J.E. Cousins, J.E. French, M.F. Lan, F. Chen, S.S. Wong, H.T. Mount, P.E. Fraser, D. Westaway, and P. St George-Hyslop. 2006. Cyclohexanehexol inhibitors of Abeta aggregation prevent and reverse Alzheimer phenotype in a mouse model. *Nature medicine*. 12:801-808.
- McLean, C.A., R.A. Cherny, F.W. Fraser, S.J. Fuller, M.J. Smith, K. Beyreuther, A.I. Bush, and C.L. Masters. 1999. Soluble pool of Abeta amyloid as a determinant of severity of neurodegeneration in Alzheimer's disease. *Ann Neurol*. 46:860-866.
- Meinhardt, J., C. Sachse, P. Hortschansky, N. Grigorieff, and M. Fandrich. 2009. Abeta(1-40) fibril polymorphism implies diverse interaction patterns in amyloid fibrils. *Journal of molecular biology*. 386:869-877.
- Meng, F., Y. Park, and H. Zhou. 2001. Role of proline, glycerol, and heparin as protein folding aids during refolding of rabbit muscle creatine kinase. *Int J Biochem Cell Biol*. 33:701-709.
- Merkel, O., M. Fido, J.A. Mayr, H. Pruger, F. Raab, G. Zandonella, S.D. Kohlwein, and F. Paltauf. 1999. Characterization and function in vivo of two novel phospholipases B/lysophospholipases from *Saccharomyces cerevisiae*. *The Journal of biological chemistry*. 274:28121-28127.
- Merkel, O., O.V. Oskolkova, F. Raab, R. El-Toukhy, and F. Paltauf. 2005. Regulation of activity in vitro and in vivo of three phospholipases B from *Saccharomyces cerevisiae*. *The Biochemical journal*. 387:489-496.
- Michaelis, T., G. Helms, K.D. Merboldt, W. Hanicke, H. Bruhn, and J. Frahm. 1993. Identification of Scyllo-inositol in proton NMR spectra of human brain in vivo. *NMR in biomedicine*. 6:105-109.
- Middendorp, O., C. Ortler, U. Neumann, P. Paganetti, U. Luthi, and A. Barberis. 2004. Yeast growth selection system for the identification of cell-active inhibitors of beta-secretase. *Biochimica et biophysica acta*. 1674:29-39.
- Mikhaleva, N.I., V.V. Golovastov, S.N. Zolov, M.V. Bogdanov, W. Dowhan, and M.A. Nesmeyanova. 2001. Depletion of phosphatidylethanolamine affects secretion of *Escherichia coli* alkaline phosphatase and its transcriptional expression. *FEBS letters*. 493:85-90.
- Miravalle, L., M. Calero, M. Takao, A.E. Roher, B. Ghetti, and R. Vidal. 2005. Amino-terminally truncated Abeta peptide species are the main component of cotton wool plaques. *Biochemistry*. 44:10810-10821.
- Mishra, R., R. Seckler, and R. Bhat. 2005. Efficient refolding of aggregation-prone citrate synthase by polyol osmolytes: how well are protein folding and stability aspects coupled? *The Journal of biological chemistry*. 280:15553-15560.
- Mizuguchi, M., K. Ikeda, and S.U. Kim. 1992. Differential distribution of cellular forms of beta-amyloid precursor protein in murine glial cell cultures. *Brain research*. 584:219-225.
- Moats, R.A., T. Ernst, T.K. Shonk, and B.D. Ross. 1994. Abnormal cerebral metabolite concentrations in patients with probable Alzheimer disease. *Magn Reson Med*. 32:110-115.
- Moens, P.B. 1971. Fine structure of ascospore development in the yeast *Saccharomyces cerevisiae*. *Canadian journal of microbiology*. 17:507-510.
- Moens, P.B., and E. Rapport. 1971. Spindles, spindle plaques, and meiosis in the yeast *Saccharomyces cerevisiae* (Hansen). *The Journal of cell biology*. 50:344-361.

- Mogi, T., K. Saiki, and Y. Anraku. 1994. Biosynthesis and functional role of haem O and haem A. *Molecular microbiology*. 14:391-398.
- Molin, M., J. Norbeck, and A. Blomberg. 2003. Dihydroxyacetone kinases in *Saccharomyces cerevisiae* are involved in detoxification of dihydroxyacetone. *The Journal of biological chemistry*. 278:1415-1423.
- Montine, K.S., C.N. Bassett, J.J. Ou, W.R. Markesbery, L.L. Swift, and T.J. Montine. 1998. Apolipoprotein E allelic influence on human cerebrospinal fluid apolipoproteins. *Journal of lipid research*. 39:2443-2451.
- Morgan, D., G. Landreth, and P. Bickford. 2009. The promise and perils of an Alzheimer disease vaccine: a video debate. *J Neuroimmune Pharmacol*. 4:1-3.
- Mori, C., E.T. Spooner, K.E. Wisniewsk, T.M. Wisniewski, H. Yamaguch, T.C. Saido, D.R. Tolan, D.J. Selkoe, and C.A. Lemere. 2002. Intraneuronal Abeta42 accumulation in Down syndrome brain. *Amyloid*. 9:88-102.
- Morimoto, A., K. Irie, K. Murakami, Y. Masuda, H. Ohigashi, M. Nagao, H. Fukuda, T. Shimizu, and T. Shirasawa. 2004. Analysis of the secondary structure of beta-amyloid (Abeta42) fibrils by systematic proline replacement. *The Journal of biological chemistry*. 279:52781-52788.
- Morley, J.F., H.R. Brignull, J.J. Weyers, and R.I. Morimoto. 2002. The threshold for polyglutamine-expansion protein aggregation and cellular toxicity is dynamic and influenced by aging in *Caenorhabditis elegans*. *Proceedings of the National Academy of Sciences of the United States of America*. 99:10417-10422.
- Mullner, H., G. Deutsch, E. Leitner, E. Ingolic, and G. Daum. 2005. YEH2/YLR020c encodes a novel steryl ester hydrolase of the yeast *Saccharomyces cerevisiae*. *The Journal of biological chemistry*. 280:13321-13328.
- Mullner, H., D. Zweytick, R. Leber, F. Turnowsky, and G. Daum. 2004. Targeting of proteins involved in sterol biosynthesis to lipid particles of the yeast *Saccharomyces cerevisiae*. *Biochimica et biophysica acta*. 1663:9-13.
- Murray, M., and M.L. Greenberg. 2000. Expression of yeast INM1 encoding inositol monophosphatase is regulated by inositol, carbon source and growth stage and is decreased by lithium and valproate. *Molecular microbiology*. 36:651-661.
- Naiki, H., and K. Nakakuki. 1996. First-order kinetic model of Alzheimer's beta-amyloid fibril extension in vitro. *Laboratory investigation; a journal of technical methods and pathology*. 74:374-383.
- Naj, A.C., G. Jun, G.W. Beecham, L.S. Wang, B.N. Vardarajan, J. Buross, P.J. Gallins, J.D. Buxbaum, G.P. Jarvik, P.K. Crane, E.B. Larson, T.D. Bird, B.F. Boeve, N.R. Graff-Radford, P.L. De Jager, D. Evans, J.A. Schneider, M.M. Carrasquillo, N. Ertekin-Taner, S.G. Younkin, C. Cruchaga, J.S. Kauwe, P. Nowotny, P. Kramer, J. Hardy, M.J. Huentelman, A.J. Myers, M.M. Barmada, F.Y. Demirci, C.T. Baldwin, R.C. Green, E. Rogaeva, P. St George-Hyslop, S.E. Arnold, R. Barber, T. Beach, E.H. Bigio, J.D. Bowen, A. Boxer, J.R. Burke, N.J. Cairns, C.S. Carlson, R.M. Carney, S.L. Carroll, H.C. Chui, D.G. Clark, J. Corneveaux, C.W. Cotman, J.L. Cummings, C. DeCarli, S.T. DeKosky, R. Diaz-Arrastia, M. Dick, D.W. Dickson, W.G. Ellis, K.M. Faber, K.B. Fallon, M.R. Farlow, S. Ferris, M.P. Frosch, D.R. Galasko, M. Ganguli, M. Gearing, D.H. Geschwind, B. Ghetti, J.R. Gilbert, S. Gilman, B. Giordani, J.D. Glass, J.H. Growdon, R.L. Hamilton, L.E. Harrell, E. Head, L.S. Honig, C.M. Hulette, B.T. Hyman, G.A. Jicha, L.W. Jin, N. Johnson, J. Karlawish, A. Karydas, J.A. Kaye, R. Kim, E.H. Koo, N.W. Kowall, J.J. Lah, A.I. Levey, A.P. Lieberman, O.L. Lopez, W.J. Mack, D.C. Marson, F. Martiniuk, D.C. Mash, E. Masliah, W.C. McCormick, S.M. McCurry, A.N. McDavid, A.C. McKee, M. Mesulam, B.L. Miller, et al. 2011. Common variants at MS4A4/MS4A6E, CD2AP, CD33 and EPHA1 are associated with late-onset Alzheimer's disease. *Nature genetics*. 43:436-441.

- Nakagami, Y., S. Nishimura, T. Murasugi, T. Kubo, I. Kaneko, M. Meguro, S. Marumoto, H. Kogen, K. Koyama, and T. Oda. 2002. A novel compound RS-0466 reverses beta-amyloid-induced cytotoxicity through the Akt signaling pathway in vitro. *European journal of pharmacology*. 457:11-17.
- Nakanishi, H., P. de los Santos, and A.M. Neiman. 2004. Positive and negative regulation of a SNARE protein by control of intracellular localization. *Molecular biology of the cell*. 15:1802-1815.
- Nakatogawa, H., Y. Ichimura, and Y. Ohsumi. 2007. Atg8, a ubiquitin-like protein required for autophagosome formation, mediates membrane tethering and hemifusion. *Cell*. 130:165-178.
- Nalivaeva, N.N., N.D. Belyaev, I.A. Zhuravin, and A.J. Turner. 2012. The Alzheimer's Amyloid-Degrading Peptidase, Neprilysin: Can We Control It? *International journal of Alzheimer's disease*. 2012:383796.
- Nash, R., S. Weng, B. Hitz, R. Balakrishnan, K.R. Christie, M.C. Costanzo, S.S. Dwight, S.R. Engel, D.G. Fisk, J.E. Hirschman, E.L. Hong, M.S. Livstone, R. Oughtred, J. Park, M. Skrzypek, C.L. Theesfeld, G. Binkley, Q. Dong, C. Lane, S. Miyasato, A. Sethuraman, M. Schroeder, K. Dolinski, D. Botstein, and J.M. Cherry. 2007. Expanded protein information at SGD: new pages and proteome browser. *Nucleic acids research*. 35:D468-471.
- Naslund, J., V. Haroutunian, R. Mohs, K.L. Davis, P. Davies, P. Greengard, and J.D. Buxbaum. 2000. Correlation between elevated levels of amyloid beta-peptide in the brain and cognitive decline. *Jama*. 283:1571-1577.
- Natter, K., P. Leitner, A. Faschinger, H. Wolinski, S. McCraith, S. Fields, and S.D. Kohlwein. 2005. The spatial organization of lipid synthesis in the yeast *Saccharomyces cerevisiae* derived from large scale green fluorescent protein tagging and high resolution microscopy. *Mol Cell Proteomics*. 4:662-672.
- Nebauer, R., I. Schuiki, B. Kulterer, Z. Trajanoski, and G. Daum. 2007. The phosphatidylethanolamine level of yeast mitochondria is affected by the mitochondrial components Oxa1p and Yme1p. *The FEBS journal*. 274:6180-6190.
- Necula, M., L. Breydo, S. Milton, R. Kaye, W.E. van der Veer, P. Tone, and C.G. Glabe. 2007a. Methylene blue inhibits amyloid Abeta oligomerization by promoting fibrillization. *Biochemistry*. 46:8850-8860.
- Necula, M., R. Kaye, S. Milton, and C.G. Glabe. 2007b. Small molecule inhibitors of aggregation indicate that amyloid beta oligomerization and fibrillization pathways are independent and distinct. *The Journal of biological chemistry*. 282:10311-10324.
- Neiman, A.M. 1998. Prospore membrane formation defines a developmentally regulated branch of the secretory pathway in yeast. *The Journal of cell biology*. 140:29-37.
- Nevoigt, E., and U. Stahl. 1997. Osmoregulation and glycerol metabolism in the yeast *Saccharomyces cerevisiae*. *FEMS microbiology reviews*. 21:231-241.
- Nilsberth, C., A. Westlind-Danielsson, C.B. Eckman, M.M. Condron, K. Axelman, C. Forsell, C. Sten, J. Luthman, D.B. Teplow, S.G. Younkin, J. Naslund, and L. Lannfelt. 2001. The 'Arctic' APP mutation (E693G) causes Alzheimer's disease by enhanced Abeta protofibril formation. *Nature neuroscience*. 4:887-893.
- Nioi, P., B.K. Perry, E.J. Wang, Y.Z. Gu, and R.D. Snyder. 2007. In vitro detection of drug-induced phospholipidosis using gene expression and fluorescent phospholipid based methodologies. *Toxicol Sci*. 99:162-173.

- Nitsch, R.M., J.K. Blusztajn, A.G. Pittas, B.E. Slack, J.H. Growdon, and R.J. Wurtman. 1992. Evidence for a membrane defect in Alzheimer disease brain. *Proceedings of the National Academy of Sciences of the United States of America*. 89:1671-1675.
- Norbeck, J., and A. Blomberg. 1997. Metabolic and regulatory changes associated with growth of *Saccharomyces cerevisiae* in 1.4 M NaCl. Evidence for osmotic induction of glycerol dissimilation via the dihydroxyacetone pathway. *The Journal of biological chemistry*. 272:5544-5554.
- Norbeck, J., A.K. Pahlman, N. Akhtar, A. Blomberg, and L. Adler. 1996. Purification and characterization of two isoenzymes of DL-glycerol-3-phosphatase from *Saccharomyces cerevisiae*. Identification of the corresponding GPP1 and GPP2 genes and evidence for osmotic regulation of Gpp2p expression by the osmosensing mitogen-activated protein kinase signal transduction pathway. *The Journal of biological chemistry*. 271:13875-13881.
- Nowotny, P., J.M. Kwon, S. Chakraverty, V. Nowotny, J.C. Morris, and A.M. Goate. 2001. Association studies using novel polymorphisms in BACE1 and BACE2. *Neuroreport*. 12:1799-1802.
- Nygard, O., S.E. Vollset, H. Refsum, I. Stensvold, A. Tverdal, J.E. Nordrehaug, M. Ueland, and G. Kvale. 1995. Total plasma homocysteine and cardiovascular risk profile. The Hordaland Homocysteine Study. *Jama*. 274:1526-1533.
- O'Hare, E., D.I. Scopes, J.M. Treherne, K. Norwood, D. Spanswick, and E.M. Kim. 2010. RS-0406 arrests amyloid-beta oligomer-induced behavioural deterioration in vivo. *Behavioural brain research*. 210:32-37.
- O'Nuallain, B., A.K. Thakur, A.D. Williams, A.M. Bhattacharyya, S. Chen, G. Thiagarajan, and R. Wetzel. 2006. Kinetics and thermodynamics of amyloid assembly using a high-performance liquid chromatography-based sedimentation assay. *Methods in enzymology*. 413:34-74.
- Oakley, H., S.L. Cole, S. Logan, E. Maus, P. Shao, J. Craft, A. Guillozet-Bongaarts, M. Ohno, J. Disterhoft, L. Van Eldik, R. Berry, and R. Vassar. 2006. Intraneuronal beta-amyloid aggregates, neurodegeneration, and neuron loss in transgenic mice with five familial Alzheimer's disease mutations: potential factors in amyloid plaque formation. *J Neurosci*. 26:10129-10140.
- Oddo, S., A. Caccamo, J.D. Shepherd, M.P. Murphy, T.E. Golde, R. Kaye, R. Metherate, M.P. Mattson, Y. Akbari, and F.M. LaFerla. 2003. Triple-transgenic model of Alzheimer's disease with plaques and tangles: intracellular Abeta and synaptic dysfunction. *Neuron*. 39:409-421.
- Oddo, S., A. Caccamo, I.F. Smith, K.N. Green, and F.M. LaFerla. 2006. A dynamic relationship between intracellular and extracellular pools of Abeta. *The American journal of pathology*. 168:184-194.
- Odorizzi, G., M. Babst, and S.D. Emr. 2000. Phosphoinositide signaling and the regulation of membrane trafficking in yeast. *Trends in biochemical sciences*. 25:229-235.
- Oelkers, P., A. Tinkelenberg, N. Erdeniz, D. Cromley, J.T. Billheimer, and S.L. Sturley. 2000. A lecithin cholesterol acyltransferase-like gene mediates diacylglycerol esterification in yeast. *The Journal of biological chemistry*. 275:15609-15612.
- Oh, S., H.S. Hong, E. Hwang, H.J. Sim, W. Lee, S.J. Shin, and I. Mook-Jung. 2005. Amyloid peptide attenuates the proteasome activity in neuronal cells. *Mechanisms of ageing and development*. 126:1292-1299.
- Ohyagi, Y., Y. Tsuruta, K. Motomura, K. Miyoshi, H. Kikuchi, T. Iwaki, T. Taniwaki, and J. Kira. 2007. Intraneuronal amyloid beta42 enhanced by heating but counteracted by formic acid. *Journal of neuroscience methods*. 159:134-138.

- Olgiati, P., A.M. Politis, G.N. Papadimitriou, D. De Ronchi, and A. Serretti. 2011. Genetics of late-onset Alzheimer's disease: update from the alzgene database and analysis of shared pathways. *International journal of Alzheimer's disease*. 2011:832379.
- Ono, K., M.M. Condron, and D.B. Teplow. 2009. Structure-neurotoxicity relationships of amyloid beta-protein oligomers. *Proceedings of the National Academy of Sciences of the United States of America*. 106:14745-14750.
- Ostrander, D.B., D.J. O'Brien, J.A. Gorman, and G.M. Carman. 1998. Effect of CTP synthetase regulation by CTP on phospholipid synthesis in *Saccharomyces cerevisiae*. *The Journal of biological chemistry*. 273:18992-19001.
- Ostrowski, S.M., B.L. Wilkinson, T.E. Golde, and G. Landreth. 2007. Statins reduce amyloid-beta production through inhibition of protein isoprenylation. *The Journal of biological chemistry*. 282:26832-26844.
- Outeiro, T.F., and S. Lindquist. 2003. Yeast cells provide insight into alpha-synuclein biology and pathobiology. *Science (New York, N.Y.)*. 302:1772-1775.
- Owen, O.E., S.C. Kalhan, and R.W. Hanson. 2002. The key role of anaplerosis and cataplerosis for citric acid cycle function. *The Journal of biological chemistry*. 277:30409-30412.
- Ozier-Kalogeropoulos, O., F. Fasiolo, M.T. Adeline, J. Collin, and F. Lacroute. 1991. Cloning, sequencing and characterization of the *Saccharomyces cerevisiae* URA7 gene encoding CTP synthetase. *Mol Gen Genet*. 231:7-16.
- Palade, G.E. 1956. The endoplasmic reticulum. *The Journal of biophysical and biochemical cytology*. 2:85-98.
- Park, S.K., S.D. Pegan, A.D. Mesecar, L.M. Jungbauer, M.J. LaDu, and S.W. Liebman. 2011. Development and validation of a yeast high-throughput screen for inhibitors of Abeta(4)(2) oligomerization. *Disease models & mechanisms*. 4:822-831.
- Parnetti, L., R. Tarducci, O. Presciutti, D.T. Lowenthal, M. Pippi, B. Palumbo, G. Gobbi, G.P. Pelliccioli, and U. Senin. 1997. Proton magnetic resonance spectroscopy can differentiate Alzheimer's disease from normal aging. *Mechanisms of ageing and development*. 97:9-14.
- Patton-Vogt, J. 2007. Transport and metabolism of glycerophosphodiester produced through phospholipid deacylation. *Biochimica et biophysica acta*. 1771:337-342.
- Paulus, H., and E.P. Kennedy. 1960. The enzymatic synthesis of inositol monophosphate. *The Journal of biological chemistry*. 235:1303-1311.
- Perocchi, F., E. Mancera, and L.M. Steinmetz. 2008. Systematic screens for human disease genes, from yeast to human and back. *Molecular bioSystems*. 4:18-29.
- Perry, R.J., and N.D. Ridgway. 2005. Molecular mechanisms and regulation of ceramide transport. *Biochimica et biophysica acta*. 1734:220-234.
- Pittet, M., and A. Conzelmann. 2007. Biosynthesis and function of GPI proteins in the yeast *Saccharomyces cerevisiae*. *Biochimica et biophysica acta*. 1771:405-420.
- Poirier, J., J. Davignon, D. Bouthillier, S. Kogan, P. Bertrand, and S. Gauthier. 1993. Apolipoprotein E polymorphism and Alzheimer's disease. *Lancet*. 342:697-699.
- Ponka, P. 1999. Cell biology of heme. *The American journal of the medical sciences*. 318:241-256.

- Poorkaj, P., T.D. Bird, E. Wijsman, E. Nemens, R.M. Garruto, L. Anderson, A. Andreadis, W.C. Wiederholt, M. Raskind, and G.D. Schellenberg. 1998. Tau is a candidate gene for chromosome 17 frontotemporal dementia. *Ann Neurol.* 43:815-825.
- Preitschopf, W., H. Luckl, E. Summers, S.A. Henry, F. Paltauf, and S.D. Kohlwein. 1993. Molecular cloning of the yeast OPI3 gene as a high copy number suppressor of the cho2 mutation. *Current genetics.* 23:95-101.
- Preuss, D., J. Mulholland, C.A. Kaiser, P. Orlean, C. Albright, M.D. Rose, P.W. Robbins, and D. Botstein. 1991. Structure of the yeast endoplasmic reticulum: localization of ER proteins using immunofluorescence and immunoelectron microscopy. *Yeast (Chichester, England).* 7:891-911.
- Price, D.L., R.E. Tanzi, D.R. Borchelt, and S.S. Sisodia. 1998. Alzheimer's disease: genetic studies and transgenic models. *Annual review of genetics.* 32:461-493.
- Prince, M., R. Bryce, and C. Ferri. 2011. World Alzheimer Report 2011. *Alzheimer's Disease International.*
- Prinz, W.A., L. Grzyb, M. Veenhuis, J.A. Kahana, P.A. Silver, and T.A. Rapoport. 2000. Mutants affecting the structure of the cortical endoplasmic reticulum in *Saccharomyces cerevisiae*. *The Journal of cell biology.* 150:461-474.
- Purdue, P.E., and P.B. Lazarow. 2001. Peroxisome biogenesis. *Annual review of cell and developmental biology.* 17:701-752.
- Qi-Takahara, Y., M. Morishima-Kawashima, Y. Tanimura, G. Dolios, N. Hirotsu, Y. Horikoshi, F. Kametani, M. Maeda, T.C. Saido, R. Wang, and Y. Ihara. 2005. Longer forms of amyloid beta protein: implications for the mechanism of intramembrane cleavage by gamma-secretase. *J Neurosci.* 25:436-445.
- Querfurth, H.W., and F.M. LaFerla. 2010. Alzheimer's disease. *The New England journal of medicine.* 362:329-344.
- Rajakumari, S., K. Grillitsch, and G. Daum. 2008. Synthesis and turnover of non-polar lipids in yeast. *Progress in lipid research.* 47:157-171.
- Rajendran, L., M. Honsho, T.R. Zahn, P. Keller, K.D. Geiger, P. Verkade, and K. Simons. 2006. Alzheimer's disease beta-amyloid peptides are released in association with exosomes. *Proceedings of the National Academy of Sciences of the United States of America.* 103:11172-11177.
- Rayapuram, N., and S. Subramani. 2006. The importomer--a peroxisomal membrane complex involved in protein translocation into the peroxisome matrix. *Biochimica et biophysica acta.* 1763:1613-1619.
- Reid, P.C., Y. Urano, T. Kodama, and T. Hamakubo. 2007. Alzheimer's disease: cholesterol, membrane rafts, isoprenoids and statins. *Journal of cellular and molecular medicine.* 11:383-392.
- Reynolds, S.M., L. Kall, M.E. Riffle, J.A. Bilmes, and W.S. Noble. 2008. Transmembrane topology and signal peptide prediction using dynamic bayesian networks. *PLoS computational biology.* 4:e1000213.
- Richard, P., B. Teusink, H.V. Westerhoff, and K. van Dam. 1993. Around the growth phase transition *S. cerevisiae*'s make-up favours sustained oscillations of intracellular metabolites. *FEBS letters.* 318:80-82.
- Riffle, M., L. Malmstrom, and T.N. Davis. 2005. The Yeast Resource Center Public Data Repository. *Nucleic acids research.* 33:D378-382.

- Robenek, H., O. Hofnagel, I. Buers, M.J. Robenek, D. Troyer, and N.J. Severs. 2006. Adipophilin-enriched domains in the ER membrane are sites of lipid droplet biogenesis. *Journal of cell science*. 119:4215-4224.
- Robinson, M.D., J. Grigull, N. Mohammad, and T.R. Hughes. 2002. FunSpec: a web-based cluster interpreter for yeast. *BMC bioinformatics*. 3:35.
- Robinson, S.R., G.M. Bishop, and G. Munch. 2003. Alzheimer vaccine: amyloid-beta on trial. *Bioessays*. 25:283-288.
- Roheim, P.S., M. Carey, T. Forte, and G.L. Vega. 1979. Apolipoproteins in human cerebrospinal fluid. *Proceedings of the National Academy of Sciences of the United States of America*. 76:4646-4649.
- Rose, M.D., L.M. Misra, and J.P. Vogel. 1989. KAR2, a karyogamy gene, is the yeast homolog of the mammalian BiP/GRP78 gene. *Cell*. 57:1211-1221.
- Roses, A.D. 2006. On the discovery of the genetic association of Apolipoprotein E genotypes and common late-onset Alzheimer disease. *J Alzheimers Dis*. 9:361-366.
- Rosenberger, S., M. Connerth, G. Zellnig, and G. Daum. 2009. Phosphatidylethanolamine synthesized by three different pathways is supplied to peroxisomes of the yeast *Saccharomyces cerevisiae*. *Biochimica et biophysica acta*. 1791:379-387.
- Roses, A.D., A.M. Saunders, M.A. Alberts, W.J. Strittmatter, D. Schmechel, E. Gorder, and M.A. Pericak-Vance. 1995. Apolipoprotein E E4 allele and risk of dementia. *Jama*. 273:374-375; author reply 375-376.
- Ross, C.A., and M.A. Poirier. 2004. Protein aggregation and neurodegenerative disease. *Nature medicine*. 10 Suppl:S10-17.
- Ross, C.A., and M.A. Poirier. 2005. Opinion: What is the role of protein aggregation in neurodegeneration? *Nature reviews. Molecular cell biology*. 6:891-898.
- Roth, A.F., J. Wan, A.O. Bailey, B. Sun, J.A. Kuchar, W.N. Green, B.S. Phinney, J.R. Yates, 3rd, and N.G. Davis. 2006. Global analysis of protein palmitoylation in yeast. *Cell*. 125:1003-1013.
- Rudek, M.A., W.D. Figg, V. Dyer, W. Dahut, M.L. Turner, S.M. Steinberg, D.J. Liewehr, D.R. Kohler, J.M. Pluda, and E. Reed. 2001a. Phase I clinical trial of oral COL-3, a matrix metalloproteinase inhibitor, in patients with refractory metastatic cancer. *Journal of clinical oncology : official journal of the American Society of Clinical Oncology*. 19:584-592.
- Rudek, M.A., M. Horne, W.D. Figg, W. Dahut, V. Dyer, J.M. Pluda, and E. Reed. 2001b. Reversible sideroblastic anemia associated with the tetracycline analogue COL-3. *American journal of hematology*. 67:51-53.
- Ruepp, A., A. Zollner, D. Maier, K. Albermann, J. Hani, M. Mokrejs, I. Tetko, U. Guldener, G. Mannhaupt, M. Munsterkotter, and H.W. Mewes. 2004. The FunCat, a functional annotation scheme for systematic classification of proteins from whole genomes. *Nucleic acids research*. 32:5539-5545.
- Saba, J.D., F. Nara, A. Bielawska, S. Garrett, and Y.A. Hannun. 1997. The BST1 gene of *Saccharomyces cerevisiae* is the sphingosine-1-phosphate lyase. *The Journal of biological chemistry*. 272:26087-26090.
- Sabo, S.L., A.F. Ikin, J.D. Buxbaum, and P. Greengard. 2001. The Alzheimer amyloid precursor protein (APP) and FE65, an APP-binding protein, regulate cell movement. *The Journal of cell biology*. 153:1403-1414.

- Sachse, C., C. Xu, K. Wieligmann, S. Diekmann, N. Grigorieff, and M. Fandrich. 2006. Quaternary structure of a mature amyloid fibril from Alzheimer's Abeta(1-40) peptide. *Journal of molecular biology*. 362:347-354.
- Sahlin, C., A. Lord, K. Magnusson, H. Englund, C.G. Almeida, P. Greengard, F. Nyberg, G.K. Gouras, L. Lannfelt, and L.N. Nilsson. 2007. The Arctic Alzheimer mutation favors intracellular amyloid-beta production by making amyloid precursor protein less available to alpha-secretase. *Journal of neurochemistry*. 101:854-862.
- Saito, T., T. Suemoto, N. Brouwers, K. Sleegers, S. Funamoto, N. Mihira, Y. Matsuba, K. Yamada, P. Nilsson, J. Takano, M. Nishimura, N. Iwata, C. Van Broeckhoven, Y. Ihara, and T.C. Saido. 2011. Potent amyloidogenicity and pathogenicity of Abeta43. *Nature neuroscience*. 14:1023-1032.
- Sambrook J, Fritsch E, Maniatis T (1989) Molecular cloning: A laboratory manual Cold Spring Harbor Laboratory press. *New York, N.Y.*: 931-957
- Sandager, L., M.H. Gustavsson, U. Stahl, A. Dahlqvist, E. Wiberg, A. Banas, M. Lenman, H. Ronne, and S. Stymne. 2002. Storage lipid synthesis is non-essential in yeast. *The Journal of biological chemistry*. 277:6478-6482.
- Sandberg, A., L.M. Luheshi, S. Sollvander, T. Pereira de Barros, B. Macao, T.P. Knowles, H. Biverstal, C. Lendel, F. Ekholm-Petterson, A. Dubnovitsky, L. Lannfelt, C.M. Dobson, and T. Hard. 2010. Stabilization of neurotoxic Alzheimer amyloid-beta oligomers by protein engineering. *Proceedings of the National Academy of Sciences of the United States of America*. 107:15595-15600.
- Sandhoff, R., B. Brugger, D. Jeckel, W.D. Lehmann, and F.T. Wieland. 1999. Determination of cholesterol at the low picomole level by nano-electrospray ionization tandem mass spectrometry. *Journal of lipid research*. 40:126-132.
- Santiago, T.C., and C.B. Mamoun. 2003. Genome expression analysis in yeast reveals novel transcriptional regulation by inositol and choline and new regulatory functions for Opi1p, Ino2p, and Ino4p. *The Journal of biological chemistry*. 278:38723-38730.
- Santos, M.J., R.A. Quintanilla, A. Toro, R. Grandy, M.C. Dinamarca, J.A. Godoy, and N.C. Inestrosa. 2005. Peroxisomal proliferation protects from beta-amyloid neurodegeneration. *The Journal of biological chemistry*. 280:41057-41068.
- Saraiva, M.J. 2001. Transthyretin amyloidosis: a tale of weak interactions. *FEBS letters*. 498:201-203.
- Sato, T., N. Dohmae, Y. Qi, N. Kakuda, H. Misonou, R. Mitsumori, H. Maruyama, E.H. Koo, C. Haass, K. Takio, M. Morishima-Kawashima, S. Ishiura, and Y. Ihara. 2003. Potential link between amyloid beta-protein 42 and C-terminal fragment gamma 49-99 of beta-amyloid precursor protein. *The Journal of biological chemistry*. 278:24294-24301.
- Saudou, F., S. Finkbeiner, D. Devys, and M.E. Greenberg. 1998. Huntingtin acts in the nucleus to induce apoptosis but death does not correlate with the formation of intranuclear inclusions. *Cell*. 95:55-66.
- Schafer, F.Q., and G.R. Buettner. 2001. Redox environment of the cell as viewed through the redox state of the glutathione disulfide/glutathione couple. *Free Radic Biol Med*. 30:1191-1212.
- Schatz, G., and B. Dobberstein. 1996. Common principles of protein translocation across membranes. *Science (New York, N.Y.)*. 271:1519-1526.
- Schellenberg, G.D. 1995. Genetic dissection of Alzheimer disease, a heterogeneous disorder. *Proceedings of the National Academy of Sciences of the United States of America*. 92:8552-8559.

- Scherzer-Attali, R., R. Pellarin, M. Convertino, A. Frydman-Marom, N. Egoz-Matia, S. Peled, M. Levy-Sakin, D.E. Shalev, A. Caflisch, E. Gazit, and D. Segal. 2010. Complete phenotypic recovery of an Alzheimer's disease model by a quinone-tryptophan hybrid aggregation inhibitor. *PLoS ONE*. 5:e11101.
- Scheuner, D., C. Eckman, M. Jensen, X. Song, M. Citron, N. Suzuki, T.D. Bird, J. Hardy, M. Hutton, W. Kukull, E. Larson, E. Levy-Lahad, M. Viitanen, E. Peskind, P. Poorkaj, G. Schellenberg, R. Tanzi, W. Wasco, L. Lannfelt, D. Selkoe, and S. Younkin. 1996. Secreted amyloid beta-protein similar to that in the senile plaques of Alzheimer's disease is increased in vivo by the presenilin 1 and 2 and APP mutations linked to familial Alzheimer's disease. *Nature medicine*. 2:864-870.
- Schipper, H.M. 2000. Heme oxygenase-1: role in brain aging and neurodegeneration. *Exp Gerontol*. 35:821-830.
- Schmidt, M., C. Sachse, W. Richter, C. Xu, M. Fandrich, and N. Grigorieff. 2009. Comparison of Alzheimer A β (1-40) and A β (1-42) amyloid fibrils reveals similar protofilament structures. *Proceedings of the National Academy of Sciences of the United States of America*. 106:19813-19818.
- Schneider, R., B. Brugger, R. Sandhoff, G. Zellnig, A. Leber, M. Lampl, K. Athenstaedt, C. Hrastnik, S. Eder, G. Daum, F. Paltauf, F.T. Wieland, and S.D. Kohlwein. 1999. Electrospray ionization tandem mass spectrometry (ESI-MS/MS) analysis of the lipid molecular species composition of yeast subcellular membranes reveals acyl chain-based sorting/remodeling of distinct molecular species en route to the plasma membrane. *The Journal of cell biology*. 146:741-754.
- Seilheimer, B., B. Bohrmann, L. Bondolfi, F. Muller, D. Stuber, and H. Dobeli. 1997. The toxicity of the Alzheimer's beta-amyloid peptide correlates with a distinct fiber morphology. *Journal of structural biology*. 119:59-71.
- Selhub, J., P.F. Jacques, A.G. Bostom, R.B. D'Agostino, P.W. Wilson, A.J. Belanger, D.H. O'Leary, P.A. Wolf, E.J. Schaefer, and I.H. Rosenberg. 1995. Association between plasma homocysteine concentrations and extracranial carotid-artery stenosis. *The New England journal of medicine*. 332:286-291.
- Selkoe, D.J. 1991. Amyloid protein and Alzheimer's disease. *Scientific American*. 265:68-71, 74-66, 78.
- Selkoe, D.J. 2002. Alzheimer's disease is a synaptic failure. *Science (New York, N.Y.)*. 298:789-791.
- Selkoe, D.J. 2004. Cell biology of protein misfolding: the examples of Alzheimer's and Parkinson's diseases. *Nature cell biology*. 6:1054-1061.
- Selkoe, D.J. 2008. Soluble oligomers of the amyloid beta-protein impair synaptic plasticity and behavior. *Behavioural brain research*.
- Selkoe, D.J. 2011. Resolving controversies on the path to Alzheimer's therapeutics. *Nature medicine*. 17:1060-1065.
- Selley, M.L. 2007. A metabolic link between S-adenosylhomocysteine and polyunsaturated fatty acid metabolism in Alzheimer's disease. *Neurobiology of aging*. 28:1834-1839.
- Serrano, R. 1988. H⁺-ATPase from plasma membranes of *Saccharomyces cerevisiae* and *Avena sativa* roots: purification and reconstitution. *Methods in enzymology*. 157:533-544.
- Serretti, A., P. Artioli, R. Quartesan, and D. De Ronchi. 2005. Genes involved in Alzheimer's disease, a survey of possible candidates. *J Alzheimers Dis*. 7:331-353.
- Seshadri, S., A. Beiser, J. Selhub, P.F. Jacques, I.H. Rosenberg, R.B. D'Agostino, P.W. Wilson, and P.A. Wolf. 2002. Plasma homocysteine as a risk factor for dementia and Alzheimer's disease. *The New England journal of medicine*. 346:476-483.

- Seshadri, S., A.L. Fitzpatrick, M.A. Ikram, A.L. DeStefano, V. Gudnason, M. Boada, J.C. Bis, A.V. Smith, M.M. Carassquillo, J.C. Lambert, D. Harold, E.M. Schrijvers, R. Ramirez-Lorca, S. DeBette, W.T. Longstreth, Jr., A.C. Janssens, V.S. Pankratz, J.F. Dartigues, P. Hollingworth, T. Aspelund, I. Hernandez, A. Beiser, L.H. Kuller, P.J. Koudstaal, D.W. Dickson, C. Tzourio, R. Abraham, C. Antunez, Y. Du, J.I. Rotter, Y.S. Aulchenko, T.B. Harris, R.C. Petersen, C. Berr, M.J. Owen, J. Lopez-Arrieta, B.N. Varadarajan, J.T. Becker, F. Rivadeneira, M.A. Nalls, N.R. Graff-Radford, D. Campion, S. Auerbach, K. Rice, A. Hofman, P.V. Jonsson, H. Schmidt, M. Lathrop, T.H. Mosley, R. Au, B.M. Psaty, A.G. Uitterlinden, L.A. Farrer, T. Lumley, A. Ruiz, J. Williams, P. Amouyel, S.G. Younkin, P.A. Wolf, L.J. Launer, O.L. Lopez, C.M. van Duijn, M.M. Breteler, C. Consortium, G. Consortium, and E. Consortium. 2010. Genome-wide analysis of genetic loci associated with Alzheimer disease. *Jama*. 303:1832-1840.
- Sharma, S.C. 2006. Implications of sterol structure for membrane lipid composition, fluidity and phospholipid asymmetry in *Saccharomyces cerevisiae*. *FEMS yeast research*. 6:1047-1051.
- Shen, H., and W. Dowhan. 1997. Regulation of phospholipid biosynthetic enzymes by the level of CDP-diacylglycerol synthase activity. *The Journal of biological chemistry*. 272:11215-11220.
- Shen, H., P.N. Heacock, C.J. Clancey, and W. Dowhan. 1996. The CDS1 gene encoding CDP-diacylglycerol synthase in *Saccharomyces cerevisiae* is essential for cell growth. *The Journal of biological chemistry*. 271:789-795.
- Sherrington, R., E.I. Rogaev, Y. Liang, E.A. Rogaeva, G. Levesque, M. Ikeda, H. Chi, C. Lin, G. Li, K. Holman, T. Tsuda, L. Mar, J.F. Foncin, A.C. Bruni, M.P. Montesi, S. Sorbi, I. Rainero, L. Pinessi, L. Nee, I. Chumakov, D. Pollen, A. Brookes, P. Sanseau, R.J. Polinsky, W. Wasco, H.A. Da Silva, J.L. Haines, M.A. Perikicak-Vance, R.E. Tanzi, A.D. Roses, P.E. Fraser, J.M. Rommens, and P.H. St George-Hyslop. 1995. Cloning of a gene bearing missense mutations in early-onset familial Alzheimer's disease. *Nature*. 375:754-760.
- Shetty, H.U., H.W. Holloway, and M.B. Schapiro. 1996. Cerebrospinal fluid and plasma distribution of myo-inositol and other polyols in Alzheimer disease. *Clinical chemistry*. 42:298-302.
- Shi, J., C.W. Heegaard, J.T. Rasmussen, and G.E. Gilbert. 2004. Lactadherin binds selectively to membranes containing phosphatidyl-L-serine and increased curvature. *Biochimica et biophysica acta*. 1667:82-90.
- Sikorski, R.S., and P. Hieter. 1989. A system of shuttle vectors and yeast host strains designed for efficient manipulation of DNA in *Saccharomyces cerevisiae*. *Genetics*. 122:19-27.
- Simmons, L.K., P.C. May, K.J. Tomaselli, R.E. Rydel, K.S. Fuson, E.F. Brigham, S. Wright, I. Lieberburg, G.W. Becker, D.N. Brems, and et al. 1994. Secondary structure of amyloid beta peptide correlates with neurotoxic activity in vitro. *Molecular pharmacology*. 45:373-379.
- Sinha, G. 2011. Peering inside Alzheimer's brains. *Nature biotechnology*. 29:384-387.
- Sinha, S., J.P. Anderson, R. Barbour, G.S. Basi, R. Caccavello, D. Davis, M. Doan, H.F. Dovey, N. Frigon, J. Hong, K. Jacobson-Croak, N. Jewett, P. Keim, J. Knops, I. Lieberburg, M. Power, H. Tan, G. Tatsuno, J. Tung, D. Schenk, P. Seubert, S.M. Suomensari, S. Wang, D. Walker, J. Zhao, L. McConlogue, and V. John. 1999. Purification and cloning of amyloid precursor protein beta-secretase from human brain. *Nature*. 402:537-540.
- Smith, M.A., A. Nunomura, X. Zhu, A. Takeda, and G. Perry. 2000. Metabolic, metallic, and mitotic sources of oxidative stress in Alzheimer disease. *Antioxidants & redox signaling*. 2:413-420.
- Sorger, D., K. Athenstaedt, C. Hrastnik, and G. Daum. 2004. A yeast strain lacking lipid particles bears a defect in ergosterol formation. *The Journal of biological chemistry*. 279:31190-31196.

- Soto, C., E.M. Sigurdsson, L. Morelli, R.A. Kumar, E.M. Castano, and B. Frangione. 1998. Beta-sheet breaker peptides inhibit fibrillogenesis in a rat brain model of amyloidosis: implications for Alzheimer's therapy. *Nature medicine*. 4:822-826.
- Stamer, K., R. Vogel, E. Thies, E. Mandelkow, and E.M. Mandelkow. 2002. Tau blocks traffic of organelles, neurofilaments, and APP vesicles in neurons and enhances oxidative stress. *The Journal of cell biology*. 156:1051-1063.
- Stefani, M., and C.M. Dobson. 2003. Protein aggregation and aggregate toxicity: new insights into protein folding, misfolding diseases and biological evolution. *Journal of molecular medicine*. 81:678-699.
- Steiner, H. 2004. Uncovering gamma-secretase. *Current Alzheimer research*. 1:175-181.
- Steinmetz, L.M., C. Scharfe, A.M. Deutschbauer, D. Mokranjac, Z.S. Herman, T. Jones, A.M. Chu, G. Giaever, H. Prokisch, P.J. Oefner, and R.W. Davis. 2002. Systematic screen for human disease genes in yeast. *Nature genetics*. 31:400-404.
- Stokes, C.E., and J.N. Hawthorne. 1987. Reduced phosphoinositide concentrations in anterior temporal cortex of Alzheimer-diseased brains. *Journal of neurochemistry*. 48:1018-1021.
- Stolz, L.E., C.V. Huynh, J. Thorner, and J.D. York. 1998. Identification and characterization of an essential family of inositol polyphosphate 5-phosphatases (INP51, INP52 and INP53 gene products) in the yeast *Saccharomyces cerevisiae*. *Genetics*. 148:1715-1729.
- Storey, M.K., K.L. Clay, T. Kutateladze, R.C. Murphy, M. Overduin, and D.R. Voelker. 2001. Phosphatidylethanolamine has an essential role in *Saccharomyces cerevisiae* that is independent of its ability to form hexagonal phase structures. *The Journal of biological chemistry*. 276:48539-48548.
- Strahl, T., and J. Thorner. 2007. Synthesis and function of membrane phosphoinositides in budding yeast, *Saccharomyces cerevisiae*. *Biochimica et biophysica acta*. 1771:353-404.
- Stukey, J.E., V.M. McDonough, and C.E. Martin. 1990. The OLE1 gene of *Saccharomyces cerevisiae* encodes the delta 9 fatty acid desaturase and can be functionally replaced by the rat stearoyl-CoA desaturase gene. *The Journal of biological chemistry*. 265:20144-20149.
- Summers, E.F., V.A. Letts, P. McGraw, and S.A. Henry. 1988. *Saccharomyces cerevisiae* cho2 mutants are deficient in phospholipid methylation and cross-pathway regulation of inositol synthesis. *Genetics*. 120:909-922.
- Sunde, M., and C.C. Blake. 1998. From the globular to the fibrous state: protein structure and structural conversion in amyloid formation. *Quarterly reviews of biophysics*. 31:1-39.
- Sunde, M., L.C. Serpell, M. Bartlam, P.E. Fraser, M.B. Pepys, and C.C. Blake. 1997. Common core structure of amyloid fibrils by synchrotron X-ray diffraction. *Journal of molecular biology*. 273:729-739.
- Surma, M.A., C. Klose, R.W. Klemm, C.S. Ejlsing, and K. Simons. 2011. Generic sorting of raft lipids into secretory vesicles in yeast. *Traffic (Copenhagen, Denmark)*. 12:1139-1147.
- Sutton-Tyrrell, K., A. Bostom, J. Selhub, and C. Zeigler-Johnson. 1997. High homocysteine levels are independently related to isolated systolic hypertension in older adults. *Circulation*. 96:1745-1749.
- Takahashi, R.H., T.A. Milner, F. Li, E.E. Nam, M.A. Edgar, H. Yamaguchi, M.F. Beal, H. Xu, P. Greengard, and G.K. Gouras. 2002. Intraneuronal Alzheimer abeta42 accumulates in multivesicular bodies and is associated with synaptic pathology. *The American journal of pathology*. 161:1869-1879.

- Takami, M., Y. Nagashima, Y. Sano, S. Ishihara, M. Morishima-Kawashima, S. Funamoto, and Y. Ihara. 2009. gamma-Secretase: successive tripeptide and tetrapeptide release from the transmembrane domain of beta-carboxyl terminal fragment. *J Neurosci.* 29:13042-13052.
- Tanzi, R.E., and L. Bertram. 2005. Twenty years of the Alzheimer's disease amyloid hypothesis: a genetic perspective. *Cell.* 120:545-555.
- Tanzi, R.E., R.D. Moir, and S.L. Wagner. 2004. Clearance of Alzheimer's Abeta peptide: the many roads to perdition. *Neuron.* 43:605-608.
- Tardiff, D.F., M.L. Tucci, K.A. Caldwell, G.A. Caldwell, and S. Lindquist. 2012. Different 8-hydroxyquinolines protect models of TDP-43 protein, alpha-synuclein, and polyglutamine proteotoxicity through distinct mechanisms. *The Journal of biological chemistry.* 287:4107-4120.
- Tauchi-Sato, K., S. Ozeki, T. Houjou, R. Taguchi, and T. Fujimoto. 2002. The surface of lipid droplets is a phospholipid monolayer with a unique Fatty Acid composition. *The Journal of biological chemistry.* 277:44507-44512.
- Tebar, F., S.K. Bohlander, and A. Sorkin. 1999. Clathrin assembly lymphoid myeloid leukemia (CALM) protein: localization in endocytic-coated pits, interactions with clathrin, and the impact of overexpression on clathrin-mediated traffic. *Molecular biology of the cell.* 10:2687-2702.
- Terry, R.D., E. Masliah, D.P. Salmon, N. Butters, R. DeTeresa, R. Hill, L.A. Hansen, and R. Katzman. 1991. Physical basis of cognitive alterations in Alzheimer's disease: synapse loss is the major correlate of cognitive impairment. *Ann Neurol.* 30:572-580.
- Terzi, E., G. Holzemann, and J. Seelig. 1997. Interaction of Alzheimer beta-amyloid peptide(1-40) with lipid membranes. *Biochemistry.* 36:14845-14852.
- Teter, S.A., K.P. Eggerton, S.V. Scott, J. Kim, A.M. Fischer, and D.J. Klionsky. 2001. Degradation of lipid vesicles in the yeast vacuole requires function of Cvt17, a putative lipase. *The Journal of biological chemistry.* 276:2083-2087.
- Thal, D.R., U. Rub, M. Orantes, and H. Braak. 2002. Phases of A beta-deposition in the human brain and its relevance for the development of AD. *Neurology.* 58:1791-1800.
- Thieringer, R., H. Shio, Y.S. Han, G. Cohen, and P.B. Lazarow. 1991. Peroxisomes in *Saccharomyces cerevisiae*: immunofluorescence analysis and import of catalase A into isolated peroxisomes. *Molecular and cellular biology.* 11:510-522.
- Thomas, D., and Y. Surdin-Kerjan. 1997. Metabolism of sulfur amino acids in *Saccharomyces cerevisiae*. *Microbiol Mol Biol Rev.* 61:503-532.
- Tiwari, A., and R. Bhat. 2006. Stabilization of yeast hexokinase A by polyol osmolytes: correlation with the physicochemical properties of aqueous solutions. *Biophysical chemistry.* 124:90-99.
- Tong, A.H., M. Evangelista, A.B. Parsons, H. Xu, G.D. Bader, N. Page, M. Robinson, S. Raghibizadeh, C.W. Hogue, H. Bussey, B. Andrews, M. Tyers, and C. Boone. 2001. Systematic genetic analysis with ordered arrays of yeast deletion mutants. *Science (New York, N.Y.)* 294:2364-2368.
- Tong, A.H., G. Lesage, G.D. Bader, H. Ding, H. Xu, X. Xin, J. Young, G.F. Berriz, R.L. Brost, M. Chang, Y. Chen, X. Cheng, G. Chua, H. Friesen, D.S. Goldberg, J. Haynes, C. Humphries, G. He, S. Hussein, L. Ke, N. Krogan, Z. Li, J.N. Levinson, H. Lu, P. Menard, C. Munyana, A.B. Parsons, O. Ryan, R. Tonikian, T. Roberts, A.M. Sdicu, J. Shapiro, B. Sheikh, B. Suter, S.L. Wong, L.V. Zhang, H. Zhu, C.G. Burd, S. Munro, C. Sander, J. Rine, J. Greenblatt, M. Peter, A. Bretscher, G. Bell, F.P. Roth, G.W. Brown, B. Andrews, H. Bussey, and C. Boone. 2004. Global mapping of the yeast genetic interaction network. *Science (New York, N.Y.)* 303:808-813.

- Townsend, M., J.P. Cleary, T. Mehta, J. Hofmeister, S. Lesne, E. O'Hare, D.M. Walsh, and D.J. Selkoe. 2006. Orally available compound prevents deficits in memory caused by the Alzheimer amyloid-beta oligomers. *Ann Neurol.* 60:668-676.
- Travers, K.J., C.K. Patil, L. Wodicka, D.J. Lockhart, J.S. Weissman, and P. Walter. 2000. Functional and genomic analyses reveal an essential coordination between the unfolded protein response and ER-associated degradation. *Cell.* 101:249-258.
- Treusch, S., D.M. Cyr, and S. Lindquist. 2009. Amyloid deposits: protection against toxic protein species? *Cell cycle.* 8:1668-1674.
- Treusch, S., S. Hamamichi, J.L. Goodman, K.E. Matlack, C.Y. Chung, V. Baru, J.M. Shulman, A. Parrado, B.J. Bevis, J.S. Valastyan, H. Han, M. Lindhagen-Persson, E.M. Reiman, D.A. Evans, D.A. Bennett, A. Olofsson, P.L. DeJager, R.E. Tanzi, K.A. Caldwell, G.A. Caldwell, and S. Lindquist. 2011. Functional links between A β toxicity, endocytic trafficking, and Alzheimer's disease risk factors in yeast. *Science (New York, N.Y.)* 334:1241-1245.
- Trotter, P.J., J. Pedretti, and D.R. Voelker. 1993. Phosphatidylserine decarboxylase from *Saccharomyces cerevisiae*. Isolation of mutants, cloning of the gene, and creation of a null allele. *The Journal of biological chemistry.* 268:21416-21424.
- Trotter, P.J., J. Pedretti, R. Yates, and D.R. Voelker. 1995. Phosphatidylserine decarboxylase 2 of *Saccharomyces cerevisiae*. Cloning and mapping of the gene, heterologous expression, and creation of the null allele. *The Journal of biological chemistry.* 270:6071-6080.
- Trotter, P.J., and D.R. Voelker. 1995. Identification of a non-mitochondrial phosphatidylserine decarboxylase activity (PSD2) in the yeast *Saccharomyces cerevisiae*. *The Journal of biological chemistry.* 270:6062-6070.
- Tzagoloff, A., and C.L. Dieckmann. 1990. PET genes of *Saccharomyces cerevisiae*. *Microbiological reviews.* 54:211-225.
- Umeda, M., and K. Emoto. 1999. Membrane phospholipid dynamics during cytokinesis: regulation of actin filament assembly by redistribution of membrane surface phospholipid. *Chemistry and physics of lipids.* 101:81-91.
- Urano, Y., I. Hayashi, N. Isoo, P.C. Reid, Y. Shibasaki, N. Noguchi, T. Tomita, T. Iwatsubo, T. Hamakubo, and T. Kodama. 2005. Association of active gamma-secretase complex with lipid rafts. *Journal of lipid research.* 46:904-912.
- Vagenende, V., M.G. Yap, and B.L. Trout. 2009. Mechanisms of protein stabilization and prevention of protein aggregation by glycerol. *Biochemistry.* 48:11084-11096.
- Valla, J., J.D. Berndt, and F. Gonzalez-Lima. 2001. Energy hypometabolism in posterior cingulate cortex of Alzheimer's patients: superficial laminar cytochrome oxidase associated with disease duration. *J Neurosci.* 21:4923-4930.
- Van Broeckhoven, C., J. Haan, E. Bakker, J.A. Hardy, W. Van Hul, A. Wehnert, M. Vegter-Van der Vlis, and R.A. Roos. 1990. Amyloid beta protein precursor gene and hereditary cerebral hemorrhage with amyloidosis (Dutch). *Science (New York, N.Y.)* 248:1120-1122.
- van der Does, C., J. Swaving, W. van Klompenburg, and A.J. Driessen. 2000. Non-bilayer lipids stimulate the activity of the reconstituted bacterial protein translocase. *The Journal of biological chemistry.* 275:2472-2478.
- van Es, M.A., and L.H. van den Berg. 2009. Alzheimer's disease beyond APOE. *Nature genetics.* 41:1047-1048.

- van Ham, T.J., R. Breitling, M.A. Swertz, and E.A. Nollen. 2009. Neurodegenerative diseases: Lessons from genome-wide screens in small model organisms. *EMBO molecular medicine*. 1:360-370.
- van Meer, G., D.R. Voelker, and G.W. Feigenson. 2008. Membrane lipids: where they are and how they behave. *Nature reviews*. 9:112-124.
- Van Vickle, G.D., C.L. Esh, W.M. Kalback, R.L. Patton, D.C. Luehrs, T.A. Kokjohn, F.G. Fifield, P.E. Fraser, D. Westaway, J. McLaurin, J. Lopez, D. Brune, A.J. Newel, M. Poston, T.G. Beach, and A.E. Roher. 2007. TgCRND8 amyloid precursor protein transgenic mice exhibit an altered gamma-secretase processing and an aggressive, additive amyloid pathology subject to immunotherapeutic modulation. *Biochemistry*. 46:10317-10327.
- Vance, D.E., C.J. Walkey, and Z. Cui. 1997. Phosphatidylethanolamine N-methyltransferase from liver. *Biochimica et biophysica acta*. 1348:142-150.
- Vance, J.E. 2003. Molecular and cell biology of phosphatidylserine and phosphatidylethanolamine metabolism. *Progress in nucleic acid research and molecular biology*. 75:69-111.
- Vassar, R., B.D. Bennett, S. Babu-Khan, S. Kahn, E.A. Mendiaz, P. Denis, D.B. Teplow, S. Ross, P. Amarante, R. Loeloff, Y. Luo, S. Fisher, J. Fuller, S. Edenson, J. Lile, M.A. Jarosinski, A.L. Biere, E. Curran, T. Burgess, J.C. Louis, F. Collins, J. Treanor, G. Rogers, and M. Citron. 1999. Beta-secretase cleavage of Alzheimer's amyloid precursor protein by the transmembrane aspartic protease BACE. *Science (New York, N.Y.)*. 286:735-741.
- Vicinanza, M., G. D'Angelo, A. Di Campli, and M.A. De Matteis. 2008. Phosphoinositides as regulators of membrane trafficking in health and disease. *Cell Mol Life Sci*. 65:2833-2841.
- Vizeacoumar, F.J., W.N. Vreden, J.D. Aitchison, and R.A. Rachubinski. 2006. Pex19p binds Pex30p and Pex32p at regions required for their peroxisomal localization but separate from their peroxisomal targeting signals. *The Journal of biological chemistry*. 281:14805-14812.
- Voelker, D.R. 2005. Bridging gaps in phospholipid transport. *Trends in biochemical sciences*. 30:396-404.
- von der Haar, T., L. Josse, P. Wright, J. Zenthon, and M.F. Tuite. 2007. Development of a novel yeast cell-based system for studying the aggregation of Alzheimer's disease-associated Abeta peptides in vivo. *Neuro-degenerative diseases*. 4:136-147.
- Waechter, C.J., and R.L. Lester. 1973. Differential regulation of the N-methyl transferases responsible for phosphatidylcholine synthesis in *Saccharomyces cerevisiae*. *Archives of biochemistry and biophysics*. 158:401-410.
- Wakabayashi, M., T. Okada, Y. Kozutsumi, and K. Matsuzaki. 2005. GM1 ganglioside-mediated accumulation of amyloid beta-protein on cell membranes. *Biochemical and biophysical research communications*. 328:1019-1023.
- Waldo, G.S., B.M. Standish, J. Berendzen, and T.C. Terwilliger. 1999. Rapid protein-folding assay using green fluorescent protein. *Nature biotechnology*. 17:691-695.
- Walsh, D.M., I. Klyubin, J.V. Fadeeva, M.J. Rowan, and D.J. Selkoe. 2002b. Amyloid-beta oligomers: their production, toxicity and therapeutic inhibition. *Biochemical Society transactions*. 30:552-557.
- Walsh, D.M., I. Klyubin, J.V. Fadeeva, W.K. Cullen, R. Anwyl, M.S. Wolfe, M.J. Rowan, and D.J. Selkoe. 2002a. Naturally secreted oligomers of amyloid beta protein potently inhibit hippocampal long-term potentiation in vivo. *Nature*. 416:535-539.
- Walsh, D.M., and D.J. Selkoe. 2004. Deciphering the molecular basis of memory failure in Alzheimer's disease. *Neuron*. 44:181-193.

- Walsh, D.M., and D.J. Selkoe. 2007. A beta oligomers - a decade of discovery. *Journal of neurochemistry*. 101:1172-1184.
- Walsh, D.M., M. Townsend, M.B. Podlisny, G.M. Shankar, J.V. Fadeeva, O. El Agnaf, D.M. Hartley, and D.J. Selkoe. 2005. Certain inhibitors of synthetic amyloid beta-peptide (Abeta) fibrillogenesis block oligomerization of natural Abeta and thereby rescue long-term potentiation. *J Neurosci*. 25:2455-2462.
- Walsh, D.M., B.P. Tseng, R.E. Rydel, M.B. Podlisny, and D.J. Selkoe. 2000. The oligomerization of amyloid beta-protein begins intracellularly in cells derived from human brain. *Biochemistry*. 39:10831-10839.
- Walsh, J.S., H.G. Welch, and E.B. Larson. 1990. Survival of outpatients with Alzheimer-type dementia. *Annals of internal medicine*. 113:429-434.
- Walther, T.C., and R.V. Farese, Jr. 2009. The life of lipid droplets. *Biochimica et biophysica acta*. 1791:459-466.
- Wang, H.T., P. Rahaim, P. Robbins, and R.R. Yocum. 1994. Cloning, sequence, and disruption of the *Saccharomyces diastaticus* DAR1 gene encoding a glycerol-3-phosphate dehydrogenase. *Journal of bacteriology*. 176:7091-7095.
- Wang, J., G.W. Farr, D.H. Hall, F. Li, K. Furtak, L. Dreier, and A.L. Horwich. 2009. An ALS-linked mutant SOD1 produces a locomotor defect associated with aggregation and synaptic dysfunction when expressed in neurons of *Caenorhabditis elegans*. *PLoS genetics*. 5:e1000350.
- Wang, J.Z., and F. Liu. 2008. Microtubule-associated protein tau in development, degeneration and protection of neurons. *Progress in neurobiology*. 85:148-175.
- Ward, J.E., R. Ren, G. Toraldo, P. Soohoo, J. Guan, C. O'Hara, R. Jasuja, V. Trinkaus-Randall, R. Liao, L.H. Connors, and D.C. Seldin. 2011. Doxycycline reduces fibril formation in a transgenic mouse model of AL amyloidosis. *Blood*. 118:6610-6617.
- Waschuk, S.A., E.A. Elton, A.A. Darabie, P.E. Fraser, and J.A. McLaurin. 2001. Cellular membrane composition defines A beta-lipid interactions. *The Journal of biological chemistry*. 276:33561-33568.
- Watkins, P.A., J.F. Lu, S.J. Steinberg, S.J. Gould, K.D. Smith, and L.T. Braiterman. 1998. Disruption of the *Saccharomyces cerevisiae* FAT1 gene decreases very long-chain fatty acyl-CoA synthetase activity and elevates intracellular very long-chain fatty acid concentrations. *The Journal of biological chemistry*. 273:18210-18219.
- Watkins, S.M., X. Zhu, and S.H. Zeisel. 2003. Phosphatidylethanolamine-N-methyltransferase activity and dietary choline regulate liver-plasma lipid flux and essential fatty acid metabolism in mice. *The Journal of nutrition*. 133:3386-3391.
- Weber, U., C. Eroglu, and M. Mlodzik. 2003. Phospholipid membrane composition affects EGF receptor and Notch signaling through effects on endocytosis during *Drosophila* development. *Developmental cell*. 5:559-570.
- Wegiel, J., I. Kuchna, K. Nowicki, J. Frackowiak, B. Mazur-Kolecka, H. Imaki, J. Wegiel, P.D. Mehta, W.P. Silverman, B. Reisberg, M. Deleon, T. Wisniewski, T. Pirttilla, H. Frey, T. Lehtimäki, T. Kivimäki, F.E. Visser, W. Kamphorst, A. Potempska, D. Bolton, J.R. Currie, and D.L. Miller. 2007. Intraneuronal Abeta immunoreactivity is not a predictor of brain amyloidosis-beta or neurofibrillary degeneration. *Acta neuropathologica*. 113:389-402.
- Welander, H., J. Franberg, C. Graff, E. Sundstrom, B. Winblad, and L.O. Tjernberg. 2009. Abeta43 is more frequent than Abeta40 in amyloid plaque cores from Alzheimer disease brains. *Journal of neurochemistry*. 110:697-706.

- Welch, W.J., and C.R. Brown. 1996. Influence of molecular and chemical chaperones on protein folding. *Cell stress & chaperones*. 1:109-115.
- Welihinda, A.A., A.D. Beavis, and R.J. Trumbly. 1994. Mutations in LIS1 (ERG6) gene confer increased sodium and lithium uptake in *Saccharomyces cerevisiae*. *Biochimica et biophysica acta*. 1193:107-117.
- Wenk, M.R. 2005. The emerging field of lipidomics. *Nature reviews. Drug discovery*. 4:594-610.
- Wertkin, A.M., R.S. Turner, S.J. Pleasure, T.E. Golde, S.G. Younkin, J.Q. Trojanowski, and V.M. Lee. 1993. Human neurons derived from a teratocarcinoma cell line express solely the 695-amino acid amyloid precursor protein and produce intracellular beta-amyloid or A4 peptides. *Proceedings of the National Academy of Sciences of the United States of America*. 90:9513-9517.
- Wheeler, D.L., T. Barrett, D.A. Benson, S.H. Bryant, K. Canese, V. Chetvernin, D.M. Church, M. Dicuccio, R. Edgar, S. Federhen, M. Feolo, L.Y. Geer, W. Helmberg, Y. Kapustin, O. Khovayko, D. Landsman, D.J. Lipman, T.L. Madden, D.R. Maglott, V. Miller, J. Ostell, K.D. Pruitt, G.D. Schuler, M. Shumway, E. Sequeira, S.T. Sherry, K. Sirotkin, A. Souvorov, G. Starchenko, R.L. Tatusov, T.A. Tatusova, L. Wagner, and E. Yaschenko. 2008. Database resources of the National Center for Biotechnology Information. *Nucleic acids research*. 36:D13-21.
- Williams, A.D., E. Portelius, I. Kheterpal, J.T. Guo, K.D. Cook, Y. Xu, and R. Wetzel. 2004. Mapping abeta amyloid fibril secondary structure using scanning proline mutagenesis. *Journal of molecular biology*. 335:833-842.
- Willingham, S., T.F. Outeiro, M.J. DeVit, S.L. Lindquist, and P.J. Muchowski. 2003. Yeast genes that enhance the toxicity of a mutant huntingtin fragment or alpha-synuclein. *Science (New York, N.Y.)*. 302:1769-1772.
- Winderickx, J., C. Delay, A. De Vos, H. Klinger, K. Pellens, T. Vanhelmont, F. Van Leuven, and P. Zabrocki. 2008. Protein folding diseases and neurodegeneration: lessons learned from yeast. *Biochimica et biophysica acta*. 1783:1381-1395.
- Winzeler, E.A., D.D. Shoemaker, A. Astromoff, H. Liang, K. Anderson, B. Andre, R. Bangham, R. Benito, J.D. Boeke, H. Bussey, A.M. Chu, C. Connolly, K. Davis, F. Dietrich, S.W. Dow, M. El Bakkoury, F. Foury, S.H. Friend, E. Gentelen, G. Giaever, J.H. Hegemann, T. Jones, M. Laub, H. Liao, N. Liebundguth, D.J. Lockhart, A. Lucau-Danila, M. Lussier, N. M'Rabet, P. Menard, M. Mittmann, C. Pai, C. Rebischung, J.L. Revuelta, L. Riles, C.J. Roberts, P. Ross-MacDonald, B. Scherens, M. Snyder, S. Sookhai-Mahadeo, R.K. Storms, S. Veronneau, M. Voet, G. Volckaert, T.R. Ward, R. Wysocki, G.S. Yen, K. Yu, K. Zimmermann, P. Philippsen, M. Johnston, and R.W. Davis. 1999. Functional characterization of the *S. cerevisiae* genome by gene deletion and parallel analysis. *Science (New York, N.Y.)*. 285:901-906.
- Wiradjaja, F., L.M. Ooms, J.C. Whisstock, B. McColl, L. Helfenbaum, J.F. Sambrook, M.J. Gething, and C.A. Mitchell. 2001. The yeast inositol polyphosphate 5-phosphatase Inp54p localizes to the endoplasmic reticulum via a C-terminal hydrophobic anchoring tail: regulation of secretion from the endoplasmic reticulum. *The Journal of biological chemistry*. 276:7643-7653.
- Wirths, O., G. Multhaup, C. Czech, V. Blanchard, S. Moussaoui, G. Tremp, L. Pradier, K. Beyreuther, and T.A. Bayer. 2001. Intraneuronal Abeta accumulation precedes plaque formation in beta-amyloid precursor protein and presenilin-1 double-transgenic mice. *Neuroscience letters*. 306:116-120.
- Wolfe, M.S., W. Xia, B.L. Ostaszewski, T.S. Diehl, W.T. Kimberly, and D.J. Selkoe. 1999. Two transmembrane aspartates in presenilin-1 required for presenilin endoproteolysis and gamma-secretase activity. *Nature*. 398:513-517.
- Wolozin, B. 2004. Cholesterol and the biology of Alzheimer's disease. *Neuron*. 41:7-10.

- Woods, J.S. 1976. Developmental aspects of hepatic heme biosynthetic capability and hematotoxicity. *Biochem Pharmacol.* 25:2147-2152.
- Wright S, Franke-Snyder M, Morton J, Upadhyaya A (1996) Time-course study and partial characterization of a protein on hyphae of arbuscular mycorrhizal fungi during active colonization of roots. *Plant and Soil* 181: 193-203.
- Wu, W.I., and G.M. Carman. 1994. Regulation of phosphatidate phosphatase activity from the yeast *Saccharomyces cerevisiae* by nucleotides. *The Journal of biological chemistry.* 269:29495-29501.
- Wurth, C., N.K. Guimard, and M.H. Hecht. 2002. Mutations that reduce aggregation of the Alzheimer's Abeta42 peptide: an unbiased search for the sequence determinants of Abeta amyloidogenesis. *Journal of molecular biology.* 319:1279-1290.
- Xie, Z., U. Nair, and D.J. Klionsky. 2008. Atg8 controls phagophore expansion during autophagosome formation. *Molecular biology of the cell.* 19:3290-3298.
- Xu, H., P. Greengard, and S. Gandy. 1995. Regulated formation of Golgi secretory vesicles containing Alzheimer beta-amyloid precursor protein. *The Journal of biological chemistry.* 270:23243-23245.
- Yamamoto, N., U. Igbabvoa, Y. Shimada, Y. Ohno-Iwashita, M. Kobayashi, W.G. Wood, S.C. Fujita, and K. Yanagisawa. 2004. Accelerated Abeta aggregation in the presence of GM1-ganglioside-accumulated synaptosomes of aged apoE4-knock-in mouse brain. *FEBS letters.* 569:135-139.
- Yancey, P.H., M.E. Clark, S.C. Hand, R.D. Bowlus, and G.N. Somero. 1982. Living with water stress: evolution of osmolyte systems. *Science (New York, N.Y.* 217:1214-1222.
- Yang, F., G.P. Lim, A.N. Begum, O.J. Ubeda, M.R. Simmons, S.S. Ambegaokar, P.P. Chen, R. Kayed, C.G. Glabe, S.A. Frautschy, and G.M. Cole. 2005. Curcumin inhibits formation of amyloid beta oligomers and fibrils, binds plaques, and reduces amyloid in vivo. *The Journal of biological chemistry.* 280:5892-5901.
- Yang, H., M. Bard, D.A. Bruner, A. Gleeson, R.J. Deckelbaum, G. Aljinovic, T.M. Pohl, R. Rothstein, and S.L. Sturley. 1996. Sterol esterification in yeast: a two-gene process. *Science (New York, N.Y.* 272:1353-1356.
- Yeung, T., G.E. Gilbert, J. Shi, J. Silvius, A. Kapus, and S. Grinstein. 2008. Membrane phosphatidylserine regulates surface charge and protein localization. *Science (New York, N.Y.* 319:210-213.
- Yi, P., S. Melnyk, M. Pogribna, I.P. Pogribny, R.J. Hine, and S.J. James. 2000. Increase in plasma homocysteine associated with parallel increases in plasma S-adenosylhomocysteine and lymphocyte DNA hypomethylation. *The Journal of biological chemistry.* 275:29318-29323.
- Yorimitsu, T., and D.J. Klionsky. 2005. Autophagy: molecular machinery for self-eating. *Cell death and differentiation.* 12 Suppl 2:1542-1552.
- York, J.D., S. Guo, A.R. Odom, B.D. Spiegelberg, and L.E. Stolz. 2001. An expanded view of inositol signaling. *Advances in enzyme regulation.* 41:57-71.
- Younkin, S.G. 1995. Evidence that A beta 42 is the real culprit in Alzheimer's disease. *Ann Neurol.* 37:287-288.
- Younkin, S.G. 1998. The role of A beta 42 in Alzheimer's disease. *Journal of physiology, Paris.* 92:289-292.

- Yrjanheikki, J., R. Keinänen, M. Pellikka, T. Hokfelt, and J. Koistinaho. 1998. Tetracyclines inhibit microglial activation and are neuroprotective in global brain ischemia. *Proceedings of the National Academy of Sciences of the United States of America*. 95:15769-15774.
- Yu, C., N.J. Kennedy, C.C. Chang, and J.A. Rothblatt. 1996. Molecular cloning and characterization of two isoforms of *Saccharomyces cerevisiae* acyl-CoA:sterol acyltransferase. *The Journal of biological chemistry*. 271:24157-24163.
- Yu, H., P. Braun, M.A. Yildirim, I. Lemmens, K. Venkatesan, J. Sahalie, T. Hirozane-Kishikawa, F. Gebreab, N. Li, N. Simonis, T. Hao, J.F. Rual, A. Dricot, A. Vazquez, R.R. Murray, C. Simon, L. Tardivo, S. Tam, N. Svrzikapa, C. Fan, A.S. de Smet, A. Motyl, M.E. Hudson, J. Park, X. Xin, M.E. Cusick, T. Moore, C. Boone, M. Snyder, F.P. Roth, A.L. Barabasi, J. Tavernier, D.E. Hill, and M. Vidal. 2008. High-quality binary protein interaction map of the yeast interactome network. *Science (New York, N.Y.)*. 322:104-110.
- Zhang, H., H. Komano, R.S. Fuller, S.E. Gandy, and D.E. Frail. 1994. Proteolytic processing and secretion of human beta-amyloid precursor protein in yeast. Evidence for a yeast secretase activity. *The Journal of biological chemistry*. 269:27799-27802.
- Zhang, H., Q. Ma, Y.W. Zhang, and H. Xu. 2012. Proteolytic processing of Alzheimer's beta-amyloid precursor protein. *Journal of neurochemistry*. 120 Suppl 1:9-21.
- Zhang, R., X. Hu, H. Khant, S.J. Ludtke, W. Chiu, M.F. Schmid, C. Frieden, and J.M. Lee. 2009. Interprotofilament interactions between Alzheimer's Abeta1-42 peptides in amyloid fibrils revealed by cryoEM. *Proceedings of the National Academy of Sciences of the United States of America*. 106:4653-4658.
- Zhang, W., D. Espinoza, V. Hines, M. Innis, P. Mehta, and D.L. Miller. 1997. Characterization of beta-amyloid peptide precursor processing by the yeast Yap3 and Mkc7 proteases. *Biochimica et biophysica acta*. 1359:110-122.
- Zhu, S., I.G. Stavrovskaya, M. Drozda, B.Y. Kim, V. Ona, M. Li, S. Sarang, A.S. Liu, D.M. Hartley, D.C. Wu, S. Gullans, R.J. Ferrante, S. Przedborski, B.S. Kristal, and R.M. Friedlander. 2002. Minocycline inhibits cytochrome c release and delays progression of amyotrophic lateral sclerosis in mice. *Nature*. 417:74-78.
- Zinser, E., and G. Daum. 1995. Isolation and biochemical characterization of organelles from the yeast, *Saccharomyces cerevisiae*. *Yeast (Chichester, England)*. 11:493-536.
- Zinser, E., F. Paltauf, and G. Daum. 1993. Sterol composition of yeast organelle membranes and subcellular distribution of enzymes involved in sterol metabolism. *Journal of bacteriology*. 175:2853-2858.

APPENDIX A

ORFs whose deletants were not screened using A β ₄₂GFP

YHL047C	YHR030C	YHR114W	YHR202W	YGR097W	YKR030W	YLR432W	YJR075W
YHL046C	YHR031C	YHR115C	YHR203C	YGR100W	YKR031C	YLR433C	YJR078W
YHL045W	YHR033W	YHR116W	YHR204W	YGR101W	YKR032W	YLR434C	YJR079W
YHL044W	YHR034C	YHR117W	YHR206W	YGR102C	YKR033C	YLR435W	YJR082C
YHL043W	YHR035W	YHR120W	YHR207C	YGR104C	YKR035C	YLR436C	YJR083C
YHL042W	YHR037W	YHR121W	YHR209W	YGR105W	YKR042W	YLR437C	YJR088C
YHL041W	YHR038W	YHR123W	YHR210C	YGR107W	YKR043C	YLR438W	YJR092W
YHL040C	YHR039C	YHR124W	YGR027C	YGR108W	YKR044W	YLR441C	YJR102C
YHL038C	YHR043C	YHR125W	YGR031W	YGR109C	YKR045C	YLR443W	YJR103W
YHL037C	YHR044C	YHR126C	YGR033C	YGR111W	YKR047W	YLR444C	YJR105W
YHL036W	YHR046C	YHR129C	YGR034W	YGR112W	YKR048C	YLR445W	YJR108W
YHL035C	YHR047C	YHR130C	YGR035C	YGR118W	YKR049C	YLR446W	YJR110W
YHL034C	YHR048W	YHR132C	YGR036C	YGR121C	YKR050W	YLR447C	YJR111C
YHL033C	YHR049W	YHR134W	YGR037C	YGR122W	YKR051W	YLR448W	YJR115W
YHL032C	YHR049C-A	YHR135C	YGR039W	YKL191W	YKR052C	YLR449W	YJR127C
YHL031C	YHR050W	YHR136C	YGR041W	YKL197C	YKR054C	YLR450W	YJR128W
YHL030W	YHR051W	YHR137W	YGR042W	YKL198C	YKR055W	YLR452C	YJR129C
YHL029C	YHR057C	YHR138C	YGR043C	YKL199C	YKR056W	YLR453C	YJR130C
YHL028W	YHR060W	YHR139C	YGR044C	YKL205W	YKR057W	YLR454W	YJR135C
YHL027W	YHR061C	YHR139C-A	YGR045C	YKL200C	YKR058W	YLR456W	YJR137C
YHL026C	YHR066W	YHR142W	YGR049W	YKL206C	YKR059W	YLR460C	YJR146W
YHL023C	YHR073W	YHR143W	YGR051C	YKL207W	YKR060W	YLR461W	YJR147W
YHL022C	YHR075C	YHR147C	YGR052W	YKL208W	YKR061W	YML009C	YJR149W
YHL021C	YHR076W	YHR150W	YGR054W	YKL211C	YKR064W	YML010C-B	YJR152W
YHL020C	YHR077C	YHR151C	YGR055W	YKL212W	YKR065C	YML021C	YJR154W
YHL019C	YHR078W	YHR133C	YGR056W	YKL213C	YKR087C	YML081C-A	
YHL017W	YHR079C	YHR152W	YGR057C	YKL214C	YKR088C	YMR060C	
YHL016C	YHR080C	YHR153C	YGR058W	YKL216W	YKR089C	YMR158C-B	
YHL014C	YHR081W	YHR154W	YGR059W	YKL217W	YKR090W	YMR169C	
YHL013C	YHR082C	YHR155W	YGR061C	YKL218C	YKR091W	YMR174C	
YHL012W	YHR086W	YHR156C	YGR062C	YKL221W	YKR092C	YMR175W	
YHL010C	YHR087W	YHR157W	YGR064W	YKL222C	YKR093W	YMR194C-A	
YHL009C	YHR091C	YHR158C	YGR066C	YKR001C	YKR097W	YMR326C	
YHL008C	YHR092C	YHR159W	YGR067C	YKR003W	YKR098C	YNR032C-A	
YHL007C	YHR093W	YHR160C	YGR068C	YKR005C	YKR099W	YNR050C	
YHL006C	YHR094C	YHR161C	YGR069W	YKR006C	YKR100C	YNR051C	
YHL005C	YHR095W	YHR163W	YGR070W	YKR007W	YKR101W	YNR056C	
YHL003C	YHR096C	YHR167W	YGR071C	YKR009C	YKR103W	YNR057C	
YHR001W-A	YHR097C	YHR176W	YGR072W	YKR011C	YKR104W	YNR058W	
YHR010W	YHR100C	YHR177W	YGR076C	YKR012C	YKR105C	YNR059W	
YHR011W	YHR103W	YHR178W	YGR077C	YKR013W	YLL018C-A	YNR060W	
YHR012W	YHR104W	YHR179W	YGR078C	YKR014C	YLR262C-A	YNR061C	
YHR013C	YHR105W	YHR182W	YGR079W	YKR015C	YLR422W	YNR062C	
YHR014W	YHR106W	YHR183W	YGR080W	YKR016W	YLR423C	YNR063W	
YHR015W	YHR108W	YHR184W	YGR081C	YKR017C	YLR425W	YNR064C	
YHR018C	YHR109W	YHR189W	YGR084C	YKR018C	YLR426W	YNR065C	
YHR021C	YHR110W	YHR195W	YGR085C	YKR020W	YLR427W	YNR066C	
YHR022C	YHR112C	YHR198C	YGR087C	YKR021W	YLR428C	YNR067C	
YHR028C	YHR111W	YHR199C	YGR088W	YKR024C	YLR429W	YNR068C	
YHR029C	YHR113W	YHR200W	YGR096W	YKR026C	YLR431C	YJR073C	

APPENDIX B

Mutants exhibiting weak/faint A β ₄₂GFP-associated fluorescence

ORF	Gene name	Description
<i>YDL243C</i>	<i>AAD4</i>	Putative aryl-alcohol dehydrogenase with similarity to <i>P. chrysosporium</i> aryl-alcohol dehydrogenase, involved in the oxidative stress response
<i>YGL234W</i>	<i>ADE5,7</i>	Bifunctional enzyme of the 'de novo' purine nucleotide biosynthetic pathway, contains aminoimidazole ribotide synthetase and glycinamide ribotide synthetase activities
<i>YDR408C</i>	<i>ADE8</i>	Phosphoribosyl-glycinamide transformylase, catalyzes a step in the 'de novo' purine nucleotide biosynthetic pathway
<i>YDR226W</i>	<i>ADK1</i>	Adenylate kinase, required for purine metabolism; localised to the cytoplasm and the mitochondria; lacks cleavable signal sequence
<i>YBR288C</i>	<i>APM3</i>	Mu3-like subunit of the clathrin associated protein complex (AP-3); functions in transport of alkaline phosphatase to the vacuole via the alternate pathway
<i>YMR119W</i>	<i>ASI1</i>	Putative integral membrane E3 ubiquitin ligase; genetic interactions suggest a role in negative regulation of amino acid uptake
<i>YCR068W</i>	<i>ATG15</i>	Lipase, required for intravacuolar lysis of autophagic bodies; located in the endoplasmic reticulum membrane and targeted to intravacuolar vesicles during autophagy via the multivesicular body (MVB) pathway
<i>YJL180C</i>	<i>ATP12</i>	Molecular chaperone, required for the assembly of alpha and beta subunits into the F1 sector of mitochondrial F1F0 ATP synthase
<i>YML081C-A</i>	<i>ATP18</i>	Subunit of the mitochondrial F1F0 ATP synthase, which is a large enzyme complex required for ATP synthesis; termed subunit I or subunit j; does not correspond to known ATP synthase subunits in other organisms
<i>YDR298C</i>	<i>ATP5</i>	Subunit 5 of the stator stalk of mitochondrial F1F0 ATP synthase, which is a large, evolutionarily conserved enzyme complex required for ATP synthesis; homologous to bovine subunit OSCP (oligomycin sensitivity-conferring protein)
<i>YER177W</i>	<i>BMH1</i>	14-3-3 protein, major isoform; binds proteins and DNA, involved in regulation of many processes including exocytosis and vesicle transport, Ras/MAPK signaling during pseudohyphal development, rapamycin-sensitive signaling, and others
<i>YNR027W</i>	<i>BUD17</i>	Protein involved in bud-site selection; diploid mutants display a random budding pattern instead of the wild-type bipolar pattern
<i>YDR241W</i>	<i>BUD26</i>	Dubious open reading frame, unlikely to encode a protein; not conserved in closely related <i>Saccharomyces</i> species; 1% of ORF overlaps the verified gene SNU56; diploid mutant displays a weak budding pattern phenotype in a systematic assay
<i>YCR063W</i>	<i>BUD31</i>	Protein involved in bud-site selection; diploid mutants display a random budding pattern instead of the wild-type bipolar pattern
<i>YKL005C</i>	<i>BYE1</i>	Negative regulator of transcription elongation, contains a TFIIIS-like domain and a PHD finger, multicopy suppressor of temperature-sensitive <i>ess1</i> mutations, probably binds RNA polymerase II large subunit
<i>YER061C</i>	<i>CEM1</i>	Mitochondrial beta-keto-acyl synthase with possible role in fatty acid synthesis; required for mitochondrial respiration
<i>YBR003W</i>	<i>COQ1</i>	Hexaprenyl pyrophosphate synthetase, catalyzes the first step in ubiquinone (coenzyme Q) biosynthesis
<i>YNR041C</i>	<i>COQ2</i>	Para hydroxybenzoate: polyprenyl transferase, catalyzes the second step in ubiquinone (coenzyme Q) biosynthesis
<i>YLR201C</i>	<i>COQ9</i>	Mitochondrial inner membrane protein required for ubiquinone (coenzyme Q) biosynthesis, which in turn is required for respiratory growth; exhibits genetic interaction with ABC1, suggesting a possible common function
<i>YGL263W</i>	<i>COS12</i>	Protein of unknown function, member of the DUP380 subfamily of conserved, often subtelomerically-encoded proteins
<i>YPL132W</i>	<i>COX11</i>	Mitochondrial inner membrane protein required for delivery of copper to the Cox1p subunit of cytochrome c oxidase; association with mitochondrial ribosomes suggests that copper delivery may occur during translation of Cox1p

<i>YLL018C-A</i>	<i>COX19</i>	Protein required for cytochrome c oxidase assembly, located in the cytosol and mitochondrial intermembrane space; putative copper metallochaperone that delivers copper to cytochrome c oxidase
<i>YHR051W</i>	<i>COX6</i>	Subunit VI of cytochrome c oxidase, which is the terminal member of the mitochondrial inner membrane electron transport chain; expression is regulated by oxygen levels
<i>YBR036C</i>	<i>CSG2</i>	Endoplasmic reticulum membrane protein, required for mannosylation of inositolphosphorylceramide and for growth at high calcium concentrations
<i>YJR048W</i>	<i>CYC1</i>	Cytochrome c, isoform 1; electron carrier of the mitochondrial intermembrane space that transfers electrons from ubiquinone-cytochrome c oxidoreductase to cytochrome c oxidase during cellular respiration
<i>YBR112C</i>	<i>CYC8</i>	General transcriptional co-repressor, acts together with Tup1p; also acts as part of a transcriptional co-activator complex that recruits the SWI/SNF and SAGA complexes to promoters
<i>YDL117W</i>	<i>CYK3</i>	SH3-domain protein located in the mother-bud neck and the cytokinetic actin ring; mutant phenotype and genetic interactions suggest a role in cytokinesis
<i>YOR065W</i>	<i>CYT1</i>	Cytochrome c1, component of the mitochondrial respiratory chain; expression is regulated by the heme-activated, glucose-repressed Hap2p/3p/4p/5p CCAAT-binding complex
<i>YDR320C-A</i>	<i>DAD4</i>	Essential subunit of the DASH microtubule ring complex, couples kinetochores to the force produced by MT depolymerization thereby aiding in chromosome segregation; is transferred to the kinetochore prior to mitosis
<i>YKR034W</i>	<i>DAL80</i>	Negative regulator of genes in multiple nitrogen degradation pathways; expression is regulated by nitrogen levels and by Gln3p; member of the GATA-binding family, forms homodimers and heterodimers with Deh1p
<i>YDL101C</i>	<i>DUN1</i>	Cell-cycle checkpoint serine-threonine kinase required for DNA damage-induced transcription of certain target genes, phosphorylation of Rad55p and Sml1p, and transient G2/M arrest after DNA damage; also regulates postreplicative DNA repair
<i>YPR023C</i>	<i>EAF3</i>	Esa1p-associated factor, nonessential component of the NuA4 acetyltransferase complex, homologous to Drosophila dosage compensation protein MSL3
<i>YNL136W</i>	<i>EAF7</i>	Subunit of the NuA4 histone acetyltransferase complex, which acetylates the N-terminal tails of histones H4 and H2A
<i>YKL204W</i>	<i>EAP1</i>	eIF4E-associated protein, binds eIF4E and inhibits cap-dependent translation, also functions independently of eIF4E to maintain genetic stability; plays a role in cell growth, implicated in the TOR signaling cascade
<i>YBR078W</i>	<i>ECM33</i>	GPI-anchored protein of unknown function, has a possible role in apical bud growth; GPI-anchoring on the plasma membrane crucial to function; similar to Sps2p and Pst1p
<i>YDR512C</i>	<i>EMI1</i>	Non-essential protein of unknown function required for transcriptional induction of the early meiotic-specific transcription factor IME1, also required for sporulation
<i>YNL280C</i>	<i>ERG24</i>	C-14 sterol reductase, acts in ergosterol biosynthesis; mutants accumulate the abnormal sterol ignosterol (ergosta-8,14 dienol), and are viable under anaerobic growth conditions but inviable on rich medium under aerobic conditions
<i>YBR026C</i>	<i>ETR1</i>	2-enoyl thioester reductase, member of the medium chain dehydrogenase/reductase family; localised to in mitochondria, where it has a probable role in fatty acid synthesis
<i>YFR019W</i>	<i>FAB1</i>	1-phosphatidylinositol-3-phosphate 5-kinase; vacuolar membrane kinase that generates phosphatidylinositol (3,5)P ₂ , which is involved in vacuolar sorting and homeostasis
<i>YBR040W</i>	<i>FIG1</i>	Integral membrane protein required for efficient mating; may participate in or regulate the low affinity Ca ²⁺ influx system, which affects intracellular signalling and cell-cell fusion during mating
<i>YER109C</i>	<i>FLO8</i>	Transcription factor required for flocculation, diploid filamentous growth, and haploid invasive growth; genome reference strain S288C and most laboratory strains have a mutation in this gene

<i>YER145C</i>	<i>FTR1</i>	High affinity iron permease involved in the transport of iron across the plasma membrane; forms complex with Fet3p; expression is regulated by iron
<i>YJR040W</i>	<i>GEF1</i>	Chloride channel localised to late- or post-Golgi vesicles, involved in iron metabolism; highly homologous to voltage-gated chloride channels in vertebrates
<i>YDL198C</i>	<i>GGC1</i>	Mitochondrial GTP/GDP transporter, essential for mitochondrial genome maintenance; has a role in mitochondrial iron transport; member of the mitochondrial carrier family; (putative) mitochondrial carrier protein
<i>YML094W</i>	<i>GIM5</i>	Subunit of the heterohexameric co-chaperone prefoldin complex which binds specifically to cytosolic chaperonin and transfers target proteins to it
<i>YJL184W</i>	<i>GON7</i>	Protein of unknown function, proposed to be involved in the transfer of mannosylphosphate groups onto N-linked oligosaccharides; also proposed to be involved in responding to osmotic stress
<i>YKL109W</i>	<i>HAP4</i>	Subunit of the heme-activated, glucose-repressed Hap2p/3p/4p/5p CCAAT-binding complex, a transcriptional activator and global regulator of respiratory gene expression; provides the principal activation function of the complex
<i>YCR065W</i>	<i>HCM1</i>	Forkhead transcription factor involved in cell cycle specific transcription of SPC110; dosage-dependent suppressor of calmodulin mutants with specific defects in SPB assembly; involved in telomere maintenance
<i>YLR192C</i>	<i>HCR1</i>	Dual function protein involved in translation initiation as a substoichiometric component of eukaryotic translation initiation factor 3 (eIF3) and required for processing of 20S pre-rRNA; binds to eIF3 subunits Rpg1p and Prt1p and 18S rRNA
<i>YDR317W</i>	<i>HIM1</i>	Protein of unknown function involved in DNA repair
<i>YMR172W</i>	<i>HOT1</i>	Transcription factor required for the transient induction of glycerol biosynthetic genes GPD1 and GPP2 in response to high osmolarity; targets Hog1p to osmostress responsive promoters; has similarity to Msn1p and Gcr1p
<i>YKL138C-A</i>	<i>HSK3</i>	Essential subunit of the DASH microtubule ring complex, couples kinetochores to the force produced by MT depolymerization thereby aiding in chromosome segregation; is transferred to the kinetochore prior to mitosis
<i>YBR272C</i>	<i>HSM3</i>	Protein of unknown function, involved in DNA mismatch repair during slow growth; has weak similarity to Msh1p
<i>YCR046C</i>	<i>IMG1</i>	Mitochondrial ribosomal protein of the small subunit, required for respiration and for maintenance of the mitochondrial genome
<i>YBR107C</i>	<i>IML3</i>	Protein with a role in kinetochore function, localises to the outer kinetochore in a Ctf19p-dependent manner, interacts with Chl4p and Ctf19p
<i>YIR005W</i>	<i>IST3</i>	Component of the U2 snRNP, required for the first catalytic step of splicing and for spliceosomal assembly; interacts with Rds3p and is required for Mer1p-activated splicing
<i>YJR097W</i>	<i>JJJ3</i>	Protein of unknown function, contains a J-domain, which is a region with homology to the <i>E. coli</i> DnaJ protein
<i>YNL104C</i>	<i>LEU4</i>	Alpha-isopropylmalate synthase (2-isopropylmalate synthase); the main isozyme responsible for the first step in the leucine biosynthesis pathway
<i>YJR070C</i>	<i>LIA1</i>	Deoxyhypusine hydroxylase, a HEAT-repeat containing metalloenzyme that catalyses hypusine formation; binds to and is required for the modification of Hyp2p (eIF5A); complements <i>S. pombe</i> mmd1 mutants defective in mitochondrial positioning
<i>YFL018C</i>	<i>LPD1</i>	Dihydrolipoamide dehydrogenase, the lipoamide dehydrogenase component (E3) of the pyruvate dehydrogenase and 2-oxoglutarate dehydrogenase multi-enzyme complexes
<i>YCL051W</i>	<i>LRE1</i>	Protein involved in control of cell wall structure and stress response; inhibits Cbk1p protein kinase activity; overproduction confers resistance to cell-wall degrading enzymes
<i>YAL024C</i>	<i>LTE1</i>	Putative GDP/GTP exchange factor required for mitotic exit at low temperatures; acts as a guanine nucleotide exchange factor (GEF) for Tem1p, which is a key regulator of mitotic exit; physically associates with Ras2p-GTP
<i>YDL182W</i>	<i>LYS20</i>	Homocitrate synthase isozyme, catalyzes the condensation of acetyl-CoA and alpha-ketoglutarate to form homocitrate, which is the first step in the lysine biosynthesis pathway; highly similar to the other isozyme, Lys21p
<i>YMR021C</i>	<i>MAC1</i>	Copper-sensing transcription factor involved in regulation of genes required for high affinity copper transport

<i>YDR318W</i>	<i>MCM21</i>	Protein involved in minichromosome maintenance; component of the COMA complex (Ctf19p, Okp1p, Mcm21p, Ame1p) that bridges kinetochore subunits that are in contact with centromeric DNA and the subunits bound to microtubules
<i>YJR010W</i>	<i>MET3</i>	ATP sulfurylase, catalyzes the primary step of intracellular sulfate activation, essential for assimilatory reduction of sulfate to sulfide, involved in methionine metabolism
<i>YOR211C</i>	<i>MGM1</i>	Mitochondrial GTPase related to dynamin, present in a complex containing Ugo1p and Fzo1p; required for normal morphology of cristae and for stability of Tim11p; homolog of human OPA1 involved in autosomal dominant optic atrophy
<i>YBR084W</i>	<i>MIS1</i>	Mitochondrial C1-tetrahydrofolate synthase, involved in interconversion between different oxidation states of tetrahydrofolate (THF); provides activities of formyl-THF synthetase, methenyl-THF cyclohydrolase, and methylene-THF dehydrogenase
<i>YLL006W</i>	<i>MMM1</i>	Mitochondrial outer membrane protein required for normal mitochondrial morphology and mtDNA stability; involved in tethering mitochondria to the actin cytoskeleton and in anchoring mtDNA nucleoids
<i>YBR098W</i>	<i>MMS4</i>	Subunit of the structure-specific Mms4p-Mus81p endonuclease that cleaves branched DNA; involved in recombination and DNA repair
<i>YBR098W</i>	<i>MMS4</i>	Subunit of the structure-specific Mms4p-Mus81p endonuclease that cleaves branched DNA; involved in recombination and DNA repair
<i>YGL257C</i>	<i>MNT2</i>	Mannosyltransferase involved in adding the 4th and 5th mannose residues of O-linked glycans
<i>YDR347W</i>	<i>MRP1</i>	Mitochondrial ribosomal protein of the small subunit; MRP1 exhibits genetic interactions with PET122, encoding a COX3-specific translational activator, and with PET123, encoding a small subunit mitochondrial ribosomal protein
<i>YPL118W</i>	<i>MRP51</i>	Mitochondrial ribosomal protein of the large subunit; MRP51 exhibits genetic interactions with mutations in the COX2 and COX3 mRNA 5'-untranslated leader sequences
<i>YBL038W</i>	<i>MRPL16</i>	Mitochondrial ribosomal protein of the large subunit
<i>YNL252C</i>	<i>MRPL17</i>	Mitochondrial ribosomal protein of the large subunit
<i>YKR085C</i>	<i>MRPL20</i>	Mitochondrial ribosomal protein of the large subunit
<i>YOR150W</i>	<i>MRPL23</i>	Mitochondrial ribosomal protein of the large subunit
<i>YCR003W</i>	<i>MRPL32</i>	Mitochondrial ribosomal protein of the large subunit
<i>YBR268W</i>	<i>MRPL37</i>	Mitochondrial ribosomal protein of the large subunit
<i>YLR439W</i>	<i>MRPL4</i>	Mitochondrial ribosomal protein of the large subunit
<i>YPR100W</i>	<i>MRPL51</i>	Mitochondrial ribosomal protein of the large subunit
<i>YHR091C</i>	<i>MSR1</i>	Mitochondrial arginyl-tRNA synthetase
<i>YDL107W</i>	<i>MSS2</i>	Peripherally bound inner membrane protein of the mitochondrial matrix, required for export of C-terminal tail of Cox2p through the inner membrane
<i>YMR287C</i>	<i>MSU1</i>	RNase, component of the mitochondrial degradosome along with the ATP-dependent RNA helicase Suv3p; the degradosome associates with the ribosome and mediates turnover of aberrant or unprocessed RNAs
<i>YNL119W</i>	<i>NCS2</i>	Protein with a role in urmylation and in invasive and pseudohyphal growth; inhibits replication of Brome mosaic virus in <i>S. cerevisiae</i> , which is a model system for studying replication of positive-strand RNA viruses in their natural hosts
<i>YPR072W</i>	<i>NOT5</i>	Subunit of the CCR4-NOT complex, which is a global transcriptional regulator with roles in transcription initiation and elongation and in mRNA degradation
<i>YNL091W</i>	<i>NST1</i>	Protein of unknown function, mediates sensitivity to salt stress; interacts physically with the splicing factor Msl1p and also displays genetic interaction with MSL1
<i>YER154W</i>	<i>OXA1</i>	Translocase of the mitochondrial inner membrane, mediates the insertion of both mitochondrial- and nuclear-encoded proteins from the matrix into the inner membrane, interacts with mitochondrial ribosomes; null is respiratory deficient

<i>YCR077C</i>	<i>PAT1</i>	Topoisomerase II-associated deadenylation-dependent mRNA-decapping factor; also required for faithful chromosome transmission, maintenance of rDNA locus stability, and protection of mRNA 3'-UTRs from trimming; functionally linked to Pab1p
<i>YDL179W</i>	<i>PCL9</i>	Cyclin, forms a functional kinase complex with Pho85p cyclin-dependent kinase (Cdk), expressed in late M/early G1 phase, activated by Swi5p
<i>YGR004W</i>	<i>PEX31</i>	Peroxisomal integral membrane protein, involved in negative regulation of peroxisome size; partially functionally redundant with Pex30p and Pex32p; probably acts at a step downstream of steps mediated by Pex28p and Pex29p
<i>YBR168W</i>	<i>PEX32</i>	Peroxisomal integral membrane protein, involved in negative regulation of peroxisome size; partially functionally redundant with Pex31p; genetic interactions suggest action at a step downstream of steps mediated by Pex28p and Pex29p
<i>YDL236W</i>	<i>PHO13</i>	Alkaline phosphatase specific for p-nitrophenyl phosphate, involved in dephosphorylation of histone II-A and casein
<i>YNL082W</i>	<i>PMS1</i>	ATP-binding protein required for mismatch repair in mitosis and meiosis; functions as a heterodimer with Mlh1p, binds double- and single-stranded DNA via its N-terminal domain, similar to <i>E. coli</i> MutL
<i>YDR300C</i>	<i>PRO1</i>	Gamma-glutamyl kinase, catalyzes the first step in proline biosynthesis
<i>YDL214C</i>	<i>PRR2</i>	Protein kinase with a possible role in MAP kinase signaling in the pheromone response pathway
<i>YDL230W</i>	<i>PTP1</i>	Phosphotyrosine-specific protein phosphatase that dephosphorylates a broad range of substrates in vivo, including Fpr3p; localised to the cytoplasm and the mitochondria
<i>YPR191W</i>	<i>QCR2</i>	Subunit 2 of the ubiquinol cytochrome-c reductase complex, which is a component of the mitochondrial inner membrane electron transport chain; transcription is regulated by Hap1p, Hap2p/Hap3p, and heme
<i>YDR529C</i>	<i>QCR7</i>	Subunit 7 of the ubiquinol cytochrome-c reductase complex, which is a component of the mitochondrial inner membrane electron transport chain; oriented facing the mitochondrial matrix; N-terminus appears to play a role in complex assembly
<i>YDL104C</i>	<i>QRI7</i>	Putative metalloprotease, similar to O-sialoglycoprotein metallopeptidase from <i>P. haemolytica</i>
<i>YER173W</i>	<i>RAD24</i>	Checkpoint protein, involved in the activation of the DNA damage and meiotic pachytene checkpoints; subunit of a clamp loader that loads Rad17p-Mec3p-Ddc1p onto DNA; homolog of human and <i>S. pombe</i> Rad17 protein
<i>YJR035W</i>	<i>RAD26</i>	Protein involved in transcription-coupled repair nucleotide excision repair of UV-induced DNA lesions; homolog of human CSB protein
<i>YJR052W</i>	<i>RAD7</i>	Protein that recognises and binds damaged DNA in an ATP-dependent manner (with Rad16p) during nucleotide excision repair; subunit of Nucleotide Excision Repair Factor 4 (NEF4)
<i>YGL246C</i>	<i>RAI1</i>	Nuclear protein that binds to and stabilises the exoribonuclease Rat1p, required for pre-rRNA processing
<i>YJR033C</i>	<i>RAV1</i>	Subunit of the RAVE complex (Rav1p, Rav2p, Skp1p), which promotes assembly of the V-ATPase holoenzyme; required for transport between the early and late endosome/PVC and for localization of TGN membrane proteins; potential Cdc28p substrate
<i>YBR073W</i>	<i>RDH54</i>	DNA-dependent ATPase, stimulates strand exchange by modifying the topology of double-stranded DNA; involved in the recombinational repair of double-strand breaks in DNA during mitosis and meiosis; proposed to be involved in crossover interference
<i>YNL090W</i>	<i>RHO2</i>	Non-essential small GTPase of the Rho/Rac subfamily of Ras-like proteins, involved in the establishment of cell polarity and in microtubule assembly
<i>YFL033C</i>	<i>RIM15</i>	Glucose-repressible protein kinase involved in signal transduction during cell proliferation in response to nutrients, specifically the establishment of stationary phase; originally identified as a regulator of IME2
<i>YEL024W</i>	<i>RIP1</i>	Ubiquinol-cytochrome-c reductase, a Rieske iron-sulfur protein of the mitochondrial cytochrome bc1 complex; transfers electrons from ubiquinol to cytochrome c1 during respiration
<i>YGL107C</i>	<i>RMD9</i>	Mitochondrial protein required for sporulation
<i>YNL072W</i>	<i>RNH201</i>	Ribonuclease H2 catalytic subunit, removes RNA primers during Okazaki fragment synthesis; cooperates with Rad27p nuclease
<i>YIL119C</i>	<i>RPI1</i>	Putative transcriptional regulator; overexpression suppresses the heat shock sensitivity of wild-type RAS2 overexpression and also suppresses the cell lysis defect of an mpk1 mutation

<i>YGL135W</i>	<i>RPL1B</i>	N-terminally acetylated protein component of the large (60S) ribosomal subunit, nearly identical to Rpl1Bp and has similarity to <i>E. coli</i> L1 and rat L10a ribosomal proteins; rpl1a rpl1b double null mutation is lethal
<i>YDR289C</i>	<i>RTT103</i>	Protein that interacts with exonuclease Rat1p and Rai1p and plays a role in transcription termination by RNA polymerase II, has an RPR domain (carboxy-terminal domain interacting domain); also involved in regulation of Ty1 transposition
<i>YJR004C</i>	<i>SAG1</i>	Alpha-agglutinin of alpha-cells, binds to Aga1p during agglutination, N-terminal half is homologous to the immunoglobulin superfamily and contains binding site for a-agglutinin, C-terminal half is highly glycosylated and contains GPI anchor
<i>YGL126W</i>	<i>SCS3</i>	Protein required for inositol prototrophy, appears to be involved in the synthesis of inositol phospholipids from inositol but not in the control of inositol synthesis
<i>YKR029C</i>	<i>SET3</i>	Defining member of the SET3 histone deacetylase complex which is a meiosis-specific repressor of sporulation genes; necessary for efficient transcription by RNAPII; one of two yeast proteins that contains both SET and PHD domains
<i>YIR001C</i>	<i>SGN1</i>	Cytoplasmic RNA-binding protein, contains an RNA recognition motif (RRM); may have a role in mRNA translation, as suggested by genetic interactions with genes encoding proteins involved in translational initiation
<i>YNL032W</i>	<i>SIW14</i>	Tyrosine phosphatase that plays a role in actin filament organization and endocytosis; localised to the cytoplasm
<i>YBR172C</i>	<i>SMY2</i>	Protein of unknown function that interacts with Myo2p; has similarity to <i>S. pombe</i> Mpd2
<i>YDR477W</i>	<i>SNF1</i>	AMP-activated serine/threonine protein kinase found in a complex containing Snf4p and members of the Sip1p/Sip2p/Gal83p family; required for transcription of glucose-repressed genes, thermotolerance, sporulation, and peroxisome biogenesis
<i>YBR169C</i>	<i>SSE2</i>	Member of the heat shock protein 70 (HSP70) family; may be involved in protein folding; localised to the cytoplasm; highly homologous to the heat shock protein Sse1p
<i>YCR030C</i>	<i>SYPI</i>	Protein with a potential role in actin cytoskeletal organization; overexpression suppresses a pfy1 (profilin) null mutation
<i>YJL004C</i>	<i>SYS1</i>	Integral membrane protein of the Golgi required for targeting of the Arf-like GTPase Arl3p to the Golgi; multicopy suppressor of ypt6 null mutation
<i>YPL129W</i>	<i>TAF14</i>	Subunit (30 kDa) of TFIID, TFIIF, and SWI/SNF complexes, involved in RNA polymerase II transcription initiation and in chromatin modification, contains a YEATS domain
<i>YBR150C</i>	<i>TBS1</i>	Probable Zn-finger protein
<i>YGL049C</i>	<i>TIF4632</i>	Translation initiation factor eIF4G, subunit of the mRNA cap-binding protein complex (eIF4F) that also contains eIF4E (Cdc33p); associates with the poly(A)-binding protein Pab1p, also interacts with eIF4A (Tif1p); homologous to Tif4631p
<i>YBR162C</i>	<i>TOS1</i>	Covalently-bound cell wall protein of unknown function; identified as a cell cycle regulated SBF target gene; deletion mutants are highly resistant to treatment with beta-1,3-glucanase; has sequence similarity to YJL171C
<i>YNL079C</i>	<i>TPM1</i>	Major isoform of tropomyosin; binds to and stabilises actin cables and filaments, which direct polarised cell growth and the distribution of several organelles; acetylated by the NatB complex and acetylated form binds actin most efficiently
<i>YLR435W</i>	<i>TSR2</i>	Protein with a potential role in pre-rRNA processing
<i>YCR084C</i>	<i>TUP1</i>	General repressor of transcription, forms complex with Cyc8p, involved in the establishment of repressive chromatin structure through interactions with histones H3 and H4, appears to enhance expression of some genes
<i>YGR019W</i>	<i>UGA1</i>	Gamma-aminobutyrate (GABA) transaminase (4-aminobutyrate aminotransferase) involved in the 4-aminobutyrate and glutamate degradation pathways; required for normal oxidative stress tolerance and nitrogen utilization
<i>YPL045W</i>	<i>VPS16</i>	Subunit of the homotypic vacuole fusion and vacuole protein sorting (HOPS) complex; part of the Class C Vps complex essential for membrane docking and fusion at both the Golgi-to-endosome and endosome-to-vacuole stages of protein transport

<i>YJL029C</i>	<i>VPS53</i>	Component of the GARP (Golgi-associated retrograde protein) complex, Vps51p-Vps52p-Vps53p-Vps54p, which is required for the recycling of proteins from endosomes to the late Golgi; required for vacuolar protein sorting
<i>YJR044C</i>	<i>VPS55</i>	Late endosomal protein involved in late endosome to vacuole trafficking; functional homolog of human obesity receptor gene-related protein (OB-RGRP)
<i>YJR126C</i>	<i>VPS70</i>	Protein of unknown function involved in vacuolar protein sorting
<i>YGL104C</i>	<i>VPS73</i>	Mitochondrial protein of unknown function involved in vacuolar protein sorting
<i>YIL173W</i>	<i>VTH1</i>	Putative membrane glycoprotein with strong similarity to Vth2p and Pep1p/Vps10p, may be involved in vacuolar protein sorting
<i>YDR369C</i>	<i>XRS2</i>	Protein required for DNA repair; component of the Mre11 complex, which is involved in double strand breaks, meiotic recombination, telomere maintenance, and checkpoint signaling
<i>YNL107W</i>	<i>YAF9</i>	Subunit of both the NuA4 histone H4 acetyltransferase complex and the SWR1 complex, may function to antagonise silencing near telomeres; interacts directly with Swc4p, has homology to human leukemogenic protein AF9, contains a YEATS domain
<i>YPR024W</i>	<i>YME1</i>	Subunit, with Mgr1p, of the mitochondrial inner membrane i-AAA protease complex, which is responsible for degradation of unfolded or misfolded mitochondrial gene products; mutation causes an elevated rate of mitochondrial turnover
<i>YGL259W</i>	<i>YPS5</i>	Protein with similarity to GPI-anchored aspartic proteases such as Yap1p and Yap3p
<i>YGR285C</i>	<i>ZUO1</i>	Cytosolic ribosome-associated chaperone that acts, together with Ssz1p and the Ssb proteins, as a chaperone for nascent polypeptide chains; contains a DnaJ domain and functions as a J-protein partner for Ssb17p and Ssb2p
<i>YCR016W</i>	-	Unknown function
<i>YDL218W</i>	-	Unknown function
<i>YDR262W</i>	-	Unknown function
<i>YAL056C-A</i>	-	Unknown function
<i>YCL075W</i>	-	Unknown function
<i>YCL076W</i>	-	Unknown function
<i>YJR098C</i>	-	Unknown function
<i>YJR100C</i>	-	Unknown function
<i>YJR107W</i>	-	Unknown function
<i>YJR119C</i>	-	Unknown function
<i>YDL133W</i>	-	Unknown function
<i>YJL007C</i>	-	Unknown function
<i>YJL016W</i>	-	Unknown function
<i>YJR054W</i>	-	Unknown function
<i>YNR025C</i>	-	Unknown function
<i>YNR029C</i>	-	Unknown function
<i>YBR053C</i>	-	Unknown function
<i>YBR062C</i>	-	Unknown function
<i>YIL100W</i>	-	Unknown function
<i>YIL110W</i>	-	Unknown function
<i>YIL166C</i>	-	Unknown function

<i>YIL168W</i>	-	Unknown function
<i>YKL202W</i>	-	Unknown function
<i>YKR040C</i>	-	Unknown function
<i>YKR041W</i>	-	Unknown function
<i>YBR090C</i>	-	Unknown function
<i>YBR280C</i>	-	Unknown function
<i>YCR061W</i>	-	Unknown function
<i>YER137C</i>	-	Unknown function
<i>YER185W</i>	-	Unknown function
<i>YER186C</i>	-	Unknown function
<i>YER187W</i>	-	Unknown function
<i>YGL101W</i>	-	Unknown function
<i>YPL183W-A</i>	-	Unknown function
<i>YBR099C</i>	-	Unknown function
<i>YBR108W</i>	-	Unknown function
<i>YGR012W</i>	-	Unknown function
<i>YGR015C</i>	-	Unknown function
<i>YGR016W</i>	-	Unknown function
<i>YGR017W</i>	-	Unknown function
<i>YGR021W</i>	-	Unknown function
<i>YGL262W</i>	-	Unknown function
<i>YGR001C</i>	-	Unknown function
<i>YGR153W</i>	-	Unknown function
<i>YGR206W</i>	-	Unknown function
<i>YIL039W</i>	-	Unknown function
<i>YBR284W</i>	-	Unknown function
<i>YBR300C</i>	-	Unknown function
<i>YCL001W-A</i>	-	Unknown function
<i>YDR537C</i>	-	Unknown function
<i>YDR271C</i>	-	Unknown function
<i>YOR331C</i>	-	Unknown function
<i>YOR333C</i>	-	Unknown function
<i>YJR039W</i>	-	Unknown function
<i>YMR118C</i>	-	Unknown function
<i>YER087W</i>	-	Unknown function
<i>YGR150C</i>	-	Unknown function
<i>YJR120W</i>	-	Unknown function

<i>YJL022W</i>	-	Unknown function
<i>YNR020C</i>	-	Unknown function
<i>YML090W</i>	-	Unknown function
<i>YLR149C</i>	-	Unknown function
<i>YLR235C</i>	-	Unknown function
<i>YMR293C</i>	-	Unknown function
<i>YOR199W</i>	-	Unknown function
<i>YPR123C</i>	-	Unknown function
<i>YDL068W</i>	-	Unknown function
<i>YDR532C</i>	-	Unknown function
<i>YDL062W</i>	-	Unknown function
<i>YDR442W</i>	-	Unknown function
<i>YDR458C</i>	-	Unknown function
<i>YDR048C</i>	-	Unknown function
<i>YDR307W</i>	-	Unknown function
<i>YDR319C</i>	-	Unknown function
<i>YDR336W</i>	-	Unknown function
<i>YDR348C</i>	-	Unknown function
<i>YDR370C</i>	-	Unknown function
<i>YAL016C-B</i>	-	Unknown function
<i>YCR075W-A</i>	-	Unknown function
<i>YER053C-A</i>	-	Unknown function
<i>YHR050W-A</i>	-	Unknown function
<i>YIL002W-A</i>	-	Unknown function
<i>YJL136W-A</i>	-	Unknown function
<i>YBR287W</i>	-	Protein of unknown function; mutation results in a zinc sensitive phenotype
<i>YJR080C</i>	-	The authentic, non-tagged protein was localised to the mitochondria